Multipass Laboratory Simulation of Steel Plate Hot Rolling for Improved Productivity

By

Bin Xiao

Thesis submitted for the Degree of
Doctor of Philosophy

At

Department of Materials Science and Engineering
The University of Sheffield

December 2013

Summary

The advanced thermomechanical controlled processing (TMCP) of high strength low alloy (HSLA) steels has been successfully implemented into the commercial hot rolling steel plate production for many decades, despite its major drawback on the low productivity due to a long holding period (HP) often being necessary between the high temperature rough rolling and the low temperature finish rolling stages to avoid the deformation taking place in the partial-recrystallisation temperature range. The long HP also enhances the local austenite coarsening towards the much hotter plate centre, thus exacerbating the microstructure heterogeneity (the prior austenite grain sizes being significantly increased towards plate centre) prior to the finishing stage, and results in non-uniform ferrite grain sizes across the thickness of as-rolled steel plate. Therefore, one of key objectives for this PhD research project, which is fully sponsored and supported by the Tata Steel Europe Company (formerly Corus) Research Development &Technology, was to apply the intermediate forced cooling (IFC) during the HP to increase productivity of heavy plate hot rolling and investigate the effects on the prior austenite grain size (PAGS) at the end of HP and the subsequent ferrite grain size.

In the present study, two complete industrial heavy plate hot rolling schedules (from the reheating, to roughing, HP cooling, and finishing, to post-rolling cooling) with different total applied strains were found possible to be closely translated into the laboratory multistage simulations. Most of the experiments were carried out through the continuous cooling multipass PSC tests that were conducted on the sophisticated Thermomechanical Compression (TMC) machine. One of the commercial hot rolling schedules for producing the 60mm Nb steel plate 8AK39 has 15 rolling passes (10-pass roughing and 5-pass finishing), which has been closely replicated, modified and analysed through some 8-pass PSC tests and one 11-pass PSC test with the same total applied strain and similar deformation temperatures and strain rates. Furthermore, significant modelling efforts from different simulation models were carried out in this project to evaluate the temperature, strain and strain rate gradients present in heavy plates during the hot rolling process of 60mm Nb steel 8AK39, particularly in predicting the temperature profiles through thickness of the partially as-rolled plate during the HP under conditions of different applied cooling rates. These predicted results (such as the calculated IFC temperature profile during the HP) were then used as the input values for the continuous cooling multipass PSC tests to investigate the different flow curves and the corresponding microstructures at the specific positions across plate thickness (mainly at the plate centre and sub-surface) during roughing and the HP.

In general, the results have shown great consistency and reliability of recorded temperature profiles and the corresponding flow curves in many similar multipass PSC tests, which is essential to correctly analyse the microstructural evolution following the continuous cooling 8-pass PSC test and the effects of different rolling parameters on the PAGS and the subsequent ferrite grain sizes. Moreover, application of the novel IFC rather than the natural-air slow cooling during the long HP indeed increased productivity, reduced the kinetics of austenite grain growth during the HP (i.e. a faster cooling rate produces a small austenite grain size at the end of the HP) and refined the subsequent average ferrite grain size. More importantly, according to the results, the applied cooling rate of acceleration cooling (ACC) after deformation was the most dominant factor to achieve small ferrite grain size compared to the results of the others rolling factors, such as different steel chemical composition, application of the IFC during the HP, increasing applied strain per pass and reducing the average deformation temperature of 5-pass finishing.

It is important to emphasise that the successfully developed continuous cooling multipass (up to 13 passes so far and most tests were 8-pass) PSC testing is the state-of-the art on the laboratory replication of industrial hot rolling steel production as most similar simulations are only carried out on the multipass hot torsion tests.

Acknowledgement

I would like to acknowledge a deep debt of gratitude to the people and organisation that have made this PhD work possible and to whom I owe so much.

I would like to express my sincere gratitude and appreciation to my two supervisors Dr. Eric J. Palmiere and Prof. Andy A. Howe for giving me this great opportunity to work at the Department of Materials Science and Engineering in University of Sheffield and for their patience, invaluable guidance, constant support, encouragement and understanding during all these years of my PhD, particularly at the final difficult stage of thesis writing. I am also greatly appreciative that Eric and Andy gave me the great opportunity to attend and present my works at several national symposiums and international conferences: HSLA' Steel 2011, Thermec 2011 and TMP 2012, and also thanks to Eric present my latest work at the REX&GG 2013 on my behalf. I would also like to thank the travel grants from the SMEA and the Ironmongers' Foundation.

I am also very grateful to the Tata Steel Europe (formerly Corus), Research Development and Technology, for the full sponsorship to undertake this research, and technical and materials support. In particular, special thanks are due to Dr. Heathery Carey, Dr. Sally Parker (using the IMPress model) and Mr. Roger Beaverstock for many inspiring discussions and kindly help throughout this work.

I would like to thank the members of the past research organisation (till March 2013): IMMPETUS (The Institute for Microstructural and Mechanical Process Engineering: The University of Sheffield), especially Dr. Richard Thackray, Dr. Krzysztof Muszka (for the Abaqus/Explict finite element simulation supports), Dr. Lin Sun and Dr. John Hinton for their stimulating conversations, help and friendship. Especially thanks to my colleagues in office H6, for the friendly and enjoyable research atmosphere.

I would also like to express many thanks to the technical staff of The Department of Materials Science and Engineering for their time, and technical assistance, especially Mr. Ian. Watts for help handling the heavy cast ingots, Mr. Stuart Bater for the laboratory Hille mill hot rolling practices and materials heat treatment tests, Mr. Phil Staton with specimen preparation and training in optical microscopy, Mr. Dave Manvell and Mr. Deano Haylock for the TMC machine maintenance.

Finally but not least, I would like to thank my wife, Jiang Jiang Jia (Rita), for her constant praying, patience, understanding, supporting and the endless love, without whom this PhD thesis could not have been achieved. I dedicate this work to her.

Nomenclature

ACC …..…….....Accelerated Cooling

DQ ……..……....Direct Quenching

DRX …..…….....Dynamic Recrystallisation

FD …..…….....Finite Difference

FE …..…….....Finite Element

FTTU ……..…….....Fast Thermal Treatment Unit

HSLA ……...…….....High Strength Low Alloy

HP ……..…….....Holding Period

HTC ……..…….....Heat Transfer Coefficient (W/m^2K)

IAC …….....Interrupted Accelerated Cooling

IFC …….....Intermediate Forced Cooling

MAE …….....Microalloyed Elements

MDRX ..…….....Metadynamic Recrystallisation

MFS …….…….....Mean Flow Stress (MPa)

PSC …….....Plane Strain Compression

PAGS …….…….....Prior Austenite Grain Size (μm)

RCR …….....Recrystallisation Controlled Rolling

RD …….....Rolling Direction

SIP …….....Strain Induced Precipitation

SRX ……Static Recrystallisation

TD …….....Transverse Direction

TMC …….....Thermomechanical Compression

TMCP ….....Thermomechanical Controlled Rolling Process

WQ ….....Water Quench

T_{def} …….....Deformation Temperature (°C)

T_{DISS} ……..….....Dissolution Temperature for Precipitates (°C)

T_{GC} ……...….....Grain Coarsening Temperature (°C)

T_{RH} …….....Reheating Temperature (°C)

$T_{0.95X}$ ….....95% or Fully Recrystallisation Temperature (°C)

$T_{0.05X}$ …….....5% or Non–Recrystallisation Temperature (°C)

Ar_3 …….....Austenite to Ferrite Transformation Temperature (°C)

C_r …….....Cooling Rate (°C/s)

d_r …….....Austenite grain size (μm)

D_0 …….....Initial austenite grain size (μm)

d_i …….....Austenite grain size after the i^{th} pass ($i \geq 1$) (μm)

d_{rex} …….....Statically recrystallised austenite grain size (μm)

d_{gg} …….....Austenite grain size after grain growth (μm)

d_α …….....Ferrite grain size (μm)

m …….....Rolling shape factor

R …….....Universal Gas constant = 8.314kJ/(kg mol K)

$t_{0.95X}$ …….....Time for 95% static recrystallisation (s)

$t_{0.5X}$ …….....Time for 50% static recrystallisation (s)

$t_{0.05X}$ …….....Time for 5% static recrystallisation (s)

$t_{0.05P}$ ……..….....Time for 5% strain induced precipitation (s)

X …….....Volume fraction of static recrystallisation

Z …….....Zener Hollomon parameter

ε …….….....Strain

ε_{evm} …….….....Equivalent Strain

ε_c …….....Critical strain for the dynamic recrystallisation

ε_{eff} …….....Effective strain for the static recrystallisation

ε_p …….....Peak strain

ε_r …….....Retained strain prior to the phase transformation

ε_{Total} …….….....Total applied strain

$\dot{\varepsilon}$ …….....Deformation strain rate (s^{-1})

List of Figures

Figure Number **Page Number**

List of Tables

Table Number **Page Number**

Table of Contents

Chapter 1 - Introduction

1.1. Thermomechanical Controlled Processing (TMCP) of HSLA Steel Plate

There is a large and continuous strong demanding market for High Strength Low Alloy (HSLA) steels with thick gauge (generally the thickness of heavy plate is greater than 25mm, and can be up to 120mm), in particular the heavy plate for ship building, offshore platforms, pipelines for gas and oil transportation, building construction and bridges but also a lot of other application fields [1-3, 5, 7]. It is well recognised that the Thermomechanical Controlled Processing (TMCP) of HSLA steels is the modern integrated technique which utilises the advantages of microalloying elements (MAE), thermal and mechanical control during hot rolling and post-deformation controlled accelerated cooling (ACC). The technique of TMCP has been widely employed in the production of plate to optimise properties such as high strength, low ductile to brittle transition temperature, great impact toughness and good weldability for many decades [6, 8-12]. Nowadays, this technology in steels has also been applied to the strip, section, bar, rod and forging industry with considerable success [8].

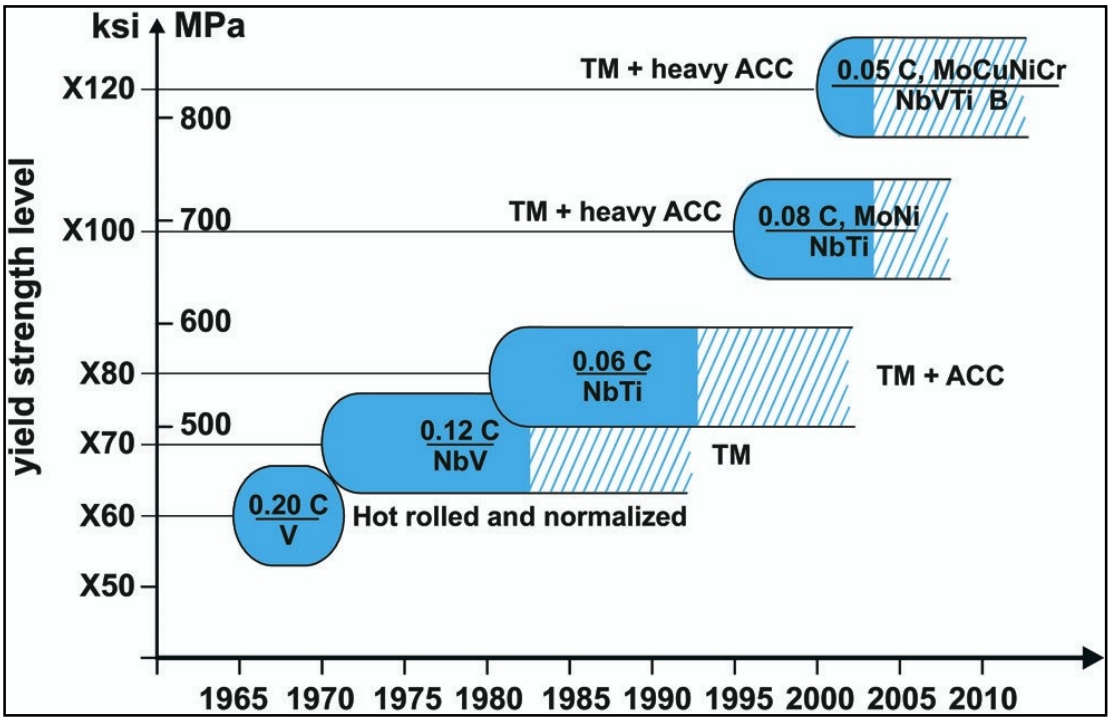

Figure 1: Historical development of HSLA steels as results of advanced microalloying elements, thermomechanical treatment (TM) and accelerated cooling (ACC) [5]

The Figure 1 clearly shows the developing history of increasing yield strength level in HSLA steels as a result of advanced microalloying, thermomechanical treatment (TM) and ACC. The targets of mechanical properties of TMCP are not only increased strength of HSLA plate steel but also improved toughness simultaneously, as well as low carbon equivalent for good weldability. Therefore, grain refinement of ferrite and precipitation hardening during and after phase transformation are the two obvious strengthening mechanisms to be used in TMCP for achieving the desired mechanical properties. In general, the main concept of TMCP is based on metallurgical phenomena such as static and/or dynamic recrystallisation and grain growth, phase transformation and precipitation, which utilise many common strengthening mechanisms in steel such as solid solution hardening, precipitation hardening, dislocation hardening, and particularly for the grain refinement [6-12].

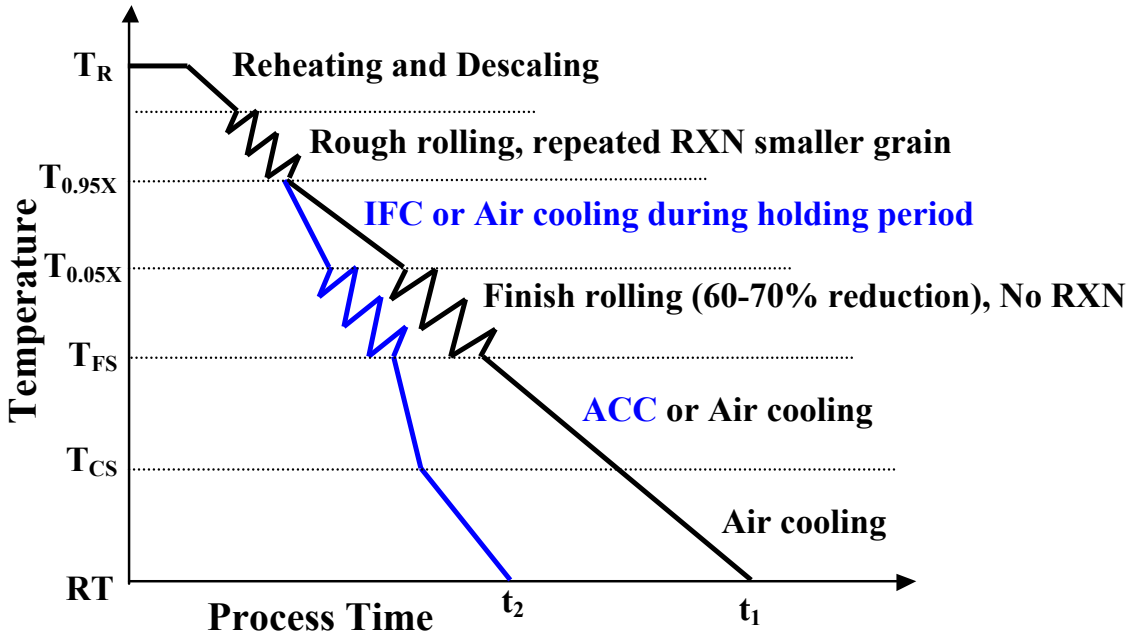

Figure 2: Two different hot rolling profiles of TMCP including critical temperatures

In the above Figure 2, T_R, $T_{0.95X}$, $T_{0.05X}$, T_{FS}, T_{CS} and RT refer to the slab reheating, fully or 95% austenite recrystallisation, 5% or non-recrystallisation, finish rolling, accelerated cooling stop and room temperatures, respectively. It also indicates that the conventional TMCP has longer process time, t_1 than the modified TMCP (water or forced cooling during holding period and after finish rolling), t_2, and more detailed information of the above figure are explained in the following and next chapter (Literature Review).

1.2. Problems in Commercial Heavy Plate Production through TMCP

Despite the many advantages through applying the TMCP into heavy plate production, one major drawback is the excessive process time, resulting in low productivity [13-18]. This problem is much worse in a reversible one stand rolling mill due to a long holding period between the high temperature (roughing) and the low temperature (finishing) rolling stages, and if the distance between the roughing stand and finishing stand is short. That is because in order to produce the smallest ferrite grain size as possible it usually requires a large reduction (usually more than 60%) during finishing below recrystallisation stop temperature, $T_{0.05X}$, shown in Figure 2, with deformation sometimes taking place below the austenite to ferrite transformation temperature, Ar_3, resulting in intercritical rolling [7-11]. Therefore, after the roughing stage at the high temperature region, the rolling schedule requires a long and critical holding period (HP) to allow the temperature of partially rolled plate to fall sufficiently to suppress recrystallisation during the finishing stage, which can have a significant impact on production rate because rolling mill delays can be up to twenty minutes [16]. Recently, the SIMENS VAI Company has built new plate mill [17] to improve productivity (air cooling several partial rolled plates during HP), shown below in Figure 3, in which there is a long distance between the roughing and finishing stands and a spacing of 105 meters was reported in the AG der Dillinger hot rolling plate mill [19].

Figure 3: Long space required for maximising productivity during holding period [17]

Moreover, the biggest challenge for the hot rolled heavy plate is the ability of achieving high strain penetration (reduction >15-30%) in the heavy plate centre region in order to promote good through-thickness grain size homogeneity and annihilation of central porosity [17-21].

It is considered that the overall reduction from initial slab to final plate should be a minimum of 3:1 to give reasonable consolidation and to refine the ferrite microstructure at the centreline of thick plate [18, 22]. For the modern powerful plate mill, the refinement of heavy plate centre quality is possible if the maximum possible per-pass reductions so called HSF (High Shape Factor), m, is applied during deformation, especially at the roughing stage [18-21]. It has been shown that the local reduction at the plate mid-thickness in one pass rolling can be treated as a function of the rolling shape factor m, which is defined as

$$m = \frac{2\sqrt{R_r \times \left(h_i - h_f\right)}}{h_i + h_f} = \frac{2\sqrt{R_r \times \Delta h}}{h_i + h_f} \tag{1}$$

Where R_r is the work roll radius; h_i and h_f are the plate thickness before and after the each rolling pass respectively. In the case of HSF (m>0.8) rolling, the centre of the rolled product was reportedly deformed thoroughly resulting in good toughness and high tensile strength in the thickness direction [18-21]. However, a value of $m > 0.8$ is still difficult to achieve under normal conditions in early roughing passes with thick plate even with high rolling load and torque [18, 21]. To overcome the limitations of developing a refined ferrite grain size and improved properties at the centreline of heavy plate, the use of 'Force Cooling' prior to first pass of rough rolling is commonly applied by heavy plate producers which have accelerated cooling units already and the benefits of this type of rolling schedule were reported to be an improvement in the mid-thickness consolidation, ferrite grain size and toughness of heavy plate [18, 20, 21].

1.3. Introduction of Water Cooling during and after Hot Rolling

In the modern hot-rolled heavy steel plate industry, water is defined as "the most effective microalloying addition to steel" [13] and water-cooling techniques can be applied at the different stages of conventional TMCP to replace natural-air cooling to increase production rate and improve final plate properties, which are introduced in more detail in the literature review chapter. As it can be seen from Figure 4 forced cooling has been adopted at: descaling (remove oxide layers at the plate surface after dropout from the reheating furnace and chill the plate surface) before roughing mill, intermediate forced cooling (IFC) at the delaying period between roughing and finishing mill, accelerated cooling after finishing mill, and also water cooling can take place at relatively long inter-pass times between rough rolling passes which depends on the specific hot rolling schedule.

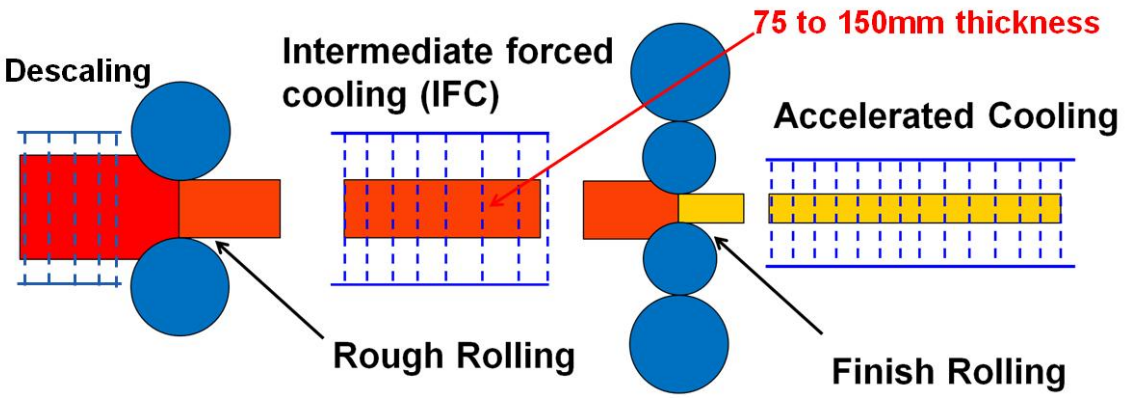

Figure 4: Schematic water-cooling applied at the different stage of hot rolling process

In order to reduce the long holding time, and increase productivity, a number of plate producers have examined the possibility of applying the ACC unit to cool partially rolled plate during the HP, known as 'Intermediate Forced Cooling' [13, 15, 16, 18]. Compared with the significant amount of research that has been carried out on accelerated cooling (ACC) after finish rolling, the IFC technique to reduce the long HP has been paid much less attention. Based on the limited published papers and research reports [16, 23-30] on the IFC, the HP can be shortened through application of water spraying without any deterioration in bulk plate mechanical properties and can improve the through thickness homogenisation of thick plate, and eliminate the need for expensive post-heat treatments.

The primary novel aspect of employing IFC instead of normal air-cooling into TMCP is that good levels of grain refinement can be also achieved through reduced austenite grain growth during HP [23]. This includes cooling the plate surface below the temperatures required for the remaining finishing passes and then allowing the surface to reheat through diffusion of heat from the much hotter core [24-30]. Under conventional natural-air cooling conditions, a large variation of prior austenite grain size may occur throughout the plate thickness as a result of different cooling rates from surface to centre of plate during HP. This variation cannot be sufficiently reduced during finish rolling and in turn causes differences in ferrite grain size across thickness in final plate microstructure and reduce toughness. On the other hand, under IFC conditions, chilling the surface of plate possibly increase thickness penetration during HP [18, 20, 21], and also relatively increase average cooling rate from surface towards centre (but most likely the cooling rate at plate centre is not affected by the IFC) of plate comparing to air cooling, which in turn maybe reduce the variation of prior austenite grain size distribution and relatively improve homogenisation of microstructure.

1.4. Multipass Laboratory Simulation of Industrial Rolling Schedules

Sections 1.1 to 1.3 have introduced the industrial aspects of this study, and alongside these was one of the main objectives – the development of advanced laboratory based experimental simulation of a complete commercial hot rolling steel plate production as close as possible. It is well recognised that the costs associated with industrial trials are extremely high, and also the rolling schedules of trials are difficult to control and monitor and the trials may also be constrained by the capability of existing rolling mills.

It is important to emphasis that normally the industrial rolling schedules were simulated by multistage laboratory hot torsion test due to larger strain can be applied compared to the strain limit in plane strain compression (PSC) testing. However, PSC testing is chosen for this project due to the deformation state is much closer to the industrial flat hot rolling process. The laboratory simulations of two completed industrial hot rolling schedules, varying in chemical composition, deformation (strain and strain rate), temperature, number of passes and interpass time, have been successfully developed and well performed by multipass (up to 13 passes so far and most tests were 8 passes) PSC tests on the Thermomechanical Compression (TMC) machine. It is the state-of-the-art on the laboratory multipass PSC simulation as most reported PSC deformations so far were only up to 4 passes.

Clearly, it is impossible to simulate all the aspects of industrial hot rolling steel plate production in the laboratory standard 10 or 12mm PSC specimens, such as temperature and strain distributions across thickness of heavy plate. Therefore, most of the tests were conducted using rolling parameters calculated by finite element modelling as relevant to specific positions (such as plate surface and centre) through the heavy plate thickness. Extremely useful results were obtained from the laboratory simulation of the multistage hot rolling process, shown in the results chapter.

Chapter 2 - Literature Review

2.1. Overview of Literature Survey

The historical developments and fundamental metallurgy of TMCP in HSLA steels since 1970's have been numerously reported and summarised in several books [8, 9, 31-36], conference proceedings [10-13, 37-45] and papers [2, 46-53]. It is important to be reminded from these numerous literatures that the primary objective of the TMCP for heavy plate is to achieve a very fine and uniform ferrite grain size as much as possible across the thickness with the desired high strength and toughness properties, and good weldability. The following literature review includes various aspects of TMCP in heavy plate hot rolling: underlying strengthening mechanisms and metallurgical phenomena taken place during hot deformation of steel heavy plate, detailed information of water cooling and heat transfer during and after hot rolling production, physical-based modelling of austenite and ferrite grain sizes and an introduction of plane strain compression (PSC) tests on the TMC machine. Finally, in the summary of the literature survey, reasons and the challenges for the present work were also included at the end of this chapter.

2.2. The Roles of Microalloying Elements and the Key Strengthening Mechanisms in Hot Rolling HSLA Steels

2.2.1. The Roles of Microalloying Elements

It is well recognised that it is difficult to achieve small ferrite grain size and good mechanical properties steels through the TMCP without the addition of correct microalloying elements (MAE), and on the other hand the steels with addition of MAE, but without applying accurate TMCP technique into production, can even display lower toughness than their plain-carbon steel counterparts [8, 36]. Therefore it is crucial to fully integrate advanced microalloying technique into the precise TMCP to obtain the desired as-rolled microstructures and properties. In general, the definition of HSLA steels is containing small amounts of MAE such as aluminium, niobium, titanium and vanadium, copper (whose total composition is less than 1wt%), for their much better ability to increase the strength and toughness of the as-rolled steel plate compared to mild or plain carbon steel [8, 35, 39]. Moreover, HSLA steels usually have either low or extra low carbon concentration, which lead to greatly improve in weldability and ductility.

The roles of the MAE in HSLA steels are well documented in many literatures in which there are two main purposes on mechanical properties: to improve strength and toughness through ferrite grain refinement and to increase strength through strengthening mechanisms. In terms of grain size refinement, the MAE can suppress austenite grain coarsening during reheating step, delay static recrystallisation and grain growth during intervals of multipass deformation. That is because the MAE can be presented either as forming fine precipitates (strong pining force) induced by deformation to stop austenite recrystallisation or dissolving in the austenite matrix as solutes (weak pinning force) to impede the movement of dislocations [42, 54]. Moreover, if at end of finishing stage there is still amount of MAE in solid solution, these elements can enhance further strength through precipitation hardening, also increase hardenability and lower transformation temperatures.

In terms of increasing the yield strength σ_y of hot rolled HSLA ferrite – pearlite steels [8] (ferrite is the dominant phase with small amount of pearlite in the final as-rolled transformed microstructure), the functions of MAE can be described by the following semi-empirical equation (cannot be applied to steel microstructures with large amount of pearlite or low temperature transformed products) in which different hardening mechanisms are included:

$$\sigma_y = \sigma_0 + \Delta\sigma_S + \Delta\sigma_P + \Delta\sigma_D + \Delta\sigma_T + k_y d_\alpha^{-\frac{1}{2}} \quad (2)$$

where σ_0 is the lattice friction stress required to move dislocations along the slip planes in the pure iron crystal lattices and $\Delta\sigma_S, \Delta\sigma_P, \Delta\sigma_D$, and $\Delta\sigma_T$ are the strengthening increments caused by solid solution, precipitation, dislocation and texture effects, respectively, and the last term $k_y d_\alpha^{-\frac{1}{2}}$ is the effect of average ferrite grain size to the yield strength [8, 12, 46].

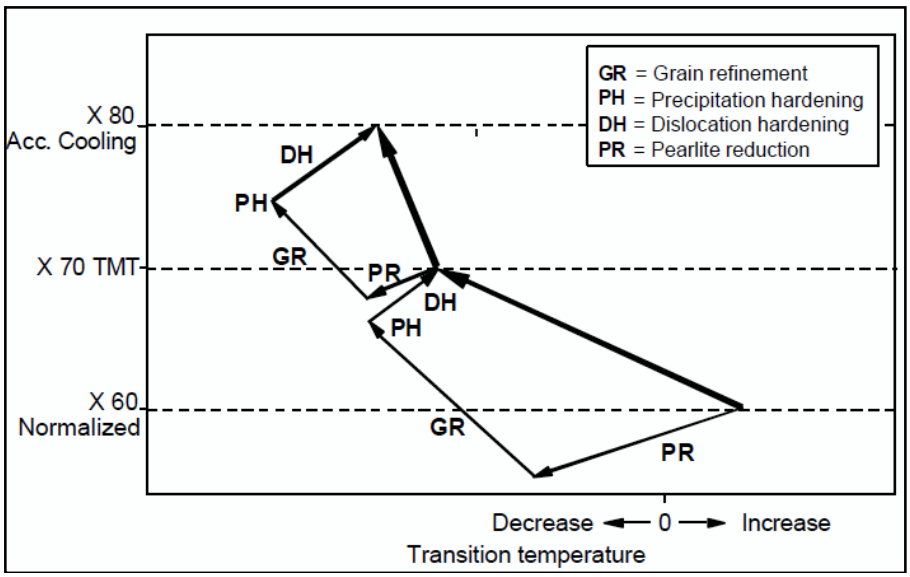

Figure 5: The effects of different microstructures in steel to improve strength and toughness properties [5]

It is also well documented that only the ferrite grain refinement can simultaneously improve the as-rolled steel strength and toughness, while all others strengthening mechanisms in some extent decrease steel toughness, shown in Figure 5. In the following parts three common strengthening mechanisms for hot rolling steel plate: solid solution strengthening, grain size refinement, and precipitation hardening are in brief introduced.

2.2.2. Solid Solution Strengthening

The nature of solid solution strengthening is a recognised fact through adding solute elements into the crystal structure of iron matrix for increasing lattice resistance to deformation [9, 31]. As the solutes are introduced to the matrix, the lattice becomes elastically distorted and the atoms of solute tend to concentrate at dislocations to reduce mobility and pin the movement of dislocations, increasing the stress necessary to move dislocations [9, 31, 55-57]. Depending on the size of the solute, there are two types of solid solution strengthening: substitutional and interstitial solid solutions, shown in Figure 6. It has been reported that the solutes of both types obey the relationship that increase of strength is proportional to the square root of solute concentration, and increases with a larger difference in atomic size between iron atoms and solute atoms [31]. Moreover, frequently the substitutional solutes can be interacted with interstitial solutes to form compounds such as TiN, TiC, Nb(C, N), etc. which will decrease the overall solid solution strengthening effect but this may be compensated by some degree of precipitation hardening [31].

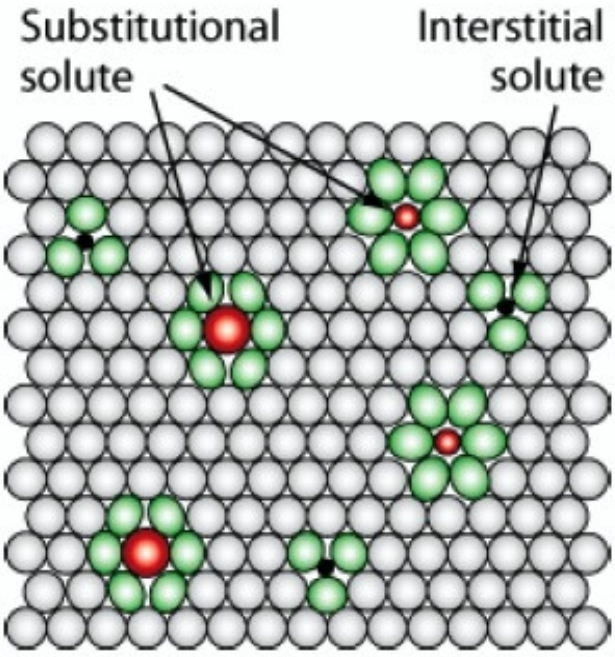

Figure 6: Schematic atoms structures of substitutional and interstitial solutes added into parent matrix in solid solution strengthening [58]

Firstly, substitutional solid solution strengthening occurs when the atoms size of solute have roughly similar size to parent iron atoms (that is within ±15% different in atomic size) and the solute atoms do not combine C and N elements to form carbides, nitrides or other compounds, merely for substitute the solvent Fe atoms [31, 63], such as Mn and Si. Secondly, interstitial solid solutions take place when the solute atoms, such as C, N and B, are considerably smaller than the solvent atoms (Fe) and to be accommodated into the interstitial sites of Fe crystal structure. The interstitial elements have a higher strengthening effect, which apparently produces 10 -100 times that of substitutional atoms [31, 57], shown in the following Figure 7. However, it must be noticed that both C and N have limited solubility in ferrite, which cannot be used to a great extent and with adverse effect on toughness. Thus, of the remaining elements in Figure 7, only Si and Mn are the most cost-effective elements to increase solid solution strengthening [57]. It is illustrated in Figure 7 that Ni and Al in solid solution have very little influence on the yield stress, while the addition of Cr even reduced the yield stress but the original author [6, 31] and later researchers [36, 56, 63] did not explain the possible reasons in their works.

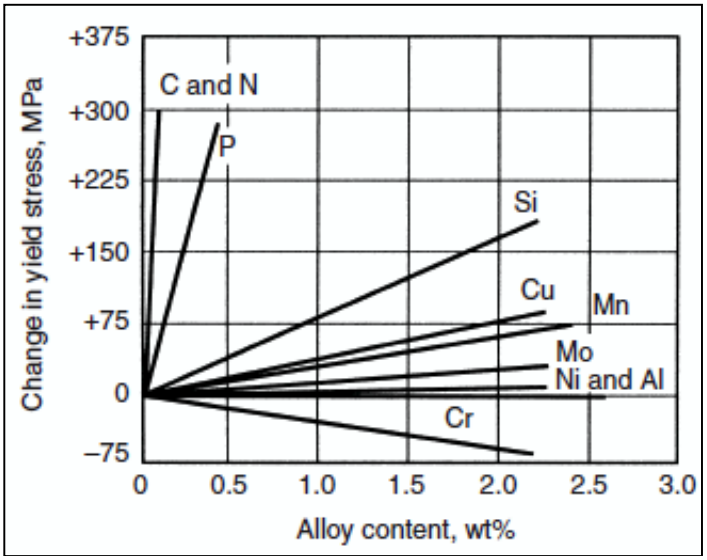

Figure 7: Solid solutions strengthening effects of different alloying elements in ferrite-pearlite high strength low alloy steels containing 0.25 wt% C and 1.5wt% Mn [36, 56, 63]

2.2.3. Grain Size Refinement

Grain size refinement has been extensively used as one of the main strengthening mechanisms in the development of HSLA steels for its unique function that improves both strength and toughness simultaneously since 1950s. The increment in strength due to ferrite grain refinement is because the ferrite grain boundaries are the effective barriers to the dislocation movements, and the smaller ferrite grain sizes produce the greater number of

grain boundaries and greater force of barriers. The effect of ferrite grain size d_α on yield strength σ_y is properly quantified by the well-known Hall-Petch relationship shown in Equation 3 in which σ_0 and k_y are constants. As mentioned previously the small ferrite grain size also reduced the ductile-to-brittle impact transition temperature, shown in Equation 4 in which β and C are constants [56]. According to the following Figure 8, when the ferrite grain size reduced from 10μm to 3μm, the yield strength of steel increased from 245MPa to 385MPa while the ductile-to-brittle impact transition temperature (ITT) is reduced from -40°C to -130°C. In hot rolling steel processes, there are a number of ways to refine the ferrite grain size, which depends on many factors. However, based on Figure 8 there is obviously a limit to the amount of strengthening that can be obtained via this mechanism [56], which are explained and described in detail in later sections of this thesis.

$$\sigma_y = \sigma_0 + k_y d_\alpha^{-\frac{1}{2}} \tag{3}$$

$$\beta T = \ln\beta - \ln C - \ln d_\alpha^{-\frac{1}{2}} \tag{4}$$

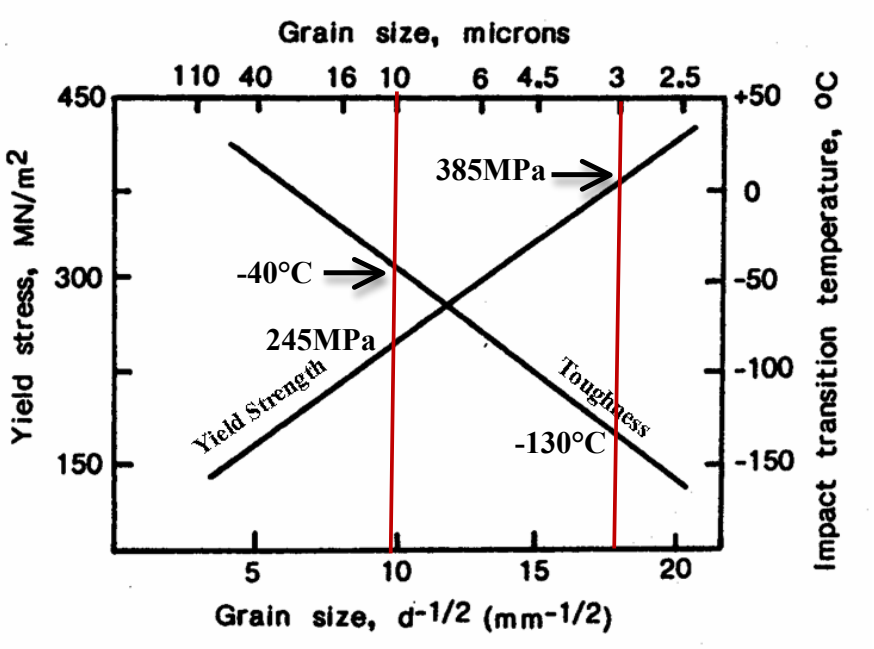

Figure 8: Effects of ferrite grain size on yield strength and impact transition temperature (ITT) [57]

2.2.4. Precipitation Strengthening

Apart from the grain size refinement, precipitation hardening of fine, second phase particles in the Fe matrix is another very important strengthening mechanism in HSLA steels. Microalloyed particles were precipitated out of solid solution either in the austenite, or during

the austenite to ferrite phase transformation because when the temperature of as-rolled plate is continuously reduced, the solubility of microalloyed (Nb and V) particles decreased. The presence of precipitates can impede dislocation movements, as a greater force is required to move the dislocation through an array of particles, thus causing the strength of as-rolled plate to increase [31, 55-57, 59]. In HSLA steels, precipitation strengthening is usually achieved through fine and randomly dispersed small carbides, nitrides and/or carbonitride of small additions of MAE (Ti, Nb, Al and V) in the Fe matrix, and the strengthening effect of these precipitates is dependent on both the volume fraction and particle size. It is illustrated in Figure 9 that there are two ways of interaction between dislocations and precipitate particles: a) dislocation can slide through particles and shear them, b) dislocation can loop between fine-spaced hard particles and bypass them (known as the Orowan mechanism) [32, 57]. According to the relationship in Figure 10, the stress increases as the volume fraction of precipitates increase and precipitate size decreases.

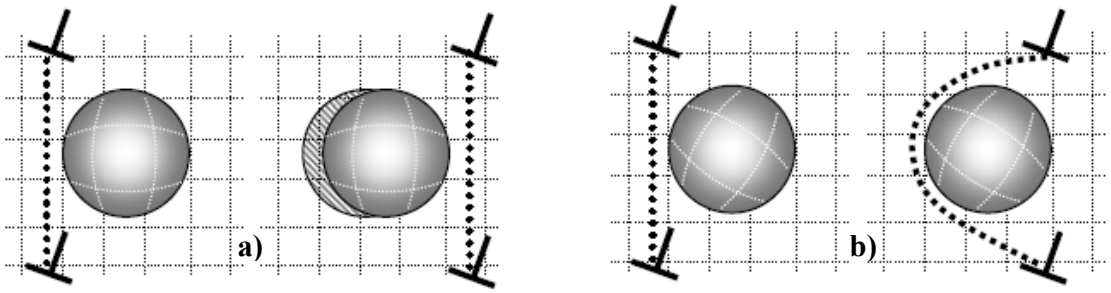

Figure 9: Interactions between dislocations and precipitate particles [57]

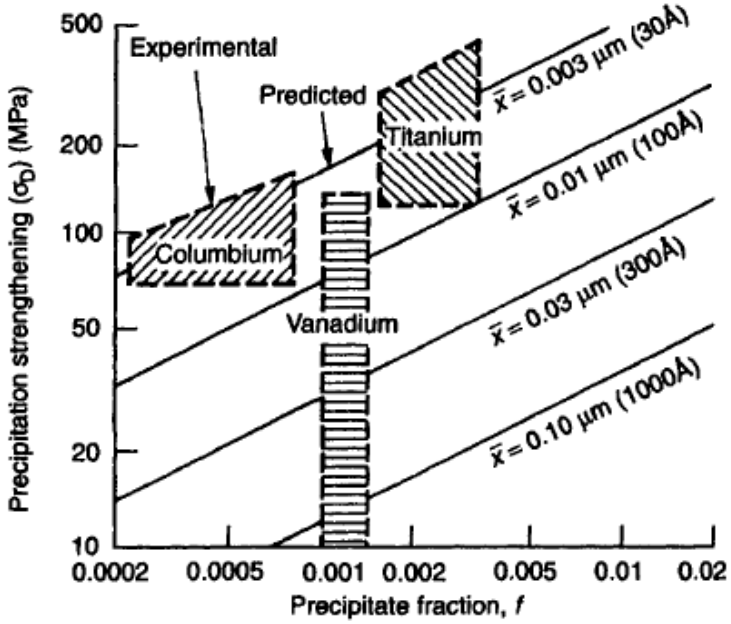

Figure 10: The dependence of precipitation strengthening on precipitate size and volume fraction according to the Ashby - Orowan mechanism, compared with experimental observation for given microalloyed additions [56]

2.3. Metallurgical Phenomena and Microstructure Evolution during Hot Working

2.3.1. Introduction

For many decades hot working has been the most common method of metal forming and has been widely used to not only reduce the thick slabs down to their required dimensions but also to achieve desired mechanical properties through the deliberate design and controls of the hot rolling processing [8, 36]. Hot working steel generally involves changing the shape of as-reheated slab through a sequence of multipass deformation in the temperature range 1200°C to 750°C, when the steel is fully austenitic or in the austenitic plus ferrite two phase condition. Hot working is more economical compared with cold working as it is much easier to deform the slab at high temperature, and therefore the lower working power is required.

2.3.1.1. Iron Carbon Equilibrium Phase Diagram

The equilibrium phases presented in the plain carbon and HSLA steels (approximately) at each temperature as a function of carbon composition can be simply represented by the fundamental binary Fe-C phase diagram, in which there are many constituents like austenite, ferrite, cementite, and graphite [9, 63-67], shown in Figure 11. It is widely accepted that when the carbon addition is less than 2.14 wt% it is known as steel, otherwise, it is called cast iron. It should be noted that analysing the microstructures of most steels usually require the basic knowledge of Fe-C phase diagram, which is vital in understanding the critical temperatures in hot rolling schedules and phase transformation during and after hot rolling process, and the most importantly is the foundation of studying some complex as-rolled microstructures.

According to the temperature axis in Figure 11, pure Fe exists in two different crystal forms as function of temperature. From the room temperature up to 912°C, the Fe atoms are in the body centred cubic (BCC) pattern, which is known as alpha iron (or ferrite in steel). Above 912°C the ferrite transforms to gamma iron (austenite) that has a face centred cubic (FCC) crystal structure. Further increasing temperature until it reaches at 1394°C the gamma iron reverts back to BCC form and called delta iron which is stable until the melting point 1538°C [9, 63-67]. It is important to notice that the solid solubility of carbon in ferrite is much smaller, with a maximum concentration of 0.022wt% at 723°C than in austenite phase with a maximum value of 2.14wt% at 1147°C (shown Figure 11). Consider the HSLA steels containing 0.085wt% carbon concentration in this project, the temperature of as-rolling steel plate progressively reduced from reheating temperature and slowly reached the A_3

temperature boundary line, proeutectoid ferrite [64] started to nucleate and growth mostly from the austenite grain boundary. Because only little amount of carbon can be dissolved in proeutectoid ferrite phase, the rest of the austenite is gradually enriched in carbon until the Ar_1 temperature (723°C) is reached. Under slow cooling rate the rest of austenite transformed into pearlite, which is not a phase but it is a eutectoid mixture, which comprises alternate lamellae of ferrite and iron carbide or cementite (Fe_3C) through the eutectoid reaction that describes the phase transformation of one solid into two different solids [63-67]. The ferrite in the pearlite is called eutectoid ferrite to be distinguished from the proeutectoid ferrite which formed firstly above 723°C [64]. According to the level rule in phase diagram and different carbon contents in ferrite and the eutectoid point (0.76wt%), the weight percentage of proeutectoid and eutectoid ferrite can be determined as the following steps.

$$\text{wt \% total ferrite} = \frac{6.67 - 0.085}{6.67 - 0.022} \times 100\% = 99\% \text{ (6.67wt\% is the carbon content in } Fe_3C)$$

$$\text{wt\% proeutectoid ferrite} = \frac{0.76 - 0.085}{0.76 - 0.022} \times 100\% = 91.5\%$$

wt % eutectoid ferrite = total ferrite – proeutectoid ferrite = 7.5%

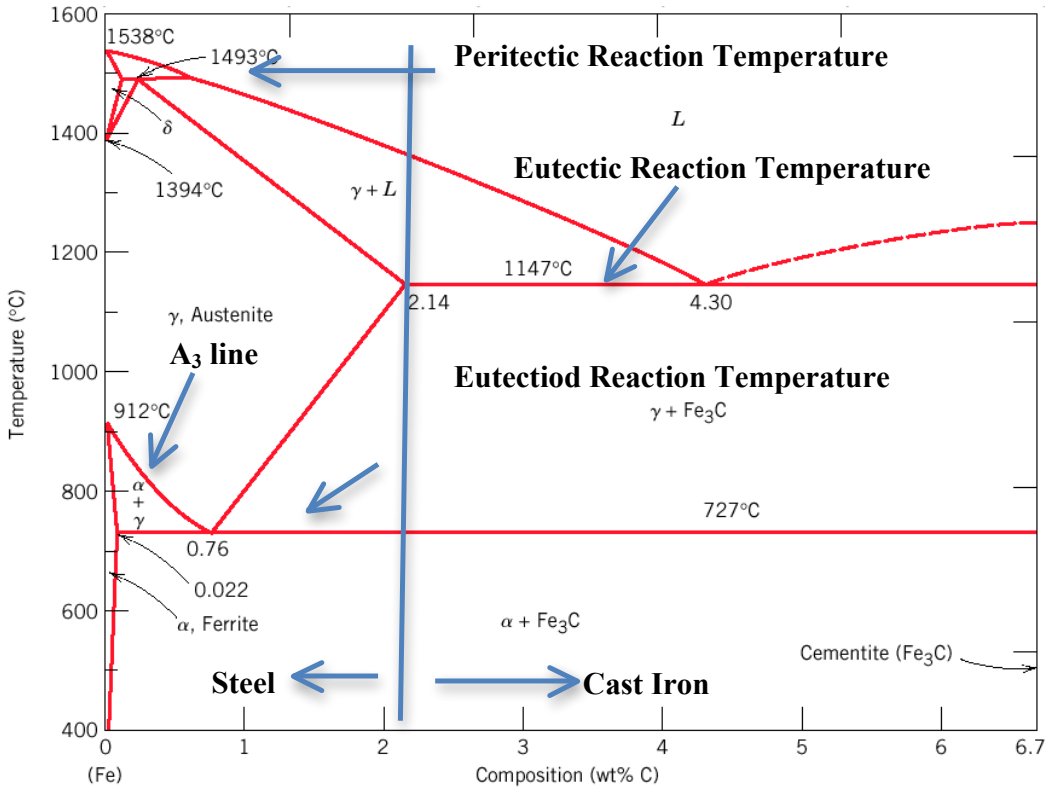

Figure 11: The modified iron - carbon (Fe-C) phase diagram up to 6.7wt% of carbon with different constituents [63-67]

2.3.1.2. Work Hardening and Softening in Stress-Strain (Flow) Curve

During the hot rolling deformation the applied compressive force from the rolls induced generation, movement and blocking of dislocations within as-rolling steel plate, which causes the strength of the steel to increase and is called work hardening [36]. This phenomenon of increasing strength occurs because the generated dislocations interacted with each other, and pile-up at the grain boundaries, which making further deformation more difficult. However, the increment of dislocation density within grains also raised the stored energy and left the deformed steel in unstable or non-equilibrium state [54, 68]. Therefore naturally there is a thermodynamic driving force to reduce the energy accumulated during deformation through either the dynamic recovery and/or dynamic recrystallisation (DRX) within the roll gap if the applied strain has achieved the corresponding critical strain, or static recovery and static recrystallisation (SRX) during the delay period after deformation [54, 69].

It is clearly shown in Figure 12 that the characteristic shape and values of the macroscopic flow stress are function of strain and the Zener –Hollomon parameter, Z. The following Equation 5 indicates that the value of Z depends upon strain rate and temperature of deformation, and $\dot{\varepsilon}$ is the strain rate of deformation, R_{gas} is the ideal gas constant, Q_{def} is the apparent activation energy for deformation and T_{def} = absolute temperature at which deformation occurs.

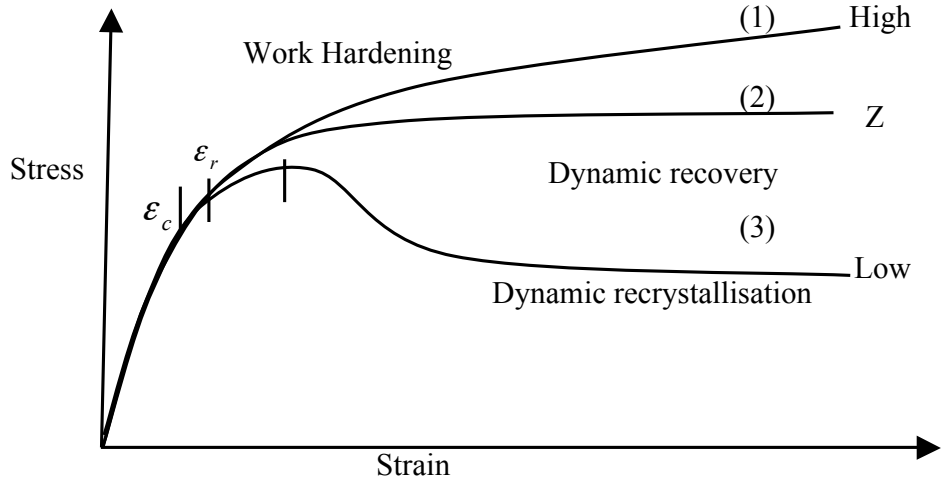

Figure 12: Typical flow curve (stress-strain) of hot deformation [43, 54]

$$Z = \dot{\varepsilon}\exp\left(\frac{Q_{def}}{R_{gas}T_{def}}\right) \quad (5)$$

As can be seen from Figure 12, the initial rapid rise in stress is associated with an increment in dislocation density as a result of work hardening effect at the region of relatively low strain, which is below the critical strains for the onset of dynamic recovery ε_r [54]. As the applied

strain continues to increase, three distinguishable shapes of flow curves can appear depending on the conditions of Z. The first one is the flow stress continuously raise as applied strain increase under high Z condition (low T_{def}, high $\dot{\varepsilon}$) in which the deformed austenite grains will be "pancake shape", highly dislocated and elongated, which can later be restored by the static recovery and SRX processes when the stain is unload at the gap time [36]. The second case is the appearance of a steady state stress with no further increase for subsequent applied strain, which indicates the work hardening is being offset by dynamic recovery. The last case is the appearance of a maximum stress followed by reduction of stress till a lower steady state stress (independent of strain) is achieved, which means DRX is being taken place. For the DRX occurring, the deformation was usually carried on under low Z conditions (high T_{def}, low $\dot{\varepsilon}$) and the applied strain had to be exceeded the corresponding critical strain ε_R, just below the peak strain ε_P. However, the strain required for DRX is too large to be found in plate rolling but may occur in strip and rod rolling where the applied strain and strain rates are significantly greater [36].

2.3.1.3. Overview of Hot Rolling Processes and Physical Metallurgy

It is well reported that the reduction in ferrite grain size is a complex process dependant on many factors such as deformation temperature, strain, strain rate, interpass time, steel composition and accelerated cooling rate. In accordance with many literature reviews [8-12, 31-53], there are five important stages to control the microstructures in final products in the hot rolling process of HSLA steels:

1. Heavy slab is reheated to a suitably high temperature for a certain time to take all or most of the MAE additions into solid solution in the austenite phase and ensure the temperature homogenisation throughout heavy slab, and reasonable (not too large) initial austenite grain size after the reheating step.
2. A series of relatively high temperature roughing passes to continually reduce the thickness of plate and refine the as-reheated coarse austenite grains by repeated SRX between each pass.
3. Holding (or time delay of) the partially - rolled plate at the defined thickness in order to pass through the intermediate temperature range where partial recrystallisation may occur between the passes if deformation continues, so that the finish rolling can take place at the lower temperature usually below the recrystallisation-stop temperature.
4. Low temperature controlled finish rolling in the austenite where recrystallisation is sufficiently retarded so that highly dislocated, and elongated austenite grains are developed to provide a high density of nucleation sites for the ferrite transformation during cooling after rolling.

5. Finally, controlled accelerated cooling to form fine and uniform ferrite grains from such pancaked austenite grains and achieve associated mechanical properties.

2.3.1.4. Different Types of Industrial Hot Rolling Processes

Figure 13 graphically illustrates the five different types of hot rolling process that can be implemented into commercial plate mills, and apply which rolling process depends on many factors such as the deformation temperature, total reduction, rolling power and cooing capability of plate mills. In here, only the conventional controlled rolling (CCR) and recrystallisation controlled rolling (RCR) of plate production are briefly mentioned here, shown in Figure 13 the process B and D respectively. The first one is the CCR that involves three stages: roughing rolling at high temperature, a holding period after roughing and a finish rolling below recrystallisation-stop temperature. The steels designed for the CCR should have a possibly high recrystallisation stop temperature to minimise the rolling power required at low temperature deformation [68]. The other one is RCR, that represents entire deformation is above the recrystallisation limit ($T_{0.95X}$) temperature but below austenite grain coarsening temperature (see Section 2.3.2.3.) and the applied reduction in each rolling pass was relatively small. Thus, a benefit of RCR over CCR is that it can be used in relatively old heavy plate mills that are not sufficiently powerful for the low temperature controlled rolling. The main objective of RCR is to reach the limit of austenite grain refinement through the repeated sequence of deformation and completely static recrystallisation of austenite at higher rolling temperatures, and above all that the fine austenite microstructure can be retained during interpass delays and during cooling down to Ar_3 by suitable dispersion of second phase particles [70]. It is important to make sure the steel has a low recrystallisation stop temperature for the RCR to ensure the full SRX occurred at the end of deformation.

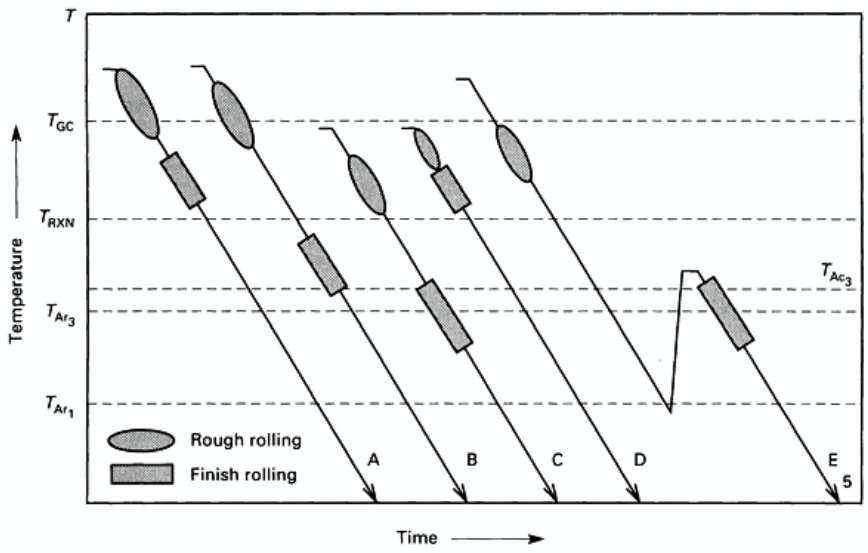

Figure 13: Different types of the hot rolling process [36]

In the following section, the focus is on the important metallurgical factors on austenite grain size development and its effects on subsequent transformation of ferrite, which based microstructures at the three important stages of TMCP: reheating, rough rolling and finish rolling. The others two stages: holding period and austenite to ferrite phase transformation will be explained later in more detail next Section 2.4.

2.3.2. Structural Changes during Reheating

2.3.2.1. Reheating Process of Heavy Steel Slab

Following casting process, there are four ways by which the as-casted heavy steel slabs can be charged into the reheating furnace: cold charging, warm charging, hot charging and direct charging. It is well accepted that in commercial heavy plate mills, the cold charging method is the most popular way due to much easier to handle cold slab [71]. In general, the cold slabs are reheated in a gas-fired furnace to a defined temperature within the 1100°C to 1250°C range for a certain time (1 to 3 hours), which depends on steel chemical composition, thickness and quantity of slab. In addition, the reheating process has to be closely controlled to achieve a homogeneous target temperature throughout the heavy plate.

The reheating step of HSLA steels can serve three major purposes in hot rolling process: firstly, the heavy slabs must be hot enough to allow the later roughing deformation easier (decrease the resistance to deformation) with suitable loads, and secondly most of the precipitates of the MAE (Ti, Nb and V), typically carbides, nitrides and/or carbonitrides, which formed during previous solidification process, were taken into solid solution at the austenite phase allow the relevant microalloyed particles to precipitate later on in the hot rolling process. Finally, the initial austenite grain size and its distribution were controlled or limited to some certain values through exploiting some un-dissolved precipitates. For example, TiN particles do not dissolve at 1200°C due to its limited solubility, and can serve to inhibit the austenite coarsening during reheating through pinning the movements of the austenite grain boundaries.

2.3.2.2. Solubility Products

Following the reheating step, the temperature of the steel plate decreases continuously during the roughing and finishing stages, as does the solubility of the microalloyed particles in the austenite phase decreases. These particles gradually become supersaturated (that is the difference between the amount of particles dissolved at the reheating temperature and that in equilibrium at the deformation temperature and the greater difference the more potential for

strain induced precipitation taken place) [59], and the driving force for precipitation at a given temperature is the solute supersaturation at that temperature [59, 72]. According to Figure 14, which describes the precipitation potentials of four different microalloyed element systems from the stable or highly insoluble titanium nitride TiN to the unstable and very soluble vanadium carbide VC, and niobium carbide NbC is somewhere between TiN and VC. These precipitated particles can have strong impacts on heavy plate microstructure development during different stages of hot rolling processes. For examples, TiN particles are considered to be more effective in retarding austenite grain coarsening during the high temperature reheating stage, while Nb is the most widely and effectively used to control the recrystallisation of austenite during the finishing passes of hot rolling, and Nb and V also can further increase the strength by precipitation strengthening either during and/or after subsequent phase transformation.

As mention previously, the MAE particles can be fully or partially, or even hardly at all dissolved into solid solution at the specific target reheating temperature, which can be explained through solubility products (k_s) of different MAE compounds. A number of authors [8, 32, 54, 73-78] have investigated the solubility of many microalloyed particles in austenite, illustrated in Figure 15, and various solubility product equations (in Table 1) have been produced but with the general format, shown in Equation 6. Such equation can be used to calculate the dissolution temperature (in Equation 7) of microalloyed particle, and the amount of an element in solution at a particular temperature.

$$Log([M]\times[X]) = \log k_s = A - \frac{B}{T_{DISS}} \tag{6}$$

$$T_{DISS} = \frac{B}{A - Log([M]\times[X])} \tag{7}$$

Where M is the concentration of metal element (V, Nb, Ti…) in austenite solid solution and X is the concentration of the non-metal element (usually C or N), and A, B are constants, T_{DISS} is the absolute dissolved temperature of compound. The T_{DISS} of microalloyed element can be determined by rearranging the Equation 6 into Equation 7. For the well-known compound Nb(C, N), Equation 8 has taken the effect of Mn into account of solubility product [79]. In fact, there are considerable discrepancies (different values of constants in Equation 6) between the solubility products of the same compound obtained by different workers, which have been analysed by Palmiere et al. [73] and they suggested the dissimilarities may be attributed partly to the different techniques used for measurement and partly to differences in steel composition.

$$Log\left([Nb]\times\left[C+\frac{12}{14}N\right]\right) = 2.15 - \frac{6770}{T_D} + 0.248Mn \tag{8}$$

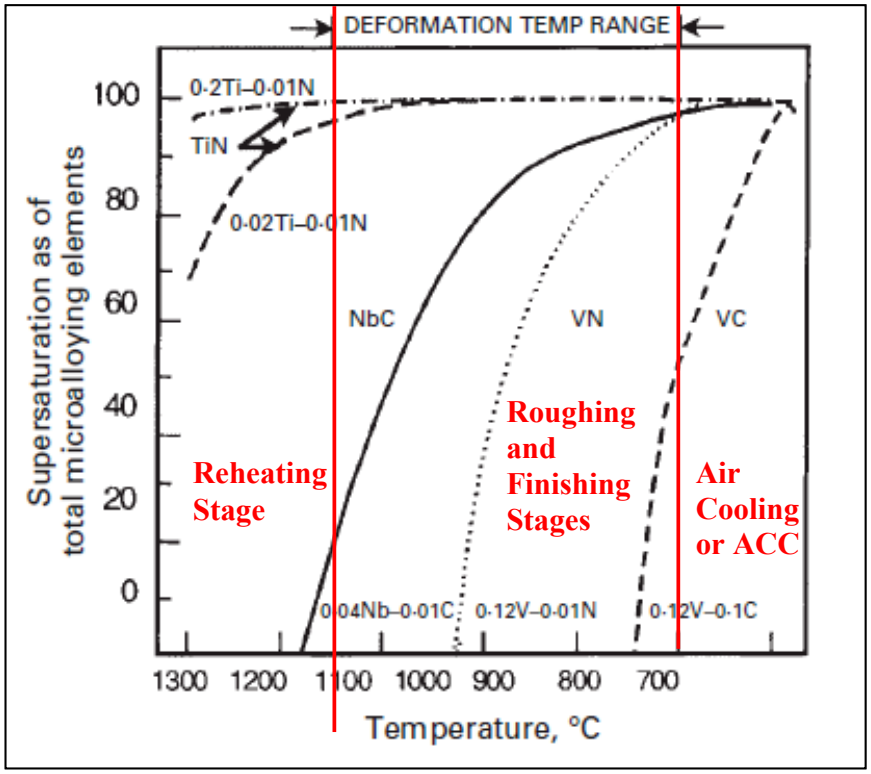

Figure 14: Precipitation potential of four different microalloyed element systems [50]

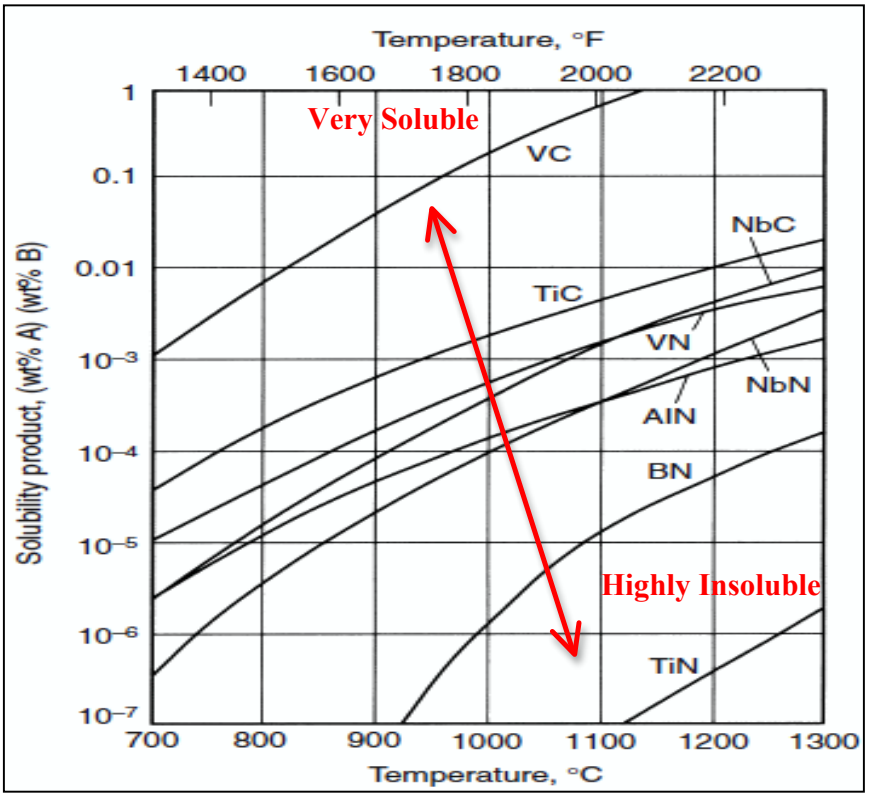

Figure 15: Selected solubility products of carbides and nitrides as function of temperatures [36]

Table 1: Typical values of A and B constants for selected carbide, nitrides and carbonitrides

MX	A	B	References
TiN	3.82	15020	[74]
NbN	2.80	8500	[73, 78]
	4.04	10230	[73, 76]
	3.79	10150	[63, 73]
AlN	1.03	6770	[74, 78]
VN	3.63	8700	[74]
	3.46	8330	[76]
	3.02	7840	[78]
BN	5.24	13970	[63, 77]
TiC	2.75	7000	[63, 75]
NbC	3.42	7900	[73]
	3.04	7290	[73, 76]
	4.37	9290	[73, 76]
VC	6.72	9500	[78]
Nb (C, N)	2.26	6770	[74,75]

2.3.2.3. Austenite Grain Growth and Grain Coarsening Temperature

Since the reheating of steel slabs represents the initial stage for any subsequent deformation process, the precise controls of the initial austenite grain size and its uniform distribution at the end of reheating step are important through the proper MAE, reheating temperature and time controls. Cuddy [74] has reported that in extreme cases, the coarse or non-uniform grain structures in the reheated slab have been found difficult to refine by subsequent hot rolling due to the limited reduction in heavy plate. It is widely accepted that austenite grain growth is a thermally activated diffusion process and that the rate of coarsening strongly depends both on reheating temperature and holding time. Also, the presence of the second phase MA particles may affect the migration of the austenite grain boundaries during the growth process due to the interaction between grain boundaries and the particles [80]. In general, and depending on the steel chemical composition, the austenite grain coarsening process can be classified into two categories – normal (continuous) and abnormal (discontinuous) grain coarsening. The influences of the various MAE and increasing concentrations of some typical precipitates on the austenite grain coarsening during reheating are shown in Figure 16 and Figure 17, respectively, and the hatched region on each curve in Figure 16 indicates the grain coarsening temperature region (see later definition) of the corresponding steel.

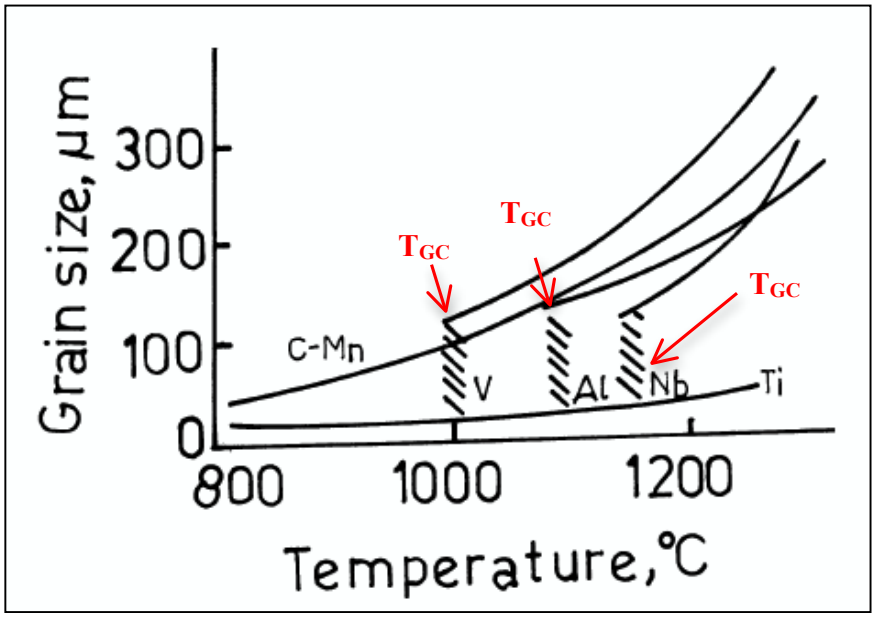

Figure 16: Austenite grain coarsening characteristics in steels containing various microalloying additions (V, Al, Nb, and Ti) [51]

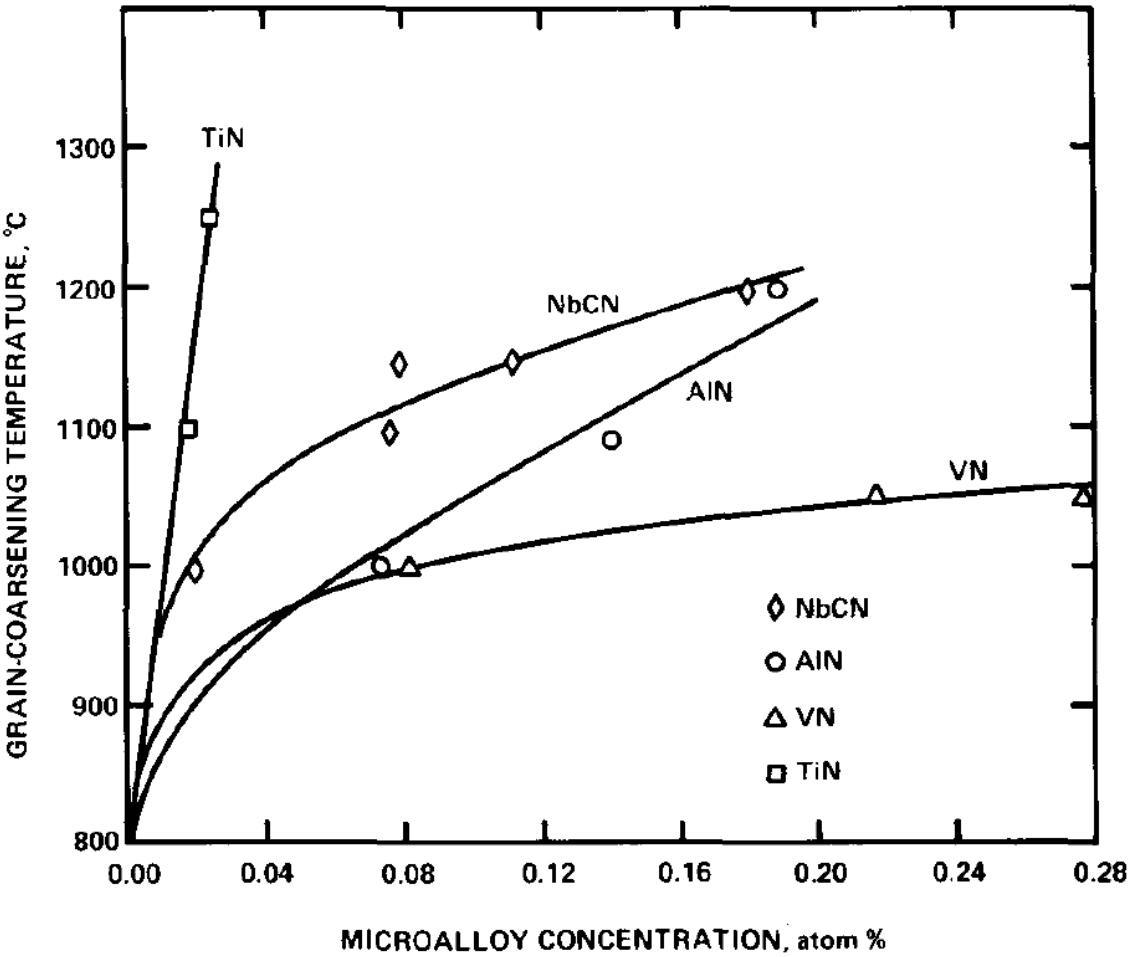

Figure 17: Increase in grain coarsening temperatures of four different microalloyed compounds with increase in the microalloy concentration [74]

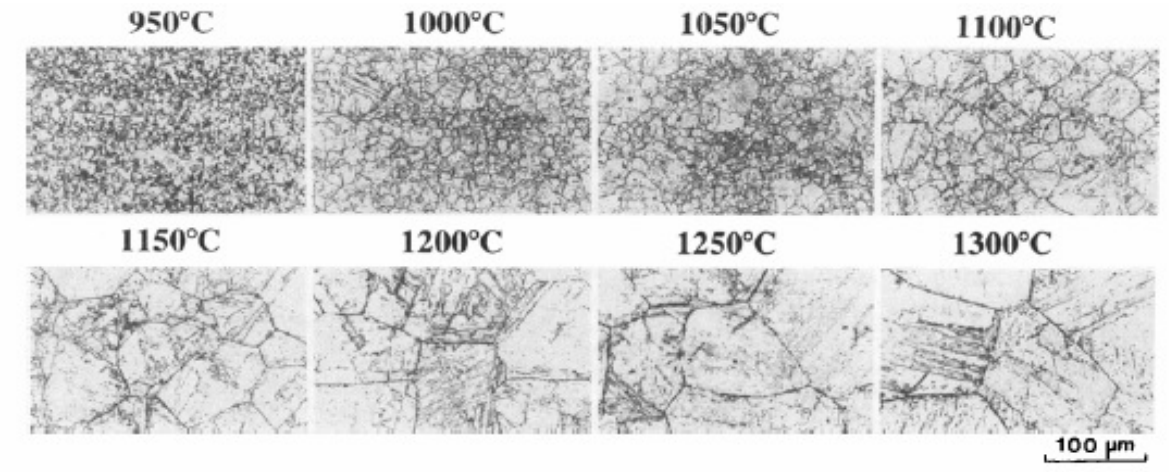

Figure 18: Prior austenite grain size for microalloyed steel (0.09C-1.49Mn-0.41Si-0.049Nb) after isothermally reheating to the above temperatures and water quenching [73]

According to the Figure 16, the normal grain growth is usually taken place on plain C-Mn steel in which uniform and similar equiaxed austenite grains continuously and gradually increase in size while increasing reheating temperature even above 1200°C. The opposite however, is the abnormal grain growth that can be defined as non-uniform growth of austenite grains in which a small amount of grains growing more rapidly as compared to the majority of the grains. In order for the abnormal growth to take place the normal grain growth has to be inhibited usually by introduction second phase of particles at the lower temperature and the target reheating temperature is above austenite grain coarsening temperature, T_{GC}. Figure 16 and Figure 17 indicate that Ti or TiN is very effective to suppress austenite grain coarsening even at above normal reheating temperature range, and Nb or Nb (C, N) can prohibit austenite grain coarsening roughly below 1150°C.

The T_{GC} is defined as that temperature above which abnormal or discontinuous austenite grain growth or secondary recrystallisation commences and related to the temperature above which the un-dissolved precipitate can not longer suppress grain growth and produce coarse grain structure at an accelerated rate [8, 57, 81, 82]. As it is illustrated from the Palmiere's work in Figure 18, the austenite grain coarsening occurred abruptly at 1100°C, which was the T_{GC} for that specific microalloyed steel. That is because at the sufficient high temperature and reheating time, the pinning force of MAE particles on austenite grain boundary can be lost due to the precipitates may dissolved or the size of particles grow larger, thus limiting their ability to pin. Therefore, the grain coarsening temperature is determined by the stability and solubility of the second phase precipitates at the reheating stage [83], which can be explained through the following equation developed by Gladman [81, 84].

$$r_C = \frac{6R_0 f}{\pi}\left(\frac{3}{2} - \frac{2}{Z}\right)^{-1} \tag{9}$$

where r_C is the maximum effective size of particles to pin movements of austenite grain boundaries, r_0 is the mean radius of austenite grain, f is the volume fraction of second phase particles and Z is the heterogeneity factor that is ratio of the radii of coarsening and average pinned austenite grains [74, 80]. It has observed that the value of Z is in the range $\sqrt{2}$ to 2 during grain coarsening process and for most polygonal metals a value of Z = 1.5 was assumed [80]. According to the Equation 9, the size of a given dispersion of particles above the r_C, the primary austenite grain will no longer be suppressed and abnormal grain coarsening will take place [81]. Cuddy et al. [74] have reported that a linear relationship of increase in the observed T_{GC} with the computed temperature for complete solution of microalloyed particles in the austenite, shown in Equation 10 in which A and B are constants of the corresponding particles. Later, Palmiere et al. [73] studied grain coarsening in Nb-microalloyed steels and have also developed a relationship between the grain coarsening temperature (T_{GC}) of austenite and the dissolution of temperature (T_{DISS}) of particles in Equation 11.

$$T_{GC} = A + BT_{DISS} \tag{10}$$

$$T_{GC} = T_{DISS} - 125^{\circ}\text{C} \tag{11}$$

$$T_{GC} = T_{RH} - 175^{\circ}\text{C} \tag{12}$$

In commercial hot rolling practices, it is normal to design the reheating temperatures T_{RH} at least 50°C higher [36] than the corresponding T_{DISS} determined from Equation 7. Thus, the Equation 12 shows the relation between T_{RH} and T_{GC}, and the choice of T_{RH} may determine the amount of MAE dissolved, and T_{GC} as well as the initial austenite grain size. Many researchers [85] reported that intensive grain growth was avoided, and toughness and productivity were improved at a reduced reheating temperature, however, it reduced the level of supersaturation as less Nb and V particles were taken into solution, and resulted in some loss of strain induced precipitation during deformation to retard recrystallisation and precipitation hardening during phase transformation. For example, for a Ti-V-N microalloyed steel it has been found that a reduction in reheating temperature from 1200°C to 1100°C reduced the yield stress by about 40MPa while the decreased the ductile to- brittle transition temperature (ITT) by 15°C [70].

To summarise, Palmiere [54] has pointed out that while some of the MAE should be use the control the T_{GC} by particle grain boundary interaction, a portion should remain in solution for precipitation during subsequent hot deformation, and these two needs are perhaps best served by multiple MAE additions.

2.3.3. High Temperature Roughing

2.3.3.1. Industrial Rough Rolling Process

In general, once the heavy slab dropped out the reheating furnace and passed through the descaling water box to remove oxide scales on plate surfaces, the slab then entered a reverse 2- high roughing mill. The first step was to achieve the required width through vertical rolls and this process is known as broadsiding. After that the heavy slab was rotated through 90˚ on a turntable and passed through the rollers with compressive force so the length and thickness reduction can be attained. For most HSLA steels the temperature region of rough rolling is from 1200°C down to about 950°C depends on steel composition and heavy plate thickness. Furthermore roughing rolling at such elevated temperatures large reduction can be achieved with relatively low rolling loads, and completely austenite recrystallisation was taken place.

In order to obtain the optimum strength and toughness at room temperature it is essential that the final ferrite grain size of the steel plate is small, which in turn is related to small austenite grain size at end of roughing process. Therefore, the metallurgical objectives of rough rolling stage are the same as the previously mentioned RCR process, that is, to achieve the finest possible recrystallised austenite grain size at the end of roughing stage through intensive repeated recrystallisation occurring between reversed rolling passes and retard austenite grain growth during holding period before entering the finishing stage. In general, the coarser the initial austenite grain size and thicker the slab, the higher is the rolling reduction required to refine the grains. In the case of rough rolling very thick plates, bulk temperature of heavy plate may decrease by a small amount over entire roughing stage and reduction in each rolling pass was only 5% due to insufficient rolling power, and such low reductions can enhance coarsening of the grain during the gap time between the early passes [86].

2.3.3.2. Static Recovery, Recrystallisation and Grain Growth

It has been shown that high temperature flow curves (Figure 12) are characterised by an initial work hardening stage followed by a continuous increasing, constant or decreasing stress level. As shown in Figure 19, prior to the start of hot deformation, steel microstructure consists of coarse and strain free equiaxed grains of austenite. When the hot slab is deformed between roll gap the austenite grains are flattened and elongated at the rolling direction by the compressive force, the area of grain boundaries, dislocation density within grains and other defects were increased to a thermodynamically unstable high-energy state. Therefore, restoration processes are taken place as a response to these work hardening effects.

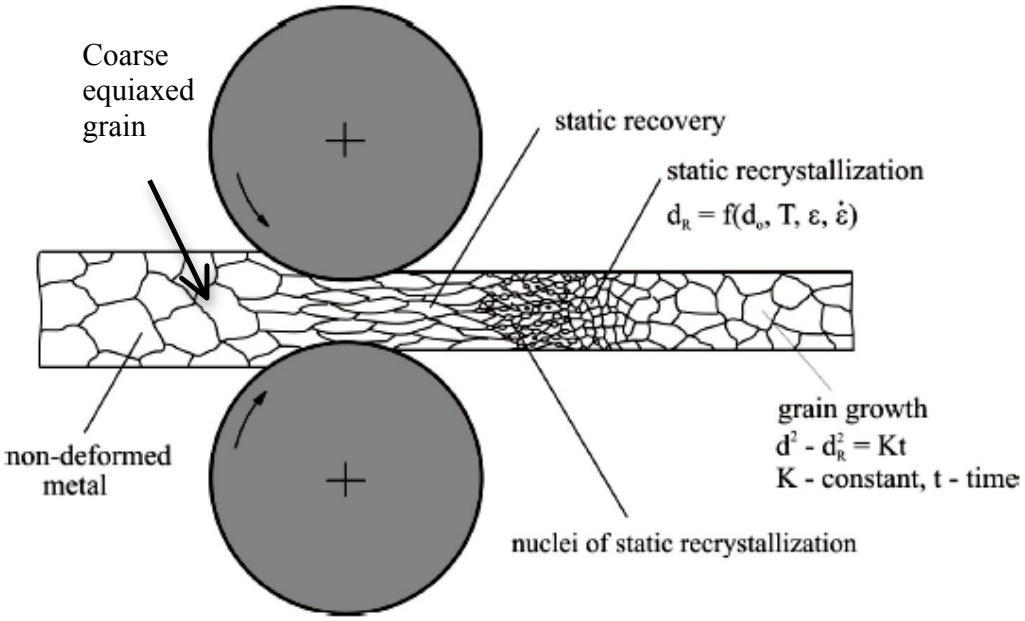

Figure 19: Physical metallurgy (static recovery, recrystallisation and grain growth) of hot rolling steel plate [87, 88]

During multipass hot rolling, there were three possible types of restoration or recrystallisation processes may take place during and between passes as following:

1) Dynamic recrystallisation (DRX) may start and complete during deformation in the roll gap
2) Metadynamic recrystallisation (MDRX) if it occurred, would start during deformation in the roll gap and complete in the time interval between deformation [8, 35]
3) Static recrystallisation (SRX) process which might start and complete during the time period between passes

In terms of industrial steel heavy plate hot rolling schedules with relatively low strain, strain rates and long interpass time, the first two types of softening processes are unlikely to take place during the rolling stage due to insufficient reduction of each roughing pass and total accumulated strain to reach critical strain for initiate dynamic restoration. According to an opinion of DeArdo et al. [8, 89], the time required for substantial amounts of DRX to occur is orders of magnitude longer than the times actually available in the roll gap. Jonas [90, 91] has also summarised that longer interpass (plate rolling) periods favour SRX and strain induced precipitation, while short interpass time (strip and rod rolling) prompt strain accumulation for initiating DRX followed by MDRX. Therefore, static recrystallisation (SRX) is the most likely restoration process that may occur after the as-deformed plate exited from the roll gap. As mentioned previously, the raised stored energy due to the accumulated dislocations and other defects during deformation provides the driving force for subsequent static restoration process: static recovery and static recrystallisation and grain growth.

Firstly, after deformation static recovery takes place immediately with no incubation period and is a process that involves the continuous annihilation and rearrangement of dislocations to lower the raised stored energy with no movement of high angle grain boundaries, shown in Figure 20 where there are five stages and have been clearly studied and summarised by Humphreys el at. [92]: a) dislocation tangles, b) cell formation, c) annihilation of dislocation within cells, d) sub-grain formation, and e) sub-grain growth. Static recovery is a thermally activated process, which depends on the strain rate, temperature and stacking fault energy (SFE) of the material [59]. Since the SFE of austenite is relatively low (75mJ/m) [93-95], which means the ability for dislocations to cross-slip or climb is difficult [93, 94, 96], softening attributed to static recovery would be limited, or even can be neglected [96] so that fractional softening and recrystallisation are numerically the same. However, the overall softening during interpass is caused by static recovery and static recrystallisation (SRX), and it is difficult to fully distinguish and measure individual percentages of softening caused by static recovery and SRX. For examples, Sellars [97] in his early paper mentioned the static recovery process accounts for up to 40-50% of total softening at high strain while at the low strains the stored energy is insufficient to cause (SRX) and only limited static recovery takes place. Later Lenard et al. [98, 99] have considered that static recovery only accounts for a maximum 20% of the whole softening process during holding. The criterion that 20% of the overall softening is due to recovery has been adopted Palmiere [93-95] to study static softening through double hit compression tests and one of examples is shown in Figure 21. During subsequent recrystallisation, these sub-grains can act as nuclei of recrystallisation and because raised stored energy is the driving force for both static recovery and SRX, the progress of static recovery decreases the driving force available for SRX [100]. Therefore, static recovery and SRX are competing events.

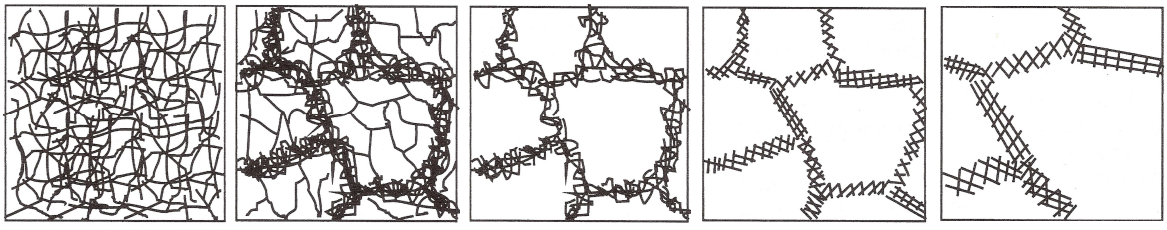

Figure 20: Schematic of 5 different stages in recovery process of deformed materials [62, 92]

Secondly, a definition of SRX by Doherty et al. [101] involves the formation of new strain-free, low dislocation density and smaller grains in a deformed material by the formation and migration of high angle grain boundaries driven by stored energy of deformation. The process of SRX usually described as taking place in two stages - nucleation of new grains and growth of new grains at the expense of the deformed grains, illustrated in a sigmoidal shape [102] of recrystallized curve in Figure 22.

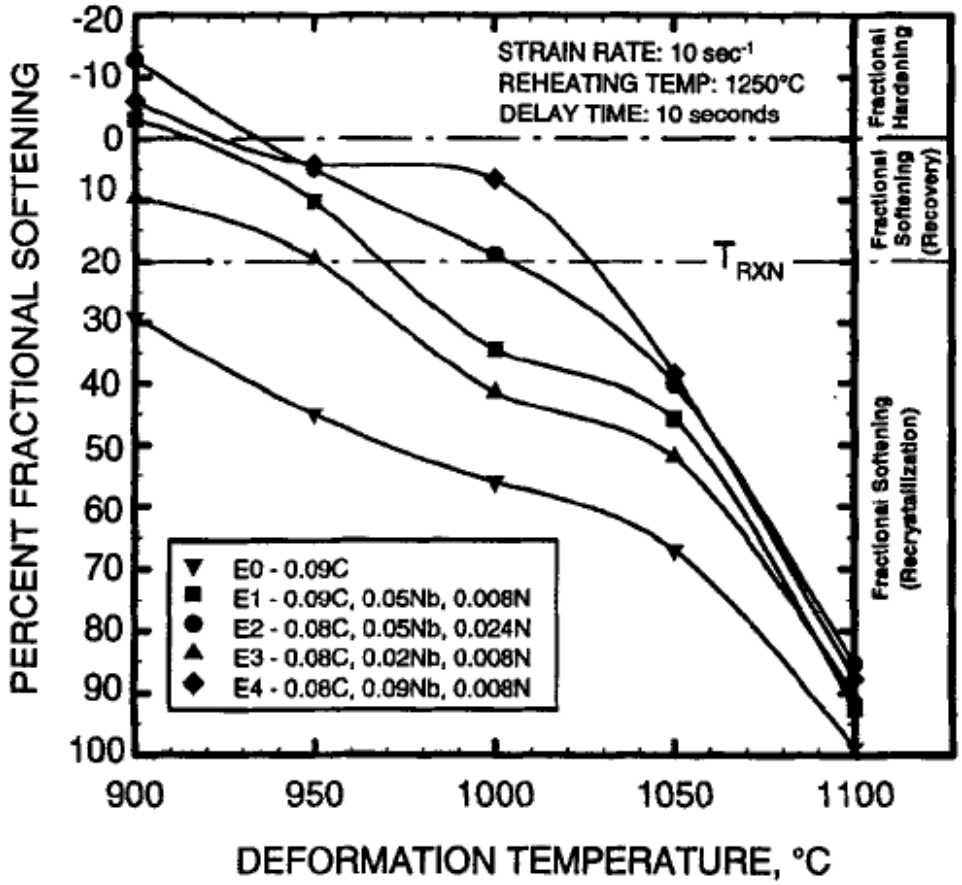

Figure 21: Percentage fractional softening of austenite as determined from interrupted compression testing [94]

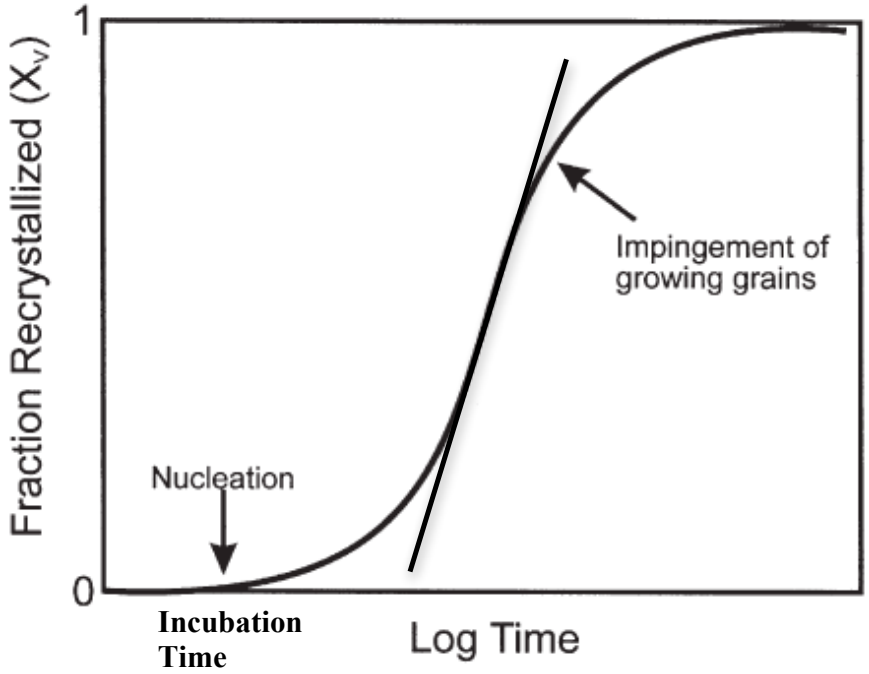

Figure 22: Typical recrystallisation kinetics during isothermal annealing [92]

There is a time gap before static recrystallisation can begin, termed the incubation (Figure 22) or nucleation time in which static recovery occurs to a great extent and provides nuclei of SRX. Nucleation of SRX is initiated heterogeneously at sites with a high stored energy [59], preferentially at the triple junctions of grains [46], austenite grain boundaries, twin boundaries, and on deformation bands. Once these new strain-free grains have nucleated, they are capable of moving into the old deformed grains, increasing in volume and consuming the deformed grains [59]. The migration rate of such new austenite grain boundaries is sensitive to the presences of MAE solutes and undissolved stable particles because the driving force of moving grain boundaries has to overcome the dragging forces from solutes and the pinning force from particles. The driving force for static recrystallisation (F_{RXN}) is the difference in dislocation density between the old deformed grains region and the new recrystallized grain region [50], which is often given by the following Equation 13 [50, 94, 95] in which μ is the shear modulus of austenite, b is the burgers vector, and $\Delta\rho$ is the increase in dislocation density due to deformation and can be estimated from increase in flow stress $\Delta\sigma$ in Equation 14 [95]. Although both Equations 13 and 14 show no direct temperature dependence, the value of $\Delta\rho$ decreased by increased temperature, which in turn caused the F_{RXN} decreased to some degree with increased temperature [94].

$$F_{RXN} = \frac{\mu b^2 \Delta\rho}{2} \tag{13}$$

$$\Delta\rho = \frac{25\left(\Delta\sigma\right)^2}{\mu^2 b^2} \tag{14}$$

The kinetics of SRX under isothermal condition as a function of the holding time after deformation can be described by the Johnson-Mehl-Avrami-Kolmogorov (JMAK) Equation 15 in which t is the gap time between rolling passes, and t_X is the time for a given volume of recrystallized fraction, X, is the amount of recrystallized volume fraction at end of gap time. Additionally, $A = \ln X$, and k is the Avrami exponent [98] that are dependent on steel composition. The most common recrystallisation fraction model has been developed shown in Equation 16 in which X =0.5, and thus $A = \ln\left(0.5\right) = -0.693$. The exponent k, typically 1 to 2, is not very sensitive to deformation parameters [103]. Four of classical models for determining the time to reach a 50% recrystallized fraction $t_{0.5}$ in C-Mn and C-Mn-Nb steels suggested by Sellars [37, 98, 103-105] and Hodgson [79, 98, 106-109] shown in Equations 17-20. Recently, a series of work have been carried out by the Rodriguez-Ibabe research group [110-115] to modify Sellars's Equation 19 through taking account of solute drag effect of common Nb, Ti and V elements into Equations 21 and 22.

$$X = 1 - \exp\left(At^k\right) = 1 - \exp\left[A\left(\frac{t}{t_x}\right)^k\right] \quad (15)$$

$$X = 1 - \exp\left[-0.693\left(\frac{t}{t_{0.5}}\right)^2\right] \quad (16)$$

for C-Mn steel

Sellars: $$t_{0.5} = 2.5\times10^{-19}d_{\circ}^{2}\varepsilon_{eff}^{-4}\exp\left(\frac{300000}{RT}\right) \quad (\varepsilon < 0.8\varepsilon_p) \quad (17)$$

Hodgson: $$t_{0.5} = 2.3\times10^{-15}d_{\circ}^{-2}\varepsilon_{eff}^{-2.5}\exp\left(\frac{230000}{RT}\right) \quad (18)$$

for C-Mn-Nb steel

Sellars: $$t_{0.5} = 2.5\times10^{-19}d_{\circ}^{2}\varepsilon_{eff}^{-4}\exp\left(\frac{300000}{RT}\right)\exp\left\{\left[\left(\frac{2.75\times10^5}{T}\right)\text{-}185\right][Nb]_{sol}\right\} \quad (19)$$

Hodgson: $$t_{0.5} = \left(-5.24 + 550[Nb]\right)\times10^{-18}d_{\circ}^{2}\varepsilon_{eff}^{\left(-4+77[Nb]\right)}\exp\left(\frac{330000}{RT}\right) \quad (20)$$

for Nb, Ti and V steels

$$t_{0.5} = 9.92\times10^{-11}d_0\varepsilon_{eff}^{\left(-5.6d_0^{-0.15}\right)}\dot{\varepsilon}^{-0.53}\exp\left(\frac{180000}{RT}\right)\exp\left\{\left[\left(\frac{2.75\times10^5}{T}\right)\text{-}185\right][MAE]\right\} \quad (21)$$

$$[MAE] = [Nb] + 0.374[Ti] + 0.0585[V] \quad (22)$$

Finally, if the recrystallisation fraction X is more than 95% it is assumed that SRX is completed and provided enough time between passes completed SRX immediately followed by grain growth of new recrystallised grains, which is a process involving the migration of grain boundaries in which the recrystallised grains coarsen, and the relative area grain boundaries are lowered and leaving a new structure with a low dislocation density. The driving force of grain growth is solely the reduction of the free energy associated with area of grain boundaries itself [101]. The following Equation 23 is for Nb steels proposed by Hodgson et al. [79] was used to determine at the end of interpass time the austenite grain size

after grain coarsening, d_{gg}, which in turn will be the initial grain size d_0 or d_{i-1} for the subsequent i^{th} rolling pass. Later Hodgson et al. [34, 107, 116, 117] have developed Equations 24 and 25 to obtain more realistic d_{gg} in C-Mn steels with different grain growth time t_{gg} due to a large difference between the rate of grain growth during the first second of the interpass interval and the remaining time [117]. As indicted in Equations 23 - 25, the d_{gg} value depends on statically recrystallised grain d_{rex}, which was calculated from the Equations 26 [103], 27 [36, 118] and 28 [113] depend upon the steel composition. The time in which grain growth can occur t_{gg} was determined from Equations 29 in which $t_{0.95}$ is the time for 95% static recrystallisation, which was calculated using Equations 30 [99]. However, if $X < 0.95$ then essentially two different austenite grain sizes will exist: unrecrystallised, and recrystallised grains. Beynon and Sellars [103] have developed Equation 31 to determine the mean statically grain size d_{MSRX}.

$$\mathrm{d}_{\mathrm{gg}}^{4.5} = \mathrm{d}_{\mathrm{rex}}^{4.5} + 4.05\times10^{23}\times t_{gg}\times\exp\left(-\frac{435000}{RT}\right) \quad \text{for C-Mn-Nb steels} \tag{23}$$

$$\mathrm{d}_{\mathrm{gg}}^{2} = \mathrm{d}_{\mathrm{rex}}^{2} + 1.1\times10^{7}\times t_{gg}\times\exp\left(-\frac{113000}{RT}\right) \quad \text{for C-Mn steels} \quad (t_{gg} < 1s) \tag{24}$$

$$\mathrm{d}_{\mathrm{gg}}^{7} = \mathrm{d}_{\mathrm{rex}}^{7} + 1.5\times10^{27}\times t_{gg}\times\exp\left(-\frac{400000}{RT}\right) \quad \text{for C-Mn steels} \quad (t_{gg} > 1s) \tag{25}$$

$$\mathrm{d}_{\mathrm{rex}} = 0.743\mathrm{d}_{\circ}^{0.67}\varepsilon_{\mathrm{eff}}^{-1} \quad \text{for C-Mn steels and} \, (\varepsilon < 0.8\varepsilon_p) \tag{26}$$

$$\mathrm{d}_{\mathrm{rex}} = 6.2 + 55.7\mathrm{d}_{\circ}^{0.15}\varepsilon_{\mathrm{eff}}^{-0.65}\left[\exp\left(\frac{350000}{RT}\right)\right]^{-1} \quad \text{for C-Mn steels} \tag{27}$$

$$\mathrm{d}_{\mathrm{rex}} = 1.4\mathrm{d}_{\circ}^{0.56}\varepsilon_{\mathrm{eff}}^{-1} \quad \text{for C-Mn-Nb steels} \tag{28}$$

$$t_{gg} = t - t_{0.95} \tag{29}$$

$$t_{0.95} = \left[\frac{\ln\left(1-0.95\right)}{\ln\left(0.5\right)}\right]^{\frac{1}{2}}\times t_{0.5} \tag{30}$$

$$d_{MSRX} = d_{SRX}\left(X\right)^{\frac{4}{3}} + d_{i-1}\left(1-X\right)^{2} \tag{31}$$

2.3.3.3. Austenite Conditions at the End of Roughing Stage

As noted earlier, the aim during the roughing stage is to produce a uniform austenite structure exhibiting a relatively small grain size. It is important to note that the large austenite grains at the end of a reheating cycle is the starting point for rough rolling, and after that the refinement of large initial austenite grain size only can be obtained during the roughing stage through strain induced austenite recrystallisation during and after deformation [119], and uniformity of final microstructure critically depends on the austenite conditions at end of roughing stage [120]. Based on previously physical based equations in Section 2.3.3.2, refinement of the statically recrystallised grain size d_{rex} can be achieved by increasing the effective strain ε_{eff}, decreasing the initial austenite grain size d_0 and deformation temperature (within completed recrystallisation range), and solute drag effect from MAE addition. It is widely accepted that a minimum reduction (15-20%) or critical strain per pass is required to ensure full recrystallisation [36, 44, 120, 121], which depends on d_0 shown in Equations 26-28 (the larger d_0 the higher critical strain is required for completed SRX for a single pass). However, many researchers [36, 44, 122] have agreed that in practice, the initial austenite grain size has little influence on the recrystallised grain size because after several passes the values of d_{rex} are similar regardless of different initial grain sizes (20μm -200μm), shown in Figure 23 below. Moreover, for good cross sectional austenite conditioning the total reduction in the roughing stage should be 60% with a relatively heavy draught at the last pass of roughing were reported [123]. Nevertheless, even with optimum composition and adopting large reduction (more than 60% reduction), grain refinement does not process indefinitely [124] and there seems to be a limit to the degree of SRX that can be achieved by repeated recrystallisation [36, 44. 124] between passes and the finest recrystallized austenitic grain sizes were reported about 15μm [11] within the processing capabilities of conventional mills.

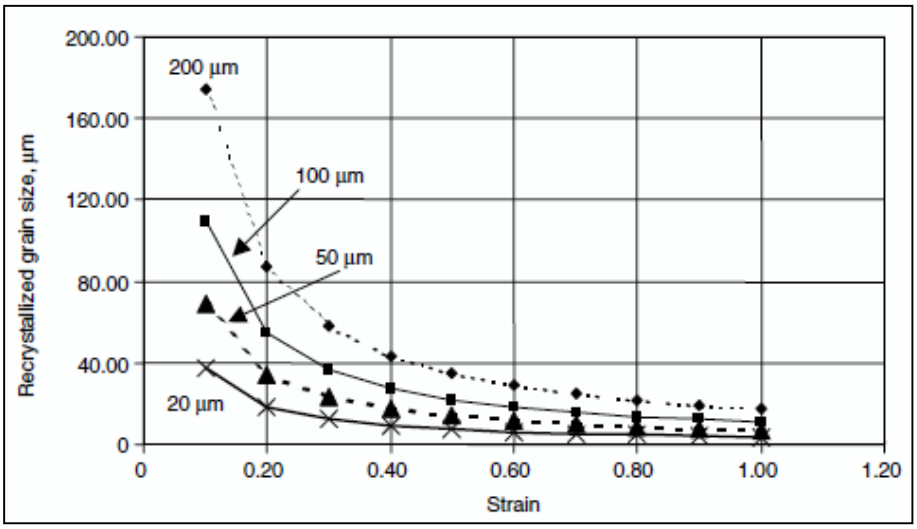

Figure 23: Effects of single pass strains on recrystallised grain size for various initial grain sizes [36]

2.3.4. Suppression of Austenite Recrystallisation during Low Temperature Finish Rolling

2.3.4.1. Deformation of Austenite in the Non-Recrystallisation Region

As mentioned earlier, limited austenite grain size refinement can occur by finishing the whole deformation above 95% recrystallisation temperature $T_{0.95X}$ (RCR process). In order to further refine the ferrite grain size through increasing the number of nucleation sites, the fine recrystallised austenite grains obtained from the previous roughing stage are deformed in the subsequent low temperature finish rolling stage with maximum possible total reduction (60-85%) below recrystallisation temperature [125]. The purpose of such low temperature finishing rolling operation is to accumulate the rolling strain in the regime where no further recrystallisation of the austenite grains occur between two successive rolling passes, so that the previously recrystallized austenite equiaxed grains would be flattened (pancaked), highly elongated in the direction of rolling, and as the applied strain increases, near planar crystalline defects such as (sub-grain boundaries, deformation bands and incoherent twin boundaries) [69] and high dislocation density possible be produced inside the deformed and elongated austenite grain. Therefore, it provides more austenite grain boundary surface area to volume ratio than the equiaxed recrystallized grains, which gives rise to more potential sites for ferrite nucleation and produce a much finer ferrite grain size on transformation, explained in greater detail in Section 2.3.4.4.

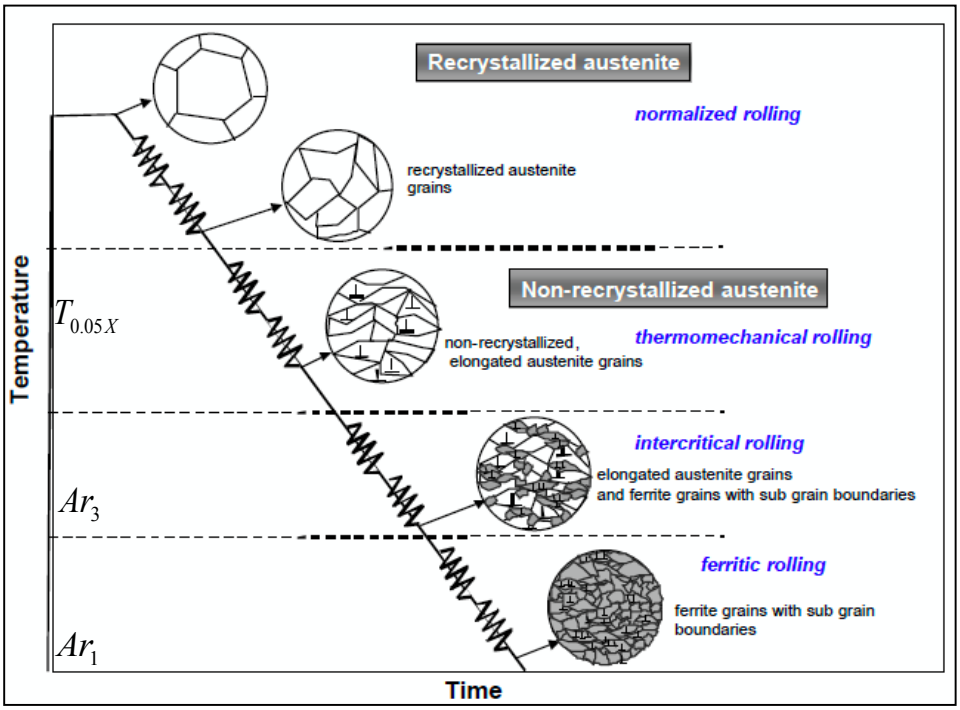

Figure 24: Temperature regions of hot rolling process and the resulting microstructures [125]

Depending on the final microstructures and properties requirement, as well as the power capacity of the plate mill, there are four possibility of finish rolling temperatures, and corresponding rolling processes with resulting microstructures shown in Figure 24: a) normalized rolling - high temperature fully austenite recrystallisation, b) thermomechanical rolling - relatively low temperature below $T_{0.05X}$, c) intercritical rolling - two phases region of ferrite plus ferrite, and d) low or warm temperature ferritic rolling. It is clearly illustrated in Figure 24 that as the deformation temperature reduces the resulting microstructures form more sub-grain structure with more potential nucleation sites for ferrite grains. However, since deformations are at such low temperatures, the process requires high rolling loads as the steel slab becomes increasing difficult to deform and maybe above the power capacity of some heavy plate mills. Williams et al. [21] have mentioned that no metallurgical advantage of heavy finishing reduction ratio has been established at Port Kemla and a number of disadvantages have been found. For examples, he stated [21] that excessive holding periods were required for the commencement of finish rolling start temperature, and there was reduced opportunity for reaching the finest recrystallized austenite grain size in heavy plate with 40-50mm thickness.

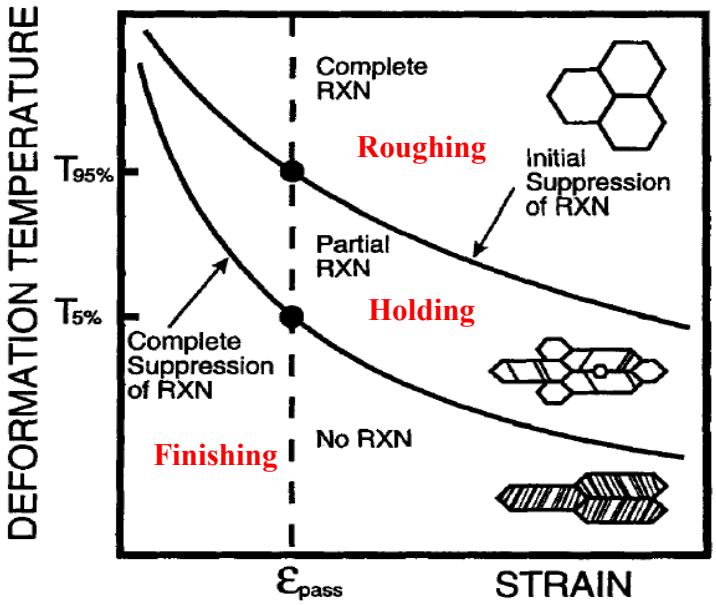

Figure 25: Schematic illustration of austenite microstructures resulting from different deformation temperatures at a constant level of strain [94]

The above Figure 25 illustrates the influences of both deformation temperature and amount of applied strain on the microstructures of statically recrystallised austenite [54, 93, 94]. It can be observed from Figure 25 that for constant deformation variables such as strain, strain rate and interpass holding time, the austenite microstructure will be completely recrystallised at high deformation temperatures if the last pass of roughing above $T_{0.95X}$. As the deformation temperature is decreased such that the progress of austenite recrystallisation becomes

increasingly difficult, a partially recrystallisation microstructure is observed, which is often referred to as being duplex because of a non-uniform grain size [54, 93, 94]. Finally, a completely unrecrystallised microstructure is present when deformation occurs below $T_{0.05X}$. Therefore, the generally rules for finishing rolling process are for the first pass of finish rolling the temperature must below $T_{0.05X}$ so that there is not any recrystallisation of austenite in finish rolling, and from the industrial production standpoint, it is advantage to keep the $T_{0.05X}$ as high as possible to enable large reductions to take place below this temperature without causing excessive mill loads.

2.3.4.2. Recrystallisation Stop Temperature of Austenite

There is no doubt that the recrystallisation stop temperature $T_{0.05X}$ is one of the most important parameters in TMCP of HSLA steels. Cuddy [126] defined the $T_{0.05X}$ as the temperature at which after a particular rolling sequence, recrystallisation was less that 5% in 15 seconds between two successive rolling passes [44], which depends on intrinsic parameters such as steel composition, which determines the precipitation potential [93] and the deformation parameters. Cuddy has shown in Figure 26 that microalloying elements such as Al, Nb, Ti and V initially dissolved in austenite during reheating stage can increase the $T_{0.05X}$. It is clearly presented that small addition of Nb caused the most pronounced effect of increasing the $T_{0.05X}$ due to Nb (C, N) shows the largest supersaturation in austenite (in Figure 14) possible precipitated out of solid solution by strain-induced at the temperatures that well situated within hot rolling stage and [43].

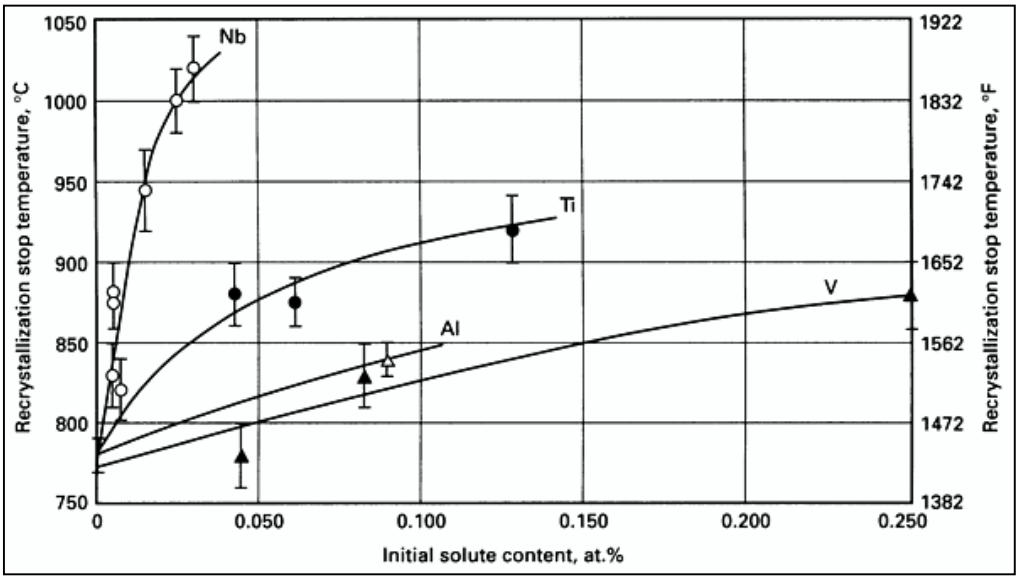

Figure 26: The increase in recrystallisation stop temperature (minimum required temperature to complete recrystallisation) with increase in the level of microalloy solutes in 0.07% C, 1.4% Mn and 0.25% Si steel and deformation per pass 10-15% [36, 126]

Therefore, in designing industrial hot rolling schedules of HSLA steels it is essential to know the value of $T_{0.05X}$ as close as possible to avoid start of finish rolling taken place at the partial recrystallisation region (in Figure 25). In general, $T_{0.05X}$ can be determined from empirical regression equation [127, 128], rolling mill logs data [129], the most commonly multistage hot torsion testing [113, 127-135], and measurement of recrystallisation or softening fraction (less than 20%) during intervals of passes [93-95]. Boratto et al. [127] have developed the first empirical correlation between $T_{0.05X}$ and the chemical composition (shown in Equation 32 and based on 17 different steel compositions) through simulated an industrial rolling schedule using 17-pass hot torsion tests under continuous cooling conditions. They plotted the mean flow stress (MFS) produced from the stress-strain curve (Figure 27- a) to against inverse deformation temperature to determine the $T_{0.05X}$, which is the intersection of the two straight regression lines through the points the corresponding to regions I and II [113, 136], and an example of such test is presented in the following Figure 27.

To convert stress-strain curve into MFS versus 1/T, MFS for each deformation step between ε_1 and ε_2 has to be determined first by Equation 33 and it is defined as the area under each stress-strain curve divided by the pass strain [113]. Originally, Misaka introduced prediction of MFS for C-Mn steels during hot strip rolling by Equation 34. Later Jonas research group [117, 137, 138] have modified Misaka's equation to take account of the effects of MAE, such as Nb, Ti and Mn as well as softening attributable dynamic recrystallisation X_{dyn} into Equation 35, which is valid over the following concentration ranges: 0.02 to 0.08 wt% Nb, 0.35 to 1.33 wt% Mn and 0 to 0.024 wt% Ti.

$$T_{0.05X}\left(^{\circ}C\right) = 887 + 464C + 890Ti + 363Al - 357Si + 6445Nb - 644Nb^{0.5} + 732V - 230V^{0.5} \qquad (32)$$

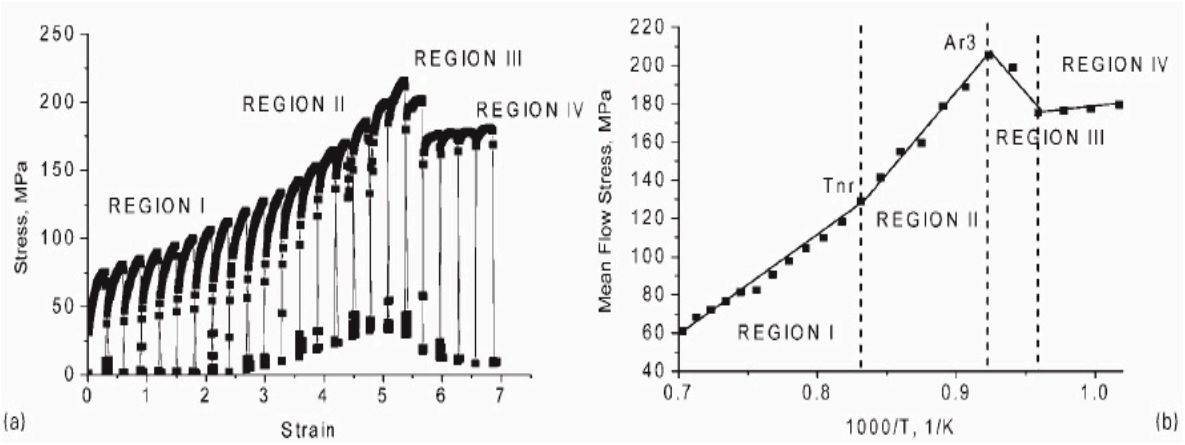

Figure 27: a) The typical stress-strain curve obtained in a 23-pass torsion test including 4 different regions as deformation temperature reduced; b) mean flow stress against inverse absolute temperature [136]

$$MFS = \overline{\sigma} = \frac{1}{\varepsilon_2 - \varepsilon_1}\int_{\varepsilon_1}^{\varepsilon_2} \sigma \, d\varepsilon \tag{33}$$

$$MFS_{Misaka} = \exp\left(0126 - 1.75C + 0.594C^2 + \frac{2851 + 2968C - 1120C^2}{T}\right)\varepsilon^{0.21}\dot{\varepsilon}^{0.13} \tag{34}$$

$$MFS_{New} = MFS_{Misaka}\left(0.768 + 0.51[Nb] + 4.217[Ti] + 0.137[Mn]\right) \times \left(1 - X_{dyn}\right) + K\sigma_{SS}X_{dyn} \tag{35}$$

$$T_{0.05X}\left({}^{0}C\right) = 932.36 + 1091.43[Nb] + 15.65[C] + 13.8[Mn] - 13.94\varepsilon - 0.22\dot{\varepsilon} - 11.93t \tag{36}$$

Recently, Vervynckt et al. [136] have reviewed the fundamental mechanisms that control $T_{0.05X}$, and they stated that unlike phase transition temperature, $T_{0.05X}$ is not an exact quantity and it represents the start of the inhibition of complete SRX during cooling between rolling passes. It should be noted that the actual intersection of two straight lines is not always that obviously and sharply revealed. Instead, the transition from complete recrystallisation in region I to recrystallisation stop region II is more gradual than shown in Figure 27–b) [136]. It is now widely recognised that $T_{0.05X}$ is not depends on chemical composition alone, but also affected by effective strain in each pass, strain rate, interpass time and reheating temperature [136, 139]. Radovic et al. [128] have developed Equation 36 that has taken account of strain, strain rate, and interpass time on $T_{0.05X}$.

2.3.4.3. Retardation of Austenite Recrystallisation by Solute Drag and Strain Induced Precipitation (SIP)

It is well known that MAE plays an important role in the restoration process in HSLA steel. In contrast to those rolling parameters, such as increasing deformation temperature, strain and strain rate, which enhance SRX, increases in MAE solutes have been shown to suppress SRX [54]. The recrystallisation retardation due to MAE, particular Nb, has been the subject of considerable interest by many researchers through different testing methods, it has been attributed to solute drag effect, strain induced precipitation (SIP), and the combined effects of solute drag and SIP. In earlier 1980s, Akben and Andrade et al. [140, 141] have investigated the influences of MAE dissolved in solid solution on recovery and recrystallisation in austenite. They have found that the retarding effect of Nb in solution on recrystallisation is to shift the kinetic curves of recrystallisation start and stop temperatures to the right-hand side of recrystallisation-temperature-time (RTT) diagram with respected to that of typical plain C steel [140], indicated in Figure 28, and such a shift caused intersection of recrystallisation and precipitation curves, thus precipitation may take place. They also have stated that the greatest

solute retardation or solute drag effect is produced by Nb additions, followed by that of Mo and then V elements. Almost at the same time, Yomamoto et al. [143] have also reported that the retarding rates of several MAE solutes are in the following descending order Nb>Ti>Mo>V>Mn>Cr>Ni, and Nb, V and Ti in solution retard recovery in deformed austenite and consequently delay the onset of recrystallisation but less than their effects on the progress of recrystallisation. Later, Bai et al. [132] have examined the influences of interpass time on the recrystallisation stop temperature under continuous cooling conditions, and they have found that when the interpass times are short (<12 seconds), solute atoms control the rate of recrystallisation. On the other hand, strain induced precipitation takes place and retards the recrystallization when the interpass times are long (12s<t<50s). However, in practices during finish rolling heavy steel plate the interpass is about 10-13 seconds, it maybe difficult to clearly distinguish the solute drag and SIP on the overall retardation of austenite recrystallisation based on Bai's work.

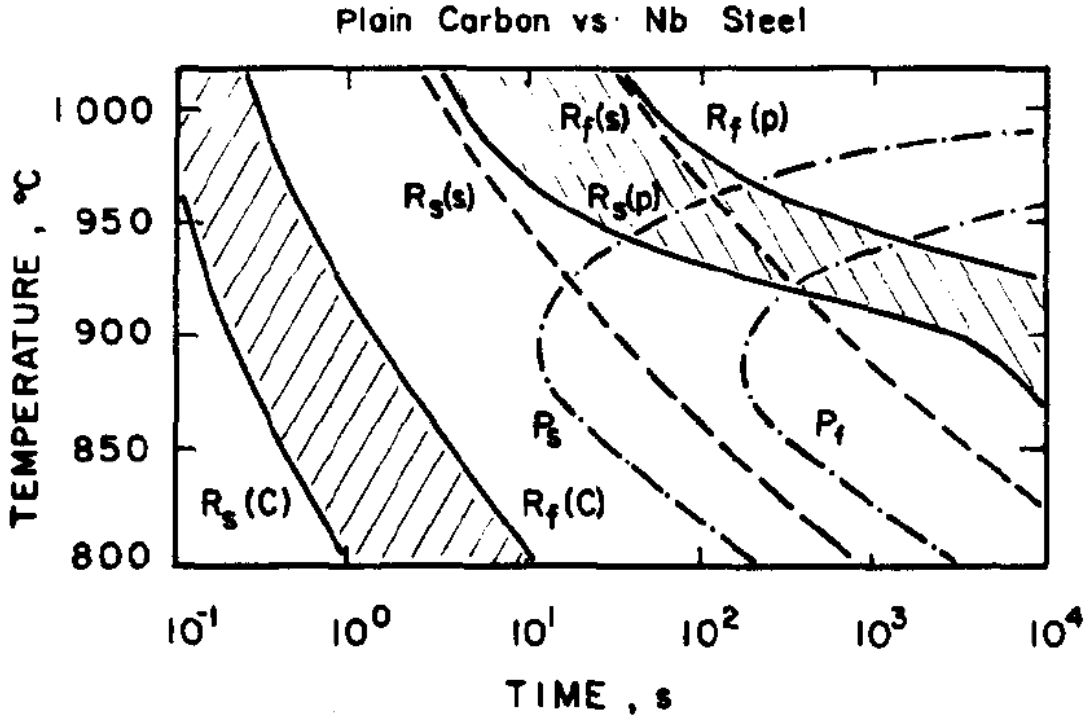

Figure 28: Precipitation-Temperature-Time (PTT) diagram for the present 0.035Nb-1.25Mn steel shown in relation to RTT diagram for the typical plain C and Nb steels [140]

Most researchers [44, 140-147] have agreed that Nb in solid solution only can retard austenite recrystallisation to some extent by solute drag effect until the SIP could begin, but the most dramatic retardation or pinning effect results from SIP of fine Nb (C, N) particles (<25nm in diameter) that takes place prior to or during early stages of recrystallisation. For example, DeArdo [42] has mentioned that when the Nb is in solution, the measured delay of static recrystallisation was less than 1.5 second at 1000°C, whereas the delay caused by precipitates

was on the order of several minutes. In order for the SIP to take place in deformed austenite, LeBon et al. [147] have shown that the presence of Nb in solution prior to deformation is a necessary criterion for recrystallisation retardation. However, if the Nb is precipitated as Nb (C, N) particles prior to deformation, the pinning effect is lost. Later, Hansen et al. [143, 144] have suggested that a critical level of precipitate supersaturation is required for significant SIP to occur and the degree of pinning effect increases with the concentration of dissolved Nb prior to deformation. In term of nucleation of the SIP, Kwon et al. [145] have reported the SIP were taken place in the localised areas with high dislocation density, such as prior austenite grain boundaries, deformation bands and austenite subgrain boundaries. Hansen et al. [143, 144] also mentioned general precipitation commences in the matrix of the unrecrystallised austenite after the high-energy areas were occupied by Nb (C, N) precipitates at the initial stage of nucleation. This renders the assumption of uniform precipitate distribution invalid and it is challenge to measure and predict the correct volume fraction of precipitates [95].

2.3.4.4. Interaction Between Austenite Recrystallisation and Strain Induced Precipitation

During the finish rolling stage, both austenite recrystallisation and the SIP may take place at the interpass time, and greatly interact with each other. For example, Zurob et al. [100, 148] and Veryncket et al. [136] mentioned since the strain-induced heterogeneous precipitation often occurs on dislocations in the matrix, a decrease in dislocations through recrystallisation reduces the numbers of nucleation sites for precipitation and thus retards the onset and rate of precipitation. Moreover, features (near planar crystalline defects) formed in the deformed (unrecrystallised) austenite can provide nucleation sites for precipitation thus accelerating the reaction of SIP, while the precipitates (if of sufficient fineness and quantity) tend to pin the substructure and thus inhibits recrystallisation [38]. Whichever process first sets in, recrystallisation or SIP, will delay the onset of the other. Therefore, it is no surprise that such complex interactions between recrystallisation and SIP has a profound implication for the controls on the conditions of austenite and subsequent ferrite microstructure, and has been drawn considerable attention by many researchers [143-154].

In general, austenite recrystallisation will be suppressed when the pinning force (F_{PIN}) exerted by the heterogeneously distributed second phase particles on austenite grain and subgrain boundaries exceeds the driving force (F_{RXN}) for recrystallisation [54]. The interaction between F_{PIN} and F_{RXN} hold the key in deciding if retardation of austenite recrystallisation would occur. The equation for determining F_{RXN} has been introduced at the previous Section 2.3.3.2, and the values for F_{RXN} ranged from 22 MN/m^2 at 1100°C to 30

MN/m^2 at 900°C according to Palmiere' work [54, 93, 94]. The F_{PIN} are given by the following Equations 37 using the most realistic subgrain boundary pinning force model in which σ is interfacial energy per unit area of boundary, f_v is the volume fraction of precipitates, l is the average intercept distance between the subgrains, r is the radius of precipitates [49. 94, 95]. Therefore, the large pinning force can be promoted by the small precipitate size and the high volume fraction of precipitate, and much higher magnitudes of F_{PIN} from those with very high-localised values of f_v [50]. Palmiere et al. [50, 93, 94] have measured the local volume fraction and particles size of Nb (C, N) on austenite grain boundaries and in the grain interiors of two different steels with varied Nb addition (steels E3 and E4 with 0.02 and 0.09wt% Nb respectively), and reported that at 10°C below the $T_{0.05X}$ of steel E4, the F_{PIN} calculated through using Equation 37 at austenite grain boundaries was approximately 19MN/m^2 greater than the F_{RXN}; on the other hand, the F_{PIN} calculated from grain interiors was about 1 MN/m^2 less than the F_{RXN}. These results are summarised in Figure 29 in which data to the right hand side of F_{RXN} curve resulted in complete suppression of recrystallisation; while data to the left hand side of F_{RXN} caused a partially or fully recrystallised austenite microstructure [54, 93, 94].

$$F_{PIN} = \frac{3\sigma f_v l}{2\pi r^2} \tag{37}$$

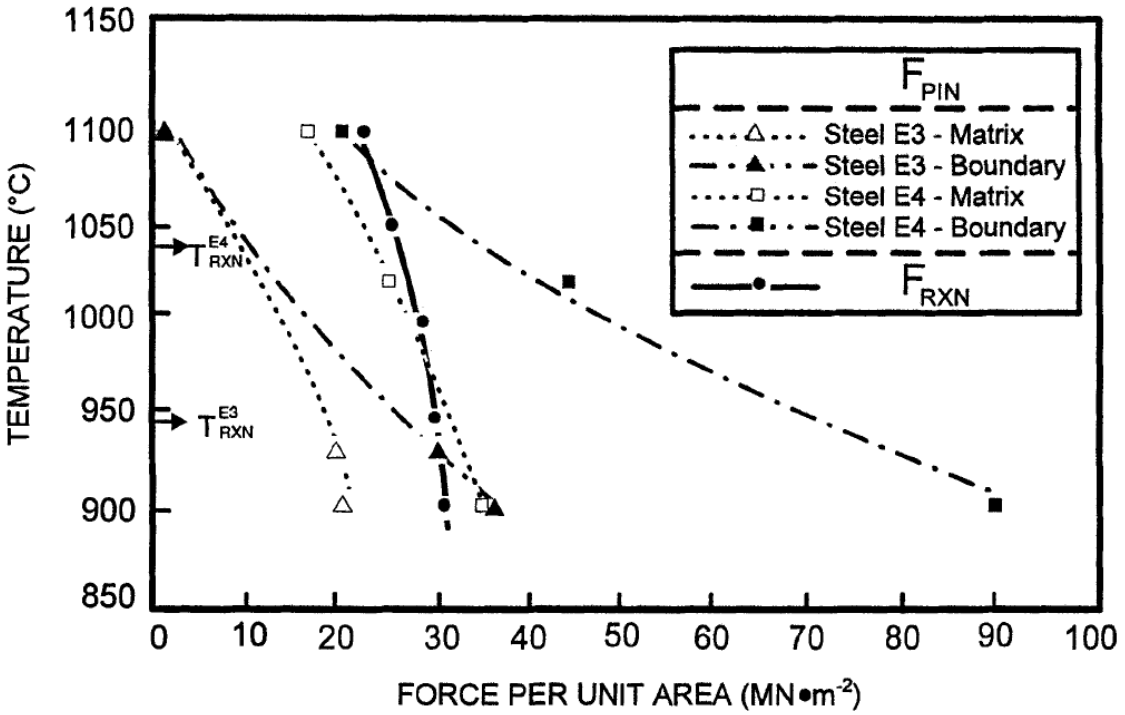

Figure 29: Comparison between F_{PIN} and F_{RXN} versus deformation temperature at austenite grain boundary and in matrix [54, 93, 94]

However, Palmiere et al. [95] have also mentioned that precise determination of precipitates volume fraction cannot be achieved by direct measurement using the extraction replicas techniques, which are dependent on the extraction efficiency, and the fine precipitates (<2nm) [155] nucleated on dislocation, subgrain boundaries and deformation bands maybe beyond the resolution of electron microscopic. It is well recognised that the size of precipitate is one of critical factor to retard recrystallisation and Hansen et al. [143, 144], suggested that recrystallisation proceed only after Nb (C, N) precipitates reach a large enough size to lose their effectiveness.

The progress and complex interaction of the two completing processes: recrystallisation and SIP have traditionally been explained with the aid of generalised recrystallisation-precipitation-temperature-time (RPTT) diagram [143, 145]. One typical example is shown in Figure 30 in which both the kinetic curves of recrystallisation and precipitation are superimposed [145]. In Figure 30 below, R_s and R_f refer to the start and finish of recrystallisation, respectively, in microalloyed steels; $R_s^{'}$ and $R_f^{'}$ refer to the start and finish of recrystallisation, respectively, in plain carbon steels; $P_s^{'}$ and $P_f^{''}$ refer to the hypothetical precipitation start times in deformed and undeformed austenite, respectively. P_s is the actual precipitation start time [145]. Also in the Figure 30, there are three different temperatures: T_{sol}, $T^{'}$ and T_R, which are respectively the solution temperature above which Nb-rich precipitates are completely dissolved in the austenite; the temperature below which recrystallisation and precipitation compete; and the temperature below which precipitation occurs prior to recrystallisation [145], and these three temperatures have divided the diagram into three stages.

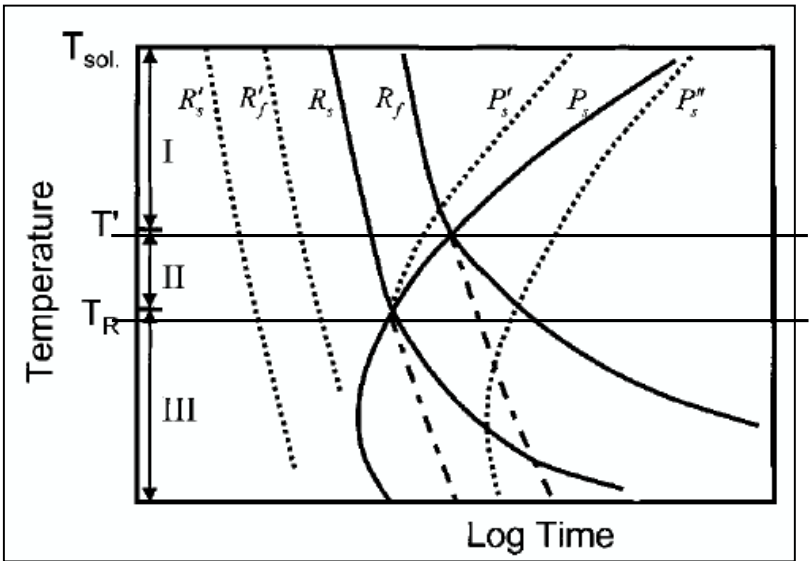

Figure 30: Recrystallisation-precipitation-time-temperature (RPTT) diagram showing the interaction between precipitation and recrystallisation [50, 145]

In stage I, recrystallisation is completed before the actual start of precipitation. However, since precipitation takes place in the completely fine recrystallised austenite, the start of precipitation may be accelerated gradually, shifting the hypothetical curves $P_f^{''}$ to left $P_s^{'}$. In stage II, precipitation occurs after partial recrystallisation. Hence, the precipitation kinetic is also accelerated in this stage due to the presence of substructure in the partially recrystallised austenite. Deformations in the stage can produce a duplex microstructure, which should be avoided. In last stage III, precipitation commences prior to recrystallisation because pinning force is thought to be high enough to impede the retard the initiation and progress of recrystallisation.

Medina et al. [133-135, 156-159] have established another method of representing the interaction between precipitation and recrystallisation. They found the conventional sigmoidal shape (in earlier Figure 22) usually associated with recrystallisation kinetics did not show at specific deformation temperature but showed a plateau on the curve when SIP takes place in Figure 31 [59]. They also defined the static recrystallisation critical temperature (SRCT) at which the inhibition of static recrystallisation begins as consequence of SIP start under isothermal condition, which is approximately the same as $T_{0.05X}$. The precipitation-time-temperature (PTT) diagram illustrated in Figure 32 also has been determined from the recrystallisation against time curves through identified the start and finish of the plateau as the start time P_s and finish time P_f of the SIP [156-159].

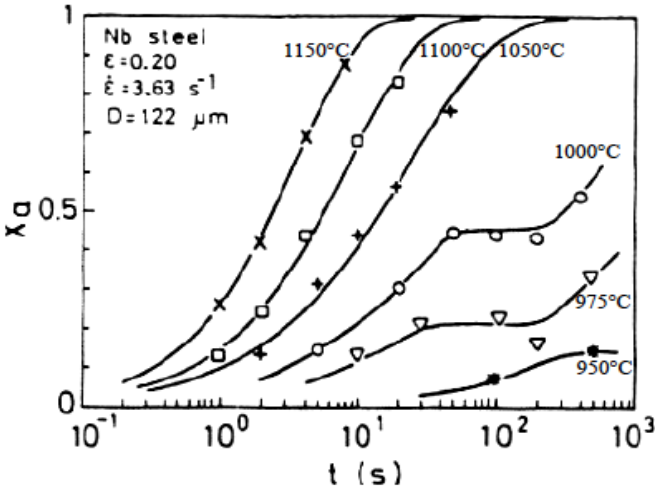

Figure 31: Recrystallisation fraction verse time as function of temperatures in which plateaux show the start and finish of SIP [59]

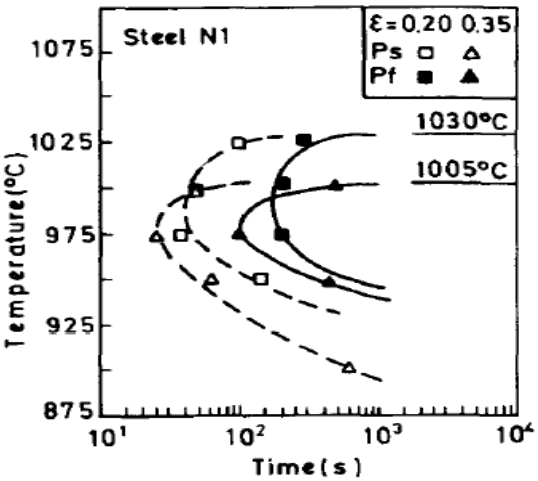

Figure 32: Precipitation-time-temperature (PTT) diagram of Nb steel of different strains 0.2 and 0.35 [157]

Dutta and Sellars [160-164] used thermodynamic data and classic nucleation and growth theory to proposed a physical based model, which describes isothermal SIP kinetics of Nb(C, N) from supersaturated austenite, and the model is able to predict the interaction between recrystallisation and SIP during interpass time by calculating the different start times required

for 5% recrystallisation $t_{0.05X}$ and 5% precipitation $t_{0.05P}$ as a function of process variable and composition. The calculations for determining these two values are expressed in Equations 38 to 41, in which Z is the Zener-Holloman parameter; A is constant is equal to 3 x 10^{-6} or 6 x10^{-6} by Hodgson [98, 105, 109], or approximately determined by Equation 39 in which T_R is the reheating temperature or the last final roughing temperature for industrial processing [161, 162]; k_s represents the supersaturation ratio of [Nb][C+12/14N] in solution at the reheating stage to the equilibrium solubility product at the deformation temperature T, which determine the chemical driving force for SIP. It has assumed [98, 109] that if $t_{0.05P} < t_{0.05X}$ SIP was considered to have occurred and no recrystallisation takes place; if $t_{0.05X} < t_{0.05P} < t_{0.95X}$ recrystallisation is started before beginning of the SIP but recrystallisation is incomplete; if $t_{0.95X} < t_{0.05P} < t$ recrystallisation proceeds completely before reaction of SIP starts during time available between passes. The completion time of precipitation progress is reported about two orders of magnitude greater than $t_{0.05P}$ [162]. They have also defined the recrystallisation stop temperature (RST) is related with SIP and determined when $t_{0.05X}$ is equal to $t_{0.05P}$.

$$t_{0.05P} = A \times [Nb]^{-1} \varepsilon^{-1} Z^{0.5} \exp\left(\frac{270000}{RT}\right) \exp\left(\frac{2.5 \times 10^{10}}{T^3 (\ln(k_s))^2}\right) \tag{38}$$

In which, $A = 200 \exp\left(\frac{-200000}{RT_R}\right)$ (39)

$$\text{and } k_s = \frac{\left[[Nb]\left([C] + \frac{12}{14}[N]\right)\right]_{sol}}{10^{2.26 - \frac{6770}{T}}}, \text{ remember } T \le 1350K \tag{40}$$

$$t_{0.05} = 6.75 \times 10^{-20} d_\circ^2 \varepsilon_{eff}^{-4} \exp\left(\frac{300000}{RT}\right) \exp\left\{\left[\left(\frac{2.75 \times 10^5}{T}\right) - 185\right][Nb]_{sol}\right\} \tag{41}$$

2.3.4.5. Conditions of Austenite Prior to Phase Transformation

The subsequent post-deformation phase transformation of the "conditioned austenite" determines the final ferrite grain sizes, which are controlled by several important parameters such as the austenite grain size and morphology, cooling rate during transformation and temperature range of transformation [11]. In general, by increasing the ferritic nucleation rate and decreasing the ferritic growth rate, which were generally achieved by good conditioned austenite prior to transformation and controlled cooling during phase transformation, it is able to achieve a finer ferritic grain size. It is widely accepted that the good conditioned austenite are the results of relatively small initial austenite grain size at the reheating stage, grain size

refinement through repeated austenite recrystallised at rough rolling stage, and high density of near planer crystalline defects (NPD) within heavily deformed unrecrystallised and pancaked austenite grain.

A parameter S_V, which is defined as the total interfacial area per unit volume (mm^2/mm^3 or mm^{-1}) of NPD such as grain boundaries (GB), deformation bands (DB) and incoherent twin boundaries (TB) [43, 49, 54], has been introduced to quantify the effectiveness of austenite conditioning prior to phase transformation. The importance of S_V in regards to the recrystallisation behaviour of austenite can be illustrated using the schematic diagram shown in Figure 33 in which depending on whether the deformation temperature T_ε is above or below none recrystallisation temperature T_{RXN}, there can be differences in the final austenite structure and different expressions for the S_V [54]. When T_ε is more than T_{RXN}, the total S_V was only a function of the recrystallised grain size, while when $T_\varepsilon < T_{RXN}$ the total S_V is a function of NPD in addition to the contribution due to austenite grain boundaries. It is also showed that the minimum reduction required below the T_{RXN} to form deformation bands was on the order of 30% [54]. As mentioned previously it is now well understood that these NPD can be acted as nucleation sites for ferrite during transformation. Therefore, the larger values of S_V as result of large reduction below $T_{0.05X}$ were found to be associated with finer ferrite grains [49].

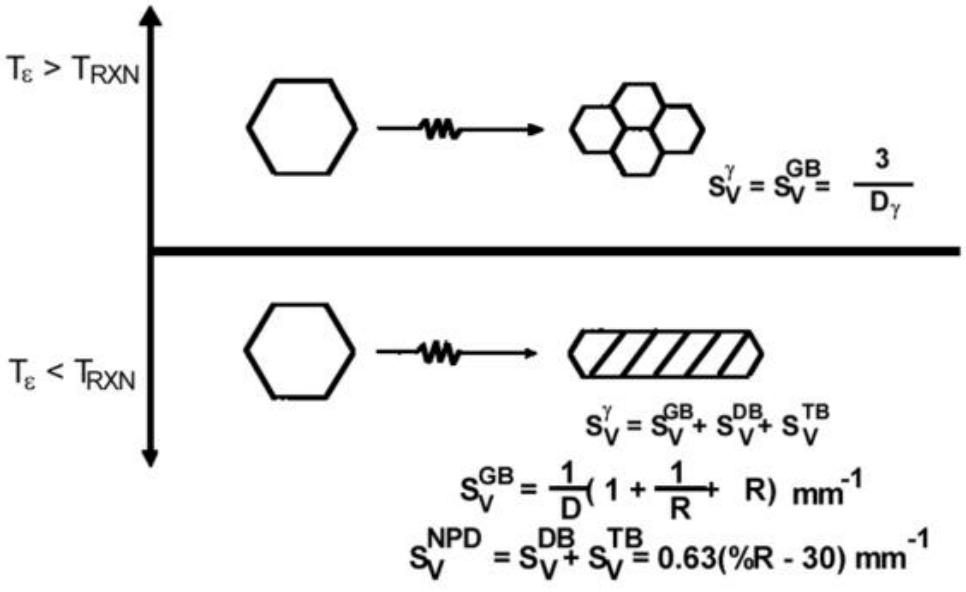

Figure 33: Schematic representation of austenite microstructure when deformed above or below the recrystallisation stop temperature of austenite (D is the grain size and R is the average aspect ratio of deformed austenite grain) [49, 57, 83]

2.4. Intense Water Cooling during and after Hot Rolling Steel Plate

2.4.1. Forced Cooling Prior to Roughing

It is well recognised that in commercial heavy plate production, when the heavy slab was dropped out from the reheating furnace, the surfaces of slab were covered with thick layers of oxide scales that can be detrimental to the surface properties if carried on and rolled into the steel in later deformation. Thus, the oxides scales were usually removed through a set of vertical and horizontal scale breakers by high pressure water spraying [165]. As mentioned in the Introduction, some industrial heavy plate mills reported that prior to the first roughing pass, when applied forced cooling to the surface of heavy plate for a certain time, it has reduced the oxide scales, as well as promoted mid-thickness deformation and refinement [18, 20, 21]. The reason [18] for increasing the strain penetration was that after forced cooling the colder surfaces of plate were harder to deform than the softer region of mid-thickness thereby increased the effective arc of contact and the rolling shape factor, m (in Equation 1).

2.4.2. Intermediate Forced Water during Holding Period

2.4.2.1. The Critical Holding Period in TMCP

As mentioned previously, while successively lowering the deformation temperature, austenite recrystallisation will become first partially and then completely suppressed. It is widely accepted that in order to avoid formation of duplex microstructures that result from partial recrystallisation, the last pass of rough rolling should be finished above fully or 95% recrystallisation temperature and the first pass of finish rolling should be below the recrystallisation stop temperature. Therefore, the holding period (HP) is a critical step in which the partially rolled slab is allowed to cool from complete austenite recrystallisation at a high roughing temperature to relatively low finishing temperature, which is below the recrystallisation stop temperature and only grain flattening occurs. The improper selection of the holding temperature range would produce a partly recrystallised structure during holding, which would not be eliminated but rather be intensified by the subsequent reductions and would finally transform in to the mixed ferrite grain structure.

However, due to a generally 3:1 or 4:1 thickness reduction [10, 86] is required to be performed in the finishing stage to assure pancake shape of unrecrystallised austenite and the occurrence of NPD, under natural air-cooled condition a HP as long as fifteen to twenty minutes [16] can occur on 120mm-160mm partially rolled thick plates, which causes serious

disruption to the production rate [166]. The exact length of the HP depends upon the slab soaking temperature, cooling rate of as-rolling heavy plate between roughing passes, holding thickness of partially rolled heavy plate, and the temperature of the first finishing pass, which in turn depends upon the rolling schedule required to meet the desired microstructure and specified properties [29]. Therefore, there is a strong driving force in commercial heavy plate mills for reducing this long holding period with little effect or without sacrificing the final material properties. Apart from time concerns, the fine recrystallised austenite grains produced at the end of the roughing pass naturally are influenced by grain growth during holding period, and the resultant grain coarsening is more pronounced if the temperature of the last roughing pass is increased due to an increase in grain growth rate [53]. Furthermore, long holding periods may promote local grain growth for non-uniform grain size distribution, which is highly undesirable. However, some researchers [86] argued that the undissolved TiN particles in microalloyed steel could inhibit the growth of recrystallised austenite grains during the long holding period under the natural air-cooling condition.

2.4.2.2. The Development and Operation of IFC Technique

The first report about implementing the water spray cooling process during HP to augment the air cooling of partially rolled plates was studied by Fegredo [29] in 1977, and in his investigation, different water cooling rates were applied into 32mm and 44.5mm thick plate in the holding period with promising results. Later, Fegredo et al. [28] have published another paper on the effects of holding period accelerated cooling on the microstructure and mechanical properties of Nb and V HSLA steels, and they showed that the HP was decreased by a factor 2-3 through water-spray cooling with smaller ferrite grain size and improved strength and toughness compared with normally air-cooling processed plate. Other published studies [14-16, 23-30, 167-170] have also reported significant benefits of using the IFC. For examples, several researchers [21, 25, 27, 167, 168] from the former Bethlehem Steel Corporation (now ArcelorMittal) have described that water spray cooling practices have been developed to accelerate the cooling rate of heavy plates up to 80mm thickness prior to commencement of finish rolling stage without any adverse effects on plate temperature homogeneity and mechanical properties of the finished plate. Accelerated cooling was applied on both HP and after finish rolling has been reported by Dilg et al. [26] at the plate mills of Dillinger Huttenwerke GTS. In their study, they showed that the application of intermediate force cooling during the long HP and ACC produced a finer grain structures and more homogeneous distribution of bainite because the high cooling rates during HP suppressed the recovery and diffusion processes, which coarsen the grains when the partially rolled plate is air cooled [25].

The brief operations of applying IFC into HP were described by Abel et al. [25], and they mentioned that as the partial-rolled plate leaves the roughing stand and enters the holding area with water cooling unit, the heavy plate is oscillated back and forth for a fixed time while water is sprayed on surfaces of the plate. After the spray water is turned off, in the first 10 seconds air nozzles remove the excess water on the surface of the plate, which continues to oscillate for a sufficient time prior to rolling in the finish mill to allow the plate temperature to equilibrate. The intermittent application of water-cooling may continue if the temperature of the heavy slab has not achieved its target temperature under the initial forced cooling [25]. Abel [25] also mentioned that it is important to make sure that during the IFC process, the surface temperature of heavy plate is not dropped below 649°C in order to avoid cooling the plate at the transition boiling period in which two different mechanisms (film and nucleate boiling) with significantly different cooling heat fluxes may operate together and result in difficult to control heat fluxes [171, 172].

2.4.2.3. Temperature Change and Distributions inside Partial Rolled Plate During HP

Under conventional air-cooling condition during HP, the centre of the partially rolled heavy plate is much hotter than that of the surface at the beginning of finish rolling stage. This temperature gradient cannot be eliminated in the subsequent processing, and causes microstructure inhomogeneity in the final products. In general, the application of IFC into HP initially introduces a much greater temperature gradient from the surface towards the interior of the heavy plate, and then when water spraying stops, the hot centre quickly reheats the cold surfaces but the rate of reheating gradually decreases as new thermal equilibrium temperature is approaching.

The Figure 34 shows schematic curves of temperature changing and distributions inside of thick plate at the air (black curves) and water-cooling (blue curves) conditions, and the exact temperature profiles strongly depend on the heat transfer mechanisms of different cooling media during HP (it will be explained more in details later in Section 2.5). During a normal IFC operation, an online computer model probably determines the optimal strategy to cool the heavy plate to a target finishing mill entry temperature after rolling in the roughing mill, but how close the predicted temperature profiles and actual temperature reading inside heavy plate during holding period has not been mentioned in the published literature. Generally speaking, there are three stages in the temperature profiles inside the thick plate that is subjected the IFC during the holding period. Firstly, the cooling stage includes chilling the plate surfaces with water spraying at a defined cooling rate and short cooling time (t_C), and in this stage the surface temperature may below Ar_3 but the centre of heavy plate takes some

time to response without obviously temperature dropping. Secondly, it is the recovery or recalescence stage in which water spraying was stopped and it is under natural air-cooling condition. Because there is a huge temperature difference between surface and centre of plate, the plate surface is gradually reheated (reheating rate mainly depends on plate thickness and severity of cooling) through diffusion of the heat flow from much hotter centre of thick plate that is not affected directly by chilling surface. Finally it is the equilibrium or homogenisation stage when temperatures across thick plate are more or less equalised after a sufficient recovery time (t_R) and the plate is ready for finish rolling. Therefore, the total holding period (t_H) via IFC is the short water-cooling plus recalescence time, i.e. $t_H = t_c + t_R$. On the other hand, for the natural air cooling condition the length of HP (t_A) depends on the cooling time required for the centre of thick plate reduces to the target temperature of first pass of finish rolling (T_1), which obviously is longer than the time spent in the IFC conditions ($t_A > t_H$). Additionally, at the end of the HP, the temperature difference between the surface and centre of the plate still is large, which in turn may cause uneven austenite grain size distribution throughout the thickness of plate prior to finish rolling.

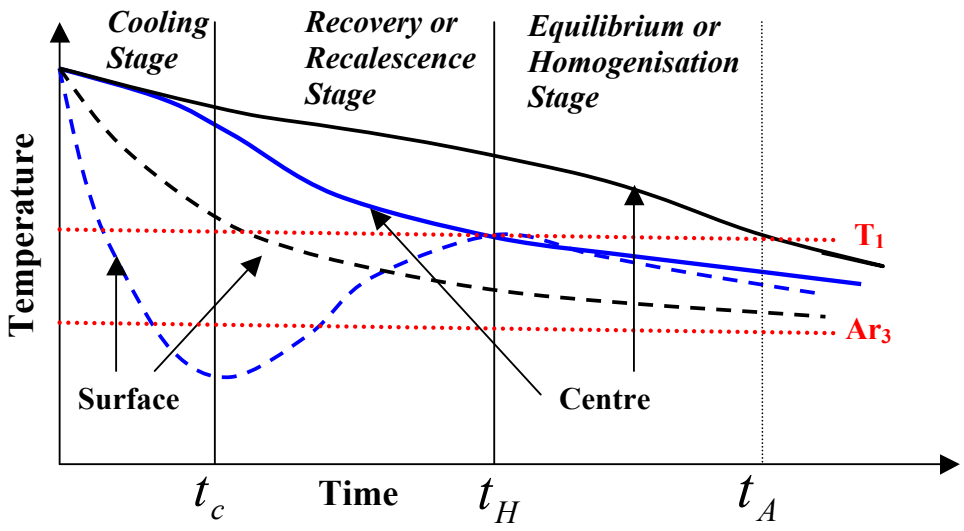

Figure 34: Comparisons of schematic cooling profiles at the surface and centre of plate in air and water-cooling during holding period

2.4.2.4. Microstructure Evolution and Concerns of Applying IFC

As mentioned previously, applying the IFC into the HP of heavy plate production not only can improve productivity significantly, but also refine the microstructure and improve the mechanical properties of plate. In general, for the IFC treated heavy plate, only a thin layer (typically 500μm) [28] of heavily deformed and very fine ferrite grain size is formed at the plate surface, which is considerably finer than that in the centre of plate. This non-uniform grain size distribution has not caused notable reduction of the bulk plate mechanical

properties (possibly bendability) [13, 28-30]. However, there are still some concerns about the severity of IFC over the microstructure and properties of heavy plate. For example, if the plate surface is already suffered from decarburisation and over chilled by heavy water spray, no sufficient recovery time provided and a low finish rolling temperature is used, a thin surface layer with hard, elongated and pancaked grained structure will form at the plate surface but not at the interior of thick plate, so there is a risk of tensile stresses occurring at the surface [24, 29, 30, 170] and a danger of initiating hydrogen-induced cracking at the surface because of high hardness [28]. Fegredo [28, 29] has explained two possible reasons for the formation of fine grain size layer in the Nb microalloyed steel heavy plate rather than in V microalloyed steel.

Firstly, because the IFC puts the surface through a high, low and high again rapid local temperature cycle [24, 28] and there is a possibility that the surface was cooled below the Ar_3 and ferrite is formed near surface if heavy spraying is applied, and also initiates early precipitation. By contrast, the surfaces of the plate given by the air-cooling condition remain above the Ar_3 during the HP, shown in Figure 34. Then, when the water spraying is stopped, the quickly reheated surface temperature may not reach the ferrite to austenite transformation temperature Ac_3(which increases in rapid reheating rate) to transform back into austenite grain during the recalescence stage. If the temperature of the first finishing pass is below the elevated Ac_3 (i.e. the surface layers are less than 100% austenitic) then elongated pancaked ferrite grains are formed firstly at plate surface at the preliminary finishing passes [29], which are indicative of deformed unrecrystallised ferrite. On the other hand, if the equilibrium temperature is above elevated Ac_3(i.e. the surface layers are 100% austenitic), then a very fine austenite grain size is formed at the start of finish rolling.

Secondly, Fegredo [28, 29] and Gorni et al. [24] also mentioned that the early precipitates formed at the water quenching stage could not re-dissolve into solid solution, such as Nb (C, N) when the plate was thermally equalised, which probably in turn retard austenite static recrystallisation and raise the local Ar_3temperature at the surface of plate [24, 28, 29]. Under the same conditions, for the V-HSLA steels, the VC precipitates form in the surface can re-dissolve into solid solution when the plate is homogenised at 890°C-940°C because of higher solubility of VC in austenite compared with that of Nb (C, N) [28]. Fegredo [28, 29] has suggested that softer water spraying over plate surface can solve this problem through induce smaller temperature gradients from surface to centre so it requires shorter time for temperature homogenisation and make sure the surface is fully austenitic at end of holding period. Additionally, this problem of surface layer formation is not occurred in plain steels with similar IFC conditions due to no microalloyed precipitation available [29].

2.4.2.5. Advantages and Critical Parameters of Applying IFC

As described above, there is no doubt that the production rate of heavy steel plates can be increased significantly when the IFC is applied during the long holding periods and this technique has been successfully adopted in a number of industrial plate mills and shows positive results. For example, the COSIPA steelworks [24, 170] in Brazil have applied the IFC using cooling rates of 3.5°C/s to 5°C/s into an industrial plate mill to increase productivity, and they did report a 40% reduction in the delaying time and up to 17% decrease in total production time. In Figure 35 below, it indicates that almost 50% and 20% reduction in HP and total processing time respectively for light plate compared to those of 20% and 8% reduction respectively for heavy plate. Furthermore, the IFC has also been applied in production at Bethlehem Steel Corporation, and shows at least 37% reduction in process times with no notably deterioration in bulk plate properties [25]. Additionally, IFC perhaps refines the austenite grain and its distribution across thickness as a result of lowering austenite grain growth rate, which maybe caused by the reduced average temperature of the whole plate during HP compared to that of natural air cooling.

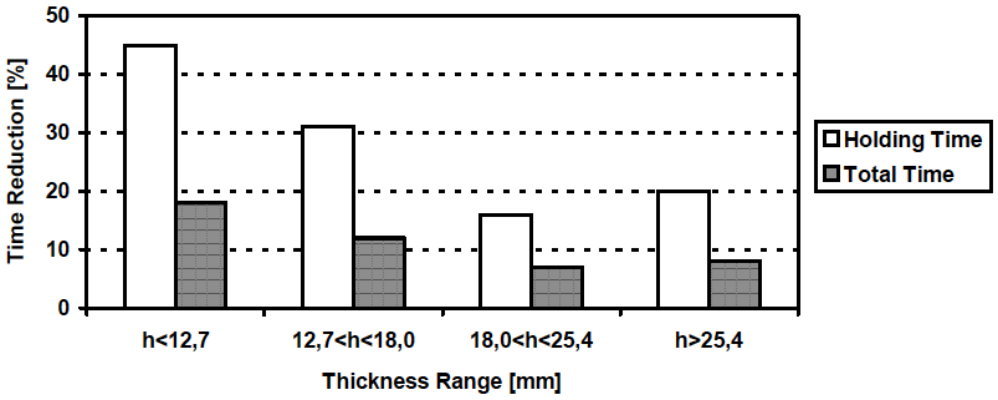

Figure 35: Reduction in the holding time and total processing time associated with the application of IFC during HP of TMCP [170]

The IFC technique has been also applied to reduce oxide scale thickness by reducing the HP, and Abel et al. [25] explained that in theory, application of IFC should reduce the oxide scale growth rate because the plate surface is exposed to a high temperature range for a shorter period of time. This attempt was confirmed by optical measurements that showed the scale thickness is 0-4μm for the IFC plate and 10-15μm for the air -cooled plate [25]. A specialised TMCP has been developed on the Nippon Steel Corp. [173-176], illustrated in Figure 36-a), which initially involves an IFC step applied after roughing, in order to induce a large temperature gradient from plate surface to centre, and then when the surface temperature is reheated just above Ac_3, the finishing stage starts, i.e., rolling in the two phase region. Ferrite in the plate surface is deformed at an increasing temperature, which can make the ferrite

achieve recovery and recrystallisation, and results in surface layers with ultra-fine grains (SUF) shown in Figure 36-b). Therefore, the steel plate with SUF has excellent toughness and crack arrestability. Another advantage of using IFC was mentioned by Abel [25] is that the thicker plates would not have to be normalised when the furnaces are at full capacity due to the IFC can provided required toughness property.

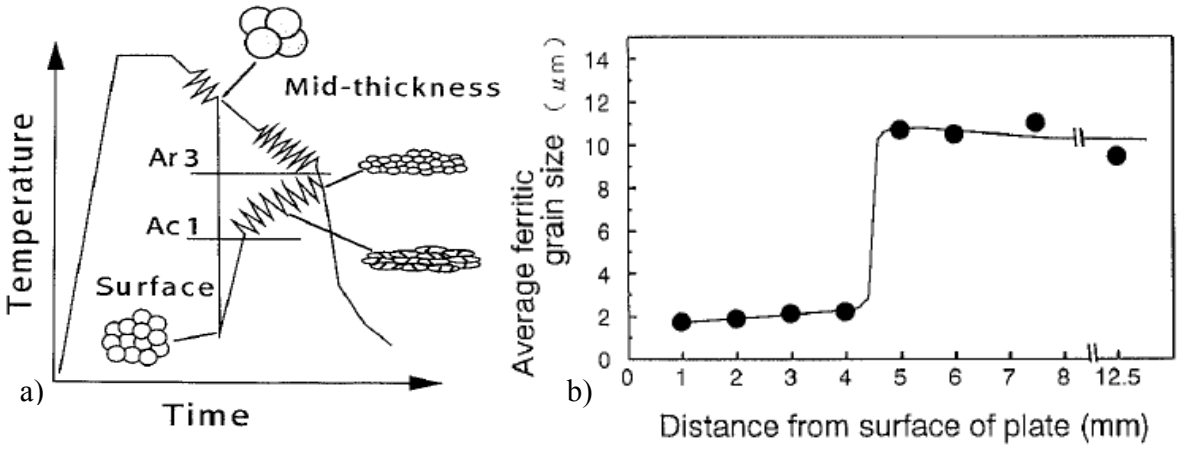

Figure 36: a) Schematic process of SUF steel plates with different deformation profiles in plate surface and mid-; b) cross-sectional distribution of the average ferrite grain size in a SUF steel plate of 25mm [173-175]

2.4.3. Accelerated Cooling after Deformation

2.4.3.1. Effects of ACC on Final as-Rolled Microstructures

After the desired conditioning of the austenite is achieved at the end of finish rolling, the as-rolled plate exits the finish stand, and enters the run-out tables or cooling banks for austenite to ferrite transformation. Accelerated cooling (ACC) of after controlled rolling of HSLA steel plate, is one of the most essential parts of TMCP, and has been intensively studied for many decades and is widely adopted into plate and strip mills to further increase both strength and toughness due to enhanced ferrite grain refinement at the lower transformation temperature and induce second strong phase into softer ferrite matrix. This ACC technology allows an overall reduction in carbon equivalent and MAE contents, resulting in better toughness and weldability at a given strength level. Three specific conference proceedings [165, 173, 177] and many published papers [2, 72,116, 178-189] are related to ACC of steel plate or strip during phase transformation, which has been taken much more attention compared the application IFC during HP. Therefore, the effects of ACC on final microstructure are only briefly mentioned in the following.

It is a well-recognised fact that the austenite to ferrite phase transformation is typically controlled by diffusion process and takes place through thermally activated nucleation and growth, which can be described by the JMAK equation. Therefore, lowering the Ar_3 by MAE and ACC (start cooling temperature above Ar_3) the kinetics of ferrite grain growth are reduced while the nucleation rate of new ferrite grain size is enhanced, and hence a finer ferrite grain size is formed. For a given austenite condition prior to transformation, both the rate of ACC and the stop temperature of ACC extensively influence the final transformed as-rolled microstructures and corresponding properties, which based on steel composition (hardenability) and its corresponding continuous-cooling-transformation (CCT) diagram. To prevent formation of a large amount of brittle bainite or martensite in the final product when relatively fast rate of ACC is applied, hardenability should not be high and as-rolled austenite grain size should be fine [6].

In most cases, air-cooling produces a relatively low strength with coarse equiaxed ferrite and pearlite bandings mixture microstructure. As the cooling rate increases, the growth of the grain boundary nucleated ferrite is progressively inhibited such that the later stages of transformation lead to the formation of very fine ferrite, acicular ferrite and bainite microstructures associated with higher dislocation densities and higher strength. The ferrite grain size d_α is function of the cooling rate C_r, and can be determined from the empirical Equation 42 [189], in which ε_r is the retained strain that is the amount of strain accumulated below the $T_{0.05X}$, and d_γ is the prior austenite grain size, and indicates that ferrite grain size can refined by increasing the ε_r and C_r decreasing the d_γ. Limitations of each parameter in Equation 42 are that the concentration of carbon [C] is in the range of 0.04 to 0.16wt%, and [Mn] is in 0.8~1.2wt%, and maximum ε_r is 1.2, C_r is valid from 0.3°C/s to 10°C/s and d_γ is in the range of 15μm to 90μm. Furthermore, the ferrite volume fraction X_f can be determined through Equations 43 and 44 [98, 104]. Pickering [6] also suggested that a fast cooling rate suppresses precipitation while a slow cooling rate may allow the precipitate to over-age, and the reaction is more rapid for V-steels than for Nb steels. However, Pickering did not define the exact cooling rates for the fast and slow cooling rates.

$$d_\alpha = \left(1 - 0.8\varepsilon_r^{0.15}\right) \times \left(29 - 5 \times C_r^{-0.5} + 20 \times \left(1 - \exp\left(-0.015 d_r\right)\right)\right) \tag{42}$$

$$X_f = X_f^e - 5.476 \times \left(1 - \exp\left(-0.0106 C_r\right)\right) - 0.723 \times \left(1 - \exp\left(-8.8 \times 10^{-4} d_r\right)\right) \tag{43}$$

$$X_f^e = 1 - [C] \times \left(0.789 - 0.1671[Mn] + 0.1607[Mn]^2 - 0.048[Mn]^3\right)^{-1} \tag{44}$$

2.4.3.2. The Operations of ACC in Commercial Hot Rolling Plate Mill

Depending on the severity and the stop temperature of ACC, there are several well-known cooling processes, shown in Table 2 (B_S and M_S are the formation temperatures of bainite and martensite respectively), such as direct quenching (DQ), direct quench plus self-tempering (QST), continuous ACC and interrupted accelerated cooling (IAC), which all can be achieved in one advanced equipment MULPIC (Multi-Purpose Interrupted Cooling) [19, 187, 190-193]. The target or actual cooling rate of different cooling process is controlled by the water flow rate (L/m^2s) and the stop temperature of ACC is determined by the water cooling time. Therefore, the MULPIC equipment should have a high degree of flexibility for the heat flux extraction (from soft to heavy cooling rate) [187] and capability of cooling over a wide plate thickness range (from ultra-thin to heavy plate) uniformly in the thickness, width and length directions for achieving satisfied flatness and uniform mechanical properties. In heavy plate cooling, the IAC is the most popular process characterised by allowing ACC in a given temperature region (usually from 800°C to 500°C) after finish rolling for a specified time interval, followed by natural air cooling to room temperature. Similar to the operations of IFC during HP, the excessive water left on the top surface of plate was removed by forced air blowing after water cooling finished for improving temperature homogeneity.

In general, depending on the different nozzle types for providing accelerated cooling, the as-rolled steel plate may be subjected to laminar flow cooling (an example showed in Figure 37), water curtains or with spray cooling systems [165], which were described in detail in another publications [195, 196]. The range of the practical cooling rate in heavy plate above 40mm appears to be 5°C/s-15°C/s [181] confirmed in Figure 38 [191-193], and the maximum cooling rate is close to the theoretical maximum which limited by the thermal conductivity in the steel plate [186, 190]. The heat transfer mechanism during ACC is described in later Section 2.5.4.

Table 2: Classification of different cooling process and corresponding cooling rate (depends on plate thickness) in the TMCP [181, 184]

	Stop Cooling Temperature	Cooling Rate
IAC	above M_S temperature	5-80°C/s
Continuous ACC	down to 200°C	
Interrupted Direct Quenching or QST	below B_S or M_S Temperature	10-60°C/s
DQ	down to 200°C	

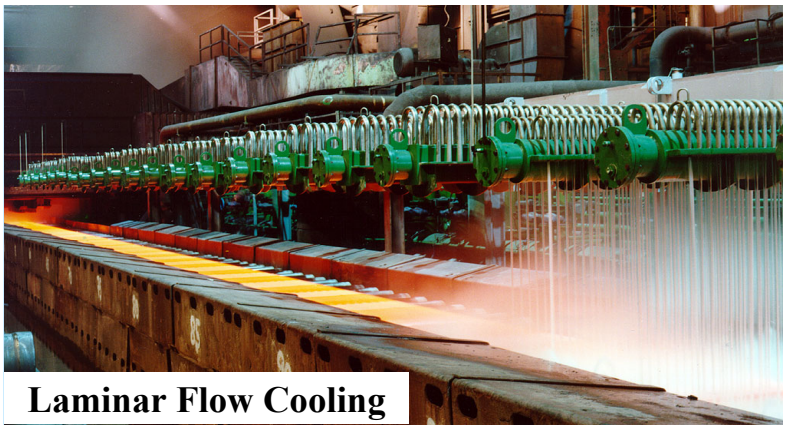

Figure 37: An example of laminar flow cooling applied in accelerated cooling stage [194]

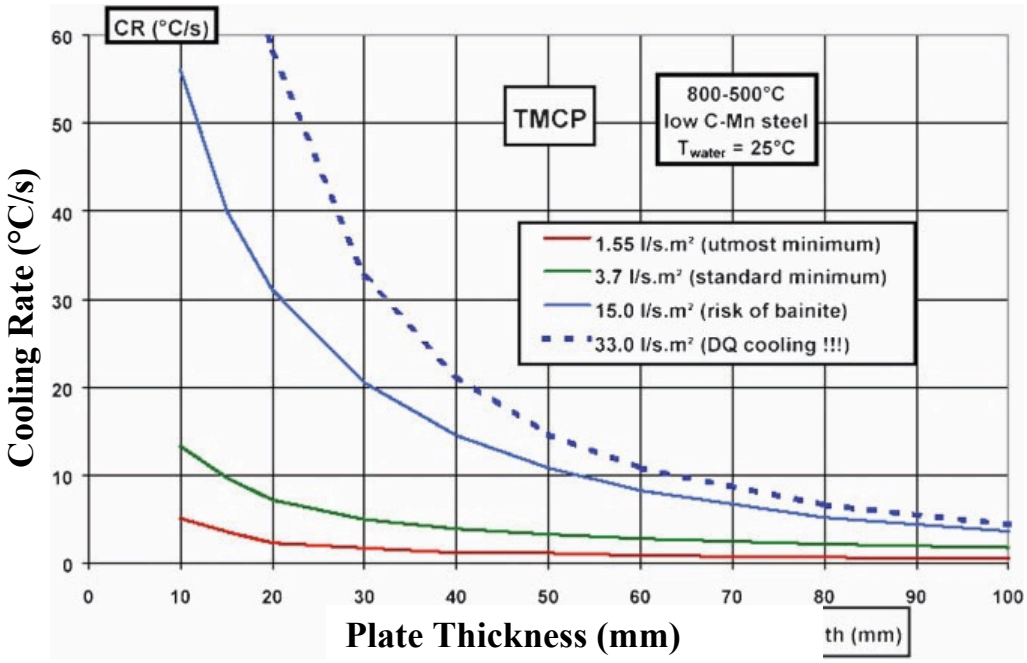

Figure 38: Typical achieve water cooling rates of the MULPIC system from SIEMENS VAI [191-193]

2.5. Temperature and Strain Distribution Models of Hot Rolling Steel Plate

2.5.1. Introduction of Heat Transfer in Hot Rolling

In the previous sections, the metallurgical aspects of hot rolling steel heavy plate were presented and most microstructure evolutions are strongly temperature dependent. In addition, the shape, surface quality and rolling power are also influenced by temperature. Therefore, knowledge of the temperature distribution and heat transfer mechanisms during hot rolling

operations is vital to evaluate the microstructural states and also the strength (flow stress) of as-rolled steel plate. Heat transfer in the hot rolling steel plate is a complicated process due to interactions between the hot slab, cold work roll and environment (air and water spraying). Many heat transfer models [197-208] have been developed to predict the temperature distribution within hot rolling steel plates, strips and rods by finite difference (FD) and finite element (FE) methods. In general, a complete heat transfer model [196-198, 207, 209], illustrated in Figure 39, in hot rolling steel plate should include heat conduction within the slab, adiabatic heat induced by plastic deformation and friction at the roll/slab interface, the cooling effects from the high pressure descaling, chilling effect by conduction from work roll and support rollers, heat lost by radiation and convection from the surfaces of the plate to the atmosphere in gap time of deformation, and rapid heat lost by convection in descaling and accelerated cooling.

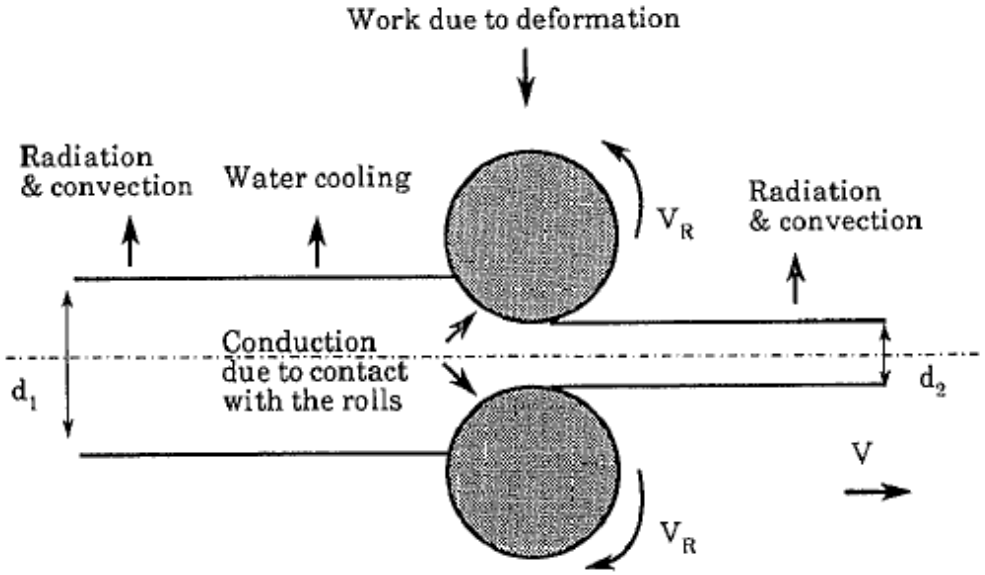

Figure 39: Different heat transfer mechanisms during hot rolling [197]

All these heat transfer phenomena in the above Figure 39 across the different interface or boundary can be described by corresponding interface heat transfer coefficients, which are affected by the oxide layer of plate surface due to it alters the efficiency of heat loss to roll and atmosphere, which is described in somewhere else [165, 199, 210-213]. It is widely agreed that the accuracy of the temperature distribution is mainly dependent on appropriate boundary and the initial temperature conditions. The initial temperature of the slab can be assumed as a uniform single value, or as a temperature distribution that from a calculation made by previous programme [103]. The boundary conditions at the different zones of hot rolling processes are described in the following sections.

2.5.2. Heat Transfer at the Roll Gap

As the hot steel plate enters the rolls gap for deformation, illustrated in Figure 39, although the contact time between the rolls and plate is short, the heat generation will still occur at the plate surface owing to the energy of plastic deformation and friction work at the contact surface [214]. Moreover, the surface of hot plate is chilled by the cold rolls and conversely the cold rolls are heated from the hot slab [197], and thus there is conductive heat transfer at the interface of roll and hot slab surface. Heat conduction, described by Fourier's Law that heat must flow downhill on the temperature scale [215], within the steel slab is governed by the partial differential Equation 45 in which q_w is the heat or energy (Wm^{-3}) generated from the plastic deformation, k_s, ρ and c_p are the thermal conductivity ($Wm^{-1}K^{-1}$), density (kgm^{-3}), and specific heat ($Jkg^{-1}K^{-1}$) of steel, respectively, which are usually assumed to be independent of temperature but this is not strictly the case [211]. x, y and z are the distances in the directions of length, width and thickness of plate, respectively.

$$k_s\left(\frac{\partial^2 T}{\partial x^2}+\frac{\partial^2 T}{\partial y^2}+\frac{\partial^2 T}{\partial z^2}\right)+q_w=\rho c_p\frac{\partial T}{\partial t} \tag{45}$$

$$q_w=\eta\bar{\sigma}\dot{\bar{\varepsilon}},\quad \eta=0.85-0.95 \tag{46}$$

$$q_{fric}=\tau A_c\left|\Delta v\right|\delta t \tag{47}$$

$$T=T_0(z)\ \text{at t=0},\ 0\le z\le\frac{H}{2} \tag{48}$$

$$-k\frac{\delta T}{\delta z}=0\quad \text{at the centreline of the slab, t>0},\ z=0 \tag{49}$$

$$-k\frac{\delta T}{\delta z}=h_{con}\left(T_s-T_r\right)-q_{fric}\ \text{at the surface of the slab, t>0},\ z=\frac{H}{2} \tag{50}$$

$$\Delta T=\frac{1}{\rho C_P}\int_{\varepsilon_0}^{\varepsilon_1}\sigma\, d\varepsilon \tag{51}$$

The q_w in Equation 45 can be calculated by the Equation 46 in which η is the efficiency of the conversion of plastic deformation into the heat, and $\bar{\sigma}$ and $\dot{\bar{\varepsilon}}$ are the effective stress and strain rate, respectively [208, 210, 214, 216]. In addition, a distributed surface flux q_{fric} that is generated from frictional sliding and only contributes small amount to the total thermal balance [210], which is determined by Equation 47 where τ is the frictional stress, A_c is the

contact area, and $|\Delta v|$ and δt are the relative velocity and time step, respectively [210, 216]. To simplify the solution process of Equation 45, a few assumptions are usually made. For example: the heat conduction along the length and width of the plate are negligible due to the high speed motion of slab and thickness of plate is much smaller in comparison with the other two dimensions [199, 204]; the rolling process was assumed to operate at steady-state conditions [198-200]; the assumption of symmetry allows only one half of the thickness to be considered. Therefore, the Equation 45 can be simplified into one-dimensional heat transfer through the thickness z direction with symmetrical cooling at the centreline. The initial state of simulation is given in Equation 48 where the temperature distribution $T_0(z)$ in the plate before it enters the roll gap is taken as the initial condition. The boundary conditions at the plate centreline and surface are given by Equations 49-50, respectively, in which h_{con} is the roll-plate interface heat transfer coefficient and H is thickness of the plate; T_r is the surface temperature of work roll, which can be simultaneously determined by another FE model [199, 200]. Finally, the adiabatic increase in temperature produced by deformation is calculated by the Equation 51, in which the integral represents the energy required to deform steel from ε_0 to ε_1 [201].

2.5.3. Heat Transfer at the Interstand Cooling

Heat transfer mechanisms at the intervals of rough and finishing rolling passes are similar to those at the roll gap, and can be also governed by the simplified partial differential Equation 52 through the thickness z direction after the assumptions. The q_w term in Equation 45 is not included in this stage in which the slab temperature drops due to heat loss to the surroundings at ambient temperature, mainly by radiation and partly by convection because Hand and Sellars [217] suggested that at the relatively high temperatures region (>827°C) the radiation heat transfer dominates, while at the low temperatures region (<527°C) where convective and radiative losses are of similar magnitudes. The initial condition of the simulation is given in Equation 53 in which the temperature distribution or single average temperature $T_1(z)$ in the plate after it leaves preceding roll gap is taken as initial state. The boundary condition at the centreline of plate is the same as Equation 49, and the surface condition under natural air cooling at the intervals is given by Equation 54 in which h is the convective heat transfer coefficient, λ is the emissivity of the steel plate, which is assumed a constant value of λ =0.85 or calculated by Equation 55 [203,207], and σ is the Stefan–Boltzmann constant (5.67 $\times 10^{-8}$W/m^{2}K^4), and T_∞ and T_s are the ambient and as-rolled heavy plate surface temperatures, respectively.

$$\frac{\partial}{\partial z}\left(k\frac{\partial T}{\partial z}\right)=\rho c_p\left(\frac{\partial T}{\partial t}\right) \tag{52}$$

$$T = T_1(z) \text{ at t=0, } 0 \le z \le \frac{H}{2} \tag{53}$$

$$-k\frac{\delta T}{\delta z} = h\left(T_s - T_\infty\right) + \lambda\sigma\left(T_s^4 - T_\infty^4\right) \tag{54}$$

$$\lambda\left(T^0C\right) = \frac{T}{1000}\left(0.125\frac{T}{1000} - 0.38\right) + 1.1 \tag{55}$$

2.5.4. Heat Transfer during Descaling and Accelerated Cooling

In terms of accelerated cooling or water quenching condition at the descaling period prior to roughing and post-deformation during phase transformation, the heat transfer mechanism is similar to the above interstand cooling stage, but with much higher value of convective heat transfer coefficient and the radiation term only contribute little amount to the overall heat balance during water quenching process [217]. It is important to note that there are five different regions of heat transfer mechanisms when the plate subjecting to water cooling, illustrated in Figure 40. However, most heat transfer models only take the region I - single phase forced convection into the simulation (possibly due to most heat flux occur in this region), the other four regions and the heat conduction between the bottom of plate and support rolls (owing to high speed motion of plate) [218] on run-out table are usually not included, thus the convection heat transfer at the plate surface determined the temperature distribution inside as-rolled steel plate. Additionally, due to the phase transformation austenite to ferrite, pearlite and/or bainite is an exothermic reaction, the heat source q_H generated by the transformation, in Equation 56 where H_t is the heat of transformation and F is the fraction of transformation, causes an increase in the temperature of steel plate [204, 207, 220]. Equation 56 is coupled with the initial condition in Equation 57 in which $T_2(z)$ is the average finish rolling temperature or the temperature distribution within plate prior to cooling. The boundary state at the centreline of plate is the same as Equation 49, while the surface condition is determined by Equation 58 where h_q is the convective heat transfer coefficient for the water quenching medium [217].

$$\frac{\partial}{\partial z}\left(k\frac{\partial T}{\partial z}\right) + q_H = \rho c_p\left(\frac{\partial T}{\partial t}\right), \quad q_H = \rho H_t\left(\frac{\partial F}{\partial t}\right) \tag{56}$$

$$T_s = T_2(z) \text{ at t=0, } 0 \le z \le \frac{H}{2} \tag{57}$$

$$-k\frac{\delta T}{\delta z} = h_q\left(T_s - T_q\right) \tag{58}$$

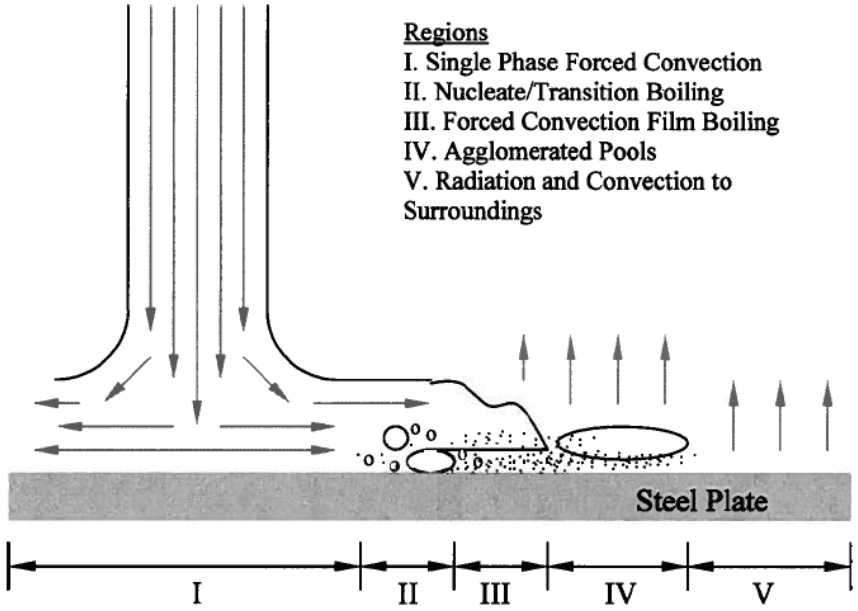

Figure 40: A schematic of different heat transfer regions on the steel plate surface being impinged by a water flow [196, 219]

2.5.5. Temperature, Strain and Strain Rate Distributions inside Heavy Steel Plate and PSC Specimen

Most of physical-based microstructure models assume a uniform temperature, strain and strain rate through the thickness of the as-rolled steel. However, during the commercial hot rolling of heavy plate, the temperature, strain and strain rate are largely different across the plate thickness, illustrated in Figures 41 and 42, which in turn cause inhomogeneity of microstructure and mechanical property distributions across heavy plate thickness in final as-rolled products. It is commonly agreed that the highest effective strain is near the surface (in Figure 41-a) and decrease towards the centre of industrial hot rolling thick plate [221-226] due to the high redundant shear associated with constraining the slab to flow through the roll gap [199, 227] and the consequent higher local strain rate distribution concentrates just beneath the plate surface [199], which normally predicted by the rigid-plastic FE models with full coupling of the thermal and deformation variables. The complete solutions of rigid-plastic approach are described in detail in references [98, 228, 230], and are based on the principle which states that for a plastically deforming body of volume V, under traction F (the friction forces), prescribed on a part of the surface S_t (the contact surface of work roll and slab), and the velocity v prescribed on the rest of the boundary, under the constraint

$\dot{\varepsilon}_V = \dot{\varepsilon}_x + \dot{\varepsilon}_y + \dot{\varepsilon}_z = 0$, the actual solution minimises the functional J in Equation 59 [98, 106, 229-231], where K is the penalty coefficient or Lagrange multiplier, and σ_i, $\dot{\varepsilon}_i$, $\dot{\varepsilon}_v^*$ are the effective stress, strain rate, and volumetric strain rate, respectively.

$$J = \int_V \left(\sigma_i \dot{\varepsilon}_i + K \dot{\varepsilon}_V \right) dV - \int_{S_t} F v \, dS \tag{59}$$

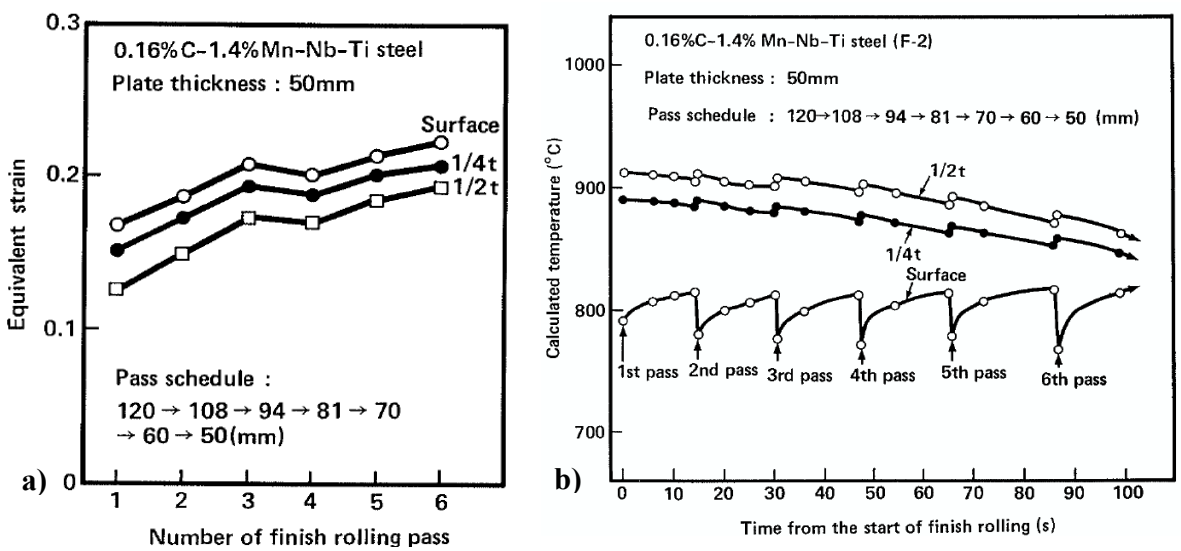

Figure 41: a) Equivalent strain at plate surface, quarter and centre of 50mm plate; b) temperature distribution inside as-rolling steel plate [221]

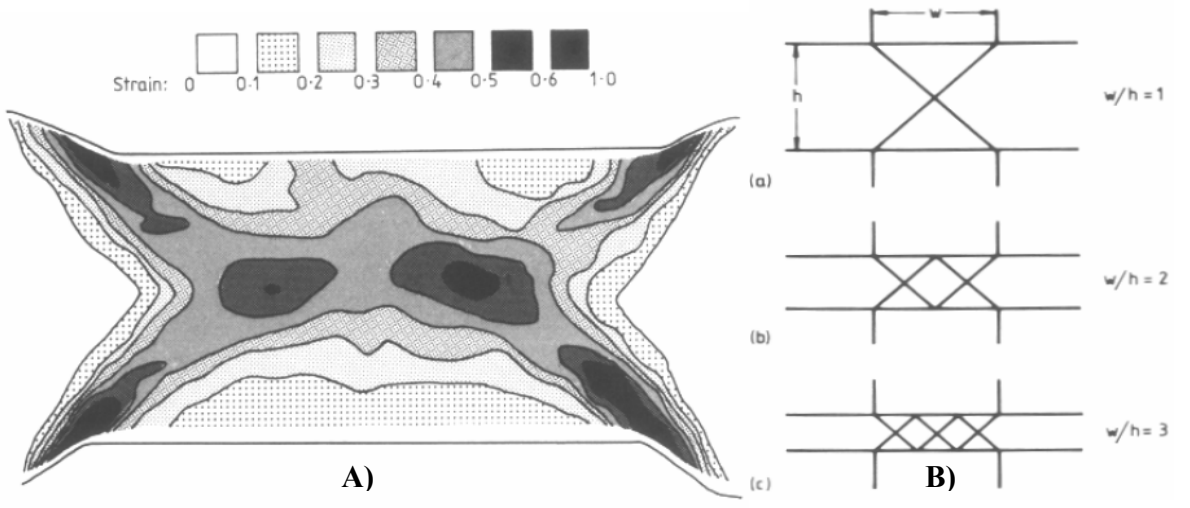

Figure 42: A)-The contour plot of predicted mean strain distribution inside deformed PSC sample with nominal strain 0.326 and w/h=2; B)-Slip line field (SLP) patterns for PSC between frictionless parallel tools with different w/h ratios [232, 233]

For the deformed PSC sample, the strain is also inhomogeneously distributed within the deformation zone, presented in Figure 42-A) in which the w/h is the ratio of the width of tool to the PSC specimen thickness. According to the Figure 42 and the work done by Sellars et al. [233-237], the large local straining occurs mainly in the diagonal (45°) regions from specimen centre to the edge of the tool [59] corresponding to the slip line field (SLF) theory, where the strain rates are also the highest. Therefore, it is important to notice that the inhomogeneous distributions of strain and strain rate within deformed PSC sample are different to those inside industrial hot rolling steel plate due to no redundant shear stress occurs at the surfaces of PSC sample if it deformed symmetrically during testing. On the contrary, there can be "dead zone" of little equivalent strain at the PSC sample surfaces.

2.6. Plane Strain Compression Testing as a Simulation of Hot Rolling

There are several different methods of laboratory-based mechanical testing for simulating industrial hot rolling steel production, which include laboratory or pilot rolling mill, axisymmetric compression, plane strain compression (PSC), torsion, and tension testing. All of these methods have been used to study the hot working of metals, and all have their own merits and drawbacks, which are not described in here but have been reviewed in the reference [98, 99, 238, 239]. The multipass PSC testing is suggested that probably the best suited method for laboratory simulation of commercial hot rolling steel plate production that is essentially a compressive process. Due to both industry and academia needs for reproducible flow stress test data for modelling, process deformation strategies and correlation with microstructural evolution studies [240], the multipass PSC testing is now widely accepted laboratory method to determine and modelling flow stress and microstructural evolution under conditions similar to industrial hot rolling steel production.

2.6.1. Plane Strain Compression Conditions

A schematic representation of the PSC testing is shown in the following Figure 43 in which the standard PSC specimen is deformed between two flat parallel tools (platens) (width of tool in room temperature is 15mm). In the following section, the mathematic descriptions of PSC conditions are briefly presented from the Good Practice Guide [240, 241]. According to the Figure 43, the equivalent strain ε_{evm}, is given by the following Equation 60:

$$\varepsilon_{evm} = \frac{\sqrt{2}}{3}\left[\left(\varepsilon_1 - \varepsilon_2\right)^2 + \left(\varepsilon_2 - \varepsilon_3\right)^2 + \left(\varepsilon_3 - \varepsilon_1\right)^2\right]^{\frac{1}{2}} \tag{60}$$

If the deformation is assumed as ideal plane strain conditions with no breadth spread, i.e. $\varepsilon_2 = 0$ and $\varepsilon_1 = -\varepsilon_3$, and $\sigma_2 = (\sigma_1 + \sigma_3)/2$ [232], then the Equation 60 becomes

$$\varepsilon_{evm}^{ideal} = \frac{\sqrt{2}}{3}\left[\varepsilon_3^2 + \varepsilon_3^2 + 4\varepsilon_3^2\right]^{\frac{1}{2}} = \frac{2}{\sqrt{3}}\varepsilon_3 = \frac{2}{\sqrt{3}}\ln\left(\frac{h}{h_0}\right) \tag{61}$$

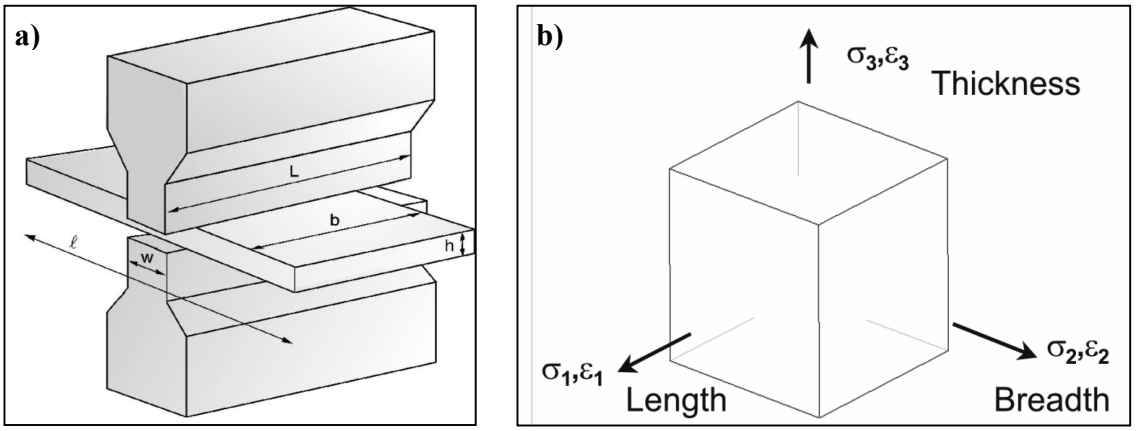

Figure 43: a) Schematic diagram of plane strain compression tests and b) schematic illustration of stress and strain axes relative to PSC specimen [240]

However, accounting for lateral spread, $\varepsilon_3 = \ln\left(\frac{h}{h_0}\right)$, $\varepsilon_2 = \ln\left(\frac{b}{b_0}\right)$, and $\varepsilon_1 = -\varepsilon_2 - \varepsilon_3$ due to constant volume conditions $\varepsilon_1 + \varepsilon_2 + \varepsilon_3 = 0$. Then by substitution, the equivalent strain ε_{evm} is given by:

$$\varepsilon_{evm} = \frac{\sqrt{2}}{3}\left[(2\varepsilon_2 + \varepsilon_3)^2 + (\varepsilon_2 - \varepsilon_3)^2 + (\varepsilon_2 + 2\varepsilon_3)^2\right]^{\frac{1}{2}} = \frac{2}{\sqrt{3}}\left[\varepsilon_2^2 + \varepsilon_2\varepsilon_3 + \varepsilon_3^2\right]^{\frac{1}{2}} \tag{62}$$

2.6.2. Thermomechanical Compression (TMC) Simulator

All the multipass simulations for this project were carried out by the PSC tests using the Thermomechanical Compression (TMC) machine, pictured in Figure 44, which is designed and built by the Servotest Ltd. to meet the specifications in Table 3 required by The University of Sheffield and delivered in 2002. The control system of the TMC is fully computer digitised to allow for the precise control of hot rolling parameters (temperature, strain, strain rate and gap time) that are appropriate to the conditions in commercial heavy plate hot rolling production, which is described more in detail in the Experimental Chapter. According to the outline structure of main components of TMC simulator shown in Figure 44,

the marked or labelled components as well as the top and bottom deformation tool (inside the test furnace) are critical for the multipass simulation, so the functions of this components are briefly introduced in the following.

The crosshead is a large moveable beam (up and down on the four large stainless steel columns) supports six accumulators: three of which are low pressure and the others three are high pressure [242, 243], which provide the driving force for the movement of the main actuator. The function of main actuator is to deform the PSC sample driven by the accumulators.

The top platen (in Figure 43-a) is mounted on to a piston or ram, which moves in the vertical direction allowing a PSC specimen placed between the platens inside test furnace to be deformed by the action of downward movement of the ram [242, 244]. The velocity and displacement of ram is controlled by a servovalve, which allows oil under hydraulic pressure into piston chamber from accumulators mounted above the piston, at a rate depends on the requirement of PSC testing. The bottom deformation tool is bolted onto a cylinder post that sits in the test furnace and is directly mounted on the maximum 500kN load cell [242, 244]. The platens are made of the nickel-based superalloy, M22 [242, 244] and strong enough to sustain the loads required for the hot deformation at high temperature.

The wedge is an adjustable mechanical stop device with different thickness. Prior to each hot deformation, the main actuator is raised so that the piston has enough distance to accelerate to the required velocity when it contacts with the PSC specimen [243], and the same time the wedge automatically moves to the correct pre-defined position for the required strain by the wedge actuator according to the defined PSC testing schedules, thus the actual deformation is not above the target strain of each pass.

The fast thermal treatment unit (FTTU) sits in front of the test furnace and consists of an induction coil and a water-quenching unit, where temperature controls of re-heating, holding and cooling processes (air blasting, water cooling or mixture of air and water) are carried out through a control thermocouple embedded into the PSC sample.

The function of robotic arms is to hold the PSC specimen firmly throughout the whole test schedules, and the robotic arms can move forward and backward between the FTTU and the test furnace. However, during the PSC testing, samples are often dropped off from the robotic arms during transportation between FTTU and test furnace, which are explained more in Experimental and Discussion Chapters.

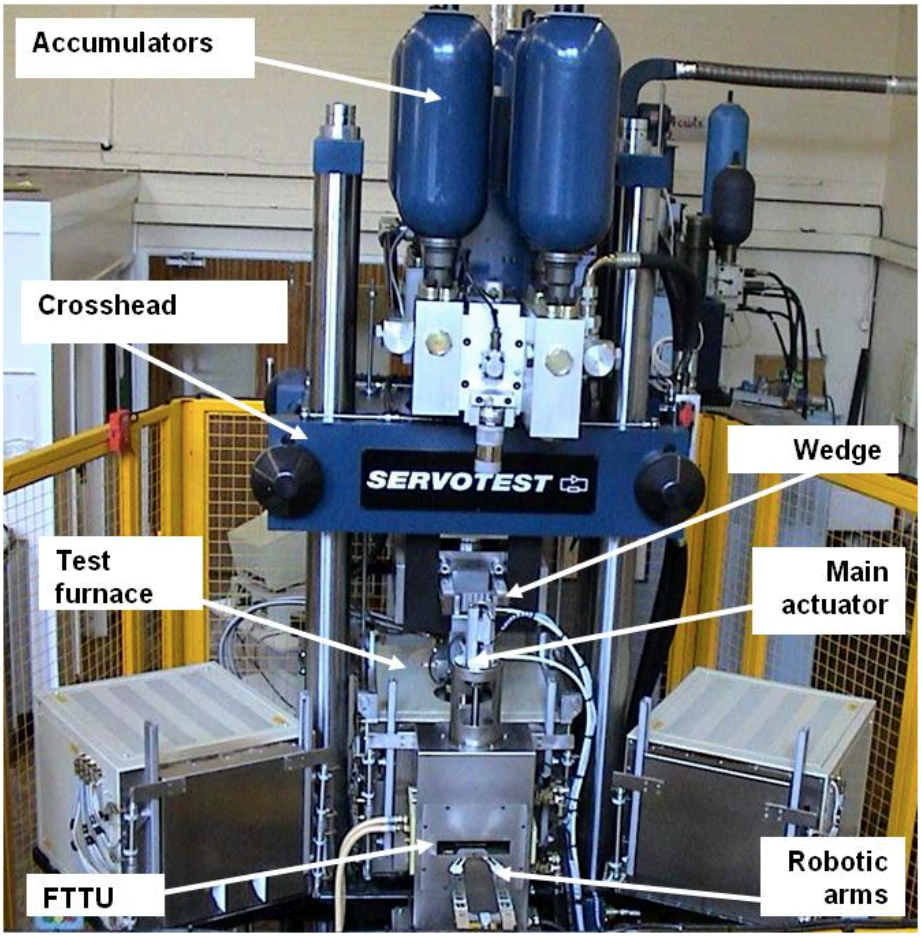

Figure 44: Outline structure of main components of TMC machine [242, 243]

Table 3: Some key features of TMC machine [242]

	Machine characteristics
Actuators	Servo-hydraulic
Maximum strain	~2
Maximum strain rate	150 – 200s^{-1}
Maximum Deformation temperature	1200°C
Maximum load	500 kN
Machine Stiffness	410 kN/mm
Maximum FTTU Reheating Temperature	1300°C
Full Quench start time	< 0.5second from end of deformation
Controllable cooling variables	Forced air, mist and water quench
Reheating rate	Rapid and controlled heating (up to 1300°C)
Atmosphere control	None (natural air)
Temperature measurement	Up to 3 thermocouples inside PSC specimen

2.6.3. PSC Samples

The dimensions of the specimens subjected to PSC testing is shown in Figures 45 and 46 below, are l=60 x b_0=30 x h_0=10mm in length, breadth and thickness respectively, and these PSC samples were machined out of a larger plate from a local engineering company and during machining the residual stress and changes in local microstructure close to the surface are minimised. The preferred dimensions of PSC samples are related to the width of tool: $h_0 \le 0.6w$, $b_0 = 5w$ and $l > 3w$ according to the best practice guide [240, 241].

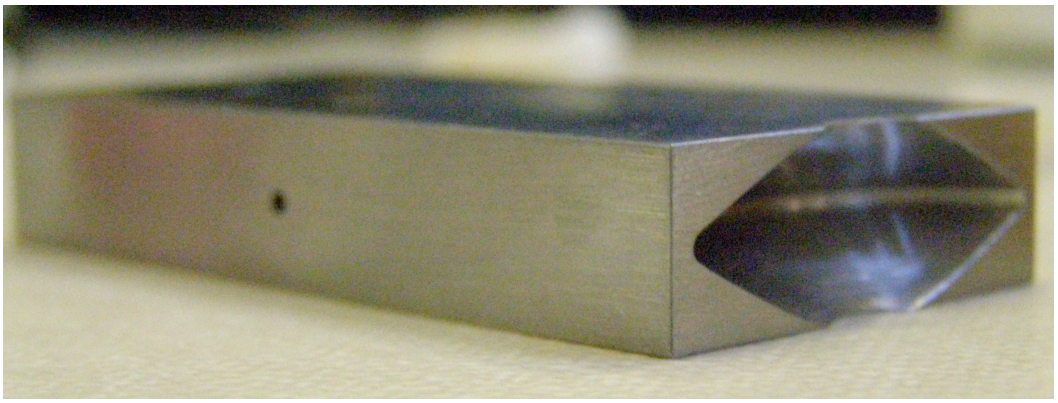

Figure 45: An example of undeformed PSC sample includes the position of thermocouple hole and the edge structure for the robotic arms

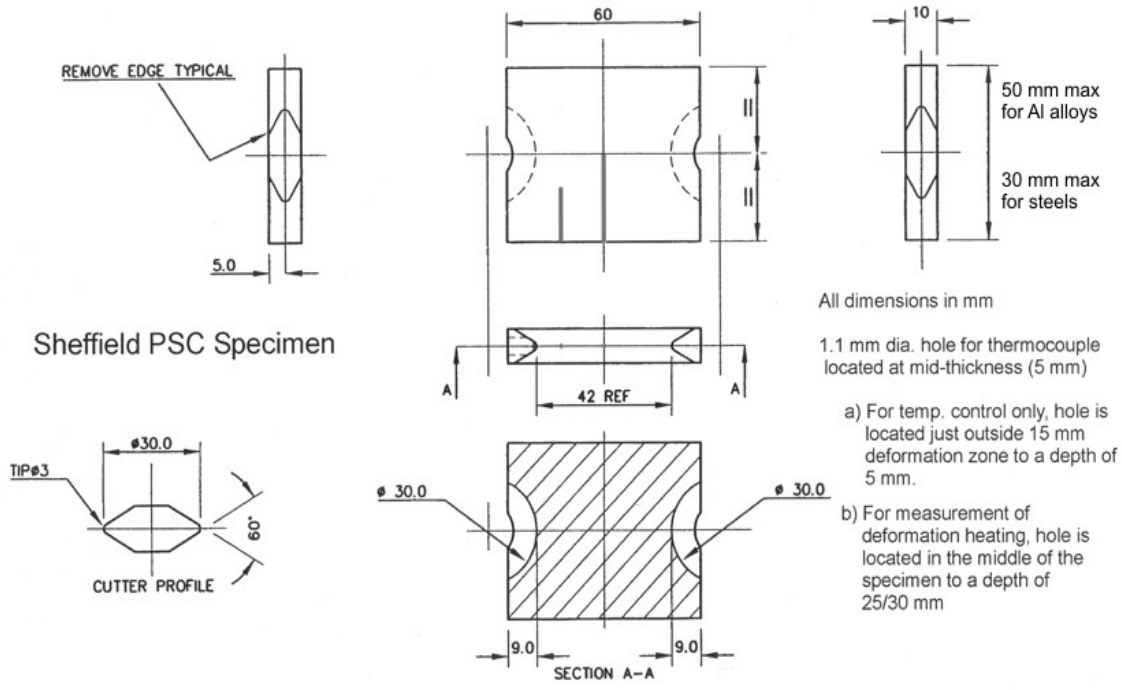

Figure 46: Detailed dimensions of PSC sample include the edges structure

2.7. Summary of Literature Review

The important points of this literature review and challenges of present work are summarized as following:

- Grain refinements of austenite and ferrite, and precipitation hardening during phase transformation are the two primary contributors to the strength and toughness in hot rolled HSLA steels, which should have a pre-existing grain boundary motion inhibition system that is small enough to permit static recrystallisation but large enough to suppress post-recrystallisation grain coarsening during the intervals of rolling passes [10].

- The highly work hardened (pancaked) austenite as the result of large reduction below recrystallisation temperature during finish rolling stage provides numerous nucleation sites for the ferrite formation and refine ferrite grain size. However, the high power requirement may above the capacity of old plate mills.

- Final ferrite grain size strongly depends on conditions of austenite and ACC (cooling rate during phase transformation and cooling stop temperature)

- Current technology for HSLA steels heavy plate hot rolling production is challenged by the long but critical holding period (HP). Based on limited published papers, the reduction of holding period can be achieved by applying the intermediate forced cooling (IFC) instead of air cooling but the effects of the IFC on austenite and ferrite grain size have not been investigated.

- So far the IFC technique only has been studied in commercial scale but not in laboratory scale. The results of such processing are only amenable to qualitative estimation at present, and require detailed experimental exploration.

- The effect of possible increases the strain penetration by chilling the heavy plate surface cannot be analysed by the 10 or 12mm PSC sample due to scale difference, but might able to be explored by the finite element models

- Some well-known physical-based empirical equations for austenite grain size evolution were mentioned in this chapter, others equations were reviewed by elsewhere [34, 98]. However, the accuracy of these equations for predicting microstructure evolution of multipass PSC testing is not well analysed and validated.

- The maximum multipass PSC testing on the advanced TMC machine before this project was only up to four passes [242], and the cooling rates capability of different cooling media inside FTTU were never been investigated, thus further explorations were required.

2.8. Statement of Objectives

Based on the knowledge gap or challenge mentioned on the summary of previous literature review chapter, the main objectives of the present investigation are

1. Fully exploration on the minimum and/or maximum controllable cooling rates of different cooling media (forced air blowing, mist and fully water quenching) during the holding period and post-deformation cooling stage.
2. Investigate the capabilities or simulation window of the thermomechanical compression (TMC) machine performing multipass plane strain compression (PSC) simulation (temperature, strain, strain rate and time controls) to the target values of hot rolling parameters.
3. Investigate through-process microstructural evolution following multipass heavy plate hot rolling simulations.
4. Development of a consistent, reliable, reproducible and state-of-the-art laboratory-based multipass (more than 4 passes) PSC simulation of the entire industrial hot rolling process (reheating, rough rolling, holding period, finish rolling and air cooling or accelerated rolling to room temperature).
5. Use of the intermediate forced cooling (IFC) during holding period to increase productivity of hot rolled steel heavy plate rolling, and investigate the effects on prior austenite grain size at the end of holding period and subsequent final ferrite grain sizes.
6. Optimise austenite and ferrite grain refinement for producing less than average 5μm ferrite grain size through thermomechanical controlled processing (TMCP) involving intermediate forced cooling (IFC) and accelerated cooling (ACC) after rolling.
7. Modelling the austenite and final ferrite grain size as function of rolling parameters in multipass PSC testing through the physical-based empirical equations, which are then compared with measured grain sizes from optical quantitative measurements.

Chapter 3 - Experimental Materials, Procedures, Equipment and Methods

3.1. Overview of Experimental Procedures

In the following sections of this chapter, the main experimental materials, test procedures and the corresponding techniques or methods that were applied to investigate the main objectives of this study (mentioned in previous Chapter 2) are introduced. This chapter covers many aspects of the work from selection of steel samples from lab-cast ingots, analysis of commercial hot rolling schedules to forced cooling tests during hot period, and from modelling temperature, strain and strain distribution inside as-rolling steel plate to multipass PSC simulations of industrial productions on the advanced TMC machine, quantitative metallography and prediction of austenite and ferrite grain sizes. It is useful to mention that most experiments and methods are included in this chapter but a summary table of many multipass PSC tests is included in Appendix A and an example of standard procedures for determination of flow curve from the multipass PSC testing is given in Appendix B.

3.2. As-Cast Steel Ingots and Initial Investigation

3.2.1. As –Received Steel Materials and Sampling

Initially, the three different steels of interest to the industrial sponsor Tata Steel Europe Company were unable to achieve the target value (0.11wt%) of carbon concentration during laboratory casting process from the Company. Therefore, four lab casts (each cast ingot was weighted 60kg), which were vacuum induction melted and were the most closer to the target composition values, were selected out of eight laboratory as-cast ingots. They were C-Mn-Nb (referred as steel A), C-Mn-Nb-Ti (referred as steel B), 2 x C-Mn (referred as steel C and D with different in carbon content) steels, shown in Table 4, and they have similar base compositions except small additions of microalloying elements Nb and Ti in steels A and B, which were measured through the chemical composition analysis at the bottom centre (about 5mm deep from the bottom surface) of as-cast ingots. In addition, the phosphorus level (0.015wt%) was intentionally kept relatively high value to aid in metallographic techniques associated with revealing prior austenite grain boundaries.

The first step of sample preparation was to section the four heavy (60kg) as-cast ingots. For the as-cast microstructural study using optical micrographs, many approximate $1cm^3$ cubes were cut from the bottom (without porosity from the previous solidification process) of each

ingot and then these small cubes were prepared through standard sample procedures (hot moulding, grinding, polishing and etching) to reveal the microstructures. During the second step, two large plates of roughly 25mm thickness were cut from the middle of ingot along the longitudinal direction on a large sawing machine, illustrated in Figure 47, so there were eight large plates in total after initial section. During the final step, 2 to 4 smaller plates (roughly 25mm in thickness, 30mm in width and 100mm in length) were cut from the each large plate, and finally these small plates were heat treated later inside a muffle furnace.

Table 4: Steel chemical compositions (wt%) of initial targets and four selected lab casts

	C	Si	Mn	P	N	Nb	Ti
C-Mn (target)	0.11	0.35	1.35	0.015	0.005	0	0
C-Mn-Nb (target)	0.11	0.35	1.35	0.015	0.005	**0.03**	0
C-Mn-Nb-Ti (target)	0.11	0.35	1.35	0.015	0.005	**0.03**	**0.015**
Steel A (Nb)	0.085	0.34	1.33	0.017	0.008	**0.028**	0.0041
Steel B (Nb + Ti)	0.083	0.34	1.33	0.017	0.005	**0.032**	**0.016**
Steel C (plain carbon)	0.085	0.33	1.34	0.016	0.006	0.003	0.0038
Steel D (plain carbon)	**0.115**	0.32	1.34	0.016	0.006	0.002	0.004

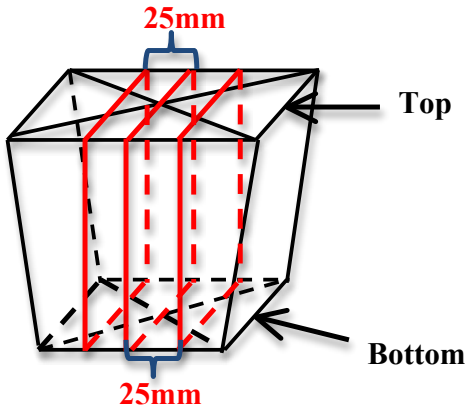

Figure 47: Schematic positions of sectioning two roughly 25mm thickness steel plates from the centre of a laboratory as-cast ingot

3.2.2. Physical Metallurgy and Properties of Steels from Predictions

In order to obtain more basic information about the selected steels and the corresponding physical properties, some empirical equations and a commercial modelling software, called JMATPro (Java-Based Materials Properties) version 4.0, were used to calculate the profiles of density, specific heat, thermal conductivity and elastic modulus of steels A, B, C and D as function of temperatures. These physical properties were calculated from the "General Steel-Quench-Properties" simulation, which is one of many functions in the JMATPro program,

and were used later in the finite element (FE) modelling of temperature distribution across thickness of hot rolling steel plate. For the prediction process, the steel compositions were entered into program first, and then the initial austenite grain size was set at the size 9 on the ASTM scale (≈16μm) and the austenitisation temperature was set at 1000°C (similar to the temperature at which holding period starts), shown in Figure 48. The last step of simulation was five cooling rates (0.01, 0.1, 1, 10 and 100°C/s or 0.5, 1, 10, 50 and 100°C/s) that were chosen during phase transformation to determine the physical properties as function decreasing temperature from 1000°C to room temperature with different cooling rates.

Also, through some basic predictions from the empirical equations, important temperatures and physical metallurgy of different steels were calculated, such as carbon equivalent (CE) by Equation 63, dissolution temperature (T_{DISS}) for microalloyed element additions (particular for the Nb element) by Equation 64, 5% recrystallisation temperature ($T_{0.05x}$), and austenite to ferrite transformation temperatures Ar_3 by Equation 65 in which the plate thickness, t, was in the range of 8mm-30mm [245]. Although these estimated temperatures are not always accurate but the values could be used as basic reference to design draft hot rolling schedules. Furthermore, the predicted temperatures ($T_{0.05x}$ and Ar_3) is then compared to the deformation temperatures of each pass in the rolling schedules to determine at which regions recrystallisation of austenite is inhibited and whether the phase change will occur.

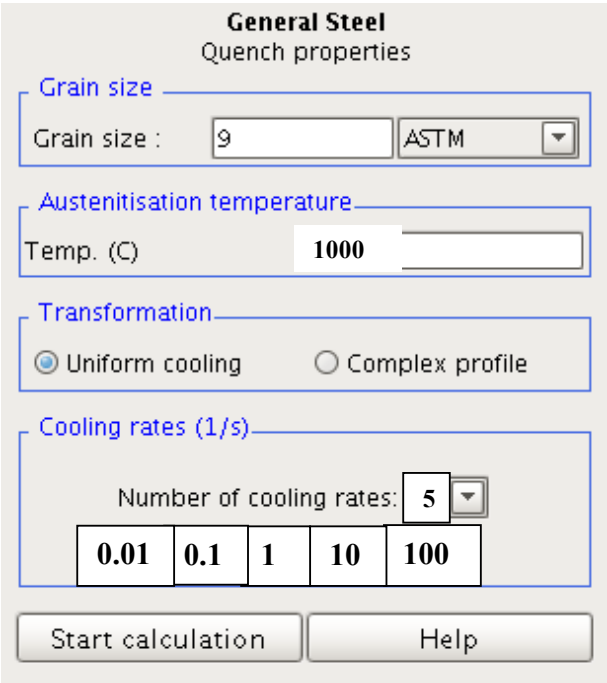

Figure 48: Input window of cooling properties of steel in JMATPro software

$$CE = C + \frac{Mn}{6} + \frac{Cr + Mo + V}{5} + \frac{Cu + Ni}{15} \qquad (63)$$

For Nb and Nb-Ti steels: $$T_{DISS} = \frac{6770}{0.248Mn + 2.15 - \log\left[Nb\left(C + \frac{12N}{14}\right)\right]} \quad (64)$$

$$Ar_3 = 910 - 310C - 80Mn - 20Cu - 15Cr - 55Ni - 80Mo + 0.35(t - 8) \quad (65)$$

3.3. Analysis of Industrial Hot Rolling Schedules and As-Rolled Samples

3.3.1. Selection and Study of Industrial Hot Rolling Schedules

As this project is sponsored by the Tata Steel Europe Company, it is necessary to understand and analyse its existing heavy plate mill production, that is the whole industrial hot rolling schedules, which whether or not can be fully simulated by utilising the fully instrumented and controlled 50-tonne Hille mill and the unique advanced TMC machine. Two industrial rolling schedules with different chemical compositions, plain carbon C-Mn (8AK43) and C-Mn-Nb (8AK36) were firstly selected out of eight commercial hot rolling schedules provided by the Company and shown in Table 5. These two specific rolling schedules were chosen for the initial study due to they were largely different in hot rolling history in terms of reheating temperature (RT) and finish rolling (FT) temperatures, initial gauge of slab (IG) and finial gauge (FG) of plates.

According to the original data sets of industrial rolling schedules for these two chosen steels, there were two different rolling schedules: the first one was a pre-rolling (targeted) schedule and the other one was actual recorded rolling schedule, which are shown in the Results chapter. The biggest different between these two schedules was the deformation temperature of each pass. A finite difference temperature model is used to calculate the temperate values in the pre-rolling schedule, while in the actual rolling schedule temperature was measured by the several pyrometers which recorded the peak temperature along the length of the plate as it passed underneath at the different steps of rolling process (before or after each rolling pass). It is important to notice that all the as-rolled samples were air-cooled slowly from the last pass of finishing rolling to room temperature, which means that the final as-rolled microstructures were all made of ferrite and pearlite. Furthermore, the following key information were extracted from these industrial hot rolling schedules as these factors were identified as being crucial to analyse the important parameters for modelling commercial hot rolling production.

1) Plate Gauge – slab thickness after each rolling pass (m)
2) Max Rolling Speed – the maximum rate of rotation of rolls (m/s)
3) Gap Time – defined as the time difference between the rolling passes (s)
4) Pass Time – Time over which the slab is being rolled (s)

5) Temperature – The surface and centre temperatures of the midpoint of the slab (K)

Table 5: Comparisons of industrial heavy plate rolling schedules in terms of chemical compositions (wt%) and rolling histories

Steel Grade	C	Si	Mn	Nb	N	RT (°C)	FT (°C)	IG (mm)	FG (mm)	Pass No.
8AK36	**0.15**	**0.348**	**1.42**	**0.03**	**0.005**	**1211**	**797**	**246**	**20**	**25**
8AK37	0.15	0.361	1.41	0.032	0.005	1200	850	253	30	21
8AK38	0.17	0.39	1.4	0.036	0.003	1186	792	223	40	22
8AK39	**0.17**	**0.39**	**1.4**	**0.036**	**0.003**	**1200**	**835**	**223**	**60**	**17**
8AK42	0.16	0.237	1.07	0.002	0.009	1188	824	250	20	23
8AK43	**0.18**	**0.242**	**1.16**	**0.002**	**0.004**	**1165**	**965**	**300**	**50**	**19**
8AK44	0.2	0.243	1.08	0.002	0.005	1167	928	296	100	17
8AK47	0.15	0.207	0.98	0.002	0.004	1175	918	300	80	17

The most frequently used in different empirical equations to predict the austenite grain size evolution are the equivalent strain ε_{evm}, equivalent strain rate $\dot{\varepsilon}$ and the well-known Zener–Hollomon parameter, Z, calculated by Equation 5 (presented at Section 2.3.1.2).

$$\varepsilon_{evm} = \frac{2}{\sqrt{3}} \ln \frac{h_0}{h_f} \quad \text{and} \quad \dot{\varepsilon} = \frac{\varepsilon V_R}{\sqrt{R\left(h_o - h_f\right)}} \tag{66}$$

Where h_0 and h_f are the initial thickness before each deformation and deformed thickness after each pass respectively, V_R is average peripheral roll speed (m/s) of each pass, and R is roll radius (in this investigation all the industrial rolling schedules were produced in a single stand mill with a diameter of 0.980m). At the first stage, a simple model was created in Microsoft Excel spreadsheet to determine these values for each pass, which were used to predict austenite grain size development during industrial hot rolling production.

3.3.2. Final Ferrite Grain Sizes Comparison

After finished comparison of two selected industrial rolling schedules, the corresponding two as-rolled samples provided by the Tata Steel Europe Company: steels 8AK36 and 8AK43 were analysed for the distribution of ferrite grain sizes at near surface (2mm below surface), quarter and middle thickness of plate. The ferrite grain size measurements were used the

standard linear grain boundaries intercept method (based on the ASTM International Standard E112-10 [246]) in parallel (longitudinal) and perpendicular (transverse) to rolling direction and the detailed procedures of ferrite grain size measurement are described in later Section 3.11.3. Furthermore, the quantitative grain size measurements were also compared with the results from the Tata Steel Company to check the reliability and consistency of ferrite grain size measurement.

3.4. Heat Treatment Samples

3.4.1. Austenite Solid Solution Heat Treatment

The as-cast plates of steels A and B were cut from the four as-cast ingots, which have been mentioned previously in Section 3.2.1, were placed in a preheated calibrated muffle furnace at the 1200°C and held constantly for 2 hours and 30 minutes to ensure that respectively the Nb and Ti microalloyed element were fully and partial dissolved into solid solution at 1200°C, and these MAE were equally distributed inside the reheating plate for microstructure homogenisation. Immediately following heat treatment, the as-reheated plates were manually withdrawal from the furnace and quenched in a tank of cold water to freeze the prior austenite microstructures developed from the reheating step. Finally, most of the heat-treated plates were sent to a local engineering company to be machined into several standard PSC samples, and a few of them were used later for the austenite grain coarsening study.

3.4.2. Austenite Grain Coarsening at Different Reheating Temperatures and Time Length

Several $1cm^3$ cubes were cut from the as-reheated plates (steels A and B) and non-reheated plate steel C, and these cubes were reheated to four different reheating temperatures (900°C, 1000°C, 1100°C and 1200°C) to analyse the resultant prior austenite grain size (PAGS) coarsening at different holding temperatures and corresponding four holding time length (2, 5, 8 and 12 minutes) inside a preheated calibrated muffle furnace, and the procedures are shown in Figure 49. Therefore, there were 48 samples in total for all the test conditions.

For each reheating temperature, 12 samples were heat-treated at the same time and these samples were divided and put on four ceramic plates as different holding time, shown in Figure 50, and in order to distinguish these cubes on each ceramic plate for all the steel B one corner of samples were trimmed off while two corners were removed for each steel C cube. During heat treatment process, one cube was wired to a calibrated K-type thermocouple to monitor the temperature changing inside furnace. That is, when the wired sample was

reached the target heat-treated temperature, the time counting started. Immediately after the samples achieved the target holding length, the corresponding ceramic plate was manually taken out from furnace and quickly dropped into a bucket of cold water to quench. Finally these cubes were then prepared for measuring the PAGS, and the results were compared with the predicted values D_0 (μm) determined by the following Equation 67 [247-249]. It is useful to mention that the Equation 67 was original developed for the plain carbon steels (0.05 – 0.2 wt% C and 0.5 – 2.0 Mn) [247] and it has also been applied in Nb-microalloyed steels in later work and reasonable predictions have been claimed by some researchers [146, 248].

$$D_0 = kt^n \exp\left(-\frac{Q}{RT}\right) = 2.93\times10^5 \times \exp\left(-\frac{94000}{RT}\right) \quad (67)$$

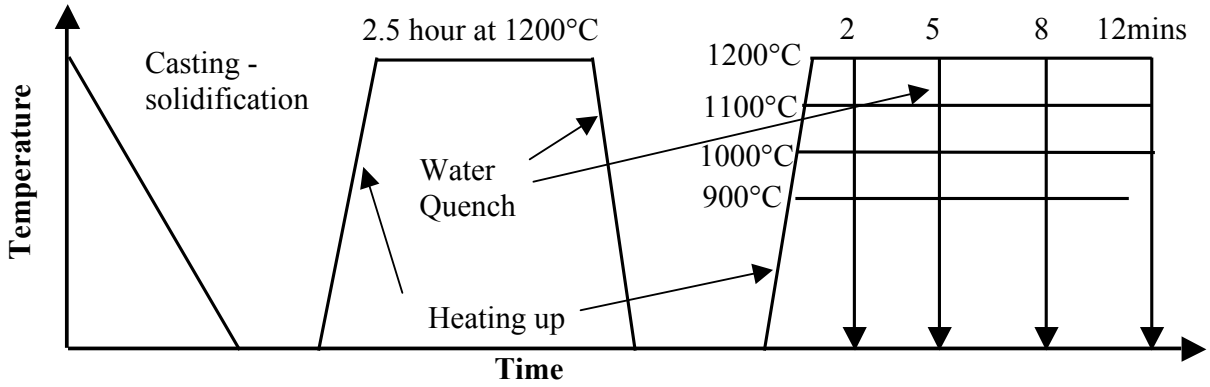

Figure 49: Experimental procedures of heat treatment samples

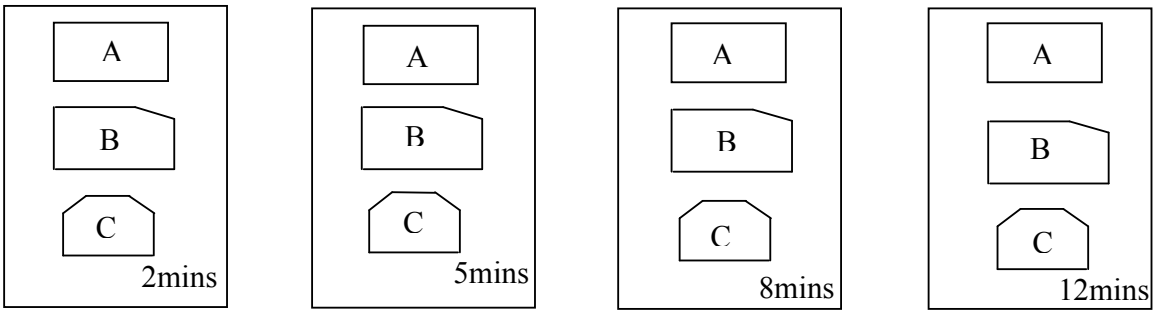

Figure 50: Layout structure of 12 samples on four ceramic plates at each reheating temperature

3.5. Forced Cooling Tests on the TMC

3.5.1. Cooling Tests of Temperature Distribution inside PSC Sample

Forced cooling tests were conducted inside the Fast Thermal Treatment Unit (FTTU) on the TMC machine in order to investigate temperature distribution inside the PSC sample during different cooling rates from 900°C to room temperature. For this study, two PSC specimens

were repeatedly used, and the dimensions of PSC specimen and positions of thermocouple holes (diameter of the hole is 1.1 mm) inside PSC samples are shown in Figure 51 in which the letters and numbers indicate different positions inside the samples: Letters T, H, M, C, B, L and R represent top, half, middle, centre, bottom, left and right, respectively. The numbers are the depths in mm from the top surface of specimen, for example, 0.6 means 0.6mm below the top surface.

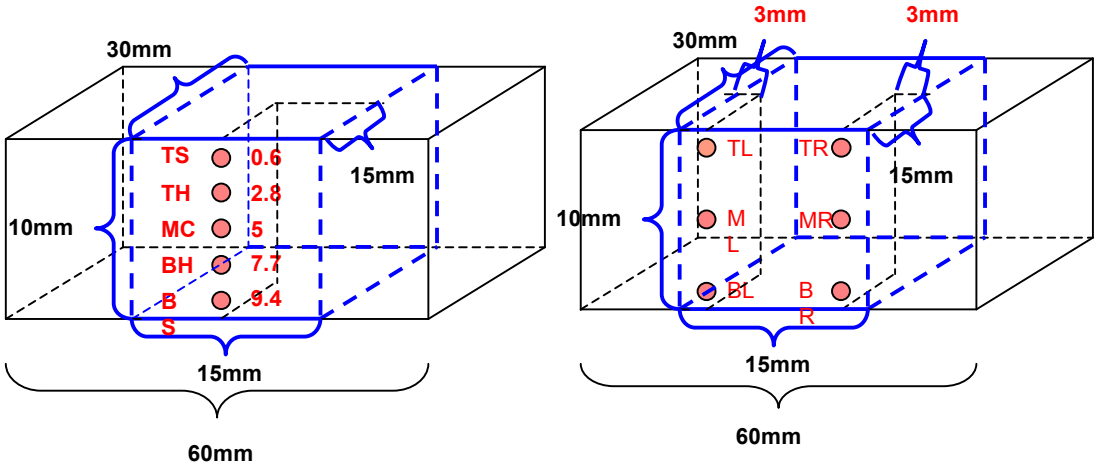

Figure 51: Schematic positions of pre-drilled holes insides the PSC specimens for measuring temperature distribution

Table 6: Four different arrangements of thermocouples inside PSC specimens

Arrangement one	**Middle centre (MC)**, top half (TH) and top surface (TS)
Arrangement two	**Middle centre (MC)**, bottom half (BH) and bottom surface (BS)
Arrangement three	**Middle left (ML)**, middle right (MR) and top right (TR)
Arrangement four	**Bottom right (BR)**, Bottom left (BL) and top left (TL)

However, for one single cooling test the computer of TMC only can monitor maximum three thermocouples at three different positions of the PSC sample. Therefore, four different arrangements of inserting thermocouples inside the specimen, shown in the following Table 6, were used to obtain almost completely temperature distribution profiles inside the PSC samples during cooling. In the Table 6, for each thermocouples arrangement the first one was the control thermocouple, and according to temperature reading of the control thermocouple the computer automatically adjusted the actual cooling rate to fit the pre-set cooling profile.

For the cooling tests, according to the layout in Figure 51 and Table 6, three thermocouples were inserted into the pre-drilled holes of PSC specimen which was reheated rapidly from room temperature to 1100°C in 60 seconds inside the FTTU and held one minute, and then sample was cooled down to 900°C in 2 minutes by forced air and then held further 1 minute.

After that, forced air has been used to reduce temperature of PSC sample to 50°C under three different cooling rates (5°C/s, 10°C/s and 15°C/s), illustrated in Figure 52. After several cooling tests, a full map of temperature distribution inside the PSC sample under each cooling rate was determined.

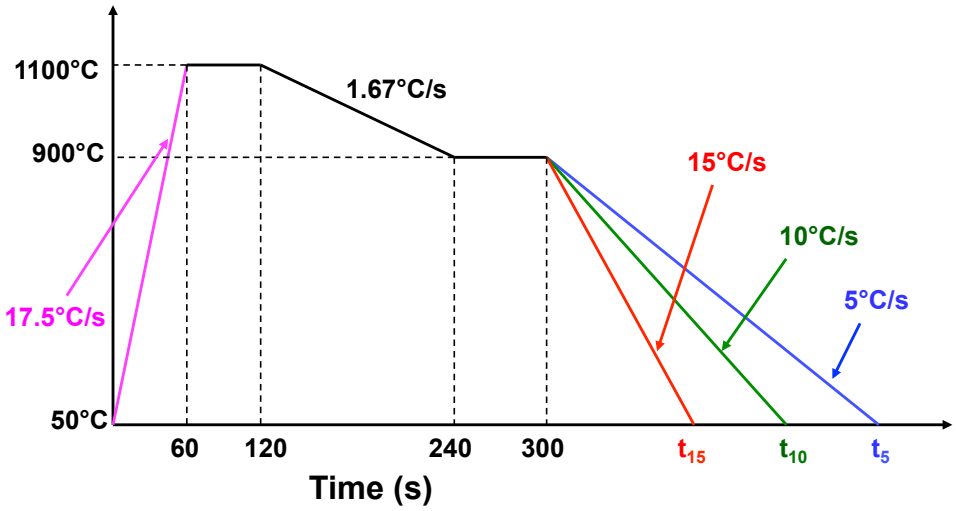

Figure 52: Reheating and cooling profiles at the different cooling rates inside FTTU

3.5.2. Cooling Capability of Different Cooling Media

Before forced cooling was applied during and after multi-pass PSC deformation, the cooling capability (minimum and/or maximum cooling rates) of three different cooling media (Forced air, mist and water cooling) during holding period and post-deformation cooling, and the corresponding accuracy in temperature control of the TMC machine were analysed first. In general, before starting the cooling capability simulation, it is important to check whether the air pressure is at the full capacity, shown in Figure 53 in which the red dot indicated that there is not enough air pressure to run the simulation so the tests had to delay (about 30 minutes) until the red dot turned to green dot, which means the full capacity of air pressure was achieved. Also two or three thermocouples were inserted into each PSC sample at its centre top and/or bottom surface (1mm below surface) and the middle centre in order to record the temperature differences through 10mm thickness under different cooling rates.

In terms of the cooling capability simulation process, firstly the PSC sample was reheated from room temperature to 1000°C in 120 seconds and then held for 1 minute at 1000°C for temperature homogenisation throughout the PSC sample. After holding, different cooling rates of three cooling media were applied from 1000°C to 800°C temperature range, and because there is not a direct cooling rate input inside the control program, the target cooling rate was determined by varying the cooling time between 1000°C to 800°C. Immediately followed by a holding period of 1 - 3 minutes at 800°C, and finally different cooling rates of

different cooling media were also applied to cool the PSC sample from 800°C to 500°C. After each cooling tests, the temperature data file from the simulation was analysed to check the differences between the real temperature and target temperature profiles.

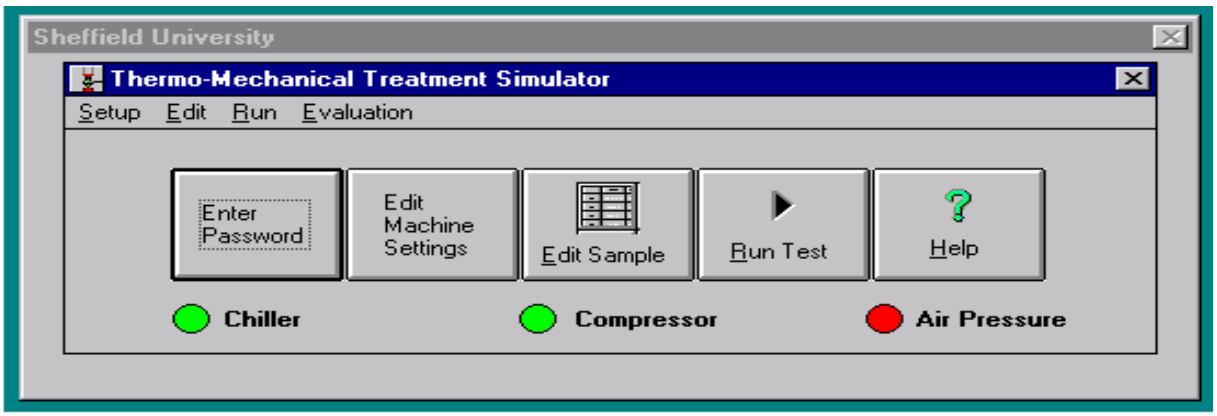

Figure 53: Control panel of TMC Machine showing insufficient air pressure [243]

3.5.3. The Effects of Control Thermocouple Location on Cooling Profiles

In normal cases, the location of the control thermocouple was embedded at the middle centre (the area can be represented as plain strain compression condition) of PSC sample. However, during industrial hot rolling production the main temperature reference usually comes from the pyrometer temperature reading at the as-rolling heavy plate surface. Therefore, by changing the position of control thermocouple to the surface (1mm below) of PSC sample, different heating and cooling profiles were expected to achieve compared to that of the normal thermocouple position. The simulation process was the same as the procedures described in Section 3.5.2, in which different cooling rates of three cooling media were applied to determine the corresponding cooling profiles.

3.6. Finite Difference and Finite Element Models in Heavy Plate Rolling

3.6.1. Temperature Distribution inside Hot Rolling Steel Plate

As the reheated heavy plate was transferred from the furnace into the water-descaling box and then deformed on rolling mill, the temperature difference between the centre and towards surface of thick plate can be very large, which have been explained and predicted by many heat transfer models in Literature review chapter Sections from 2.5.1 to 2.5.4. It is useful to mention here that the work of modelling temperature, strain, strain rate and grain size development were closely collaborated with the industrial personnel Dr. Heathery Carey, Dr. Sally Parker, and Mr. Roger Beaverstock from the Tata Steel Europe, Research, and Development and Technology, Swinden Technology Centre, and the support of Abaqus finite

element simulation from the research associate Dr. Krzysztof Muszka. Furthermore, two different heat transfer models have been studied and applied during the simulation of temperature distribution across thickness of as-rolling heavy plate.

Firstly, as mentioned previously in Section 3.3.1, in the pre-rolling (target set-up) industrial schedules, such as 8AK39, the temperature readings of the heavy plate surface and average temperature across thickness of heavy plate at the each rolling pass were calculated by the industrial in-house finite difference model, presented in next Result chapter Section 4.4.2. Secondly, a specific advanced model, IMPress, developed by the Tata Steel Europe Company for predicting microstructure development during commercial hot rolling steel process and resultant mechanical properties was also used in this work. For the IMPress simulation process, the compositions of steels A and B were first input into the program and then the industrial rolling schedule for steel 8AK39 production was also set into program, and finally an empirically corrected physical-based equation for C-Mn or C-Mn-Nb was chosen to start the prediction and the corresponding results are presented in next Result chapter.

For both models, the simulations were treated as one-dimensional heat transfer across the thickness of the heavy plate. There were four different temperature boundaries at the plate surface involved in the modelling: 1) the initial condition was assumed that uniform temperature (1200°C the same as industrial heat treated temperature) distribution across the thickness of the plate and the bottom half heat transfer was symmetrical to the top half of heavy plate; 2) The convection boundary with water cooling (next Section); 3) The radiation boundary with atmosphere (20°C) in Equation 54; 4) The conduction boundary contacted with the work rolls for which a heat transfer coefficient of 12 kW/m^2K [211] was chosen.

3.6.2. Cooling Profiles Inside Partially Rolled Heavy Plate During Holding Period

One of the main objectives was to predict the temperature distribution across the thickness of the partially rolled plate during holding period (HP). Another in-house model from Tata Steel Europe was used to calculate the temperature distribution inside the heavy plate during HP with and without intermediate forced cooling (IFC). Thus, a one-dimensional transient heat transfer model across heavy plate thickness, which describes a pure heat transfer mechanism between the hot surfaces of heavy steel plate and ambient, has been developed using the Abaqus software with the great support from Dr. Krzysztof Muszka. In this model, the finite element was based on a triangle mesh, i.e. 3-node linear heat transfer triangle. Therefore, the heavy steel plate across thickness were divided into many small meshes, which contain the steel properties and are connected by numbers of nodes, and then the solution of heat transfer

equations across plate thickness is solved by each finite element individually from the surface with defined boundary conditions towards centre of plate with time scale.

In general, according to the manual of Abaqus [250] there are 8 steps to set up the heat transfer simulation, which were: part (defined the dimension of the heavy plate), property, assembly, step, interaction, load, mesh and job. The predicted profiles of different steel properties: density, thermal conductivity, specific heat, and elastic modulus as function of temperature from the JMATPro simulation, which described earlier in Section 3.2.2, were input into the program. Moreover, the initial conditions were assumed that the whole plate across thickness was 1000°C and ambient or water temperature was 20°C. There were two steps in the simulation processes: the first stage was water or air cooling depending on the different input values of heat transfer coefficient (HTC), from 1000°C to 800°C. For the relative weak water spraying, the research in Tata Steel Europe suggested that the value of HTC is in a linear relationship with that of the heavy plate surface temperature, i.e., with value 400W/m^2K at 800°C and 200W/m^2k at 1000°C. On the other hand, for convection cooling in natural air, a static HTC value of 10$Wm^{-2}K^{-1}$ [197] was used in the program. It is important to notice that several simulation trials had to be carried out by varying the cooling time to determine the correct cooling period, at the end of which when the water spraying stopped, the centre temperature of heavy plate cooling reached 800°C. The second step was the recalescence associated with the heavy plate surface. There were also two different prediction conditions. Initially, it was assumed that no interaction between ambient and surface of plate so purely heat conduction within the plate due to the temperature differences within the plate. However, in real cooling situation when the water spraying stop, natural air cooling still takes place so the second condition was that the static HTC value of 10$Wm^{-2}K^{-1}$ still applied on boundary.

3.6.3. Effective Rolling Strain and Strain Rate Distribution inside Heavy Plate

A finite element model was built in Abaqus and used to simulate the effective rolling strain and strain rate distributions across thickness of hot rolling heavy plate, and then the corresponding predicted results of effective strain and strain rate across plate thickness (surface and centre) during the rolling was used as input values of 3-pass PSC testing and simulate specific positions through the plate thickness. It is important to be reminded that initial thickness of standard PSC sample is about 10mm (maximum 12mm) and the final deformed thickness is 2-3mm, while the heavy slab in commercial plate rolling production usually from 300-200mm rolled down to 40-100mm. Therefore, it is obviously that the strain and strain rate distributions inside the PSC samples can not fully represented the whole strain and strain rate profiles of industrial hot rolling heavy plate. In order to solve this scale problem, the FE Abaqus and IMPress models have been used to simulate the temperature

distribution inside as-rolling commercial heavy plate, particularly focusing on the surface and centre of the heavy plate, and then the results from the temperature simulation were input into the PSC settings to simulate different temperature profiles across the thickness (surface and centre) of heavy plate.

3.7. Plane Strain Compression Tests

There are several necessary steps for multipass PSC tests taken place on the TMC machine and each step had to be carefully carried out to achieve correct, reliable and reproducible multipass PSC tests and corresponding well-deformed PSC samples and flow curves. In the following section, three important areas of procedures are described here.

3.7.1. Temperature Setting for Test Furnace

Before heating up the test furnace from room temperature to the target temperature, the deformation tools (top and bottom) must be de-scaled, cleaned, lubricated and accurately aligned with each other at room temperature. This is one of the most critical steps before conducting successful multipass PSC simulation, which is explained more in the Discussion chapter. It is important to note that the temperatures of the upper and bottom tools, shown in the following Figure 54, were only governed by the temperature of the test furnace, However, due to the four heating elements were placed almost at the corners of furnace and the position of deformation tools were in the middle of test furnace, the tool temperatures were always lower than the temperature of test furnace. In general, for the high temperature PSC tests, the discrepancies of temperatures between the tools and test furnace are approximately 30°C - 60°C. Therefore, it is commonly to set the test furnace temperature higher than target deformation temperature so that the tool temperatures are close to the required deformation temperature. For example, if the intended deformation temperature was 840°C then the test furnace temperature were set at 880°C.

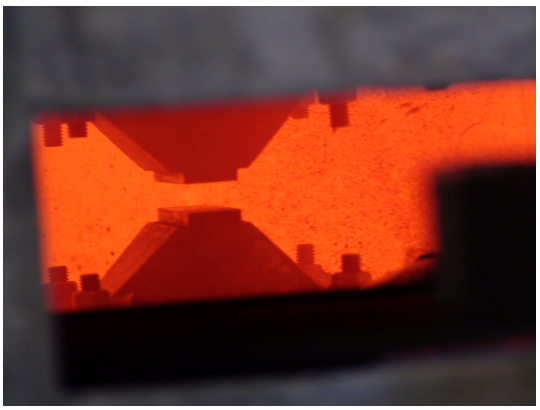

Figure 54: The upper and bottom platens for deforming PSC sample inside the reheated testing furnace

3.7.2. Designs of Deformation Schedules for PSC Testing

Before the target temperatures of the test furnace and deformation platens were achieved, which normally took 40 minutes to one hour to equilibrate, different simulation schedules were created in the TMC control program and for each schedule was a separated PSC testing which comprises of a sequence of different segments, shown in Figure 55. These segments defined the positions (FTTU and test furnace) of the PSC sample from the beginning to the end of testing. For example, if the PSC sample is set inside the FTTU, then only the temperature profiles (reheating, holding, cooling) can be controlled with no option available to deform; on the other hand, if the PSC sample is scheduled inside the test furnace then no option is available to control the temperature of deforming PSC specimen but with great capability of deformation controlled (strain and strain rate).

For the PSC deformation setting in Figure 56, five different types of testing are available, but the one that was used in this investigation is the constant true strain rate, in which the velocity of the ram (piston) is a function of the instantaneous thickness of deforming PSC specimen [242]. Equivalent strain and strain rate of each pass, interval times between pass inside test furnace are another three required variables. There is also an option of estimating initial and final forces and using the wedge as a mechanical stop in Figure 56. This estimation can be useful in multipass simulations since it allows the calculation of more accurate forces to achieve the required deformation for the last few passes. The Figure 56 also demonstrates the input window of defining temperature-cooling profile, which is decreasing temperature of PSC sample from 975°C to 814°C in 30 seconds (about 5.4°C/s) by forced air media. Finally, the TMC program has two loggers, fast and slow, and can be set at different frequencies (5Hz-20kHz). The slow logger runs through the entire simulation and 5Hz is chosen, while the fast logger (4096Hz is chosen) is only available during PSC deformations (shown in Figure 55) and records four important variables: specimen temperature, load, displacement and velocity.

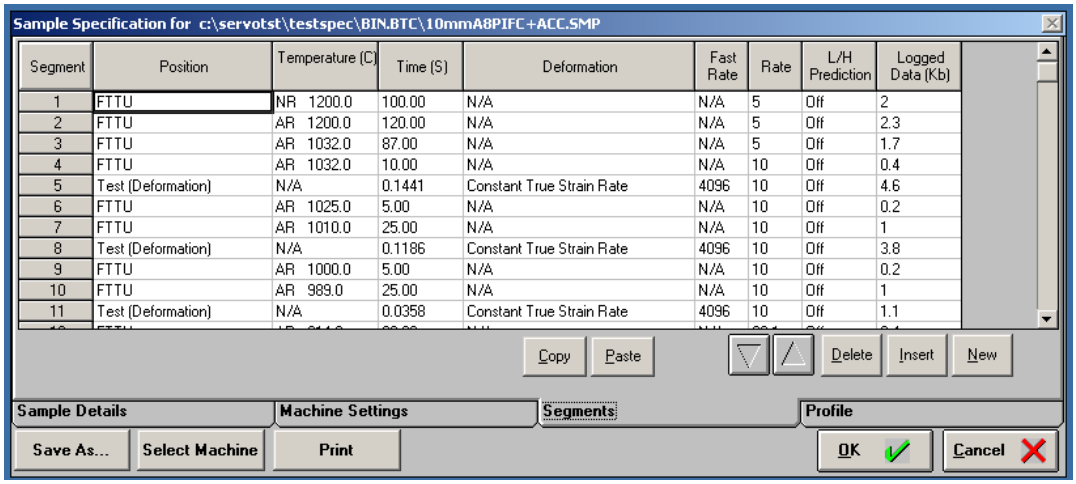

Figure 55: An example of PSC testing schedule showing a sequence of segments

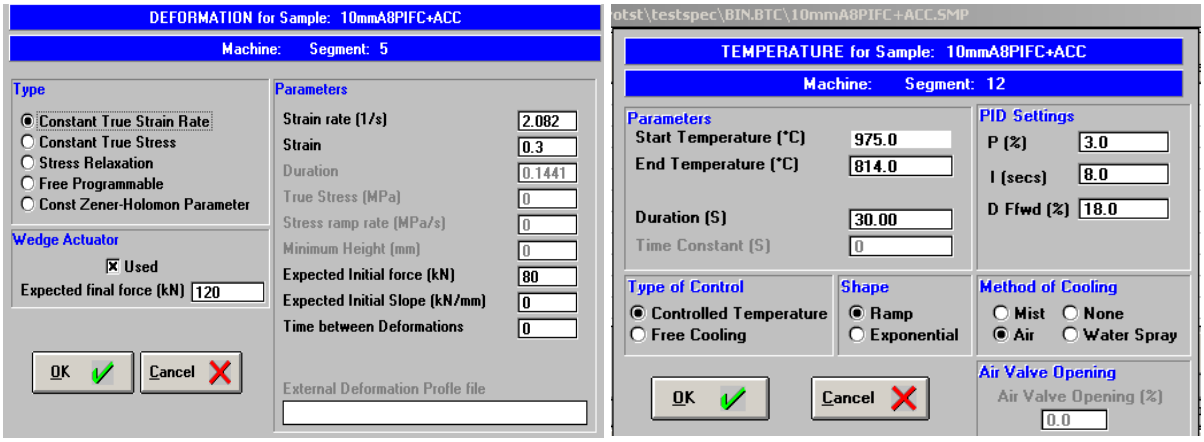

Figure 56: Examples of PSC deformation setting at the fifth segment (left hand side) and defining temperature-cooling profile at the twelfth segment (right hand side)

3.7.3. Physical Checks and Setting Before Conducting Multipass PSC Simulation

After the desired temperature of the tools was achieved and the sequence of simulation is completed, some essential physical checks must be completed before starting the actual PSC testing. First of all, the distance between the top and bottom platens must be carefully adjusted for zero offset due to thermal expansion of tools in high temperatures, and it is vital to remember that the zero offset of tools must be repeated and alignment of tools has to check prior to running each PSC test for obtaining the target strain with uniform distribution in deformed PSC sample.

Secondly, it is important to ensure there were enough clearances between the PSC specimen (10mm or 12mm) and two platens and the pathway from FTTU to test furnace so that the possibility of the sample was twisted or dropped off from the robotic arms as results of hitting the tools or other objects to during testing significantly reduced. There were several steps in this checking process:

1) A thermocouple was inserted into the measured PSC specimen, which was sprayed with very fine boron nitride powders to minimise the effects of friction during multi-pass deformation and held firmly on the robotic arms, in a predrilled hole with 1.1mm diameter and 15mm deep and situated at the exactly centre of deformation zone of PSC sample, illustrated in Figure 57.

2) Clicked *'Open Test Furnace Door'* and *'Open FTTU Door'* on the control window of diagnostics function in the TMC program (see Figure 58) to make sure that the path from FTTU to test furnace was clear, and then turned on the high pressure by clicked the HSM H.P. (Hydraulic Service Module High Pressure) key in Figure 59 and raised the top platen to

15mm or 18mm displacement for 10mm and 12mm PSC samples respectively by increased the displacement of the main actuator.

3) Removed the plastic pin from the robot arms and then manually pushed the robot arms that were holding the PSC specimen fully into the test furnace so that the sample was between the tools and then carefully checked the gap between the bottom tool and underneath surface of specimen to avoid collision (ideally should be at least 2mm above bottom platen but the distance should not be large to cause the deformation zone of PSC specimen bended or even twisted). If the gap is too small or too large, it can be adjusted through altering the weight balance by tightening or loosening the black knob on the back of the robotic arm. After the correct gap is achieved, the robotic arm was pulled back and replaced the pin. It is useful to mention that the vibration of manually pushing robotic arms into test furnace is smaller compared to the vibration occurred during actual simulation in which the automatic-controlled robotic arms moved much faster. Therefore, to further check during actual simulation whether the PSC sample would have collision with the tools or not, a few trials of automatic movement of robotic arm were carried out by clicked the “FTTU”, “Test Furnace” and “Centre (Retract)” functions in Figure 58 to determine the positions of PSC sample, and then the surfaces of sample were examined for any traces or marks of physical contacts.

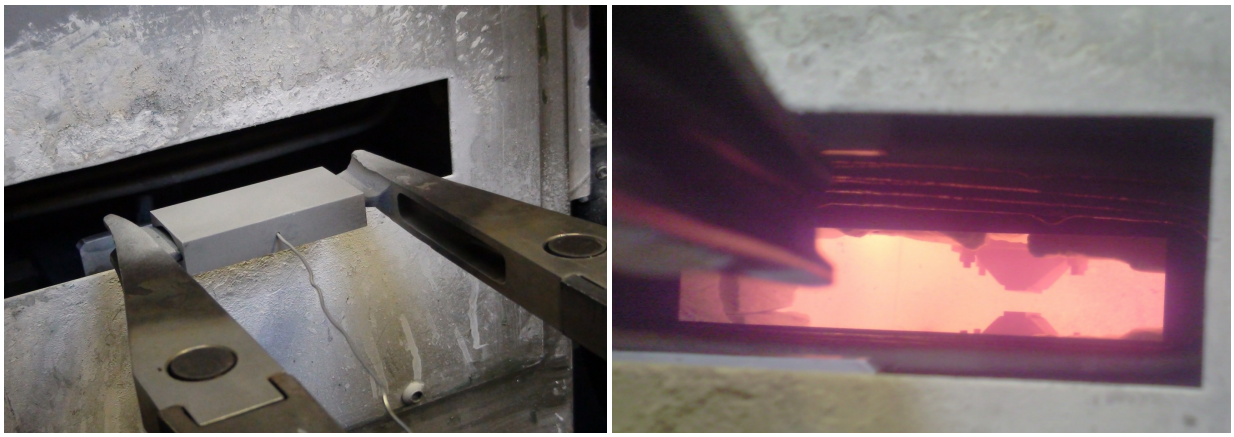

Figure 57: The pre-test PSC specimen with one thermocouple placed in the robotic arms (left hand side), and a clear pathway for transporting PSC sample from FTTU to test furnace

After all the physical checks were finished, next step was ready to conduct the multipass PSC testing, presented in Figure 60 where a specific multipass testing schedule is chosen and some parameters were input into the program, such as material (steel) and corresponding properties, expect initial and final forces (kN) of the first deformation, initial height and breadth (mm) of specimen, and for the PSC testing, tooling width 15mm and spread coefficient 0.74 were chosen.

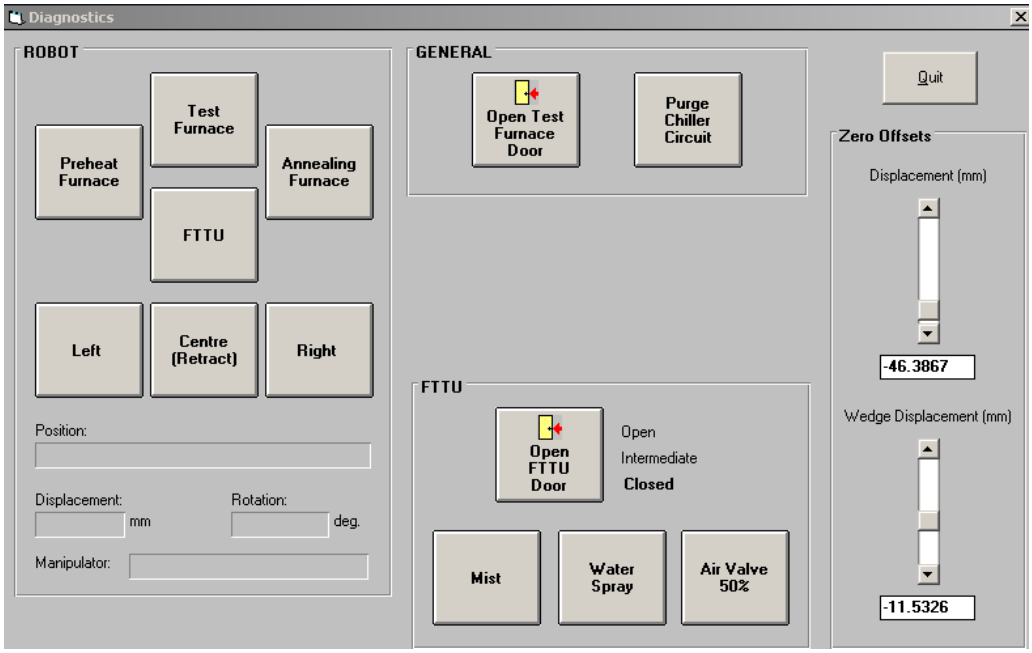

Figure 58: The control window of different diagnostics functions in TMC program

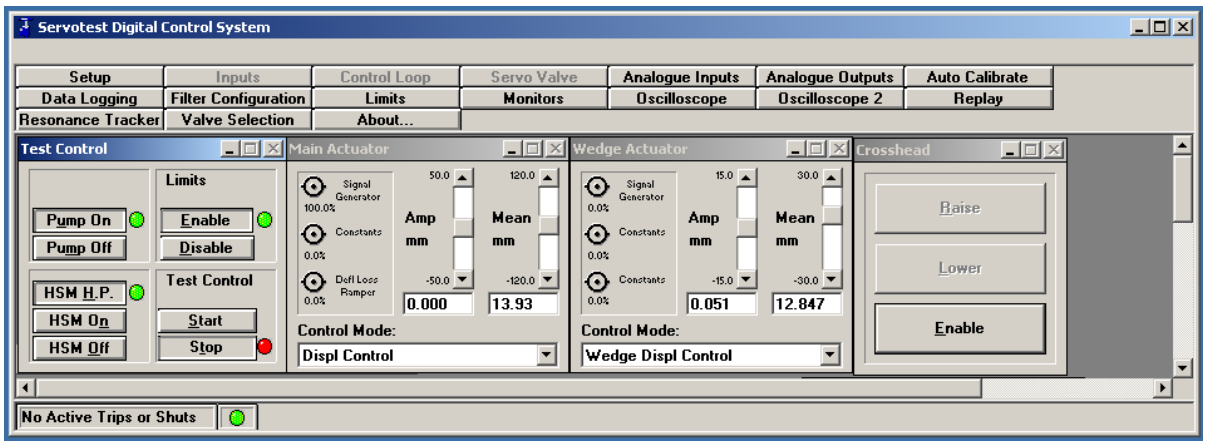

Figure 59: The window of different functions in Servotest digital control system

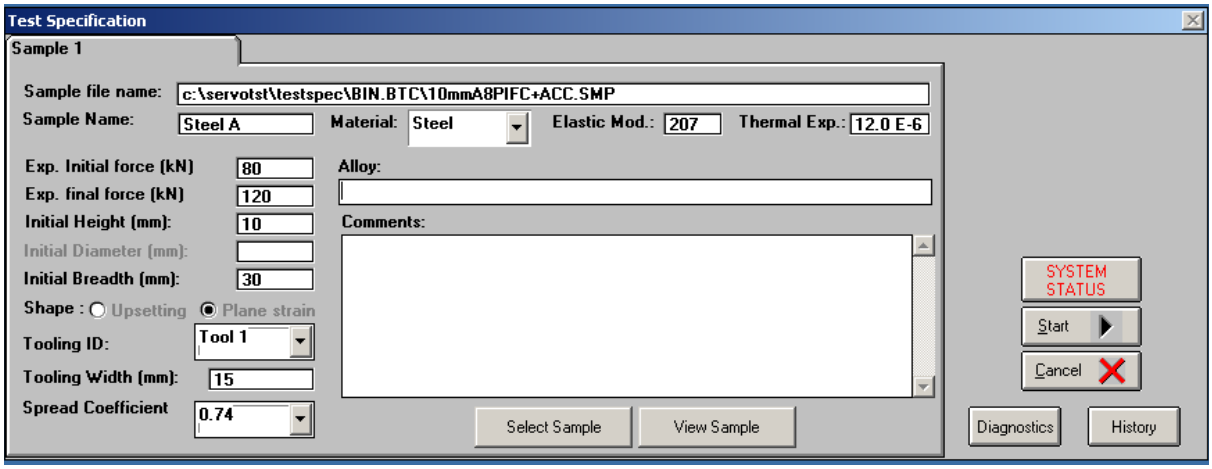

Figure 60: The control panel of setting up a specific schedule of PSC testing

3.8. Laboratory Simulation of Industrial Hot Rolling Plain Carbon Steel Plate Production

3.8.1. Overview of the Simulation Processes

The entire commercial hot rolling schedule has been successfully replicated and transferred into a laboratory scale simulation for 50mm heavy plain carbon steel plate, 8AK43 and its composition shown in Table 5. It has a higher carbon percentage with slightly lower Si and Mn concentrations compared with the lab-cast plain carbon steel C in Table 4. According to the following Figures 61 and 62, there were 18 rolling passes in total with 9-pass deformation in the roughing stage and 9 passes in the finishing stage, and there was not a long holding period in the schedule. Furthermore, in both of these two figures, there are two profiles: one is pre-rolling (intended) and another one is actual recorded rolling profile. In this simulation, the actual rolling temperatures and strains were used. It is useful to be noticed that in order to ensure the final thickness of deformed PSC sample was 2-3 mm enough for microstructure characterisations and analysis, the maximum equivalent strain can be applied in the PSC testing is about 1.6 for 10mm or 1.8 for 12mm initial thickness of PSC sample. However, the target total industrial hot rolling strain for the schedule was 2.07 above the maximum strain 1.6, seen in Figure 61, thus a method that combining the laboratory (50 tonne) Hille rolling mill and the multipass PSC deformation on the TMC machines to simulate whole industrial hot rolling plate processes has been proposed and successfully carried out. In general, there were 3 main stages in this laboratory simulation, which are described in the following sections.

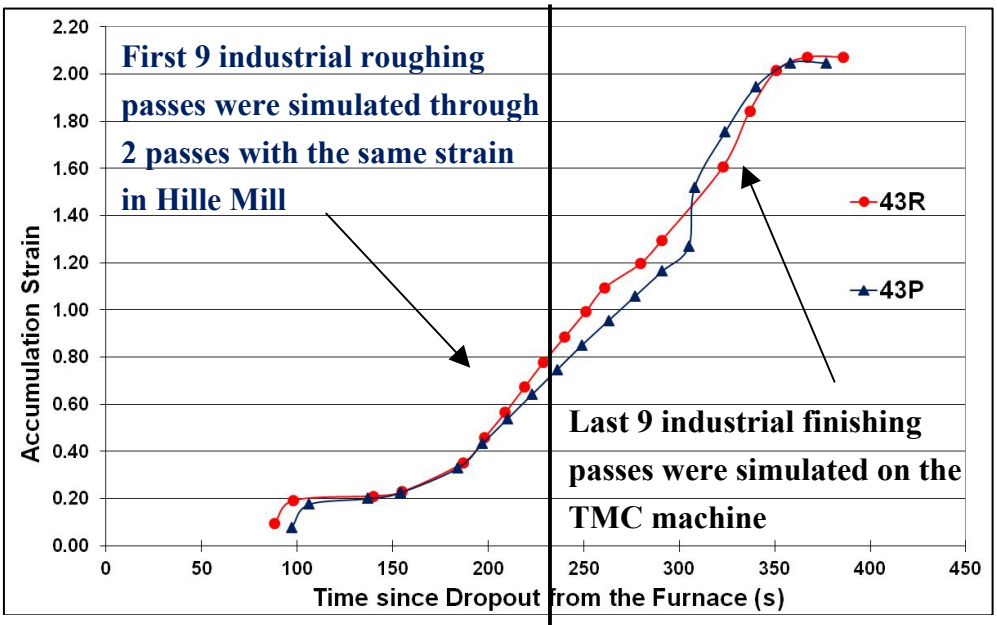

Figure 61: Comparisons pre-rolling (P) and actual rolling (R) schedules of plain carbon steel 8AK43 for accumulation strain versus time and simulation outline

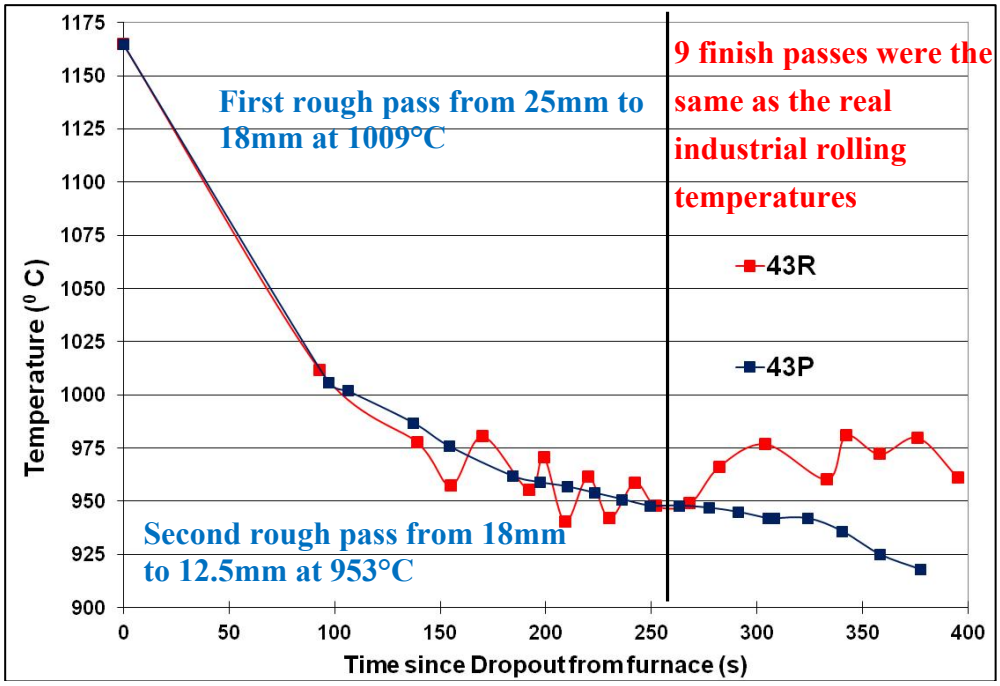

Figure 62: Comparisons pre-rolling (P) and actual rolling (R) schedules in term of temperature profiles of steel 8AK43 and simulation outline

3.8.2. Reheating and Rough Rolling on the Laboratory (50 tonne) Hille Mill

According to the rolling schedule for plain carbon steel 8AK43, shown in Figures 61 and 62, the 9 industrial roughing passes were simulated through 2 passes with the same total strain 0.8 on the laboratory Hille mill (rotation speed is up to 60 rpm, maximum roll gap is 45mm and radius of roll is 70mm). For the test one, only one thermocouple was inserted at the centre of plain carbon steel slab (roughly 25mm in thick, 32mm in width and 140mm length) to monitor and record temperature during the reheating inside the furnace and rough rolling on the Hille mill later. For the test two, two thermocouples were embedded into a slightly thicker slab (28mm) to investigate its temperature distribution during simulation: one was the middle position which is 2mm below the surface and the other one was at the middle centre of sample (14mm below surface). The rolling conditions (rotation speed, mill gap settings) of these two tests were exactly the same as described in the following.

Based on the commercial hot rolling schedule in Figure 62, the steel slabs in both tests were initially reheated at a temperature range of 1150-1175ºC (due to the intended industrial reheating temperature 1165ºC could not stay constantly) for one hour inside a muffle furnace with Argon protective atmosphere, located just beside the Hille mill. After the one hour heat treatment inside the furnace, the reheated plate was manually taken out and then waited for temperature dropped down to 1009°C (see the temperature recording on the PC screen) through air cooling for the first roughing deformation from 25 to thickness 18mm (mill gap

setting). The second roughing deformation took place when slab temperate reduced to 953°C and reduction was from 18mm to 12.5mm. After the second rough deformation, the plate was immediately put into a large water tank for quenching, and the standard 10mm PSC test samples were then machined out from the as-rolled and quenched plate. Therefore, for test one after 2-pass rough rolling from thickness about 25 rolled down to 12.5mm, the equivalent strain 0.8 was obtained within steel plate according to Equation 68. Due to the thickness of slab in the test two was higher, the equivalent strain 0.93 (reduction from 28mm to 12.5mm) was achieved.

$$\varepsilon_{evm} = \frac{2}{\sqrt{3}} \ln\left(\frac{h_i}{h_f}\right) = \frac{2}{\sqrt{3}} \ln\left(\frac{25}{12.5}\right) = 0.8 \tag{68}$$

3.8.3. TMC simulated 9-Passes Industrial Finishing Deformation

For the second stage finish rolling simulation, the temperature of the deformation furnace was set at 980°C so that about 950°C of the tools temperature can be achieved, and then two thermocouples were inserted into pre-drilled holes at the near surface (1mm below) and the middle centre of the as-roughed and quenched PSC sample that were machined out of the 2-pass roughing plate from the previous Step 3.8.2, and the control thermocouple was at the middle centre of PSC sample. For the simulation steps, the PSC sample was reheated from room temperature to 953°C in 90 seconds inside the FTTU, and then held 30 seconds for homogenisation inside the FTTU before the robotic arm carried the specimen forward and into the test furnace. The next step was performing a 9-pass PSC deformation inside test furnace according to the industrial rolling schedule presented in the Table 7, in which the PSC deformation temperatures were based on the industrially measured temperatures obtained via readings from pyrometers, which were located either before, during or after each rolling pass. In this research, it was assumed that if the industrial temperature readings were measured before and during the rolling passes then the PSC deformed temperatures were kept the same values but if the measured temperatures were obtained after rolling passes then the values of PSC deformed temperatures were 5°C lower due to deformation heat.

It is useful to emphasise that due to the 9-pass PSC tests not having been previously performed on the TMC machine before and, only few as-roughed and quenched PSC samples were available, in the earlier attempts some dummy PSC samples (not the as-roughed and quenched but still the standard PSC specimens) were used and tried to achieve the deformation temperatures were close to the real industrial rolling temperatures (up and down) as much as possible. However, because performing 9-passes that the PSC sample was in and out between the test furnace and FTTU (18 times transportation) by robotic arms had a very low successful rate due to many valuable deformed PSC samples were dropped into the test

furnace or the gap between the doors of FTTU and furnace during fast transportations between the FTTU and test furnace. Therefore, several different methods were used to improve the success rate, and the best solution was that the 9 finish passes were kept inside the test furnace with only two transportations. The other one was that the 9 passes were changed to 2 passes with the same total applied strain 1.27 and simulation time (there was a 148s holding by adding all the gap time together between the 2 passes inside the test furnace).

Table 7: Deformation schedule of 9-pass finish rolling simulation

Pass	Measured Temp. (°C)	Pyrometer location	PSC deformed Temp. (°C)	Gap time next pass (s)	Equivalent strain	Strain rate
1	959	After	954	10	0.106	2.34
2	948	Before	948	16	0.107	2.50
3	949	Before	949	14	0.102	2.61
4	966	Before	966	22	0.104	2.75
5	977	During	977	29	0.099	2.83
6	960	After	955	9	0.311	4.96
7	981	After	976	16	0.236	5.28
8	972	Before	972	18	0.172	4.12
9	980	After	975		0.056	2.97

3.8.4. Simulation of Air-Cooling 50mm as-Rolled Steel Plate

As there is no temperature measurement after the finish rolling, the Company has provided some calculated sub-surface and centre cooling profiles of 60 and 40mm steel plates through phase transformation without recalescence (PSC sample is too small to be recalescence) based on the FE model under air cooling conditions. However, the final plate thickness for 8AK43 was 50mm, thus a centre cooling profile of 50mm plate has been produced by interpolated (calculated the mean values) between the centre cooling profiles of 40 and 60mm steel plates, which is shown in the Results chapter. According to the predicted 50mm centre cooling profile, the average cooling rate above 760°C was about 0.56°C/s, and from 760°C to 400°C the mean cooling rate was 0.38°C/s, and then cooling periods in defined temperature ranges were determined and used as input parameters of post-deformation cooling simulation inside FTTU in Figure 56, followed by water quenched to room temperature to complete the laboratory simulation of whole industrial hot rolling plain carbon steel plate production.

3.9. Multi-Pass Simulation of Hot Rolling Heavy Plate Production Including Forced Cooling and Accelerated Cooling

3.9.1. Overview PSC Test Schedules of Microalloyed Steels

The 8AK39 grade is an industrial as-rolled heavy plate with 60mm final thickness, and it has a higher carbon concentration (shown in Table 5) than the steels A, B and C that are laboratory as-cast samples (shown in Table 4). The main differences between the industrial plain carbon steel (8AK43) production and microalloyed steel (8AK39) process were the total applied effective strain, which were 2.07 and 1.6 respectively, and there was a critical holding period (266 seconds), and much lower finish rolling temperatures in microalloyed steel hot rolling schedule. Therefore, the whole commercial hot rolling schedule of microalloyed steel 8AK39 with its lower total applied strain of 1.6 can be simulated through multipass PSC tests on the TMC machine without pre-roughing on the laboratory Hille mill.

Steel slabs (roughly about 30mm in thickness, 32mm in width and 140mm in length) of microalloyed steels A and B were heat treated for 2 hours and 30 minutes in muffle furnace at 1200°C in order to ensure Nb and Ti microalloyed elements were mostly dissolved in austenite, followed by an immediate water quenched to room temperature as described previously in Section 3.4.1. Two different initial thicknesses (10mm and 12mm) of PSC samples were machined out of the heat-treated samples and a thermocouple hole of 1.1mm diameter was drilled at the mid-thickness of PSC specimen.

The intended industrial rolling schedule for the production of 8AK39 steel plate, presented in Figure 63, has been chosen, modified and simulated as close as possible through multipass PSC tests on the TMC machine, illustrated in Figure 64 in which there are several test segments, such as reheating, 3-pass PSC testing simulating the 10-pass industrial rough rolling, cooling during holding period, 5-pass PSC testing replicating the 5-pass industrial finish rolling (combined the last two passes with small reductions into the 8th PSC deformation) and post-deformation air cooling or accelerated cooling. Furthermore, the main input parameters (deformation temperature, strain, strain rate and gap time) and test schedules of multipass PSC test schedules on the TMC machine are presented in Table 8. For all the multipass PSC tests, the PSC samples were quickly reheated inside the FTTU, according to the pre-deformation heat treatment step, from room temperature to 1200°C in 100 seconds and then held constantly at the 1200°C for 120 seconds inside the FTTU for the thermal equilibration inside PSC sample. Next step the PSC samples were cooled down to 1035°C from 1200°C in 87 seconds and hold for 10 seconds (the same time length 97 seconds as the reheated heavy plate drop out from the furnace to the first roughing pass in the industrial rolling schedule) and then different multi-pass PSC deformations (3-pass or 8-pass) were

performed for the investigation of the effects of different rolling parameters, which are described in the following sections.

Due to the many different multipass PSC tests which were carried out, thus for the traceability purposes, every deformed PSC sample was labelled with the alphabet letter indicating the steel grade followed by the individual sample number. For instance, B36 means the 36th PSC testing of Nb+Ti steel B.

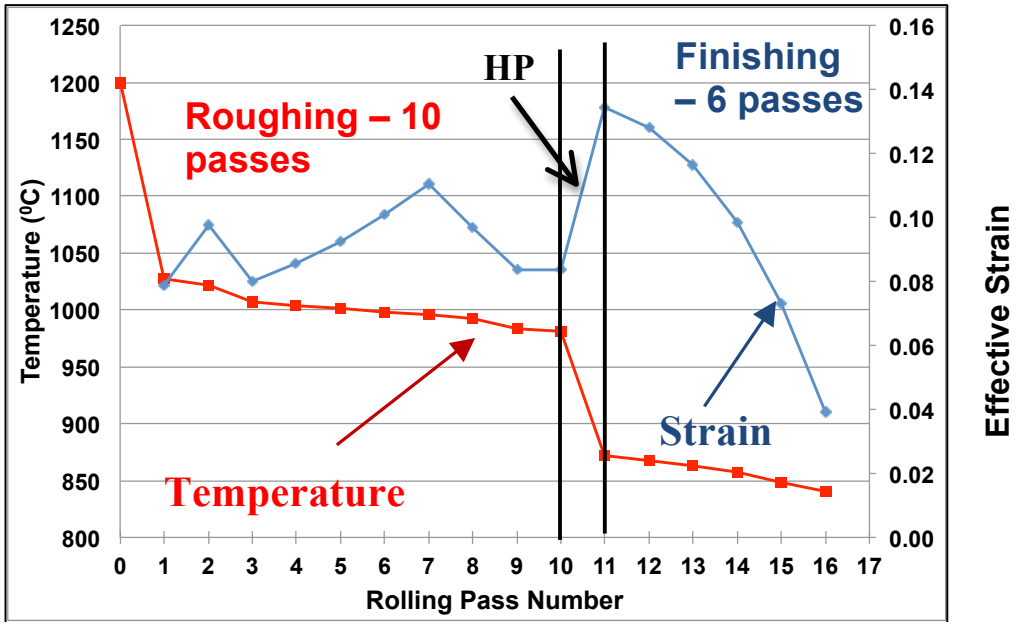

Figure 63: Industrial rolling schedule of microalloyed steel 8AK39 in terms of temperature and effective strain each pass

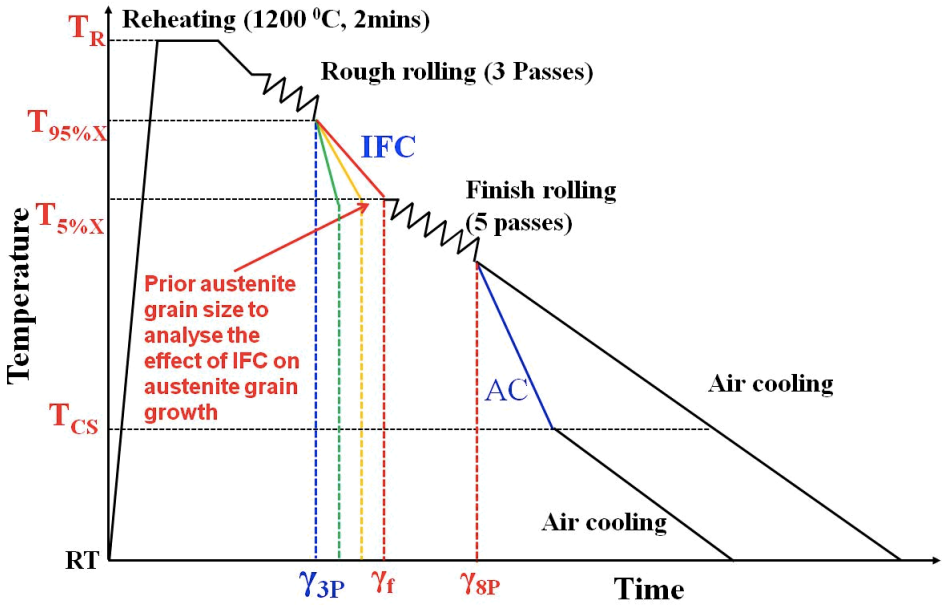

Figure 64: Schematic of multipass PSC test simulation schedules of plain carbon and microalloyed steels on the TMC machine

Table 8: A summary of simulation parameters and schedules in the most laboratory multipass PSC testing schedules including IFC and ACC

Reheating and Cooling inside FTTU					
Reheating rate		Reheating temperature (°C)	Reheating time (s)		Air Cooling time to first roughing pass (s)
10~12 °C/s		1200	120		97
TMCP inside Test Furnace					
	Pass	Average deformation temperature (°C)	Applying target strain (10/12mm)	Input Strain rate (s^{-1})	Interpass time (s)
Roughing	1	1032	0.3/0.4	2.08	5 or 46
	2	1000	0.3/0.4	2.53	5 or 46
	3	978	0.1/0.1	2.79	
Holding	Air cooling or intermediated forced cooling (IFC) Different cooling rates were applied from 978°C to 872°C				
Finishing	4	872	0.14/0.2	3.8	12
	5	868	0.13/0.17	3.91	12
	6	863	0.12/0.16	3.93	12
	7	857	0.12/0.16	3.79	14
	8	848	0.12/0.14	2.22	
Air Cooling or Accelerated cooling inside FTTU					
Cooling Stop Temperature was 400°C Cooling Rate was from 0.3°C/s –44°C/s					

3.9.2. 3-Pass Roughing and Holding Simulation

3.9.2.1. The Effects of 3-Pass Roughing on the Prior Austenite Grain Size

Before performing the 8-pass PSC tests, many 3-pass PSC simulations of industrial 10-pass rough rolling, with the same total applied strain 0.9 (0.4+0.4+0.1) and similar deformation temperature region (1032°C-978°C), were taken place first for investigating the prior austenite grain size evolution. In order to have consistent test conditions for the later 8-pass simulation where the deformation temperature of the 8th pass was 848°C (see Table 8), the temperature of test furnace was always set at 880°C so that the tool temperatures are around 845°C. Moreover, initially the PSC sample was fed into the test furnace to compress and also left in there for all three rough rolling passes to reduce the possibility of PSC sample hitting

the platens and dropping off from the robotic arms, which is similar to procedures of 9-pass finish rolling as described previously in Section 3.8.3. Another reason for keeping the 3 passes inside the test furnace all the while was to avoid the temperature of deformed PSC specimen dropping too quickly between passes. That was because the temperature differences between these 3 passes were only about 25°C-30°C and there was about 160°C difference between the target deformation temperatures and the platen temperature. After several attempts, a relatively short interval time, 5 seconds, between passes was found to best fit the testing schedule in Table 8. In terms of the simulation processes, after 10 seconds holding the PSC sample at 1040°C or 1035°C for 10 or 12mm PSC specimen respectively, 3-pass roughing (3R) deformation were carried out inside the test furnace and immediately followed by water quenched (WQ) the deformed PSC sample to room temperature, i.e. 3R+WQ.

At the end of the research timeframe, the multipass (more than 4 passes) PSC deformation has pushed over the limit of TMC machine, which are described more in later 8-pass simulation and Discussion chapter, the updated version of TMC software and hardware were installed by the Servotest Ltd. and try to solve the multipass PSC issues and resulted in a relatively better successful rate. Therefore, an updated 3-pass roughing schedule with 46 seconds gap time and after each pass was carried out and the deformed PSC sample was moved back to FTTU for temperature control of next pass, and which was then followed by fast water quenching to room temperature.

3.9.2.2. Different Strain Arrangement during 3-Pass Roughing

Some researchers [21, 22, 121] have reported that with the same total applied strain but with the highest strain applied at the last pass of rough rolling can cause more homogeneous microstructures through the thickness direction of heavy plate. Therefore, two different strain arrangements with the same total strain of 0.9: 0.4+0.4+0.1 (B4) and 0.1+0.4+0.4 (B8) were chosen with 5 seconds gap time to analyse this effect. After the 3-pass roughing deformation, the deformed PSC sample was slowly cooled down till 870°C in 300 seconds and then immediately WQ to room temperature.

3.9.2.3. Analyse the Effect of Cooling Rate on the Prior Austenite Grain Size during Holding Period

The effects of the intermediate forced cooling (IFC) on the prior austenite grain size (PAGS) at the end of holding period are described in here. The PAGS was expected to be larger with increasing holding period or decreasing cooling rate. Firstly, the deformed PSC samples after 3 roughing passes (3R) were carried back into FTTU and then reduced the temperature to

870°C by different cooling rates (varied the cooling period inside FTTU) and then water quenched (WQ) the sample to get the PAGS as function of cooling rates. For example, after 3-pass roughing, steel B samples B2, B3 and B4 were allowed to cool until reached 870°C for varying duration of time: 40, 90 and 300 seconds respectively before WQ to room temperature. The below Figure 65 shows an example of a uniformly deformed PSC sample after 3 roughing passes being subjected to the forced cooling during the HP prior to WQ. As mentioned in Literature review chapter Section 2.4.2.3, when applying the IFC during the HP there are two stages of the temperature profile of heavy plate surface: cooling and recalescence steps, illustrated in the following Figure 66 in which the actual temperature profile in red was really close to the target profile in black.

Figure 65: An example of deformed PSC sample at the holding period after 3 roughing passes

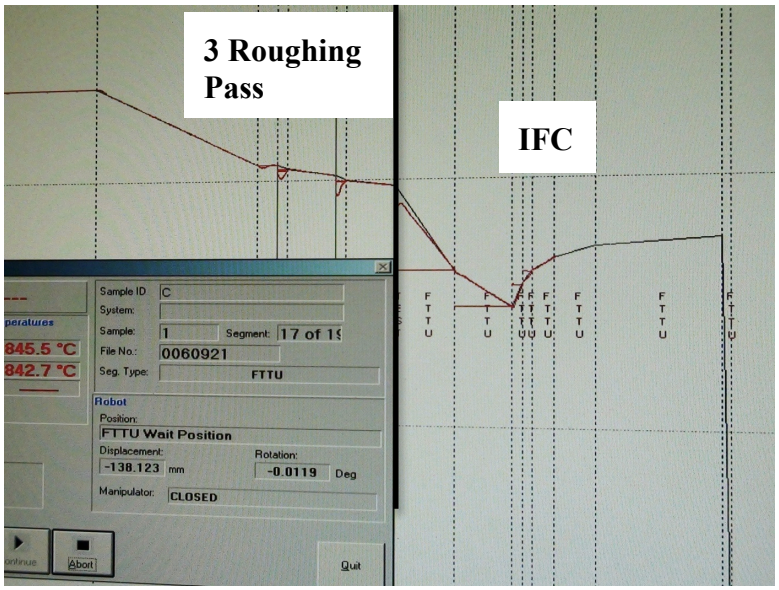

Figure 66: An example of temperature profile of multipass PSC simulation included IFC

3.9.2.4. Simulations of Heavy Plate Surface and Centre during Rough Rolling and Holding Period

According to the predicted results from the IMPress model, the input values of deformation temperatures, strain and strain rate for each pass at sub-surface (1mm below), quarter thickness and centre of heavy plate were different in the multipass PSC test settings. For instance, for the first roughing pass, the calculated deformation temperatures were 1030°C, 1120°C and 1200°C, at subsurface, quarter and centre respectively. Furthermore, from centre of heavy plate towards surface, the effective strain and strain rate increase and based the simulation results from IMPress model, it is impossible to simulate entire effective strain profile through whole rolling schedule at heavy plate surface and quarter positions by using only 12mm PSC sample due to the corresponding total required strain were 2.1 and 1.9 respectively, which are above the strain limit of PSC tests on the TMC machine. Therefore, the simulation of industrial heavy plate surface and centre deformation profiles only covered the rough rolling and holding period. In terms of simulation process, it was similar to the previous procedures in Section 3.9.2.3, with only different values in temperature, strain, and strain rate in 3 roughing passes and different cooling profiles during holding period.

3.9.3. 8-Pass PSC and Cooling After Deformation

3.9.3.1. The Effects of Finish Rolling on the Prior Austenite Grain Size

After the 3-pass roughing (3R) and cooling during holding period (HP) were successfully simulated, the multipass PSC simulation was extended to the 5-pass finish (5F) rolling stage, i.e. performing the 8-pass PSC tests (3R+HP+5F). In here, the partially deformed PSC sample was fed into the test furnace for the entire duration of the finish rolling stage with different intervals (presented in Table 8) between the 5 finishing passes, and an example of uniform deformed PSC sample after 8 passes prior to the accelerated cooling is shown in the following Figure 67.

Figure 67: Deformed PSC sample inside FTTU after 8-pass simulation before cooling

The influence of the 5-pass finishing deformation on the steel microstructure evolution and the corresponding flow curves can be seen from the examples of tests A21 and A23, which were 3-pass (3R+WQ) and 8-pass (3R+IFC+5F+WQ) respectively. Since test A21 was deformed above the recrystallization temperature, the PAGS is expected to be equiaxed while test A23 was compressed further below the recrystallisation stop temperature. Thus, the microstructure of test A23 should be elongated or pancake in the rolling direction. However, similar to the previous 9-pass finish rolling simulation of plain carbon steel production described in Section 3.8.3, at the earlier stage of project the deformed PSC samples frequently fall off from the robotic arms during the 6 to 8 passes deformation. A small modification of using thin wires to hold PSC samples more securely on the robotic arms through the pre-drilled holes on edges of samples and robot arms was done and the success rate increased relatively 40%. However, even with this modification sometimes after 8-pass deformation and the deformed PSC specimen became very thin about 3mm, and robotic arms could not retrieve automatically from test furnace back to FTTU for the last stage accelerated cooling simulation due to the deformed PSC sample stuck between the platens, which will be explained more in the Discussion chapter.

3.9.3.2. The Effects of Chemical Composition on Flow Curve and Ferrite Grain Size

It is well known that the addition of microalloyed Nb and Ti elements in the HSLA steels greatly increase the austenite recrystallisation temperature and the pinning forces for restricting austenite recrystallisation and subsequent austenite grain growth, which in turn reduces the prior austenite grain size, and produces a pancaked microstructure leading to the refinement of the final ferrite grain size. Therefore, some multipass PSC tests had exactly the same multipass PSC test conditions but with different compositions of PSC samples, such as tests A26, B32 and C8 in Appendix A. As mentioned before, many dummy PSC samples were used in multipass PSC tests, one of them was steel E, which is a Fe-30wt% Ni based steel with 0.05wt% carbon and 0.38wt% niobium, and different flow curves and optical microstructures were formed (presented in Results chapter Section 4.6.3.4) compared to the interested steels.

3.9.3.3. Variation of Applied Strain on the Ferrite Grain Size

The effects of having a variation in the applied strains on the ferrite grain size were determined from the two different initial thicknesses of PSC samples, 10mm and 12mm, with different strain values of each pass presented in Table 8. For example, both tests B31 and B32 were 8-pass (3R+HP+5R) PSC simulation with similar processing parameters (deformation temperature, strain rate, gap times and the same post-deformation accelerated cooling rate) apart from applied strain given at each pass.

3.9.3.4. Different Cooling Rates after 8-Pass Simulation

One of the major objectives was to analyse the effect of water-cooling or forced cooling after hot rolling to improve steel production. Although the influences of accelerated cooling on the transformation microstructure were investigated significantly last 30 years, no previous work has been carried out on analysing accelerated cooling after more than 8-pass PSC testing on the laboratory scale with precise controls of industrial hot rolling parameters. Therefore, after the 8-pass PSC deformation inside the test furnace, the deformed PSC specimen returned to the FTTU for the last stage of simulation: cooling down to the target temperature (usually at 400°C) in the defined periods (specific cooling rates), through applying slow natural air cooling, or ACC, and then water quenching the deformed sample to room temperature, which is shown in Figure 68. Because there is not cooling facility inside the test furnace, a slight delay of approximate 0.5 second from the finish of the deformation to the start of cooling inside FTTU, but the exact time and temperature dropping can be determined from the test data file. For instance, test samples A20, A22 and A27 had similar processing parameters only different in the post-deformation cooling rate, which were 10°C/s, 5°C/s and 0.3°C/s respectively.

Figure 68: An example of deformed PSC sample after 8-pass simulation and followed by accelerated cooling and water quenched (WQ) to room temperature

3.9.3.5. The Effects of Air Cooling and IFC During HP on the Ferrite Grain Size

It is relatively easier for replicating the temperature distributions under natural air-cooling on the TMC machine due to the cooling rates are more or less constant at near surface, quarter thickness and centre of heavy plate. However, for the IFC condition, the temperature profile at the plate surface is complex through the HP and the corresponding temperature profile was similar to the Figure 69. The surface temperature dropped significantly at beginning of forced cooling, and then quickly recovered (recalescence) when water spraying stopped because of

the heat flow from the much hotter core of heavy plate. As it shows in Figure 69, the commencement of finish rolling under IFC condition was 100 seconds earlier than that of air-cooling situation, and the TMC machine is able to simulate the complex IFC temperature profile, which was the result of finite element simulation of temperature distribution inside partially rolled heavy plate during the HP.

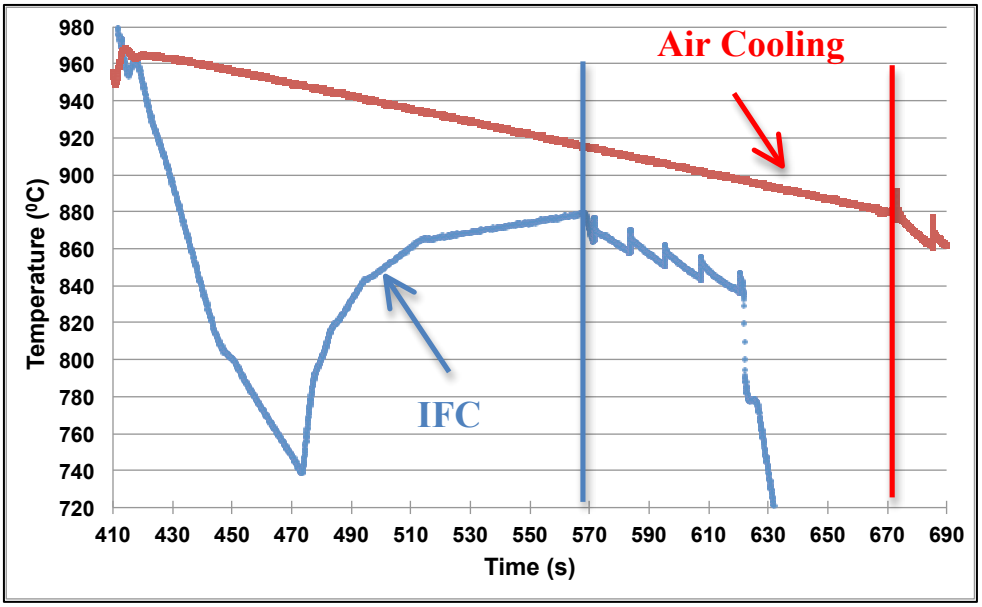

Figure 69: Different heavy plate surface cooling profiles under air cooling and IFC during holding period

Test samples A24 and A25, B32 and B35, C8 and C9 were all 8-pass simulation included 3-pass roughing, air cooling or IFC during HP, 5-pass finishing and 10°C/s accelerated cooling rate (i.e., 3R+Air/IFC+5F+10°C/s). The only variation was the cooling during HP, presented in above Figure 69, thus the effects of air-cooling and IFC during HP on ferrite grain size in different steels can be determined. Furthermore, the effect of different cooling time during HP on final microstructure can be also seen from the test samples B27 and B28, which were 3R+HP+5F+natural air cooling with only difference in the length of HP: 20 and 266 seconds respectively.

3.9.4. 10 to 13 –Pass PSC Deformation on the TMC Machine

At the last stage of the project, after the new updated version of TMC program had been installed, the successful rate of multipass PSC tests more than 4 passes was greatly increased and the maximum passes (above 8 passes) that can be achieved in the standard 10mm PSC sample was gradually determined. The additional passes were added at the roughing stage due to initially the 10-pass industrial rough rolling was simulated by 3-pass PSC test. For

example, Figure 70 shows the actual and target temperature profiles (almost the same) of continuous cooling 11-pass PSC simulation of industrial heavy plate hot rolling consists of 6-passes roughing (each pass with 0.12 strain and 2.5s^{-1} strain rate), IFC during HP, 5-passes finishing and 10°C/s accelerated cooling rate.

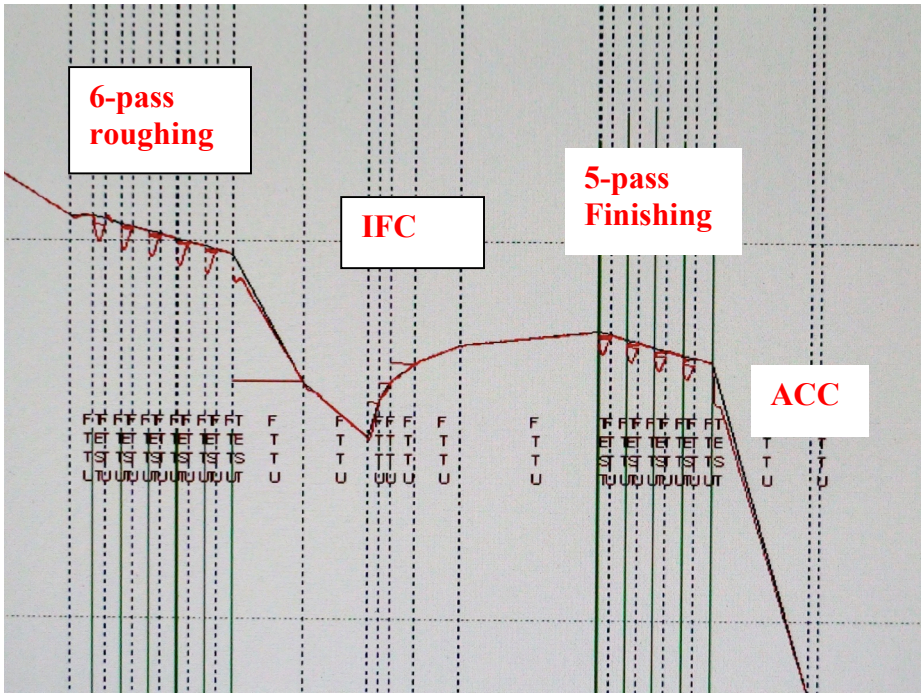

Figure 70: Actual and target temperature profiles of 11-pass simulation including IFC during HP and ACC

3.10. Compute Flow Curve from Multipass PSC Testing

After each multipass PSC test was finished, the data logging that records at each time step (depends on frequency setting) the specimen temperature, load, displacement and velocity of the ram was automatically saved in data file, which then was transferred into the Microsoft Excel spreadsheet to determine the flow curve (equivalent stress versus equivalent strain) for each multipass PSC test. For the single pass PSC testing, a good practice guide on measurement of flow curve was published in 2006 [241], which has been employed and modified for determining flow curves in the multipass PSC tests. However, care must be taken with procedures of analysing the data of multipass deformation, particular for the interpretation of the measured load-displacement relationship at each deformation temperature, in order to accurately determine the multipass stress-strain flow curves. An example of determining and correcting multipass flow curve step by step is shown in the Appendix B.

3.11. Optical and Quantitative Metallography

3.11.1. Samples Preparation

Figure 71: Sectioned PSC samples after first two cuts at the abrasive cutter

All the deformed PSC specimens were cut off the undeformed sides through using a large abrasive cutter and the positions of cutting were shown in above Figure 71 in which the arrows point at. Due to some heat may produce during the fast cutting, which could damage the as-quenched microstructure, the new Struers Accutom- IsoMet 5000 precision cutting wheels were used to slice areas of interest (the deformation zone), presented in Figure 72. Also if the length of section is too long for the mountable size (maximum in 32mm long), the extra areas at the sides of sample were further trimmed off by using the IsoMet precision cutter. It is important to remember that the centre region of the deformed PSC sample is the only area that experience plane strain compression.

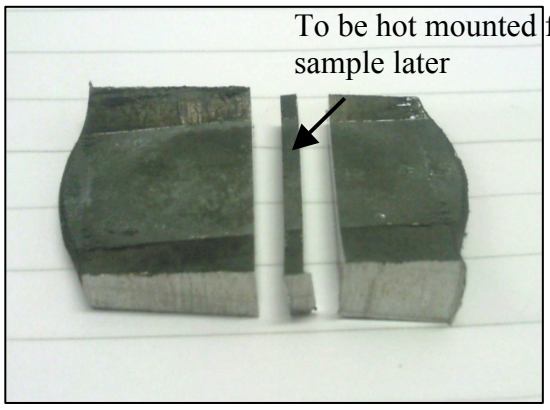

Figure 72: Sectioned sample after two precision cuts at the IsoMet 5000

The cut sample was then hot mounted in the mounting press before engraving the sample's identity at the back of the mount. These steps were repeated for every sample associated with this project. For example, the 38th sample of Nb+Ti steel B was engraved as B38.

Next, the hot mounted samples were mechanically ground using different silicon carbide papers of 120, 240, 400, 800 and 1200 grit in this order. Upon grinding using successively finer grit papers, the samples were position perpendicular to the previous grit on the grinding direction, resulting in the grinding lines from the previous grit to be easily observed if still present. The sample surface was sprayed with Iso-Propanol solution to aid drying followed by air blowing under a hand dryer.

When completed, the ground samples were then polished using diamond paste of 6μm on a fine polish cloth until all of the grinding lines were no longer visible. Before progressing to the next stage, the samples were thoroughly washed to ensure no undesirable particles were present for the next polishing stage. Subsequently, the samples progressed to polishing using diamond paste 1μm on a different polish cloth to avoid contamination of 6μm diamond particles. Pressure on the sample from this stage onwards should not be too high as to avoid introducing unintentional scratches and/or embedding of diamond particle on the metal surface. Finally, the sample is carefully polished using the Silco colloidal silica of 0.06μm to obtain a high quality, scratch-free, mirror finish.

3.11.2. Etching the Deformed PSC Samples

In general, etching must be adequate to reveal the true optical microstructure without significant distortion. To reveal ferrite grain size standard 2% Nital solution is commonly used. A clean and small container was used to hold the 2% Nital solution where the sample surface was submerged into for 10 seconds. The samples were then inspected under an optical microscope to determine the conditions of etching. Under-etched samples were re-etched at 3 to 5 seconds interval resuming with microscopic inspection. Over-etched samples were have to re-grinded using 1200 grit silicon carbide paper until traces of etching are completely removed followed by polishing to 0.06μm finish again before re-etching.

Several etchants were used but the best one to reveal prior austenite grain boundary from the as-quenched martensitic microstructure was the etching solution made of 25% teepol (soap solution) as wetting agent (an additive in etchants for better etching uniformity) and 75% saturated picric acid plus 1-3 drops of hydrochloric acid (36%). The beaker of 200ml volume was filled with 50ml (20 – 25% of total volume) of soap solution as wetting agent with the remaining volume made up of picric acid solution. Three drops of hydrochloric acid of 36%

concentration were later added to the picric acid solution before raising the temperature of the etchant to between 70°C and 90°C, illustrated in below Figure 73. A thermometer was used to measure solution temperature. This mixed solution was then heated to about 80- 90°C and the temperature was kept in that range. Finally, the sample was put into the etching solution for several minutes until the prior austenite grain boundaries were reasonably revealed under optical microscopy. However, if the sample was over etched, the sample was re-polished and then re-etched again. If the resulting structure was not clear, specimens were heated at 490°C for 24 hours inside tube furnace in the presence of argon to allow the segregation of element P on the grain boundaries to improve the response of the etching and then re-etched.

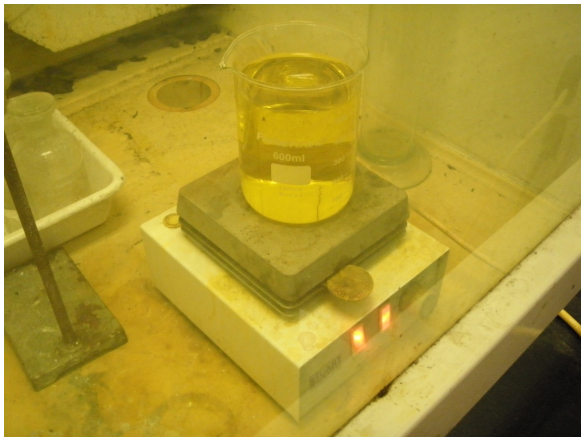

Figure 73: 75% saturated picric acid with 25% soap solution as wetting agent and 3 drops of 36% hydrochloric acid in a glass breaker, heated up to 80°C for etching.

3.11.3. Optical Microscopic Image Analysis

All of the test specimen from the isothermal reheating studies and PSC tests were observed and analysed under a Polyvar optical microscope, which can provide quantitative analysis of microstructural evolution throughout the hot rolling process route. For measurement, at least 15 optical microstructure images were captured of each test conditions for further quantitative metallography analysing (prior austenite grain size, ferrite grain size and volume fraction of ferrite and pearlite).

3.11.4. Ferrite Fraction Measurement

A free image analyser software ImageJ [251] has been used to determine volume (area in 2 dimensional) fractions of ferrite, pearlite and other phases in the post-deformation cooling microstructures. The measurement of ImageJ software is relied on the correct contrast between the dark and light area on the image taken from the Polyvar optical microscope, i.e.,

determining the percentage of black area (pearlite and other phases) against the whole selected background, which is shown in Figure 74 in which the ferrite fraction is about 88%. The detail processes of measuring the area fraction are not included in here but can be found inside the user-guide of ImageJ [251]. However, despite some errors in calculation due to the black areas also including the ferrite grain boundaries and impurity, it was still considered that the contrast between the ferrite and pearlite or other phases was sufficient to conclude that ImageJ was a viable tool for volume fraction analysis.

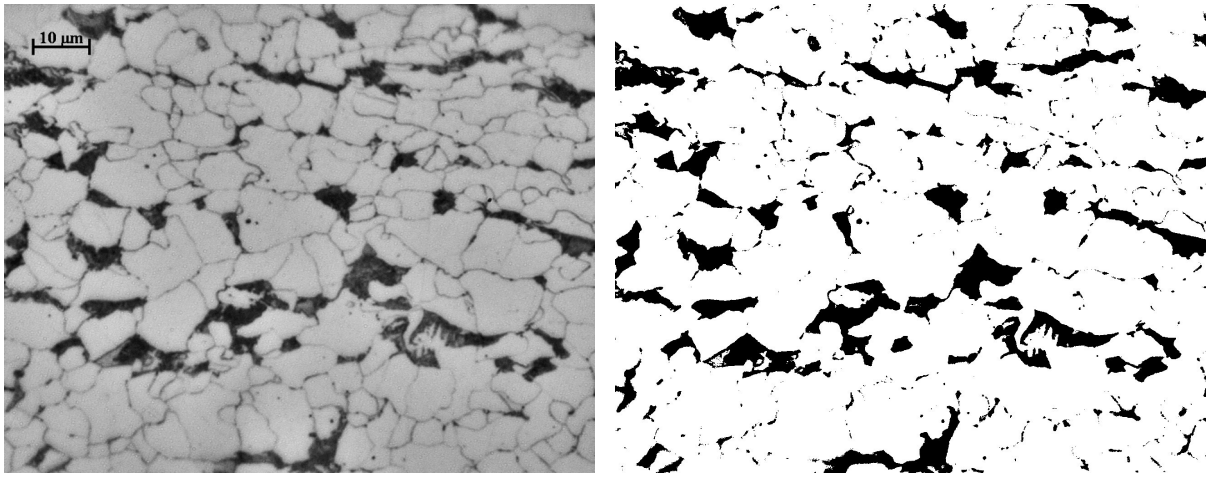

Figure 74: An example of comparison of original optical microstructure (left hand side) and the binary image (black and white) produced by ImageJ

3.11.5. Grain Size Measurement

In general, the common and fast practice for grain size measurements is determined on several 2-dimentional images of optical microstructures with ignoring the fact that the microstructures exist in 3-dimensional. There are several different techniques to measure grain size manually or automatically, but the manual mean linear intercept (MLI) method was chosen in this project for better accuracy although time consuming. The free analyser software ImageJ can be also used to determine grain size through function "Analyse Particles", and calculated results were compared to manually measured grain size. Due to the procedures of quantitative measurement of grain size through linear intercept method are well known [246, 252-254], the processes of measuring prior austenite grain size and ferrite grain size from each multipass PSC deformed sample are not described in here. It may useful to mention that for obtaining reliable results at least 50 lines in total were drawn on image of all test conditions. The aspect ratio, expressed as longitudinal (rolling direction) grain size / transverse grain size, was also calculated for determining the degree of pancaking at end of finish rolling. Errors were also introduced in measurement, particularly when the grain boundaries were only partly revealed.

3.12. Physical Based Modelling the Microstructural Evolution During Hot Rolling

A previous physical-based model [104] for predicting the austenite development through industrial hot rolling schedule and final ferrite grain size and the corresponding physical properties has been updated with new empirical equations (mentioned in the Literature review chapter), and most importantly the new model has considered continuous cooling condition during holding period. It is well known that most empirical equations, such as Sellars' and Hogdson', were established under the isothermal condition, however during industrial hot rolling heavy plate production, particular at the long HP, the temperature of heavy plate decreases significantly. In the following Figure 75, a cooling curve is divided into increment of time, Δt_i and the temperature drop for each time step is ΔT_i to detemine the austenite static recrystallisation and grain growth during the HP as a series of short, isothermal steps, and then the predicted results were compared to the measured prior austenite grain size at the end of HP, presented in Discussion chapter Section 5.5.2.1.

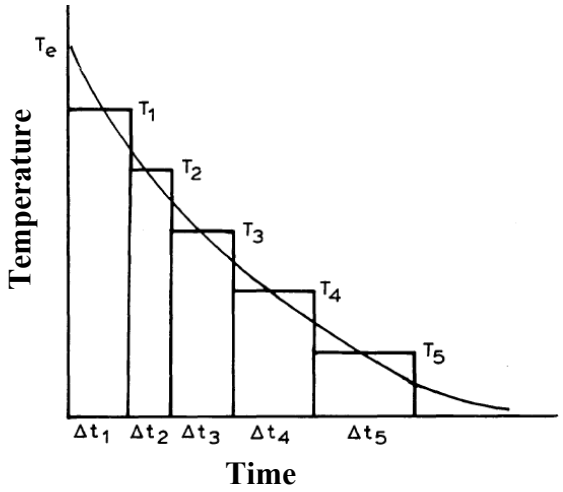

Figure 75: Schematic relationship between isothermal and continuous cooling conditions [183]

3.13. Summary of Experimental Procedures and Methods

This chapter describes some detailed and reproducible experimental procedures and techniques, which are used to achieve the objectives of this research project, particular focus on simulating the whole industrial hot rolling microalloyed heavy steel plate production through multi-pass PSC tests on the TMC machine in a laboratory scale. The key experiment work are summarised as following:

- Initial characterisations of the interested steels, and determination of maximum cooling rates capability of different cooling media (forced air, mist and water quenching) from 1000°C to 800°C and post-deformation accelerated cooling rate on the TMC machine
- An industrial hot rolling plain carbon steel plate production was simulated as closely as possible by 2-pass roughing the laboratory Hille mill, 9-pass finish rolling and post-deformation air cooling on the TMC machine.
- Temperature, strain and strain rates distributions inside the industrial hot rolling steel plate and temperature variations across the different thickness of intermediate or partially as-rolled steel plate during holding period (HP) were determined through different models, and the predicted values were used as the input values in multipass PSC test settings for simulating different flow curves and microstructure development at specific positions (plate surface and centre) through the plate thickness.
- An industrial hot rolling schedule of microalloyed steel has been closely simulated through mainly 8-pass (up to 13-pass) PSC tests and several different cooling rates have been applied during the HP simulation to investigate the effects of air-cooling and IFC on the austenite grain size and final ferrite grain size.
- The TMCP parameters such as deformation temperature, strain, strain rate, post deformation cooling rate and steel composition on the prior austenite and ferrite grain size were studied on the multipass PSC testing.
- Optical microscopy and images processing were performed to characterise the microstructure evolution during the multipass PSC simulation.

Chapter 4 – Results

4.1. Outline of Results Chapter

Five important areas of results from the experiments are covered in this chapter as following:

a. Initial characterisations of the interested steels, and the analysed results of minimum and maximum cooling rates capability of different cooling media (forced air, mist and water quenching) at the holding period from 1000°C to 800°C on the TMC machine.

b. Simulation of temperature, strain and strain rate distributions inside the industrial hot rolling steel plate and temperature variations across the thickness of intermediate as-rolled steel plate during holding period (HP).

c. Simulation of an industrial hot rolling plain carbon steel plate production with total effective strain 2.1 as close as possible through combination of 2-pass roughing on the laboratory Hille mill and 9-pass finishing PSC simulation on the advanced TMC machine.

d. Simulation of a commercial hot rolling schedule for microalloyed steel plate production with total applied strain 1.65 on the TMC machine including different cooling rates during holding period and accelerated cooling after multipass PSC deformation.

e. The effects of employing IFC on the development of prior austenite size at end of the holding period (HP) and ACC on the ferrite grain size

Not all the relevant results are included in this chapter: several results such as some optical microstructures and multipass flow curves are given in next Discussion chapter.

4.2. Initial Characterisation of Steels

4.2.1. Physical Metallurgy and Properties of Steels from Prediction

In Table 9 it shows initial investigation in comparisons of target and actual selected lab casts in terms of compositions, carbon equivalent (CE), dissolution temperature (T_{DISS}) of Nb(C, N) particles, 5% recrystallisation temperature ($T_{0.05X}$), and transformation temperatures Ar_3. Although these estimated temperatures were from empirical equations and are not always accurate, the predicted values could be used as basic reference to analyse hot rolling schedules. The Table 9 also shows that for the plain C-Mn steels C and D the recrystallisation stop temperatures were about 810°C while the microalloyed Nb and Nb +Ti steels are around

900°C. It is important to note that the difference between $T_{0.05X}$ and Ar_3 defines the temperature range of finish rolling stage for optimum grain refinement. For the Nb- and Nb+Ti- steels the difference were 112°C and 141°C respectively while 40°C – 60°C for the C-Mn steels. Therefore, there is relatively larger process window for Nb and Nb+Ti steel rolling at the un-recrystallisation of austenite region in the finish mill as expected.

Table 9: Compositions (wt%) and critical temperatures (°C) of target and actual selected lab casts

	C	Si	Mn	Nb	Ti	CE	T_{DISS}	$T_{0.05X}$	Ar_3
C-Mn-target	0.11	0.35	1.35	0.003	0	0.36	865	808	768
C-Mn-Nb-target	0.11	0.35	1.35	0.03	0	0.36	1095	906	768
C-Mn-Nb-Ti-target	0.11	0.35	1.35	0.03	0.015	0.36	1095	919	768
Steel A - Nb	0.085	0.34	1.33	0.028	0.004	0.33	1062	889	777
Steel B - Nb+Ti	0.083	0.34	1.33	0.032	0.016	0.33	1072	917	778
Steel C – plain carbon	0.085	0.33	1.34	0.003	0.004	0.33	846	808	776
Steel D – plain carbon	0.115	0.32	1.34	0.002	0.004	0.36	837	825	767

The reason to choose dissolution temperature of Nb addition rather than Ti element in the above table 9 is because Nb(C, N) precipitates had a relatively higher dissolution temperature (1072°C) than that of TiC (971°C) in C-Mn-Nb-Ti steel determined by using the following Equation 69. Moreover, it is assumed that the most stable compound TiN is present in the steel B during reheating process for control of reheated grain size; Ti can also form joint precipitates with Nb, which would have a higher dissolution temperature. However, such low Ti levels should have little effects on C and N concentrations regarding to the formation of the strain induced precipitation of Nb(C, N) particles.

For TiC dissolution temperature: $T_D = \frac{7000}{2.75 - \log([Ti] \times [C])}$ (69)

The equilibrium physical thermal properties (such as specific heat, thermal conductivity and density) are dependent of temperatures and chemical compositions and the actual ones also depend on the thermal history. These were predicted by the commercial JMATPro software version 4 and some examples of predicted profiles are shown in the following Figures 76-78. As seen in these figures, in the different temperature regions the thermal properties had different responses to the cooling rates. When temperatures above 800°C and below 350°C, the specific heat, thermal conductivity and density are in different linear relationships with temperature. On the other hand, from 350°C to 800°C, these physical thermal properties showed non-linear functions as temperature. Furthermore, in Figure 78 it displays that microalloyed steels A and B, and plain carbon steels C and D had different thermal conductivities profiles from 350 to 800°C. These dramatically changes in the curves possible reflect the phase (and magnetic) transformations. For examples, Bs and Ms in these figures perhaps indicated that the start formation temperatures of bainite and martensite, respectively.

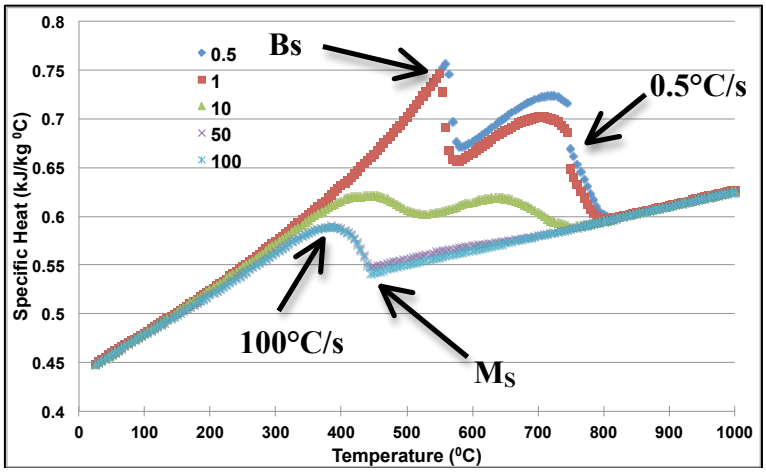

Figure 76: Predicted specific heat of steel A (Nb) as function of temperature at five different cooling rates (0.5, 1, 10, 50, 100°C/s) from the JMATPro programme

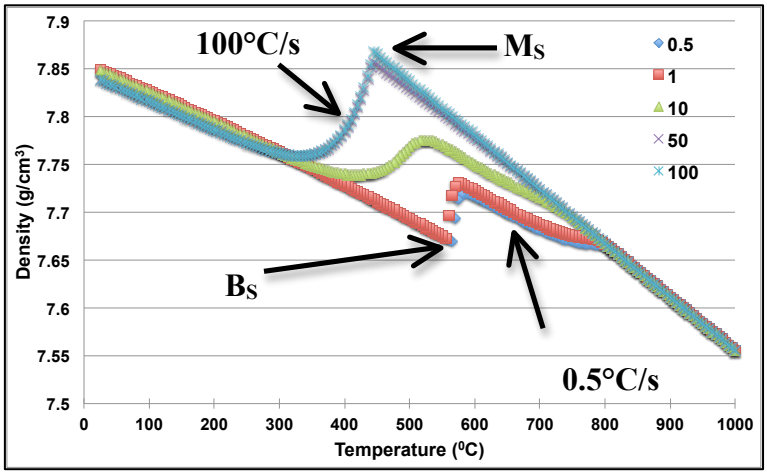

Figure 77: Predicted density of steel B (Nb+Ti) as function of temperature at five different cooling rates (0.5, 1, 10, 50, 100°C/s) from the JMATPro programme

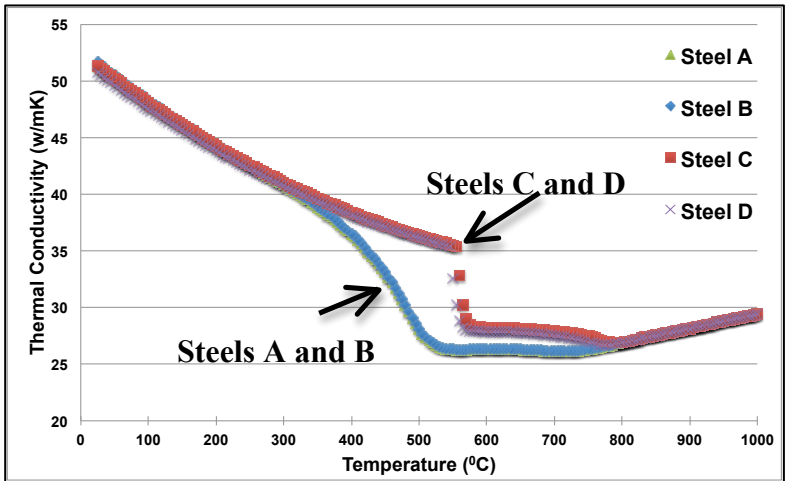

Figure 78: Predicted thermal conductivities of four different steels (steels A, B, C, and D) under cooling rate 10°C/s as function of temperature from the JMATPro programme

4.2.2. Industrial Hot Rolling Schedules of Heavy Steel Plate Production

As mentioned in the previous Experimental chapter Section 3.3.1, there were eight different industrial hot rolling schedules of heavy plate production along with some corresponding commercial hot rolled samples provided by the Tata Steel Europe Company, which have been analysed for temperature, strain and strain rate profiles. For example, the different target plate surface temperature profiles of 8 schedules are shown in the following Figures 79 and 80, where the 8AK36, 8AK37, 8AK38 and 8AK39 are the microalloyed steels with relatively lower finishing rolling temperatures while 8AK42, 8K43, 8AK44 and 8AK47 are the plain carbon steels.

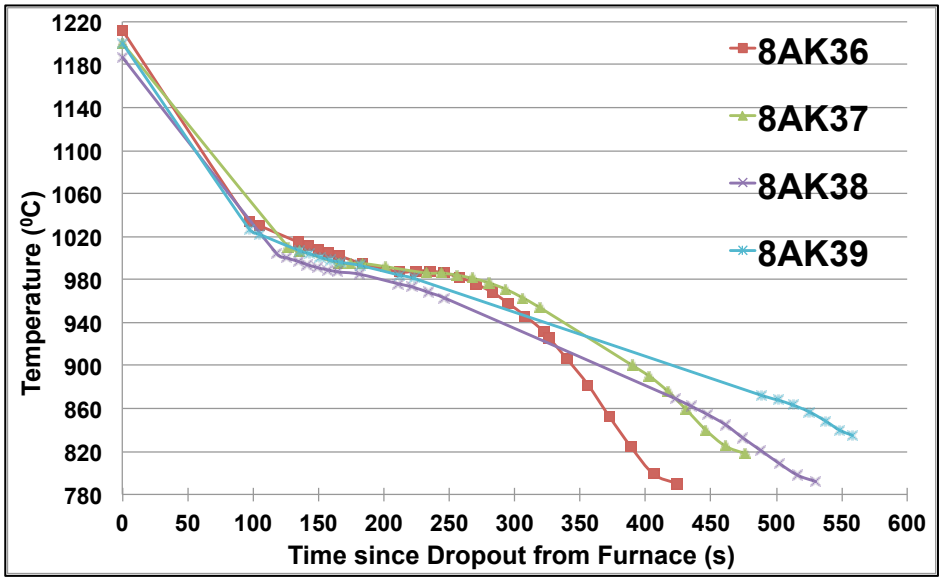

Figure 79: Predicted plate surface temperature profiles of four industrial hot rolling schedules for microalloyed steel plate production

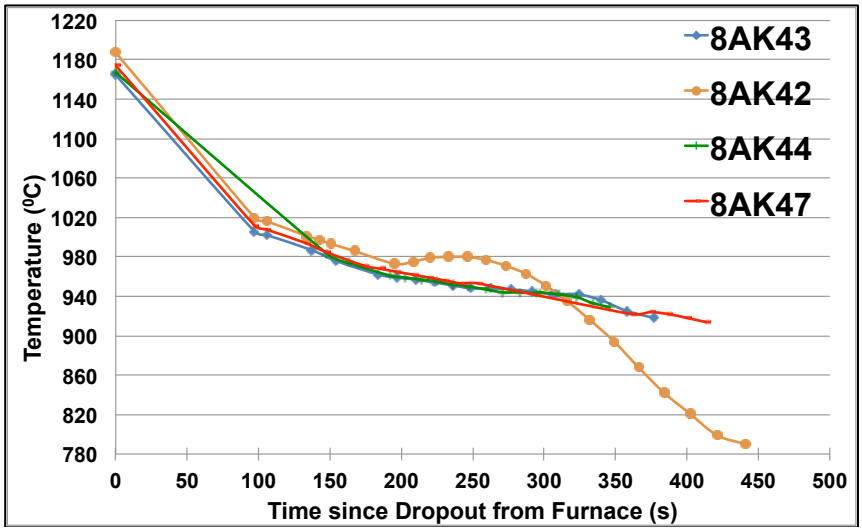

Figure 80: Predicted plate surface temperature profiles of four industrial hot rolling schedules for plain steel plate production

Based on the analysed results of eight industrial hot rolling schedules, a brief summary is given in the below Table 10 in which T_{DISS}, $T_{0.05X}$ and Ar_3 are the dissolution temperature of Nb(C, N) particles, 5% recrystallisation temperature and austenite to ferrite phase transformation temperature respectively. The steel grades 8AK39, 8AK43 and 8AK39 were chosen for further investigation.

Table 10: Selected chemical element concentrations (wt%), total reduction and total equivalent strain $\bar{\varepsilon}_t$ of eight as-rolled steel plates and predicted important temperatures

Steel Grade	C	Si	Mn	Nb	Total Reduction	$\bar{\varepsilon}_t$	T_{DISS}	$T_{0.05X}$	Ar_3
8AK36	**0.15**	**0.348**	**1.42**	**0.03**	**0.92**	**2.90**	**1127**	**925**	**747**
8AK37	0.15	0.361	1.41	0.032	0.88	2.46	1136	931	749
8AK38	0.17	0.39	1.4	0.036	0.82	1.98	1166	941	744
8AK39	**0.17**	**0.39**	**1.4**	**0.036**	**0.79**	**1.51**	**1166**	**941**	**744**
8AK42	0.16	0.237	1.07	0.002	0.92	2.91	876	870	773
8AK43	**0.18**	**0.242**	**1.16**	**0.002**	**0.83**	**2.07**	**880**	**875**	**759**
8AK44	0.2	0.243	1.08	0.002	0.66	1.25	893	888	759
8AK47	0.15	0.207	0.98	0.002	0.73	1.53	873	874	783

4.2.3. Received Commercial As-Rolled Steel Plates Microstructures

Before the interested as-cast ingots arrived, the commercial as-rolled plates plain carbon steel 8AK43 and Nb steel 8AK36 were specific chosen for comparisons in terms of industrial hot rolling schedules and as-rolled optical microstructures. Regarding to the hot rolling history, the Nb steel plate was heat treated at a relatively higher reheating temperature (1211°C) for the complete dissolution of Nb and much lower finish-rolling temperature (840°C) for grain refinement with strain-induced precipitation than those (1165°C and 940°C respectively) of the plain carbon steel plate. Moreover, total slab reduction (92%) of the Nb steel was higher than that of the plain carbon steel (83%) according to Table 10. The results of optical microstructures are presented in Figure 81 and 82, and the corresponding ferrite grain size measurement through using the average linear grain boundaries intercept method at the near surface (2mm below surface), quarter thickness and centre of commercial as-rolled plates are shown in the following Table 11, and few differences are noteworthy.

Table 11: 95% confidence limit in ferrite grain sizes (μm) at near surface, quarter thickness and middle centre of plates of C-Mn (8AK43) and C-Mn-Nb (8AK36) steels

	Plain C-Mn steel plate (50mm)		C-Mn-Nb steel plate (20mm)	
	Longitudinal	Transverse	Longitudinal	Transverse
Near surface	25.7 ± 4.7	21.1 ± 1.4	7.4 ± 1.0	4.9 ± 0.3
Quarter thickness	25.8 ± 8.0	24.2 ± 3.0	8.74 ± 0.9	6.8 ± 0.4
Middle thickness	27.9 ± 5.1	29.5 ± 5.5	10.7 ± 1.6	8.7 ± 0.7

Firstly, in the longitudinal (or rolling) and transverse directions (it is perpendicular to the rolling direction), the average ferrite grain sizes across thickness of Nb steel plate were about 3 to 5 times smaller than those of C-Mn steel plate, which are because the additional Nb element was effective in retarded austenite recrystallisation by precipitated as fine Nb(C, N) carbonitrides particles which can pin austenite grain boundaries movement, and higher reduction at the lower finish rolling temperature produced much larger amount of ferrite nucleation sites, which in turn decreases the final average ferrite grain size.

Secondly, the ferrite grain size increased from the near surface towards the middle thickness in both steel plates, particularly at the transverse directions, which indicates less strain penetration towards interior, and also due to a reduction in the cooling rates from the surface towards the plate centre when natural-air cooling was applied after finish rolling. Moreover, there was not a significant variation of ferrite grain size between the longitudinal and

transverse directions, which suggests that most of the ferrite grains are equiaxed, and only few of the relatively deformed grains are found to be parallel to the rolling direction at the near surface regions. The reason for this phenomenon is the applied strain or strain rate was not high enough to produce elongated pancaked ferrite grains at the centre of the Nb steel plate while for the C-Mn steel, even at the near surface, ferrite grains are almost all equiaxed according to the results in Table 11.

Thirdly, the Table 11 also shows high values of ferrite grain size deviation in the plain carbon steel, which means non-uniform ferrite grain size and duplex microstructures (some of grains were small or fine and the others are large or coarse), and even occurred at near surface of the plate. It is well accepted that non-uniform ferrite grain size distribution across thickness decrease toughness of final as-rolled products.

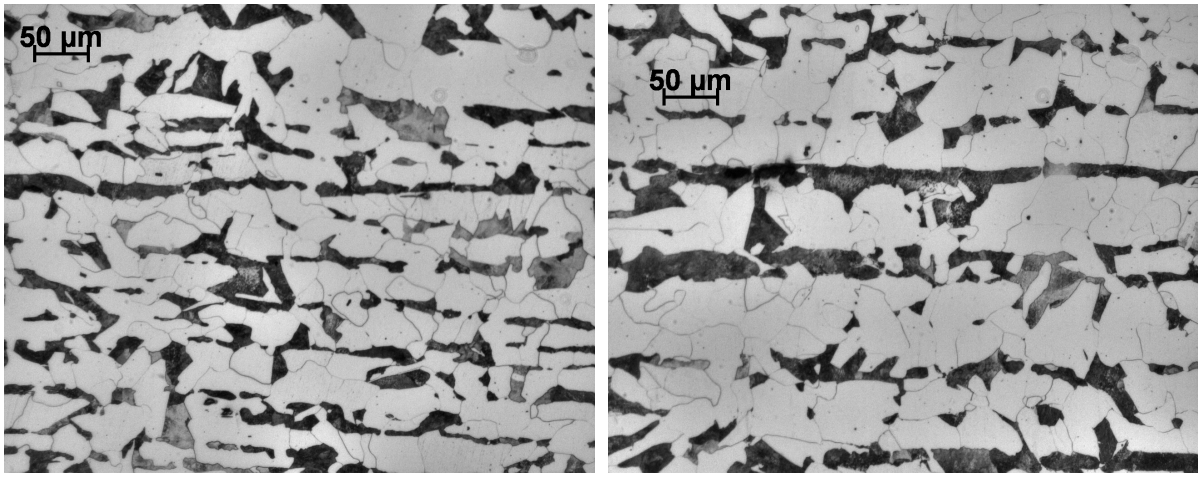

Figure 81: Optical microstructures at the sub-surface 2mm (left hand side) and centre (right hand side) of 50mm plain carbon steel (8AK43) plate

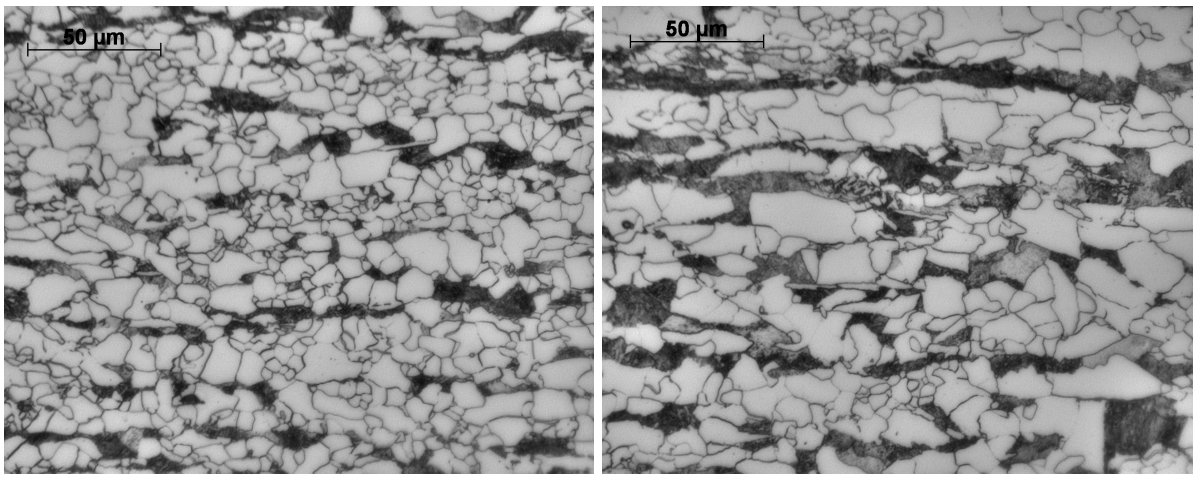

Figure 82: Optical microstructures at the sub-surface 2mm (left hand side) and centre (right hand side) of 20mm microalloyed steel (8AK36) plate

4.2.4. Results of Austenite Grain Coarsening

The results of the austenite grain coarsening of three different steels (steel A, B and C) at the different reheating temperature and the corresponding holding time are described in this Section. It is perhaps useful to emphasise that at the earlier stage of research revealing prior austenite grain size (PAGS) clearly from the 48 different as-quenched martensitic microstructures for quantitative analysis was really difficult and it was extremely time consuming. The special etching solution was described in Experimental Section 3.11.2 for revealing the PAGS was not always working properly, particularly for the heat treated samples only without deformation, even after the as-quenched samples were subjected to temper treatment and then etched. An example of unsuccessful etching is shown in Figure 83 in which the target PAGS are unable to be distinguished from the confused tempered microstructures. Therefore, only few successful etched optical microstructures of PAGS of plain carbon steel C are included in here. Furthermore, the empirical Equation 67 in Experimental Section 3.4.2 for predicting the prior austenite grain size at the reheating process (temperature and holding time) does not take account of steel composition (effects of Nb and Ti elements).

For example, two samples of the plain carbon-steel C were reheated at 900°C and were held for 15 and 30 minutes respectively, successfully revealed that the PAGS that increased from 12.6±1.9 to 18.6±1.8μm as the holding time increased from 15 to 30 minutes in Figure 84. Another illustration of PAGS development is presented in Figure 85, in which the steel C were reheated at 1100°C and held 15 and 30 minutes respectively, and the PAGS were also increased from 30.3± 2.3 to 38.5±3.1μm. However, these measured values were significantly smaller than the predicted PAGS by the Equation 67, presented in Figure 86. For example, according to the predicted curve at 1100°C in Figure 86, the estimated PAGS was 333μm (almost 10 times larger than measured value) at 30 minutes (1800s). Thus, for the present steel compositions, the Equation 67 cannot be used and applied in predicting the PAGS.

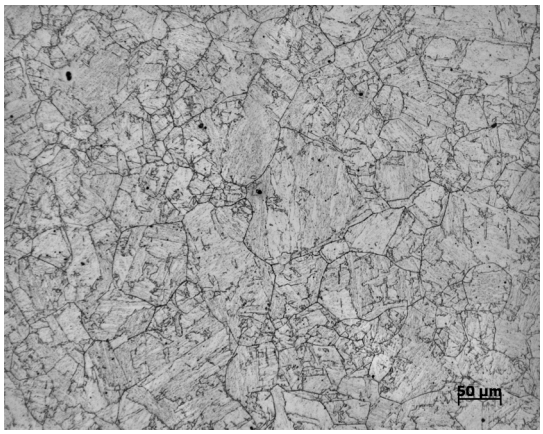

Figure 83: PAGS of Nb+Ti-steel B reheated at 900°C and hold 2 minutes in the isothermal condition

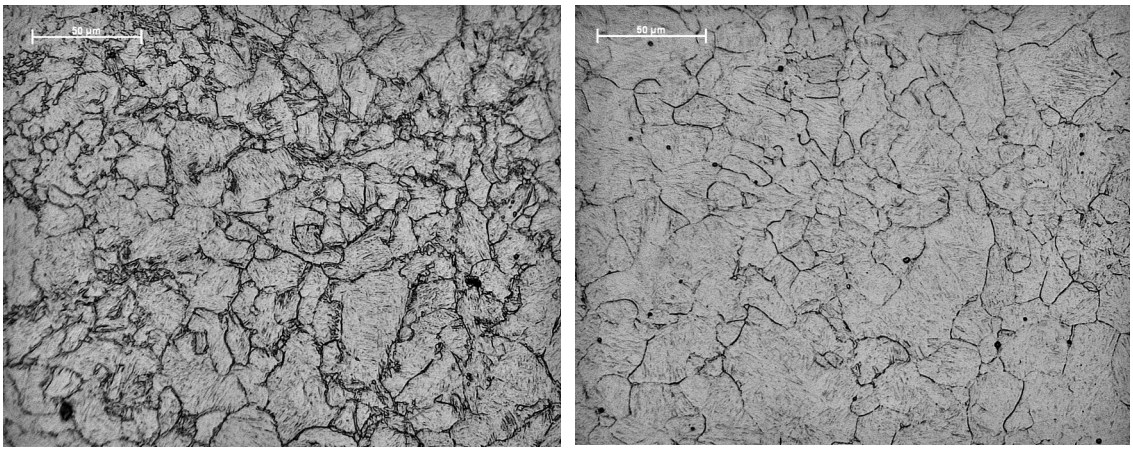

Figure 84: PAGS of plain carbon-steel C reheated at 900°C and hold 15 (left hand side) and 30 minutes (right hand side) in the isothermal condition

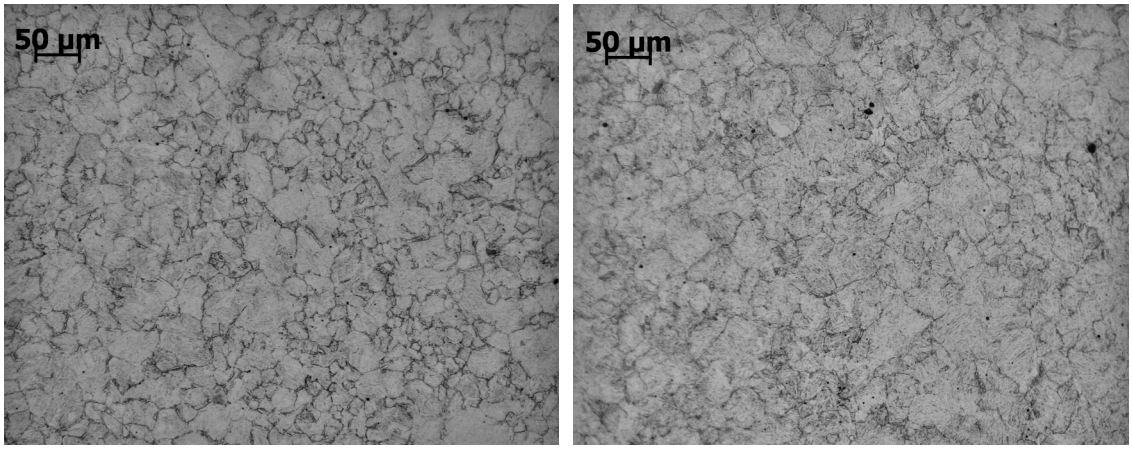

Figure 85: PAGS of plain carbon- steel C reheated at 1100°C and hold 15 (left hand side) and 30 minutes (left hand side) under the isothermal holding condition

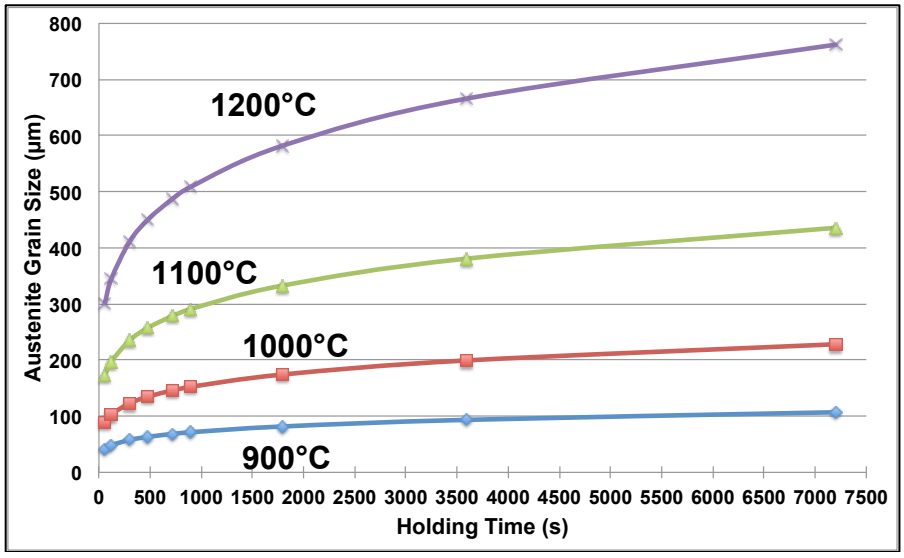

Figure 86: Predicted austenite grain sizes at the different reheating temperatures and holding time lengths by the empirical Equation 67 (showed at Section 3.4.2)

4.3. Cooling Profiles of Different Cooling Media during Holding Period and Accelerated Cooling

The maximum controllable cooling rates of three different cooling media: forced air, mist and full water quench were determined from a series of similar cooling tests taken place inside the FTTU of TMC machine, and the corresponding results are showed in here.

4.3.1. Forced Air Cooling Condition

In the following Figures 87-91, different temperature-time profiles from 1000°C to 800°C under variant forced-air cooling rates are presented. There is no doubt that the long cooling period can be significantly reduced when increased the cooling rate of forced-air from 0.5°C/s to 5°C/s (see Figure 87). However, as the applied cooling rate increased, the temperature difference between subsurface (1mm below surface) and centre of 10mm PSC sample during the cooling stage were also increased, illustrated in Figure 88, 89 and 91. To sum up, the maximum controllable forced-air cooling can be applied up to 20°C/s-25°C/s from 1000°C to 800°C, and the corresponding average temperature differences between the subsurface and centre of the sample increased from 2°C (under 0.5°C/s applied cooling rate) to 30°C. Furthermore, Figure 90 presents that the recalescence and holding profiles of surface and centre of PSC sample when the cooling stage finished. However, due to holding temperature was scheduled to hold constant at 800°C and if temperature reading of control thermocouple inserted in PSC sample (at the centre) was more than 5°C lower than target 800°C after the cooling stage, then the sample was reheated by the induction coil in FTTU, shown in Figure 90.

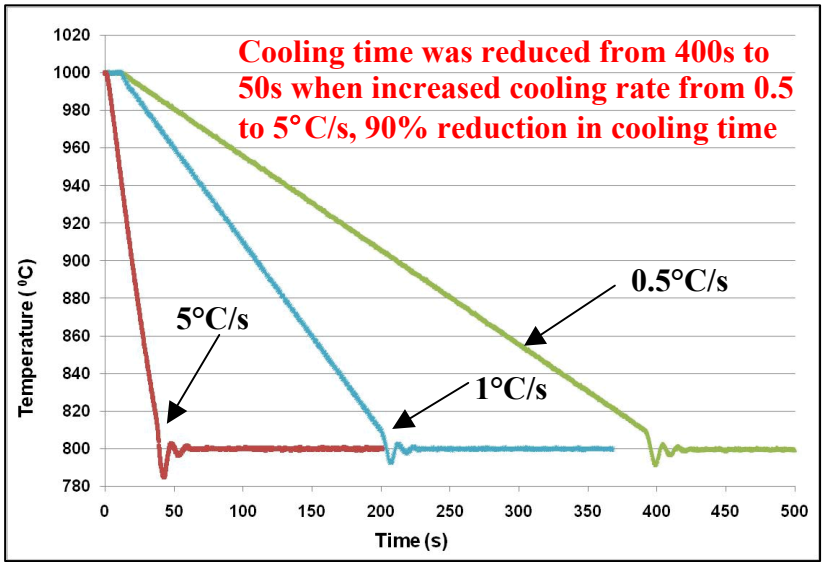

Figure 87: Temperature profiles at the centre of PSC sample at different forced-air cooling rates (0.5°C/s, 1°C/s and 5°C/s) from 1000°C to 800°C on the TMC machine

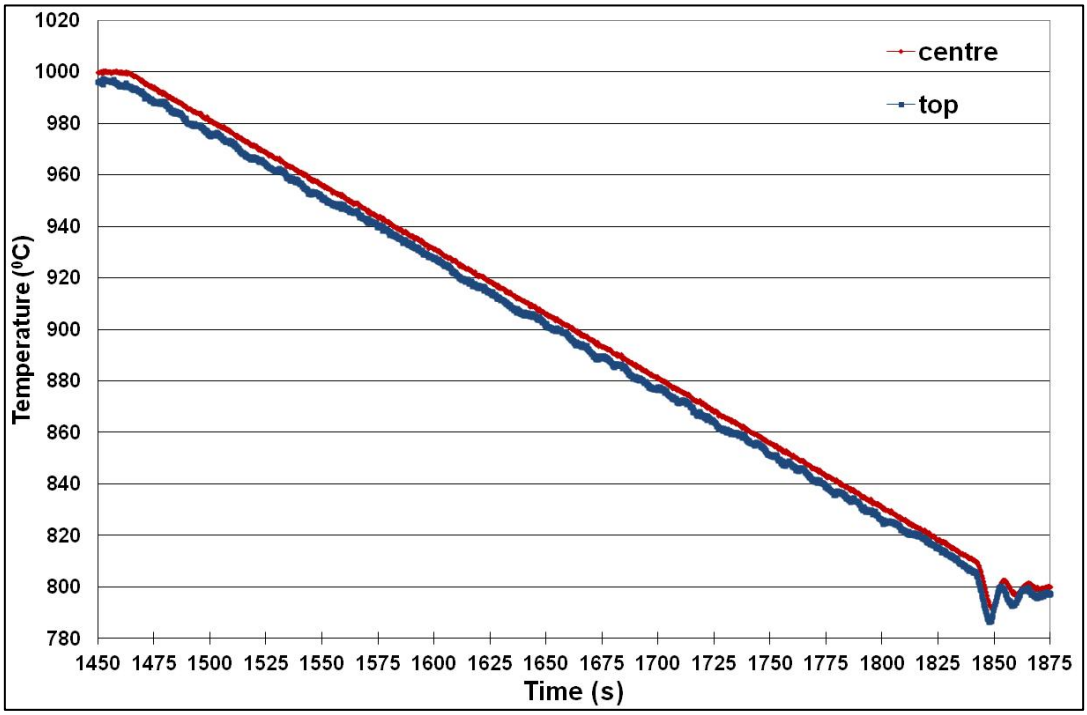

Figure 88: Recorded temperature profiles of top surface and centre of PSC sample at the 0.5°C/s slow air cooling rate from 1000°C to 800°C

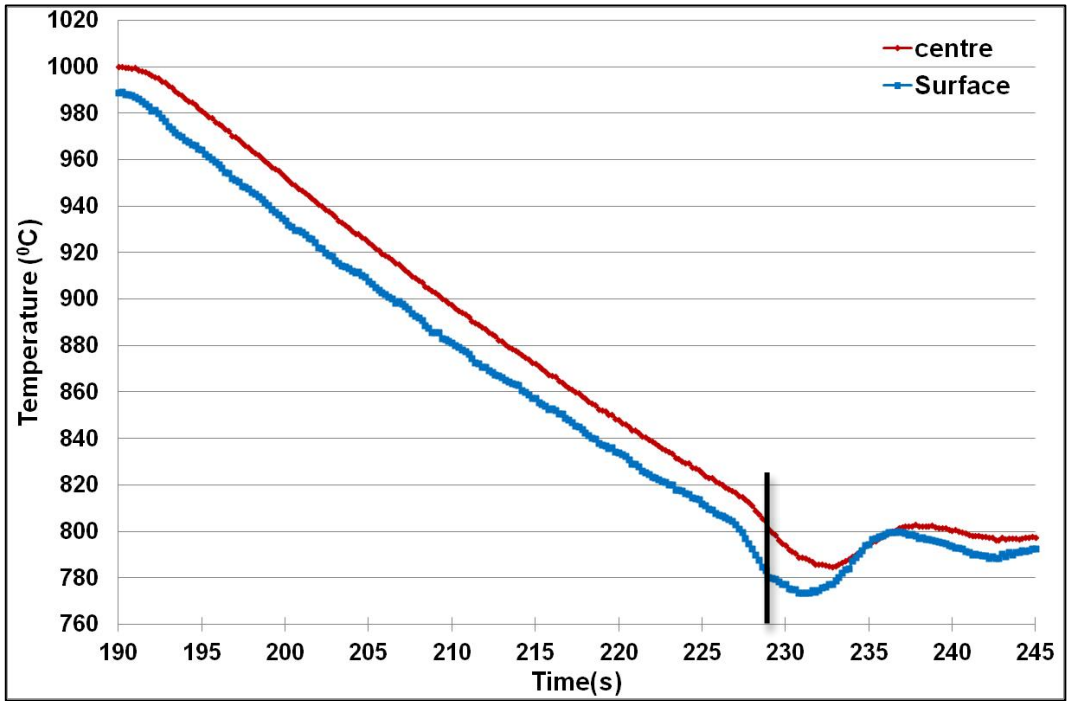

Figure 89: Recorded temperature profiles of surface and centre of PSC sample at the 5°C/s forced-air cooling rate from 1000°C to 800°C

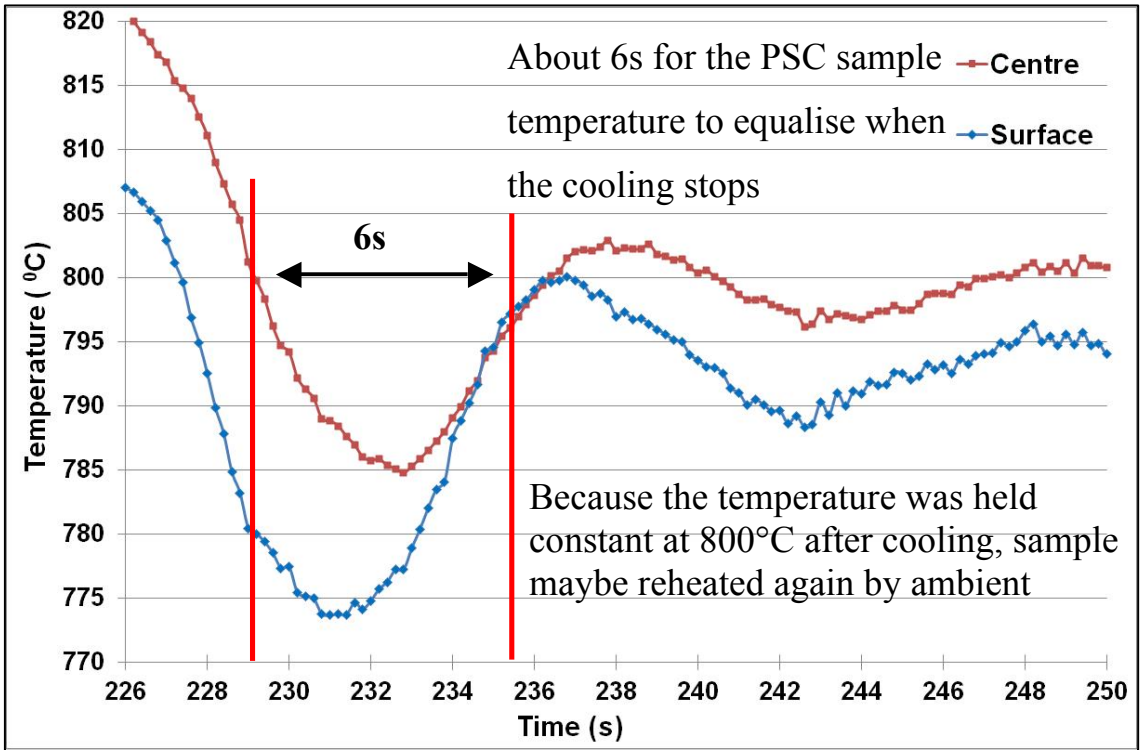

Figure 90: Recalescence and holding profiles of surface and centre of PSC sample after the 5°C/s linear forced-air cooling from 1000°C to 800°C

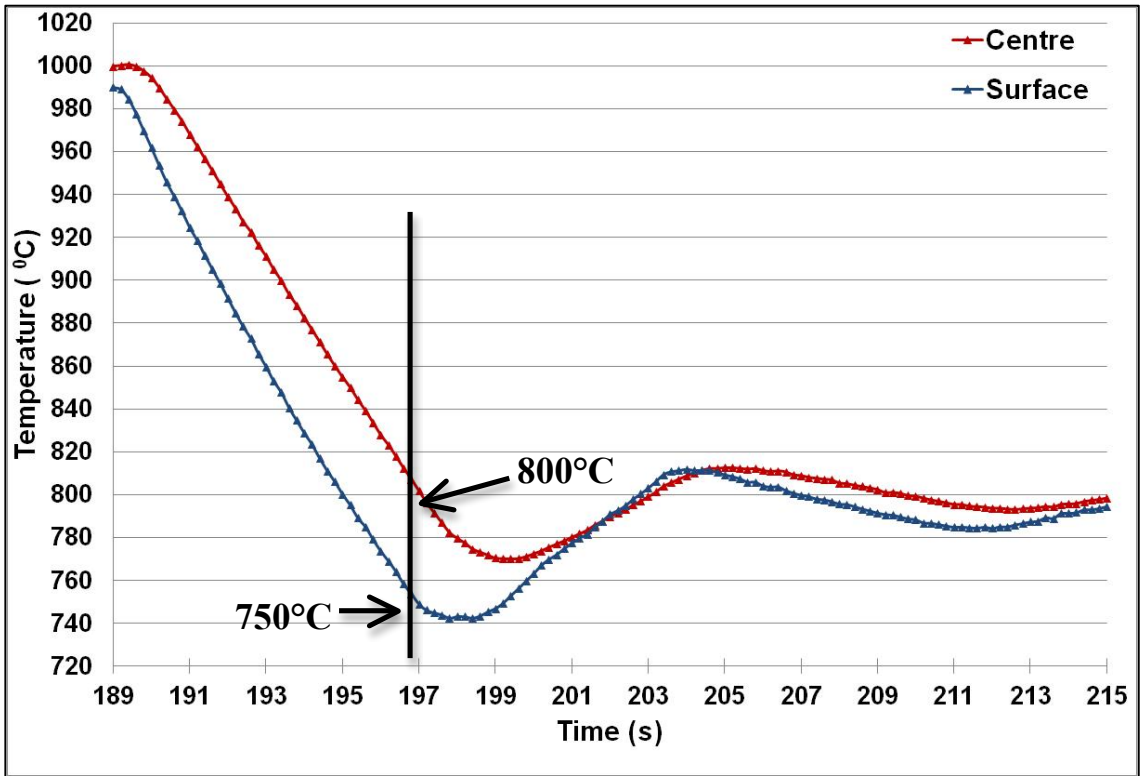

Figure 91: Temperature profiles of surface and centre of PSC sample at the 25°C/s linear forced-air cooling rate from 1000°C to 800°C

4.3.2. Mist Cooling

Under the mist (mixture of forced air and water)-cooling situation and the same cooling range 1000°C to 800°C, the maximum controllable average cooling rate at the centre of PSC sample can be applied up to 67°C/s (the control thermocouple was also located at the centre of PSC sample), but the target cooling rate of mist cooling media was difficult to control compared to forced-air cooling, shown in the following Figures 92-95. It maybe useful to mention that the actual mist-cooling rate is based on the reading and recording of control thermocouple at the centre of PSC sample and determined by different portions of forced air and spraying water in the mist, which means for the relatively higher target mist cooling rate the amount of water spraying in the mixture is larger.

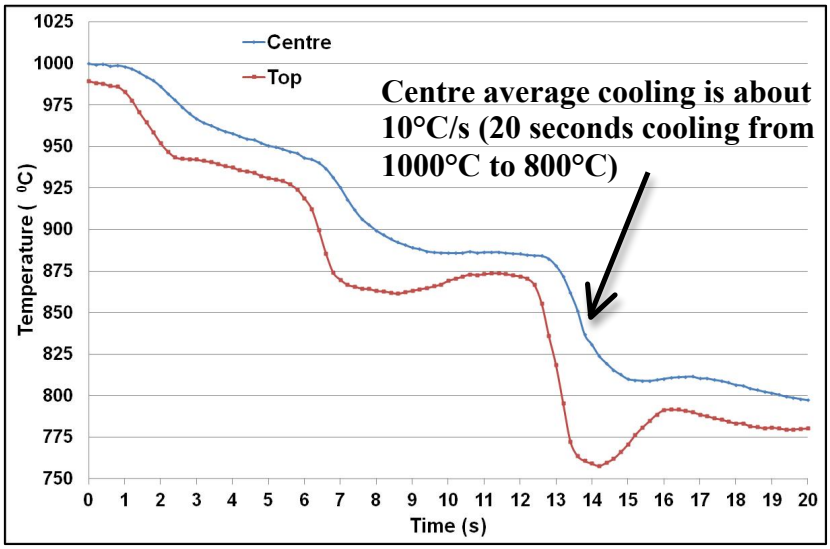

Figure 92: Temperature profiles of top surface and centre of PSC sample at the average 10°C/s applied mist cooling rate from 1000°C to 800°C

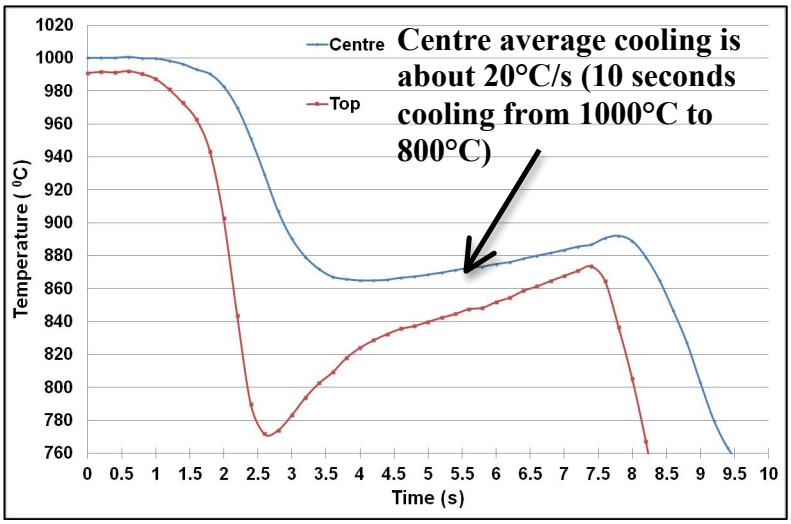

Figure 93: Temperature profiles of top surface and centre of PSC sample at the average 20°C/s applied mist cooling rate from 1000°C to 800°C

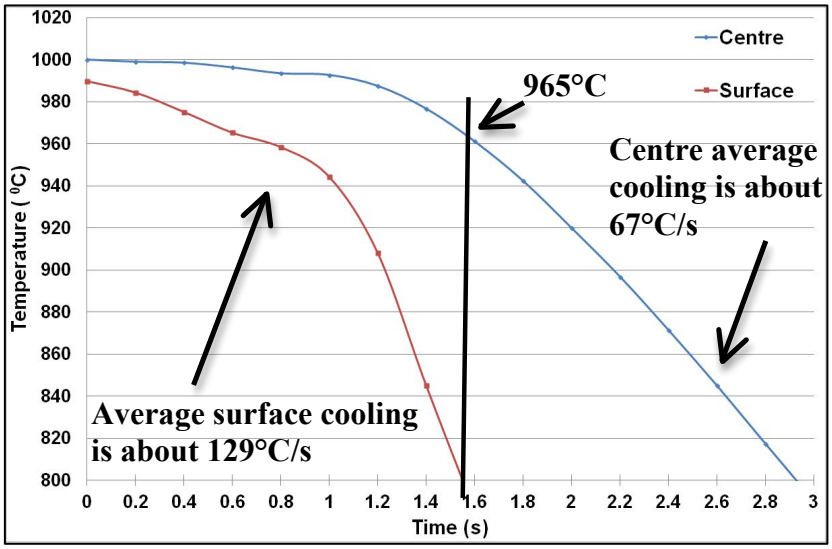

Figure 94: Temperature profiles of surface and centre of 10mm PSC sample at the average 67°C/s mist cooling rate from 1000°C to 800°C

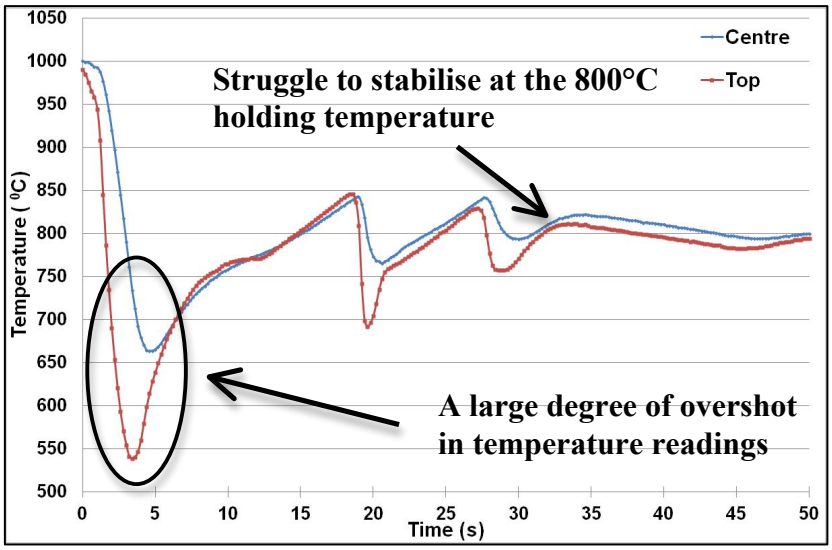

Figure 95: Recalescence and holding temperature profiles of surface and centre of 10mm PSC sample after the 67°C/s mist cooling rate from 1000°C to 800°C

As clearly shown in these Figures 92-94, the temperature differences between the surface and centre of the 10mm PSC sample were larger than those of forced-air cooling (see Figure 91), and the higher applied mist cooling rate the large temperature difference was produced inside the sample when the cooling stopped, as well as longer time required for the temperature stabilised at 800°C holding temperature (see Figure 95). Moreover, Figure 92 and 93 present that at the relatively low mist cooling rates (10°C/s and 20°C/s) the actual temperature profiles (cooled-reheated-cooled) were difficult to follow the target linear cooling profiles due to water spraying in the mist caused dramatically temperature dropping of PSC sample.

4.3.3. Full Water Quench

The last cooling media was the full water quenching, and the corresponding temperature profiles inside PSC sample are shown in the following Figure 96 and 97 in which the centre cooling rate is about 80°C/s or 105°C/s depends on at which point cooling start (centre cooling delayed almost 0.8 second compared to surface cooling in Figure 97 below), and the surface cooling rate is about 200°C/s. Therefore, a huge temperature difference between the top surface and centre of 10mm PSC specimen was induced, illustrated in Figure 97 where the centre temperature was 990°C when the surface temperature already reached 800°C.

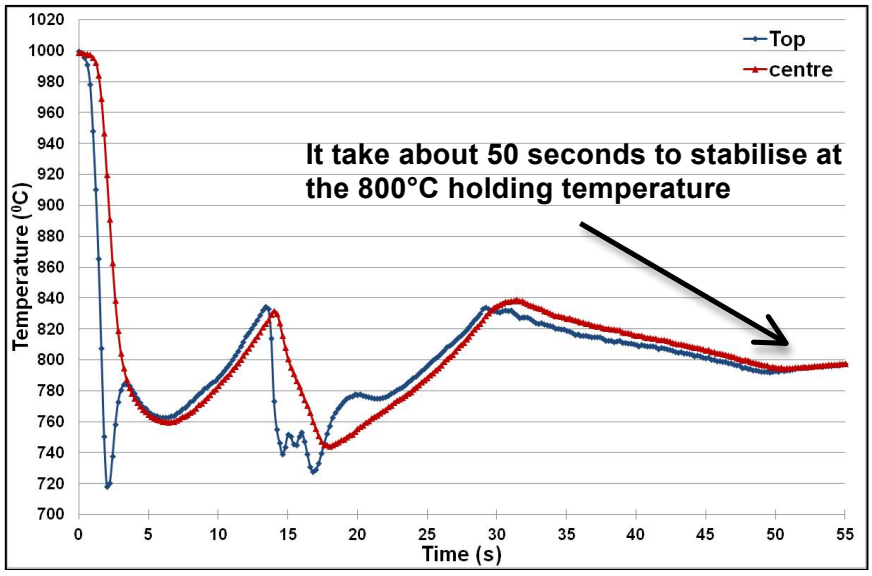

Figure 96: Temperature profiles of surface and centre of 10mm TMC sample from 1000°C to 800°C at the full water quenching

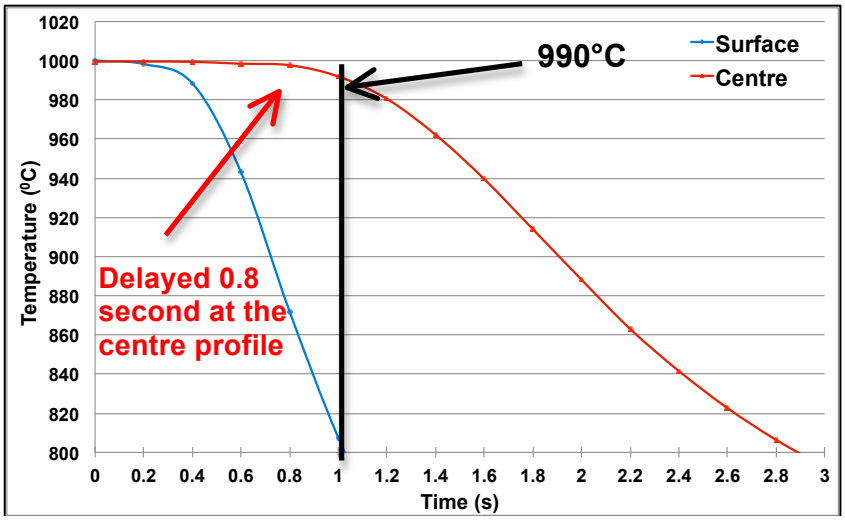

Figure 97: Temperature profiles of surface and centre of 10mm PSC sample from 1000°C down to 800°C at the full water quenching

4.3.4. Effects of the Position of Controlled Thermocouple inside the PSC Sample

In the following Figures 98-100, the location of control thermocouple (CT) changed from centre of PSC sample to the pre-drilled sub-surface (1mm below surface) of specimen, and the results indicate that when the CT is located at the sub-surface of sample, the actual measured cooling rate seems to had better controls than those of the CT were inserted at the middle centre of PSC sample, as well as took relatively shorter time to stabilise PSC sample at the 800°C holding temperature.

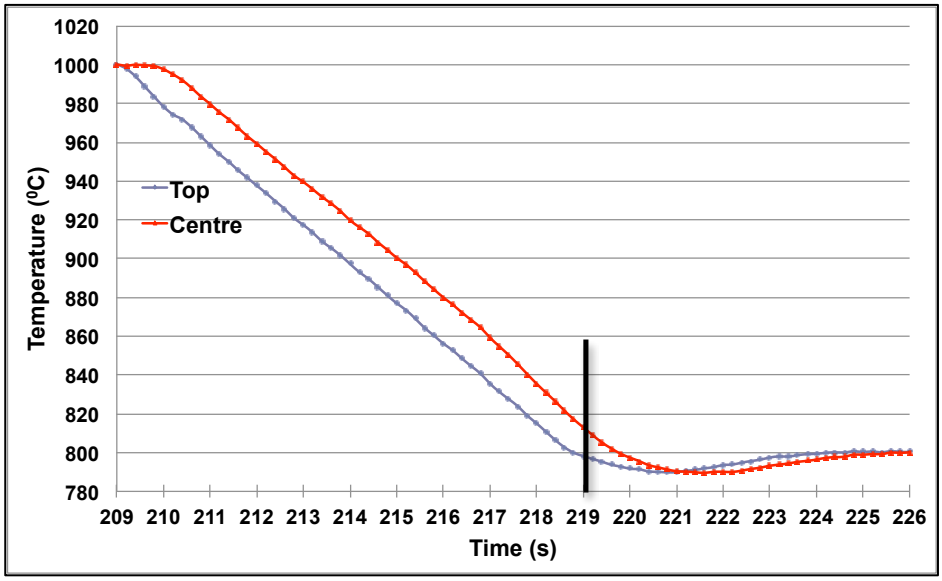

Figure 98: Temperature profiles of top surface and centre of PSC sample at the average 20°C/s forced-air cooling rate from 1000°C to 800°C with the CT at sub-surface of specimen

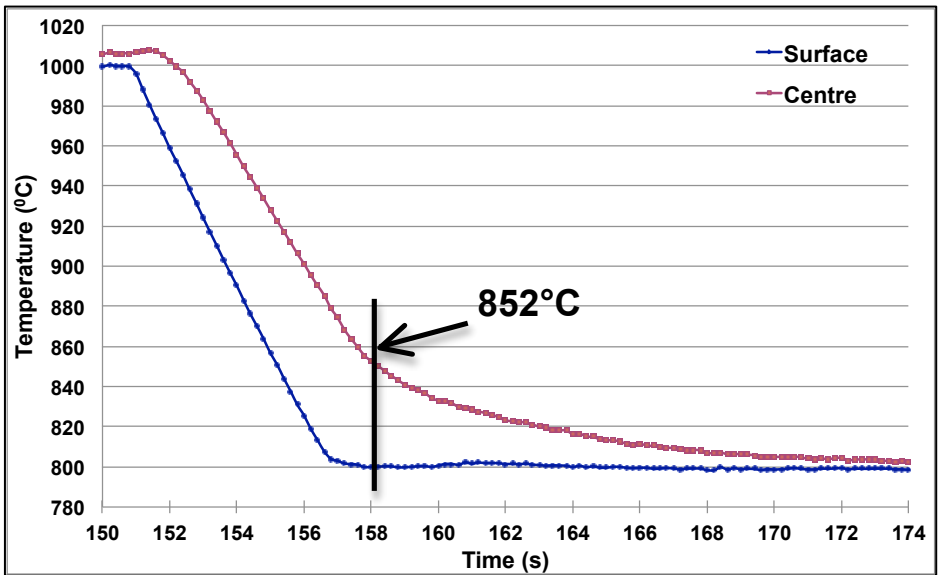

Figure 99: Temperature profiles of top surface and centre of PSC sample at the average 35°C/s forced-air cooling rate from 1000°C to 800°C with the CT at sub-surface of specimen

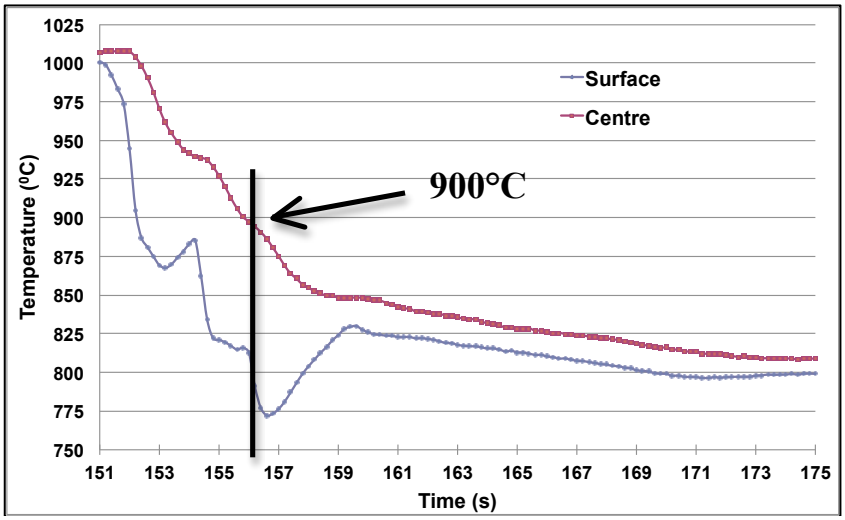

Figure 100: Temperature profiles of top surface and centre of PSC sample at the average 40°C/s mist cooling rate from 1000°C and 800°C with the CT at sub-surface of specimen

4.3.5. Cooling Profiles inside PSC Specimens at the Accelerated Cooling Temperature Range

As mentioned in Experimental chapter Section 3.5.1, cooling profiles from 900°C to room temperature at the different locations of PSC samples under three different cooling rates (5, 10 and 15°C/s) were determined and display in the following Figures 101-103 in which the letters S, T, H, C and B, represent surface, top, half (quarter), centre and bottom through thickness, while L, M and R means, left, middle and right, across width respectively. For examples, TS means at the top surface while BH indicates at the bottom half of PSC sample.

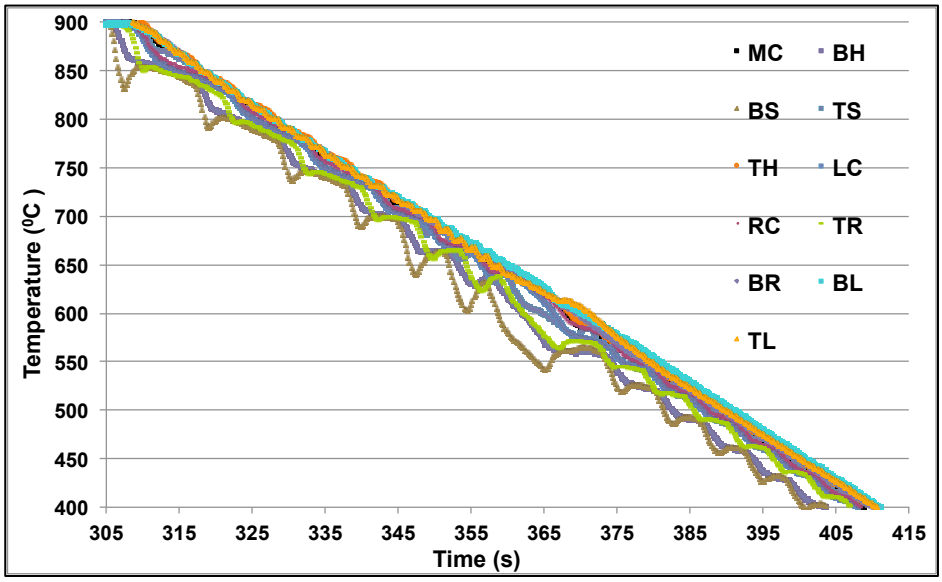

Figure 101: Cooling profiles at the different positions of standard 10mm PSC sample under 5°C/s linear cooling rate

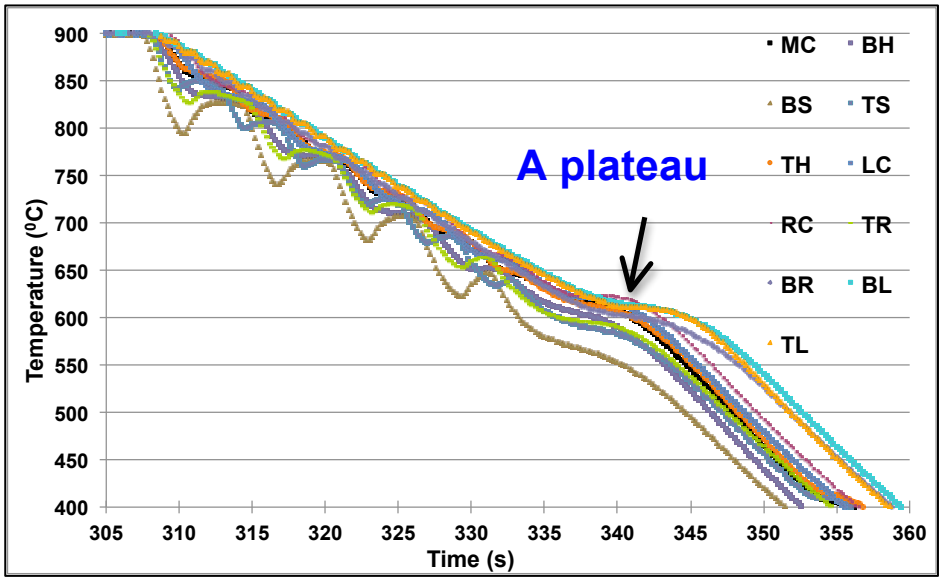

Figure 102: Cooling profiles at the different positions of standard 10mm PSC sample under 10°C/s linear cooling rate

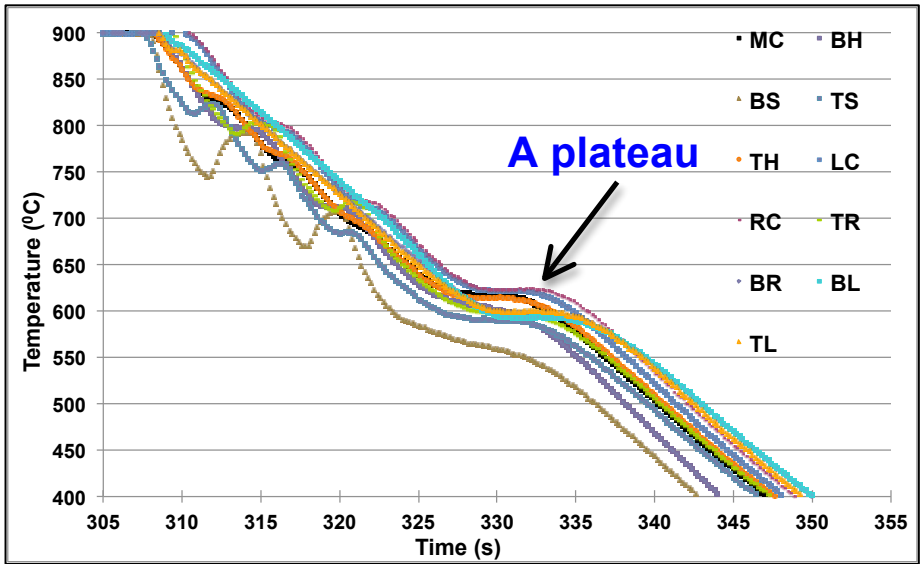

Figure 103: Cooling profiles at the different positions of standard 10mm PSC sample under 15°C/s cooling rate

Due to a maximum of only three thermocouples inserted into the pre-drilled holes of the PSC specimen in one cooling test, so the temperature distributions at the 11 different locations of the whole PSC samples shown in the above Figures 101-103 were combined all the thermocouples temperature readings from four similar cooling tests with the same test conditions and forced-air cooling rate (only dissimilarity was the locations of inserted thermocouples described in Experimental chapter Section 3.5.1 at Table 6). As the applied cooling rate increased from 5°C/s to 10°C/s and then to 15°C/s, the temperature differences of 11 specified locations inside the 10mm thickness of PSC specimen increased due to higher applied cooling rate induced larger temperature gradient across thickness. Moreover, in

Figures 102 and 103 there were plateaus (temperature was almost constant for a certain time) around 600°C at the cooling curves which possible indicate the phase transformation (pearlite formation releasing extra latent heat) of C-Mn steel. However in the Figure 101, at the applied cooling rate, 5°C/s, there was not a plateau at the cooling curve (possible the cooling control system was able to counter the tendency to exhibit a platen).

As shown in Table 12 at which under two different applied cooling rates, 5°C/s and 15°C/s, the exactly temperature readings and distributions inside PSC specimen at the two different testing times: 380th and 330th second respectively were observed and analysed. The results show that from the top and the bottom surfaces towards the interior of PSC sample, the temperature generally increased and temperature difference was larger when the applied cooling rate increased from 5°C/s to 15°C/s. However, there was an exception when the cooling rate was 5°C/s, the hottest place was at the left hand side of bottom surface. Additionally, the hottest locations were at the right and left sides of middle specimen possible due to the hot handles (robotic arms) perhaps provided extra heat through heat conduction when they were holding the edges of the PSC specimen.

Table 12: Temperature distributions inside PSC sample at the different testing time and two applied cooling rates: 5°C/s (left hand side) and 15°C/s (right hand side)

At the 380th second, temperature (°C) distribution in PSC sample at the cooling rate 5°C/s			
	Left	Centre	Right
Top Surface	548	543	523
Top Half		548	
Middle	535	543	541
Bottom Half		520	
Bottom Surface	555	521	544

At the 330th second, temperature (°C) distribution in PSC sample at the cooling rate 15°C/s			
	Left	Centre	Right
Top Surface	600	590	598
Top Half		614	
Middle	622	618	623
Bottom Half		602	
Bottom Surface	595	559	600

Therefore, from the results of these forced cooling tests through compressed air blowing starting from 900°C to room temperature, the FTTU inside the TMC machine is capable of carrying out the well-controlled cooling practices with at the different applied cooling rates.

4.4. Finite Element Modelling Temperature Distributions inside Partially Rolled Steel Plates during Holding Period

In the following sections, different predicted temperature profiles across the different thickness (mainly at the surface and centre) of the partially as-rolled heavy plate were determined from the commercial Abaqus finite element (FE) program, and a in-house simulation model developed by Tata Steel Europe RD&T, which were explained clearly at Section 3.6.2. In general, these results indicate that the Abaqus FE model can predict the temperature distribution or profiles from the surface towards the centre of heavy plate as long as the correct boundary conditions, such as heat transfer coefficients between the plate surface and ambient (natural-air or spraying water), were defined in the simulation. There were two different initial conditions: uniform and non-uniform temperature distributions inside heavy plate prior to simulation, which are described in the following sections.

4.4.1. Modelling Temperature Distributions at the Uniform Temperature of Initial Conditions

First, it may useful to mention again that the initial conditions for the following results of the holding period cooling simulation were uniform temperature across different thickness at the beginning of prediction, i.e., 1000°C from surface to centre; the ambient temperature is 20°C, and heat transfer only takes place on the top and bottom surfaces of steel plate. Moreover, the first stage-cooling period stopped at which the centre temperature of plate reached 800°C followed by the second stage-homogenisation period where it was assumed that there is no interaction between the ambient and surface of plate so purely heat conduction within the plate due to the temperature differences within the plate. Figure 104 presents an example of Abaqus FE predicted results of the temperature distribution across 10mm steel plate under forced cooling, and then the temperature readings at the specific chosen locations across thickness can be plotted against cooling time into different temperature profiles.

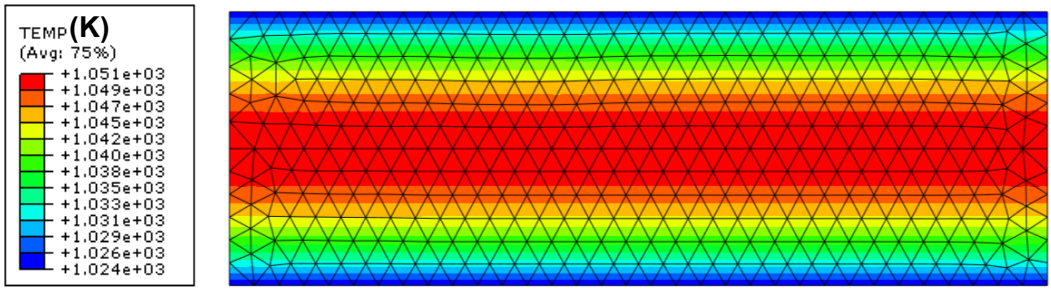

Figure 104: An example of predicted temperature (in Kevin) distribution across 10mm steel plate after cooling by the Abaqus finite element (FE) model

The following Figure 105 consists of dissimilar plate surface and centre temperature profiles of 10 steel plates with 10 different thicknesses (from 10, 20, 30…till 100mm) under the same initial, boundaries and forced cooling conditions, which were described at Section 3.6.2. It is clearly shown in Figure 105 that as the plate thickness increased the degree of variations between plate surface and centre temperature profiles were getting larger. Additionally, the plate surface temperature at the end of the first cooling stage is significantly lower as the increased in plate thickness took longer time to reduce the centre temperature down to 800°C. For the second homogenisation or surface recalescence stage, for the thicker steel plate, a longer time period was required for the plate surface to reach the same temperature as the centre value.

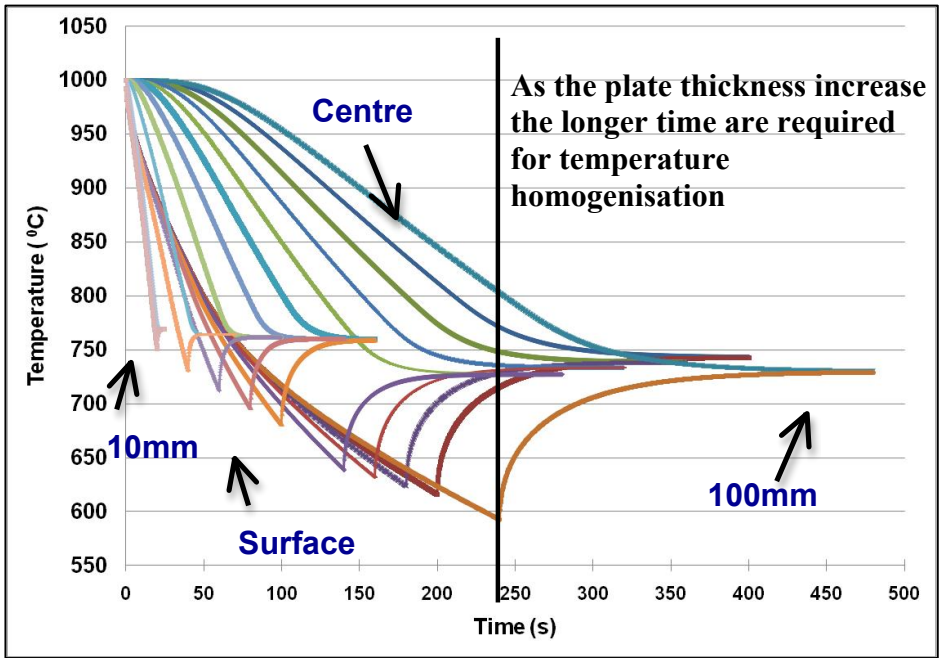

Figure 105: Centre and surface cooling profiles from 1000°C to 800°C of different plate thicknesses (from 100mm down to10mm plates) with HTC of 200 - 400W/m^{2}K

According to the centre temperature profiles of the 10 different plate thicknesses in Figure 105 above, the cooling time for the centre temperature reducing from 1000°C to 800°C of each plate thickness was easily determined, and presented in Figure 106 where a relationship of cooling time as function of thickness is also included. Next, the corresponding average cooling rate from 1000°C to 800°C was calculated by the temperature gap 200°C divided by the centre cooling time, and the result is shown in Figure 107 in which the cooling rate is in a power function of plate thickness and the relationship suggests that at the same amount forced cooling power, i.e. the same heat transfer coefficient applied at the surface, average cooling rate decrease as the plate thickness increase. Furthermore, when the plate thickness is above 50mm, the centre average cooling rate is below 2°C/s, presented in Figure 107.

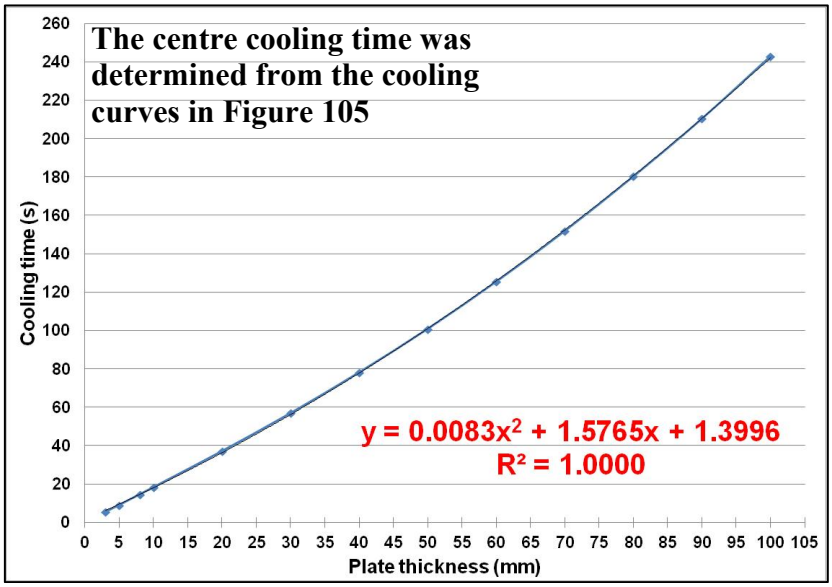

Figure 106: Centre cooling time 1000°C to 800°C under the same cooling condition as function of plate thickness

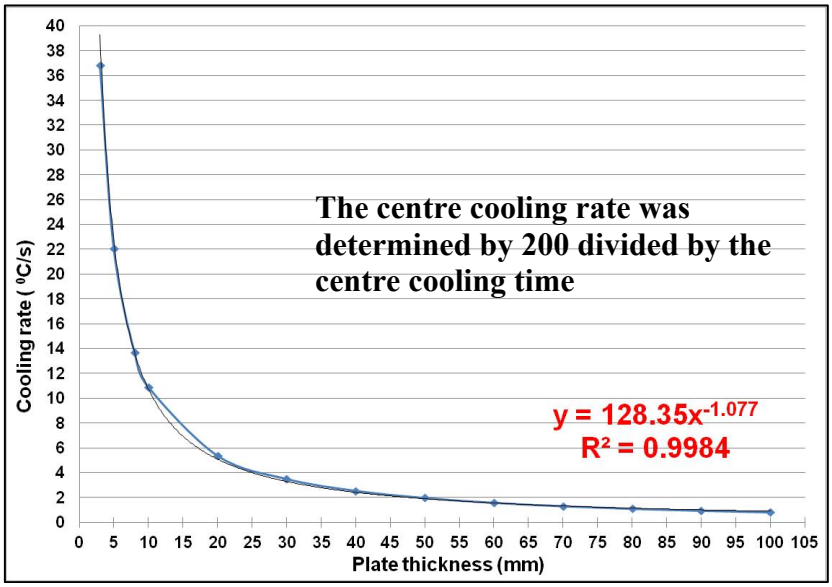

Figure 107: Average centre cooling rate 1000°C to 800°C under the same cooling condition as function of plate thickness

Due to the 100mm was the programmed holding thickness during the holding period at the commercial hot rolling schedule of microalloyed steel 8AK39, further temperature distribution across 100mm thickness under different cooling conditions were carried out. Firstly, under natural-air cooling situation, much smaller heat transfer coefficient ($10Wm^{-2}K^{-1}$) was applied at the boundary condition and different temperature cooling profiles at the specific locations of 100mm heavy plate are displayed in Figure 108. Second, to compare with natural-air cooling condition, forced cooling simulation of 100mm heavy plate was also taken place, and the value of heat transfer coefficient was in a linear relationship with heavy

plate surface temperature, i.e., from the maximum value 400W/m^{2}K at 800°C down to a minimum value of 200W/m^{2}K at 1000°C. It is clearly shown in Figures 109 and 110 that centre temperature profile reached 800°C at the considerably faster cooling time (in 240s) compared to the profile under natural-air cooling situation in Figure 108 (in 690s), but induced a significantly larger temperature gradient (ΔT=210°C) across the 100mm thickness at the end of cooling stage compared to the temperature difference (ΔT=50°C) in Figure 108.

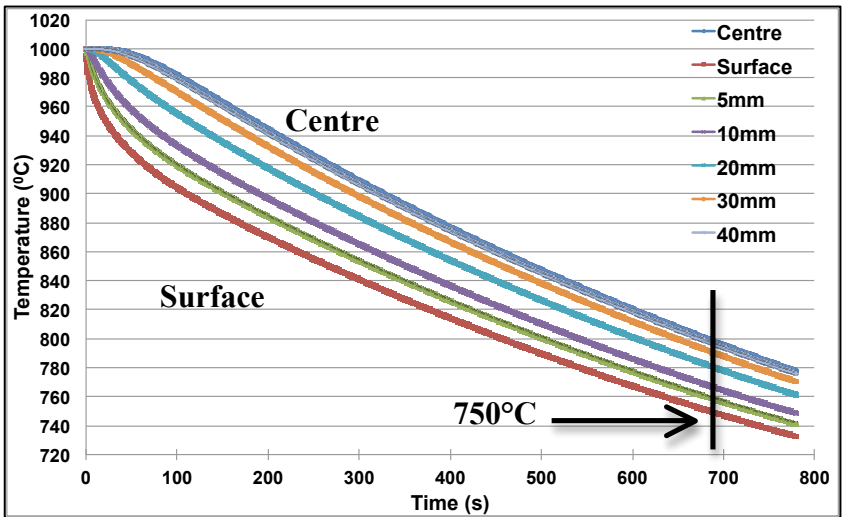

Figure 108: Temperature distributions across 100mm heavy plate under natural-air cooling simulation predicted by Abaqus FE model with HTC of 10Wm^{-2}K^{-1}

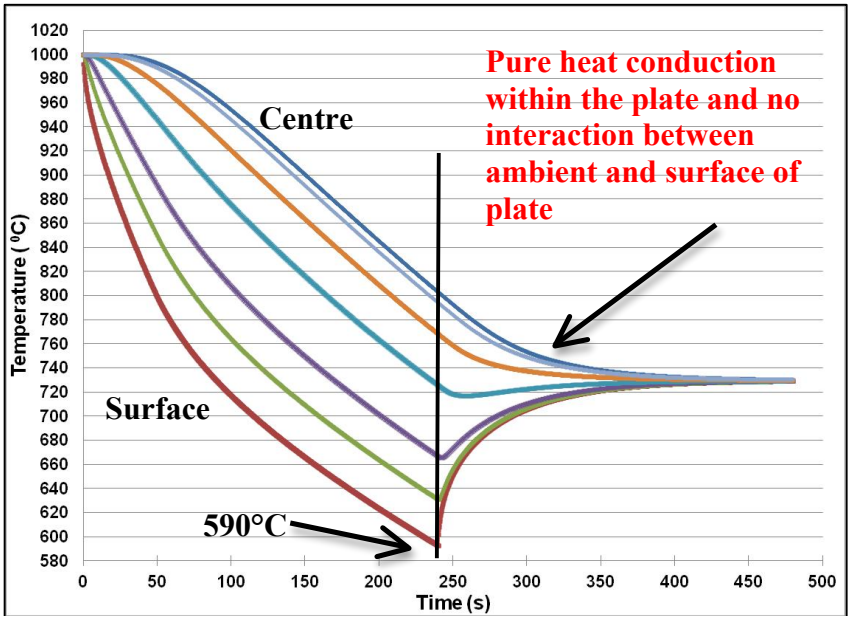

Figure 109: Temperature profiles of the different positions of 100mm steel plate during forced cooling (with HTC of 200 - 400W/m^{2}K) and isothermal holding stages

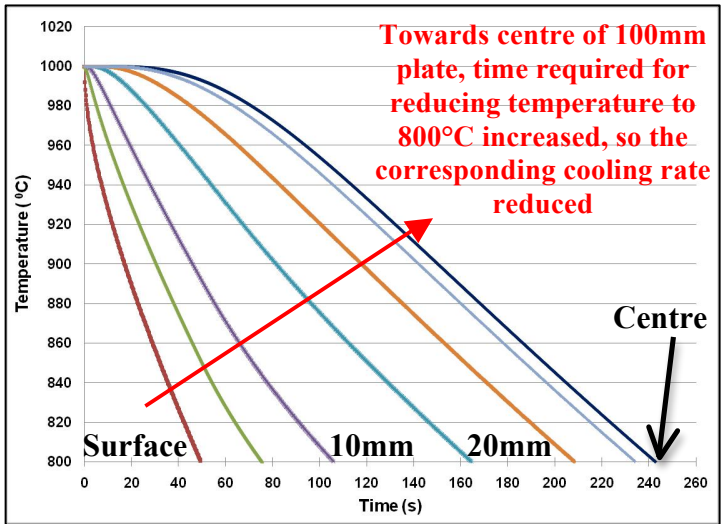

Figure 110: Time required for the plate centre cooling down 1000°C to 800°C at the different positions of 100mm plain carbon plate

As illustrated in Figures 105 and 109, at the second homogenisation stage the boundary condition was assumed that no heat transfer takes place between the plate surface and ambient. However, it is a well-known fact that after the initial forced cooling stage, the heavy plate surface is still subjected to the natural-air cooling. Therefore, at the second stage, radiation heat transfer was taken place between the plate surface and ambient (20°C) with emissivity λ=0.85, and the heat transfer coefficient was a constant value of $10 Wm^{-2}K^{-1}$. The associated results of the temperature distributions across the 100mm and 10mm plates are shown in the following Figures 111 and 112 respectively, and there are still some temperature gradients across thickness after the second natural-air cooling simulation stage. Moreover, the simulation time was significantly shorter for the intermediated forced cooling (IFC) followed by natural-air cooling than the time required for the nature-air cooling only reaching the same target temperature in Figure 112.

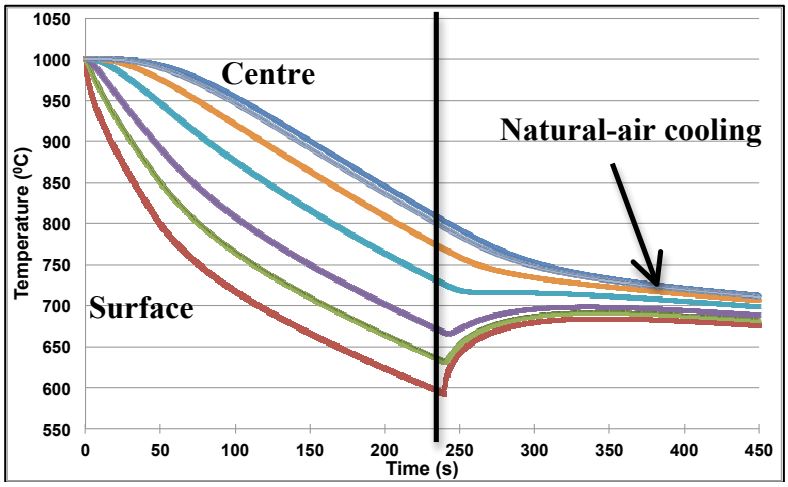

Figure 111: Temperature profiles of the different positions of 100mm steel plate during water spraying and natural-air cooling stages

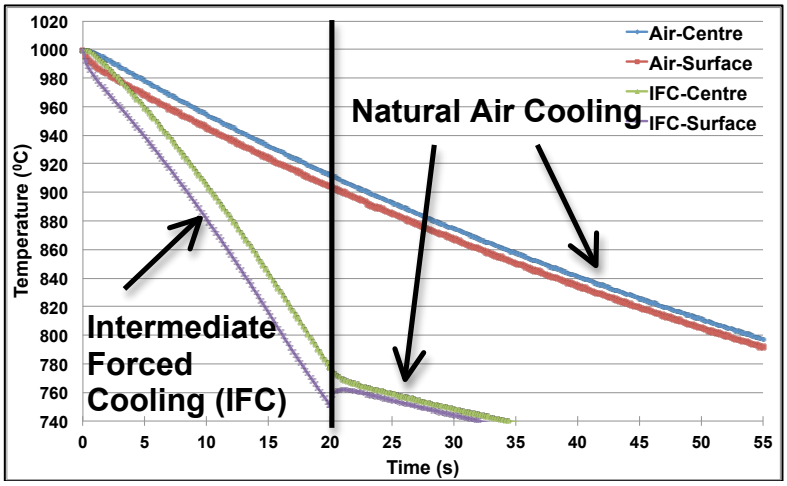

Figure 112: Centre and surface cooling profiles of 10mm plate during holding period during different cooling conditions: natural-air cooling and the IFC followed by natural air cooling

4.4.2. Temperature Distributions at the Non-Uniform Initial Conditions

For the second initial simulation conditions, the temperature distribution inside the partially rolled (after high temperature rough rolling) heavy plate at the start of holding period (HP) was set to be not uniform, which means the initial temperature of interior was much hotter than the cold surface of heavy plate. Therefore, the industrial hot rolling schedule of the Nb steel 8AK39 was inputted into another in-house simulation model developed by Tata Steel Europe RD&T to predict the temperature distribution across as-rolling heavy plate from roughing to finishing, particular focused on temperature profiles inside the 100mm thickness of partially rolled plate during holding period under natural-air cooling and IFC cooling conditions, presented in Figures 113 and 114 respectively.

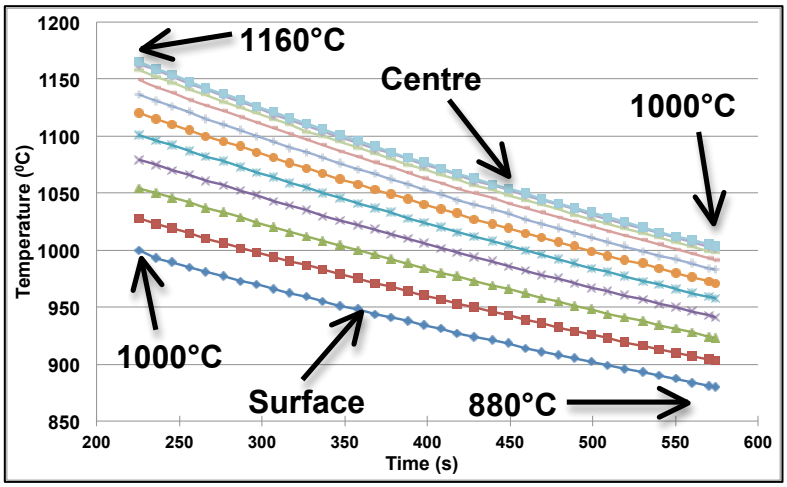

Figure 113: Temperature distribution of 100mm partial-rolled heavy plate during HP under natural-air cooling condition predicted by industrial in-house model

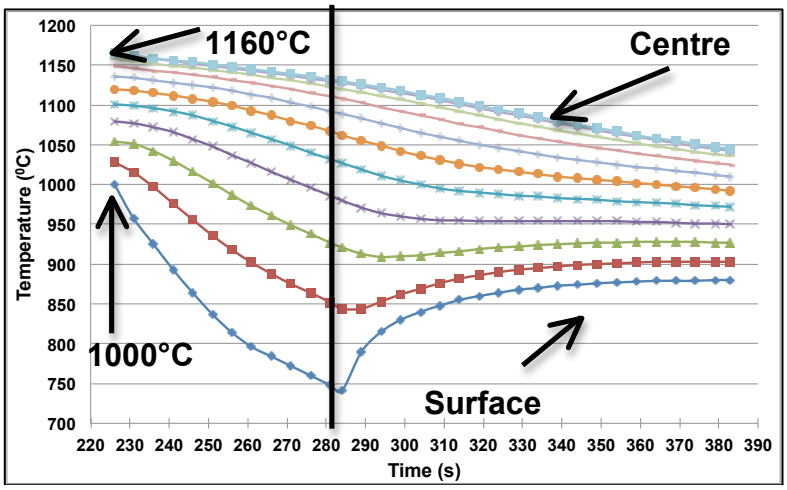

Figure 114: Predicted temperature distribution of 100mm partial-rolled heavy plate during HP under the IFC condition (water spraying and then natural-air cooling)

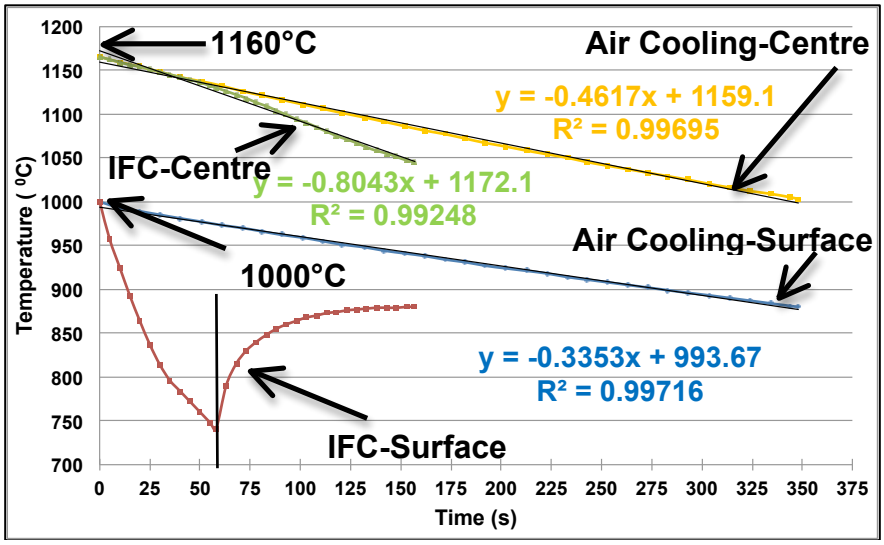

Figure 115: Predicted centre and surface temperature profiles of 100mm intermediate as-rolled plate under natural-air and water cooling situations

As shown in Figures 113 to 115, during the HP, the temperature differences between the surface and interior of the heavy plate are large (with different initial cooling start temperatures - 1160°C and 1000°C respectively) regardless of natural-air cooling or the IFC was applied during holding period cooling simulation. Furthermore, by comparing the Figures 113 and 114 to the previous Figure 111, the in-house model provides a larger temperature variation across the thickness and a higher plate centre and surface temperatures at the end of holding period compared to the results of Abaqus FE model, which is possibly due to the different initial conditions and dissimilar heat transfer coefficients were used in these two models. According to the average centre cooling rates in Figure 115, the centre temperature was reduced nearly twice as fast (0.80°C/s) in the IFC situation than that of natural-air cooling (0.46°C/s).

The following Figures 116 and 117 present the predicted temperature profiles from two Tata steel in-house simulation models. It may be helpful to mention that the first model which has been used for designing the commercial hot rolling schedule calculated the mean and surface temperature profiles at the roughing and finishing stages in both figures. The other three temperature profiles were the result of holding period cooling simulation at the surface, quarter and centre of 100mm partially rolled heavy plate under natural-air cooling and the IFC in Figures 116 and 117 respectively, which were predicted by the same in-house model for obtaining the temperature distribution across the thickness during the HP shown in the previous Figures 113-115. Moreover, the simulated temperature profiles at the surface and quarter thickness of heavy plate during the HP fit close to the surface and mean profiles in both Figures 116 and 117. Finally, the temperature profiles at the quarter and centre of plate only changed slightly when applied increased cooling rate from natural-air cooling in Figure 116 to IFC in Figure 117.

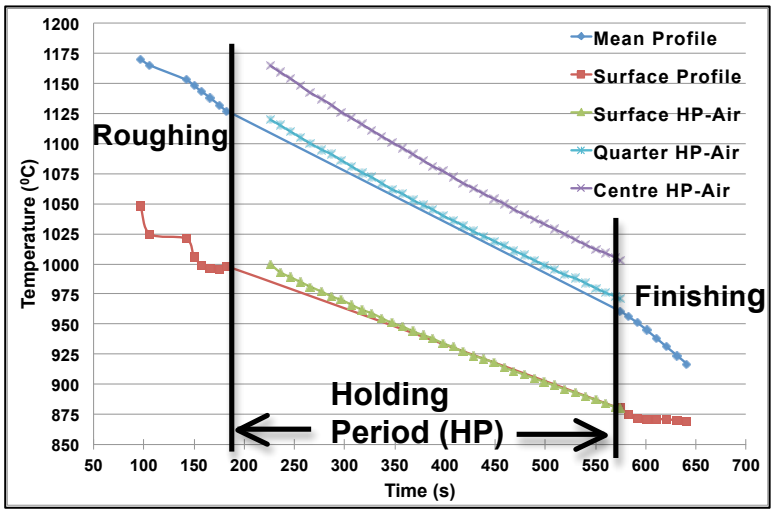

Figure 116: Different predicted temperature profiles across thickness of as-rolling heavy plate with natural-air cooling during the HP from two in-house models

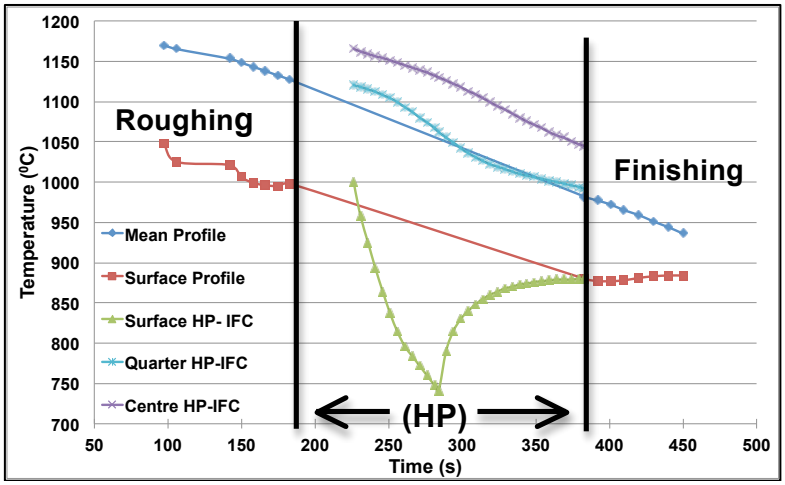

Figure 117: Different predicted temperature profiles across thickness of as-rolling heavy plate with the IFC during the HP from two in-house models

4.5. Simulation of Industrial Hot Rolling Plain Carbon Steel Production

In general, the laboratory simulation process of commercial hot rolling plain carbon steel plate (8AK43) production involved three important stages: started with 2-pass roughing of plain carbon steel C with the same total amount of industrial roughing strain 0.8 on the laboratory Hille mill due to exact replication of the commercial roughing process is not important (Literature review Section 2.3.3.3); and then the as-roughed and water quenched plate was machined into several standard 10mm PSC samples for the 9-pass PSC testing with exactly the same parameters of the industrial finish rolling process was taken place on the TMC machine; and finally, post-deformation natural-air cooling simulation of the 50mm as-rolled plate, the results of which are descried in the following sections.

4.5.1. Temperature Profile of 2-pass Roughing on the Hille Mill

For the first test, after a one hour heat-treatment at about 1165°C for the temperature homogenisation inside a roughly 25mm steel plate, the first 9 industrial roughing passes were simulated through 2 passes with the same total applied strain ε_{total}=0.8 on the 50 tonnes laboratory Hille mill, and the recorded temperature profile at the plate centre during simulation is presented in Figure 118 below. It may useful to describe again that as soon as the second reduction was finished, the deformed plate was then quickly manually dropped into a large cold-water tank to quickly freeze the 2-pass as-rolled microstructure at about 124°C/s from 950°C to 350°C (see Figure 119) and then the as-rolled plate was machined into two or three standard 10mm PSC samples for later 9-pass PSC finishing simulation.

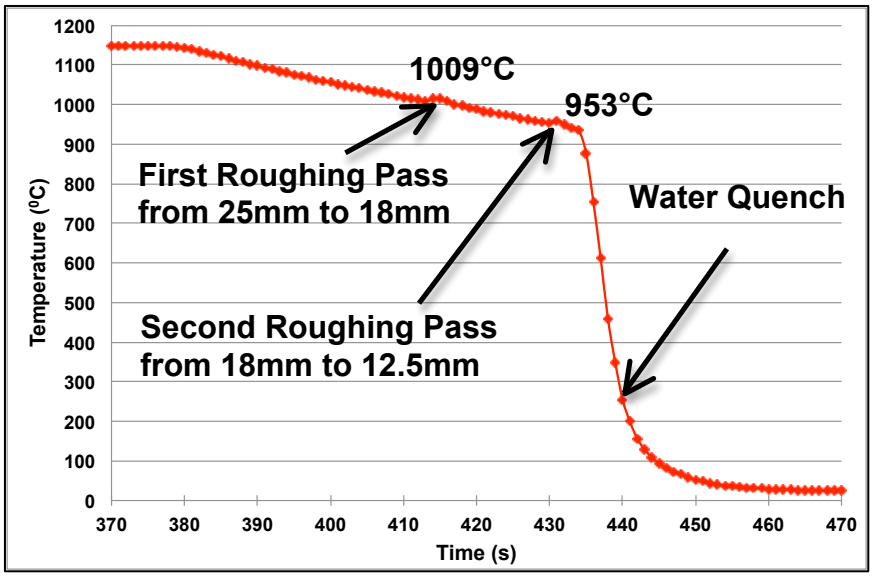

Figure 118: Recorded centre temperature profile (roughing and water quenching) of 2-pass roughing of plain carbon steel C on the laboratory Hille mill

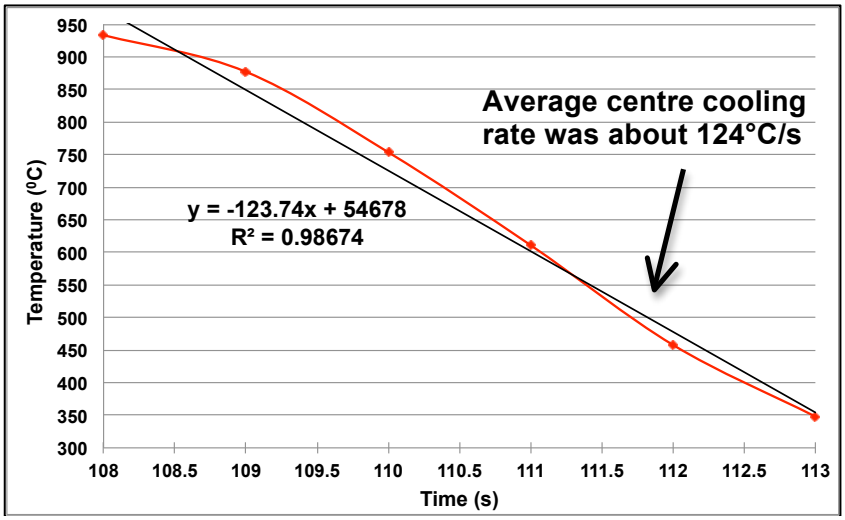

Figure 119: Centre cooling rate of water quenched as-roughed 12.5mm steel plate

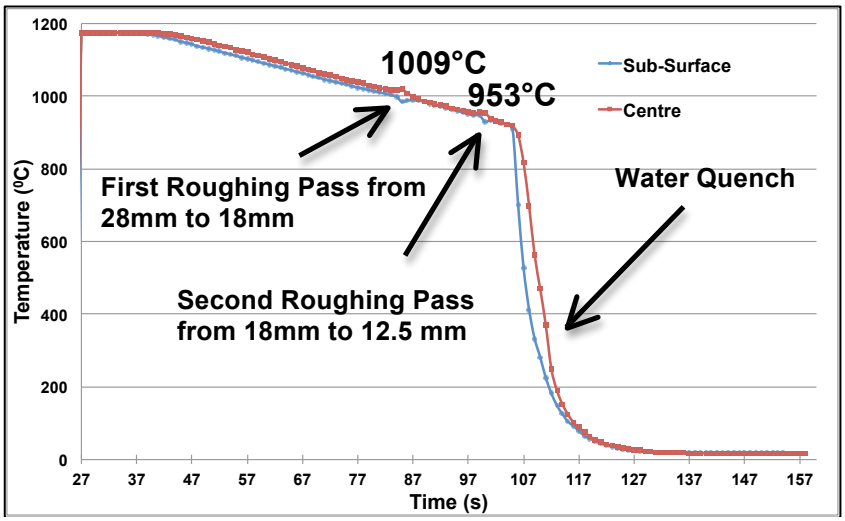

Figure 120: Recorded temperature profiles of sub-surface (2mm below surface) and centre of steel plate during 2-pass roughing and water quenched the as-roughed 12.5mm plate

For the second test, with the same 2-pass laboratory rough rolling settings on the Hille mill as in test one, two thermocouples were embedded into a slightly thicker 28mm plain carbon steel C plate to investigate and record its temperature distribution during the 2-pass roughing simulation: one was 2mm below the middle surface and the other one was at the middle centre of plate (14mm below surface), shown in Figures 120 and 121 in which similar temperature profiles are found as same as the first test in earlier Figure 118. Furthermore, it is clearly presented in Figure 121 that during cooling from the reheating temperature 1165°C to the first reduction there was a small temperature difference (about 20°C) between the sub-surface and centre of plate, and a little amount of deformation heat increased centre temperature somewhat during the two roughing passes in which temperature dropped slightly at the sub-surface due to the chilling effect from the cold work roll. After each reduction temperatures were equalised quickly at the sub-surface and centre of plate.

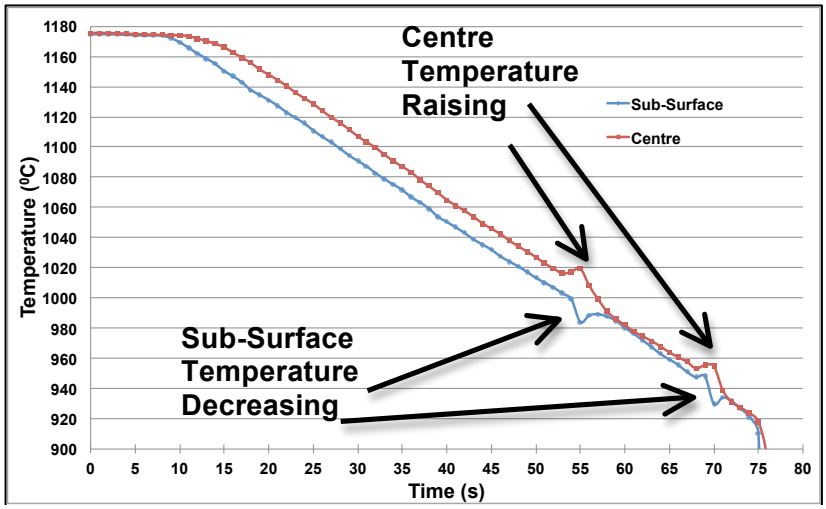

Figure 121: Recorded temperature profiles at the sub-surface and centre of as-roughing plain carbon steel C plate prior to water quenching

4.5.2. 9-pass and 2-Pass PSC Simulation on the TMC Machine

The second stage of simulation was to use a 2-pass roughed (2R) and water quenched PSC sample for replicating the actual 9-pass industrial finish rolling (Experiment Chapter 3.8.3) on the TMC machine. Before conducting the multipass PSC testing, two thermocouples were inserted into the sub-surface (1mm below surface) and centre (5mm below surface- the controlled thermocouple) of the samples to monitor the temperature profiles during whole simulations. Due to the fact that more than 4-pass PSC deformations were never previously carried out on the TMC machine, the PSC samples frequently dropped off from the robotic arms during the transfers (18 times for the 9-pass deformation) between the FTTU and test furnace, or stuck between the deformation platens to cause the corresponding deformed microstructures to be either inaccessible or damaged (see more in Discussion chapter). Therefore, after many testing trials, and before the new updated TMC program was finally installed at the last stage of this research project, the best solution was that the 9-pass PSC tests were performed inside the test furnace and required only 2 transfers in and out of test furnace without taking out into the FTTU for temperature control at each gap time of 9-pass deformation.

Before showing the flow curves (equivalent stress versus equivalent strain) of different PSC tests, the associated recorded temperature profiles of 9-pass finishing (9F) and 2-pass finishing (2F) PSC tests, were analysed and compared first, and shown in the following Figures 122-124 in which three multipass PSC tests with dissimilar test schedules or different initial conditions were included. For example, in Figure 122 it presents the temperature profiles of test one that the 9-pass PSC deformations were kept inside the test furnace whole time, nearly the same temperature raising profiles were found at the sub-surface (1mm below

surface) and centre of deforming PSC sample of plain carbon steel C that has been previously 2-pass roughed (2R) and water quenched on the laboratory Hille mill. However, the biggest disadvantage for keeping the PSC sample all the while inside the test furnace during the 9-pass deformations, the actual temperature profiles of deforming PSC sample in Figure 122 were gradually increased compared to the target 9-pass finishing rolling temperatures should be up and down presented in the Experimental Chapter at Table 7.

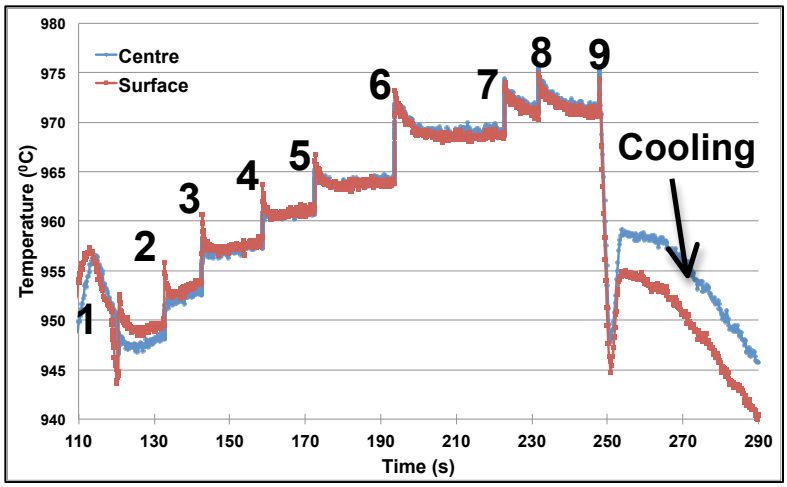

Figure 122: Measured temperature profiles at the centre and surface of deformed PSC sample (plain carbon steel C) during 9-pass PSC simulation inside the test furnace

As mentioned earlier there were many failures on performing the 9-pass PSC tests under the condition that the PSC sample was scheduled to transfer in and out the test furnace and FTTU 18 times, only one trial test was done successfully at the earlier stage of project and the corresponding complex centre and sub-surface temperature profiles inside the successful dummy PSC specimen are displayed in Figure 123 in which there are some errors on the centre temperature reading (possible some issues on temperature coupling). Moreover, at the last 3 passes (from the 7^{th} to 9^{th} pass), the temperature differences between sub-surface and centre of specimen were greater than those in previous 6 passes.

Finally, the third successful test was a 2-finish (2F) pass PSC test with the same total applied strain $\varepsilon_{Total} = 1.27$ and simulation time as the 9-pass PSC test, and the corresponding surface and centre temperature profiles presented in Figure 124. Due to a 148 seconds gap time between the two passes was carried out inside the test furnace, the sample temperature slowly increased from 961°C to 965°C and the peak centre temperature (987°C) of the second deformation temperature in Figure 124 was higher than the peak temperature (975°C) of the 9^{th} pass in above Figures 122. Moreover, it is clearly shown in Figure 121 to Figure 124 that after the last pass, the temperature dropped about 35°C during the transfer from test furnace to the FTTU so more accurate temperature controls during multipass PSC simulation are required (described more in next Discussion Chapter).

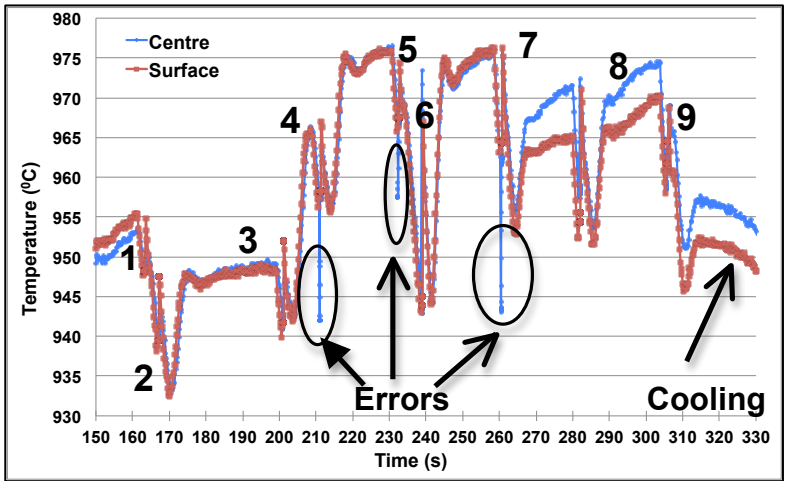

Figure 123: Complex recorded temperature profiles at the centre and surface of PSC sample during 9-pass PSC test with deforming specimen in and out of the test furnace

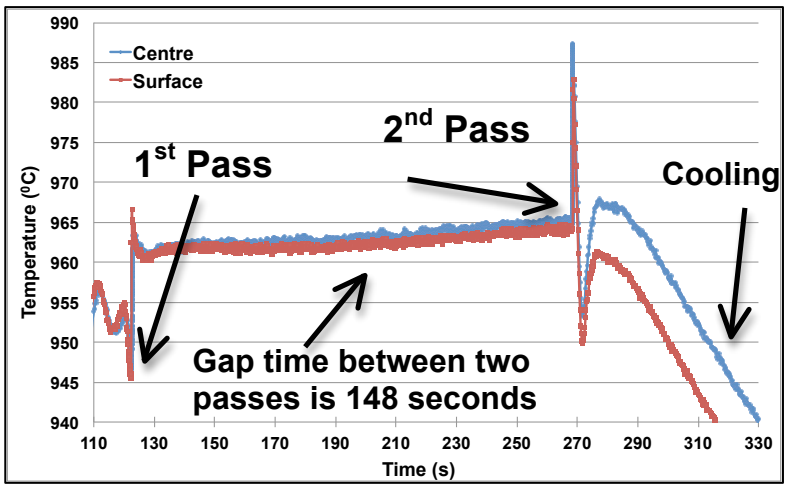

Figure 124: Measured temperature profiles at the centre and surface of deformed PSC sample during 2-pass PSC simulation inside the test furnace

The flow curves of two PSC tests (2R+9F, 2R+2F) are presented in Figure 125 in which with almost the same total applied strain ε_{Total} =1.2, the 2-finish (2F) passes had a higher flow stress than the value of 9-finish (9F) passes. By comparing the flow curve of 2R+2F in Figure 125 or Figure 126 to the schematic flow curve of dynamic recrystallisation (DRX) in Figure 12 (Literature review chapter Section 2.3.1.2), it suggests that the DRX occurred during the deformations of 2-finishing passes due to the large applied and accumulated strain 0.5 and 0.7 at the first and second pass respectively and excessed the peak strain ε_c of each pass for initiating the DRX, illustrated clearly in Figure 126. Additionally, it is clearly displayed in both Figures 125 and 126 that static softening took place at the each interval or gap time of flow curves because the deformation temperatures were too high to retain work or strain hardening. Furthermore, during the deformation the temperature inside the PSC sample was nominally constant but gradually increased due to the deformation heat, shown in Figure 126,

and the magnitude of temperature increment depends on the applied strain and test furnace temperature.

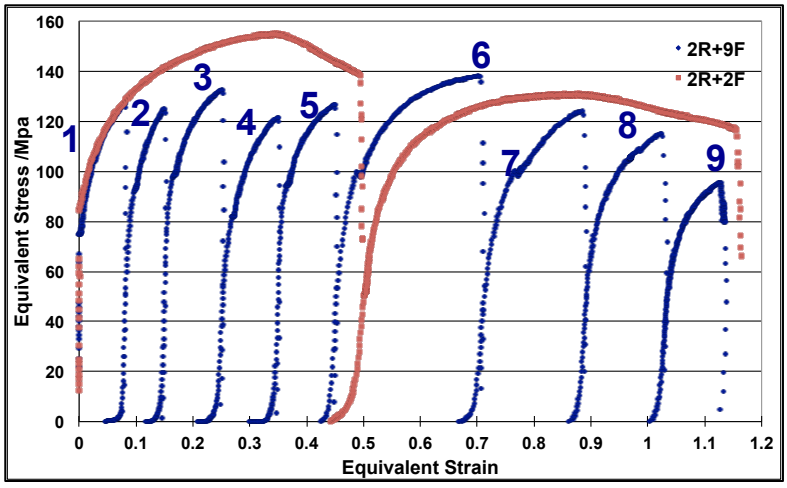

Figure 125: Comparison of flow curves between 2- and 9- finish passes with the same total finishing strain and simulation time

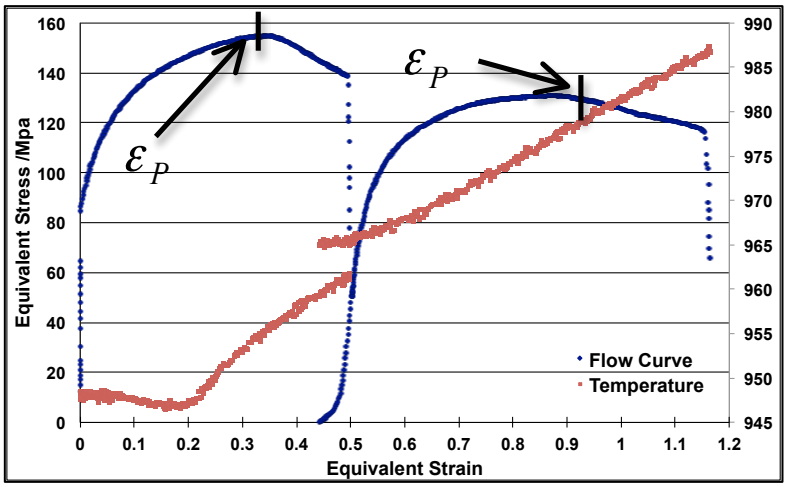

Figure 126: Relationship between flow curve and deformation temperatures under test conditions of 2R+2F

4.5.3. Post-Deformation Air Cooling Profiles

The last stage of industrial plain carbon steel production was to replicate post-rolling natural-air cooling profile of 50mm steel plate. As described in the Experimental chapter Section 3.8.4, the centre air-cooling profile for the 50mm plate was determined by interpolated (calculated the mean values) between the predicted temperature cooling profiles from the 40mm and 60mm steel plates in Figure 127 in which both cooling profiles were predicted by a Tata Steel Europe in-house finite difference model with conditions of 0.16C-0.3Si-0.84Mn steel composition, 30µm prior austenite grain size (PAGS) prior to cooling, heat transfer coefficient of 10W/m^{2}K, and ambient temperature of 20°C. According to the predicted 50mm

centre cooling profile in Figures 128 and 129, the average centre-cooling rate above 760°C was about 0.56°C/s, and from 760°C to 400°C the mean cooling rate was 0.38°C/s.

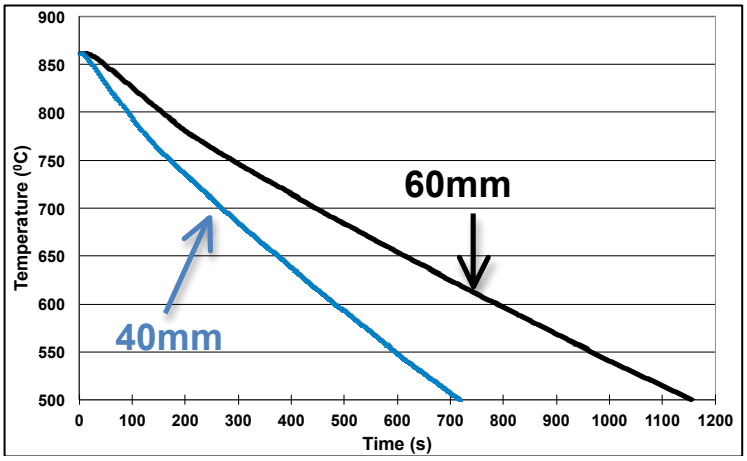

Figure 127: Predicted centre cooling profiles of 60mm and 40mm steel plates through phase transformation

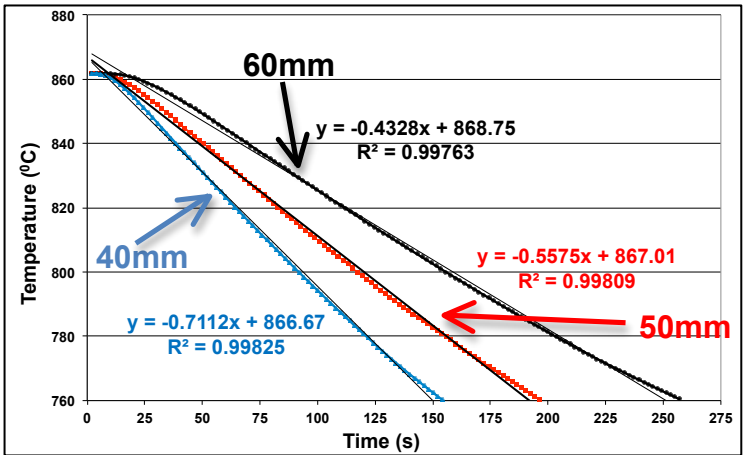

Figure 128: Average centre cooling profiles of 60mm, 50mm and 40mm steel plates above 760°C under natural-air cooling condition

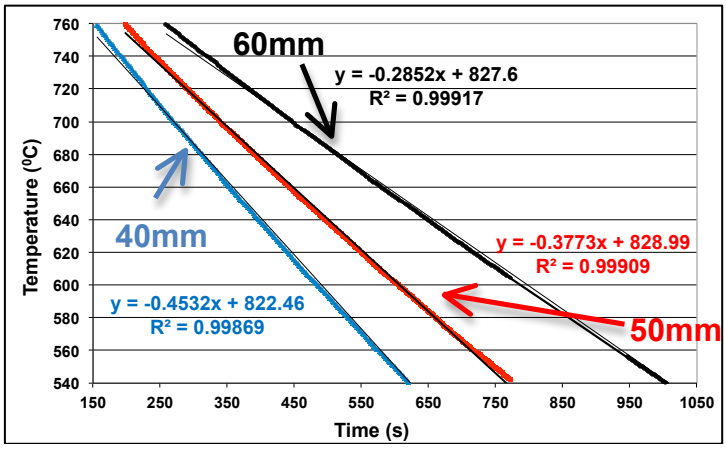

Figure 129: Average centre cooling profiles of 60mm, 50mm and 40mm steel plates below 760°C under natural-air cooling condition

4.5.4. Optical Microstructures and Ferrite Grain Size Measurement

It may be useful to notice again that the non-uniform microstructure distribution across the thickness of the deformed PSC sample (Literature review chapter Section 2.5.5), and an example of showing inhomogeneous microstructures at the surface and centre of deformed PSC specimen are clearly presented in the following Figures 130 and 131 respectively. Therefore, it is essential to choose the correct regions of the deformed sample for taking optical microstructures otherwise significantly errors could be induced in later ferrite grain size quantitative measurements.

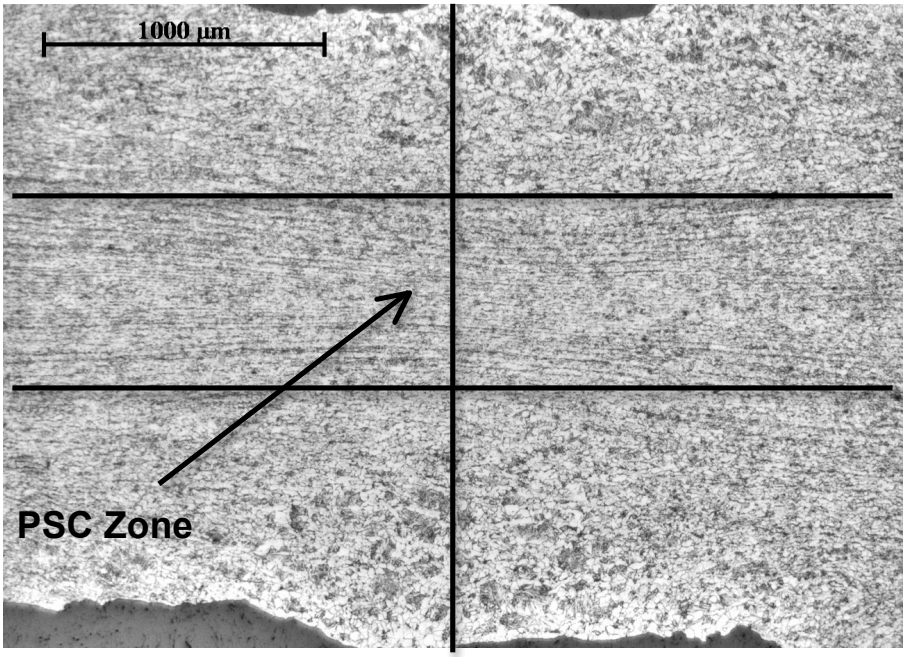

Figure 130: An example of microstructures across thickness of 2.8mm deformed PSC sample

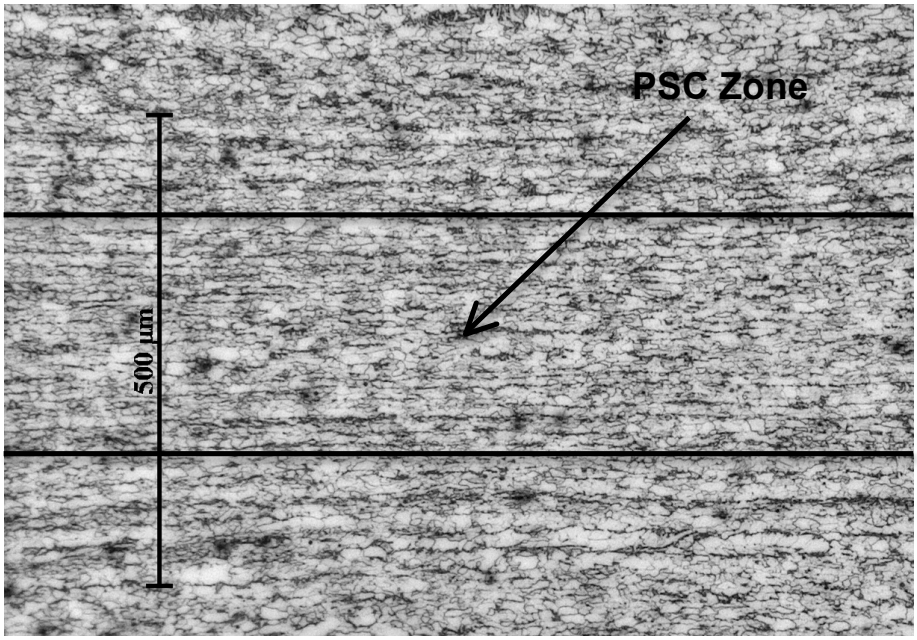

Figure 131: Plane strain compression (PSC) region inside the deformed PSC sample

As mentioned previously, only the centre of deformed PSC sample was subjected to the plane strain compression (PSC), which is similar to the condition inside industrial hot rolling steel plate and indicated as the PSC zone in Figures 130 and 131 where the observed ferrite grains in the PSC zone are much finer than those towards surface of PSC sample.

The different optical microstructures of 2R+9F and 2R+2F tests, which had the same total applied effective strain $\varepsilon_{Total} = 1.2$ and the identical post-deformation natural air cooling rates (above 760°C was about 0.56°C/s, and from 760°C to 400°C the mean cooling rate was 0.38°C/s), are showed in below Figures 132. According to the results of applying average linear intercept method in many correct optical images that were taken at the centre of deformed PSC samples, the test of 2R+9F+natural-air cooling gave a ferrite grain size of 15.8μm in rolling direction (RD) and 15.2μm in transverse direction (TD), while the test of 2R+2F+natural-air cooling gave finer grain size 11.6μm in the RD and 12.2μm in the TD. There was much more dynamic recrystallisation evident (see flow curves in earlier Figure 125) in the latter, which might explain the difference in finer average ferrite grain size. Moreover, Figure 132 shows that more distinguish pearlite-banding structures are found in the test of 2R+2F+natural-air cooling than those in 2R+9F+natural-air cooling.

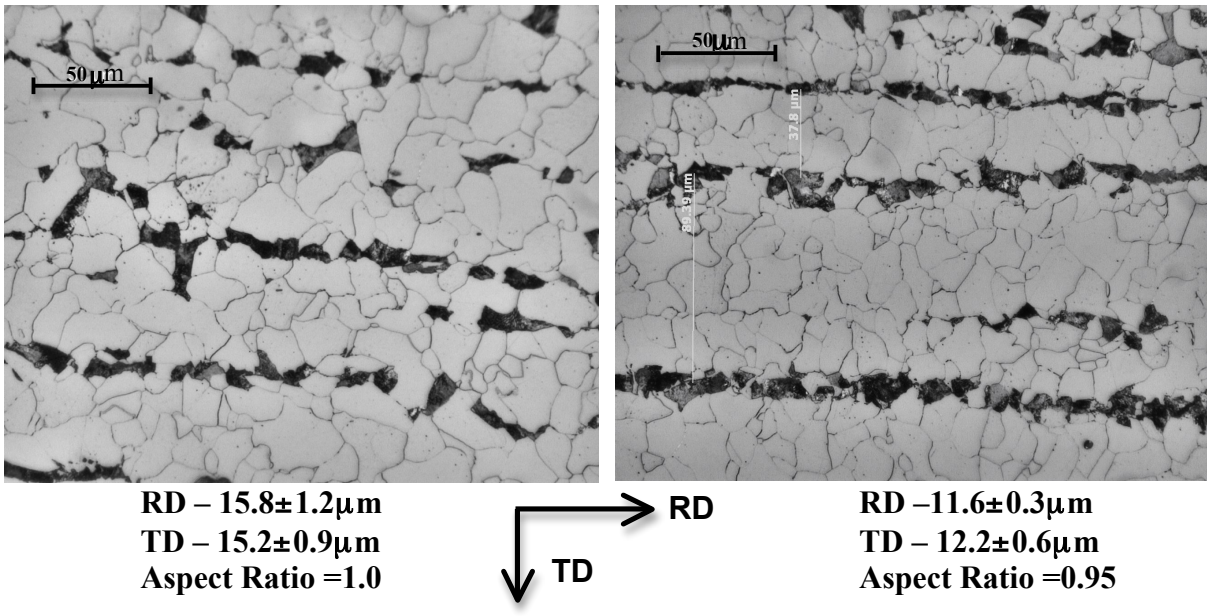

Figure 132: Optical microstructures of plain carbon steel C after 2 rough passes + 9 finish passes + natural-air cooling (left hand side) and after 2 rough passes + 2 finish passes + natural-air cooling with some banding structures (right hand side)

4.6. Multi-Pass Simulation of Microalloyed Steel Hot Rolling

Many multipass PSC tests (at least 3 passes) were carried out to replicate the microstructures development during the industrial 60mm microalloyed Nb steel plate (8AK39) hot rolling production with total applied effective strain ε_{Total} =1.65 as close as possible on the advanced TMC machine, and investigate the effects of different important hot rolling parameters, such as deformation temperature, applied strain, applying the intermediate forced cooling (IFC) on the prior austenite grain structures, flow curves and final as-rolled microstructures. These sophisticated multi-pass PSC tests represented the major portion of this research program and opened a new field of simulating the whole commercial hot rolling steel plate production.

4.6.1. Industrial Hot Rolling Schedule of Microalloyed Steel

According to the analysed results of 16-pass commercial hot rolling schedule for producing 60mm Nb steel plate 8AK39, presented in the following Figures 133-135, the whole hot rolling process was divided into four simulation stages on the TMC machine, and the detail testing schedules described clearly in earlier Table 8 and in Figures 63 and 64 of Experimental chapter Section 3.9.1. It may useful to mention again that according to the pre-rolling (intended) profile in Figure 133 below, the first 10 industrial roughing passes with total applied strain 0.9 were simulated through 3-pass PSC test with strain arrangement 0.4+0.4+0.1 was considered as stage one-roughing simulation, and then different cooling rates were applied during the holding period between the 10th and 11th pass was stage two.

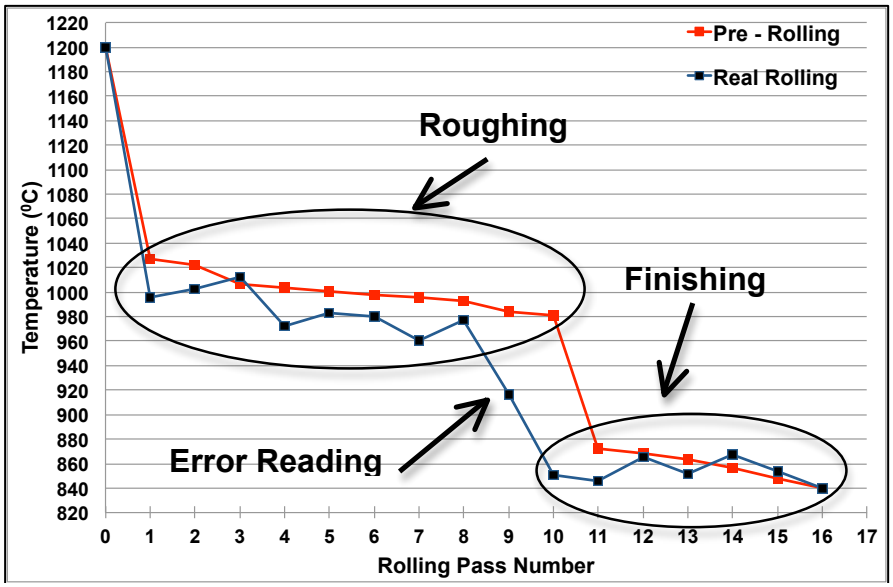

Figure 133: Differences in temperature profiles between industrial pre-rolling (intended) and actual hot rolling schedules

Moreover, the third stage was to perform the 5-pass (nominally 6 finishing passes but the last two passes with small reductions were combined into the 8th deformation) PSC finish rolling simulation with the same industrial finish rolling parameters, such as deformation temperatures in Figure 133, and reduction each pass in Figure 134. Finally, the last stage was to simulate post-deformation natural-air cooling (or applying the accelerated cooling in some tests) of 60mm as-rolled heavy plate. The corresponding simulation results of these four stages are presented in the later sections.

It is clearly shown in the Figures 134 and 135 that the applied reduction and rolling shape factor, m, of each pass in this chosen industrial hot rolling schedule were relatively low, particularly during the first 10-pass rough rolling with all the reductions were less than 10%. Additionally, due to the values of m in all 16 passes were less than the critical value of 0.8 (particularly the first 10 roughing passes m < 0.6) in Figure 135, inhomogeneous microstructures across thickness were most likely formed in the final as-rolled heavy plate.

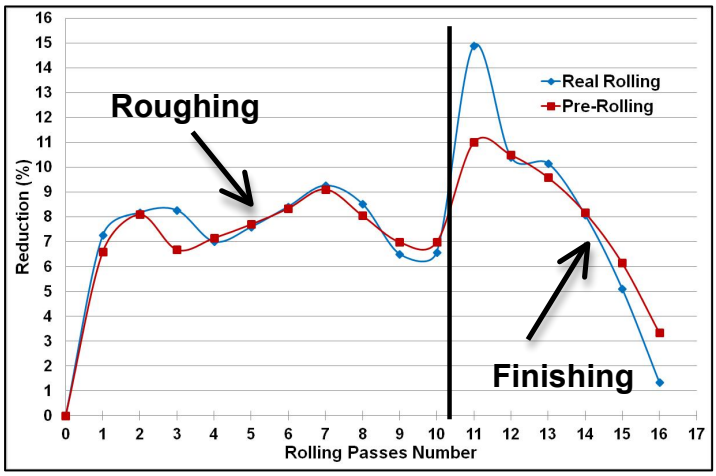

Figure 134: Differences in rolling reduction per pass (%) between industrial pre-rolling (intended) and real rolling schedules of microalloyed steel 8AK39

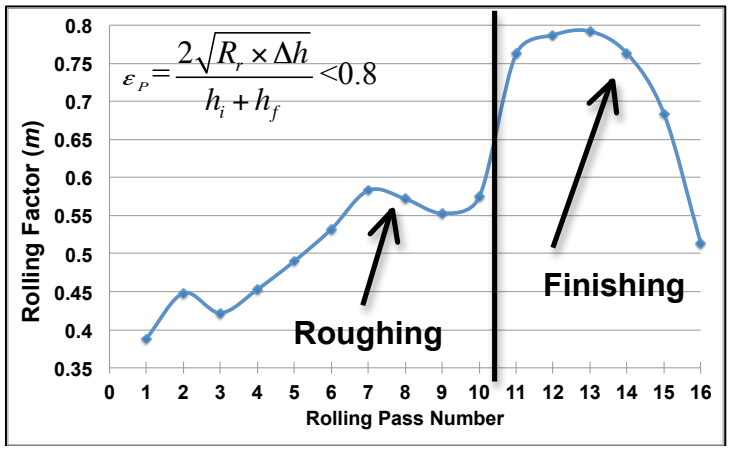

Figure 135: The rolling shape factor (m) of each rolling pass in the commercial hot rolling schedule of microalloyed steel 8AK39

Furthermore, non-uniform microstructures are confirmed in the below Figure 136 in which the ferrite and pearlite microstructures at the sub-surface and centre of the 60mm Nb steel 8AK39 heavy plate are presented, and the figure clearly illustrates that the average ferrite grain size at the near surface is much finer compared to the ferrite grains at the centre, and the associated ferrite grain sizes in the rolling directions are 18.0±1.3μm and 25.4±1.8μm respectively. Moreover, the volume fractions of pearlite at the near surface and centre of the 60mm plain carbon steel plate are roughly 20% and 25% respectively.

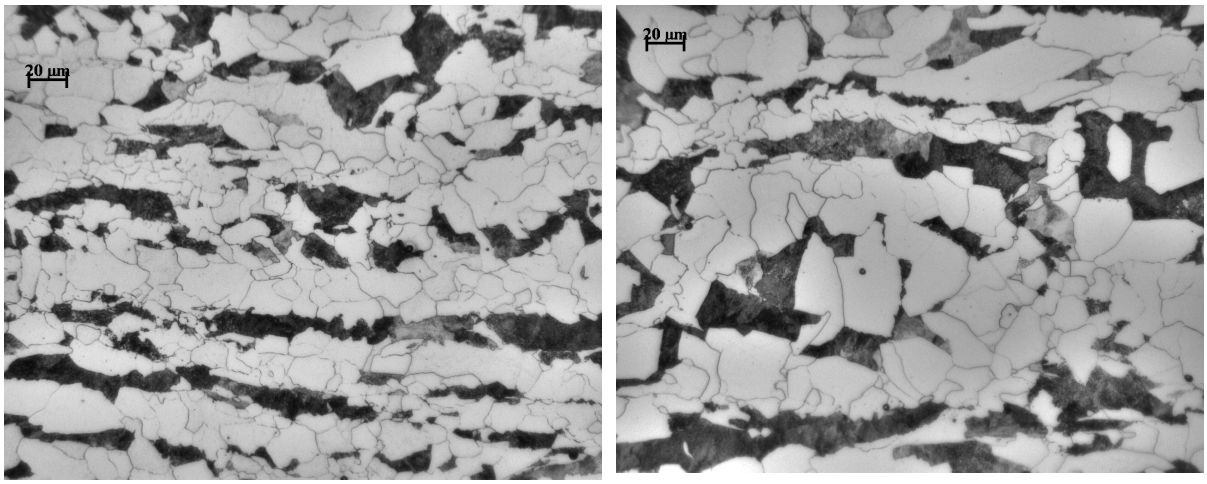

Figure 136: Optical microstructure at the near surface (left hand side) and the centre (right hand side) of 60mm Nb steel 8AK39 Nb steel plate

4.6.2. PSC Deformed Sample after Multipass Simulation

The following Figures 137-139 show an example of a successfully deformed 8-pass PSC sample during and after multipass simulation, which clearly demonstrated that the new updated version of TMC program installed at the end of research program is able to carry out complex multipass PSC tests with uniform reduction or thickness at the deformation zone of the PSC sample in Figures 137 and 139. Moreover, the noticeable platen imprints on the deformed PSC sample presented in Figure 138 indicate the successful 8-pass PSC reductions.

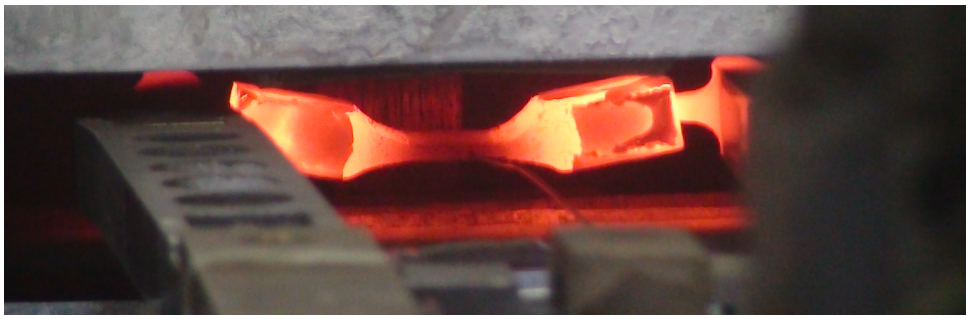

Figure 137: Uniform deformed PSC sample after 8-pass PSC deformation

Figure 138: A successfully deformed PSC sample of showing the platen imprints of 8-pass deformation (CT was the control thermocouple during testing)

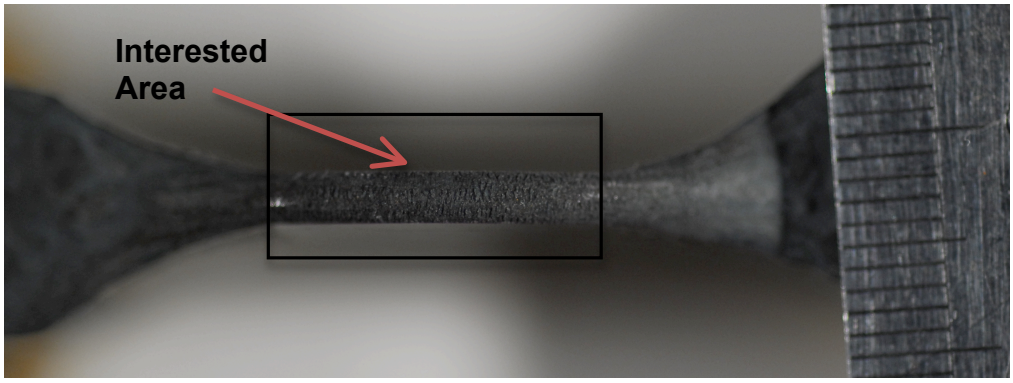

Figure 139: Cross-thickness view of uniform deformed PSC sample after 8-pass deformation

In order to obtain accurate microstructures of deformed PSC samples that can fully represent the corresponding multipass PSC testing, it is important to make sure that the interested areas, which were subjected to all the PSC deformations (such as a 8-pass PSC test is illustrated in Figures 138 and 139) by the platens, are flat and uniform without misalignment or shear.

4.6.3. Development of Prior Austenite Grain Size in Multipass PSC Simulation

The development of the prior austenite grain size (PAGS) at the different stages of multipass PSC simulation are shown in this section, which are at the end of reheating, roughing, and holding period and finishing stages. All the as-quenched microstructures appeared to be fully martensitic with no evidence of proeutectoid ferrite formation along prior austenite grain boundaries.

4.6.3.1. Prior Austenite Grain Size at the End of Reheating Stage

The PAGS of steel A and steel B after 2 minutes holding at 1200°C are shown in Figures 140 and 141, which were considered as the initial PAGS prior to later four stages of multipass PSC tests. However, in both figures, the PAGS were not clearly revealed even after 24 hours tempering treatment at 490°C in Figure 141. Therefore, based on some provided values of PAGS in different HSLA steels from the literatures [51, 74, 113], the PAGS for microalloyed steels A, B and plain carbon steel C after 2 minutes holding at 1200°C were assumed as 280μm, 200μm, and 350μm respectively. The effects of the initial PAGS on the final ferrite grain size during multipass industrial hot rolling (see Figure 23 in Literature Review chapter Section 2.3.3.3) and 8-pass PSC simulation are not noticeable, which will be described more in next Discussion Chapter.

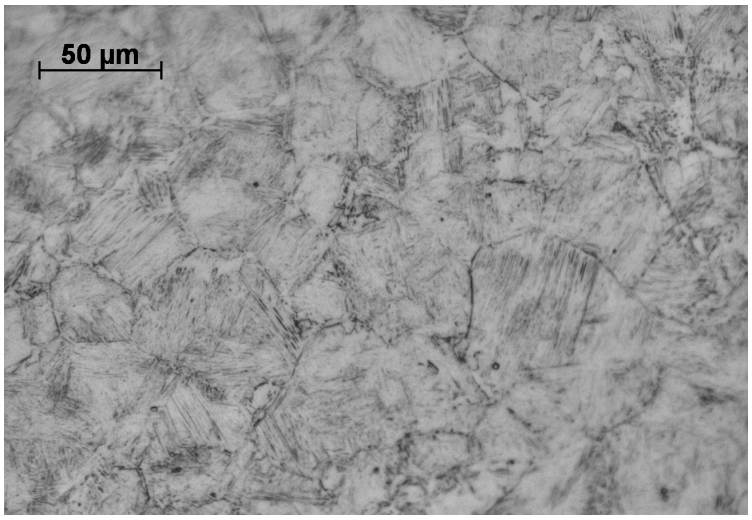

Figure 140: Prior austenite grain size of Nb steel A after 2 minutes holding at the 1200°C

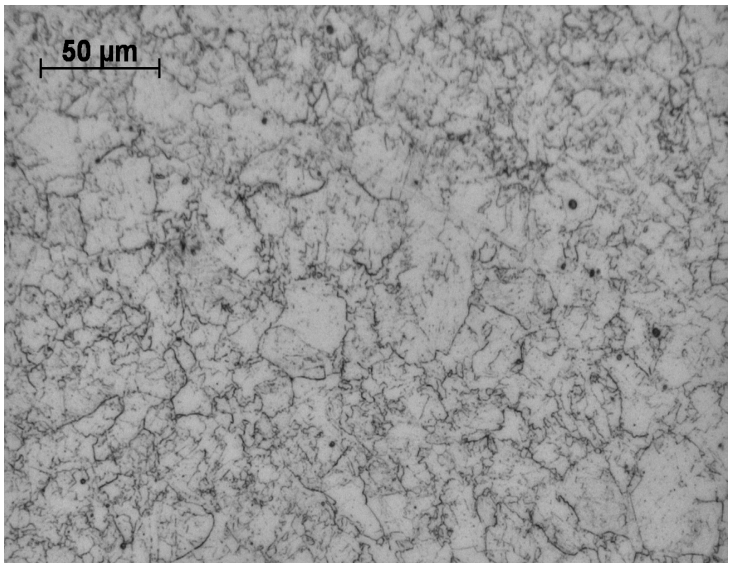

Figure 141: Prior austenite grain size of Nb+Ti steel B after at the 2 minutes holding at 1200°C and tempering treatment at 490°C

4.6.3.2. Prior Austenite Grain Size at the End of Roughing Stage

In general, the stage one was a 3-pass PSC roughing simulation with the applied strain arrangement 0.4+0.4+0.1 (the final 0.1 strain was specific chosen as same as small roughing reduction in the industrial heavy plate rolling schedule) and gap time 5 or 46 seconds at the deformation temperatures 1030°C, 1000°C and 978°C repspectively and then the deformed PSC samples were immediately quenched to room temperature inside the FTTU to analyse the prior austenite grain size (PAGS) at the end of roughing stage.

Initially, the 3-pass PSC deformations were kept inside the test furnace in order to better control deformation temperatures in just 5 seconds intervals and a success example of tempeature profiles at the centre and sub-surface (1mm below surface) of PSC sample during roughing and quenching stages are shown in the following Figures 142 and 143.

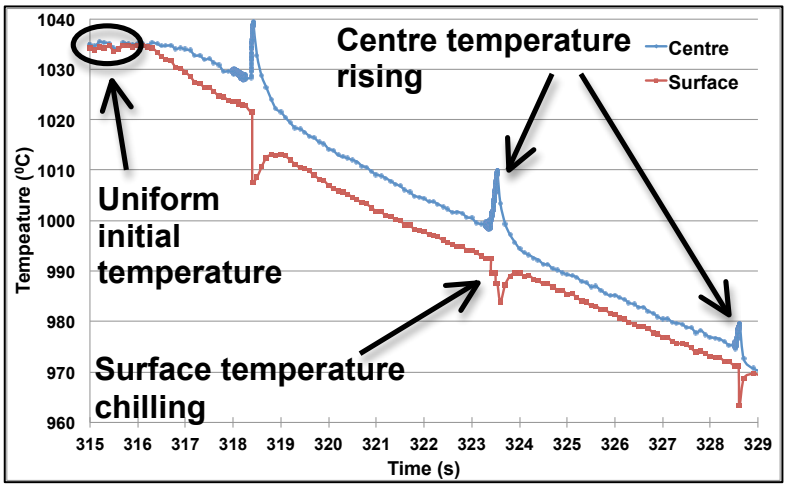

Figure 142: Recorded centre and sub-surface temperature profiles during the 3-pass roughing (0.4+0.4+0.1) test with 5 seconds gap time inside the test furnace

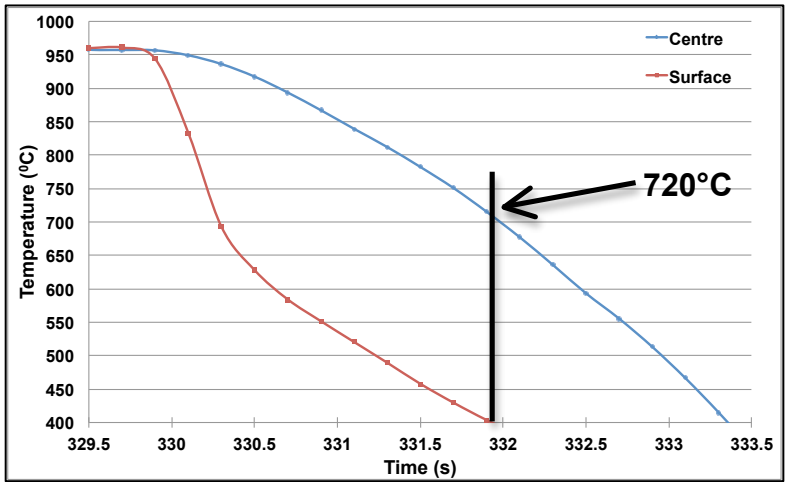

Figure 143: Centre and sub-surface temperature profiles inside a 5.3mm deformed PSC sample during post-deformation water quenching

Clearly presented in Figure 142, at the end of 2 minutes isothermal holding at 1200°C, the sub-surface (1mm below surface) and centre temperatures of undeformed 10mm PSC sample were almost the same, and then during the intervals cooling and 3-pass PSC deformation, the centre temperature was higher than the sub-surface temperature. Furthermore, a much greater temperature difference occurred at the last segment of testing sequences, i.e., water quenched the 5.3mm deformed PSC specimen into room temperature, illustrated in Figure 143 in which the temperature at the sub-surface of 5.3mm deformation sample reached 400°C whereas the centre was still at 720°C. The average surface cooling rate from 950°C to 400°C was about 250°C/s while the mean centre cooling was roughly 136°C/s, thus fully martensitic microstructures were expected to form at the centre of the as-quenched 5.3mm deformed PSC sample.

The following Figure 144 shows very good agreement in three 3-pass PSC tests with exactly the same test settings and the only difference was the steel compositions (steels A, B and C), thus any variation in the observed optical microstructures of PAGS in Figures 145-147 may be attributed to the steel composition only rather than incompatibility between the multipass PSC tests. For traceability purposes, every deformed PSC sample was labelled with alphabet letter indicating different steel grade followed by individual test number. For example, A8 means the 8th PSC test and the corresponding deformed PSC specimen of Nb steel A.

According to the results of the quantitative measurements of the PAGS in Figure 145 to 147, similar equiaxed shaped PAGS were produced immediately after the 3-pass roughing simulation in microalloyed steel A and B, and plain carbon steel C, where are 22.1±0.6μm, 18.4±0.5μm and, 22.3±0.7μm respectively. Thus, the steel B with Ti and Nb had the finest PAGS, which indicates that the Ti restricted the austenite grain growth during the high temperature deformation. The Nb steel A had similar grain size as the plain carbon steel C, which probably due to NbC had not yet precipitated out of solution during roughing.

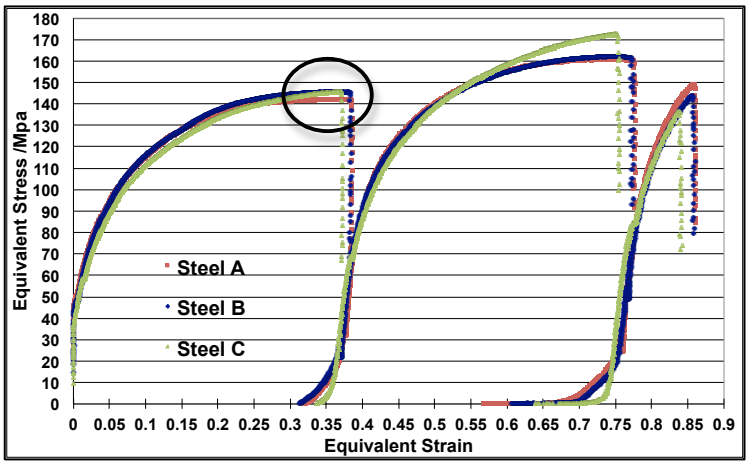

Figure 144: Comparison of flow curves of 3 roughing passes with same test conditions but different in steel compositions

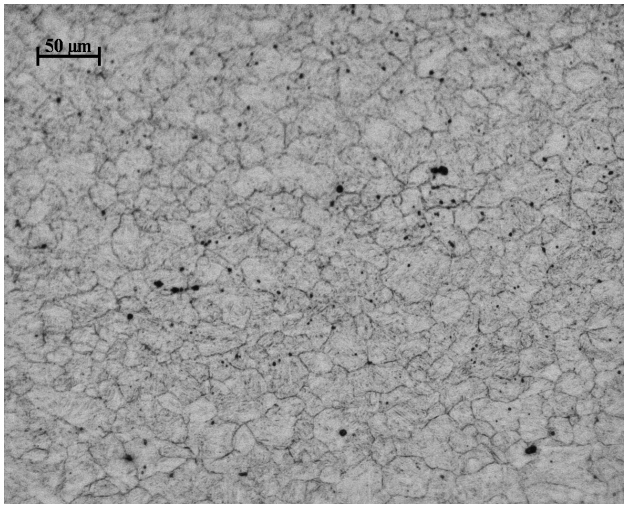

RD – 22.1±0.6µm
TD – 16.6±0.9µm
Aspect Ratio =1.3

Figure 145: Prior austenite grain size of steel A (Nb) immediately after 3 roughing passes (0.4+0.4+0.1+WQ)

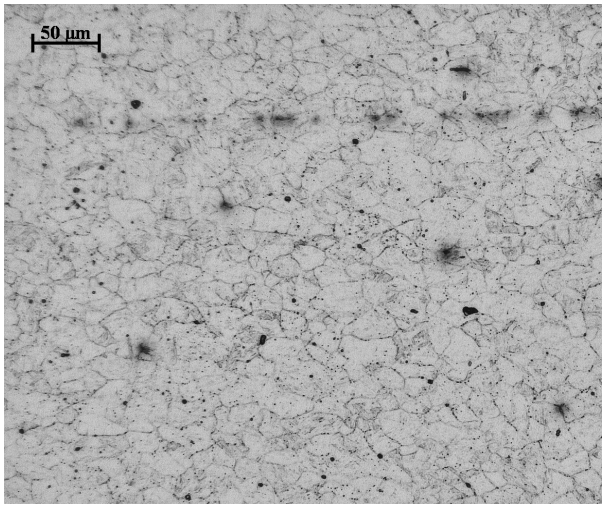

RD – 18.4±0.5µm
TD – 16.6±0.9µm
Aspect Ratio =1.1

Figure 146: Prior austenite grain size of steel B (Nb+Ti) immediately after 3 roughing passes (0.4+0.4+0.1+WQ)

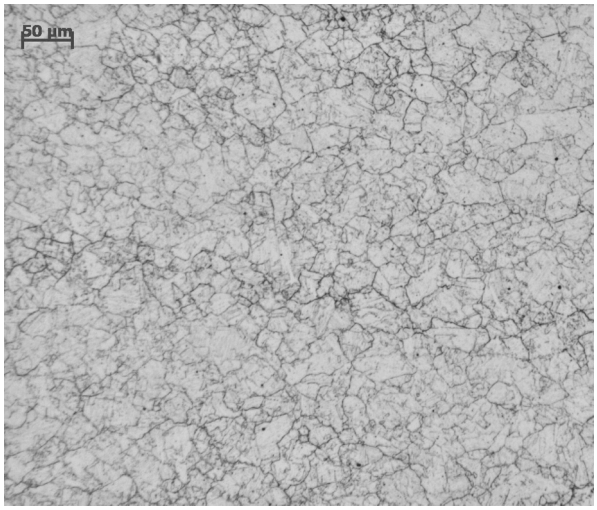

RD – 22.5±0.7µm
TD – 16.6±0.9µm
Aspect Ratio =1.4

Figure 147: Prior austenite grain size of plain carbon steel C immediately after 3 roughing passes (0.4+0.4+0.1+WQ)

4.6.3.3. Prior Austenite Grain Coarsening during the Hold Period

The development of the austenite grain growth during the hold period (HP) under different cooling rates is one of the essential objectives of this research program. It is a well-known fact for the common industrial practice after roughing stage the partially rolled heavy plate is cooled by natural-air during the HP till the average temperatures across the thickness of the heavy plate reaches the target finishing roll temperature. However, the corresponding HP could be 15 minutes long depends on the plate thickness, a sufficiently long time to allow for austenite grain coarsening to take place at the end of HP. Therefore, the results of shortening the long HP through the application of some faster forced cooling rates on the PAGS at the end of HP are also shown.

An example of a target HP cooling profile was to reduce the 3-pass roughed PSC sample from about 980°C to 880°C in 30 seconds and then slowly cooled to 870°C in 10 seconds immediately followed by water quenched to room temperature for determining the PAGS at the end of HP. The actual recorded temperature profiles in Figure 148 show great temperature controls in term of exactly following the target cooling profile during the HP simulation. Moreover, the flow curves of the four different tests B1 to B4 in Figure 149 display similar multipass flow stress behaviours, which are expected due to these four tests had exactly same 3-pass roughing conditions (0.4+0.4+0.1) prior to the HP. Notice that only the flow curve of test B4 reached the exactly defined strain 0.4 at the end of the first roughing pass, which is due to the actual recorded strain is normally slightly lower (0.05 in this case) than the setting or input value, and the more PSC passes are carried out, more deviation occurred between the actual total strain (0.73-0.8) than the defined or nominal value (0.9) in Figure 149. Therefore, to reach the target strain in the deformed PSC sample, the general rule is the input value of applied strain should be always 0.05-0.1 higher than the nominal value and described more in next Discussion chapter.

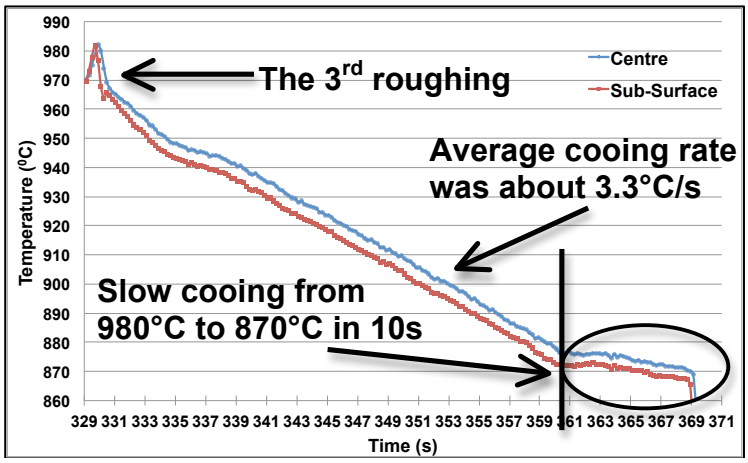

Figure 148: Centre and sub-surface (1mm below surface) temperature profiles inside the 5.5mm deformed PSC sample during HP

For these four 3-pass PSC tests, B1 is the reference test to determine the PAGS immediately after the 3-pass roughing passes (3R+W). The rest of three tests B2, B3 and B4 were allowed to carry on cooling until the deformed PSC sample reached 870°C by varying the duration of time: 40, 90 and 300 seconds respectively before WQ to room temperature (3R+HP+W). Thus, by comparing the PAGS from tests B1 to B4, the austenite grain coarsening at the continuous cooling HP from 980°C to 870°C were determined and shown in Figure 150 (40 seconds HP) and Figure 151 (300 seconds HP). The PAGS in the rolling direction for B1, B2, B3 and B4 were 18.4±0.5μm, 20.5±0.8μm, 22.9±0.8μm and 26.2±0.8μm, which have confirmed that the PAGS increased with increasing holding period.

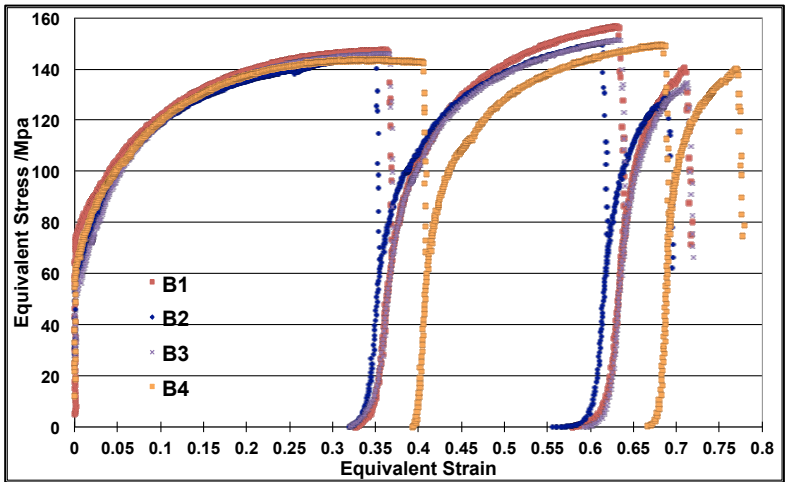

Figure 149: Flow curves of four similar 3-pass roughing tests (tests B1 to B4) but with different cooling rates during holding period

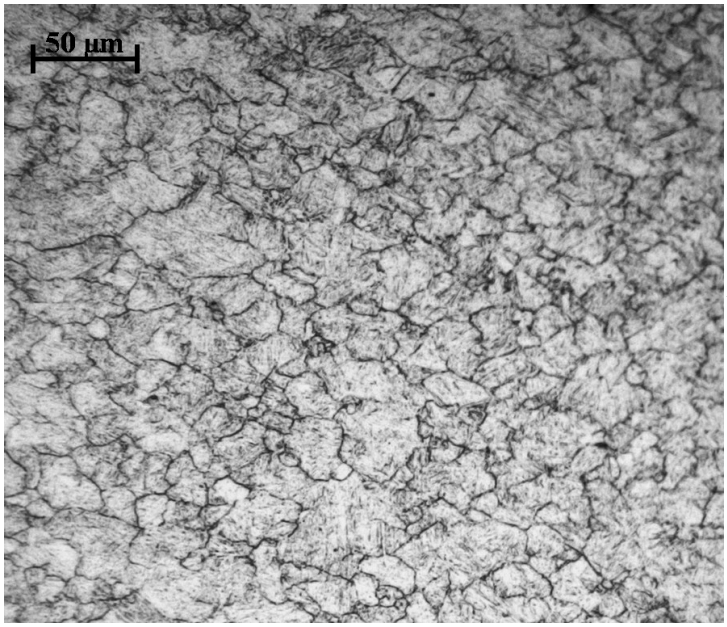

RD – 18.4±0.5μm
TD – 17.1±0.4μm
Aspect Ratio =1.1

Figure 150: PAGS after 3 roughing passes +40 seconds HP + water quenching (test B2)

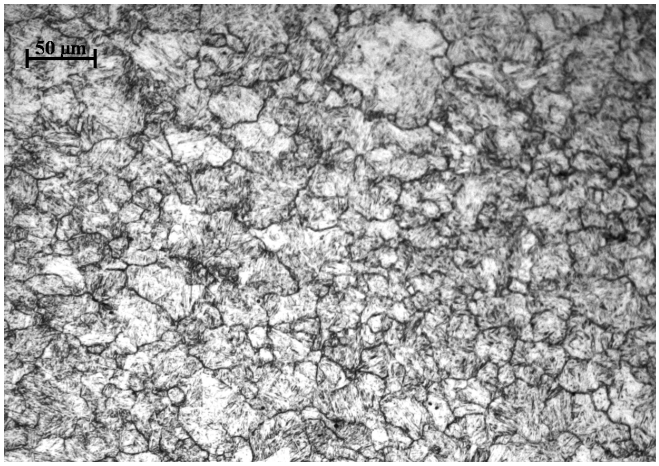

RD – 26.2±0.8µm
TD – 24.6±0.6µm
Aspect Ratio =1.1

Figure 151: PAGS after 3 roughing passes +300 seconds HP + water quenching (test B4)

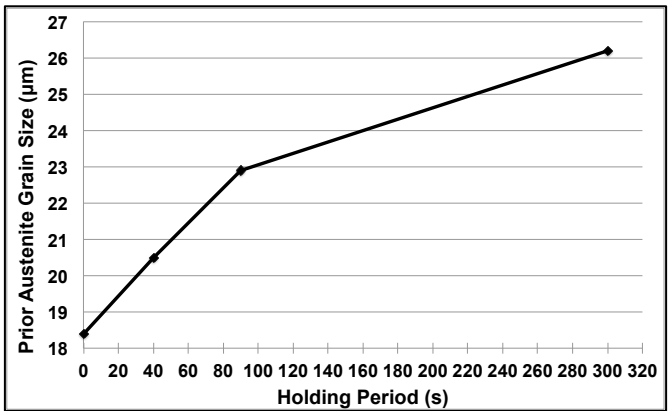

Figure 152: The measured PAGS in the rolling direction as function of the time (till 300 seconds) during continuous cooling from 980°C to 880°C

Plotting the PAGS against the cooling time during the HP (above Figure 152) indicates that the highest slope or austenite grain growth rate was during the first 40 seconds of the HP. Furthermore, the period from the 90 seconds and 300 seconds of HP in Figure 152 shows only a slightly increase in the PAGS from about 23µm to 26µm due to the coarsening rate being reduced. Therefore, it may suggest that the PAGS possible only rise to small extent even further increase the HP above 300 seconds, such as 15 minutes cooling from 980°C to 880°C, and no tests were carried out for investigating the development of PAGS during the long HP.

Secondly, another particular simulation (test B8) with a different strain sequence (0.1+0.4+0.4) during 3-pass roughing (described in Experimental Section 3.9.2.2) was performed, and was compared with test B4 (0.4+0.4+0.1) on the flow curve and the PAGS at the end of same HP, which are presented in the following Figure 153 and 154 respectively. Figure 153 shows an attractive result that for the same nominal total applied strain $\varepsilon_{total} = 0.9$ (however the actual measured total strain was about 0.8 in both tests), strain rate, deformation temperatures and intervals, applying a relatively larger strain 0.4 instead of 0.1 at the last

roughing pass before entering the holding period provided a higher flow stress (20MPa). Moreover, indeed this new strain arrangement (0.1+0.4+0.4) reduced the austenite grain growth in the HP, which gave PAGS of 21.8±1.0μm shown in below Figure 154 compared to the PAGS of 26.2±0.8μm in test B4. However, this technique only could be carried out on a powerful rolling mill. Of note, the flat stress at the initial 0.4 strain (Figure 153 below) suggested possibly the dynamic recovery was taking place.

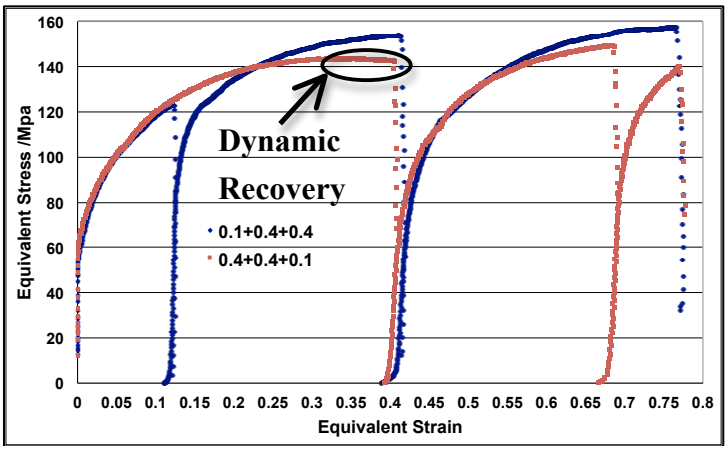

Figure 153: Flow curves comparison of 3 rough passes with the same total input strain 0.9 but different in the strain arrangement: 0.4+0.4+0.1 and 0.1+0.4+0.4

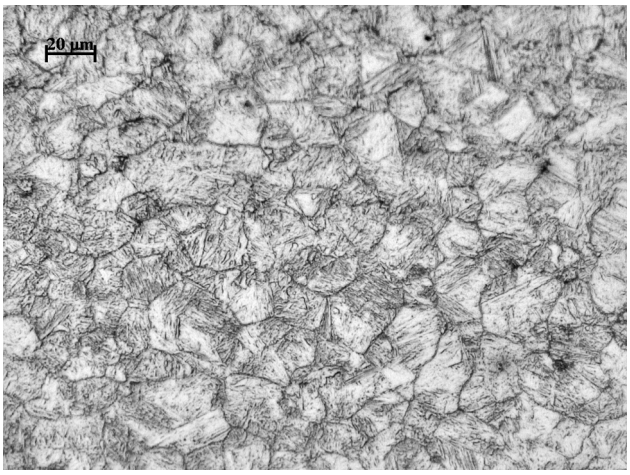

RD – 21.8±1.0μm
TD – 17.8±1.4μm
Aspect Ratio =1.2

Figure 154: The prior austenite grain size of steel B (test B8) after 3-pass roughing with strain arrangement: 0.1+0.4+0.4 and 300 seconds cooling from 1000°C to 870°C

Third, in terms of the PAGS development in the Nb steel A during the 266 seconds cooling from 980°C to 880°C, the following Figure 155 and Figure 156 indicate some similarity (as expected due to same testing conditions) in the 3-pass flow curves and variation in the PAGS respectively. As seen in Figure 155 the actual measured strain in both tests A21 (3R+W) and A28 (3R+266s+W) were closer to the nominal total 3-pass strain 0.9 and same softening degrees during the gap times, but the test A28 had higher flow stress (less than 20MPa) in the first and second passes than those of test A21.

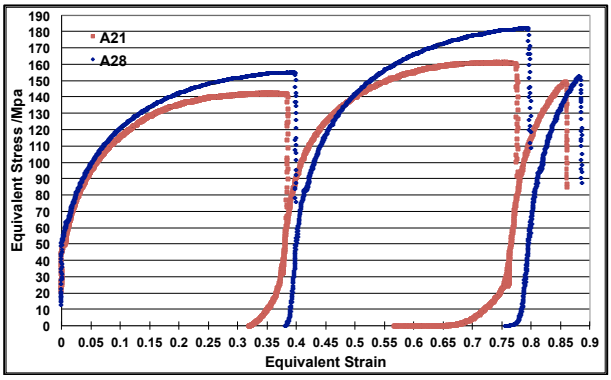

Figure 155: Flow curves of two similar 3-roughing passes A21 (3R+W) and A28 (3R+266s+W) with only difference in the holding period

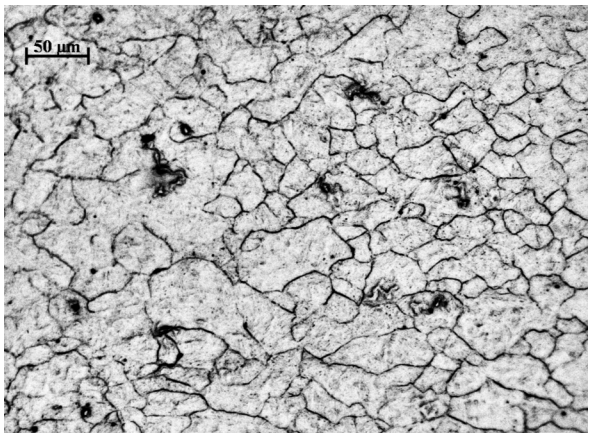

RD – 35.1±1.8µm
TD – 25.2±1.3µm
Aspect Ratio =1.4

Figure 156: The inhomogeneous PAGS of Nb steel A after 3-roughing passes and 266 seconds natural-air cooling during the HP

The PAGS of test A21 is shown in previous Figure 145 with 22.1µm in the rolling direction, while the PAGS of test A28 gave much larger PAGS of 35.1µm, which indicates considerably grain coarsening about 60% increment at the end of HP, possible due to some PAGS in Figure 156 were not able to reveal clearly to cause errors in measurement.

Fourth, a particular test A15 was also carried out to determine the PAGS evolution after 3 roughing passes (0.45+0.45+0.15) followed by a reduction in temperature to 880°C in 3.6 seconds through mist cooling and then isothermally held at the 880°C for 120 seconds. The following Figures 157, 158, 159 present a selection of actual recorded temperature profile of the 3.9mm deformed PSC sample during the HP, the associated 3-pass flow curve and the PAGS microstructures at the centre of PSC specimen respectively. As seen in Figure 157, in order to quickly reduce the temperature of deformed PSC sample that just out of the 3rd pass roughing to the target 880°C holding temperature without noticeable temperature over-shots, a fast mist cooling was applied and nicely controlled inside the FTTU. The shape of the 3-pass flow curve shown in Figure 158 is different to those of the earlier Figure 144 and Figure 149, which all had similar settings of 3-roughing PSC deformation. Usually, the maximum

flow stress σ_{max} at the third roughing pass is the lowest value in these 3-roughing passes (see Figure 144, Figure 149 and Figure 155), but in this special case the σ_{max} of the third roughing pass was the highest. Furthermore, Moreover, Figure 159 gave PAGS of 23.8±1.6μm, thus only small amount of grain coarsening occurred when the deformed PSC sample was quickly reduced to 880°C and isothermally held at 880°C for 120 seconds.

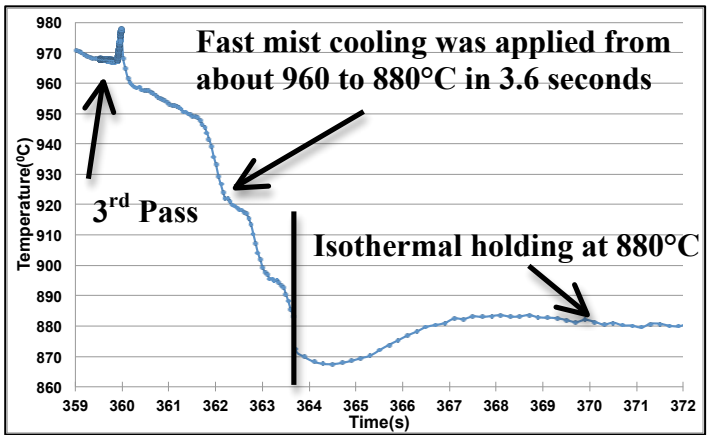

Figure 157: Temperature cooling profile of 3.9mm deformed PSC sample during the HP

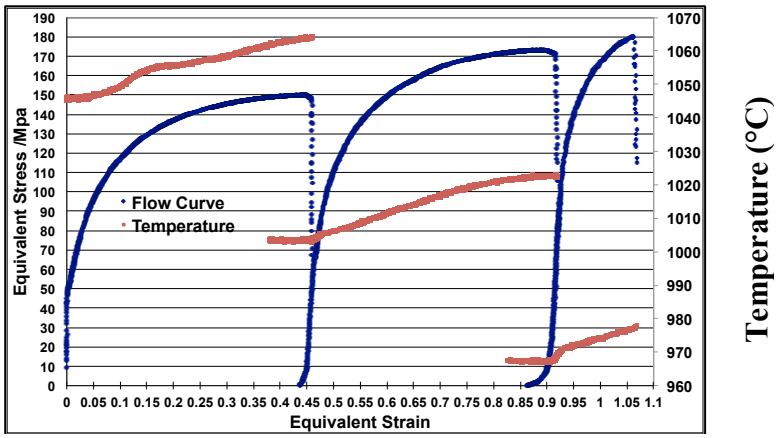

Figure 158: Flow curve and temperature profile of 3-roughing passes (0.45+0.45+0.15)

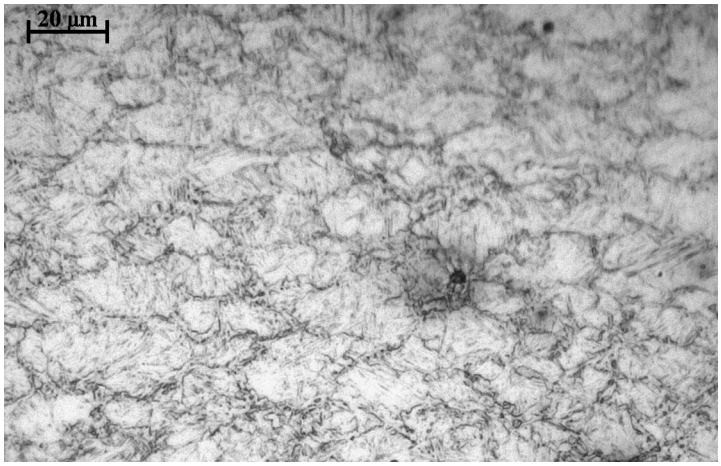

RD – 23.8±1.6μm
TD – 17.7±1.1μm
Aspect Ratio =1.3

Figure 159: The PAGS microstructure of steel A (test A15) under 3-pass roughing and 3.6 seconds cooling from 980°C to 880°C and held isothermally 120s at 880°C

Finally, the last part of holding period cooling simulation was to replicate the commercial heavy plate (100mm in this case) surface temperature profile during the HP and analyse the corresponding PAGS at the end of HP when the intermediate forced cooling (IFC) was applied. The plate surface temperature profile under the IFC condition was more complicate than the temperature cooling profile in heavy plate centre and shown in the earlier Figure 66 in Experimental chapter section 3.9.2.2, and the following Figure 160. In general, after short period of fast cooling by forced air, the much hotter core of the heavy plate gradually reheats the cold surface until the temperatures across the thickness are equalised if sufficient recalescence time is provided. The target heavy plate surface temperature cooling and recalescence profile shown in Figure 160 was the simulation result of predicted plate surface profile under the IFC condition presented at the previous Figure 115, which were divided into several small cooling segments (illustrated in small red squares in the predicted or target profile in Figure 160) and then used as the input values (start and end of cooling temperatures in a short time length) of FTTU settings. It is obviously that the actual recorded temperature test profile inside the deformed PSC sample was the same as the target profile, which means that the FTTU is able to carried out the complicated temperature profile of IFC condition.

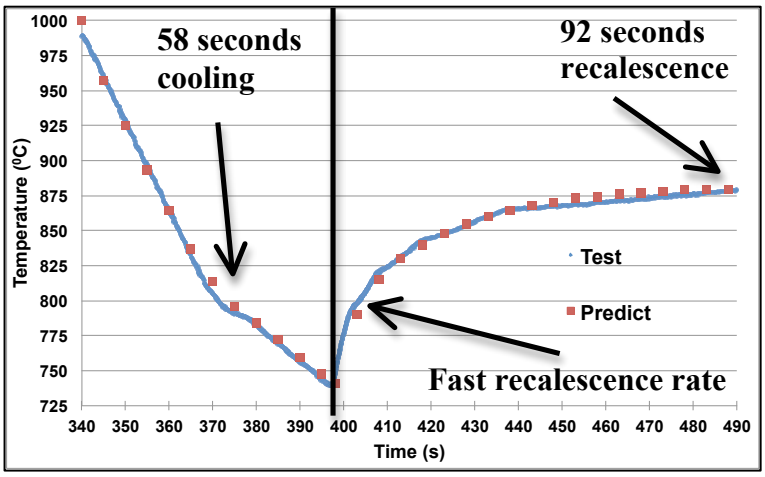

Figure 160: Comparison of the predicted heavy plate surface and actual recorded PSC sample temperature profiles during the HP simulation

The test B42 is an example of the 3-roughing passes plus applied IFC during the HP, followed by water quenched (3R+IFC+W), which are shown in the following Figure 161 and 162, and present the flow curves and the PAGS microstructure respectively. Similar flow curves, particularly the third roughing pass was found almost the same in two multipass PSC tests B33 and B42 in Figure 161, thus any difference in the measured PAGS was attributed only to the holding period cooling simulation. Moreover, the measured PAGS of test B33 shown in previous Figure 146 and that of test B42 presented in Figure 162 at the rolling direction (RD) was 18μm and 22μm respectively, thus only small amount austenite grain coarsening took place when applying the IFC during the HP.

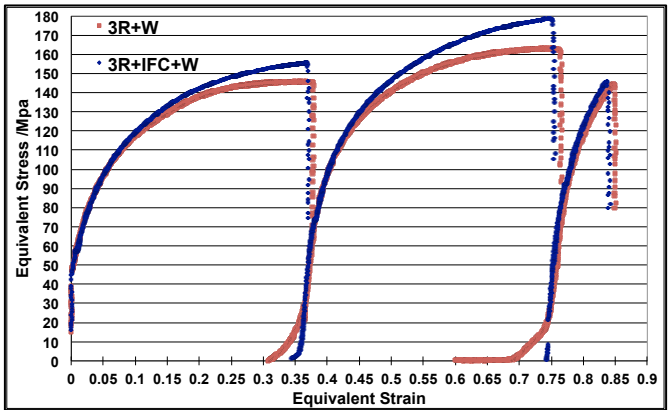

Figure 161: Flow curves of two similar 3-roughing passes B33 (3R+W) and B42 (3R+IFC+W) with only difference in the holding period

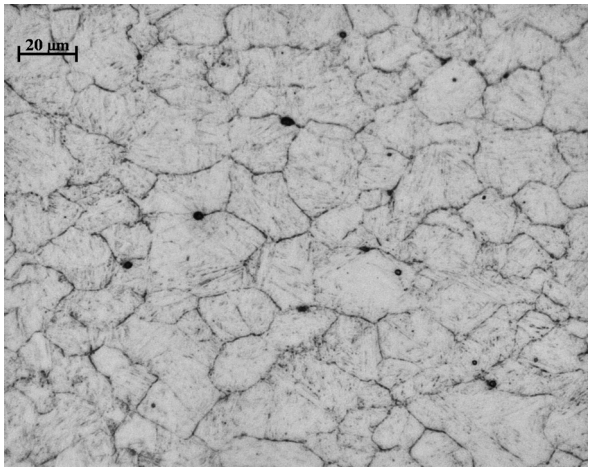

RD – 21.5±1.7µm
TD – 16.6±0.9µm
Aspect Ratio =1.3

Figure 162: The PAGS of Nb-Ti steel B after 3 roughing +IFC +water quenched (test B42)

4.6.3.4. Prior Austenite Grain Size at the Finishing Stage

The third stage of multipass PSC simulation was to replicate the 5-pass industrial finish rolling, and the corresponding prior austenite grain developments and flow curves of microalloyed steels A, B and plain carbon steels C and D after 3-pass roughing (3R), holding period cooling and 5-pass finishing (5F) prior to post-deformation cooling (3R+HP+5F+W) are shown in this section. It is important to make sure that all the as-quenched microstructures appear to be fully martensitic with no evidence of proeutectoid ferrite formation along prior austenite grain boundaries at the centre of deformed PSC sample. It is well known that the finishing rolling is the most critical stage to produce elongated or pancaked prior austenite in the rolling direction and provided sufficient number of nucleation sites for later ferrite formation during phase transformation. Furthermore, the appearances of elongated austenite also indicate the deformation temperature below the recrystallisation stop temperature, which is the one of most essential hot rolling temperatures and has been investigated by many researchers.

After some similar 3-pass (0.4+0.4+0.1) PSC tests were performed to simulate the same total strain ε_{total}=0.9 as the first 10-pass industrial rough rolling and different cooling during HP, the five intended industrial finishing passes were replicated exactly the same as a 5-pass PSC test on the TMC machine. First of all, development of PAGS of Nb steel A during the finishing rolling, and the results of recorded temperature profiles, flow curve comparisons and microstructure evolutions of three similar multipass PSC tests are shown in the following Figures 163 to 165. It is clearly shown in Figures 163 and 164 that great consistencies of the recorded temperature profiles and the corresponding flow curves are found in these three multipass PSC tests, which are the tests A1, A2 and A3 and were 3-pass (3R+HP+WQ), 4-pass (3R+HP+1F+WQ) and 5-pass (3R+HP+2F+WQ) PSC deformation respectively with similar test conditions. Furthermore, the corresponding PAGS microstructural development is shown in earlier Figure 156 for the test A1, and the following Figure 165 for the tests A2 and A3. Additionally, there are not obviously appearances of elongated or pancaked shape austenite in Figure 165, thus it would indicate that the finishing deformations were carried out above the recrystallisation stop temperature $T_{0.05X}$.

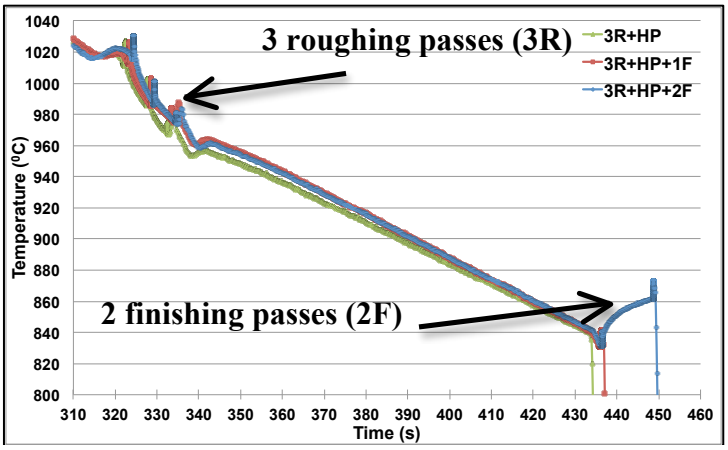

Figure 163: Similar recorded temperature profiles of three similar multipass PSC tests (3R+HP+WQ, 3R+HP+1F+WQ and 3R+HP+2F+WQ)

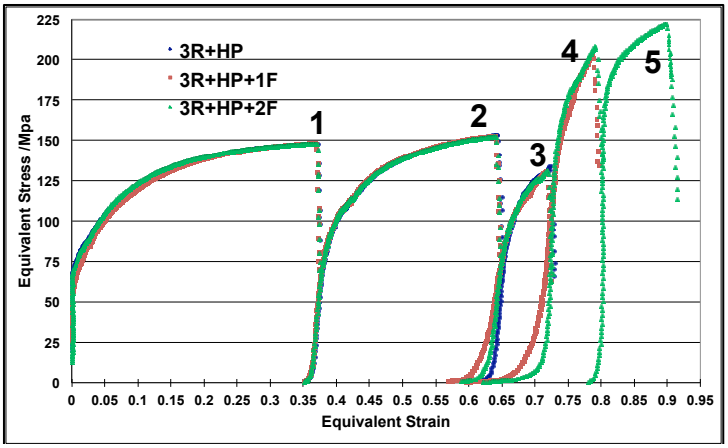

Figure 164: Flow curves of three different multipass PSC tests (3-, 4- and 5-pass deformations) and showing great consistency during multipass deformation

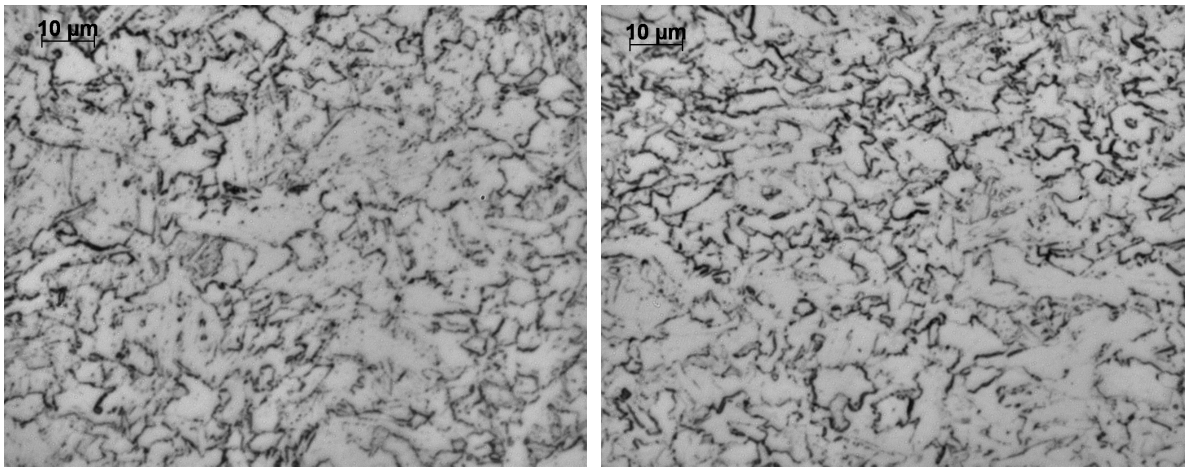

Figure 165: Optical Microstructures of Nb steel A after 4-pass (3R+HP+1F-left hand side) simulation and after 5-pass (3R+HP+2F-right hand side) PSC simulations

Furthermore, as illustrated in Figure 166, the development and good agreements of the three flow curves at the end roughing (see Figure 145), holding period (presented in Figure 159) and finishing (see later Figures 170 and 171) stages of 8-pass PSC simulation, which are the essential requirements in order to analyse the PAGS evolution at the different stages of laboratory multipass PSC testing.

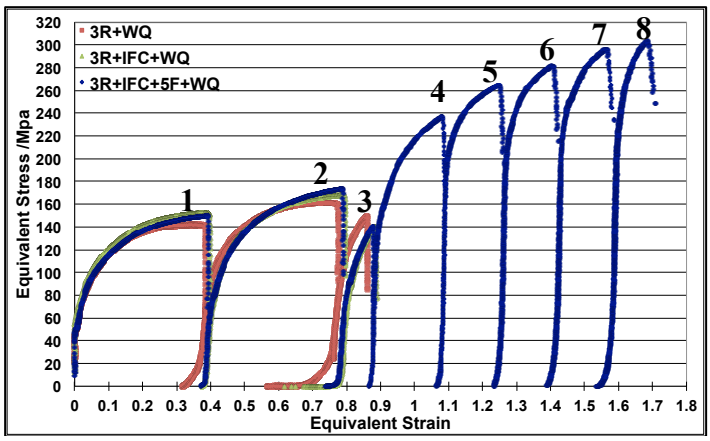

Figure 166: Flow curves of three PSC tests at the end of roughing (3R+WQ), holding period (3R+IFC+WQ) and finishing (3R+IFC+5F+WQ) stages of simulation

Some multipass PSC tests were carried out to compare the results of microalloyed steels A and B, and plain carbon steel C under exactly the same 8-pass PSC tests (3R+266s+5F+WQ), which are clearly illustrated in the following Figures 167 to 171. Furthermore, the plain carbon steel C shows a significantly lower required load (negative value in Figure 167 indicates the compressive force) and less equivalent stress to reach the same target strain compared to those of the microalloyed steels A and B presented in Figures 167 and 168. Additionally, with the same 5-pass finish rolling PSC settings, the equivalent stress of the plain carbon steel C only increased about 20MPa from the 4th to 8th pass possible due to a

gradual decrease in the finish rolling temperatures (from 980°C down to 940°C). On the other hand, as illustrated in Figures 167 and 168, the Nb steel A and Nb+Ti steel B had similar recorded compressive load-tool displacement profiles and flow curves, and the equivalent stress increased around 70MPa from the 4th to 8th pass probably owing to strain hardening in consecutive 5 finishing passes as well as reduction of deformation temperatures.

The optical microstructures of Nb steel A after 8-pass PSC deformation are shown in Figure 169 in which significantly variations in the shapes and size of PAGS are found at the sub-surface (Equiaxed PAGS) and centre (elongated PAGS) of 2.7mm deformed PSC sample due to different effective strain distribution across the thickness (i.e. the highest applied strain is at the centre of deformed PSC sample – mentioned in Literature Review chapter Section 2.5.5).

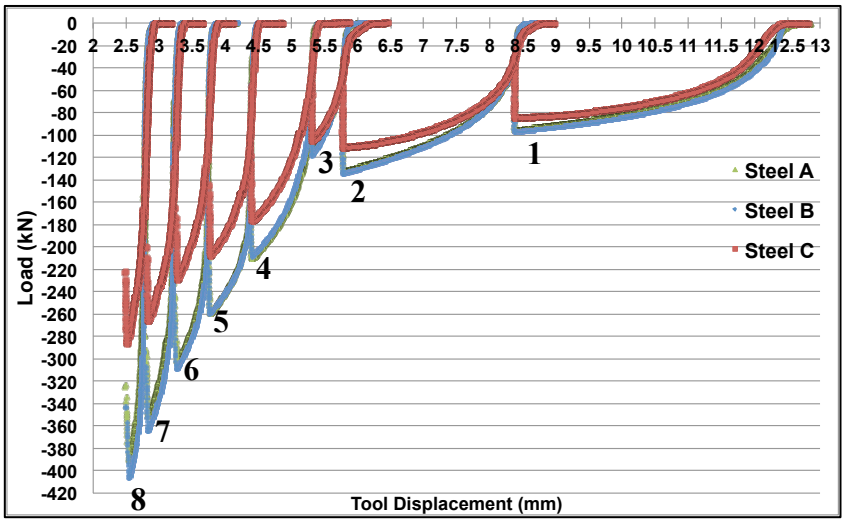

Figure 167: Relationships of tool displacements and applied compressive loads (negative values) of three different steels during 8-pass PSC tests (3R+266s+5F+WQ)

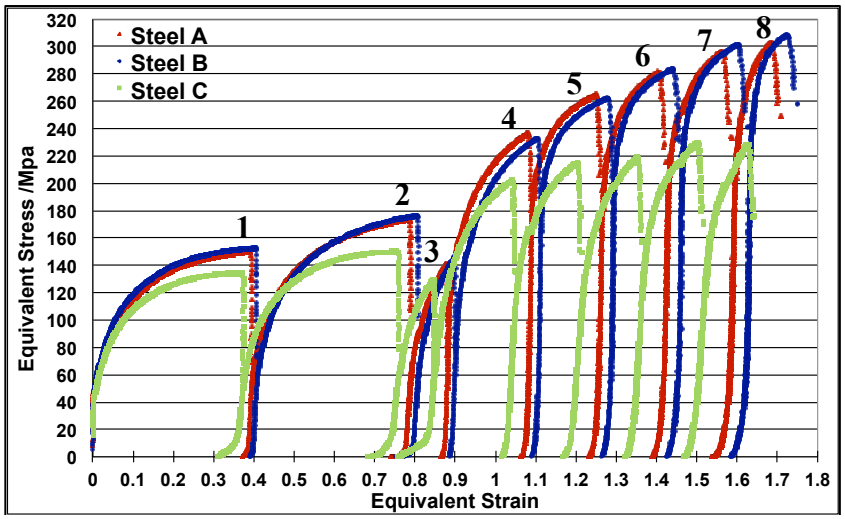

Figure 168: Flow curves comparison of three different steels under exactly the same multipass PSC test settings (3R+266 seconds+5F+WQ)

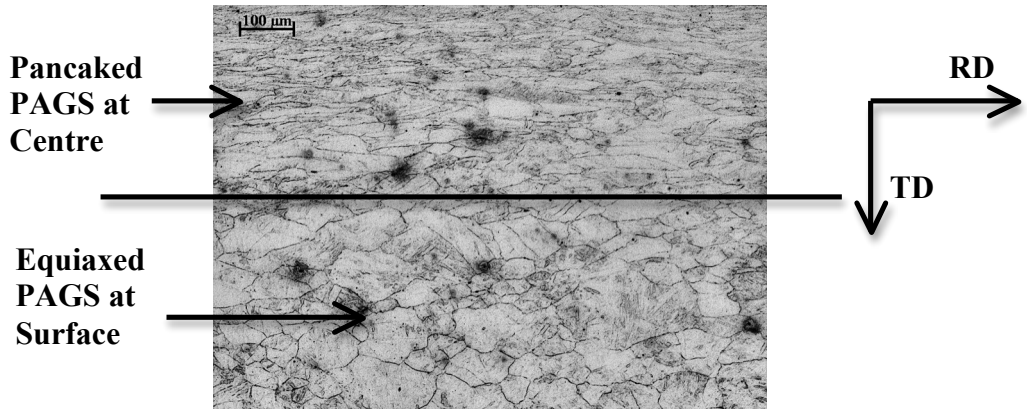

Figure 169: Prior austenite grain size distribution from the surface to centre of Nb steel A after 8-pass PSC test (3R+266 seconds+5F+WQ)

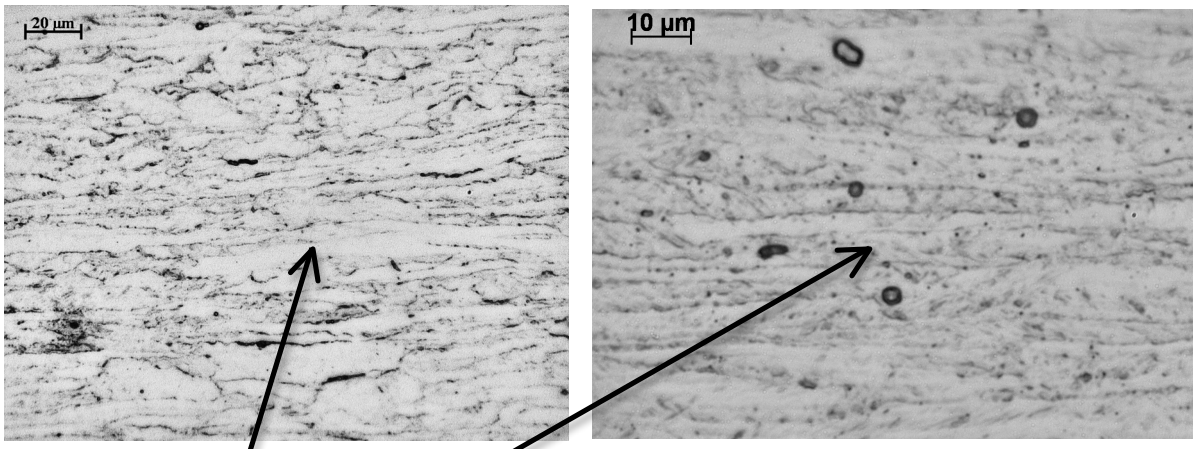

Figure 170: The elongated PAGS along the rolling direction at the centre of two deformed PSC samples (steel A at left hand and steel B at right hand) after 8-pass PSC simulation

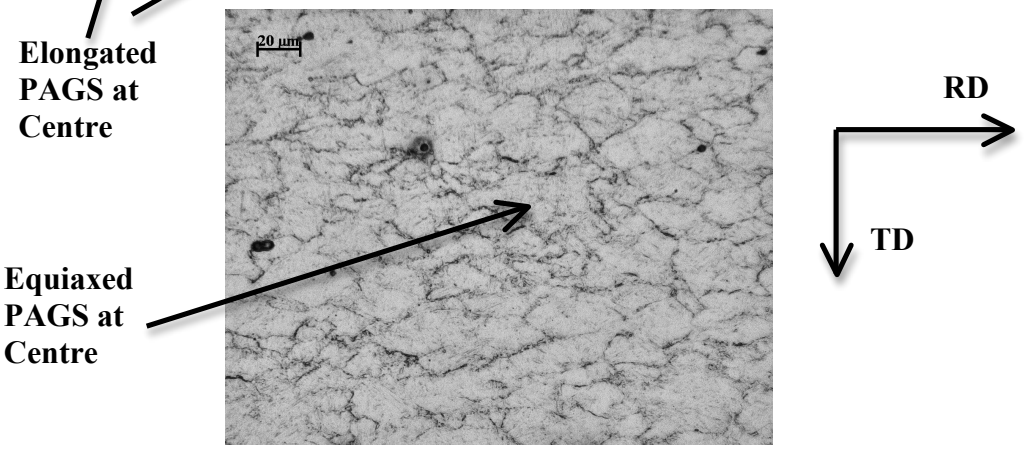

Figure 171: Prior austenite grain size of steel C after 8-pass simulation ((3R+266 seconds+5F+WQ)

Additionally, the noticeable appearances of elongated or pancaked austenite (due to the equiaxed grains were unable to initiate recrystallisation) along the rolling direction are found in above Figure 170, thus it suggests that the last few finishing passes were performed below

the important $T_{0.05X}$ of Nb steel A and Nb+Ti steel B. On the other hand, as seen in Figure 171, there are no obvious evidences of elongated austenite grain along the rolling direction in plain carbon steel C, thus it suggests that the 5-pass finish rolling temperatures (from 880°C down to 840°C) were above the $T_{0.05X}$ of plain carbon steel C. Moreover, the observed microstructures in Figures 169 to 171 have agreed the predicted $T_{0.05X}$ values of steels A, B and C in earlier Table 9, which are 889°C, 917°C and 808°C respectively.

Finally, as mentioned earlier, revealing the PAGS clearly from the as-quenched martensitic microstructure of the deformed PSC sample was challenging and time consuming, thus the similar 8-pass PSC test (3R+IFC+5F+WQ) with total applied strain ε_{Total} =1.3 was always carried out firstly on the 10mm dummy steel E (Fe-30wt%Ni-0.05wt%C-0.38wt%Nb), and the corresponding flow curve and microstructure of PAGS are shown in below Figure 172. Furthermore, the maximum equivalent stress (300MPa) at the 8th pass of the dummy steel E in Figure 172 is similar to those of steels A and B in previous Figure 168. However, different applied equivalent strains (1.24 and 1.73 in Figure 172 and Figure 168 respectively) were related to the maximum 300MPa stress due to much higher microalloyed elements additions (30wt%Ni and 0.38wt% Nb) in steel E increase its solid solution strengthening at the austenite region, thus it required much larger load (stress) to reach the same reduction.

It is widely accepted that the 30wt% Ni addition in steel E is able to stabilise the deformed austenitic microstructure during water quenching without the phase transformation into complex ferrite or martensite structure. Therefore, revealing the PAGS is much easier and quicker in steel E, and an example of the etched optical microstructures is also presented in below Figure 172 in which the measured PAGS at the rolling direction is 3.7±0.1μm.

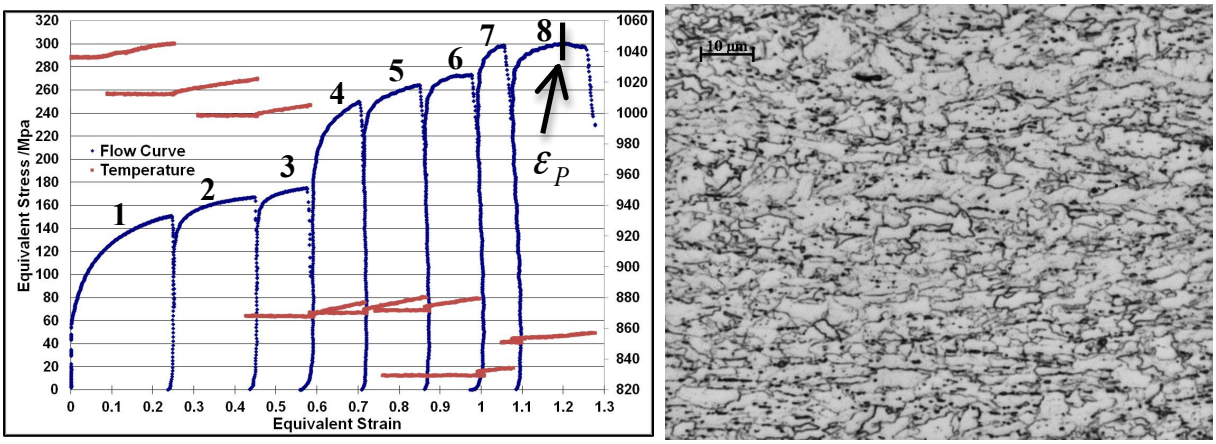

Figure 172: Flow curve and record deformation temperatures of 8-pass PSC simulation (3R+IFC+5F+WQ) of dummy steel E (test E4) Fine prior austenite grain size (pancaked) of dummy steel E after 8-pass PSC simulation (test E4)

4.6.4. The Effects of Hot Rolling Factors on As-Rolled Microstructure Evolutions

After many trials and improvements of the multipass PSC tests, the new updated version of the PSC program was installed at the last stage of this research project, and the successful rate of retrieving 8-pass deformed PSC sample from the test furnace back to FTTU for the last stage accelerated cooling simulation was greatly improved. The analysed results of many different multipass (mostly 8-pass) PSC tests in the following sections have illustrated clearly the influences of varied hot rolling parameters, such as post-deformation cooling rates, finish rolling temperature, IFC, steel chemical compositions and different total applied strains on the corresponding ferrite grain size and volume fractions of ferrite and other phases in final as-rolled microstructures. Furthermore, in order to investigate the individual and most dominant factor regarding to reduce the ferrite grain size at the similar multipass PSC conditions, the others parameters were set at the same values and are shown in the following.

4.6.4.1. Consistency of Multi-Pass PSC Simulation

Similar to the way of presenting the development of PAGS in Section 4.6.3, it is essential to make sure to these 8-pass PSC tests have good reliability and agreements from reheating, to roughing, holding period, finishing and to post-deformation cooling. Therefore, any differences in the observed microstructures and flow curves were attributed to the steel compositions or others hot rolling parameters rather than the incompatibility between the similar multipass PSC tests. An example showing high repeatability is presented in Figure 173 where there are one 3-pass roughing plus IFC during the HP (test A21), and three 8-pass PSC tests (tests A16, A17 and A18) with the same flow curves shape and almost identical values of equivalent stress and strain. These four tests had the exactly same roughing and holding period schedules, and the only difference in the three 8-passes tests were the post-deformation cooling rates (10°C/s and 20°C/s and 40°C/s).

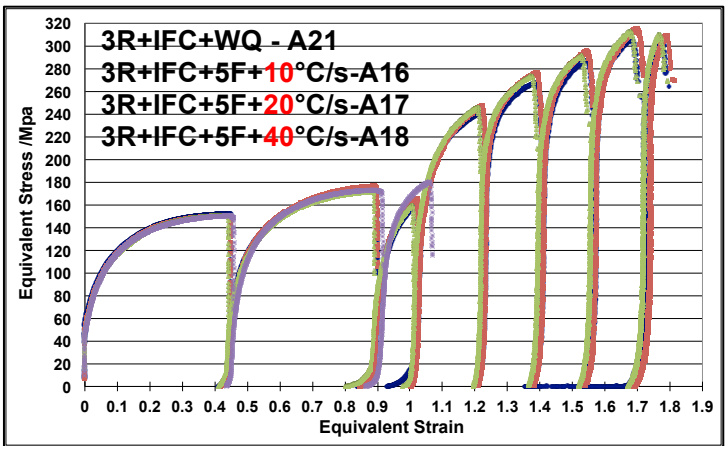

Figure 173: An example of showing great consistency of four similar 8-pass PSC tests of Nb steel A

4.6.4.2. Post-Rolling Cooling Rate

The results of the different post-rolling cooling rates (from the slow natural-air cooling to intense accelerated cooling) influenced on the final microstructures of different steel compositions (steels A, B and C) and similar 8-pass PSC tests are presented in here. It may useful to emphasise that no previous work has been carried out on analysing the accelerated cooling (ACC) after 8-pass PSC testing on the laboratory scale with precise controls of industrial hot rolling parameters (such as temperature, strain and strain rate). Investigating the effects of natural-air cooling and intense water cooling after 8-pass PSC tests to improve steel production is one of the key objectives in this research program, and it is the last stage of replicating whole industrial hot rolling steel plate process on the advanced TMC machine.

First of all, as presented in earlier Figure 173, the recorded temperature-time profiles of the first group of three similar 8-pass PSC tests A16, A17 and A18 are displayed in Figure 174 below in which the average recorded temperature cooling rates were closely agreed with the three target post-deformation cooling rates (10°C/s and 20°C/s and 40°C/s).

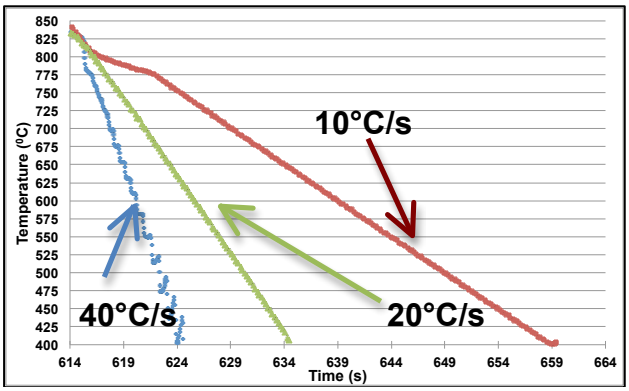

Figure 174: Recorded temperature-time profiles during the last stage accelerated cooling simulation in three similar 8-pass PSC tests

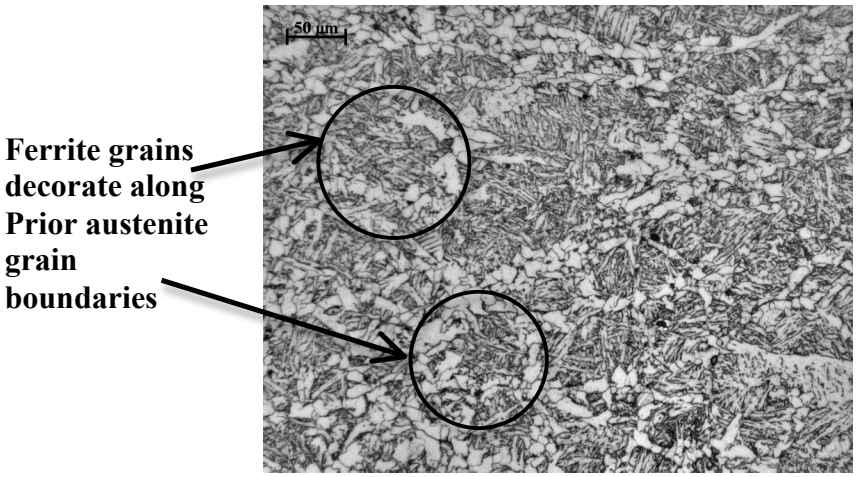

Figure 175: Complex optical microstructures at the sub-surface of 2.5mm deformed PSC sample of Nb steel A after 8-pass PSC test (test A16)

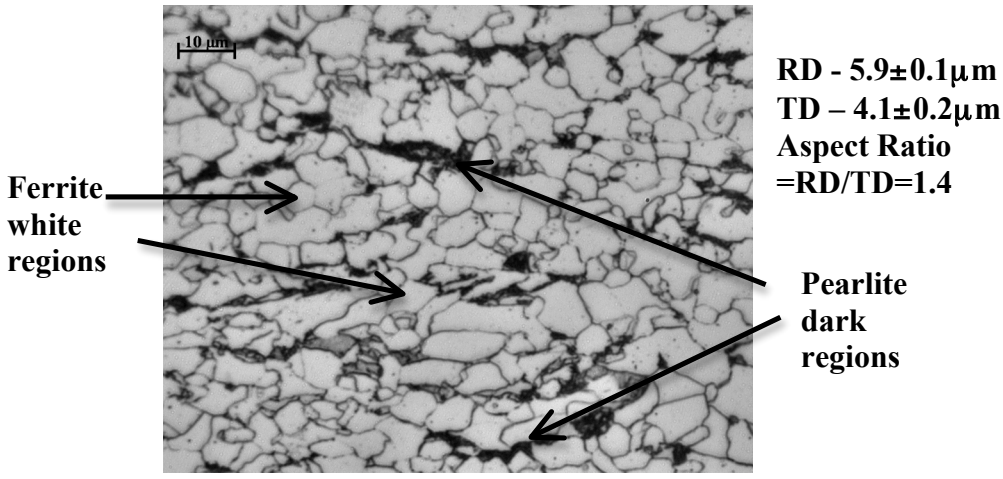

Figure 176: Optical microstructure at the centre of 2.5mm deformed PSC sample of Nb steel A after 8-pass PSC test (3R+IFC+5F) with 10°C/s accelerated cooling rate (test A16)

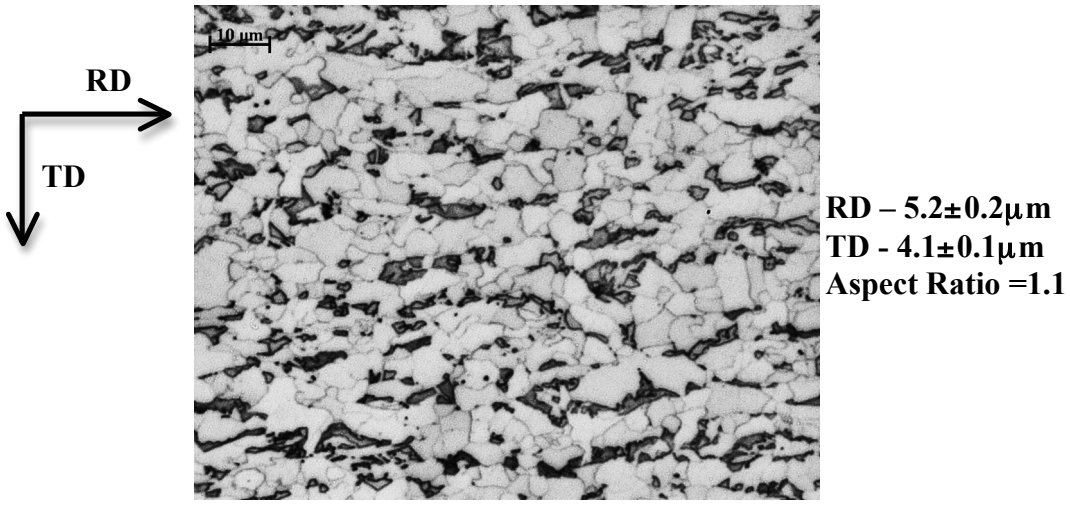

Figure 177: Optical microstructure at the centre of 2.5mm deformed PSC sample of Nb steel A after 8-pass PSC test (3R+IFC+5F) with 20°C/s accelerated cooling rate (test A17)

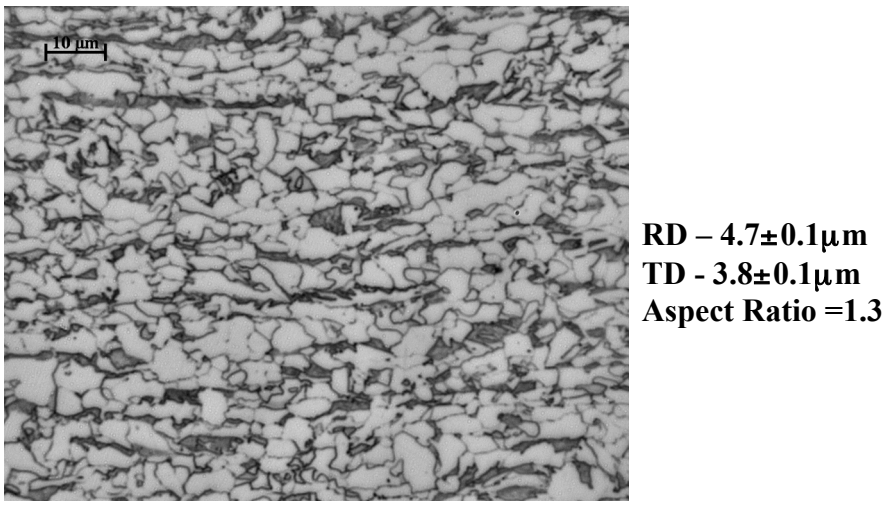

Figure 178: Optical microstructure at the centre of 2.5mm deformed PSC sample of Nb steel A after 8-pass PSC test (3R+IFC+5F) with 40°C/s accelerated cooling rate (test A18)

Similar to the PAGS distribution in Figure 169, the inhomogeneous nature of the transformed microstructures at the sub-surface and centre of 2.5mm deformed PSC specimen are presented in Figures 175 and 176 respectively (due to different applied strain and cooling rates across thickness). As presented in Figure 175, some polygonal ferrite grains were decorated along the prior austenite grain boundaries and with the harder phases (possibly acicular ferrite, bainite, or martensite) inside the PAGS. Under exactly the same 8-pass PSC testing conditions (see earlier Figure 173) prior to the ACC simulation, the ferrite grain size, determined by the average linear intercept method, was reduced from 5.9μm to 5.2μm and 4.2μm at the RD as the applied cooling rate increased from 10 to 20 and 40°C/s respectively in Figures 176, 177 and 178. Furthermore, Figure 179 presents the different ferrite grain size distributions of tests A16 and A18, and as the applied cooling rate increased from 10°C/s to 40°C/s, the ferrite grain size spreading more towards the low values range.

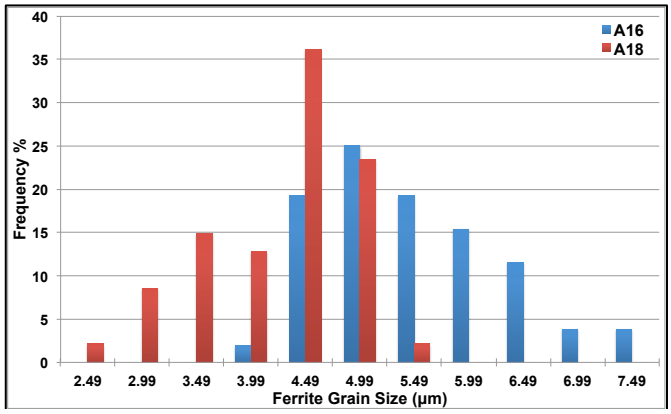

Figure 179: Measured ferrite grain size distributions of two similar 8-pass PSC tests with different accelerated cooling rates (test A16-10°C/s and test A18-40°C/s)

Furthermore, volume fractions of ferrite in these three tests were calculated by the free software ImageJ, and an example is illustrated in Figure 180 below, and the corresponding ferrite volume fractions reduced from 91%, to 86% and 80% as the applied cooling rates increased from 10°C/s to 20°C/s and 40°C/s respectively.

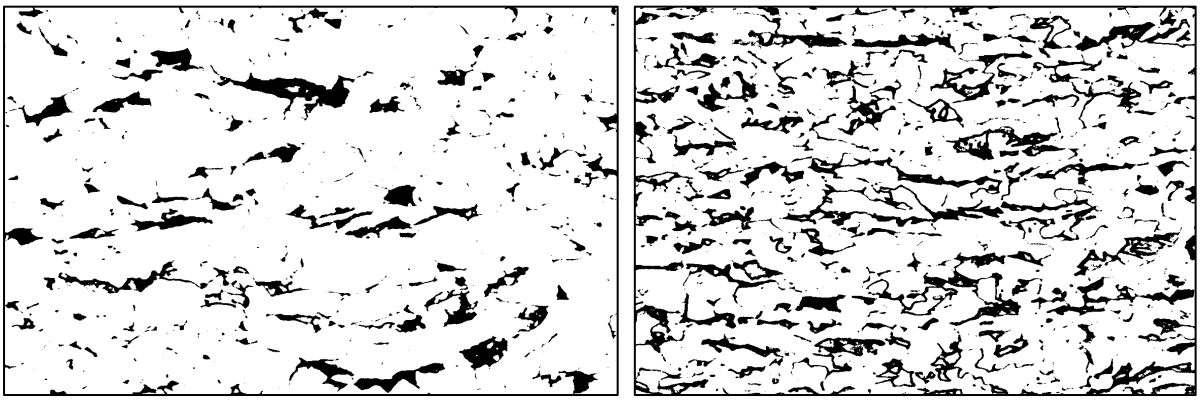

Figure 180: Comparison of volume fractions of ferrite (white regions) and the other phases (dark regions) in tests A16 (left hand side-10°C/s) and A18 (right hand side-40°C/s)

Secondly, another group (266 seconds linear cooling profile was used rather than the implement of complex IFC profile during the HP in the first group tests) of three similar 8-pass PSC tests of Nb steel A were carried out with three different applied post-rolling cooling rates, 0.3°C/s, 5°C/s and 10°C/s, and the corresponding results of multipass flow curves, optical microstructures are shown in the following Figures 181 to 184. It is important to emphasise again that the reliability and good agreements of these three 8-pass PSC tests are essential and can be seen from Figure 181, thus any difference in the observed microstructures were only attributed to the variations in the applied post-deformation cooling rates during final phase transformation. As clearly presented in Figures 181 to 184 where three similar 8-pass PSC tests with almost the same 8-pass flow curves, the average final ferrite grain size was reduced from roughly 12.1μm to 7.3μm and to 6.7μm along the rolling direction (RD). Additionally, the corresponding volume fractions of ferrite, V_F, (measured by the ImageJ program) reduced from 88% to 85% and to 82% respectively when the applied post-deformation cooling rate increased from 0.3°C/s to 5°C/s and to 10°C/s, and the ferrite grain size distribution move towards the low values range (presented in Figure 185).

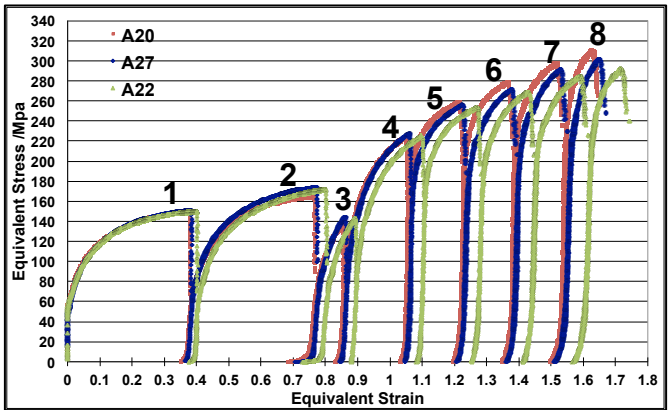

Figure 181: Similar flow curves of Nb steel A in three 8-pass PSC simulation (3R+266 seconds HP+5F) of with three different post-rolling cooling rates (0.3°C/s, 5°C/s and 10°C/s)

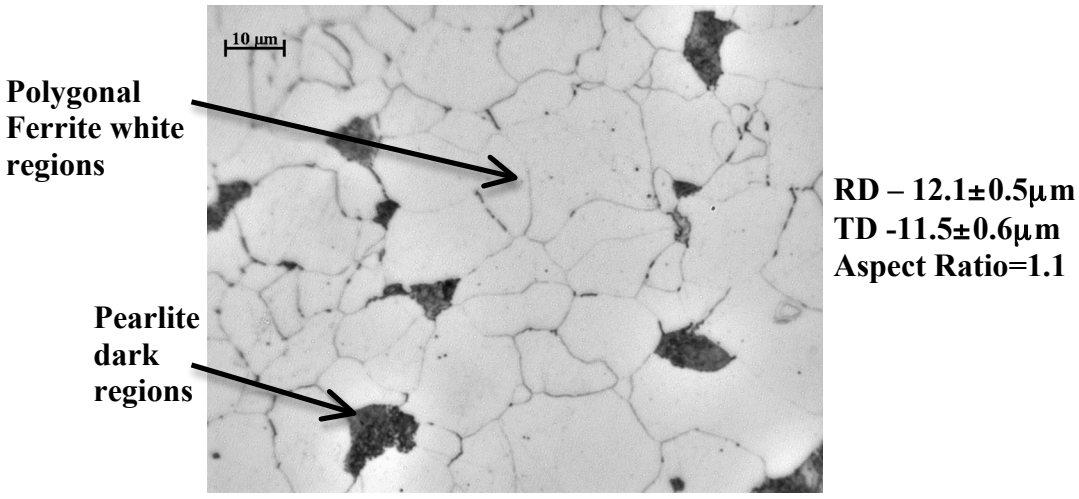

Figure 182: Large ferrite grain size of Nb steel A after 8-pass PSC simulation (3R+266s HP+5F) and with 0.3°C/s post-deformation cooling rate (test A27)

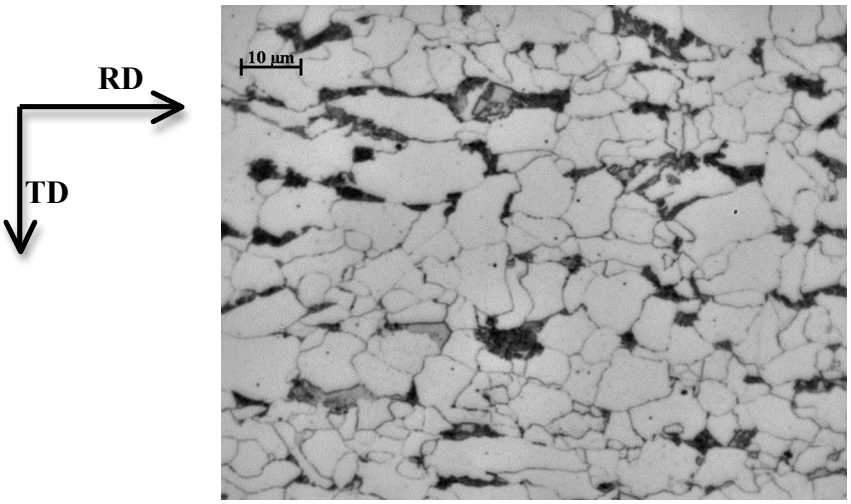

Figure 183: Finer ferrite grain size of Nb steel A after 8-pass simulation (3R+266s HP+5F) with 5°C/s post-deformation cooling rate (test A22)

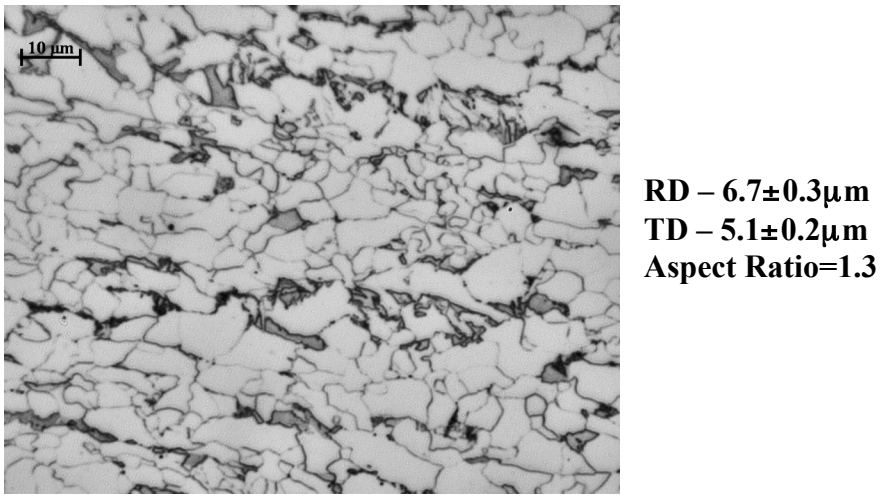

Figure 184: Small ferrite grain sizes after 8-pass simulation (3R+266s HP+5F) with 10°C/s post-deformation cooling rate of Nb steel A (test A20)

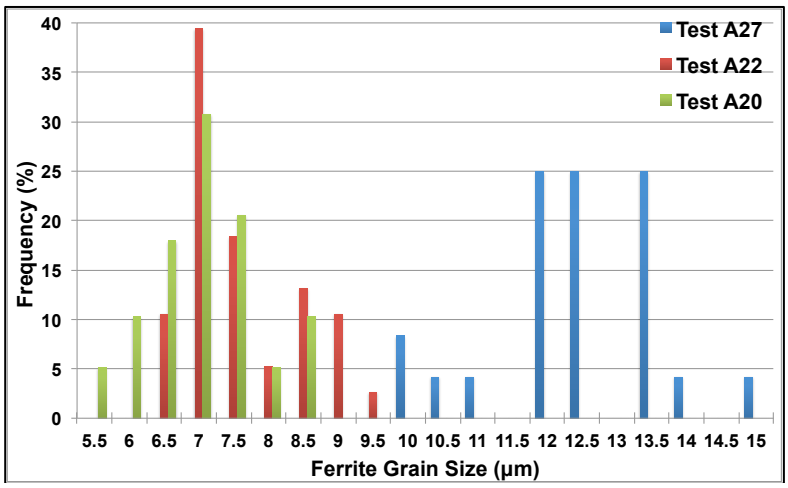

Figure 185: Measured ferrite grain size distributions of Nb steel A in three similar 8-pass PSC tests with three different post-rolling cooling rates (0.3°C/s, 5°C/s and 10°C/s)

Another three similar 8-pass PSC tests (3R+266s HP+5F) were also performed on the Nb+Ti steel B with three different accelerated cooling rates (5°C/s, 10°C/s and 20°C/s), and the corresponding results are shown in the following Figures 186 to 190. Moreover, it is clearly presented in Figure 186 where three similar 8-pass PSC tests with almost the exactly same flow curves (great test consistency), thus the subsequent variation in the average ferrite grain size and volume fraction was only due to the different applied accelerated cooling rates. According to the results of quantitative measurements, the average ferrite grain size increased from about 5.6μm to 6.4μm and to 8.4μm along the rolling direction (RD) when the applied cooling rate 20°C/s reduced to 10°C/s and to 5°C/s, and the corresponding volume fractions of ferrite, V_F, (smaller than those of Nb steel A) increased from 78% to 85% and to 90% respectively. Additionally, as the applied cooling rate increased from 5°C/s to 10°C/s and to 20°C/s, the ferrite grain size spreading more towards the low values range (see Figure 190).

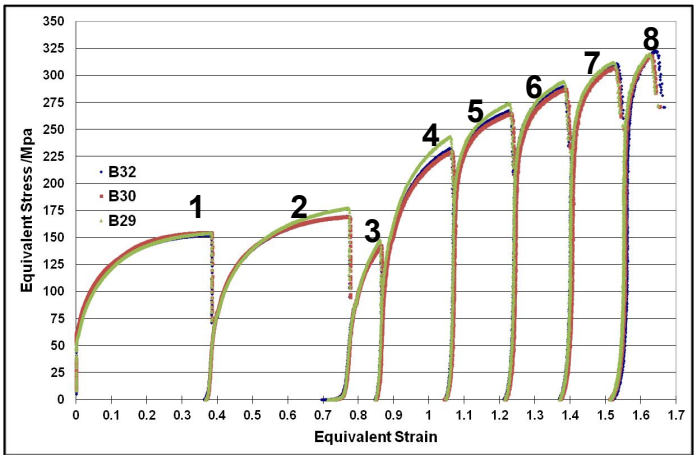

Figure 186: Three similar 8-pass PSC tests (3R+266s HP+5F) of Nb+Ti steel B with only difference in the post-deformation cooling rates (5°C/s, 10°C/s and 20°C/s)

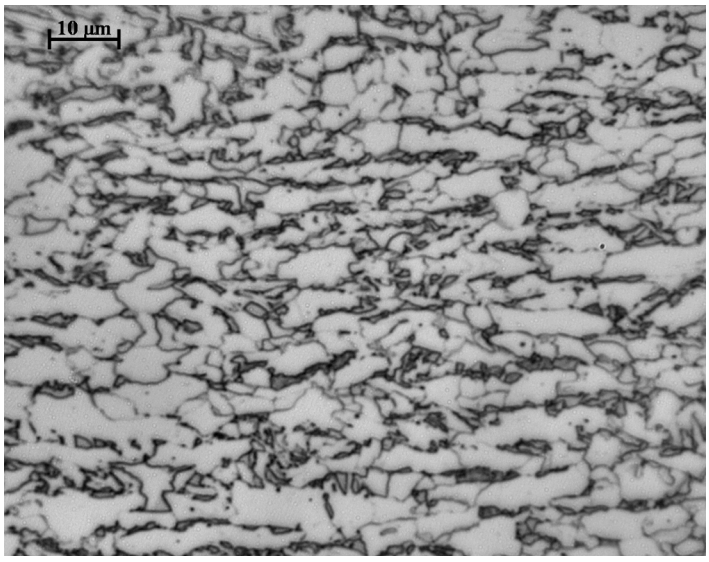

RD – 5.6±0.4μm
TD – 3.4±0.2μm
Aspect Ratio=1.6

Figure 187: Optical microstructure of Nb+Ti steel B after 8-pass PSC deformation (3R+266s HP+5F) and with 20°C/s accelerated cooling rate (test B29)

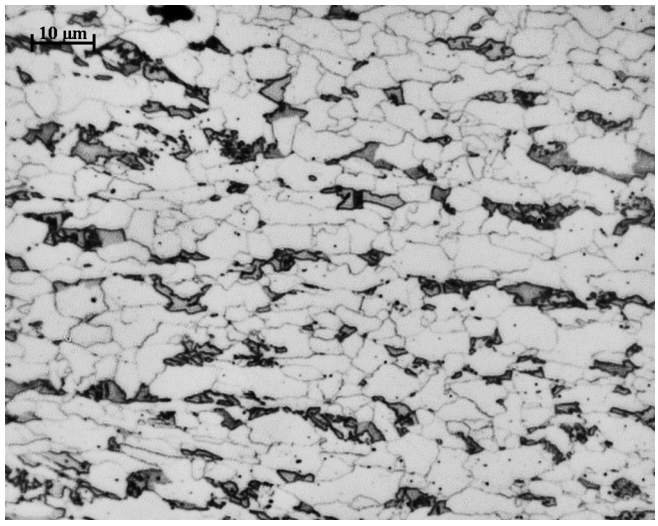

RD – 6.4±0.2µm
TD – 4.1±0.1µm
Aspect Ratio=1.6

Figure 188: Optical microstructure of Nb+Ti steel B after 8-pass PSC deformation (3R+air cooling+5F) with 10°C/s ACC (test B32)

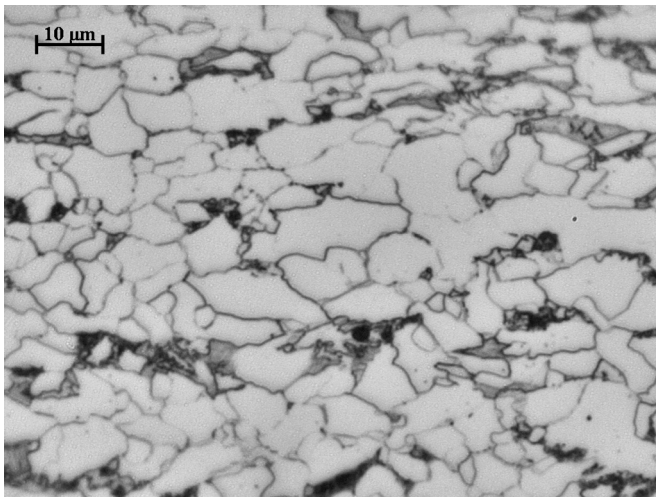

RD – 8.4±0.7µm
TD – 5.4±0.2µm
Aspect Ratio=1.5

Figure 189: Optical microstructure of steel B after 8-pass simulation (3R+air cooling+5F) with 5°C/s ACC (test B30)

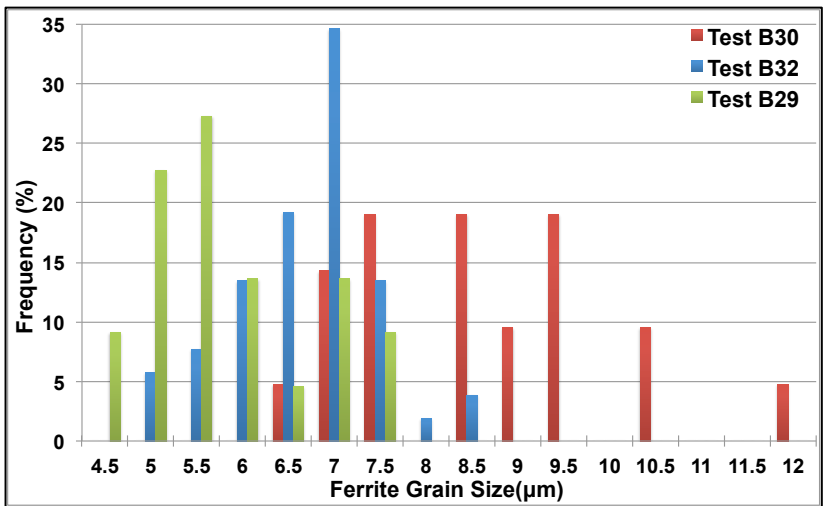

Figure 190: Measured ferrite grain size distributions at RD of steel B in three similar 8-pass PSC tests with different post-rolling cooling rates ((5°C/s, 10°C/s and 20°C/s)

Finally, two similar 8-pass PSC tests (3R+IFC+5F) with a total applied strain ε_{Total} =1.33 were also carried out on the 10mm PSC samples of the plain carbon steel C, with two different post-deformation accelerated cooling rates (5°C/s - test C13 and 10°C/s - test C11), and the flow curves, optical microstructures and ferrite grain size distributions of these two tests are shown in the following Figures 191 to 193. As seen in Figure 191, disagreements are found in the flow curves of these two 8-pass PSC tests, i.e., the test C13 with 5°C/s had relatively higher equivalent stress (about 20MPa) and larger total strain compared to those of test C11 possible due to some errors occurred during the multipass deformations. However, the average ferrite grain sizes of tests C11 still had smaller ferrite grain (6.6μm) than that (7.7μm) of C11 along the RD, shown in Figure 192. Therefore, it may suggest that the ACC is more dominant factor for controlling ferrite grain size compared to relatively larger applied stress and strain during deformation. Additionally, as the applied cooling rate increased from 5°C/s to 10°C/s, the ferrite grain size spreading more towards the low values range (see Figure 193).

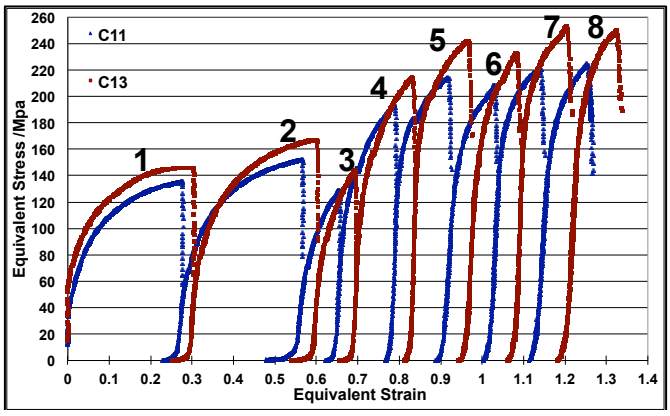

Figure 191: Flow curves of plain carbon steel C in two similar 8-pass PSC tests (3R+IFC+5F) with different accelerated cooling rates (10°C/s and 5°C/s)

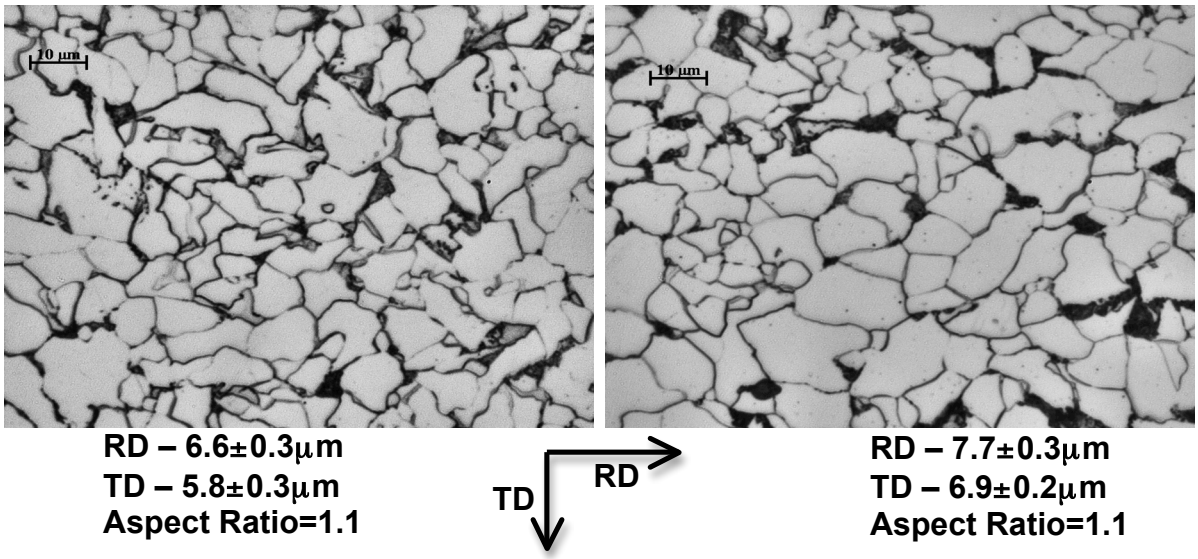

Figure 192: Optical microstructures of steel C after 8-pass simulation (3R+IFC+5F) with ACC of 10°C/s (left hand side-test C11) and with ACC of 5°C/s (right hand side-test C13)

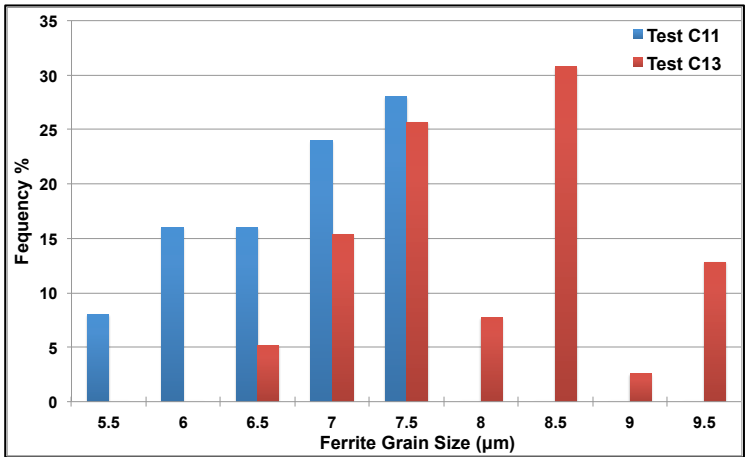

Figure 193: Comparison of ferrite grain size distributions of plain steel C in two similar 8-pass PSC tests (3R+IFC+5F) with different applied accelerated cooling rates (5°C/s –test C13 and 10°C/s -test C11)

4.6.4.3. Finish Rolling Temperatures

After the effects of the most important hot rolling parameter - accelerated cooling (ACC) rates - on the average ferrite grain size d_α and its distributions were investigated and presented in former Section 4.6.4.2, some 8-pass PSC tests with three different steel compositions (steels A, B and C) were specific performed at the relatively lower 5-pass finishing rolling temperatures, $T_{Finishing}$, (the other hot rolling factors, such as strain, strain rate and gap times were set exactly the same) to investigate the influences of deformation temperatures on the multipass flow curves and final transformed optical microstructures.

An example of two similar 8-pass PSC tests (3R+266s-HP+5F+10°C/s) with different 5-pass $T_{Finishing}$ is shown in the following Figures 194 and 195 in which the test A26 had a slightly lower average (about 30°C) $T_{Finishing}$ and post-deformation cooling start temperature than those of test A20. Therefore, the tests A20 and A26 were expected to have similar flow curves (presented in Figure 196), and the test A26 produced a smaller average d_α than that of test A20 due to lower 5-pass finishing temperatures being applied, presented in Figure 197. Indeed, the Figures 197 and 198 show that the test A26 with a relatively lower finish rolling temperature gave a marginally finer ferrite grain size of 6.1μm along the rolling direction (RD) than that of 6.7μm in the test A20. Therefore, it may suggest that the finish-rolling temperature in heavy plate hot rolling is not the most influential parameter for the refinement of the ferrite grain size. Furthermore, the volume fraction of ferrite, V_F, in the lower $T_{Finishing}$ of test A26 is 84%, smaller than that (89%) of test A20, and ferrite grain size distribution move towards low value of ferrite grain size.

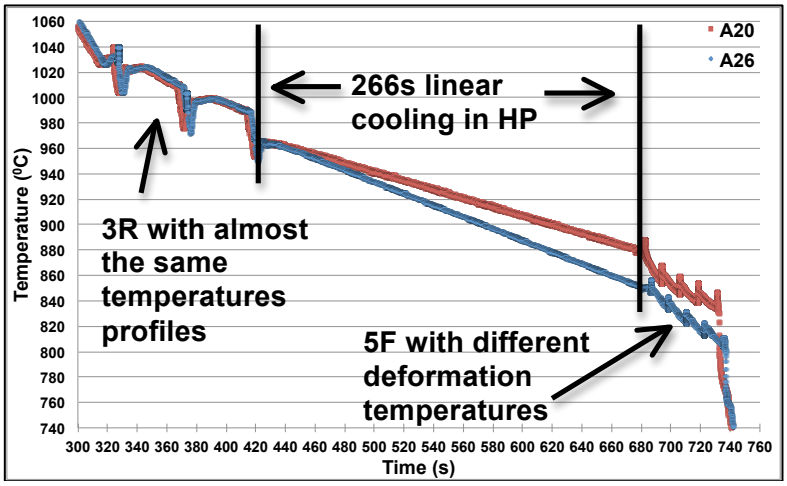

Figure 194: Similar recorded temperature profiles of two similar 8-pass PSC tests (3R+266s HP+5F+10°C/s) with different 5-pass finish rolling temperatures

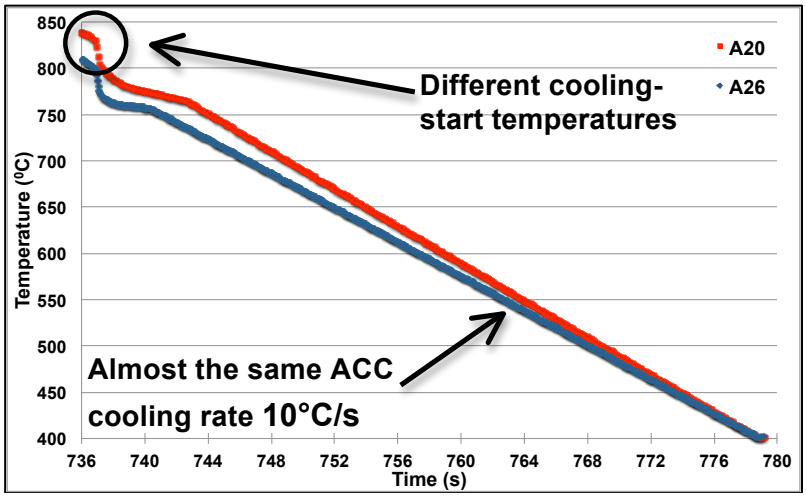

Figure 195: Recorded temperature-time profiles of two similar 8-pass PSC tests during the last stage accelerated cooling simulation

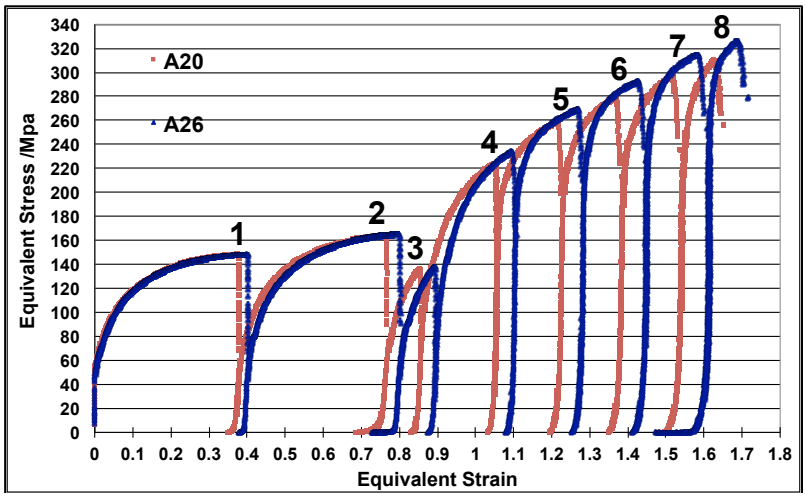

Figure 196: Flow curves comparison of two similar 8-pass PSC tests (3R+266s HP+5F+10°C/s) of Nb steel A with different 5-pass finishing rolling temperatures

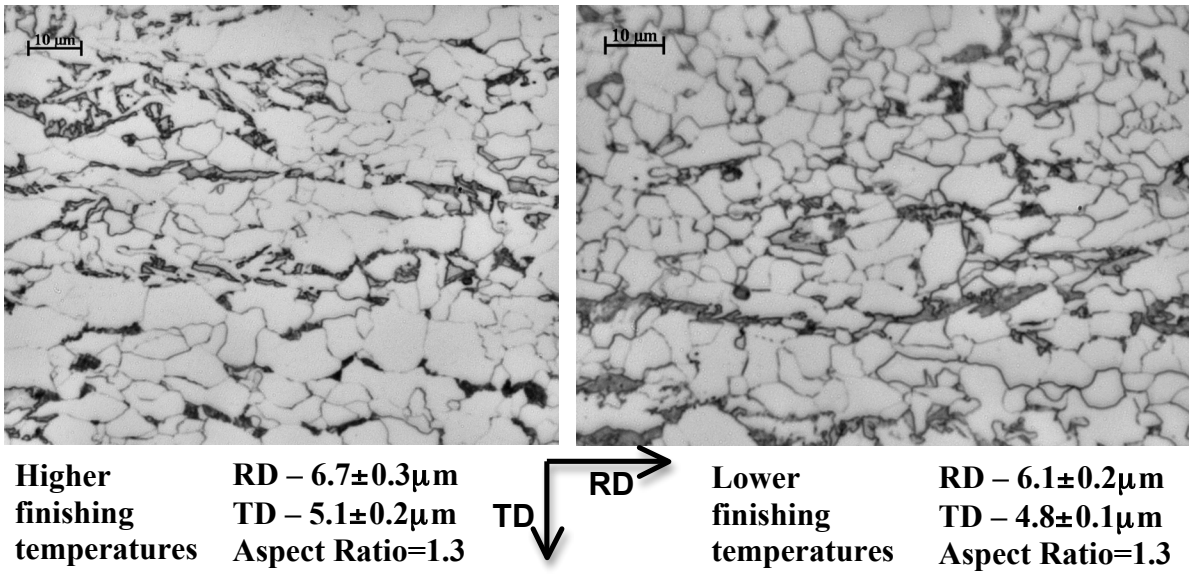

Figure 197: Optical microstructures of Nb steel A in two similar 8-pass PSC tests (3R+266s HP+5F+10°C/s) with different 5-pass finishing rolling temperatures

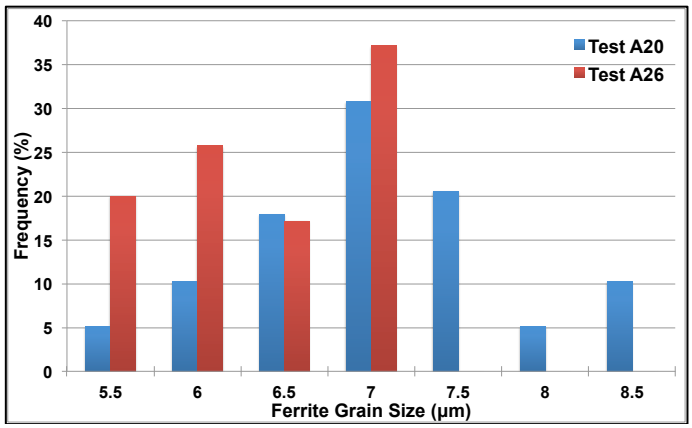

Figure 198: Comparison of ferrite grain size distribution of steel A at the RD of two 8-pass PSC tests with difference in the average temperatures of 5-pass finish rolling

Another two similar 8-pass PSC tests (3R+IFC+5F+10°C/s) with only distinction in the average temperatures $T_{Finishing}$ of 5-pass finishing deformation was also performed on the Nb+Ti steel B, and the results of temperature profiles, flow curves, optical microstructures and d_α distributions of these two tests are presented in the following Figures 199, 200, 201 and 202 respectively. It is clearly presented in Figure 199 that both tests had almost the same temperature profiles during 3-pass roughing, and the test B35 had a higher average 5-pass finishing temperatures (almost 55°C) than the $T_{Finishing}$ of test B39. Therefore, it is expected that the test B39 had a higher average equivalent stress (roughly 30MPa) than that of test B35 during the 5-pass finishing, shown in Figure 200. However, based on the quantitative measurement of the ferrite grain sizes in tests B35 and B39, which are 5.9µm and 5.3µm along the RD respectively, only a small amount of d_α refinement has been achieved when reducing the average deformation temperatures of 5-pass finishing by 55°C.

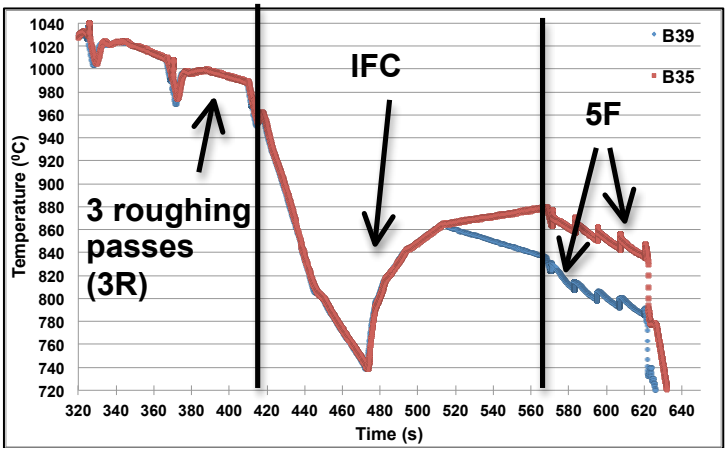

Figure 199: Similar recorded temperature profiles of two similar 8-pass PSC tests (3R+266s HP+5F+10°C/s) with different 5-pass finish rolling temperatures

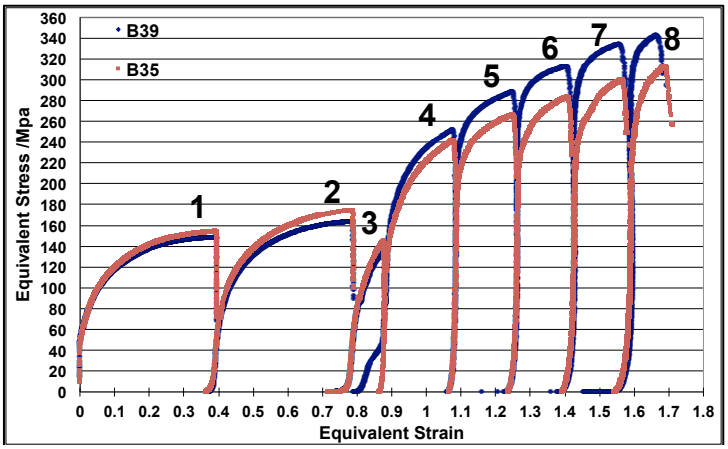

Figure 200: Flow curves of Nb+Ti steel B in two similar 8-pass PSC tests (3R+IFC+ 5F+10°C/s) with different 5-pass finish rolling deformation temperatures

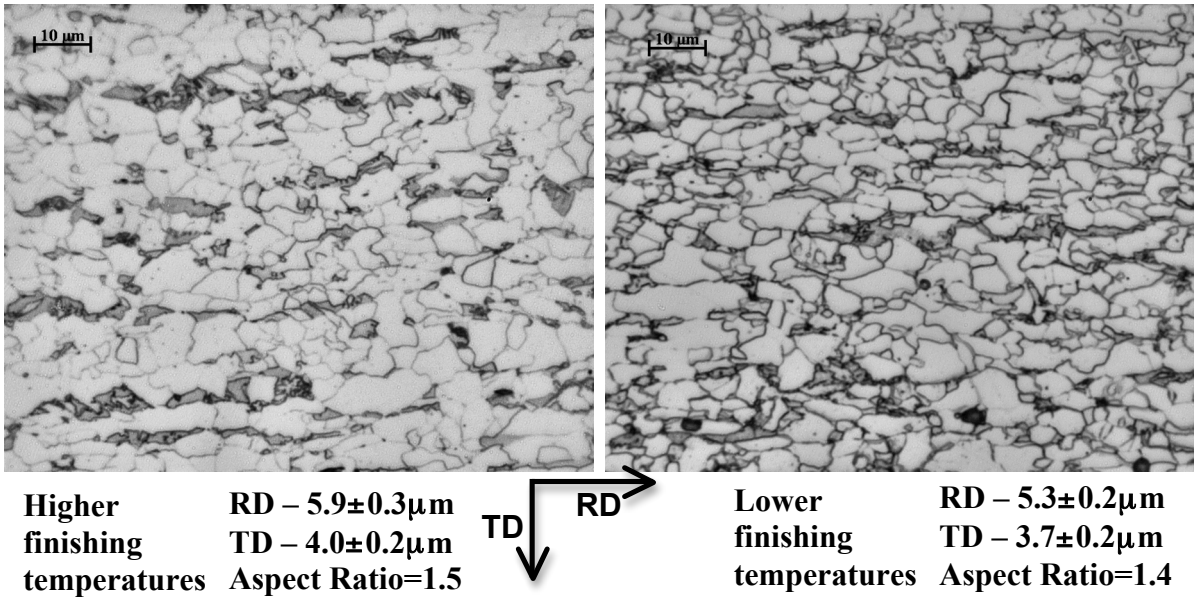

Figure 201: Optical microstructures of Nb+Ti steel B after two 8-pass PSC tests: higher finishing temperatures (left hand side) and lower finish rolling temperatures (right hand side)

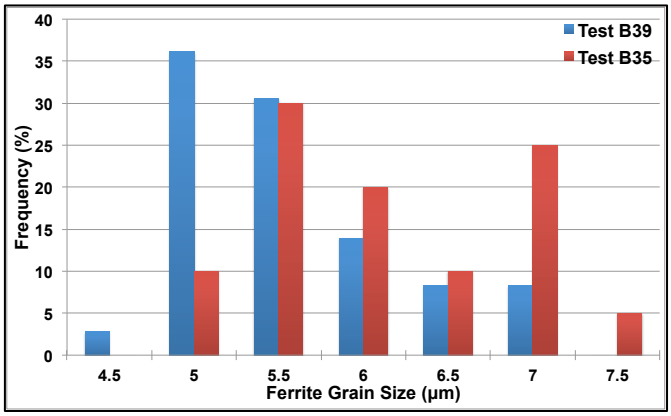

Figure 202: Ferrite grain size distributions along the RD of steel B in two 8-pass PSC tests with variation in the average temperatures of 5-pass finishing

Additionally, the volume fraction of ferrite reduced from 88% to 80% and the spreading of ferrite grain size shift marginally towards left hand side-smaller value range when lower the $T_{Finishing}$ of 5-pass finishing.

Finally, two similar 8-pass PSC tests (3R+IFC+5F+10°C/s) were performed on the plain carbon steel C with a total applied strain ε_{Total} =1.7, and the only difference between these two tests were the 5-pass finishing rolling temperatures, $T_{Finishing}$, which were 870°C, 862°C, 854°C, 848°C and 841°C for the test C9 while 826°C, 802°C, 790°C, 784°C and 777°C for the test C14. Therefore, test C14 required a higher load to deform the sample to the same total reduction owing to an increase in the deformation resistance as lowered $T_{Finishing}$, illustrated in Figure 203 below. Furthermore, according to the results of optical microstructures and ferrite grain size distributions, presented in Figure 204 and 205, respectively, the average ferrite grain size was refined from 6.5μm to 5.5μm at RD and volume fraction of ferrite decreased from 90% to 84% due to more pearlite are introduced into transformation microstructures when reduced the average $T_{Finishing}$ by about 60°C.

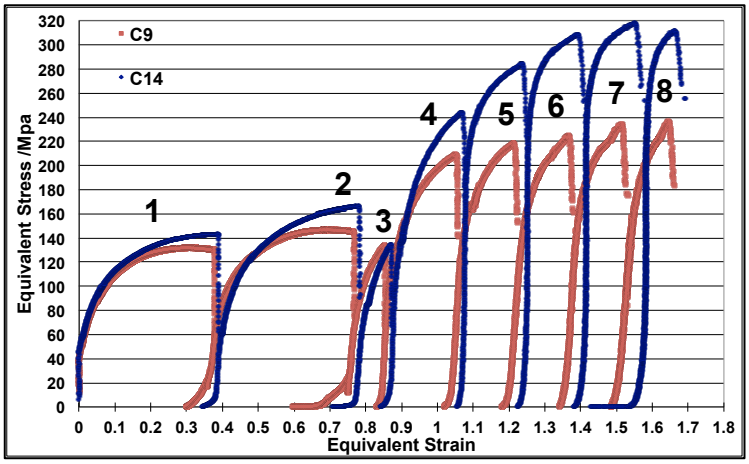

Figure 203: Flow curves comparison of steel C in two similar 8-pass PSC tests (3R+IFC+5F+10°C/s) with alterations in the finishing passes deformation temperatures

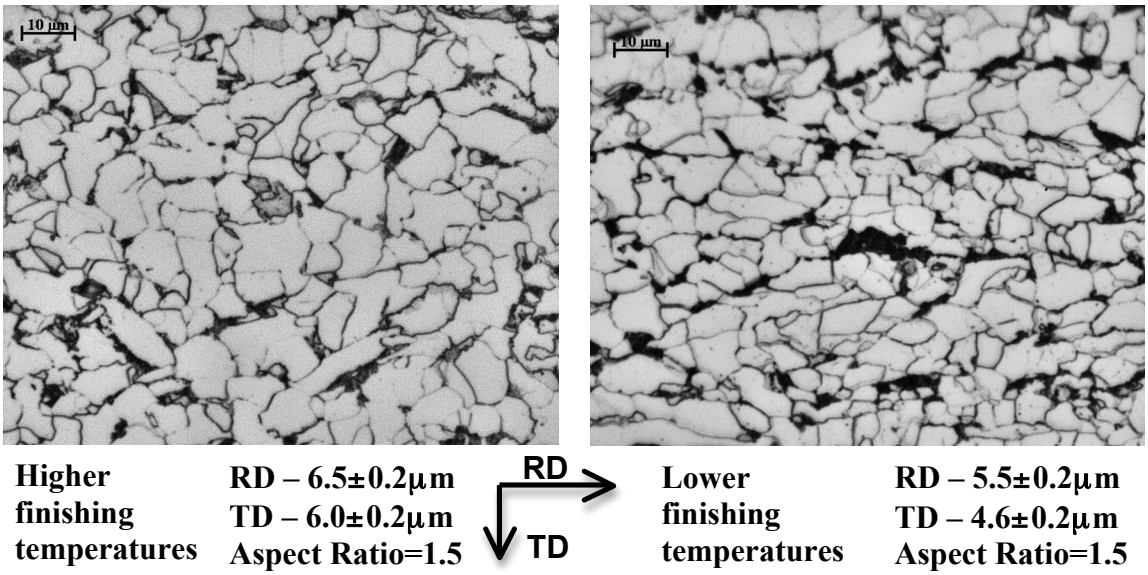

Figure 204: Optical microstructures of plain carbon steel C after two 8-pass PSC tests (3R+IFC+5F+10°C/s) with different finish rolling temperatures

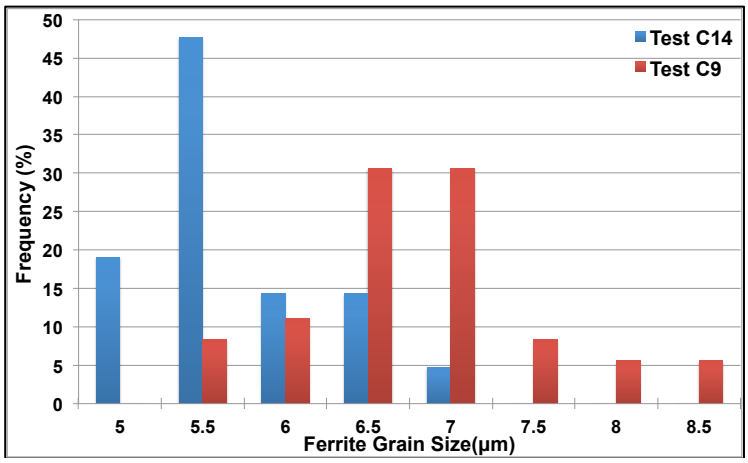

Figure 205: Ferrite grain size distributions along the RD of plain carbon steel C in two 8-pass PSC tests with variation in the average temperatures of 5-pass finish rolling

4.6.4.4. Effects of Intermediate Forced Cooling (IFC) on Ferrite Grain Size

As mentioned earlier, the first two advantages (shortening the necessary but long HP or increasing the productivity and reducing the prior austenite grain coarsening) of employing the intermediate forced cooling (IFC) during the HP were already clearly presented in previous Section 4.6.3.3. The other benefit of applying the complex IFC (forced cooling and recalescence) during the HP instead of 266 seconds linear cooling from about 980°C to 880°C on the 8-pass PSC tests to refine the final as-rolled microstructures, particularly on the reduction of ferrite grain size in different 8-pass PSC tests are shown in here. For example, the following Figure 206 presents that test A24 had the same 3-pass roughing temperature profiles but different cooling conditions during the HP and less total simulation time compared with test A25.

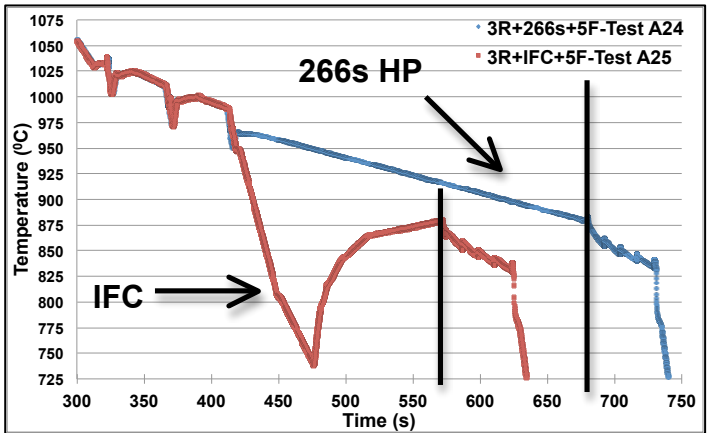

Figure 206: Recorded temperature profiles of two similar 8-pass PSC tests with different cooling conditions during the HP and total simulation time

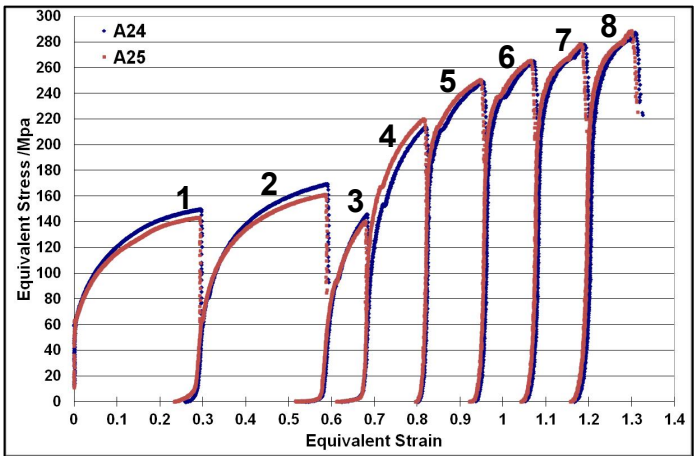

Figure 207: Similar flow curves of Nb steel A in two similar 8-pass PSC test conditions with different temperature profiles during HP

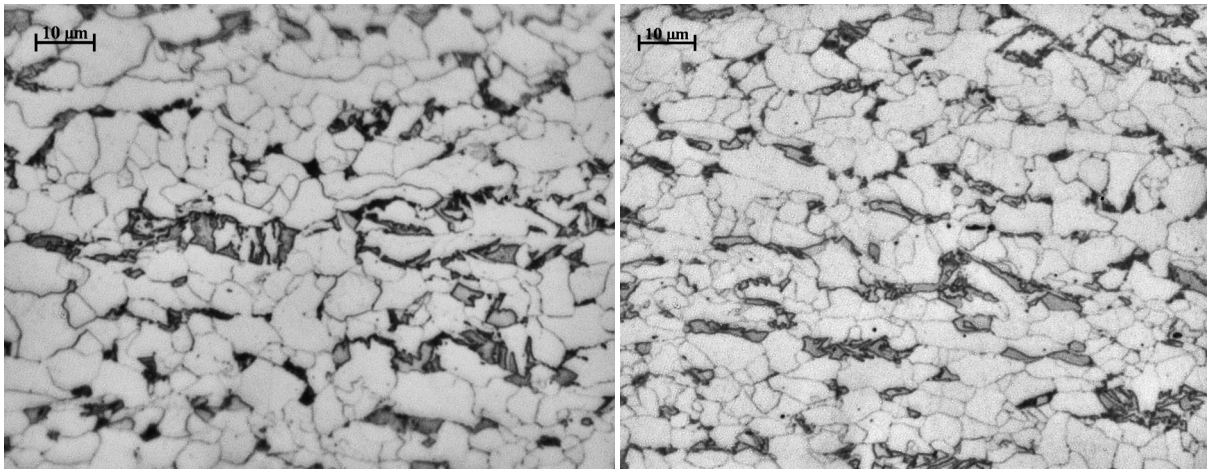

266s linear cooling in HP **RD – 6.9±0.3µm TD – 5.3±0.2µm Aspect Ratio=RD/TD=1.3**

IFC in HP **RD – 6.0±0.2µm TD – 4.5±0.2µm Aspect Ratio=1.3**

Figure 208: Optical microstructures of steel A in two 8-pass PSC tests with 266 seconds (test A24-left hand side) and with the IFC (test A25-right hand side) during HP and 10°C/s ACC

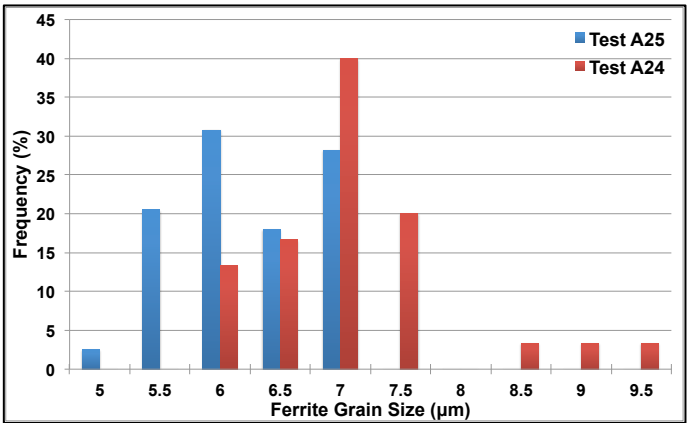

Figure 209: Ferrite grain size distributions along the RD of Nb steel A in two similar 8-pass PSC tests with variation in the average temperatures of 5-pass finishing

It is clearly presented in Figures 207 to 209 that under almost the same 8-pass flow curves and ACC of 10°C/s, a smaller average ferrite grain size (6μm) at the RD is found at the test A25 than that (6.9μm) of test A24, which attributed only to applying the complex IFC technique rather than 266 seconds linear cooling during the HP. Furthermore, the volume fraction of ferrite (90%) of test A25 with IFC is larger than that (86%) of test A24.

Secondly, two similar 8-pass PSC tests (3R+266s/IFC+5F+10°C/s) were carried out on the Nb+Ti steel B with total applied strain ε_{Total} =1.33 and two different cooling profiles (266s linear cooling and complex IFC temperature cooling and recalescence) during the HP from 980°C to 880°C (see previous Figure 206). The corresponding results of similar flow curves, optical microstructure and ferrite grain distributions of these two tests (B31- 266s and B36-IFC) are presented respectively in Figures 210, 211 and 212. Similar to the results of Nb steel A, Nb+Ti steel B also shows that implement of the IFC into long HP not only improved productivity but also refined the average ferrite grain size.

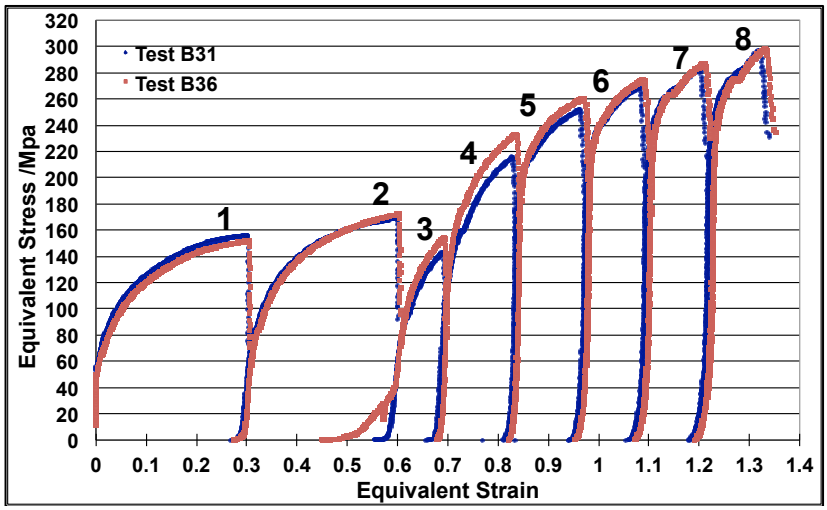

Figure 210: Flow curves of Nb+Ti steel B in two similar multipass PSC tests with only difference in the cooling conditions during HP (B31- 266s and B36- IFC)

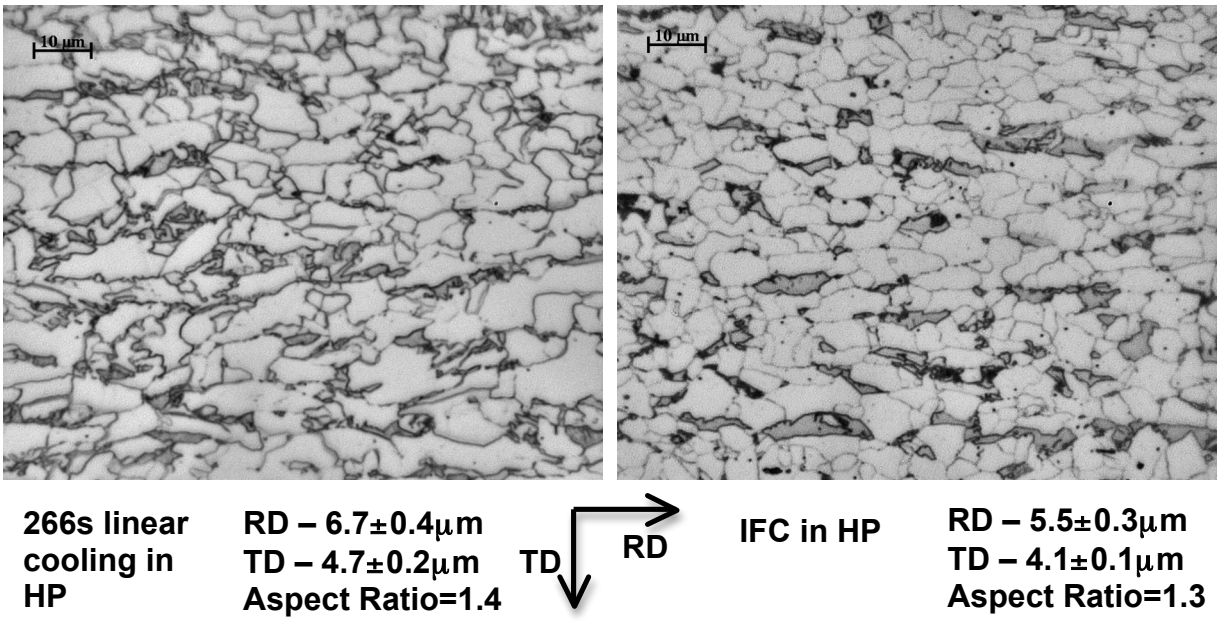

Figure 211: Optical microstructures of Nb+Ti steel B in two similar 8-pass PSC tests (3R+266s/IFC+5F+10°C/s) with different cooling conditions at the HP

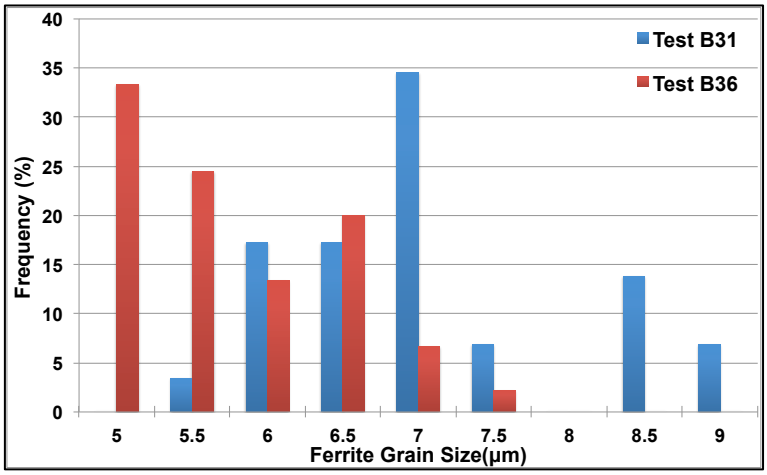

Figure 212: Ferrite grain size distributions along the RD of Nb+Ti steel B in two 8-pass PSC tests with only variation in the cooling profiles of HP

Thirdly, another two similar 8-pass PSC tests (3R+266s/IFC+5F+10°C/s) were performed on the Nb+Ti steel B but with larger total applied strain ε_{Total} =1.7, and on the two 12mm rather than 10mm initial thickness of PSC samples, so that the effect of higher total applied strain on the ferrite grain size refinement could be analysed. These two tests also had different HP cooling profiles (266s linear cooling - test B32 and complex IFC temperature cooling and recalescence - test B35). It is clearly illustrated in Figure 213 that both tests had similar flow curves or deformation history, so any variation on subsequent average ferrite grain size (presented in Figures 214 and 215) only attributed to the different cooling conditions during the HP. Moreover, the test B35 gave slightly finer (5.9µm) than that (6.4µm) of test B32, and greatly reduced the volume fractions of pearlite and others phases from 25% to 10%.

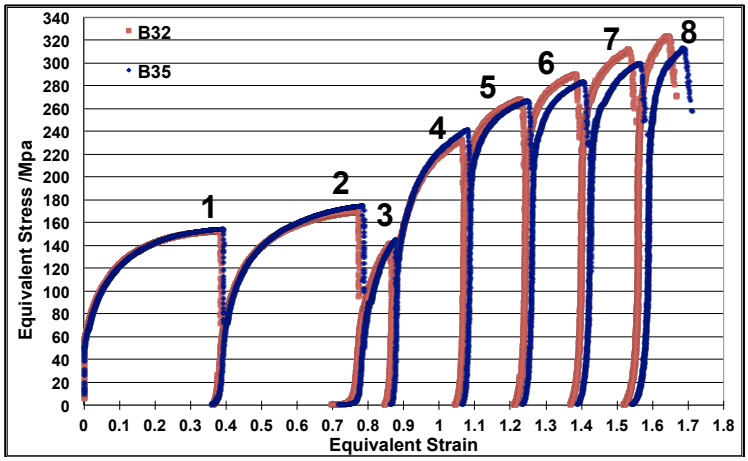

Figure 213: Flow curves of Nb+Ti steel B in two similar 8-pass PSC tests (3R+266s/IFC +5F+10°C/s) with only dissimilarity in the cooling profiles during HP

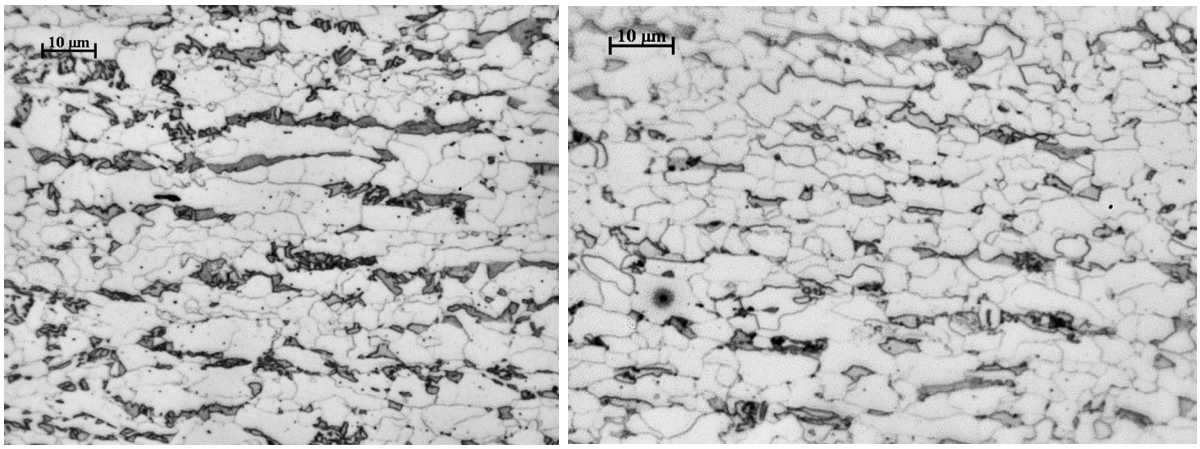

266s in HP — **RD – 6.4±0.3µm**, **TD – 4.1±0.1µm**, **Aspect Ratio=1.6**

IFC in HP — **RD – 5.9±0.3µm**, **TD – 4.0±0.2µm**, **Aspect Ratio=1.5**

Figure 214: Optical microstructures of steel B in two similar 8-pass PSC tests (3R+266s/IFC +5F+10°C/s) with same total applied strain ε_{Total} =1.7 but different HP cooling profiles

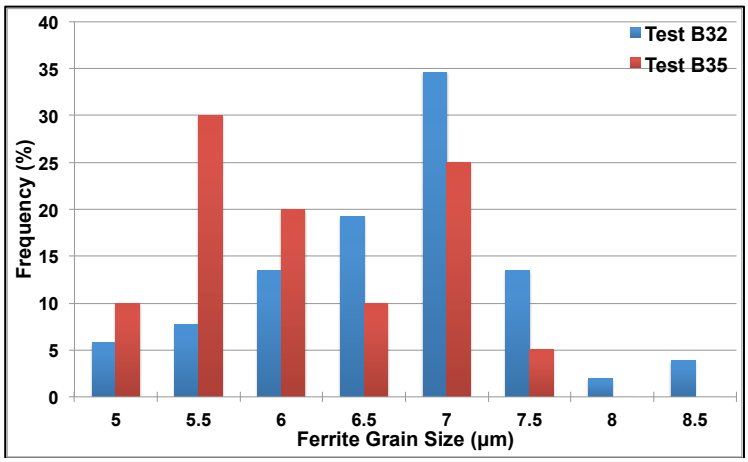

Figure 215: Ferrite grain size distributions of Nb+Ti steel B along the RD of two similar 8-pass PSC tests with only variation in the HP cooling profiles

Finally, two similar 8-pass PSC tests (3R+266s/IFC+5F+10°C/s) were also carried out on the plain carbon steel C with same total applied strain ε_{Total} =1.7 but different cooling profiles (266s linear cooling - test C8 and complex IFC temperature profile - test C9, see previous Figure 206) during the HP. Similar to former results of Nb steel A and Nb+Ti steel B, and under almost the same 8-pass flow curves and applied post-rolling ACC of 10°C/s, smaller average ferrite grain size (6.5μm) at the RD are found at the test C9 than that (7.7μm) of test C8, which are presented in the following Figures 216 to 218. Therefore, the complex IFC technique not only be employed into HP of microalloyed steel plate hot rolling production but also can be applied into plain carbon steel plate hot rolling process to further reduce average ferrite grain size.

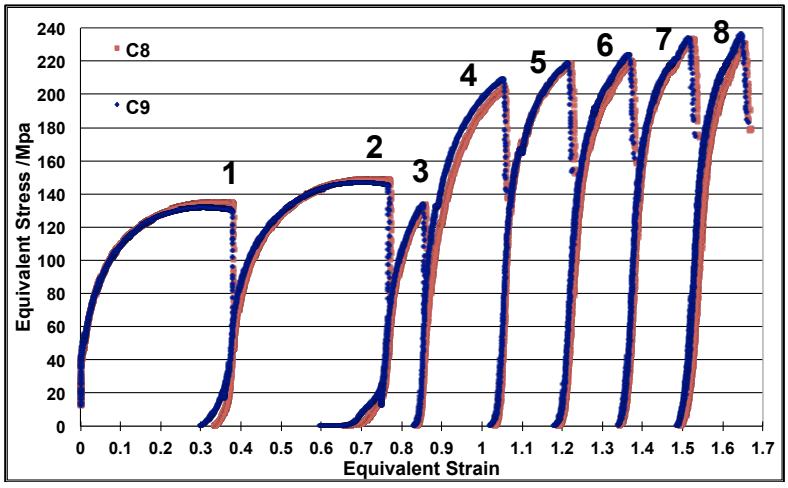

Figure 216: Flow curves of plain carbon steel C in two similar 8-pass PSC tests (3R+266s/IFC+5F+10°C/s) with different cooling during the HP

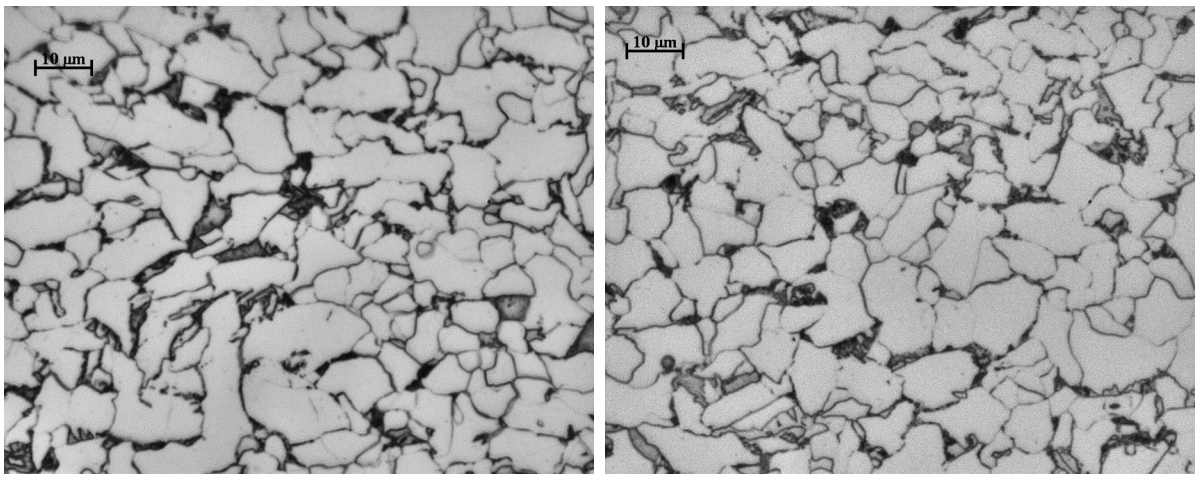

266s in HP **RD – 7.7±0.3μm TD – 6.8±0.3μm Aspect Ratio=1.5**

IFC in HP **RD – 6.5±0.2μm TD – 6.0±0.2μm Aspect Ratio=1.5**

Figure 217: Optical microstructures of plain carbon steel C in two 8-pass simulation with 266 seconds (left hand side-test C8) and IFC (right hand side-test C9) during HP

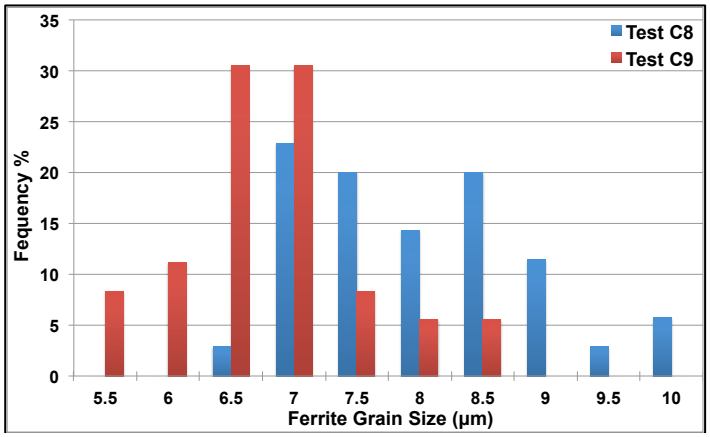

Figure 218: Ferrite grain size distributions along the RD of plain carbon steel C in two 8-pass PSC tests with variation in average temperatures of 5-pass finishing

4.6.4.5. Chemical Composition

There is no doubt that the chemical composition of the steel, particularly for the additions of MAE (Nb and Ti), plays a major role in the prior austenite grain size evolution and subsequent ferrite grain refinement processes. Hence, comparisons of the flow curves and the corresponding observed optical microstructures between the Nb steel A, Nb+Ti steel B and plain carbon steels C and D were made whenever possible and relevant. Furthermore, due to some flow curves and associated optical microstructures of similar 8-pass PSC tests but different in steel compositions were already presented at the former Sections 4.6.4.2 to 4.6.4.4, a group of four 8-pass PSC tests with the same testing schedule but different steel composition (steels A, B, C and D) is included in here. It is clearly demonstrated in Figures 219 - 222 that under exactly the same testing conditions (3R+IFC+5F+10°C/s), the Nb+Ti steel B had the largest equivalent stress and the smallest average d_α in these four steels.

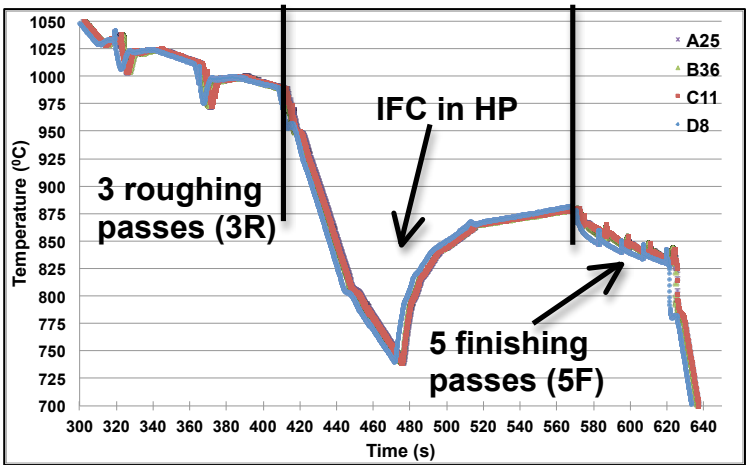

Figure 219: Almost the same recorded temperature profiles of four similar 8-pass PSC tests (3R+IFC+5F+10°C/s) with only difference in the steel compositions

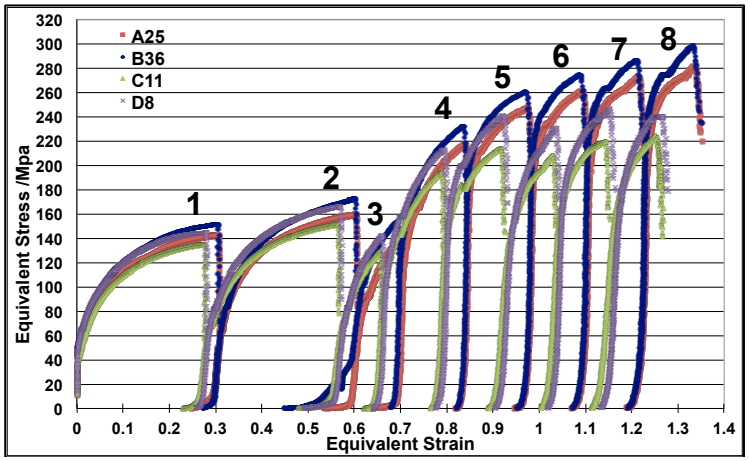

Figure 220: Similar flow curves of four 8-pass PSC simulation (3R+IFC+5F+10°C/s) with four different steel compositions

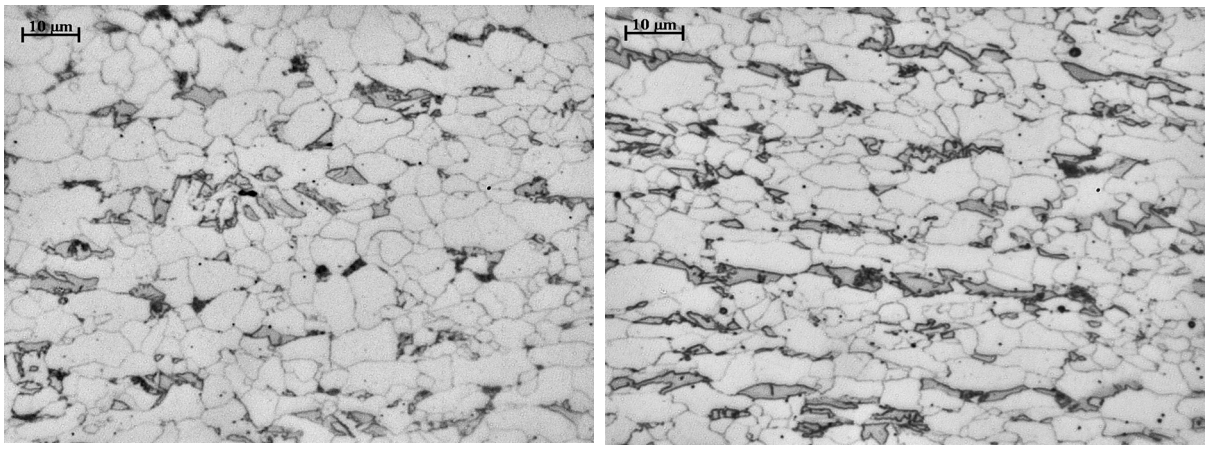

Steel A
Test A25
RD – 6.0±0.2µm
TD – 4.5±0.2µm
Aspect Ratio=1.3

Steel B
Test B36
RD – 5.5±0.3µm
TD – 4.1±0.1µm
Aspect Ratio=1.5

Figure 221: Optical microstructures of steel A (left hand side) and steel B (right and side) after the same 8-pass PSC tests (3R+IFC+5F+10°C/s)

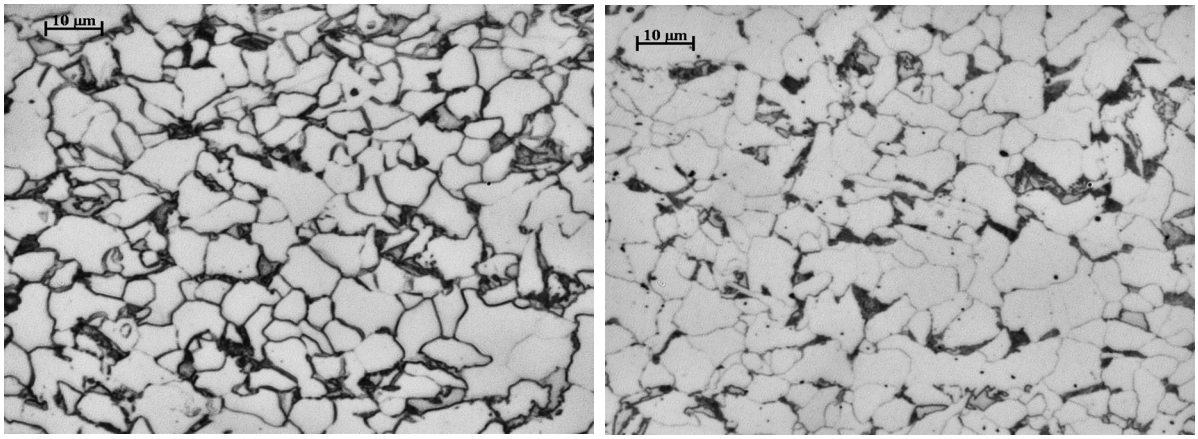

Steel C
Test C11
RD – 6.6±0.3µm
TD – 5.8±0.3µm
Aspect Ratio=1.1

Steel D
Test D8
RD – 6.3±0.4µm
TD – 5.6±0.3µm
Aspect Ratio=1.1

Figure 222: Optical microstructures of two 8-pass PSC tests (3R+IFC+5F+10°C/s) with different steel compositions

4.7. Heavy Plate Surface and Centre Profiles during Industrial Hot Rolling Production

4.7.1. Modelling Temperature, Strain and Strain Rate Distributions

It is widely recognised that at each rolling pass of commercial hot rolling steel plate processes, non-uniform distributions of important hot rolling factors, such as temperature, effective strain, accumulated metallurgical strain caused by non-completed recrystallisation, and strain rate are found across thickness of as-rolling heavy plate. These in turn caused subsequent heterogeneous ferrite grain size distribution and non-uniform mechanical properties through thickness of as-rolled plate. Furthermore, there is a lack of information available regarding industry actually recording data of these important hot rolling parameters distributions through the thickness of heavy plate. Therefore, it is very useful and necessary to predict these distributions through the finite difference (FD) and finite element (FE) methods. The following Figures 223-227 were the predicted results of the deformation temperature, effective strain, total strain, accumulation strain and strain rates respectively across the heavy plate thickness (from 230mm to 60mm) during the 16-pass commercial hot rolling process of microalloyed steel 8AK39 (see Experiment chapter Section 3.9.1). These results were determined by the IMPress model (developed by Tata Steel Europe RD&T) and the model was been taken into account of the crucial metallurgical events (such as recrystallisation, grain growth and strain induced precipitation) occurring during the hot rolling process.

First of all, theses figures have confirmed that the inhomogeneous distributions of some important parameters across thickness of heavy plate, particularly the huge deformation temperature difference (see Figure 223 below) between the sub-surface and centre of plate during the rough rolling stage (the first ten passes were rough rolling).

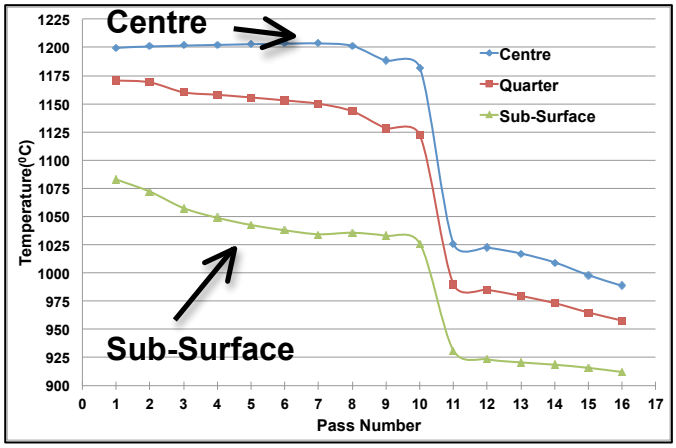

Figure 223: Different predicted temperature profiles across thickness of as-rolling heavy plate at each industrial rolling pass by the IMPress model

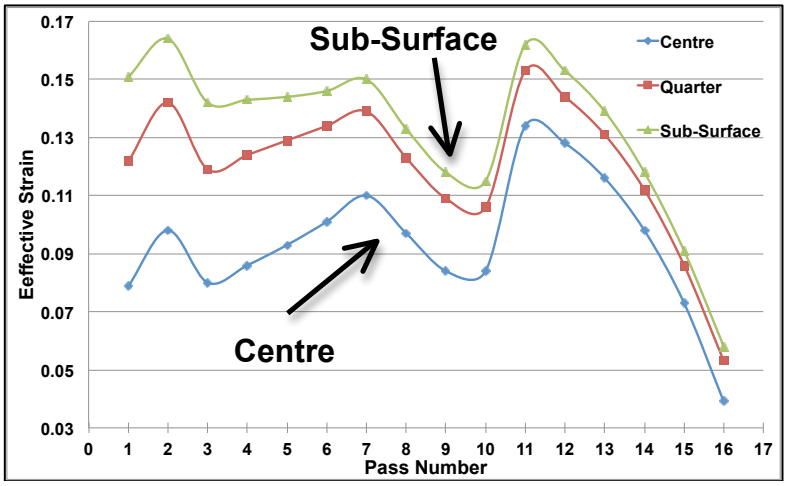

Figure 224: Different predicted effective strain profiles through thickness of as-rolling heavy plate at each industrial rolling pass by the IMPress model

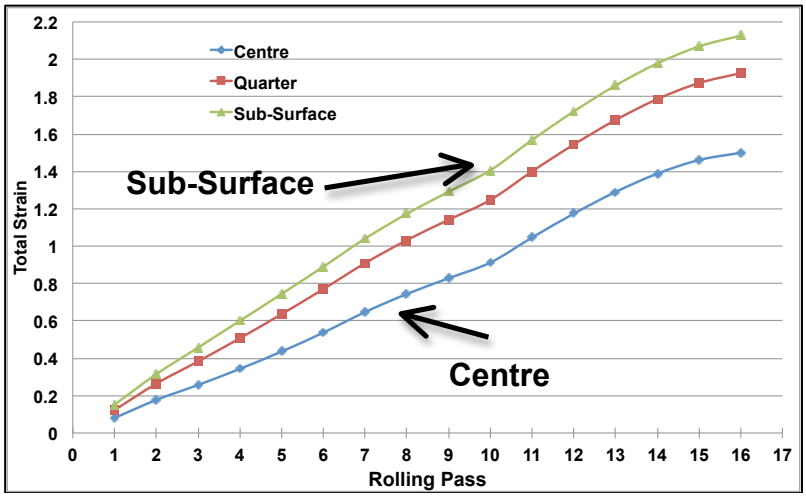

Figure 225: Different predicted effective total strain profiles through thickness of as-rolling heavy plate at each industrial rolling pass from the IMPress model

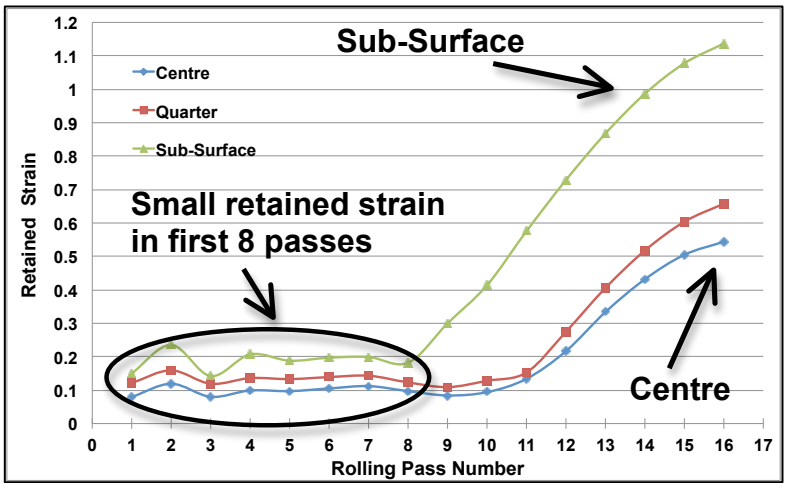

Figure 226: The predicted retained strain at the each industrial rolling pass (due to different fraction of recrystallisation at each deformation) by the IMPress model

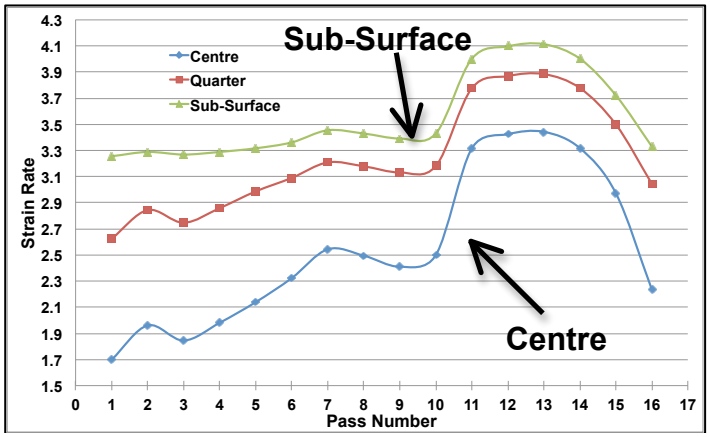

Figure 227: Predicted strain rate distribution inside industrial hot rolling schedule for 8AK39 heavy plate steel production from the IMPress model

Furthermore, much larger values of effective strain, total applied strain, accumulated metallurgical strain and strain rate are found at the heavy plate sub-surface than those at the interior of the heavy plate, illustrated in Figures 224 to 227 respectively. These predicted values were then used as the input values (deformation temperature, effective strain and strain rate) for multipass PSC tests and to simulate the flow curves and PAGS at the specific positions (such as sub-surface and centre of the plate thickness) of the plate thickness.

4.7.2. Flow Curves and PAGS of 3-Pass Roughing at Heavy Plate Surface and Centre

As clearly presented in Figure 225, the total applied strain at the heavy plate sub-surface is more than 2, which is above the maximum applied strain limit of TMC machine. Therefore, for this specific industrial hot rolling schedule, only the deformation and cooling history across the thickness of the heavy plate at the first ten roughing pass and holding period cooling can be fully simulated on the TMC machine. In terms of PSC simulation process of 3-pass roughing, the input parameters of the first PSC deformation were the average values of deformation temperatures and strain rates, as well as the total applied strains of the 1st and 2nd (1-2) industrial roughing passes, and those input values of the second and third PSC passes were the mean values of the 3rd to 7th (3-7) and 8th to 10th (8-10) industrial roughing passes, respectively. The following Table 13 shows that actual input values at the multipass PSC tests were similar to the predicted average hot rolling factors by the IMPress model, except the actual deformation temperatures dropped too much between passes for the PSC simulation at plate centre. Thus, the different flow curves at the sub-surface and centre of heavy plate at the end of roughing can be simulated through the multipass PSC tests.

Although much higher individual strains were applied at the 3-pass PSC deformation compared to the small reductions in the 10-pass industrial roughing, the two distinguish flow

curves in Figure 228 still can demonstrate the massive differences in rolling profile or deformation resistance at the heavy plate surface and centre due to the huge temperature variation. In addition, it is clearly illustrated in Figure 229 that the PAGS (21.2μm) at the sub-surface of heavy plate was more than twice smaller than that (49.3μm) of at the heavy plate centre along the RD after 3-pass roughing and different holding period cooling simulation. This result may able to explain the reason for the non-uniform microstructures distribution and properties across heavy plate thickness to some extent.

Table 13: Comparison of predicted hot rolling parameters of ten roughing passes and actual measured values at the multipass PSC testing conditions

	Predicted Values at Plate Surface	Measured Values for the Plate Surface	Predicted Values at Plate Centre	Measured Values for the Plate Centre
Average Temperatures of (1-2)/(3-7)/(8-10)	1078°C /1044°C /1031°C	1087°C /1059°C /1010°C	1200°C /1202°C /1190°C	1207°C /1154°C /1123°C
Total Strains of (1-2)/(3-7)/(8-10)	0.32/0.72/0.37	0.36/0.64/0.37	0.18/0.47/0.27	0.21/0.50/0.30
Average Strain Rates of (1-2)/(3-7)/(8-10)	$3.25s^{-1}$ /$3.34s^{-1}$ /$3.42s^{-1}$	$3.24s^{-1}$ /$3.06s^{-1}$ /$3.25s^{-1}$	$1.83s^{-1}$ /$2.17s^{-1}$ /$2.47s^{-1}$	$1.81s^{-1}$ /$2.16s^{-1}$ /$2.51s^{-1}$

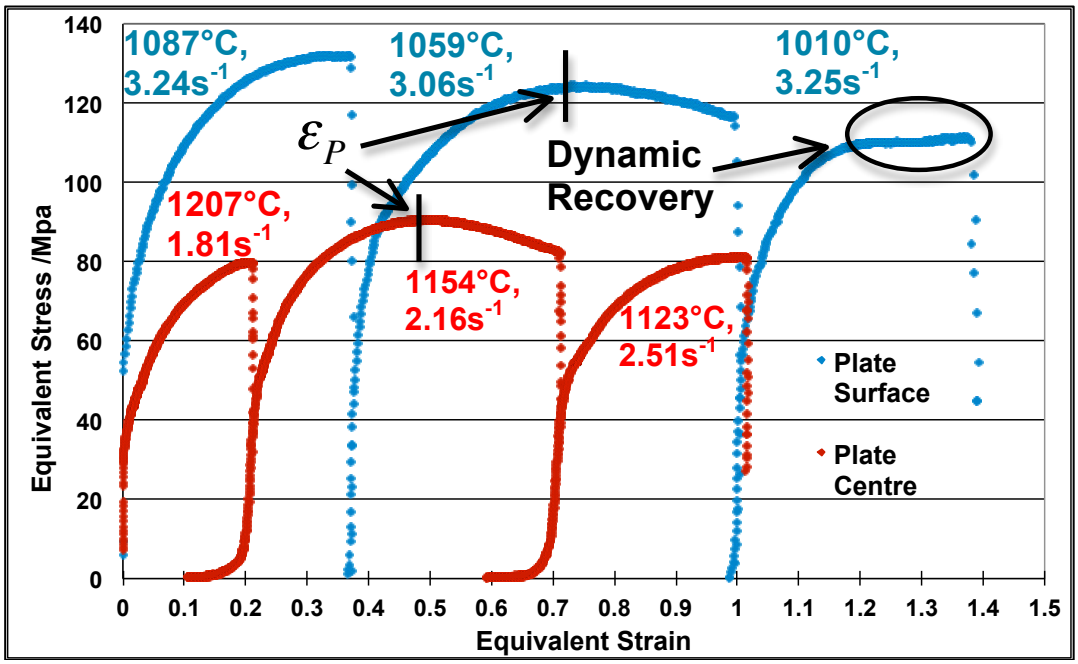

Figure 228: Flow curves of Nb+Ti steel B in two 3-pass roughing with different deformation temperature, strain and strain rate at the heavy plate surface and centre

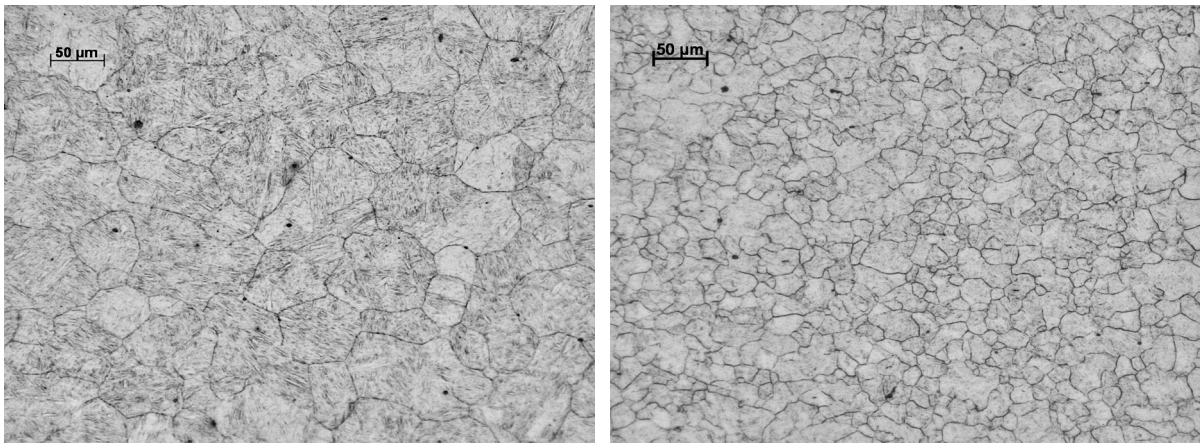

Figure 229: Large difference in PAGS of Nb+Ti steel B after 3-pass roughing and different holding period simulation at the heavy centre and the sub-surface

Finally, two particular multipass PSC tests were carried out to simulate the conditions and compare PAGS at the heavy plate sub-surface after the same roughing deformation but with different HP cooling profiles. The corresponding results are presented in the following Figures 230, 231 and 232, which are different recorded temperature profiles, almost same 3-pass flow curves, and different PAGS after the same roughing conditions but with different cooling profiles during HP (i.e. 3R+348s HP/IFC+WQ), respectively. Similar to earlier results of applying IFC during HP on the PAGS, and under almost the same 3-pass flow curves (presented in Figure 231), slightly smaller PAGS (21.2µm) at the RD are found when IFC was applied compared to that (23.4µm) of 348 seconds linear cooling during HP, shown in Figures 232.

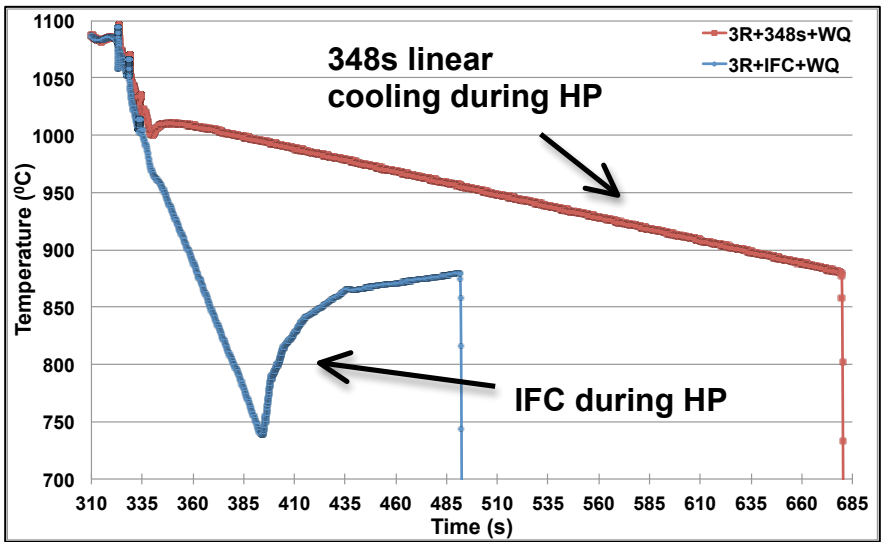

Figure 230: Recorded temperature profiles of two similar 3-pass PSC tests with almost the same 3-pass roughing temperatures but different HP cooling simulation

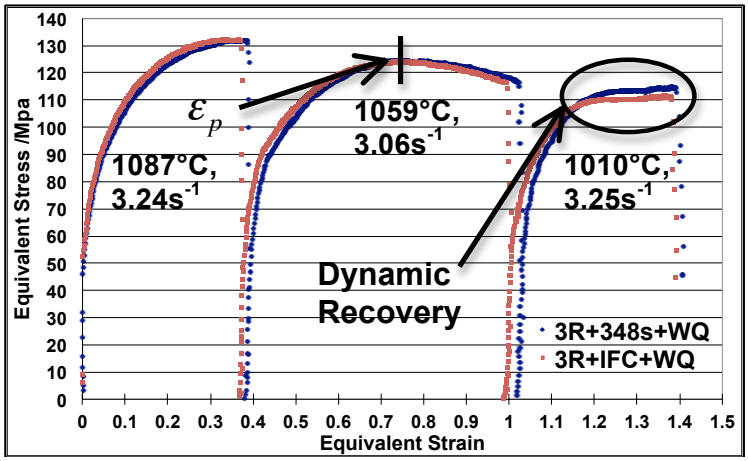

Figure 231: Flow curves of two similar 3-passes roughing at the heavy plate surface

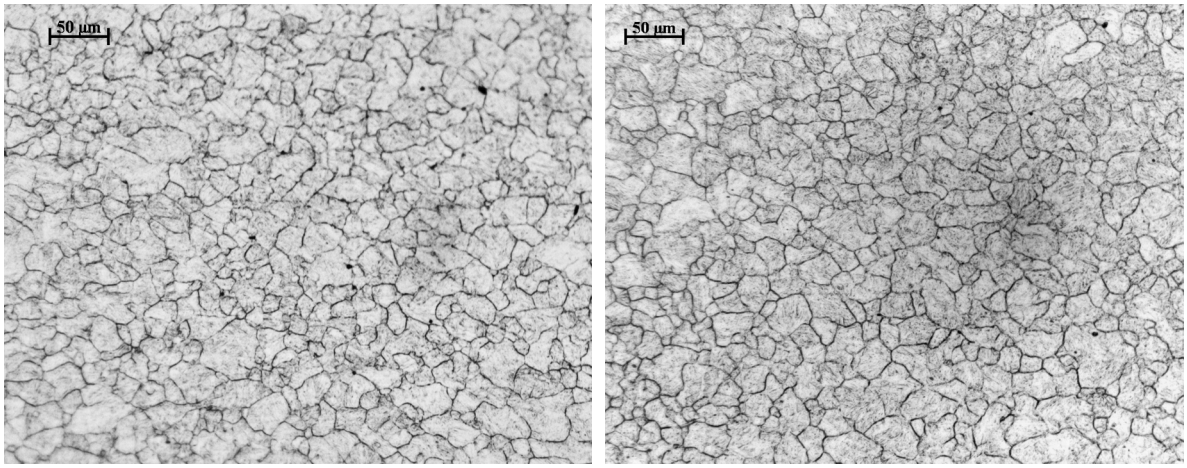

IFC during HP **RD– 21.2±0.7µm TD – 17.0±1.0µm Aspect Ratio=1.2**

348s linear air-cooling during HP **RD – 23.4±0.3µm TD – 19.5±0.1µm Aspect Ratio=1.2**

Figure 232: Comparison of the PAGS at the heavy plate surface after 3-roughing passes with IFC profile (left hand side) and 348s linear air-cooling (right hand side)

4.8. 12- and 13-Pass PSC Tests

In order to further explore the controllable testing window of maximum PSC passes that can be applied in the standard 10mm PSC sample, few tests with more than 8-pass (up to 13-pass so far and for each pass the input strain was 0.12 and strain rate was 2.5s^{-1}) deformation were also performed at end of this research project. For example, the comparison results of similar multipass flow curve and the subsequent optical microstructures (under the same post-deformation applied cooling rate - 10ºC/s) of plain carbon steel C in the continuous cooling 12- and 13-pass PSC tests are presented in the following Figures 233 and 234 respectively. It is clearly presented in Figure 234 that the 13-pass PSC test with slightly higher total applied strain (0.12 larger) and lower finishing temperature (20ºC lower) achieved a smaller average ferrite grain size (6.2µm) than that (7.1µm) of the 12-pass PSC test at the RD.

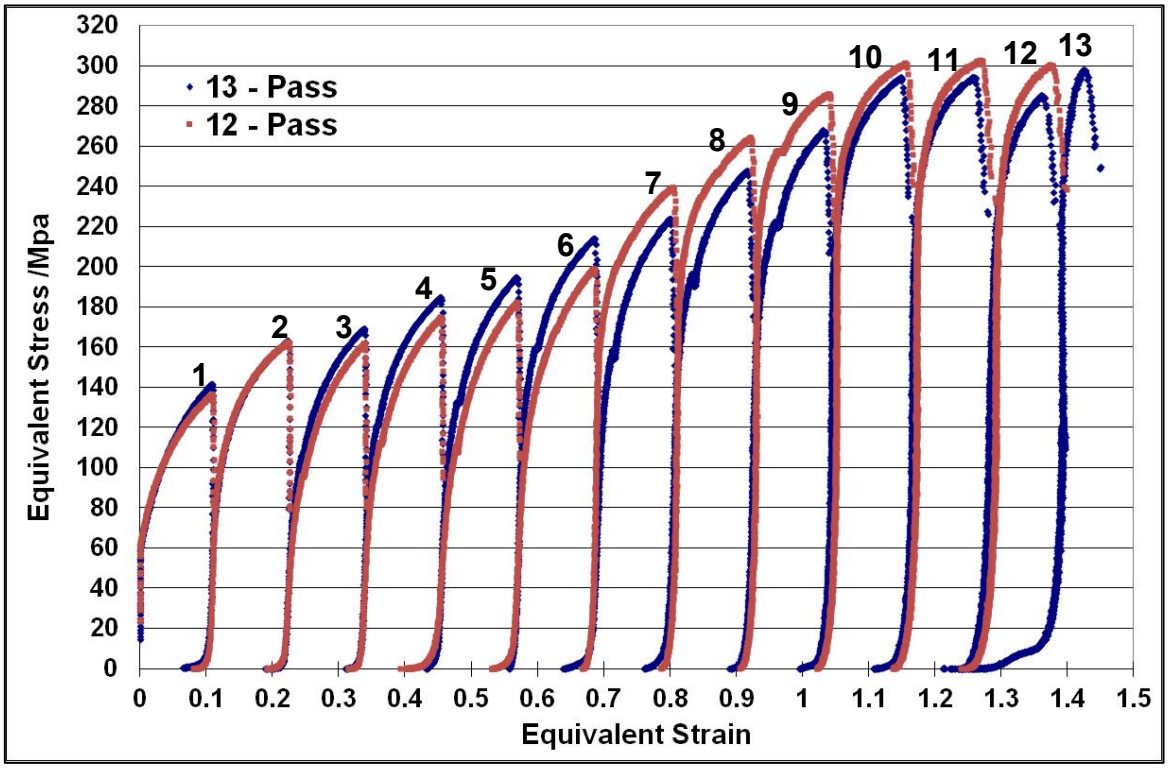

Figure 233: Similar multipass flow curves of plain carbon steel C in the continuous cooling 12- and 13-pass PSC tests

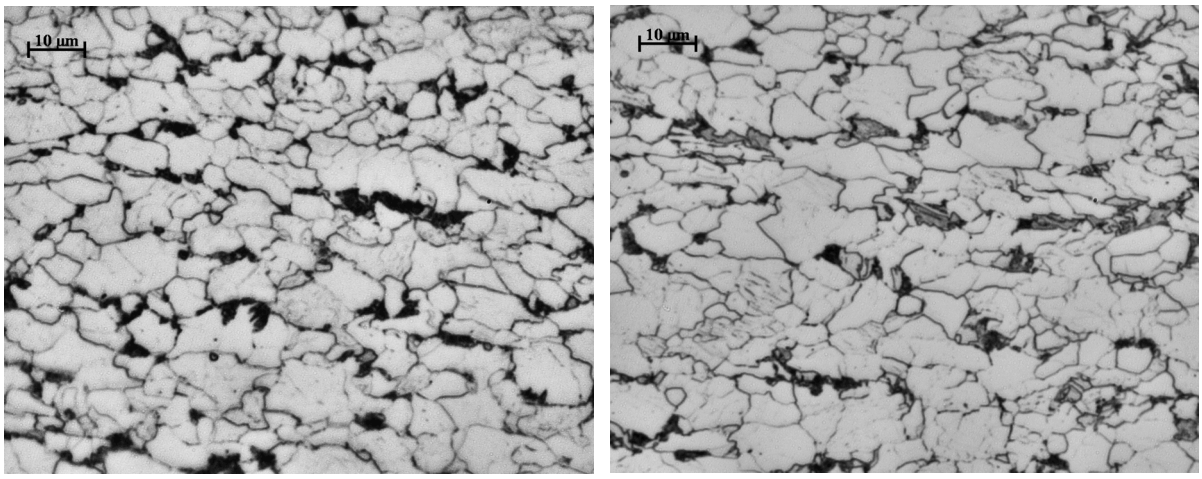

13-pass RD – 6.2±0.2µm TD – 4.8±0.2µm Aspect Ratio=1.3

TD RD

12-pass RD – 7.1±0.3µm TD – 5.6±0.5µm Aspect Ratio=1.3

Figure 234: Optical microstructures of plain carbon steel in continuous cooling 12 pass-(left hand side) and 13-pass PSC tests with the same applied 10ºC/s of ACC

4.9. Summary of Results

The following points briefly summarise this chapter and some results are going to present, discuss and compare with previous work in later Discussion chapter.

- Initial characterisation (see Section 4.2) of interested steels (steels A, B, C and D) and several industrial hot rolling schedules were carried out and the results indicated that relatively coarse (particular for the 50mm plain carbon steel plate) and non-uniform ferrite grain size distribution across the thickness of a commercial as-rolled heavy steel plate (presented in Table 11 and Figure 81, 82 and 136). The reasons for these results could be due to no water-cooling facilities were installed at the existing rolling mill, insufficient rolling reduction and non-optimised rolling schedules and will explain more in the following Discussion Chapter.
- According to the analysed results of different cooling profiles of three cooling media (forced air, mist and full water quenching) inside the 10mm PSC sample in Section 4.3, the sophisticated TMC machine is capable of cooling and reheating up the PSC specimen with a wide range of controllable heating and cooling rates.
- The commercial Abaqus software and the in-house model from Tata Steel Europe RD&T successfully predicted the sub-surface and centre cooling rates (Section 4.4) of partially rolled steel plate under different cooling conditions during holding period (HP). These predicted temperature profiles can be used as input temperature segments or sequence in the setting program of TMC machine
- The method (see Section 4.5) of combining a laboratory Hille mill for 2-pass roughing and TMC machine for 9-pass PSC test for subsequent industrial finishing and post-deformation cooling stages was successful for simulating a commercial hot rolling 50mm plain carbon steel production, and more discussion is shown in next Chapter.
- The 8-Pass PSC deformation can be closely controlled (Section 4.6) to replicate the required conditions (deformation temperature, effective strain, strain rate and cooling profiles) of commercial 60mm microalloyed Nb steel plate hot rolling production, which is the state-of-the art on the laboratory simulation.
- The results in Section 4.6 also have indicated that great consistency or good agreements of flow curves in similar multi-pass PSC tests, which is essential to analyse and compare the effects of different rolling parameters (such as the IFC and ACC) on the corresponding flow curves, austenite and ferrite microstructures.
- The TMC machine can simulate different conditions (Section 4.7) across thickness of heavy plate during roughing and holding period by using the results of FE and FD modelling, and successfully carried out the 12-pass and 13-pass PSC tests (Section 4.8).

Chapter 5 – Discussion

5.1. Overview of Discussion

It is not possible to discuss every result presented in the previous Chapter in much detail, thus only four specific areas of the results are included in the following Discussion chapter. The discussion is particularly focused on the methods, techniques and processes in the development of laboratory multipass (more than 4 passes) plane strain compression (PSC) simulations of industrial hot rolling steel (plain carbon and microalloyed steels) plate productions as close as possible on the advanced Thermomechanical Compression (TMC) machine, and the effects of employing the intermediate forced cooling (IFC) during the holding period (HP) and different post-deformation accelerated cooling (ACC) on the final as-rolled microstructures, especially on the average ferrite grain size. Furthermore, some results were compared with the previous results from the literature, and the summary of discussion were also included at the end this chapter. It is important to be recognised that 8-pass PSC testing is the state-of-the-art of laboratory simulation of whole industrial hot rolling steel plate process.

5.2. Cooling Capacity of TMC Machine and Distributions of Temperature Across Thickness of Heavy Plate

5.2.1. Cooling Capacity of Three Different Cooling Media on TMC Machine

It may useful to emphasise that the process window (upper and lower limits of controllable cooling rates) of three different cooling media (air cooling, mist-mixture of forced air and water, and full water quenching) inside the FTTU was never been previously investigated and clearly defined before this research project. Furthermore, one of main objectives of this program was to investigate the influence of applying intense or forced cooling during and after the hot rolling process on the final as-rolled transformed microstructures, thus it is necessary to know the cooling rate limits of these three cooling media, particularly the upper controllable limit of forced-air cooling prior to conduct the complex multipass PSC tests. Additionally, due to the two to three thermocouples which were inserted into the pre-drilled holes across the 10mm thickness of the PSC sample during the cooling simulation, different temperature profiles at the sub-surfaces (1mm below top surface and/or 1mm above bottom surface) and centre of the PSC sample (5mm below surface) were determined under varied applied cooling rates during the HP and ACC stages.

The following Figure 235 illustrates an example where two thermocouples were inserted into one standard 10mm PSC specimen for measuring different temperature profiles at the sub-surface (1mm below) and centre of PSC sample during the cooling capacity simulation from 1000°C to 800°C, which is similar to the normal temperature range of holding period in the commercial microalloyed steel hot rolling schedule. It is important to make sure the reading of K-type thermocouples were accurately calibrated before inserted into the pre-drilled holes of PSC sample, and that the head of thermocouples reached the centre (15mm deep) of specimen by using pliers, and checked whether there is enough air pressure at the air compressor for the forced-air cooling simulation.

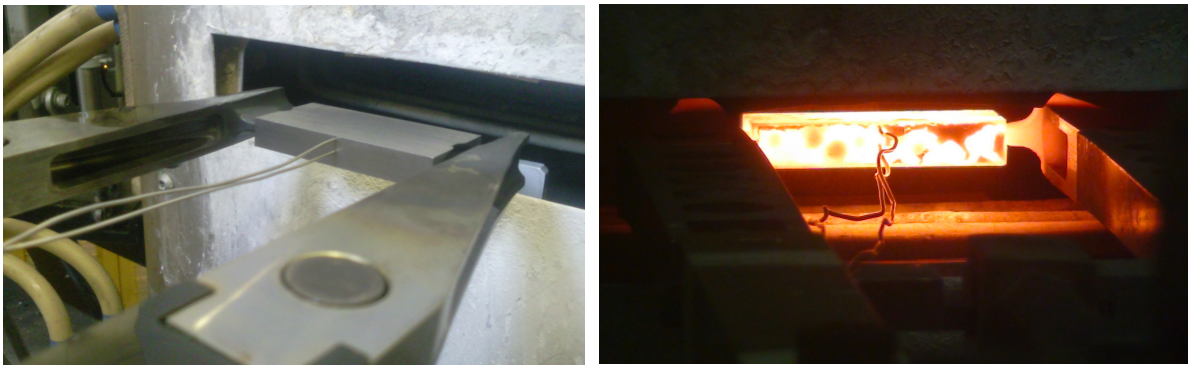

Figure 235: An example of two thermocouples were inserted the middle surface (1mm below) and centre of PSC sample to record temperature profiles before and during simulation

5.2.1.1. *Control Thermocouple at the Centre of PSC Sample*

The detailed experimental procedures of cooling capacity simulation were presented in the Experimental chapter in Section 3.5 and the corresponding results of the three different cooling medias in different applied cooling rates are shown in the Results chapter, Section 4.3. Few points have been draw into attention for further discussion when the control thermocouple (CT) was located at the centre of PSC specimen. Firstly, the forced-air cooling media has been shown that the maximum controllable linear cooling rate was about 25°C/s, and above which the actual forced air inside 10mm PSC sample struggled to achieve the target linear cooling rate from about 1000°C to 800°C, which are shown in Figure 236, where the actual average cooling rates at the sub-surface and centre of sample were presented under two different applied cooling rates (25°C/s and 40°C/s). It is clearly illustrated in Figure 236 that when the applied or intended cooling rate was set at 40°C/s (reducing temperature from 1000°C to 800°C in 5 seconds), the actual cooling rates at both sub-surface and centre of sample were less than 32°C/s. That is because the intended cooling rate from 1000°C to 800°C is controlled by the amount of forced air blowing at the specific time, which means when the intended 40°C/s is above the rate of maximum volume of forced-air blowing in 5 seconds.

Furthermore, presented in Figure 236 below, when the applied cooing rate was set at 25°C/s, the actual measured linear cooling rates were 28°C/s and 31°C/s at the sub-surface and centre of sample respectively. This indicates that slightly more volume of forced air was blown than the expected value during cooing simulation. Additionally, the results (presented in Figures 88 and 91 in Results chapter Section 4.3.1) also indicate that as the applied cooling rates increased from 0.5°C/s and 25°C/s, corresponding to an average temperature difference between the sub-surface and centre of sample increased from 4°C to 20°C (these values have been taken account of different initial temperatures at the sub-surface and centre of sample at the end of isothermal holding at 1000°C).

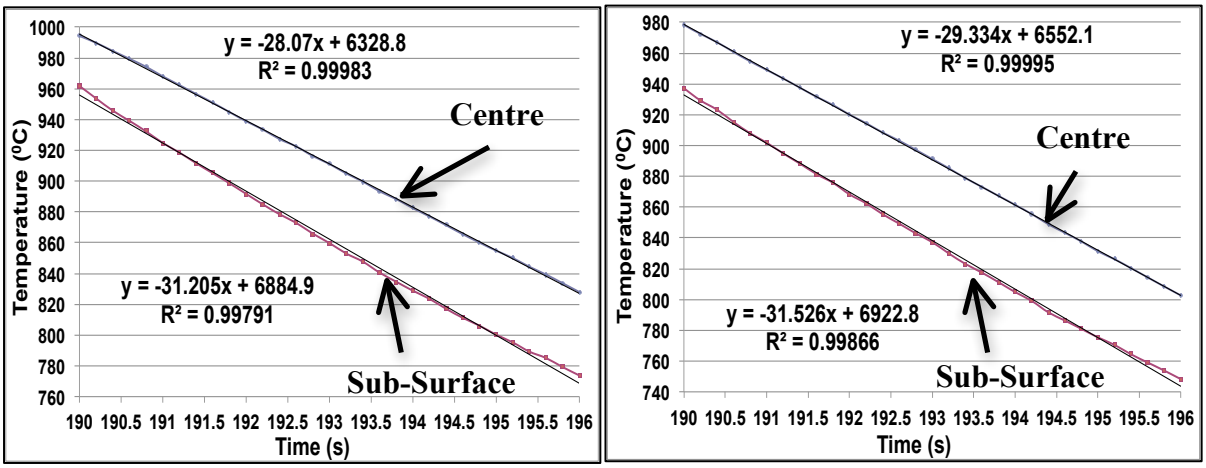

Figure 236: Temperature profiles at the sub-surface and centre of 10mm PSC sample under two different applied cooling rates: 25°C/s (left hand side) and 40°C/s (right hand side)

Secondly, although a much faster maximum average cooling rate can be achieved at the centre of 10mm PSC sample under the mist (mixture of spraying water and forced air) and fully water quench cooling conditions, which are 67°C/s and 105°C/s respectively, and can be seen from Figures 92 to 97 in Result Sections 4.3.2 and 4.3.3, the actual recorded cooling rates or profiles were found to be non-linear from 1000°C to 800°C. Moreover, the non-linear cooling profiles were more significant under the mist condition when the intended cooling rates were set at 10°C/s and 20°C/s (presented in Figures 92 and 93) than those under fully water-cooling. The reason to cause this result is that according to the signal of the control thermocouple inserted into test specimen, the TMC computer can monitor and adjust the actual testing temperature to fit or couple pre-set temperature heating and cooling profile. For example, in the mist cooling, some amount of spraying water in the mist results in temperature of PSC specimen decreased faster than the expected value, thus the induction coil inside FTTU released some heat to slow down relatively quicker cooling rate (presented in Figure 93).

Thirdly, at the higher applied mist cooling rate and fully water quenching from 1000°C to 800°C, a very large temperature difference was produced within the 10mm PSC sample when the cooling stopped, and even overcooled the sub-surface and centre of PSC sample to about 670°C and 550°C respectively at the high applied cooling rate. Additionally, after the fast cooling stage, a significantly longer holding time was required for the temperature of the PSC sample to be stabilised at the 800°C isothermal holding temperature, illustrated in Figures 95 and 96. Similar to temperature coupling during forced cooling stage when temperature reading of control thermocouple was more than 5°C lower than the target 800°C isothermal holding temperature, then the sample was quickly reheated (possible overheated) by the induction coil in FTTU.

Finally, the temperature difference at the sub-surface and centre of the PSC sample increased significantly as higher forced-cooling rates were applied from 1000°C to 800°C. For example, when the applied cooling rate increased from 0.5°C/s (slow air cooling) to 25°C/s and fully water quenching, the corresponding average temperature differences at the end of the cooling stage increased from 2°C to 30°C and to 200°C (see Figures 96 and 97) respectively. Furthermore, as the applied cooling rate increased, it took a much longer time to stabilise and equalise the temperature at the 800°C isothermal holding temperature. Therefore, according to these temperature distribution results in the 10mm thickness of a standard PSC sample, it is confident to suggest that employing the intense forced cooling into commercial hot rolling heavy steel plate production can cause significant temperature differences at the sub-surface and centre of heavy steel plate at the end of cooling, thus sufficient recalescence or equalising time after cooling must given prior to finish rolling.

5.2.1.2. Control Thermocouple Located at the Sub-Surface of PSC Sample

It was interesting to find out that when the control thermocouple (CT) was located at the sub-surface (1mm below surface) of PSC sample, the actual cooling and isothermal holding temperature profiles were much closer to the target profiles, which were presented in Figures 98-100 in Result chapter Section 4.3.4. That is because when the sub-surface rather than centre of PSC sample reached 800°C the forced cooling immediately stopped, at which the centre temperature of PSC sample is usually higher than 800°C depends on the applied cooling rate, presented in Figures 98-100. Furthermore, the main differences were lesser overcooling below the 800°C and much quicker to stabilise at the required 800°C isothermal holding temperature compared with the results when the control thermocouple was inserted at the centre of PSC sample. Therefore, for the complex heat-treatment temperature profiles, it is confident to locate the control thermocouple at the sub-surface of PSC sample for better control ability.

5.2.2. Modelling Distributions of Temperature Profiles through Thickness of Heavy Plate during Hot Rolling Production

As described in Literature review chapter Section 2.5, along with the predicted results which were presented in Results chapter Sections 4.4 and 4.7, it is widely established that during industrial hot rolling heavy plate production the temperature profiles (as well as the effective applied strain and strain rate profiles) are significantly different from the surface towards interior of heavy plate. In this research project, several different temperature prediction models, such as the commercial Abaqus finite element (FE) model, the well-built IMPress model (developed by Tata Steel Europe-TSE RD&T), and others TSE RD&T in-house models have been used to analyse and calculate the different temperature profiles across thickness of heavy plate during hot rolling process, particularly focus on the HP cooling. Furthermore, these models had different heat transfer coefficients and boundary conditions but all assumed uniform distributions along the length and width directions, and provided useful one dimension temperature distributions (mainly at the sub-surface and centre) across thickness as different input values for the multipass PSC tests (Results chapter Section 4.7.2). In the following section, the results of different predicted temperature distribution profiles through thickness are further analysed, discussed and compared with previous results from some published literatures.

Firstly, an example of showing predicted surface and mean temperature profiles inside heavy plates of two commercial hot rolling schedules are presented in below Figure 237. These two schedules had different chemical composition (Nb and plain carbon steels), hot rolling history (presented in Experimental chapter Table 5) and final plate thickness (20mm and 50mm), which were constructed by the TSE set-up model for draft hot rolling schedule.

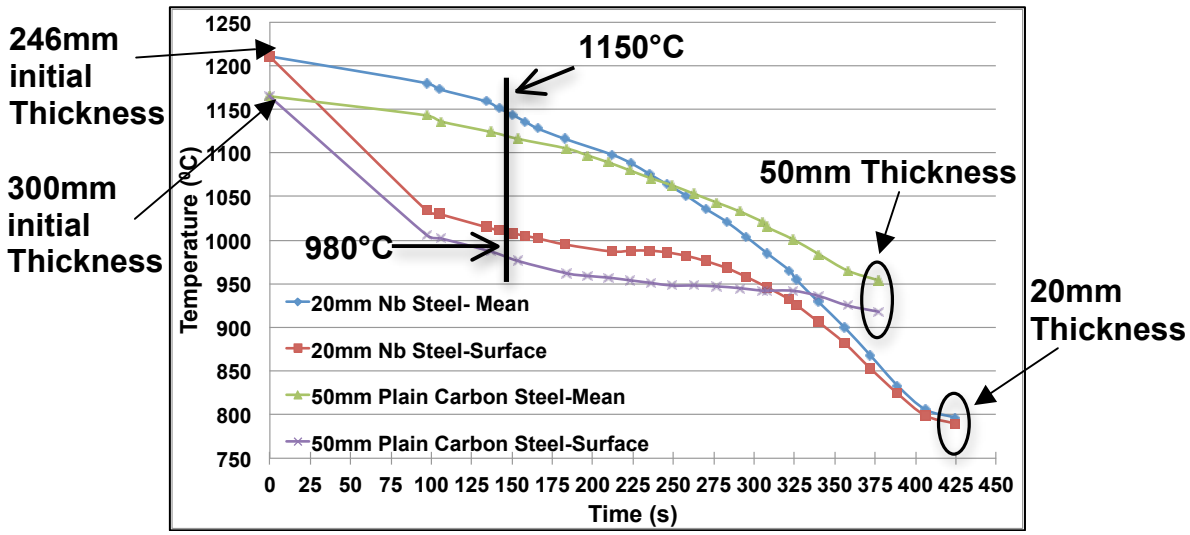

Figure 237: Predicted surface and mean (average) temperature profiles of two industrial hot rolling schedules with different chemical composition and final plate thickness

It is obviously displayed in Figure 237 that in these two draft industrial hot rolling schedules at the high temperature roughing stage, there were large temperature differences (about 150°C) between the plate surface and average temperature profiles across thickness, thus much larger temperature variations (above 200°C) would be expected to exist between the plate surface and centre of heavy plate. These predicted temperature profiles across thickness were agreed with the measured roughing temperature profiles [255] in Figure 238 in which a heavy slab with 200mm in thickness, 300mm in length and 200mm width was rolled down to 60mm in 15 roughing passes, and the corresponding different centre, quarter and surface deformation temperature profiles were clearly presented. Therefore, at the end of the roughing stage, inhomogeneous temperature profiles and the PAGS were produced through the thickness, which in turn caused non-uniform ferrite grain sizes in final as-rolled plate.

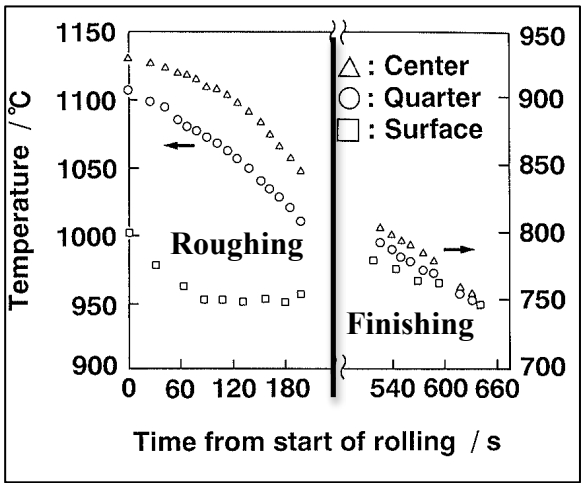

Figure 238: An example of results of temperature measurements from 200mm rolled down to 25mm [255]

Secondly, the results of the calculated temperature distribution under different cooling conditions across the different thickness of the partially rolled plates during then long HP were presented in Result Sections 4.4. In general, under the same boundary settings of forced cooling in the commercial Abaqus FE model (presented in Experimental chapter Section 3.6.2), as the plate thickness increased longer cooling time required to reduce centre temperature from 1000°C to 800°C due to heat diffusion distance from centre to surface increased. Furthermore, according to the predicted centre cooling rate profile during the HP in Figure 107 and the derived power relationship between plate thickness (X) and centre cooling rate (Y), $Y = 128.35 \times X^{-1.077}$ with $R^2 = 0.99$ (if changed to function $Y = \frac{128}{X}$ then $R^2 = 0.96$), when the plate thickness were above 50mm, the centre cooling rates were similar and all below 2°C/s. Although a faster centre cooling rate can be achieved when increased the heat transfer coefficients, a much larger temperature variation across plate thickness was produced at the end of intense water cooling stage, and longer recalescence time periods were required for the cold plate surface reheated to the similar temperature as the centre value.

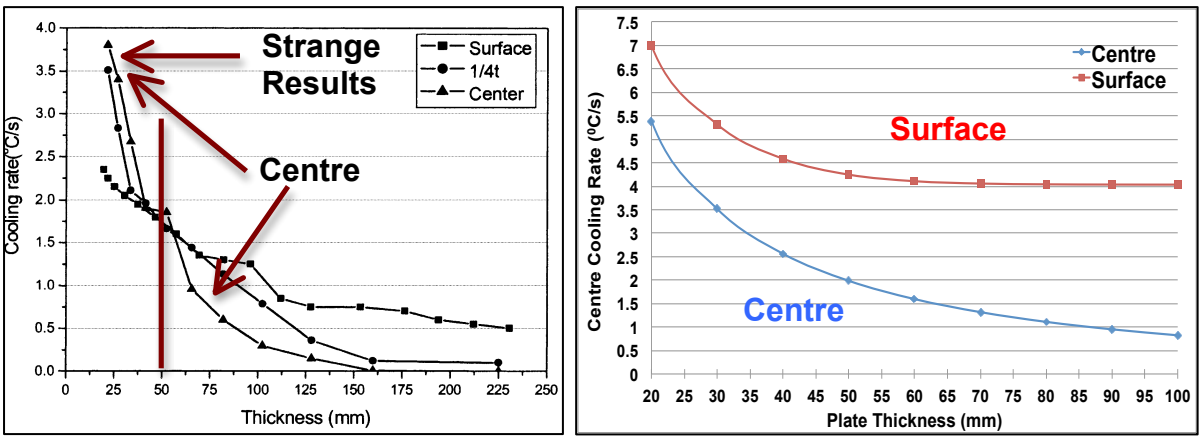

Figure 239: Predicted cooling rates comparisons of earlier work [256] (left hand side) and the results of Abaqus modelling (right hand side) across different plate thickness

However, if the Abaqus predicted average surface and centre cooling rates are compared with the published calculated cooling rates related to the plate thickness in earlier work [256], presented in above Figure 239, obviously some disagreements were found in the figure. First of all, the largest differences were that when the plate thickness was from 25mm to 50mm, the estimated cooling rate at the centre was even higher than that at the surface in earlier work (did not include the modelling process and explanation in the paper), which is a highly unlikely result, and the predicted surface (4°C/s) and centre (0.8°C/s) cooling rates of 100mm steel plate by the Abaqus FE model were higher than those in earlier work. As discussed earlier (Figure 236), the actual measured surface-cooling rate was always higher than that at the centre of 10mm PSC sample, the present work of Abaqus cooling rates modelling showed better accuracy.

As presented in Figures 108 to 111, a considerably different predicted temperature distribution profiles across the thickness of 100mm steel plate during the HP were obtained by Abaqus FE model, which was caused by the different applied heat transfer coefficient (HTC) at the plate surface. For example, with HTC of $10Wm^2K^{-1}$ under natural-air cooling, much longer cooling time and slower average centre cooling rate (0.29°C/s) was produced (shown in Figure 108) compared to that (0.83°C/s) of the forced cooling with larger input HTC of $200\text{-}400Wm^2K^{-1}$ (presented in Figure 109). Furthermore, another TSE RD&T in-house model also predicted significantly different temperature cooling profiles through thickness (presented in Figure 113-115) under natural-air cooling and IFC conditions with different initial HP start temperatures at the plate surface and centre, and the results in Figure 115 demonstrated that the average centre cooling rate (0.8°C/s) was nearly twice faster in the IFC situation than that (0.46°C/s) of natural-air cooling. However, larger temperature variations across thickness at the end of HP were produced in the in-house model due to different value of HTC was used in the simulation and insufficient homogenisation time was applied after the forced cooling.

5.3. Development of Laboratory Multi-Pass PSC Simulation of Industrial Hot Rolling Steel Production

Although there are possibly some arguments or debates regarding to the huge scale or thickness difference between commercial hot rolling heavy plate (from about 230mm rolled down to 60mm) and 10 or 12mm PSC sample, all the important hot rolling parameters such as deformation temperature, gap time, strain, strain rate and accelerated cooling profiles in the commercial hot rolling production can be precisely simulated (even better controls than those in the commercial hot rolling processes) on the cutting-edge Thermomechanical Compression (TMC) machine. Furthermore, perhaps the biggest advantage of laboratory multipass simulation on TMC machine is that the deforming PSC sample can be scheduled to extract and quench at any point in the multipass PSC testing process, and more importantly, the interval of time between the end of a given deformation and the beginning of full water quench inside FTTU is less than 0.5 seconds (no grain size coarsening took place during transferring from the test furnace to FTTU). Therefore, it enables metallographic examination of the deformed structure at the respective deformation temperature and the microstructural development in the commercial hot rolling steel production. It may useful to emphasise that there is no other facility of this type in the UK where this can be accomplished.

In terms of laboratory development in multipass PSC simulation, this research program firstly encompassed the laboratory multi-pass replication of whole industrial hot rolling production of 50mm plain carbon steel plate (8AK39) with total applied strain ε_{Total} =2.1, before concentrated on the complex multipass PSC simulation of completed commercial 60mm microalloyed steel plate production (8AK39) with total applied strain ε_{Total} =1.65. The challenged multipass PSC testing sequences of simulating microalloyed steel hot rolling schedule deliberately included the applications of intermediated forced cooling (IFC) during holding period (HP) and accelerated cooling (ACC) after hot deformation to analyse the effects of intense water cooling during and after hot rolling to improve steel production (see later discussion at Section 5.5).

Compared with the basic PSC testing sequences of performing a single hit or up to 4-pass tests with large differences of deformation temperatures (such as 1150°C, 1050°C, 850°C and 750°C) and longer gap time (10 to 50 seconds) on the TMC machine, there is no doubt that the operations of 8-pass and above PSC tests with similar industrial hot rolling steel plate schedules were much more difficult and challenge. The process of single pass PSC test has been described in elsewhere [242], and the process can be repeated and extended to create the much complex multi-pass PSC simulation as required in this research program. It is useful to emphasis in here that with the nature of these multipass PSC simulations, the whole testing schedule consists of many small input segments that defined the reheating rate, holding

temperature and time, strain and strain rate of each deformation, cooling profile and so on. Furthermore, several important issues arose regarding to the closely controls of deformation temperatures, applied strain, temperature cooling during intervals, and the length of gap time when the multipass PSC deformations were conducted. All these hot rolling parameters were defined at the testing segments, which have to be correctly adjusted through many trials. Therefore, in the following sections some critical factors on developing multipass PSC tests on the advanced TMC machine are discussed.

5.3.1. Temperature Controls in Multipass Non-Isothermic Deformation

5.3.1.1. Position of Control Thermocouple in the PSC Sample during the Multipass PSC Deformation

Although according to the results and earlier discussion on the maximum controllable cooling capacity simulation, much better temperature controls were found when the control thermocouple was inserted at the sub-surface of PSC sample, in practice the control thermocouple was still located at the centre (deformation zone) of PSC specimen to control and record the temperature profiles during the complex multipass PSC tests. That is because only the actual effective strain at the centre of deformed PSC specimen is the same as or similar to the applied strain. However, if the total applied strain is really large (more than 1.5) and final thickness of deformed sample is below 1.8mm, the thickness of control thermocouple (1.1mm in diameter) possible became an issue as claimed by Hinton in his PhD thesis [242] that due to it likely interference with the last deformation at this small thickness, leading to possible false deformation, and/or breaking of the control thermocouple to stop multipass PSC simulation.

5.3.1.2. Temperature Raising during Deformation

During the actual reduction inside the test furnace at the multipass PSC deformation, the centre temperature of deformed PSC specimen was raised by a small extent (up to 50°C) due to heat generated by the of plastic deformation and friction between the tools and sample surfaces during the contact, which can be seen in Figures 124, 126 and 142 in the Results Sections 4.5 and 4.6. This suddenly increased sample temperature resulted in a more difficult to predict post-deformation temperature of PSC sample, and disrupted the TMC computer signal feedback controls [242] for subsequent intervals cooling and deformation temperatures. Therefore, after several trials, the post-reduction temperatures can be roughly determined and some additional cooling and reheating segments were added into the intervals cooling if the deformed PSC sample was in the FTTU for the temperature cooling controls.

5.3.1.3. Temperature of PSC Sample Continuous Dropping at the Short Gap Time

Besides the temperature rise inside the deformed PSC sample during reduction, which results in some difficulty in the post-deformation temperature coupling, another big challenge for the continuous cooling 8-pass PSC test was to closely controls of intended temperature profile of deformed PSC sample during the gap time (included the HP). In general, the laboratory multipass PSC testing sequences should be close to the actual rolling schedule of industrial heavy steel plate production as much as possible, which involves many small reductions with rolling temperatures only decrease slightly after each pass in the roughing and finishing stages, as well as the some chilling effect from the cold work rolls. However, the 10mm or 12mm PSC sample is not like the industrial heavy plate at roll gap and interpass times, after each deformation the temperature of PSC specimen dropped too quickly, particularly if the tools and test furnace were set at the extreme condition - room temperature, illustrated in Figure 240 below. It is clearly shown in Figure 240 that sample temperature reduced from 951°C to 832°C and to 767°C in just about 12 seconds intervals.

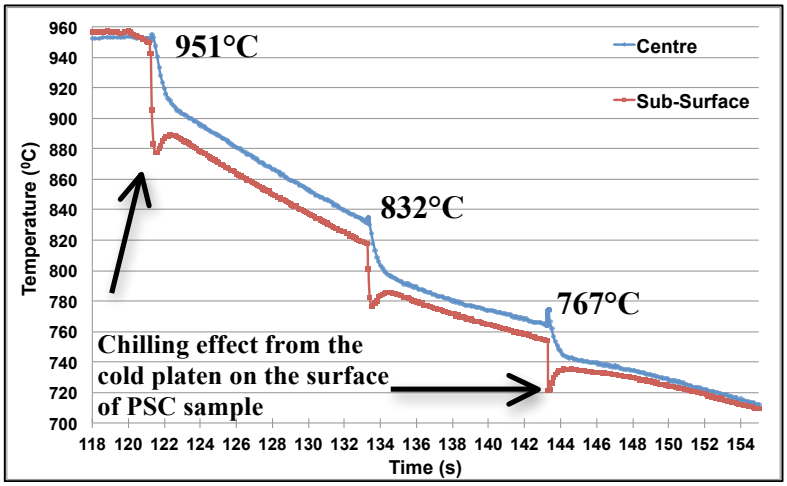

Figure 240: An extreme example of showing temperature cooling profiles inside PSC sample when the deformation platens and test furnace were both set at the room temperature

Therefore, correct settings in test furnace and tools temperatures are essential to achieve intended deformation temperature inside PSC sample. For example, in the earlier trials of 8-pass PSC simulation of microalloyed steel plate production, the furnace temperature was initially set at 865°C and it gave tools temperature about 825°C. The corresponding temperature profile at the centre of PSC sample during the first 3 roughing passes simulation is presented in Figure 241 in which the actual deformation temperatures (985°C and 955°C) of the second and third roughing passes were lower than intended values of 1000°C and 975°C respectively. That was because the chilling effects from the relatively colder tools and test furnace reduced sample temperature faster than expected. Thus, to reduce the fast chilling effects, in later practices of 8-pass simulation the test furnace temperature was usually set at

higher value of 885°C - 895°C so that upper and bottom platens temperatures, which only can be governed by the temperature of test furnace, were closer to the required deformation temperature of the last finishing pass (the 8th pass) at 840°C.

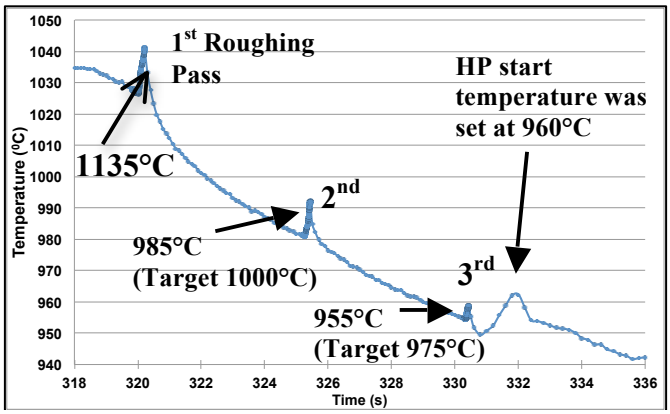

Figure 241: An example of showing temperature profile at the centre of PSC sample reduced faster than expected during the first 3-pass roughing and HP simulation

After the temperatures of the test furnace and tools were correctly adjusted, the temperatures of the PSC sample before and after deformation, start and end temperatures of HP, and length of interpass times also must be in right settings for the 8-pass continuous cooling PSC tests, especially for the first 3-pass roughing simulation due to a large temperature difference between sample and test furnace. First, prior to transferring undeform PSC sample into test furnace to conduct the first roughing pass (and transferring deformed sample for the first finishing pass), the specimen temperature should be set at 5°C (for 12mm sample) or 10°C (for 10mm sample) higher than intended deformation temperature. That is because even during the 0.5 second transporting process about 5-20°C dropping occurred inside the PSC specimen, and the magnitude of temperature dropping is higher when the sample thickness reduced and with a larger temperature difference between test furnace and PSC sample.

Second, the method of keeping the PSC sample inside the test furnace all the while (without transferring back into FTTU for more accurate temperature controls) during the 3-pass roughing simulation with relatively short interval time (5 seconds) between passes was to avoid the temperature of deformed PSC specimen dropped too quickly at the intervals, and to reduce the possibility of PSC sample hitting the platens and dropping off from the robotic arms. It is important to mention again when the PSC sample was moved into the test furnace, the temperature of intended deformation cannot be accurately controlled in the TMC program but can be roughly determined by the initial temperature of PSC sample before deformation, gap time, test furnace and tools temperatures. For instance, by shortening the gap time only from 20s to 7s and to 5s, the actual measured temperature profiles are closer to the intended deformation temperatures of the second and third roughing pass, which are displayed in the following Figure 242. It is clearly illustrated in Figure 242 that after the first roughing pass

temperature of deformed PSC sample reduced too much when the intervals were set at 20s and 7s, thus the actual deformation temperatures of second and third roughing passes were all lower than the intended values of 1000°C and 975°C respectively. Eventually when the gap time was set at 5 seconds, the actual deformation temperatures were close to the target values (see the green curve in Figure 242 below).

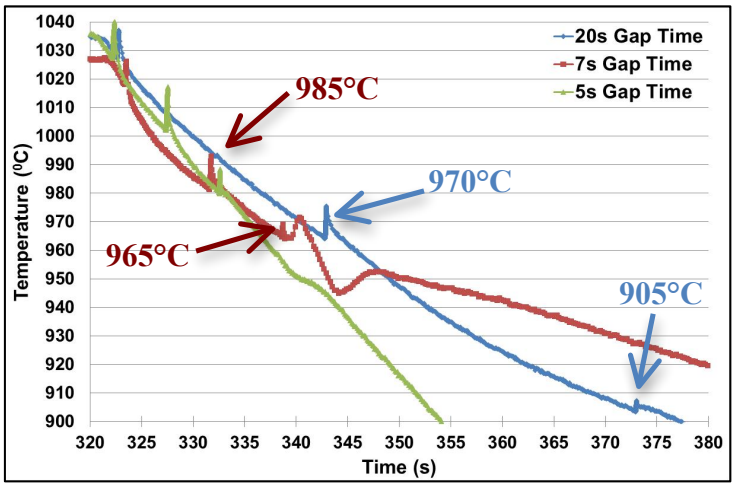

Figure 242:Temperature profiles comparison of three similar multipass PSC tests with different length of gap time and HP cooling profiles

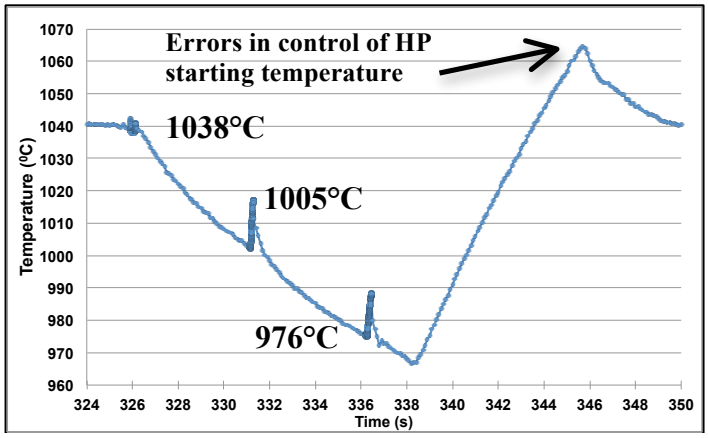

Figure 243: An example temperature profile showing the temperature control or setting error in defining start cooling temperature of HP

Finally, immediately after the 3-pass roughing deformation, the starting cooling temperature of the HP also has to set in the correct value, which should be slightly lower than the actual deformation temperature of third roughing pass. For example, if the start cooling temperature of HP did not define in the setting-up program then the computer automatically located and reheated the sample (damaged the 3-pass roughed microstructure) to the previous defined temperature, which was the value prior to the first roughing deformation and presented in Figure 243 above. Therefore, it is important to make sure the starting and ending temperatures of each testing segment were correctly defined and adjusted.

5.3.2. Strain Controls in Multipass PSC Deformation

After some complex modifications of temperature settings in the continuous cooling multipass PSC testing segments, the values of applied strains also had to be corrected. In a single pass PSC test, the actual recorded strain is normally slightly lower (0.02-0.07) than the nominal or input value, and as the more PSC passes are carried out, such as 8-pass PSC tests, the more deviation occur between the actual total measured strain than the defined value. Therefore, in order to reach the target effective strain in the deformed PSC sample, the general rule is that the input value of applied strain of each rolling pass should be always 0.05 higher than the intended strain value, particular for the first and second passes when the thickness of PSC sample is relatively high compared to later passes. However, due to the actual strain value of each pass could not be immediately obtained soon as the multipass PSC simulation finished, and normally in practices after several tests are finished the analysis and determinations of flow curves were then carried out. Perhaps more importantly to keep the consistency of multipass PSC tests, in general if the accumulated strain differences between the measured and intended values were less (or above) than 0.15 then the tests would not be repeated. There are still some precautions can be done to reduce the variance between the actual total applied strain and intended strain.

First of all, the top and bottom tools must be de-scaled, flattened, lubricated and accurately aligned with each other at the room temperature before heating up the test furnace to intended temperature. Secondly, after target temperatures of test furnace and tools were achieved, the distance between the top and bottom platens must be carefully adjusted for the zero offsetting (let the sample thickness = 0.000mm) due to thermal expansion of tools and oxide scales built up on the tools in high temperatures. Furthermore, it is vital to remember that after each test both tools must be de-scaled by using the long scraper, presented in Figure 244. Perhaps more importantly, prior to running each PSC test the process of zero offsetting of tools must be repeated for achieving the target strain in deformed PSC sample. Finally, the fine boron nitride power, which is also acted as an anti-welding agent, is sprayed evenly at the surfaces of the specimen is also important to achieve intended and uniform deformation.

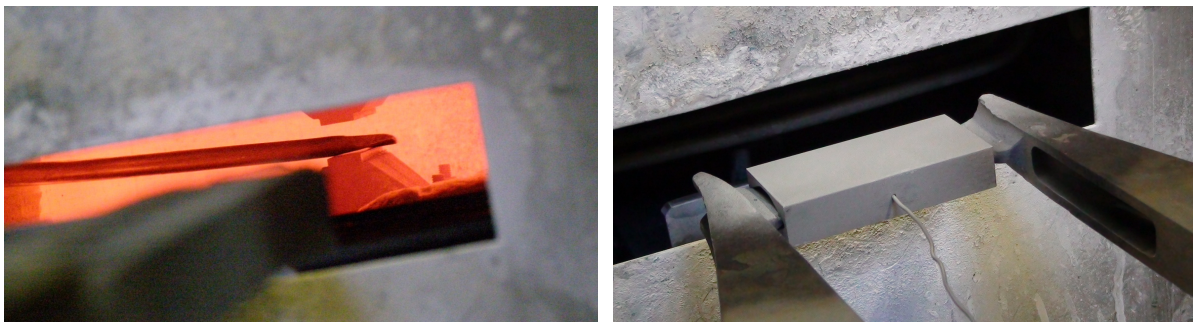

Figure 244: Demonstration of cleaning tools prior to PSC testing and illustration of spraying boron nitride powders on the top and bottom surface of PSC samples prior to testing

5.3.3. Overcome the Problems in Conducting Multipass PSC Testing

As discussed previously, when conducting the complex 8-pass continuous cooling PSC tests, the deformation temperature and effective strain of each pass and length of gap time must be in correct settings to obtain successful simulation. However, even with all the right settings in the simulation schedule there are always high possibilities that some things may go wrong during the multipass PSC tests. For examples, PSC sample hit the bottom tool and fall off from the robotic arms; platens were misaligned or rotated after several deformation; control thermocouple was broken after reduction; the door was sticking in the halfway position whilst opening and/or closing the furnace door. All these things caused unsuccessful deformation and interrupted the multipass testing sequences. Therefore, in order to achieve successful and reliable multipass PSC tests, it is essential to minimise these undesired problems during the simulation.

5.3.3.1. Tool Rotation and PSC Sample Dropping from the Robotic Arms

First of all, as these multipass PSC experiments were all conducted at the high temperature (above 800°C), high pressure, large applied force (up to 500kN) and fast movement of hydraulic ram, the tool rotated or shifted is regularly occurred after several 8-pass PSC tests due to the incoming PSC sample hit the bottom or upper tool, the bolts that fixed the tools on the posts were loosened and imbalanced sample on the robotic arms. The consequence of rotated or shifted tools was that no more tests were able to carry out until the tools were carefully re-aligned again, which only can be performed when the test furnace was shut down and the temperatures of both platens were cooled down to room temperature. This cooling process could take about 2-3 hours followed by at least one hour to re-align and then another one hour to reheat the cold platens to the intended deformation temperature, which significantly affected the progress and scheduled timeframe of research project. Therefore, it is extremely critical to minimise the issue of rotated tools by some possible solutions or precautions.

The first and very important factor regarding to the possibility of hitting the bottom or upper tools and fall off from robotic arms is the clearance (or distance) between the bottom tool and underneath surface of 10mm or 12mm PSC sample. For instances, if the position of robotic arms, which are holding PSC sample, was too high above the bottom platen and there is more than 4mm clearance, then the downward fast movement of upper platen during deformation could cause sample bended with a big curvature (possible non-uniform strain distribution) shape in the deformed specimen. On the other hand, if the robotic arms were placed too low (less than 2mm clearance) above the bottom tool, it was highly possible that the incoming specimen would hit the bottom tool, and drop off from the robotic arms as well as rotate the

bottom tool, presented in Figure 245 below [242]. As mentioned in Experimental chapter Section 3.7.3, the height of robotic arms can be carefully adjusted through altering the weight balance by tightening or loosening the black knob on the back of the robotic arm. Therefore, prior to conduct the first deformation or during the relatively long intervals, the displacement of main actuator, which controls the position of top tool, is manually raised to 15mm or 18mm displacement for 10 and 12mm PSC samples respectively so that the incoming sample would not hit the upper tool.

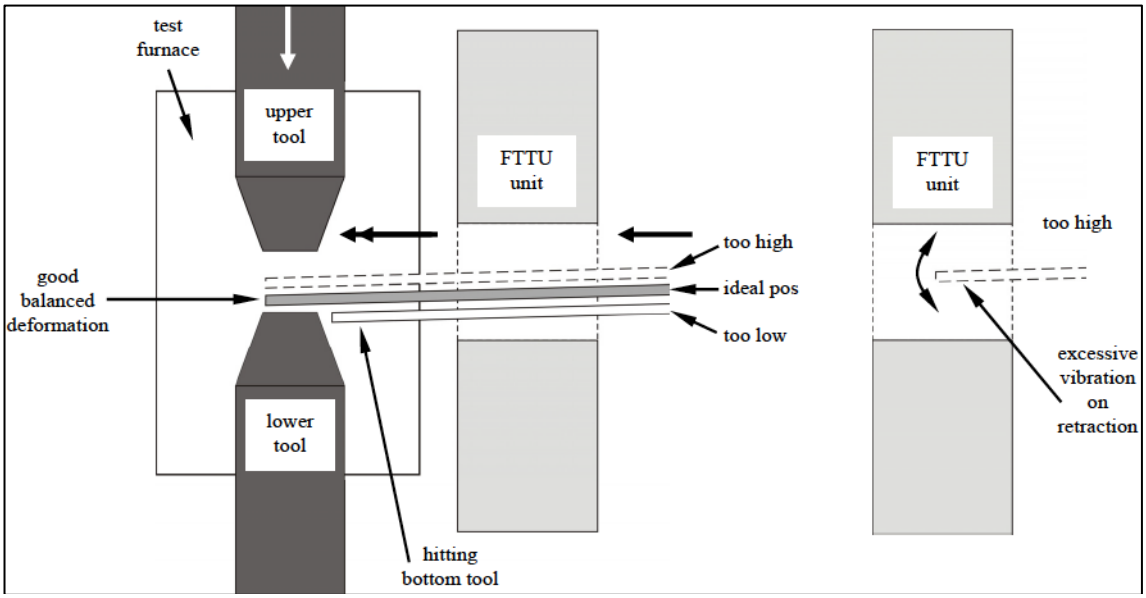

Figure 245: A schematic diagram showing the effects of position of the robotic arms and its vibration [242]

Furthermore, during the 8-pass PSC deformation, the thickness of specimen gradually reduced while its length increased progressively, so the corresponding vibration of sample after each deformation increased and more likely the sample would hit the tools as well as robotic arms would loose the grip of holding deformed sample firmly. Additionally, as Hinton [242] explained in his PhD thesis, the sudden transferring movement of robotic arms between the FTTU into test furnace sometimes caused the robotic arms to vibrate and increased the chance of sample hitting the bottom tool, see Figure 245 above.

As a result of the incoming sample hitting the tools and falling from the robotic arms, the thermocouple probably broke and the PSC sample either ended up in the test furnace, in the gap between the test furnace and the FTTU or at the bottom of the FTTU to cause the corresponding deformed microstructures inaccessible or damaged. As described in Experimental chapter Section 3.9.3, a small modification on the PSC samples was done and the success rate of incoming sample did not hit the tools and drop off from robotic arms increased relatively 40%. The modification involved drilled small holes at edges of PSC sample and robotic arms, and then through the holes four thin steel wires were used to tighten

the PSC sample more securely on the robotic arms. However, although with this modification samples are less likely to drop off from robotic arms, sometimes after 8-pass deformation the deformed PSC still stuck between the platen, which will be explained more in later Section 5.3.3.3.

5.3.3.2. Control Thermocouple Broken and Short Circuit

Because the whole testing sequence of all segments from reheating to multipass deformation, to HP cooling and to post-deformation accelerated cooling is controlled by the signal and feedback of control thermocouples inserted at the centre of PSC sample, the breaking of the control thermocouple during the testing can abort the testing sequence and stop the simulation. The reasons to cause this problem are mainly due to the sample drop from the robotic arms (already discussed previously) or deformed sample being trapped between the platen (will explain in next section). It may useful to mention here a 2m long K-type thermocouple was used repeatedly (a new live thermocouple head or junction was created in the thermocouple welder machine) in many multipass PSC tests till it is too short to link the sample on the robotic arms to the thermocouple adapter. However, for the new welded thermocouple junction at the least 2-3mm long wires were exposed without the skin protection and these wires were really brittle. Therefore, during 8-pass PSC deformation the welded thermocouple junction could break under the load and stop the simulation. One solution was to place the control thermocouple in the shoulders (undeformed regions) of PSC specimen rather than the deformation zone. This was a compromise precaution however, because the important temperature profile at deformation zone (only subjected to the PSC condition) was not recorded.

Moreover, Hinton [242, 243] also mentioned that some possible short circuit of the FTTU occurred during the test when the loosened and bent control thermocouple, PSC specimen or the robotic arms touched the induction coils inside the FTTU due to the vibration of robotic arms during the transportations between the FTTU and test furnace. He explained that the magnitude of vibration was increased at the thinner deformed sample with greater springback force or vibration of robotic arm after deformation and the fast backward retraction of robotic arm into FTTU, shown in Figure 245, which could cause the induction coils to be touched by the loosening thermocouple and the FTTU to be short circuited [242]. The consequence of this short circuit was to shut down the FTTU and ended the simulation because although the signal from the control thermocouple was present, the actual testing temperature could not be physically controlled. This was the main reason why before conducting a test the thermocouple wire had to be carefully taped down on the one side of robotic arms to prevent it loose and touch the induction coils during the simulation.

5.3.3.3. PSC Sample Trapped Between the Deformation Tools

Finally, perhaps the most difficult problem for conducting the continuous cooling 8-pass PSC tests was that after the final 8th pass, is that most likely the thin (about 2.5mm) deformed PSC sample was trapped between the platens and the control thermocouple was broken during the retraction of robotic arms. Therefore, the deformed PSC sample cannot be retrieved in a timely manner from the test furnace into FTTU to finish the last stage simulation - applying either accelerated cooling or fully water quenched to room temperature. These unsuccessful multipass tests were really frustrating because although the completed 8-pass deformation data were correctly recorded, the instantaneous microstructures immediately after the last deformation were lost and many value-deformed PSC samples were wasted.

After many failed attempts at solving this issue and asked possible causes and solutions from other researchers and the experts in the Servotest Company (developer of the TMC machine), eventually at the end of this research project we have found out the problem is caused by the requested strains (0.14 and 0.11) at the last two passes (7th and 8th) are relatively smaller compared with the elastic deformation of the TMC machine frame. For example, comparing the profiles of sample thickness (green curve) and actuator displacement (orange curve) for the last 2 deformations, presented in Figure 246, clearly the actuator displacement was still moving downwards while the calculated sample height was flat (or even was slightly increasing) during the periods where the load was increasing. This was a result of the assumed stiffness value of 390kN/mm by the control software was lower than the actual stiffness, causing the machine deflection to be over-estimated. Therefore, applying a correct (larger) value of machine stiffness in the new updated control software on the TMC machine by the experts can solve this problem and let sample thickness reduces as the load increases.

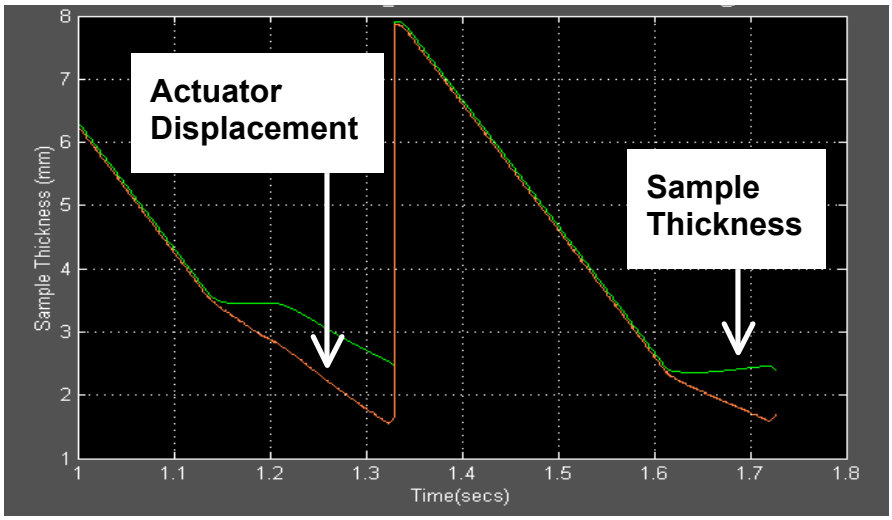

Figure 246: An example shows the differences in sample thickness and actuator displacement profiles at the last two passes of 8-pass PSC test in the fast-speed logged data file

5.3.4. Laboratory Simulation of the Whole Industrial Hot Rolling Schedule of 50mm Plain Carbon Steel Heavy Plate

After some comprehensive discussion of multipass PSC simulation in terms of temperature, effective strain and interpass time controls, and the problems solving, the results (presented in Results Section 4.5) of laboratory simulation of the entire commercial hot rolling schedule of 50mm plain carbon steel plate (8AK43) are discussed more in details in the following. It may be useful to mention again that in order to ensure the thickness of the deformed PSC sample was in the range of 2-3mm, the maximum applied effective strain for the 10mm initial thickness of PSC sample was about 1.6, which was much lower than the target total industrial applied strain of 2.07 for the schedule. Therefore, the whole laboratory testing sequences consisted of three main stages: started with the 2-pass roughing with total applied strain 0.8 on the 50 tonne laboratory Hille rolling mill; and then used the 2-pass roughed and water quenched PSC sample to carry out the 9-pass PSC deformation with the same parameters of the industrial finishing process; and finally post-deformation cooling simulation of 50mm steel plate on the TMC machine.

During commercial roughing, the early deformation passes are not metallurgically important (explained in Literature review Section 2.3.3.3), and for this reason, it was reasonable that the first 9 industrial roughing passes were simulated by just 2-pass reductions with same total applied strain (0.4+0.4=0.8) and similar deformation temperatures (1009°C and 953°C). Moreover, the results (displayed in Figures 118 and 120) showed the actual total applied strain and deformation temperatures were close to the target values, and good consistency of two similar 2-pass rouging simulations.

For the second stage, before the new updated TMC control program was finally installed at the last stage of this research project, the valuable PSC samples (maximum three PSC samples can be obtained from the each 2-pass roughing and water quenched simulation) were frequently dropped from the robotic arms during the transferring process of 9-pass deformation (18 times for the 9-pass PSC deformation) between the FTTU and test furnace. Therefore, the 9-pass and 2-pass PSC tests (with the same total applied strain 1.27 and simulation time) were performed inside the test furnace without taking out into the FTTU for precise temperature controls at each gap time, and success rate was greatly increased. In term of actual strain control, the flow curves in Figure 125 clearly shown that the actual measured strain of each pass in both tests of 9-pass and 2-pass PSC simulation were close to the intended applied strains. However, the biggest problem for keeping the PSC sample all the while inside the test furnace was that the actual deformation temperatures were gradually increased due to the generated deformation heat inside the deformed PSC sample, presented in Figures 122 and 124, which were different to the real or intended 9-pass industrial finishing temperatures and shown in the following Figure 247.

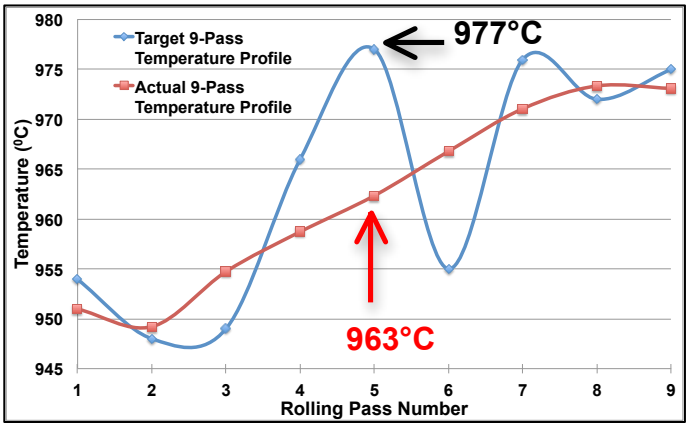

Figure 247: Comparison of target and actual temperature profiles of 9-pass PSC finishing simulation

The final stage of the simulation was to apply the predicted post-rolling natural-air cooling profile (calculated by a Tata Steel Europe in-house finite difference model) at the centre of 50mm steel plate on the roughly 3.3mm deformed PSC sample, and the intended linear cooling rates were 0.56°C/s above 760°C and 0.38°C/s from 760°C to 400°C. It is obviously illustrated in below Figure 248 that the actual recorded linear cooling rate was exactly the same as the target cooling rate - 0.56°C/s. Furthermore, the calculated linear cooling rates were much higher that the rule-of-thumb value of 6.5°C/mm/s (that is 0.13°C/s for the 50mm steel plate), which was derived from the Atlas continuous cooling transformation tables [257], and the predicted cooling rates were agreed to be more correct and realistic values.

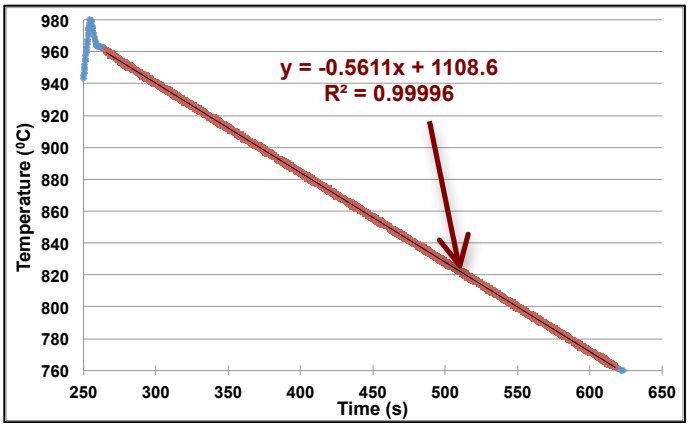

Figure 248: An example of actual measured post-deformation linear cooling rate from 960°C to 760°C was the same as the target cooling rate

Therefore, the whole industrial hot rolling production of 50mm plain carbon steel plate can be closely simulated in the well-controlled laboratory machine, and the corresponding microstructure comparisons of 9-pass and 2-pass PSC tests were presented in Figure 132 of Results Section 4.5.4. Additionally, this simulation also provided some useful information and guidance to replicate complete industrial microalloyed steel plate production as close as possible through the 8-pass PSC tests.

5.3.5. Multipass PSC Simulation of Complete Commercial 60mm Microalloyed Steel Plate Rolling Schedule

Based on experience obtained from the laboratory simulation of the whole industrial hot rolling production of 50mm plain carbon steel plate, the microstructural development of the completed industrial hot rolling schedule of 60mm microalloyed steel plate with total applied strain ε_{Total} =1.65 from roughing, to with HP cooling, and finishing, to post-rolling cooling was successfully simulated through many multipass PSC tests (Results Section 4.6) on the sophisticated TMC machine without the 2-pass pre-roughing on the laboratory Hill mill. Furthermore, the existing conventional TMCP rolling schedule was modified through applying the intermediate forced cooling (IFC) rather than natural-air cooling during the HP and employing different accelerated cooling rates after deformation.

In terms of temperature controls during the HP and ACC stages, the actual temperature profiles in Figures 160 and Figure 174 indicated the same as the target cooling profiles. It is clearly presented in the following Table 14 excellent controls in the deformation temperatures and effective strains during the 8-pass PSC tests.

Table 14: A summary table of intended and actual testing parameters in the 8-pass PSC tests

	Pass 1	Pass 2	Pass 3	HP	Pass 4	Pass 5	Pass 6	Pass 7	Pass 8	ACC
Target Temperature (°C)	1032	1003	978	Air or IFC with different applied cooling rates	872	868	863	857	848	
Actual Temperature	1027 - 1038	993 - 1010	968 - 983		883 - 872	859 - 866	850 - 860	851 - 858	848 - 840	0.3-44 °C/s
Target Strain (12mm)	0.4	0.4	0.1		0.2	0.17	0.16	0.16	0.14	
Actual Strain (12mm)	0.35 - 0.38	0.32 - 0.39	0.08 - 0.10		0.18 - 0.19	0.17 - 0.18	0.14 - 0.16	0.14 - 0.16	0.10 - 0.12	
Target Strain (10mm)	0.3	0.3	0.1		0.14	0.13	0.12	0.12	0.12	
Actual Strain (10mm)	0.25 - 0.30	0.25 - 0.30	0.08 - 0.10		0.12 - 0.14	0.12 - 0.13	0.10 - 0.12	0.09 - 0.11	0.09 - 0.10	
Target Strain Rate (s^{-1})	2.08	2.53	2.80		3.80	3.91	3.93	3.79	2.22	
Actual Strain Rate (s^{-1})	2.04	2.52	2.62		3.72	3.83	3.87	3.37	3.48	
Gap time (s)	5/46	5/46	Varied cooling time		12	12	12	13		

5.4. Effects of Roughing and Finishing Parameters on the Austenite Grain Size, Multipass Flow Curves and Ferrite Grain Size

5.4.1. Important Processing Parameters and Physical Metallurgy in the Hot Rolling Steel Plate Production

It is a well-known fact that in the commercial hot rolling steel plate production, the most important target is to achieve a fine ferrite grain size that is uniformly distributed (particularly through the thickness) in the final as-rolled heavy plate with desired strength and toughness. There are many important processing parameters that can influence the physical metallurgical events at the each stage of industrial hot rolling processing, presented in Figure 249 and Table 15, and determine final desired transformed microstructure and target mechanical properties.

As can be seen clearly from the Figure 249 and Table 15, at each stage of TMCP, different important metallurgical events take place and the corresponding processing parameters (such as deformation temperatures, strain and cooling rate etc.) must be carefully controlled to result in a small austenite and subsequent ferrite grain sizes following transformation. From the metallurgical point of view, the refinement of ferrite grain size is based on fine, strain free austenite grain size obtained from the roughing and deformed (pancaked), strained austenite from the finishing, and accelerated cooling during and after phase transformation. Furthermore, the solidification process during the casting stage is also important to attain a final homogeneous ferrite grain size distribution because it is during solidification where solute partitioning and micro-segregation can create large compositional (Microalloyed Elements-MAE) variations throughout the as-cast ingot [54], and this heterogeneous MAE distribution inside the heavy slab cannot be completely changed to homogeneous MAE distribution during next reheating stage.

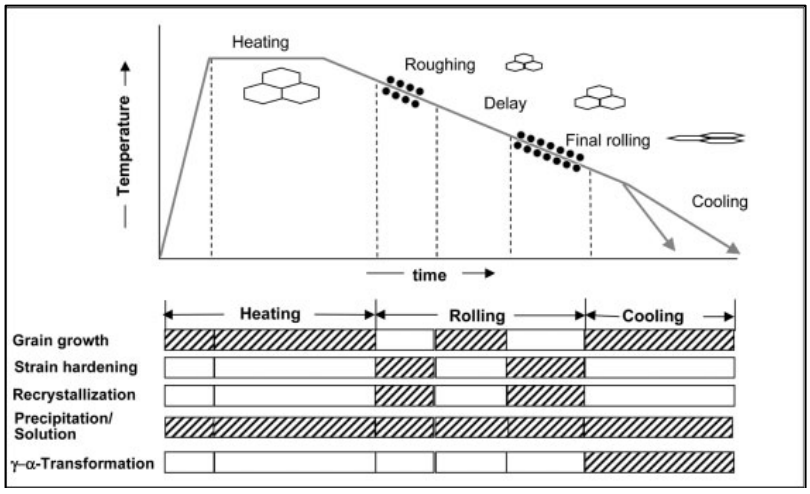

Figure 249: Important metallurgical events occurring at the different stages of hot rolling steel plate production [258]

Table 15: A summary table of critical processing factors and related physical metallurgy in the each stage of industrial hot rolling steel plate production

Processing Steps	Important Processing Parameters	Physical Metallurgy
Reheating	Slab Temperature, Reheating Time, Control Temperature Distribution	Austenitisation, Austenite Grain Coarsening, Dissolution of MA (Nb, Ti)
Descaling	Water Pressure, Spraying Time, Slab Temperature	Remove Oxidation Scale, Austenite Grain Coarsening
High Temperature Roughing	Deformation Temperature (Above the $T_{0.95X}$), Applied Strain or Reduction, Strain Rate, Interpass Time	Static Recrystallisation (SRX) of Austenite between Passes, Austenite Grain Growth
Holding Period Cooling	Cooling Rate, Sufficient Recalescence Time, Total Delay Time	Austenite Grain Growth, Austenite to Ferrite Transformation and MA Precipitation (Intense Water Cooling)
Low Temperature Finishing	Deformation Temperature (Below the $T_{0.05X}$ and above Ar_3) Applied Strain or Reduction, Strain Rate, Gap Time	Pancaked Austenite Grains, Strain Induced Precipitation (SIP), Interaction between SIP and SRX
Accelerated Cooling or Air Cooling	Start Cooling Temperature, Cooling Rate, Cooling Stop Temperature	Precipitation Hardening, Ferrite Grain Coarsening, Ferrite Transformation Products

5.4.2. Consistency of Replication in the Multipass PSC Tests

In this research project, many complicated multipass PSC tests included applying the IFC during HP were successfully performed on the advanced TMC machine to investigate the microstructures evolution and flow curves development during commercial hot rolling steel plate production, and to compare and analyse different important processing parameters on the austenite, multipass flow curves and ferrite grain size. It is critical to make sure that good consistency or agreements were found in the multipass flow curves and temperature profiles from test to test when considering the 8-pass PSC testing sequences. This was because it was necessary to know that a PSC specimen undergoing several extra steps or deformations would have the same history as those stopped earlier in the testing sequence (explained in

Figures 163, 164 and 166 of Results Section 4.6.3.4). Furthermore, to correctly analyse the effect of each processing factor, it is important to keep the others parameters at the same values, so that any differences in the multipass flow curves and/or observed optical microstructures were attributed to the investigated rolling factor only rather than incompatibility or inconsistency (many variables) between the similar multipass PSC tests.

In the following sections, the results of different roughing and finishing processing parameters, such as deformation temperature, interpass time and applied strain, on the multipass flow curves and microstructures are discussed in more details. The influences of intense water cooling during (IFC in HP) and after hot rolling (ACC) on the austenite and ferrite grain sizes are presented in next Section 5.5.

5.4.3. Effects of Different Deformation Temperatures on the Flow Curves and Ferrite Grain Size

There is no doubt that the deformation temperature is one of the most important factors in commercial hot rolling steel plate production. As obviously presented in below Figure 250, under the same steel composition (Nb steel A), applied strain, strain rate and interpass time, a higher flow stress was produced at the lower deformation temperature due to more force was required to deform the PSC sample. Furthermore, as discussed in earlier Section 5.2.1.2, during industrial heavy plate roughing stage there was a huge temperature difference between the sub-surface and centre of the heavy plate, so the flow curves of 950°C and 1190°C in Figure 250 can also represent the significant different deformation conditions at the heavy plate surface and centre respectively to some extent (assuming the uniform strain and strain rate distributions across heavy plate thickness).

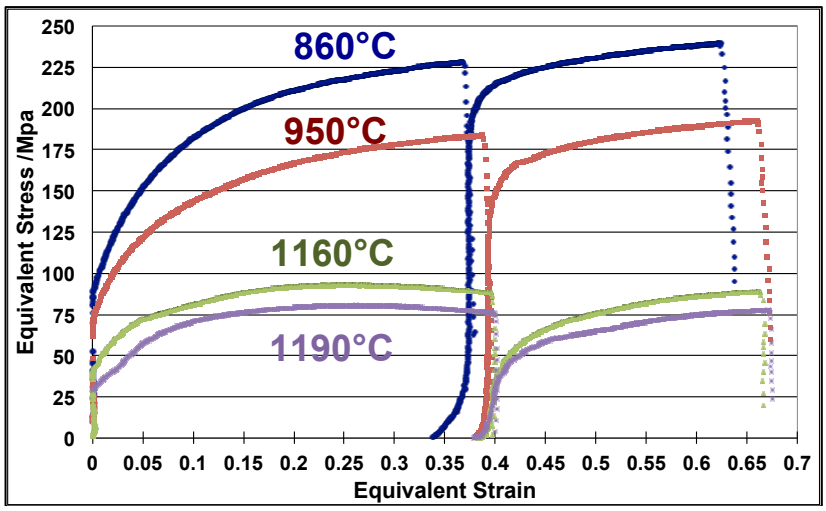

Figure 250: Flow curves comparisons of Nb Steel A in double deformations at the different deformation temperatures (860°C, 950°C, 1160°C and 1190°C)

As presented in Results Section 4.6.4.3, some 8-pass PSC tests with different 5-pass finishing deformation temperatures (strain, strain rate, gap times and post-deformation cooling rate were set exactly at the same values) were conducted to investigate the influences of 5-pass finishing rolling temperatures on the multipass flow curves and subsequent average ferrite grain sizes d_α and volume fraction of ferrite V_α.

For example, the results of the Nb+Ti steel B, which were displayed at Figures 199 to 202, possibly suggest that the finishing-rolling temperature (below the recrystallisation stop temperature, $T_{0.05X}$) in heavy plate hot rolling is not an important element on the refinement of average d_α. That is because only 0.6μm reduction from 5.9μm to 5.3μm of the average d_α was found when the average deformation temperatures of 5 finishing passes were reduced by 55°C (such as the deformation temperature of 8th pass from 840°C decreased to 785°C). Furthermore, the multipass flow curves of steel B in Figure 200 revealed that an average of only a 25MPa equivalent stress increment was found at the test of lower 5-pass finishing deformation temperatures in which the deformation temperatures of the 6th to 8th passes possible below the predicted austenite to ferrite start transformation temperatures Ar_3 of steel B (presented in later Table 16). When rolling at the two-phase regions, the replacement of some harder austenite into softer ferrite could reduce the required load to deform the sample, so further works have to be carried out on analysing the as-quenched microstructures (whether small ferrite grain sizes decorated along the prior austenite grain boundaries) at the end of finishing with low 5-pass finish temperatures. On the other hand, for the plain carbon steel C at the similar 8-pass PSC testing conditions, presented at Figures 203-205, when the average temperatures of 5-pass finishing were reduced about 60°C the average difference of equivalent stresses in these 5 finishing passes were 75MPa and also only caused average 1μm d_α refinement. The reasons for such marginally d_α reduction in both Nb+Ti steels B and plain carbon steel C are unclear, which possible due to only lowered the finishing temperatures in range of 860°C to 780°C without increased the applied finishing strain and/or changed other rolling parameters, the corresponding austenite microstructure and numbers of nucleation sites for the ferrite formation perhaps were almost the same, so further tests and investigations are required.

5.4.4. Effect of Interpass Time during 3-Pass Roughing on Flow Curves

At the end of this research program, after the new updated control software was installed, the deformed PSC sample can be more frequently transferred from the test furnace back into FTTU for the correct temperature cooling controls in longer interpass times. For example, in the following Figure 251, although different interpass times (5s, 32s and 46s) were applied after the first and second roughing passes in three similar multipass PSC tests of Nb steel A,

the corresponding multipass flow curves and magnitudes of softening caused by static recrystallisation (SRX) in the first 3 roughing passes were exactly the same. That was because according to the Equations 19 and 30 (Literature chapter Section 2.3.3.2), when the effective strain 0.45 were applies at the relatively high deformation temperatures (1037°C and 1002°C) of the first and second roughing passes, the resultant 95% SRX were completed in just 1.0 and 0.4 seconds respectively (the initial grain size was assumed at 200μm), which were less than the shortest 5 seconds applied interpass time. Furthermore, although the larger prior austenite grain size (PAGS) was produced at the longer interpass time due to the continuous grain coarsening, after the subsequent third roughing pass and identical HP cooling, similar PAGS were expected to be achieved at the end of HP according to the grain growth, Equation 66. Therefore, only shortened the intervals from 46s to 32s and to 5s in the first 3-pass roughing without altered the deformation temperatures, strain and strain rate, there were no influences on the flow curves, and the similar predicted PAGS were achieved (46μm, 43μm and 40μm respectively) at the end of the same 266s HP from 980°C to 880°C.

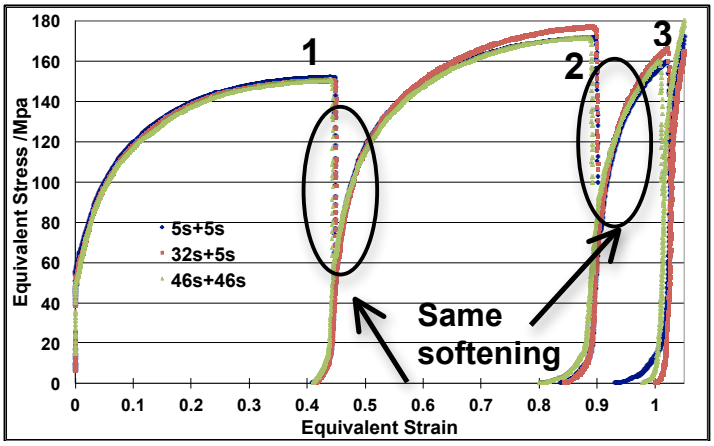

Figure 251: Flow curves comparison of three similar 8-pass PSC tests with different interpass times during the first 3-pass roughing simulation

5.4.5. Critical Applied Strain to Onset of Dynamic Recrystallisation in Multipass PSC Tests

Because the 10 industrial roughing passes with a total applied strain ε_{Total} =0.9 was simulated through only a 3-pass PSC test (0.4+0.4+0.1) in the same deformation temperatures range and strain rates, several possible dynamic recovery (flat flow curves) were found at the first and/or second roughing passes (presented in Figures 144, 149 and 153 of Results chapter Sections 4.6.3.2 and 4.6.3.3), which would not be normally occurred (due to the insufficient effective strain per pass) in the commercial heavy plate roughing stage. In order to investigate whether the dynamic recovery or dynamic recrystallisation (DRX) were actually taking place during the first and second roughing passes, several published empirical Equations 71 to 74

for determining the critical applied strain ε_c to initiate the DRX in C-Mn steel and microalloyed steels were compared under the same testing conditions and discussed as following. In general, the ε_c for the initiation of DRX is a constant fraction (0.5-0.9) of strain to the peak strain, ε_p, which is usually reported as a function of Nb and Ti contents, initial austenite gain size, and Zener-Hollomon parameter, Z.

According to the Sellars' critical strain Equation 71 [34] for the plain carbon steels C and D, in order for the DRX to take place at the first and second roughing passes (the testing conditions were shown in Table 15 and the reheated PAGS was assumed at 300μm), the applied effective strains have to be 0.56 and 0.36 respectively. Thus, most likely the DRX (or dynamic recovery) would not occur at the first roughing pass but could take place at the second roughing pass. In terms of Nb steel A and Nb+Ti steels B, the reheated PAGS was assumed at 200μm, and Equations 72-74 were used to calculate the critical strains and the corresponding predicted strains for the first roughing pass were 0.36 and 0.65 and for the second roughing pass were 0.27 and 0.66 respectively. Therefore, based on the Equations 72 and 73 the DRX took place at the first and second roughing pass; on the other hand, the predicted values from Equation 74 suggested no DRX occurred at both passes. It is important to be noted that all these equations were determined from the multipass hot torsion tests rather than the intended multipass PSC tests, thus employing these equations into the analysis of PSC deformation some errors and disagreements would be produced. A good example of comparing the Equations 73 and 74 is illustrated in Figure 252 in which two obviously peak strains (indication of the DRX) at the first and second roughing passes. As clearly presented in Figure 252, the ε_p in the first roughing pass was only about 0.28, thus ε_c=0.28X0.8=0.22, which was still considerably smaller than the predicted ε_c values of 0.61 and 0.34 respectively from the Equation 73 and 74 for the DRX to take place. Therefore, further works were required to determine the actual value of ε_c for initiating the DRX in the conditions of multipass continuous cooling PSC tests.

$$\varepsilon_c = 0.8 \times 4.9 \times 10^{-4} \times d_{i-1}^{0.5} \times Z^{0.15} = 3.92 \times 10^{-4} \times d_{i-1}^{0.5} \times \left(\dot{\varepsilon} \exp\left(\frac{312000}{RT} \right) \right)^{0.15} \quad (71)$$

$$\varepsilon_p = 2.8 \times 10^{-4} \times \frac{\left(1 + 20[Nb]\right)}{1.78} \times D_0^{0.5} \times \left(\dot{\varepsilon} \exp\left(\frac{375000}{RT} \right) \right)^{0.17} \quad (72)$$

$$\text{and } \varepsilon_c = \varepsilon_p \left(0.8 - 13[Nb]_{eff} + 112[Nb]_{eff}^2 \right) \text{ and } [Nb]_{eff} = [Nb] + \frac{[Si]}{94} - \frac{[Mn]}{120} \quad (73)$$

$$\varepsilon_c = A\varepsilon_P = 0.77\varepsilon_p = 0.77 \times 3.7 \times 10^{-3} \frac{\{1 + 20[Nb] + 0.02[Ti]\}}{1.78} d_{i-1}^{0.147} Z^{0.155} \quad (74)$$

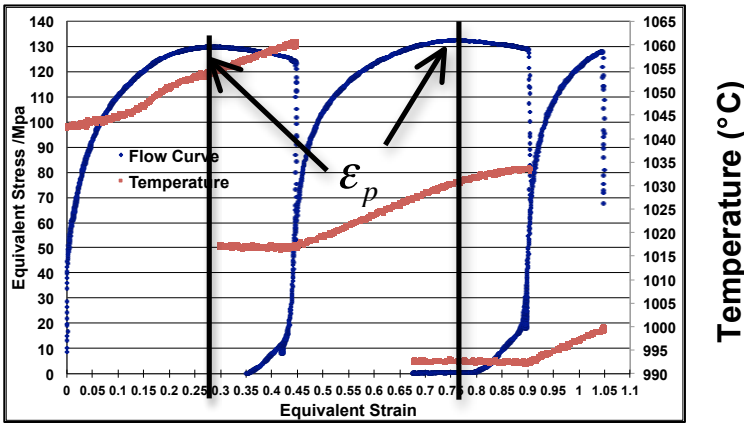

Figure 252: Flow curve and temperature profile of 3-pass PSC tests with the effective strain arrangement 0.45+0.45+0.15

5.4.6. Effects of Chemical Compositions on the Multipass Flow Curves, Prior Austenite and Ferrite Grain Sizes

There is no doubt that the chemical composition of the steel, particularly for the additions of microalloyed elements (such as Nb and Ti), plays a major role in the evolution of prior austenite grain size (PAGS) during the reheating, roughing, HP cooling and finishing stages, and the subsequent ferrite grain refinement processes. Hence, in this research, comparisons of the multipass flow curves and the corresponding observed optical microstructures between several different steels (Nb steel A, Nb+Ti steel B, plain carbon steels C and D) were made whenever relevant for the each hot rolling parameters analysing, which were clearly presented in Results Section 4.6.3 to 4.6.4. In the following section, the discussion particularly focuses on the influences of different chemical compositions on the PAGS and shapes at the end of roughing and finishing stages. The impacts of the steel composition on the PAGS at the end of HP and final transformed ferrite grain size after post-deformation cooling are discussed in the next Section 5.5.

As presented in Figures 144 to 147 in Results Section 4.6.3.2, under exactly the same testing conditions, similar multipass flow curves and the resultant equiaxed shape of the PAGS were produced immediately after the 3-pass roughing simulation in steels A, B and C, which were 22.1±0.6μm, 18.4±0.5μm and, 22.3±0.7μm respectively at the rolling direction. It is expected that the Nb+Ti steel B had the finest PAGS due to the addition of 0.015 wt% Ti, which can restrict or delay the austenite grain growth during the intervals of high temperature (above 980°C) during the 3-pass roughing deformation. Furthermore, the similar equivalent stresses in the Figure 144 suggest that the deformations were conducted at the fully recrystallisation temperature range (above $T_{0.95X}$) and the extra solid solution strengthening by the Nb and Ti elements in steel A and B did not cause large additional forces to deform the PSC samples.

However, when the subsequent 5-pass finishing rolling were taken place below the predicted recrystallisation stop temperature, $T_{0.05X}$, different multipass flow curves and prior austenite grains microstructures immediately after the 8th pass (3R+HP+5F+WQ) were observed in steels A, B and C, which were shown in Figures 167 to 171 in Results Section 4.6.3.4, and the following Figures 253 and 254.

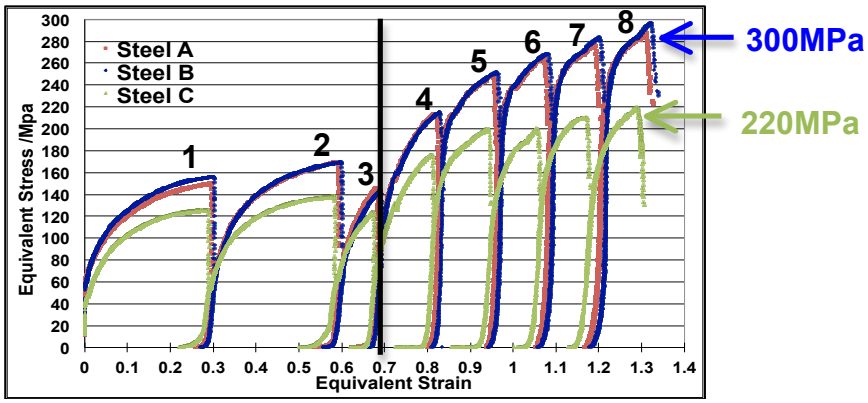

Figure 253: Flow curves of three 8-pass PSC tests (3R+266seconds+5F+10°C/s) with 10mm initial thickness of PSC sample with total strain 1.32 of three different steel compositions

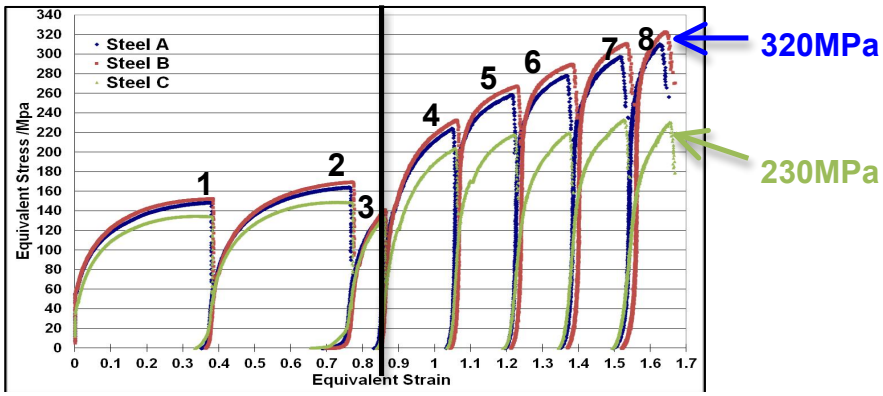

Figure 254: Flow curves of 8-pass PSC simulation (3R+266seconds+5F+10°C/s) with 12mm initial thickness of PSC sample with total strain 1.65 of three different steel compositions

It is well documented (described in Literature review Sections 2.3.4.1 and 2.3.4.5) that the finishing rolling is the most critical stage for HSLA steels to produce high density of near planer crystalline defects (NPD) within the deformed unrecrystallised and pancaked prior austenite grains, thus provided sufficient nucleation sites for later formation of small ferrite grain sizes during the phase transformation. Therefore, the noticeable appearances of elongated austenite grains at the rolling direction were produced at the centre of deformed PSC samples of steels A and B, presented in Figure 170, implied that the last few finishing passes from 860°C down to 840°C were performed below the important $T_{0.05X}$ of Nb steel A and Nb+Ti steel B and the applied strains of last few finishing passes were accumulated. On the other hand, as shown in Figure 171, there were no obvious evidences of elongated austenite grain along the rolling direction in plain carbon steel C, thus it suggested that the 5-

pass finish rolling temperatures (from 880°C down to 840°C) were still above the $T_{0.05X}$ (808°C) of steel C.

As obviously displayed in Figures 253 and 254, although different total applied strains were applied (the influences of different total applied strains on multipass flow curves and ferrite grain sizes are discussed in the next Section 5.4.7) in these two figures, the equivalent stresses of steels A and B in both figures were considerably relatively higher than the values of steel C during the lower deformation temperatures of 5-pass finishing simulation, particularly after the 8th pass (there were 80MPa to 90MPa differences in the flow stresses). That was because if compared with the relatively small solid solution strengthening in the higher temperatures 3-pass roughing, the retained work hardenings were considerably larger in the 5-pass finishing, which caused by the great pinning force exerted by the fine strain induced precipitates on the austenite grain boundaries, and then these precipitates in turn caused the suppression of static recrystallisation at the interpass time and the accumulation of applied effective strains from the 4th pass to the 8th pass in both Figures.

5.4.7. Effects of Total Applied Strains on the Multipass Flow Curves and Subsequent Average Ferrite Grain Size

As presented earlier in Figures 253 and 254, several similar 8-pass PSC tests (3R+266s HP+5F+10°C/s) were conducted in the steels A, B and C with a variation in the total applied strains (0.7+0.62=1.32 and 0.9+0.75=1.65) to determine its influences on the 8-pass flow curves and the subsequent average ferrite grain sizes d_{α}. The corresponding different input strain values of each deformation were presented in Table 8 of Experimental chapter Section 3.9.1 and in Table 14. For example, the following Figures 255 and 256 demonstrated the comparing results of Nb+Ti steel B in two similar 8-pass PSC tests with the same deformation temperatures, strain rate, gap times, HP cooling and the identical post-deformation accelerated cooling rate, apart from the applied strains given at each pass and total input strains. As showed in Figure 255, during the first 3 roughing passes the equivalent stresses were almost the same in both tests regardless of different applied strains at the first and second roughing passes, which possible suggest that dynamic recovery or DRX occurred at these two passes. Moreover, after the 8th deformation the test with the higher total applied strain gave slightly larger equivalent stress (20MPa) and the corresponding average d_{α} only reduced 0.5μm at the RD (presented in Figure 256).

Thus, for this specific 8-pass PSC testing schedule (3R+266s HP+5F+10°C/s) on the steel B, increased strain per pass at the roughing and finishing stages or total applied strain from 1.32 to 1.65 did not cause considerable differences in the equivalent stress and subsequent d_{α}.

Furthermore, the almost same measured d_α also indicated that these two 8-pass PSC tests produced similar PAGS at the end of HP and/or similar retained strain ε_r at the finishing stage according to the Equation 42 in which the d_α is a function of post-deformation cooling rate C_r, retained strain ε_r and austenite grain size D_γ in Literature review Section 2.4.3.1. Although according to the Equations 17 to 21 and Equations 26 to 28, presented in Literature review Section 2.3.3.2, at the larger applied effective strain per pass at the high temperature roughing stage, the faster kinetics of 50% static recrystallisation (smaller values of $t_{0.5}$) and smaller recrystallised austenite grain size (d_{rex}) were produced, still there is a limit of austenite grain refinement can be achieved even the whole rolling process (i.e. recrystallisation controlled rolling - RCR) were carried out above the 95% recrystallisation temperature $T_{0.95X}$, presented in Figure 23 of Literature review Section 2.3.3.3.

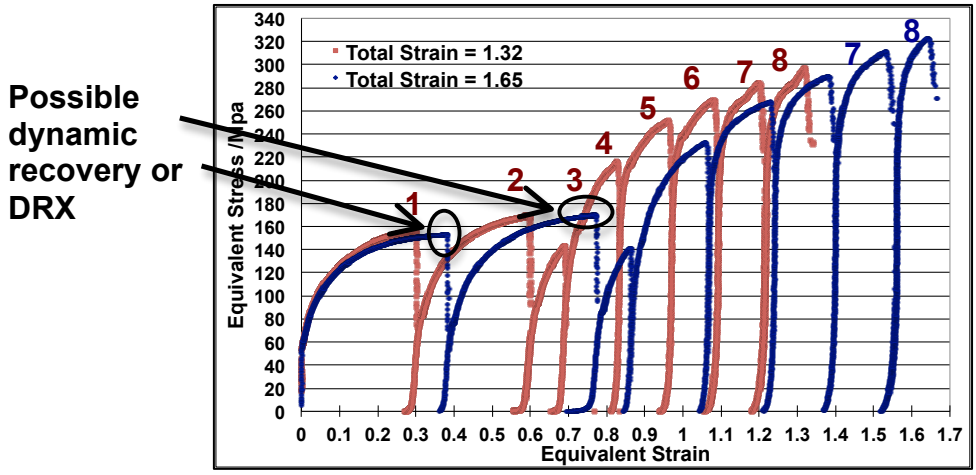

Figure 255: Flow curves comparison of Nb+Ti steel B in two similar 8-pass PSC tests with only difference in the total applied strains

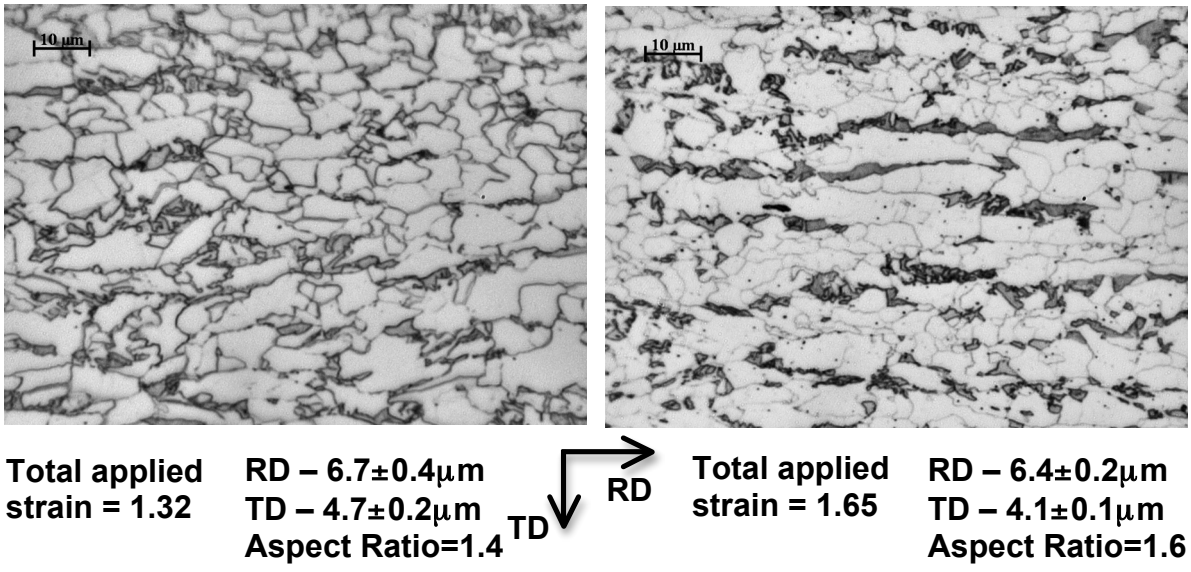

Figure 256: Optical microstructures of Nb+Ti steel B in two similar 8-pass PSC tests (3R+266s/IFC +5F+10°C/s) with different total applied strains

5.5. The Effects of Air Cooling and Forced Cooling during and after Hot Rolling on Productivity and Microstructures of Heavy Plate

After discussing the influences of some important roughing and finishing parameters (such as the different deformation temperatures, interpass time, the total applied strain and chemical composition) on the austenite evolution, multipass flow curves of the continuous cooling multipass PSC tests, and final transformed ferrite grain sizes in Section 5.4, the last vital area of this discussion chapter is to focus on the results of the most important objective of this research project – on the influence of applying the intense water cooling during HP and after hot rolling (ACC) to improve steel plate production. It is important to emphasise again that the reliability and good agreements of the 8-pass PSC tests are essential so that any difference in the final observed microstructures were only attributed to the variations in the HP cooling or the applied post-deformation cooling rates during final phase transformation.

5.5.1. Increased Productivity through Applying the IFC during Holding Period

As described in Literature review chapter Section 2.4, the conventional commercial hot rolling production of microalloyed heavy steel plate greatly suffers from the long process time or low productivity mainly due to the HP slow cooling (could be 15 to 20 minutes) and a large amount of total reduction (this gives many relatively small finishing passes and longer rolling time) is usually required at the low finishing temperatures [14].

Therefore, there is no doubt that employing the intermediated forced cooling (IFC) into the HP can shorten the necessary delay time considerably, depending on the severity of applied forced cooling, and without any significant deterioration (up to 5°C/s IFC was applied during HP) in final bulk mechanical properties [24], which were described in some published literatures [16, 24-30]. However, the reported works were conducted in the commercial steel plate mills or at the large pilot mills, the heat transfer coefficients and detail actual measured temperature profiles across different thickness of partially rolled heavy plate under air-cooling and IFC conditions were not included. Therefore, these important published works cannot be transferred and simulated on the TMC machine in this research project.

Although several other methods were also reported to increase productivity of hot rolling heavy steel plate, such as reducing the reheating temperature to about 1125°C [14, 30], and/or increasing finish-rolling temperature [30, 85], and/or rolling several heavy slabs in groups [17, 85], these options all have some limitations and/or negative impacts on desired microstructures and properties of as-rolled heavy plate. For example, the method of reducing the reheating or austenitisation temperature indeed gave higher productivity, and prevented

excessive austenite grain growth at the end of the reheating stage with more homogeneous austenite grains distribution before roughing, thus it increased toughness but decreased yield strength in a small magnitude [14]. The reason for the reduction of yield strength was the result of less amount of Nb addition was dissolved into solid solution in decreased reheating temperature, which in turn caused some loss in precipitation hardening during post-deformation phase transformation.

Another method to increase productivity was using natural-air cooling several partial rolled plates on a transfer bed during the HP while the roughing and finishing mills carried on rolling other slabs that are already for rolling, which was briefly mentioned at the Introduction chapter Figure 3, but this option is only available if there is enough space (a long spacing of 105 meters was reported in a new built heavy plate mill [19]) between the roughing and finishing stands. However, a substantial amount of austenite grain growth still took place at the end of long HP even several heavy plates were cooled at the same time.

5.5.2. Prior Austenite Grain Growth during the Holding Period

As discussion previously, when the partially rolled heavy plate is delayed 6-15 minutes during the HP, it was considerably undesirable in terms of productivity and the austenite grain coarsening at the interior of heavy plate. The reduction of prior austenite grain growth during the continuous cooling HP is very important since it determines the overall refinement of the austenite microstructure that is achieved at the end of roughing stage [53].

5.5.2.1. Austenite Grain Coarsening at the Different Cooling Conditions during the HP

It is clearly presented in the Results (Section 4.6.3.3), that several similar 3-pass roughing simulations with only difference in the cooling conditions during the HP were performed on the Nb steel A and Nb+Ti steel B. In general, all the results have confirmed that at the fully austenite phase region, increased continuous linear cooling time from 975°C to 880°C (presented in Figures 150 to 152), or increased the isothermal holding temperature from 880°C (see Figure 159) to 980°C (shown in later Figure 257), the corresponding prior austenite grains size (PAGS) increased. Therefore, these results indicated that decreasing the long cooling time indeed reduced the austenite grain growth. Although some researchers [21, 86] have claimed that the addition of 0.015wt% Ti element can form the undissolved and stable TiN particles at the prior austenite grain boundaries to inhibit the coarsening of fine recrystallised austenite produced from the roughing stage, according to the PAGS development in Figures 150 to 152, the austenite grain coarsening still occurred at the steel B during the continuous linear cooling from 975°C to 880°C.

Furthermore, the measured PAGS was a function of applied cooling time during the same HP was presented in Figure 152 in which the fastest austenite grain-coarsening rate was taking place at the first 40 seconds of HP and from the 90th second to 300th seconds of HP the PAGS only gradually increased from 23μm to 26μm. Therefore, one may confidently to suggest that the PAGS would be only increased slightly even at the end of much longer HP, such as 15 minutes slow cooling from 975°C down to 880°C. It should be noted that these results were focused on the PAGS development at the heavy plate surface during the HP, whereas different austenite grain coarsening profiles would be expected to be observed towards the centre of the heavy plate, where the corresponding temperature cooling ranges (such as from 1160°C to 1000°C) would be considerably higher during the same HP, and will be discussed in next Section.

There is no doubt that if compared with the almost linear temperature cooling profile at the 100mm heavy plate surface under the natural-air cooling during the HP, the complex (rapid forced cooling and fast recalescence) temperature profiles under the IFC condition was more challenging to be correctly simulated on the TMC machine. As illustrated in Figures 160 to 162, the target IFC temperature profile was divided into many testing segments and exactly replicated, and the measured average PAGS of steel B at the end of HP (3R+IFC+W) was 22μm at the rolling direction, which means only small amount austenite grain growth took place since the observed average PAGS immediately after 3-pass roughing was 18μm.

5.5.2.2. Physical-Based Equations Predicting the Austenite Grain Growth at the Plate Surface and Centre under Continuous Cooling and the IFC Conditions

It is useful to compare the measured PAGS at the end of HP with the predicted results from some empirical equations of modelling austenite grain growth after completed static recrystallisation, such as the widely cited Hodgson and Gibbs' Equation 23 for C-Mn-Nb steel previously mentioned in the Literature chapter (Section 2.3.3.3). However, Equation 23 was only initially applied to calculate the grain coarsening at the isothermal conditions, thus, the principles of the additivity rule [111, 113] was used to modify the isothermal holding into the continuous cooling condition, presented in Figure 75 of the Experimental chapter Section 3.12, and shown in the following Equation 75 in which $t_i(T_i)$ is the time for austenite grain growth at the time interval of temperature T_i, and T_f is the finishing temperature at end of continuous cooling delay time t_{Delay}. It has been long known that the kinetics of austenite grain growth are highly sensitive to the holding temperature due to the fact that grain coarsening is a thermally activated diffusional event. For instance, comparisons of three predicted PAGS development profiles as functions of the delaying or holding time at the different grain coarsening conditions by the Equation 23 (the d_{rex} were set at 18μm) are displayed in Figure 257.

$$\sum_{T_i}^{T_f} \frac{t_{Delay}}{t_i(T_i)} = 1 \qquad (75)$$

As presented in below Figure 257 that the simulation at the 980°C isothermal holding condition gave the largest PAGS (60μm) at the end of the same 350s grain coarsening time while the continuous slow cooling condition indeed reduced the PAGS to about 45μm due to less time at the higher temperature for the rapid grain growth. In addition, the fastest predicted growth rate was also up to about 40 seconds of holding time, which was the same as the actual measured PAGS profile in Figure 152, and the PAGS at the 40th second were almost the same regardless of isothermal holding at 980°C and continuous cooling from 980°C. In term of laboratory simulation, a specific multipass PSC test was carried out to determine the PAGS after 3 roughing passes and then isothermally held at 980°C for 350 seconds (3R+350s HP+W), and the actual measured PAGS was 33μm in the rolling direction, which was almost twice smaller than the predicted value 60μm (further analysis required).

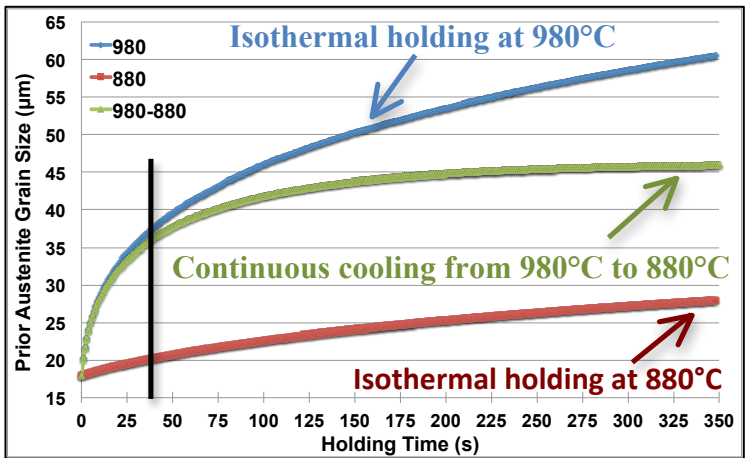

Figure 257: Comparison of predicted PAGS development profiles under three different holding and cooling conditions

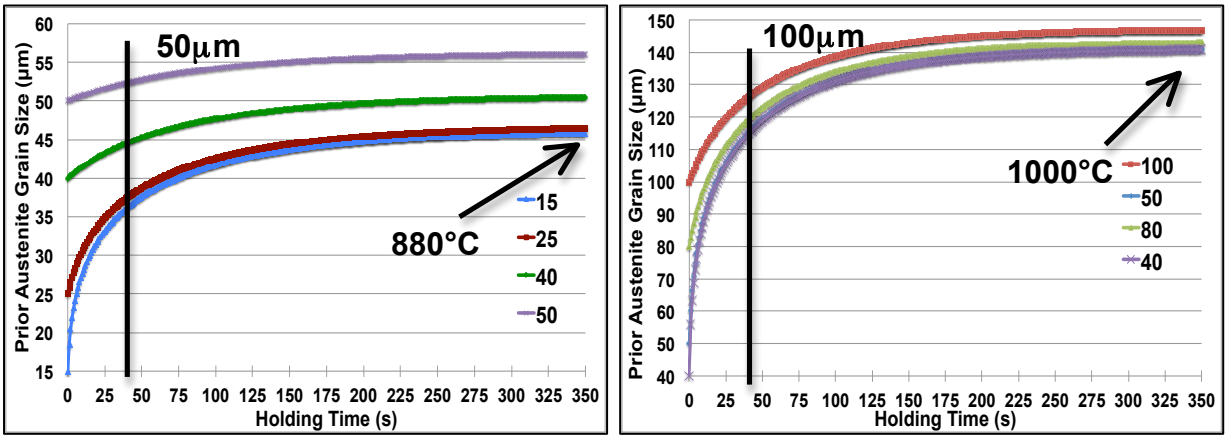

Figure 258: Predicted PAGS coarsening profiles with different initial d_{rex} and temperature ranges of HP from 980 to 880°C (left hand side) and from 1160 to 1000°C (right hand side)

By changing the values of d_{rex} and the continuous cooling temperature range from 980°C to 880°C to higher temperatures 1160°C to 1000°C in the Equation 23, the resultant different predicted PAGS coarsening profiles are shown in Figure 258. It is obviously displayed in Figure 258 that the simulation at the continuous cooling from 1160°C to 1000°C, which similar to the heavy plate centre cooling profile during HP, gave more than twice larger predicted PAGS (138μm -145μm) at the end of the same 350s grain coarsening time due to rapid grain growth at the higher holding temperature. Furthermore, even increasing d_{rex} from 40μm to 100μm (right hand side graph in Figure 258), the subsequent predicted PAGS profiles after 40 seconds were similar; on the other hand, the predicted PAGS increased from 45μm to 55μm at the continuous cooling temperature range from 980°C to 880°C when raised d_{rex} from 15μm to 50μm. Therefore, the PAGS coarsening profile is mainly determined by the continuous cooling temperature range rather than the length of cooling period, which in turn suggests that the PAGS towards plate centre can be greatly decreased when the forced water-cooling was applied during HP as the corresponding temperature profiles were reduced from the surface chilling effect.

Finally, the actual recorded complex IFC temperature profile during HP was divided into many small holding intervals and also simulated by Equation 23, and the resultant PAGS coarsening profile is presented in below Figure 259. As clearly displayed in the predicted PAGS curve, when temperature of deformed PSC sample decreased from 980°C to 880°C in 20 seconds, the predicted PAGS increased from 18μm to 24μm, and then sizes were almost same from the 20th second to 90th second. At the end of IFC cooling, the predicted size was about 25.2μm, which was still larger than the actual measured PAGS (21.5μm) of steel B after 3R+IFC+W.

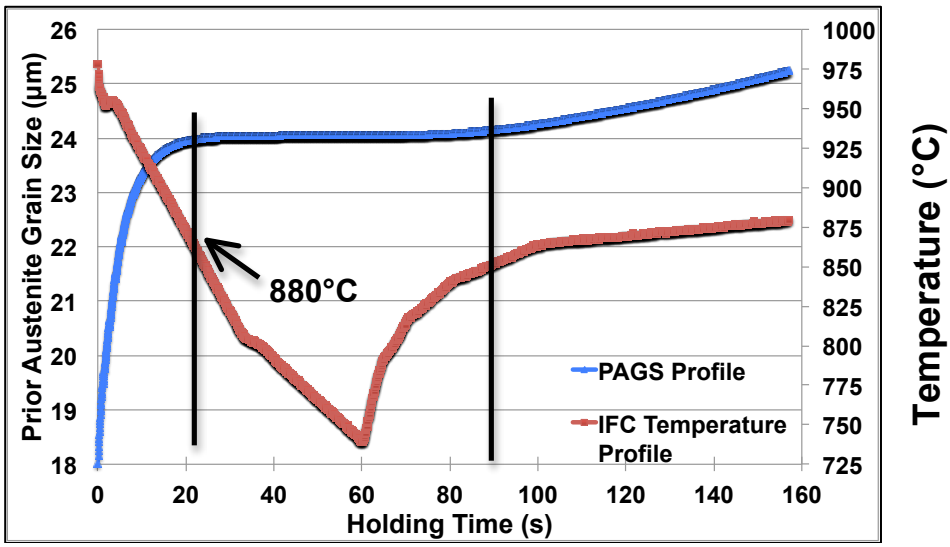

Figure 259: The predicted PAGS coarsening and the corresponding recorded IFC temperature profiles during HP

5.5.3. The Effects of Different Cooling Profiles during the HP on the Subsequent Average Ferrite Grain Size

As discussed earlier, the necessary and critical delaying time was shortened and the resultant actual measured and predicted PAGS were smaller when the linear forced and more complex IFC cooling profiles were applied during HP. In the following section, the advantage of employing the IFC temperature profile rather than the 266s linear slow cooling into the HP of 8-pass PSC tests to reduce the subsequent average ferrite grain sizes d_α are further examined. It is clearly illustrated in the Results Section 4.6.4.4 that under almost the same 8-pass flow curves (shown in Figures 207, 210, 213 and 216) and the identical post-deformation applied ACC (10°C/s), the tests with the implement of IFC profile during HP not only reduced the multipass simulation time (improved productivity) by 100 seconds but also gave slightly smaller (about 1μm finer) average D_α and larger volume fractions (roughly 5%-10% more) of ferrite in steels A, B and C. That is possibly because the marginally smaller PAGS (about 4μm finer) were produced at the end of HP when the IFC technique was applied. Further works and investigations are still required to explain the increment of ferrite volume fraction in steels A, B and C when the IFC profile was applied in the HP.

However, applying the fast forced cooling did not always reduce the average d_α, in some extreme cases when the more intense IFC temperature profiles, which was constructed from the predicted temperature distribution curves in the earlier published literatures by Abrams [27, 259] and presented in following Figure 260, were applied during the HP the resultant average d_α increased. It is clearly displayed in Figure 260 that the stop temperature of the intense IFC was 600°C (127°C below the austenite to ferrite transformation stop or pearlite formation temperature 727°C), which was also 140°C lower than the stop cooling temperature (740°C) of normal IFC profile. Moreover, similar to employing the normal IFC profile, the application of intense IFC during HP on the Nb+Ti steel B did not cause noticeable difference in the corresponding 8-pass flow curves, shown in Figures 261 in which two similar 8-pass PSC tests were carried out (3R+266s HP/Intense IFC+5F+0.3°C/s) with only dissimilarity in the HP cooling conditions. According to the observed optical microstructures in Figure 262, the test with the intense IFC profile during the HP gave larger average d_α of 8.2μm than that (6.8μm) of 266s linear cooling at the rolling direction, and gave slightly less volume fraction of pearlite in the final as-rolled slow cooling transformed microstructures.

Therefore, the optimisation of hot rolling schedule of heavy plate not only involves careful controls of the reheating, roughing and finishing operations but also requires the correct temperature cooling profile during the HP.

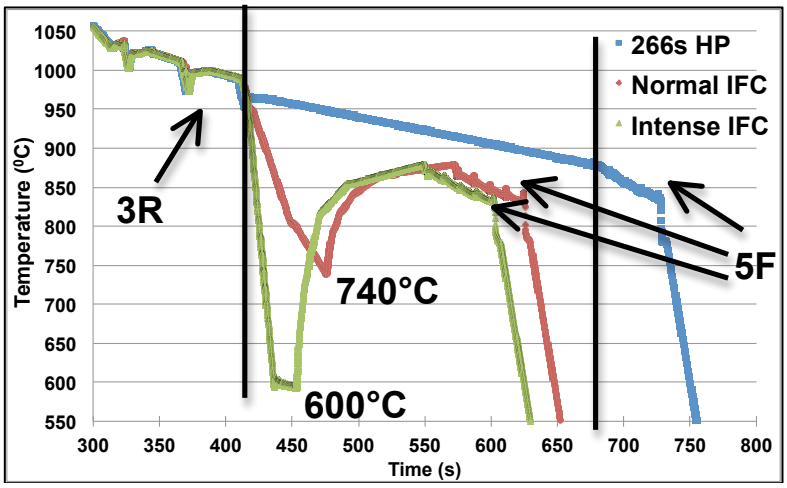

Figure 260: Temperature profiles of three similar 8-pass PSC tests (3R+266s HP/IFC/intense IFC+5F+0.3°C/s) with only variation in the HP cooling conditions

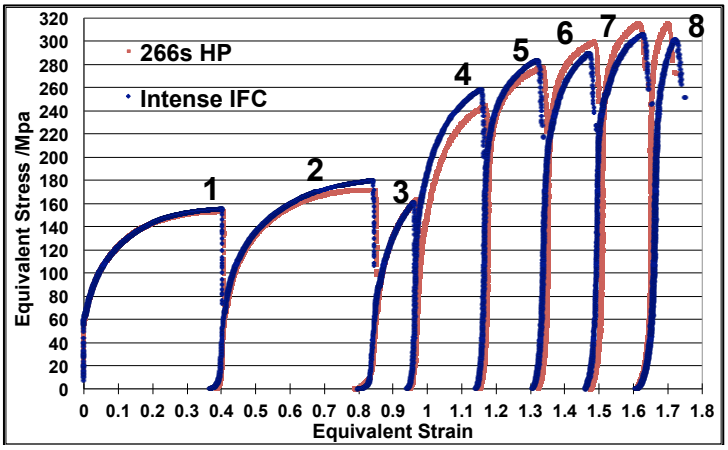

Figure 261: Flow curves comparisons of steel B in two similar 8-pass PSC test conditions (3R+266s HP/Intense IFC+5F+0.3°C/s) with different length of HP

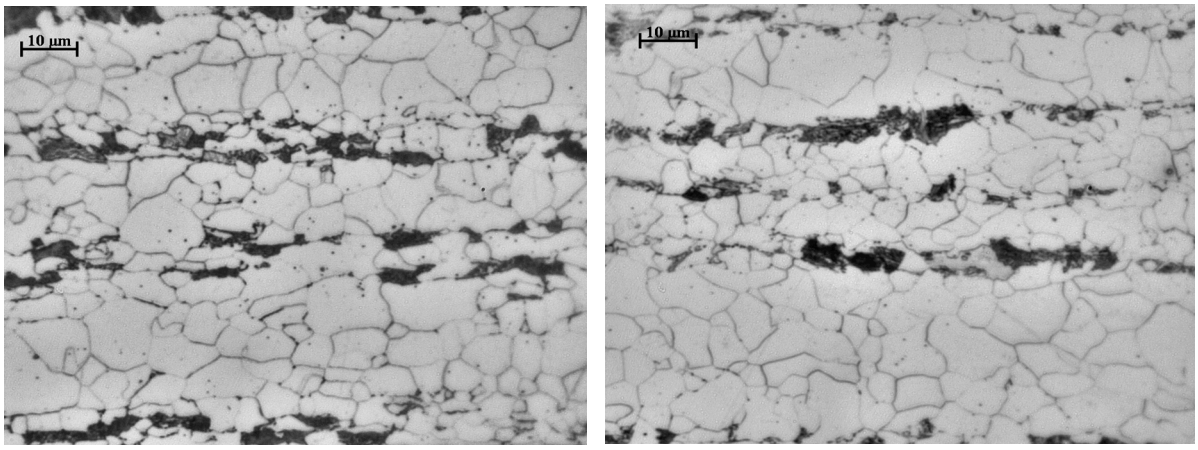

266s linear air cooling during HP

RD – 6.8±0.3µm
TD – 5.9±0.2µm
Aspect Ratio=1.2

Intense IFC during HP

RD – 8.2±0.5µm
TD – 6.5±0.2µm
Aspect Ratio=1.3

Figure 262: Optical microstructures comparison of two similar 8-pass PSC tests with 266 seconds linear cooling and with 116 seconds intense IFC profile during the HP

5.5.4. The Application of Forced Cooling into Hot Rolling Process to Improve Strain Penetration and Uniformity of Microstructure Across Heavy Plate Thickness

As mentioned in Introduction chapter Section 1.2, perhaps one of the most challenging and difficult objectives for the TMCP of commercial heavy plate is the ability to achieve a small average d_α towards plate centre and improve through-thickness grain size homogeneity and annihilate centre porosity when low total reduction ratios from the slab to final plate are usually applied [20, 21]. According to the previous discussion on the temperature distribution in Section 5.2.2, and the predicted effective strain (illustrated in Figure 41 in Literature chapter Section 2.5.5) and strain rate distributions presented in Figure 227 of Results Sections 4.7, the heavy plate centre temperatures during the roughing stage and HP were significantly higher than plate surface temperatures, and the effective strain and strain rate of each rolling pass at the plate centre were also lower than those of plate surface, not to mention the possible difference in local composition due to the segregation. Therefore, the applied deformation and subsequent grain refinement were usually concentrated near the plate surface in which a small and relatively uniform d_α were produced while the plate centre resulted in little microstructure refinement.

As displayed by Figure 228 in Results Section 4.7.2, in order to improve the uniformity of the microstructures, under the conventional processing, through heavy plate thickness, three important hot rolling factors have to be modified: decreased deformation temperatures towards plate centre, increased sufficient strain penetration or the rolling shape factor, m (ideally m should be ≥ 0.8 and determined by the applied reduction and roll radius according to the Equation 1 at the Introduction chapter) and reduced the temperature variations over the plate thickness at the end of HP and ACC cooling stages. Therefore, it requires a more sophisticated process control as well as production facilities. Normally, it is extremely difficult to reduce the deformation temperature towards the plate centre and increase the m value of each roughing pass to above 0.8 due to the long heat diffusion distance and exceedingly high rolling load and torque (most likely above the rolling mill capacity) are required. For example, as presented in Figure 135 of Results Section 4.6.1, the calculated m in all 16 industrial rolling passes were less than the critical value of 0.8 (particularly the first 10 roughing passes $m < 0.6$), inhomogeneous microstructures across thickness were expected formed in the 60mm as-rolled heavy plate (shown in Figure 136).

Many strain distribution FE models [202, 216, 223, 260] have been developed in the hot rolling steel plates and strips, and the predicted strain distribution across thickness were usually as function of various process variables, such as the plate thickness, radius of work roll and reduction ratio. Recently, Moon et al. [223] have developed an approximate model for predicting the local strain distribution through the plate thickness and suggested that the

inhomogeneity of local strain variation over the thickness was reduced as increased the shape parameter, α (clearly defined in literature). It is illustrated in Figure 263 in which at the high α, more of the plate thickness was around the strain at centre and the steep strain gradient move towards near surface, thus increased the strain homogeneity in bulk thickness.

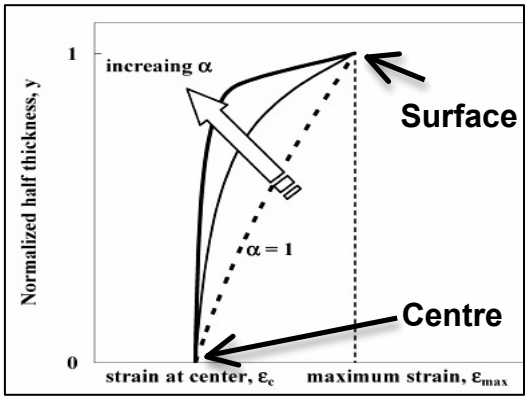

Figure 263: Effect of shape parameter (α) on the local strain variation over thickness [223]

However, the chilling effects with different applied heat transfer coefficient (HTC) applied on the plate surface to cause different strain distribution across thickness were not included in any FE model and paid much less attention. Only few heavy plate producers [18, 20, 21, 261] have reported that the application of force cooling prior to the first pass of rough rolling have improved the effective strains towards mid-thickness, centre consolidation, average d_α and toughness through thickness of heavy plate. For instance, in the experiments conducted by Williams et al. [21], steel slabs were reheated to 1200°C and rolled with a single pass reduction of 10% (the calculated m = 0.66) with and without the use of spraying water. For the normal air-cooling slab, the single deformation produced 10.5% local reduction at the subsurface region and reduced to about 7% local reduction in the mid-thickness position. In contrast, the surface water-cooled slab exhibited enhanced deformation (10% location reduction) in the centre position compared to the subsurface region (7.5% location reduction). Later, Asfahani et al. [20] also reported that water-cooling the slab surface prior to rolling effectively reduced the centre line drilled holes (increased local strain at centre) in 100mm thick plate. The main reason [18, 20, 21, 261]] for increasing the local strain towards plate centre is that the water cooling produced larger chilled surface regions below the plate surface, which are much harder to deform than the hot centre region, thus effectively increased the arc of contact of the mill rolls and the value of m at the centre. Therefore, along with increased reduction ratio, applied higher HTC of water-cooling on the heavy plate surface and lowered deformation temperature, the maximum local or shear strain increased [260] and most likely the enhanced deformation took place at the centre region of heavy plate. Further works of measuring and predicting the strain distribution over heavy plate thickness on the pilot mill have to include the chilling effect on the plate surface and corresponding variation on the strain penetration.

5.5.5. The Effects of Natural-Air Slow Cooling and Accelerated Cooling on the Final Transformed Product Morphology

After some intense discussion of applying the linear forced cooling and the complex IFC temperature profiles into the long HP on the evolution of PAGS and subsequent average d_α, in the following sections the results of different applied post-deformation cooling rates (0.3°C/s to 40°C/s) after the same 8-pass PSC deformation on the austenite to ferrite transformation start temperature Ar_3 and average d_α of different steels (Nb steel A, Nb+Ti steel B, plain carbon steels C and D) are examined in more detail.

5.5.5.1. The Effect of Applied Cooling Rate on the Austenite to Ferrite Transformation Start Temperature Ar_3

As presented in Figure 24 Literature Section 2.3.4.1, the Ar_3 temperature defined the boundary of two important deformation temperature ranges: relatively higher temperatures of non-recrystallised austenite finish rolling and lower temperature intercritical rolling. Thus, it is important to determine whether the last few finishing passes went through the Ar_3 temperature and the elongation of unrecrystallised austenite grains were occurred at the two phases (austenite + ferrite) region leading to a mixed final ferrite grain size. In general, under the equilibrium situation, the start of the austenite to ferrite transformation can be obtained from some published phase diagrams or thermodynamic calculation models (such as Thermo-Calc software). However, in the non-equilibrium or continuous cooling condition, the exact value of Ar_3 is affected by the steel chemical compositions, applied cooling rate (C_r), retained strain (ε_r) and austenite grain size (D_r). Additionally, much fewer continuous cooling transformation (CCT) diagrams are available for the HSLA steels that have been hot rolled and were taken account of the influences of MAE (such as Nb and Ti) and deformed elongated austenite with retained strain compared to those only heat-treated engineering steels [72, 74]. Hence, several researchers have measured (via the dilatometery) the austenite to ferrite transformation start and end temperatures of as-rolled steels at some given cooling rates, and derived different physical-based empirical equations for estimating the, Ar_3, which are compared as follows.

First, the most popular and widely cited empirical Equation 65 (presented in Experiments Section 3.2.2) for predicting the Ar_3 in HSLA steels based on the steel chemical composition was derived by Ouchi et al. [245] in 1982, which assumed a minimum reduction of 50% below the recrystallisation stop temperature and the corresponding investigated plate thickness was between 8mm and 30mm. Although this Equation 65 is often applied, the predicted results for different HSLA steels are relatively scattered possibly because the

equation did not include the impact of others important factors on the Ar_3. In the later work of Majta et al. [262], a more complex correlation between the Ar_3 and some process parameters was proposed in the following Equation 76 in which the D_r and ε_r were affected by steel chemical compositions and finish rolling schedules. Recently, Xuan et al. [263, 264] developed a new complex regression Equation 77 in which the Nb content (0-0.038wt%), D_r, even the time for 5% strain induced precipitation $t_{0.05p}$, $\Delta\varepsilon$ (residual or retained strain in the austenite) and C_r were all taken into account for predicting the Ar_3 of Nb steels. However, it is important to be noticed that the $t_{0.05p}$ in the Equation 77 was more or less a constant ($t_{0.05p}$ = 0.7 to 1.2) and with considerable large errors on the predicted Ar_3 values when changed the $t_{0.05p}$ possibly due to only one single reduction was carried out at the 900°C with applied strain 0.693 and strain rate $5s^{-1}$ at the reference [262]. Thus, the predicted values of Ar_3 from the Equation 77 are not included in the following Table 16.

In terms of plain carbon steels, Choo et al. [247] have developed a regression Equation 78 which was determined from the 16 kinds of plain carbon steels whose composition range: 0.05wt% - 0.2wt%[C] and 0.5wt% - 2 wt% [Mn], and the applied cooling rate was varied from 0.2°C/s - 30°C/s. Furthermore, Santos et al. [265] have also proposed another empirical Equation 79 for the plain carbon steels from 94 experimental data with high coefficient of determination (R^2 = 0.99). In order to compare the predicted Ar_3 of these Equations, the same condition of 8-pass PSC test (3R+IFC+5F) with slow C_r =0.25°C/s were applied, and the Equations 76 was applied in steels A and B while the Equations 78 and 79 were used in steels C and D, and the Equation 65 and commercial software JMATPro were applied in all four steels. As proposed in all the Equations 76-79, with smaller recrystallised austenite grain size D_r, larger residual strain $\Delta\varepsilon$ and reduced applied cooling rate C_r, the predicted values of Ar_3 were increased. For example, when changed the C_r from 0.5°C/s to 10°C/s, the predicted Ar_3 by the Equation 76 reduced 44°C.

$$Ar_3\left({}^0C\right) = 830 - 19C_r^{0.481} - 0.5\times\exp\left(\frac{0.042\times D_r + 7.8}{\left(2.11+\varepsilon_r\right)^{1.35}}\right) \tag{76}$$

$$Ar_3\left({}^0C\right) = 370\exp\left(-\frac{\sqrt{D_r}}{6.7}\right) - 198C_r^{0.1} - 6646[Nb] - 2327[Nb]^2 + 66\times\left(\frac{1}{t_{0.05p}} + \Delta\varepsilon\right) + 830 \tag{77}$$

$$Ar_3\left({}^0C\right) = 925.25 - 494.7[C] - 64.8[Mn] - 10C_r^{0.5} \tag{78}$$

$$\begin{aligned} Ar_3 = {} & 874.4 - 512.05[C] - 40.9[Mn] + 23.08[Si] + 567.1[C]^2 - 199.6[C][Mn] + 265.8[C][Si] \\ & + 4.15\times\left(-2\ln\left(0.0029D_r\right)\right) - 1.03C_r^{0.5} - 11.33\ln C_r, \text{ and } R^2 = 0.9888 \end{aligned} \tag{79}$$

Table 16: Different predicted Ar_3 (°C) of steels A, B, C and D under the same 8-pass PSC tests (C_r =0.25°C/s) from several empirical equations and JMATPro program

Predicted Ar_3	Equation 65	Equation 76	Equation 78	Equation 79	JMATPro Ae_3	JMATPro 0.1°C/s
Steel A	777	814	-	-	850	829
Steel B	778	810	-	-	852	832
Steel C	776	-	791	806	849	823
Steel D	767	-	777	788	840	815

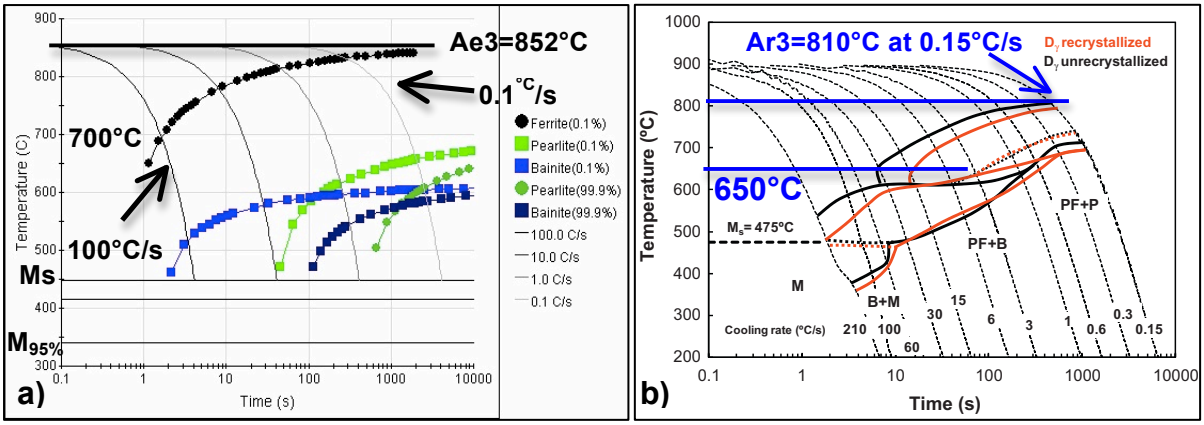

Figure 264: - a) An example of JMATPro software predicted CCT diagram of steel B with PAGS 30μm and austenitisation temperature 860°C; - b) comparison between the constructed CCT diagrams obtained for recrystallised and unrecrystallised austenite [266]

As clearly illustrated in Figure 264 of two independent studies with similar steel compositions, as the applied cooling rate increased, the cooling profile intersected the ferrite start curve at the lower temperature, which was the predicted value of Ar_3 under the specific cooling rate. Furthermore, it is clearly illustrated in Figure 264-b) that similar to the retained strain effect in Equations 76 and 77, the deformed or unrecrystallised austenite indeed increased the measured Ar_3. Therefore, according to the predicted Ar_3 values in above Table 16 and the observed PAGS microstructures after the 8th pass presented in Figures 169 and 170 (presented in Results Section 4.6.3.4) in which no ferrite grains were found along the prior austenite grain boundaries, this confirms that the austenite to ferrite start transformation did not take place in the standard continuous cooling 8-pass PSC tests of all four interest steels. Furthermore, the plain carbon steel D gave the lowest predicted Ar_3 in all estimations due to its higher carbon concentration (0.11wt%) than those (0.085wt%) of others steels. Finally, it should be mentioned that Gray and DeArdo [82] have reported that of all the common solutes, Nb in the austenite has the largest effect in reducing Ar_3, and if strain induced precipitation (SIP) of NbC or Nb(C, N) occurs during the finish rolling stage, it increased the Ar_3, thus the exact value of Ar_3 also depends on the concentration of solute Nb in the austenite during the phase transformation.

5.5.5.2. The Effects of Post-Deformation Cooling Rates on the Transformed Product Morphology

It is widely recognised that correct application of ACC is one of the most effective methods (possible the lowest production cost) to achieve the desired microstructure refinement (reduced average d_α and undesired pearlite volume fraction) and increased strength (smaller d_α and more volume fractions of lower temperature transformation products) than using much more expensive microalloyed elements such as Ni, Cu, Cr or Mo to increase steel hardenability and/or additional heat treatment process. It may useful to emphasise that the influences of employing the ACC after the finish rolling were investigated significantly in last 30 years and the advanced ACC equipment with intense water cooling rates are already installed in the modern commercial hot rolling mills for the relatively thin steel plate (below 20mm) and strip productions. However, no previous work has been conducted to analyse the effects of ACC after the continuous cooling 8-pass PSC tests, which were different to the conditions of single or less than 4-pass reductions and more closer to commercial heavy plate hot rolling production, on the laboratory scale with precise controls of important industrial hot rolling parameters. In this research, several different post-deformation cooling rates were applied after the same 8-pass PSC tests (3R+266s air/IFC+5F), and the examples of showing great consistency in several 8-pass PSC reductions prior to the last ACC stage were presented in Figures 173, 181 and 186 of the Results (Sections 4.6.4.1 and 4.6.4.2), thus any variances in the comparisons of the observed optical microstructures only attributed to the different post-deformation applied cooling rates.

According to the optical microstructures of steels A, B and C shown in Results Section 4.6.4.2, as the applied cooling rate of ACC gradually increased, the smaller average d_α were produced. For example, for Nb steel A the large (12.2μm) polygonal ferrite grains plus pearlite microstructures (presented in Figure 182) under the slow air-cooling rate of 0.3°C/s were modified into very small average d_α (4.7μm) under the 40°C/s of ACC (illustrated in Figure 178) as a result of enhanced ferrite nucleation rate and less available time for the ferrite grain growth at the high cooling rate. Furthermore, in Figure 178 the volume fraction of second phases, where were possibly bainite and/or martensite plus retained austenite (MA) constituents, was about 20%. Thus, further works are required to analyse the different phases in the transformed microstructures in more detail through the microhardness tests and electron microscopes (such as the Scanning Election Microscope-SEM).

Perhaps more importantly, compared with the effects of different chemical compositions, increased total applied strain, applying IFC into the HP and reduced average finishing temperatures (discussed in previous Sections), increased the post-deformation cooling rate was the most dominant factor to achieve small average d_α. As clearly presented in Figures

219 to 222 in Results Section 4.6.4.5, under exactly the same multipass PSC testing conditions (3R+IFC+5F+10°C/s), plain carbon steels C and D produced similar (only about 1μm difference) and fine average d_α but more equiaxed and less pancaked ferrite grains along the rolling direction (the aspect ratio of d_α was 1.1) compared to those (aspect ratio of d_α were 1.3 and 1.5 respectively) in the Nb steel A and Nb+Ti steel B. Therefore, with correct settings of multipass PSC test and ACC, fine average d_α with high strength and toughness, which possibly are similar to those of microalloyed steels, can be also achieved in the plain carbon steel without the costly MAE additions.

In addition, the microstructure refinement also indicated that the volume fraction of pearlite was gradually reduced to zero, and that the volume fraction of bainite and/or martensite increased as the applied cooling rate of ACC increased. For instance, as clearly presented in Figure 183, 189 and 192, about 11%, 10% and 16% volume fraction pearlite (dark regions) were found in all three steels A, B and C respectively when the post-deformation cooling rate was set at 5°C/s. However, these measured results did not agree with the observations from Tanaka [181] as he mentioned that the pearlite volume fraction decreased to zero when the applied cooling rate was at 4°C/s in 0.10wt%C-1.5Mn-0.04Nb steel. Furthermore, Choo et al. [247] also have developed the regression Equations 80 to 81 to calculate the volume fractions of ferrite V_f, pearlite V_p and bainite V_b in the final transformed microstructures of plain carbon steel, and predicted V_p of plain carbon steel C under 5°C/s of ACC was 11% and smaller than the measured value of V_p (16%) after the 8-pass PSC test.

$$V_P = -0.00548 + 1.31[C] + 0.0289[Mn] - 0.01842 \ln C_r \quad (80)$$

$$V_b = -0.18 + 1.2[C] + 0.09[Mn] + 0.0544 \times \ln C_r, \text{ and } V_f = 1 - V_p - V_b \quad (81)$$

Although the predicted CCT diagrams of four different steels A, B, C and D by the JMATPro software had some errors (such as the ferrite formation even still took place at the 100°C/s of ACC), these figures can still provide rough indications of pearlite and/or bainite formations at the specific cooling rates and the effect of steel composition. Due to the steels A, B and C had almost the same compositions except the additional Nb and Ti concentrations, the JMATPro program constructed almost exactly the same CCT diagrams of steel A, B and C (the curves did not move to longer time), which is presumably because according to JMATPro the Nb will already have precipitated in the austenite according to equilibrium, before the cooling simulation is calculated. Therefore, there is no Nb left in the solid solution to affect the CCT diagram and cause precipitation hardening. According to the CCT diagrams in Figures 262 and published optical and the SEM microstructures by Olasolo et al. [266], the predicted and measured transformed microstructures were fully bainitic when the applied cooling rate was at 30°C/s, but in the present investigations even the applied cooling rate was at the 40°C/s,

the optical microstructures of the Nb steel A (similar composition) were mainly the small ferrite grains (< 5μm) with possible some bainite and/or the MA islands (see Figure 178).

Additionally, Tanaka [181] mentioned that the ACC is not an isolated technology and the great benefits of applying ACC could not be fully exploited (achieved the maximum ferrite refinement) without the associated advanced deformed microstructures with high density of nucleation sites or high value of S_v made at the end of finish rolling for later ferrite formation due to the ACC greatly enhanced the nucleation rate of ferrite, and the smaller ferrite grain sizes were produced under the high value S_v as results of large reduction below the $T_{0.05x}$ [49]. Therefore, the complex interactions of D_γ, retained strain stored in the pancaked austenite, solute MAE (such as V) during the transformation, and the applied cooling rate of ACC must be optimised to ensure produced desired transformed microstructures.

5.5.6. 11-Pass PSC Tests with IFC on the HP

At the last stage of this research project, the successful rate of continuous cooling 8-pass PSC tests was improved to about 60-75%, and in order to further explore the controllable testing window of maximum PSC passes (above 8 passes) that can be applied in the standard 10mm PSC sample, the additional small passes (input strain was 0.12 and strain rate was $2.5s^{-1}$ at each added pass) were gradually added at the high temperature roughing stage. That is because initially the 10 industrial rough rolling passes were always simulated by the 3-pass PSC test (0.3+0.3+0.1) and the conditions of subsequent 5-pass industrial finishing rolling were exactly replicated by the 5-pass PSC test. For example, in the following Figures 265 and 266, the comparison results of multipass flow curves and subsequent optical microstructures of two similar 8-pass and 11-pass PSC tests with application of same IFC temperature profiles during the HP and 10°C/s of ACC are presented. As illustrated in Figures 265 and 266 that under the almost same total applied strain (only 0.05 difference) and similar flow stress during high temperature roughing stage, the 8-pass PSC test gave about 45MPa higher equivalent stress at the end of the last pass than that of the last pass in the 11-pass PSC test, and produced smaller (1.8μm further refinement) average d_α compared to the values of 11-pass PSC test. It should be noted that in these two tests the conditions of 5-pass finishing were exactly same, so the differences in the subsequent observed optical microstructures in Figure 266 were possible caused by the variations of 3-pass and 6-pass roughing simulation but as mentioned earlier the exact replication of the commercial roughing process is not expected to be metallurgically important. Therefore, more 11-pass (6R+266s/IFC HP+5F) PSC tests will be carried out to further examine the effect of roughing on the flow curve and the subsequent microstructures.

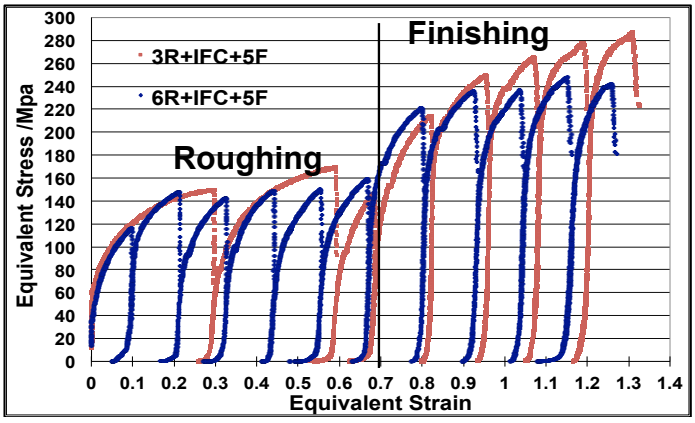

Figure 265: Flow curves comparison of 8-pass (3R+IFC+5F) and 11-pass (6R+IFC+5F) simulations including the IFC and ACC

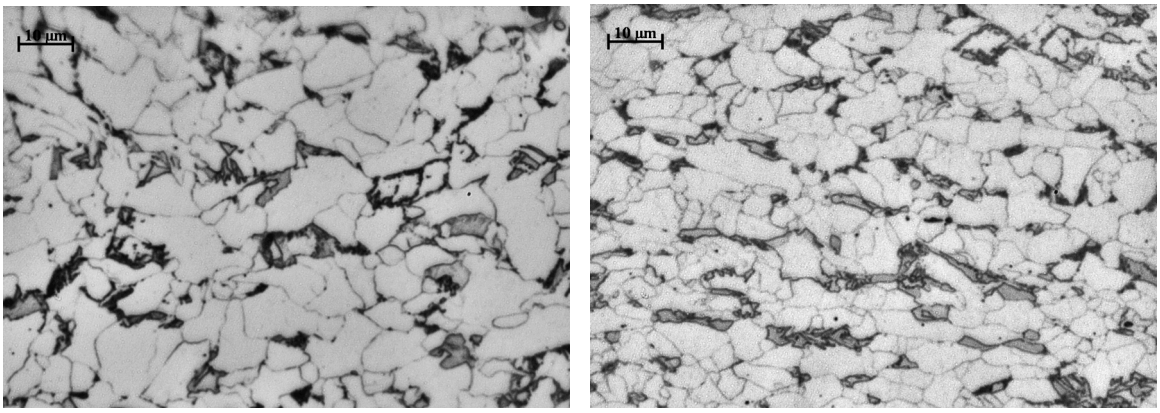

11-Pass (6 roughing passes) **RD – 7.8±0.6µm TD – 6.6±0.3µm Aspect Ratio=1.2**

8-Pass (3 roughing passes) **RD – 6.0±0.2µm TD – 4.5±0.2µm Aspect Ratio=1.3**

Figure 266: Optical microstructures comparisons of 11-pass and 8-pass PSC tests including the IFC and 10°C/s of ACC

5.5.7. Comparisons of the Average Ferrite Grain Sizes from the Multipass PSC Tests, Industrial As-Rolled Heavy Plate and Physical-Based Modelling Results

At the end of this research project, the measured average d_α and volume fractions of ferrite V_f from the 8-pass PSC test of Nb steel A, in which the post-deformation cooling profiles were set at the same values of the natural-air slow cooling of 60mm steel plates, were compared to the as-received observed microstructures of industrial 60mm Nb steel 8AK39 heavy plates. Although the commercial steel 8AK39 had higher carbon concentration (shown in Table 6) that that of the Nb steels A (presented in Table 5), the comparisons still can provide some useful information regarding to the accuracy of laboratory multipass PSC test simulating the industrial hot rolling steel plate production. Furthermore, the measured d_α were also compared with the predicted d_α from the IMPress model developed by the Tata Steel Europe RD&T and the calculated result of a series of chosen empirical equations from

the high temperature roughing to final transformed ferrite grain sizes, which were described clearly in Literature Section 2.3 and in the previous work [104].

As presented in Figure 182 of Results Section 4.6.4.2, the Nb steel A produced average d_α of 12μm in the rolling direction at the 0.3°C/s post-deformation cooling rate after the 8-pass PSC test with total applied strain ε_{Total}=1.65. On the other hand, the measured average d_α at the sub-surface and centre of 60mm Nb steel plate 8AK39 were 18μm and 25μm respectively, presented in Figure 136 (Results Sections 4.6.1). There is a reasonable 6μm difference of d_α between the 8-pass PSC test and the measured d_α at the sub-surface of commercial 60mm steel plate, and to replicate the grain size evolution at the centre of heavy plate in further works, much higher deformation temperatures and higher temperature cooling ranges during the HP (illustrated Figure 258) and post-deformation cooling have to be applied in the further 8-pass PSC tests.

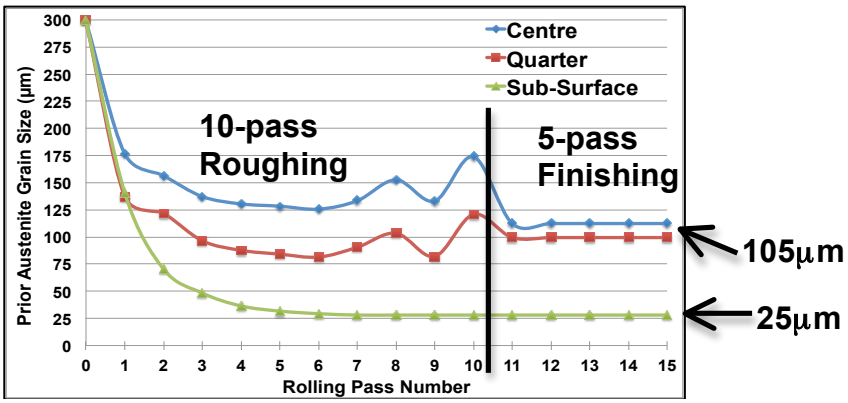

Figure 267: IMPress model predicted austenite grain size evolution at the sub-surface, quarter and centre of heavy plate during 15-pass industrial rolling of Nb steel 8AK39

As demonstrated in Figure 267, at the heavy plate surface, the IMPress model predicted PAGS (D_γ) were expected to be always smaller than the values of at the quarter thickness and centre of heavy plate, and the calculated D_γ were the same through thickness during the 5-pass finish rolling as results of the austenite recrystallisation suppression by the SIP. More importantly, there was a large difference (80μm) in the predicted D_γ at the sub-surface and centre of 60mm steel plate at the end of finishing stage. Furthermore, the final calculated average d_α under the slow air cooling rate 0.12°C/s by the IMPress model were 9.8μm, 12.3μm and 14.4μm respectively at the sub-surface, quarter and centre of heavy plate, which were much smaller than the measured values at the corresponding locations of as-rolled 60mm steel plate, but agreed with the measured value (12μm) of 8-pass PSC test. It should be noticed that the IMPress model has been tuned by many commercial data so the reasons to cause such different in the d_α of this specific 60mm steel plate were unclear. The IMPress model also predicted the average V_f was 78%, which was similar to the measured value (73%) at the centre of 60mm steel heavy plate.

In terms of empirical equations modelling, the completed simulation processes were based on the previous developed relatively simple hot rolling physical-based model [104] with some modifications. For example, the IMPress model predicted temperature, strain and strain rate profiles at the sub-surface, quarter and centre of heavy plate of each rolling pass were applied into the calculations of empirical equations, and applying the principles of the additivity rule [111, 113] to change the isothermal austenite grain growth condition during the intervals and long HP into the realistic continuous cooling conditions (Section 5.5.2.2). It is worthy to be emphasised that there is a considerable difference between the predicted recrystallised austenite grain sizes d_{rex} from the two widely cited Equations developed by Sellars et al. [161] and Lopez et al. [111, 113], and are presented in Figure 268 in which if the effective applied strain below 0.25 much larger predicted d_{rex} and higher minimum applied strain to refine the initial austenite grain sizes (50μm and 300μm) were found in the Lopez' Equation. Because in the commercial heavy plate hot rolling practices, the effective applied strain of each rolling normally is limited to about 0.15, the Sellars' equation was chosen in the simulation, and the corresponding predicted d_{rex} at the sub-surface, quarter and centre of heavy plate during the industrial rolling of Nb steel 8AK39 were shown in Figure 269.

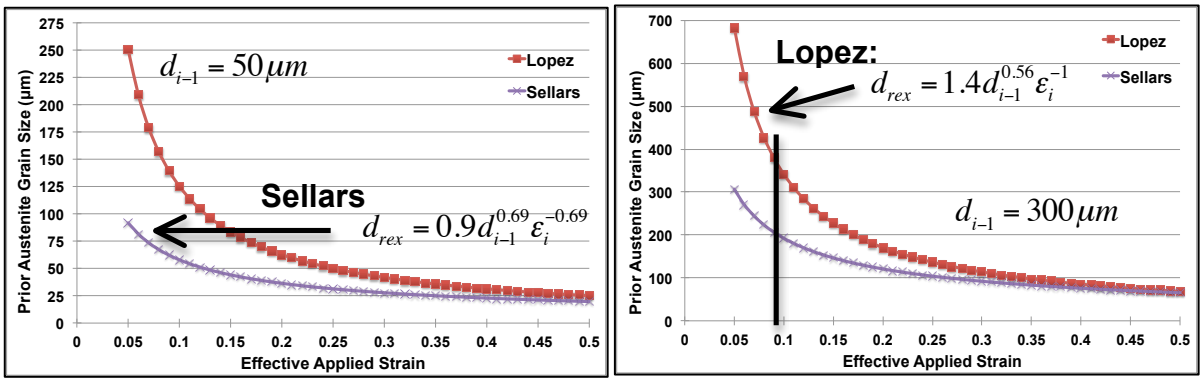

Figure 268: Predicted d_{rex} comparisons of the two well-known empirical equations with different initial austenite grain sizes: 50μm (left hand side) and 300μm (right hand side)

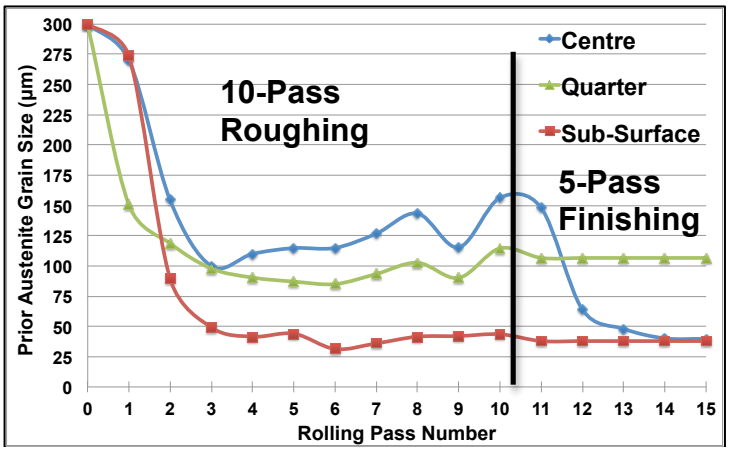

Figure 269: Predicted prior austenite grain size evolution at the sub-surface, quarter and centre of heavy plate during 15-pass industrial rolling of Nb steel 8AK39

By comparing the results in Figure 267 and Figure 269, the empirical equations calculated almost the same the PAGS profile (about 100μm at the end of rolling) as the IMPress model at the quarter thickness of heavy plate. In term of predicted PAGS profile at the sub-surface, the IMPress estimated that the SIP occurred at the 6th pass with PAGS of 25μm while in Figure 269 the SIP happened at the 11th pass with larger PAGS of 43μm. Furthermore, the biggest difference in these two figures was that in the IMPress prediction the pinning caused by the SIP was expected to take place at the plate centre at the 11th pass (Figure 267) and with much larger PAGS after the 15th pass, which were possibly due to different equation for the $t_{0.05P}$ was used in the IMPress model where modified constants based on commercial data were also applied in the equations for predicting the $t_{0.5X}$ and d_{rex}. With the same 0.12°C/s post-rolling cooling rate as IMPress model, the subsequent predicted d_α based on Equation 42 were 19μm, 20μm and 22μm respectively at the sub-surface, quarter and centre of 60mm as rolled plate, which were larger than those of IMPress prediction and closer to the measured values at the sub-surface (18μm) and centre (25μm) of 60mm as-rolled plate.

The continuous cooling 8-pass PSC test (3R+266s HP+5F+0.3ºC/s) of Nb steel A was also simulated by the empirical equations, and the corresponding predicted PAGS profiles with different initial PAGS (300μm and 100μm) are presented in Figure 270, which were similar to the sub-surface profile of 15-pass industrial rolling in Figure 269. Furthermore, it is clearly illustrated in Figure 270 that regardless of the initial PAGS, the predicted PAGS after the 2nd pass were almost the same due to repeated fast SRX took place following the first and second reductions, and the SRX were inhibited by the SIP after the first finishing pass (the 4th pass) in both simulations. With the 0.3°C/s post-rolling cooling rate, the subsequent predicted d_α was 15.2μm, which was 3.2μm larger than the measured value of the same 8-pass PSC test and 2.8μm smaller than the measured average d_α at the sub-surface of 60mm as-rolled plate. Therefore, the predicted results from the empirical equations were acceptable.

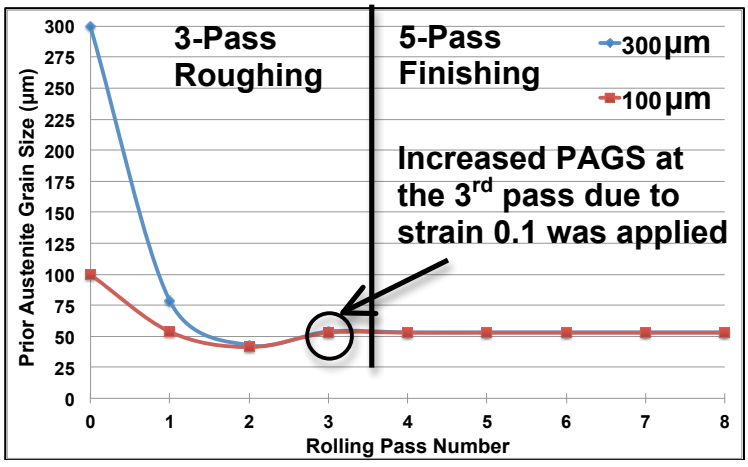

Figure 270: Predicted PAGS development profiles of the continuous cooling 8-pass PSC test with different initial PAGS (300μm and 100μm)

5.5.8. Application of Intense Water Cooling into the Commercial Hot Rolling Steel Plate Production

There is no doubt that the implementation of intense water cooling during the HP and after the finish rolling, or even prior to the first roughing pass and at the relatively long inter-pass time can considerably increase the productivity of heavy plate. This benefit was particularly significant in the single stand reversing heavy plate mill where the operations of high temperature roughing and low temperature finishing have to be executed in the same rolling stand [24]. More importantly, applying the forced cooling during and after hot rolling can also significantly refine the average ferrite grain size, which is the only strengthening mechanism that increases both strength and toughness of the steel simultaneously. Furthermore, without the expensive post-rolling heat treatment process, the desired high strength and toughness of as-rolled heavy plate can be also achieved if the intense or forced cooling was correctly integrated into the different stages of TMCP.

Due to applying the higher severity (larger values of heat transfer coefficients) of water cooling during the HP and ACC stages, larger temperature gradients over the plate thickness were produced and exacerbated the undesired inhomogeneity of microstructures, thus immediately after the short intense water spraying stage, the excess water left on the plate surface must be removed through air nozzles and then sufficient delay time was required to allow the plate temperature to equilibrate under natural-air cooling condition. Although the sufficient recalescence or delay time affect the productivity, the large temperature gradient reduced considerably and improved homogeneity of ferrite grain size distribution through thickness. In order to design and implement the novel forced cooling technique into practice on an industrial heavy plate mill and to minimise the undesired inhomogeneous d_{α} distribution and mechanical properties through final as-rolled plate thickness, the temperature distributions of the partially rolled heavy plate at the end of the HP and the 40-60mm as-rolled plate during the ACC stage must be carefully controlled. For example, Abel [25] mentioned that the surface temperature during model simulations was not allowed to fall below 649°C to avoid cooling the plate by two large different heat transfer mechanisms (film and nucleate boiling).

Therefore, significant high level computer modelling efforts were required to determine the most efficient and uniform water cooling strategy, such as water cooling time, air cooling time, number of water cooling cycles (on and off), transfer plate thickness during the HP [23]. Finally, larger scale multipass hot rolling tests (possible on the Tata Steel Europe RD&T pilot mill) with IFC cooling during HP are required to carry out to obtain correct values for temperature distributions in much larger holding period plate thickness.

5.6. Summary of Discussion

In general, the results from this research are consistent with the previous work on the commercial and pilot rolling mills [23-30], demonstrating that the IFC technique is a really powerful tool to improve steel plate production (increased the productivity and refined the average ferrite grain sizes) without the large modifications of exist reheating, roughing and finishing stages. The summary of four specific discussion areas is presented in the following.

- The process window (upper and/or lower limits of controllable cooling rates) of three different cooling media during the HP (cooling from 1000°C to 800°C) inside the FTTU and the corresponding temperature differences between the sub-surface and centre of the 10mm PSC sample (Section 5.2) were investigated at the first time, which can provide some useful information for the interval cooling (such as the HP) at the multipass PSC tests and future complex heat treatment simulation.

- In order to develop the successful, repeatable and reliable continuous cooling multipass PSC tests for simulating the industrial hot rolling steel production on the cutting-edge TMC machine, some critical factors (such as deformation temperatures, applied strain of each pass, temperature cooling of deformed PSC sample during the intervals, and the length of gap time) have to be correctly adjusted through many trials (Section 5.3.1 and 5.3.2), and more importantly, it is essential to minimise the undesired problems (Section 5.3.3) that were raised in conducting the multipass PSC tests.

- The deformation temperature and chemical composition were the two most influential factors to determine the shape and value of multipass flow curve compared to the effects of reducing interpass time and increasing applied strain per pass (Section 5.4).

- The application of the IFC during the long HP indeed can indeed reduce the corresponding PAGS coarsening profiles towards plate centre, which mainly determined by the continuous cooling temperature range (reduced by the surface chilling effect) rather than the length of continuous cooling HP period (Figure 258 in Section 5.5.2.2). It is important to emphasis that applying the intense forced cooling (presented in Figure 260) rather than the normal IFC cooling profile, the resultant average d_α did not refine but increased, thus the severity and cooling time of the IFC should be carefully controlled.

- Although with addition of MAE (Nb and Ti in this project), reducing the average deformation temperature of 5-pass finishing, increasing applied strain per pass and applying the IFC into the HP can refine the d_α, the most dominant factor to achieve small d_α is still the applied cooling rate of ACC (Section 5.5.5.2).

Chapter 6 – Conclusions

It is useful to emphasise that at the end of this research program, the 7 main objectives or aims (presented at Section 2.8) were all more or less achieved based on the results from experiments, and the following conclusions can be made regarding this PhD research project concerning intense water cooling during and after hot rolling to improve steel production:

- A critical and detailed literature survey including some important metallurgical phenomena and modelling microstructural evolution during the hot rolling steel plate production, and the application of intense water or forced cooling during and after the hot rolling and the fundamental heat transfer mechanisms, has been carried out. The knowledge gaps and challenges of present work were also mentioned at the summary, end of the Literature review chapter. The two most critical gaps identified for this work were: the IFC technique only has been studied in the commercial scale with limited information available and effects of applying the IFC during the HP on austenite and subsequent ferrite grain size have not been investigated; the cooling rates capability of different cooling media inside the FTTU of TMC machine were never been investigated, and before this project the maximum deformation number of PSC testing on the TMC machine was only up to four passes.

- The minimum and/or maximum controllable applied cooling rates of three different cooling media (forced air, mist and water quenching) from 1000°C to 800°C, which is similar to the normal temperature range of HP in the commercial microalloyed steel hot rolling schedule, were fully explored inside the FTTU of TMC machine. The corresponding temperature differences between the sub-surface and centre of the 10mm PSC sample at the different cooling rate simulations were determined. In terms of the forced-air cooling media, the maximum controllable linear cooling rate was about 25°C/s, and as the applied cooling rates increased from 0.5°C/s and 25°C/s, the corresponding average temperature gradient through thickness increased from 4°C to 20°C. Therefore, employing the intense forced cooling into the HP of commercial hot rolling heavy steel plate production can cause significant temperature differences through thickness (above 100mm) at the end of water cooling, thus the sufficient recalescence or equalising time after cooling must given prior to the finish rolling.

- More importantly the TMC machine is capable of precisely simulating the predicted complex IFC (rapid forced cooling immediately followed by the fast recalescence) temperature profile during the HP, and achieving the desired applied cooling rate of ACC by using the well controlled cooling media - compressed air blowing.

- It has been found possible to simulate an industrial hot rolling steel plate processes to produce 50mm plain carbon steel plate 8AK43 with total applied strain 2.07 as closely as possible: started with 2-pass roughing with applied strain 0.8 on the laboratory Hille mill, and then used the 2-pass roughed and as-quenched PSC sample to carry out the subsequent 9-pass PSC finish rolling with the exactly same industrial finishing parameters and finally performed the post-deformation cooling simulation of 50mm steel plate on the TMC machine.

- It has also been found possible to replicate the required conditions (such as deformation temperatures, effective strains, strain rates and post-deformation cooling rate) of another commercial hot rolling schedule for producing the 60mm Nb steel plate 8AK39 closely through many multipass PSC tests with great reliability. That is because through many trials and adjustments in the test settings (presented in Discussion Section 5.3), the capabilities or simulation window of the sophisticated TMC machine for conducting the multipass PSC tests have been successfully extended from usually less than 4-pass to above 8-pass (up to 13-pass in present study) continuous cooling deformations with great repeatability.

- The great consistency and reliability of recorded temperatures and flow curves in many similar continuous cooling multi-pass PSC tests were found to be satisfactory, which is essential to analyse the effects of various hot rolling parameters (such as steel composition, deformation temperature and HP cooling), on the PAGS and ferrite grain size thus any differences in the multipass flow curves and/or observed optical microstructures were attributed to the investigated rolling factor only rather than incompatibility (many variables) between the similar multipass PSC tests.

- The microstructure evolution, mainly the PAGS development of Nb steel A, Nb+Ti steel B and plain carbon steel C following the continuous cooling 8-pass PSC test (3R+HP cooling+5F) were determined and analysed, such as the equiaxed PAGS at the end of the 3-pass roughing, austenite grain coarsening during the HP with different applied cooling profiles, and the pancaked or elongated austenite (steels A and B) and equiaxed austenite (steel C) after the final 8^{th} pass. These results confirmed that the last few finishing passes from 860°C down to 840°C were performed below the important $T_{0.05X}$ of steels A and B, but the deformations were still above the $T_{0.05X}$ (808°C) of plain carbon steel C as expected.

- Applying the complex IFC rather than the natural-air slow cooling during the long HP, not just increased the productivity of commercial hot rolling heavy steel plate significantly by shortening the critical delay period (up to 40% reduction depending on the rolling schedule) but also reduced the austenite grain growth at the end of the HP and

the subsequent ferrite grain size. All the results of austenite grain coarsening at the different cooling conditions during the HP have confirmed by decreasing the continuous linear cooling time from 975°C to 880°C, or reducing the isothermal holding temperature from 980°C to 880°C, the corresponding PAGS reduced. It is important to emphasise that the continuous cooling temperature range rather than the length of the continuous cooling HP period mainly determines the PAGS coarsening profile.

- The austenite grain coarsening still occurred on the Nb+Ti steel B (addition of 0.015wt% Ti element) during the continuous linear cooling from 975°C to 880°C, thus the undissolved and stable TiN particles did not inhibit the coarsening of fine recrystallised austenite produced from the roughing stage during the HP, which did not agreed with the results of some researchers [21, 86]. This might be due to differences in the size and distribution density of the TiN particles, but would need to be investigated by electron metallography.

- Significant modelling efforts from different simulation models (such as Abaqus FE model and IMPress model) were carried out to evaluate the temperature, strain and strain rate gradients present in heavy plates during the hot rolling process of 60mm Nb steel 8AK39, especially in estimating the temperature profiles through thickness of the partially as-rolled plate during the HP under conditions of different applied cooling rates (from slow natural-air cooling to fast water cooling). These predicted results (much higher deformation temperature, lower effective strain and strain rate towards plate centre) were extremely useful to analyse inhomogeneity microstructures across the heavy plate thickness, and can be used as the input values (such as the predicted IFC temperature profile was applied during the HP) for the continuous cooling multipass PSC tests. Perhaps more importantly, the different multipass flow curves and the corresponding PAGS microstructures at the sub-surface and centre of heavy plate during roughing and the HP were successfully simulated through the multipass continuous cooling PSC tests, which were conducted using the calculated deformation temperatures, strains and strain rate at the heavy plate sub-surface and centre.

- Increased accelerated cooling (up to 40°C/s in present study) after the 8-pass PSC test was still the most dominant factor on reducing the average ferrite grain sizes (from 12μm refined to 4.5μm) compared to the results of the others rolling parameters, such as different steel chemical composition, application of the IFC during the HP, increasing applied strain per pass and reducing the average deformation temperature of 5-pass finishing. However, employing the intense forced cooling into a commercial hot rolling heavy steel plate production can cause significant temperature differences at the sub-surface and centre of heavy steel plate at the end of cooling, thus the severity and cooling time of water cooling should be carefully controlled, and sufficient recalescence or

equalising time after the intense forced cooling must given to reduce the temperature gradient through thickness.

- Without the large modifications of existing reheating, roughing and finishing schedule, the average d_α of 6μm was produced in the Nb steel A, Nb+Ti steel B, and plain carbon steels C and D under the 8-pass PSC tests with the IFC during the HP and 10°C/s of ACC. Therefore, with correct settings of multipass PSC test and ACC, the fine average d_α, which are similar to those of microalloyed steels, can be also achieved in the plain carbon steel without the costly MAE additions (such as Nb and Ti). Similarly, the same should be possible on suitably equipped production plant.

- The continuous cooling 8-pass PSC test (3R+266s HP+5F+0.3°C/s) of Nb steel A was simulated by the empirical equations, with application of the principles of the additivity rule that can change the isothermal austenite grain growth condition during the intervals into the realistic continuous cooling conditions, and the predicted of d_α was 15.2μm, which was 3.2μm larger than the measured value of the same 8-pass PSC test, and 2.8μm smaller than the measured average d_α at the sub-surface (2mm below surface) of the commercial 60mm as-rolled Nb steel plate. Therefore, the predicted results from the empirical equations were acceptable.

- It is important to recognise that the consistent and reliable continuous cooling 8-pass PSC testing is the state-of-the art on the laboratory simulation of industrial hot rolling steel plate process as most similar simulations are only carried out on the multipass hot torsion tests.

Chapter 7 – Further Works

A number of issues were raised during the course of this thesis warranting further investigations into the important hot rolling parameters of industrial hot rolling steel plate production through the well-developed continuous cooling multipass PSC tests. More specifically, the corresponding multipass flow curves and the resultant microstructures can be studied in more detail during (such as the HP) and after the 8-pass PSC tests regarding the following.

- More 8-pass PSC tests with lower 5-pass finishing temperatures (possibly from 800°C to 740°C) should be carried out to analyse the microstructure evolution in the two phases region, particularly focussing on the as-quenched microstructures (whether the small ferrite grain sizes decorated along the prior austenite grain boundaries) at the end of finishing, and the subsequent average ferrite grain size.

- Further work should be performed to determine the critical strain ε_c for initiating the dynamic recrystallisation (DRX) in the conditions of multipass continuous cooling PSC testing, and to derive more accurate empirical equation for estimating the ε_c under the PSC rather than the hot torsion situation. As mentioned in Figure 268 in the Discussion chapter Section 5.5.7, a considerable difference exists between the predicted recrystallised austenite grain sizes d_{rex} at the small applied strain (below 0.2) from the two widely cited empirical equations developed by Sellars et al. [161] and Lopez et al. [111, 113], thus an updated empirical equation to copy with small applied strain should be developed in further work.

- In order to explain not only the smaller average ferrite grain size but also the increment of ferrite volume fraction in the steels A, B and C when the IFC profile was applied in the HP of 8-pass PSC tests, further investigations are required.

- More 11-pass (6R+266s/IFC HP+5F) PSC tests should be carried out to further examine the effect of different roughing conditions (such as different pass number and deformation temperatures) but with the same total applied strain on the corresponding multipass flow curve and the subsequent average ferrite grain size.

- As presented in Figures 233 and 234 in the Results Section 4.8, the continuous cooling 12-pass and 13-pass PSC tests were successfully carried out on the 10mm standard PSC sample, which provided some useful information to perform more than 13-passes in PSC tests in further work. If the input effective strain for each pass is set at 0.1 (similar to commercial heavy plate condition) and the final deformed thickness of PSC sample is

about 2.5mm for the microstructure characterisation, in theory the total number of applied deformations on the 12mm PSC sample could be up to 18 passes.

- Based on present study, it is most likely the well-developed 8-pass test can be successfully extended to continuous cooling 13 to 18-pass PSC tests for simulating the industrial hot rolling steel plate production in further work, and then the corresponding flow curves and subsequent transformed microstructures between the PSC and hot torsion tests under the exactly same testing conditions can be compared for the first time. Furthermore, due to the multipass flow curve being essential for the prediction of rolling power and deformation resistance in a plate mill, the predictions of multipass flow curves under the PSC condition should be performed, and the estimated flow curves would be extremely useful for better predicting the resistance, strain and strain rate distributions through thickness and degrees of work hardening and softening at the various stages of hot rolling steel plate production.

- The PAGS development during the 8-pass PSC tests including IFC or ACC and the subsequent average ferrite grain sizes in the final transformed microstructures were the two main objectives in this research project. However, the present microstructure analysis and characterisation did not include the more detailed investigations from the SEM and transmission electron microscopy (TEM). Therefore, further analysis of microstructure evolution during and after the multipass PSC tests should take place. For example, the investigations should be particularly focused on the size and volume fraction of NbC and/or Nb (C, N) precipitates in the Nb steel A and Nb+Ti steel B on the prior austenite grain boundaries caused by the SIP at the finishing rolling stage.

- Measuring and modelling the effective strain penetration and temperature distribution through thickness at the large scale possibly will be taking place by the project's sponsors, on the pilot mill of Tata Steel Europe with different severity and cooling time of water cooling on the plate surfaces.

References

[1] F. Heisterkamp and T. Carnerio, *Niobium: Future Possibilities – Technology and the Market Place,* Proceeding of International Symposium "*Niobium Science & Technology*" held in Orlando, USA, December 2-5, 2001, Niobium 2001 Limited, p1109-1118.

[2] C. Quchi, *Development of Steel Plates by Intensive Use of TMCP and Direct Quenching Process,* ISIJ, 2001,Vol. 41, No. 6, p542-553.

[3] G. Tither, *Progress in Niobium Markets and Technology 1981-2001,* the same as the reference [1], 2001, p7-11.

[4] F. B. Pickering, *The Spectrum of Microalloyed High Strength Low Alloy Steels,* Proceedings of International Conference on "*HSLA Steels: Technology and Applications*", 1983, Philadelphia, American society for metals, p1-31.

[5] H. G. Hillenbrand, M. Gras and C. Kalwa, *Development and Production of High Strength Pipeline Steels,* the same as the reference [1], 2001, p543-556.

[6] F. B. Pickering, *High-Strength, Low-Alloy Steels-A Decade of Progress,* Proceedings of an International Symposium on "Microalloying 75 - High-Strength, Low-Alloy Steels", edited by M. Korchynsky, 1975, Union Carbide Corporation, p9-31.

[7] H. J. Kim and W. Y. Choo, *Application of TMCP Steels for Shipbuilding and Offshore Structures,* proceeding of "*Microalloyed HSLA Steels - Microalloy '88*" held in conjunction with the 1988 World Materials Congress, Chicago, USA, 1988, ASM International, p205-208.

[8] A.J. DeArdo, C. I. Garcia and E.J. Palmiere, *Thermomechanical Processing of Steels,* "Heat Treating", Volume 4, ASM Handbook, 1991, ASM International, p237-255.

[9] H. K. D. H. Bhadeshia and R. W. K. Honeycombe, *Steel Microstructure and Properties*, Third edition, 2006, Elsevier Ltd., p209-220.

[10] A. J. DeArdo, *Modern Thermomechanical Processing of Microalloyed Steel: A Physical Metallurgy Perspective*, proceeding of an international conference on "*Microalloying'95"*, 1995, Pittsburgh, USA,The Iron and Steel Society, p15-33.

[11] M. Cohen and S. S. Hansen, *On the Fundamentals of HSLA Steels*, in proceeding of International conference on "*HSLA steels: Metallurgy and Applications"*, 1985, Beijing, ASM International, p61-71.

[12] P. E. Repas, *Metallurgical Fundaments for HSLA Steels,* the same as the reference [7], 1988, p3-14.

[13] W. Roberts, *Recent Innovations in Alloy Design and Processing of Microalloyed Steels,* the same as the [4], 1983, p52-62.

[14] P. J. Heedman and A. Sjostrom, *Controlled Rolling Schedules for Increased Plate Production,* Scandinavian Journal of Metallurgy, 1980, No. 9, p21-24.

[15] W. Y. Choo and J. H. Eom, *Effect of Interrupted Cooling and Rolling on the Mechanical Properties of Accelerated Cooled Plates*, in international conference on "*THERMEC-88"*, editor: I. Tamura, Tokyo, Japan, 1988, p495-502.

[16] A. L. Sjong, et al., *Fracture behavior of Nb-V-Ti Microalloyed Plates Processed with and without Intermediate Cooling*, in Materials solutions conference, International symposium of "microalloyed steels 2002", Columbus, ASM International, p92-100.

[17] R. Doell, J. Lee, A Harvey and M. Steeper, *Microstructural Modelling Applied to the Design and Control of the Steel Plate Rolling Process*, Materials Science Forum, 2012, Vol. 715-716, p529-541.

[18] I. W. Martin, *High Penetration Rolling and Cooling Strategy During Plate Rolling,* Corus RD&T Report, 2005, reference source number-114220

[19] A. Streisselberger, V. Schwinn, and R. Hubo, *Microalloyed Structural Plate Rolling Heat Treatment and Applications,* same as the ref. [1], p625-635.

[20] R. I. Asfahani and J. R. Kahrs, *Effect of Surface Cooling and Heavy Reduction on High Penetration Rolling in Thick Plates*, 35th Mechanical Working and Steel Processing (MWSP) Conference Proceeding, ISS-AIME, 1994, p371-378.

[21] J. G. Williams, et al., *Controlled Rolling of Heavy Plates for Offshore Plateform Application*, in Processing, Microstructure and Properties of HSLA Steels, edited by A. J. DeArdo, 1987, Pittsburgh: TMS, p133-152.

[22] D. G. Stalheim, *Slab and Level 2 Automation Design Guidelines for Optimum Metallurgy and properties for Plate and Steckel Mill*, proceeding of the 6th international conference on "*HSLA Steels: Metallurgy and Applications" (HSLA'2011)*, Beijing, China

[23] B. Xiao, E. J. Palmiere, A. A. Howe and H. C. Carey, *Multi-Pass Simulation of Heavy Plate Rolling Including Intermediate Forced Cooling*, Advanced Materials Research, 2012, Vol. 409, p443-448.

[24] A. A. Gorni, et al., *Application of Forced Cooling during the Holding Phase in Controlled Rolling of Plates,* on address: http://www.gorni.eng.br/e/rif.html, latest access website on 03/10/2012

[25] C. A. Abel, and G. A. Brown, et al., *Instand Cooling during the Processing of Controlled Rolled Plates to Improve Mill Productivity*, in 39th MWSP conference proceeding, 1998, ISS-AIME, p545-554.

[26] C. Dilg, et al., *TMCP Process Including Two Accelerated Cooling Stages*. Revue de Metallurgie, 1995, July, p883-892.

[27] H. Abrams, *Accelerated Spray Cooling to a Reduced Intermediate Temperature for Controlled Rolling*, in Mechanical Working and Steel Processing Coference XXI, 1984, ISS-AIME, p423-445.

[28] D. M. Fegredo, J. D. Boyd, and M. J. Stewart, *The Effects of Accelerated Processing on the Microstructure and Mechanical Properties of V- and V+Nb HSLA Steels*, the same as the reference [4], 1983, p95-105.

[29] D. M. Fegredo, *Hold-Period Accelerated Cooling Experiments on Nb- and Ti-HSLA Steels*, Metals Technology, 1977, p417-424.

[30] P. J. Heedman, S. P. Rutqvist, and J. A. Sjostrom, *Controlled Rolling of Plate with Forced-Water Cooling during Rolling*, Metals Technology, 1981, p352-360.

[31] F. B. Pickering, *Physical Metallurgy and the Design of Steels,* Applied science publishers LTD, 1978, London, p10-25, p62-80.

[32] T. Gladman, *The Physical Metallurgy of Microalloyed Steels*. 1997, London, Maney, p230-261.

[33] I. Tamura, C. Ouchi, et al., *Thermomechanical Processing of High Strength Low Alloy Steels*, 1988, Butterworth, p22-55.

[34] J. M. Rodriguez-Ibabe, *Thin Slab Direct Rolling of Microalloyed Steels*, 2007, Switzerland: Trans Tech Publications LTD, p10-77.

[35] V. B. Ginzburg and R. Ballas, *Flat Rolling Fundamentals*, Marcel Dekker, Inc., 2000, p283-325.

[36] S. Yue, *Thermomechanical Processing of Ferrous Alloys*, in *ASM Handbook, Volume 14A: Metalworking: Bulk Forming*, 1991, p286-296.

[37] C. M. Sellars, *The Physical Metallurgy of Hot Working,* in conference proceeding of "*Hot Working and Forming Processes",* edited by C. M. Sellars and G. J. Davies, The Metals Society, London, 1980, p3-15.

[38] C. M. Sellars, *Static Recrystallisation and Precipitation during Hot Rolling of Microalloyed Steels,* in the "Deformation, Processing, and Structure" presented at the ASM materials science seminar in St. Louis, Missouri, 1982, American Society for Metals, p245-275.

[39] M. Cohen and S. S. Hansen, *Microstructural Control in Microalloyed Steels*, in conference proceeding of "*MiCon 78: Optimization of Processing, Properties, and Service Performance through Microstructural Control"*, 1978, Houston, ASTM, p34-52.

[40] M. Korchynsky, *Microstructure and Thermomechanical Treatment*, from the same reference as [21], 1987, p169-180.

[41] R. K. Amin and F. B. Pickering, *Austenite Grain Coarsening and the Effect of Thermomechanical Processing on Austenite Recrystallisation,* Proceeding of the International Conference on "Thermomechanical Processing of Microalloyed Austenite" in Pittsburgh, 1981, edited by A. J. DeArdo, G. A. Ratz and P. J. Wray, The Metallurgy society of AIME, p1-31.

[42] A. M. Sage, *The Role of Micro Alloys in Thermomechanically Processed Steels*, from the same reference as the [15], 1988, p11-19.

[43] A. J. DeArdo, *Fundamental Aspects of the Physical Metallurgy of Thermomechanical Processing of Steel*, the same as the [15], 1988, p20-29.

[44] C. M. Sellar, *Options and Constraints for Thermomechanical Processing of Microalloyed Steel,* from the same reference as the [11], 1985, p73-81.

[45] A. J. DeArdo, et al., *Thermomechanical Processing of Microalloyed Steels: Grain Refinement Revisited*, in International Conference Proceeding of "Thermomechanical Processing: Mechanics, Microstructure & Control", 2002, The University of Sheffield, p9-16.

[46] T. Tanaka, *Controlled Rolling of Steel Plate and Strip*, International Metal Reviews, 1981, No.4, p185-209.

[47] I. Tamura, *Some Fundamental Steps in Thermomechanical Processing of Steels,* Transactions ISIJ, 1987, Vol. 27, p763-779.

[48] W. B. Morrison, *Microalloy Steels the Beginning,* Materials Science and Technology, 2009, Vol. 25, p1066-1073.

[49] A. J. DeArdo, *Metallurgical Basis for Thermomechanical Processing of Microalloyed Steels,* Journal of Ironmaking and Steelmaking, 2001, Vol. 28, p138-144.

[50] A. J. DeArdo, *Niobium in Modern Steels,* International Materials Reviews, 2003, Vol. 48, p371-402.

[51] B. K. Panigrahi, *Processing of Low Carbon Steel Plate and Hot Strip – an Overview,* Journal of Bull. Mater. Sci., Vol. 24, No. 4, August 2001, p361-371.

[52] A. J. DeArdo, et al., *On Strength of Microalloyed Steels: an Interpretive Review,* Materials Science and Technology, 2009, vol. 25, p1074-1082.

[53] W. Roberts, *The Evolution of Microstructure During Controlled Rolling of Microalloyed Steels.* Scandinavian Journal of Metallurgy, 1980, No. 9, p13-20

[54] E. J. Palmiere, *PhD Thesis: Suppression of Recrystallisation during the Hot Deformation of Microalloyed Austenite*, 1991, University of Pittsburgh, Chapter 2.

[55] H. Beladi, *PhD Thesis: Ultrafine Ferrite Formation in Steels Through Thermomechanical Processing*, Deakin Univeristy, 2004, Chapter 1.

[56] D. T. Llewellyn and R. C. Hudd, *Steels: Metallurgy and Applications,* 3rd edition, Butterworth – Heinemann, 1998, Oxford, Chapter 2, p137-151, p182.

[57] K. F. Al-Hajeri, *PhD Thesis: The Grain Coarsening and Subsequent Transformation of Austenite in the HSLA Steel during High Temperature Thermomechanical Processing*, 2005, University of Pittsburgh, chapter 2.

[58] M. Ashby, H. Shercliff and D. Cebon, *Materials Engineering, Science, Processing and Design*, 2007, Elsevier Ltd., p120

[59] P. B. Martin, *PhD Thesis: Microstructural Evolution of Austenite in a Microalloyed Fe-30%Ni Alloy*, 2002, University of Sheffield, Chapter 2.

[60] R. E. Reed-Hill and R. Abbaschian, *Physical Metallurgy Principles*, 3rd edition, 1994, PWS Publishing Company, p588-597.

[61] W. B. Morrison, *Relationship between Thermomechanical Treatment and Properties of HSLA Steels,* Scandinavian Journal of Metallurgy, 1980. No. 9, p83-90.

[62] M. A. Almojil, *PhD thesis: Deformation and Recrystallisation in Low Carbon Steels*, 2010, The University of Manchester, Chapter 2.

[63] G. Krauss, *Steels: Processing, Structure, and Performance*, ASM International, 2005, chapter 8, p15- 21, p139-148.

[64] W. D. Callister, Jr., *Fundamentals of Materials Science and Engineering*, 5th Edition, John Wiley & Son, New York, p302-309.

[65] W. D. Callister, Jr. and D. G. Rethwisch, *Materials Science and Engineering An Introduction*, 8th Edition, John Wiley & Son, New York, p211-227, p319-326.

[66] W. F. Smith, *Foundations of Materials Science and Engineering*, 2nd Edtion, McGraw-Hill, Inc., 1993, Chapter 9: p423-431, Chapter 6: p238-243.

[67] A. K. Sinha, *Ferrous Physical Metallurgy*, Butterworth, 1989, Chapter 1: p1-11, Chapter 3: 87-112, Chapter 13: 609-631.

[68] R. Kaspar and A. Peters, *Efficient Steel Processing by Disciplined Hot Forming and Microalloying,* Steel Research, 1998, Vol. 69, No. 4+5, p128-135.

[69] C. Debalay, *PhD Thesis: Development of Bimodal Grain Structures and Their Effect on Toughness in HSLA Steel*, 2007, The University of Birmingham, chapter 2.

[70] T. Siwecki, B. Hutchinson, et al., *Recrystallisation Controlled Rolling of HSLA Steels,* the same as the reference [10], 1995, p197-211.

[71] J. Patel, *Microalloyed Hot Strip Mill Products – Processing and Properties*, internet address http://www.doc88.com/p-01599407401.html, last access on 15/10/2012.

[72] A. J. DeArdo, *Accelerated Cooling: Physical Metallurgy Perspective,* Canadian Metallurgical Quarterly, 1988, vol. **27, No.** 2, p141-154.

[73] E. J. Palmiere, C. I. Garcia and A. J. DeArdo, *Compositional and Microstructural Changes which Attend Reheating and Grain Coarsening in Steels Containing Niobium,* Metallurgical and Materials Transactions A, 1994, Vol. 25A, p277- 286.

[74] L. J. Cuddy and J. C. Raley, *Austenite Grain Coarsening in Microalloyed Steels,* Metallurgical and transaction A, 1983, Vol. 14A, p1989-1995.

[75] K. J. Irvine, F.B. Pickering, and T. Gladman, *Grain-Refined C-Mn Steels,* Journal of The Iron and Steel Institute, 1967, Vol., 205, No. February, p161-182.

[76] J. Strid and K. E. Easterling, *On the Chemistry and Stability of Complex Carbides and Nitrides in Microalloyed Steels*, Acta Metall., 1985, Vol. 33, No. 11, p2057-2074.

[77] D. C. Houghton, *Equilibrium Solubility and Composition of Mixed Carbonitrides in Microalloyed Austenite*, Acta Metall. Mater., 1993, Vol. 41, No. 10, p2993-3006.

[78] T. Gladman, *Grain Size Control,* 2004, IoM3, Maney Publishing, UK, chapter 5, p114-124.

[79] P. D. Hodgson and R. K. Gibbs, *A Mathematical Model to Predict the Mechanical Properties of Hot Rolled C-Mn and Microalloyed Steels.* ISIJ International, 1992, Vol. 32, No. 12, p1329-1338.

[80] T. Gladman and D. Dulieu, *Grain-Size Control in Steels,* Metal Science, 1974, Vol. 8, No. 1, p167-176.

[81] E. J. Palmiere, *Precipitation Phenomena in Microalloyed Steels*, the same as the reference [10], 1995, p307-320.

[82] J. M. Gray and A. J. DeArdo, *Austenite Conditioning Alternatives for Microalloyed Steel Products,* the same reference as [11], 1986, p83-96.

[83] J. E. G. Gonzalez, *Master Thesis: Study of the Effect of Hot Rolling Processing Parameters on the Variability of HSLA Steels*, 2002, University of Pittsburgh, Chapter 2.

[84] T. Gladman and F. B. Pickering, *Grain-Coarsening of Austenite,* Journal of The Iron and Steel Institute, 1967, Vol. 205, No. June, p653-664.

[85] P. J. Heedman, *Shorter Process Times in the Controlled Rolling of Plate,* Journal of Mechanical Woking Technology, 1978, Vol. 2, p117-128.

[86] L. J. Cuddy, *Hot Rolling: A Thermomechanical Process*, in Encyclopaedia of Materials Science and Engineering, Pergamon Press, Oxford, 1986, p2213-2217.

[87] J. Adamczyk, *Development of the Microalloyed Constructional Steels*, Journal of Achievements in Materials and Manufacturing Engineering, 2006, Vol. 14, No. 1-2, p9-20.

[88] W. Ozgowicz et al., *Metallurgical Products of Microalloy Constructional Steels*, Journal of Achievements in Materials and Manufacturing Engineering, 2011, Vol. 44, Issue 1, p7-34.

[89] G. E. Dieter, H. A. Kuhn and S. L. Semiatin, *Thermomechanical Processing by Controlled Rolling*, in Handbook of workability and process design, 2003, ASM International, Chapter 17, p248-256.

[90] J. J. Jonas, *Dynamic Recrystallization--Scientific Curiosity or Industrial Tool?,* Materials Science and Engineering: A, 1994, Vol. 184, No. 2, p155-165.

[91] J. J. Jonas, *Dynamic Recrystallisation: Laboratory Curiosity to Industrial Tool*, the same reference as the [45], 2002, p2-8.

[92] F. J. Humphreys and M. Hatherly, *Recrystallisation and Related Annealing Phenomena*, 2nd Edition, Elsevier Science Ltd, Oxford Pergamon, 2004, p215-230.

[93] E. J. Palmiere, C. I. Garcia, and A. J. DeArdo, *Suppression of Static Recrystallisation in Microalloyed Steels by Strain Induced Precipitates*, in Proceedings of International Symposium on "*Low-Carbon Steels for the 90's"*, 1993, edited by R. Asfahani and G. Tither, Pittsburgh, TMS, p121-130.

[94] E. J. Palmiere, C. I. Garcia, and A. J. DeArdo, *The Influence of Niobium Supersaturation in Austenite on the Static Recrystallization Behavior of Low Carbon Microalloyed Steels,* Metallurgical and Materials Transactions A, 1996, Vol. 27, No. 4, p951-960.

[95] Dutta, B. and E. Palmiere, *Effect of Prestrain and Deformation Temperature on the Recrystallization Behavior of Steels Microalloyed with Niobium,* Metallurgical and Materials Transactions A, 2003, Vol. 34, No. 6, p1237-1247.

[96] F. Siciliano, *PhD Thesis: Mathematical Modelling of the Hot Strip Rolling of Nb Microalloyed Steels*, 1999, McGill University, Chapter 2.

[97] C. M. Sellars, *Recrystallization of Metals during Hot Deformation,* Philosophical Transactions of the Royal Society of London. Series A, Mathematical and Physical Sciences, 1978, Vol. 288, p147-158.

[98] J. G. Lenard, M. Pietrzyk, and L. Cser, *Mathematical and Physical Simulation of the Properties of Hot Rolled Products*, 1999, Elsevier Science, p151-229.

[99] J. G. Lenard, *Primer on Flat Rolling*, 2007, Elsevier Ltd, p3-7, p78-91, 109-118.

[100] H. S. Zurob, et al., *Modeling Recrystallization of Microalloyed Austenite: Effect of Coupling Recovery, Precipitation and Recrystallization,* Acta Materialia, 2002, Vol. 50, No. 12, p 3077-3094.

[101] R. D. Doherty, et al., *Current Issues in Recrystallization: a Review,* Materials Science and Engineering A, 1997, Vol. 238, No. 2, p219-274.

[102] L. Lissel, *Master Thesis: Modeling the Microstructural Evolution during Hot Working of C-Mn and of Nb Microalloyed Steels Using a Physically Based Model*, 2006, University of Dalarna, Chapter 2.

[103] J. H. Beynon and C. M. Sellars, *Modelling Microstructure and its Effects during Multipass Hot Rolling,* ISIJ International, 1992, Vol. 32, No. 3, p359-367.

[104] B. Xiao and J. D. Plummer, et al., *MEng Group Report: Developing A Mathematical Model Capable of Predicting the Properties of TMCR Steel*, The University of Sheffield, 2007.

[105] C. M. Sellars, *Modelling Microstructural Development during Hot Rolling,* Materials Science and Technology, 1990, Vol. 6, p1072-1081.

[106] M. Pietrzyk, C. Roucoules, and P. D. Hodgson, *Modelling the Thermomechanical and Microstructural Evolution during Hot Rolling of a Nb HSLA Steel,* ISIJ International, 1995, Vol. 35, No. 5, p531-541.

[107] P. D. Hodgson, *Microstructure Modelling for Property Prediction and Control,* Journal of Materials Processing Technology, 1996, Vol. 60, No. (1-4), p27-33.

[108] P. D. Hodgson, S. H. Zahiri, and J. J. Whale, *The Static and Metadynamic Recrystallisation Behaviour of an X60 Nb Microalloyed Steel,* ISIJ International, 2004, Vol. 44, No. 7, p 1224-1229.

[109] P. Korczak and H. Dyja, *Investigation of Microstructure Prediction during Experimental Thermo-mechanical Plate Rolling,* Journal of Materials Processing Technology, 2001, Vol. 109, No. (1-2), p112-119.

[110] P. Uranga, P., B. Lopez, and J.M. Rodriguez-Ibabe, *Microalloying and Austenite Evolution during Hot Working in Near Net Shape Processed Steels,* Materials Science and Technology, 2009, Vol. 25, p1147-1153.

[111] B. Pereda, et al., *Improved Model of Kinetics of Strain Induced Precipitation and Microstructure Evolution of Nb Microalloyed Steels during Multipass Rolling.* ISIJ International, 2008, Vol. 48, No.10, p1457-1466.

[112] M. Arribas, B. Lopez, et al., *Additional Grain Refinement in Recrystallization Controlled Rolling of Ti-Microalloyed Steels Processed by Near-Net-Shape Casting Technology*, Materials Science and Engineering A, 2008, Vol. 485, p383-394.

[113] R. Abad, et al., *Interaction between Recrystallization and Precipitation during Multipass Rolling in a Low Carbon Niobium Microalloyed Steel,* ISIJ International, 2001, Vol. 41, No. 11, p1373-1382.

[114] A. I. Fernandez, et al., *Static Recrystallization Behaviour of A Wide Range of Austenite Grain Sizes in Microalloyed Steels,* ISIJ International, 2000, Vol. 40, No. 9, p893-901.

[115] M. Jonsson, *An Investigation of Different Strategies for Thermo-mechanical Rolling of Structural Steel Heavy Plates,* ISIJ International, 2006, Vol. 46, No. 8, p1192-1199.

[116] P. D. Hodgson, L. O. Hazelden, et al., *The Development and Application of Mathematical Models to Design Thermomechanical Processes for Long Products*, from the same reference as the [10], 1995, p341-353.

[117] F. Siciliano and J. Jonas, *Mathematical Modelling of the Hot Strip Rolling of Microalloyed Nb, Multiply-Alloyed Cr-Mo, and Plain C-Mn Steels,* Metallurgical and Materials Transactions A, 2000, Vol. 31, No. 2, p511-530.

[118] W. Roberts, et al., *Prediction of Microstructure Development During Recrystallisation Hot Rolling of Ti-V Steels*, from the same reference as [4], 1984, p67-84.

[119] D. G. Stalheim and R. Glodowski, *Production of Fine - Grained as-Rolled Structural Plate Steels,* Iron and Steel Technology, 2010, No. October, p78-94.

[120] L. Cuddy, *Grain Refinement of Nb Steels by Control of Recrystallization during Hot Rolling,* Metallurgical and Materials Transactions A, 1984, Vol. 15, No. 1, p87-98.

[121] D. G. Stalheim, *Metallurgical Optimization of Microalloyed Steels for Oil and Gas Transmission Pipelines*, proceeding of the 6th international conference on "*HSLA Steels: Metallurgy and Applications" (HSLA'2011)*, Beijing, China

[122] A. I. Fernandez, B. Lopez and J. M. Rodriguez-Ibabe, *Modelling of Microstructure Evolution during Multipass Rolling of Nb-Microalloyed Steels: Influence of Initial Austenite State*, the same as reference as [45], 2002, p302-308.

[123] A. M. Sage, *Developments in Control Rolling of Vanadium-Bearing Steels*, the same as the reference [37], 1980, p119-127.

[124] T. Tanaka, *Science and Technology of Hot Rolling Process of Steel*, the same as the reference [10], 1995, p165-181.

[125] R. Rittmann and K. Freier, *Niobium Containing Steels for Spiral and Electric Resistance Welded Line Pipe Productions,* the same reference as [1], 2001, p571-586.

[126] L. C. Cuddy, *The Effect of Microalloyed Concentration on the Recrystallisation of Austenite During Hot Deformation*, the same reference as the [41], 1982, p129-140.

[127] F. Boratoo, et al., *Effect of Chemical Composition on the Critical Temperatures of Microalloyed Steels*, the same as reference as [15], 1988, p383-390.

[128] N. Radovic, et. al, *Determination of Tnr Temperature on Laboratory and Industrial Scale*, on the International Conference Thermec 2000, Las Vegas, USA, CD-ROM

[129] T. M. Maccagno, et al., *Determination of Recrystallisation Stop Temperature from Rolling Mill Logs and Comparison with Laboratory Simulation Results,* ISIJ International, 1994, Vol. 34, No. 11, p917-922.

[130] A. Zaky, *Determinations of the Non-Recrystallization Temperature for X52 Steel Produced by Compact Slab Process Combined with Direct Hot Rolling,* Journal of Materials Engineering and Performance, 2006, Vol. 15, No. 6, p651-655.

[131] W. S. Sun, et al., *Measurement and Modelling of the Effects of Precipitation on Recrystallization under Multipass Deformation Conditions*, Acta Metallurgical Materials, 1993, Vol. 41, No. 12, p3595-3604.

[132] D. Bai, et al., *Effect of Deformation Parameters on the No-Recrystallisation Temperature in Nb-bearing Steels,* Metallurgical and Materials Transactions A, 1993, Vol. 24, No. 10, p 2151-2159.

[133] M. Gómez, L. Rancel, and S. Medina, *Assessment of Austenite Static Recrystallization and Grain Size Evolution during Multipass Hot Rolling of a Niobium-Microalloyed Steel,* Metals and Materials International, 2009, Vol. 15, No. 4, p689-699.

[134] M. Gomez, et al., *Static Recrystallisation and Induced Precipitation in a Low Nb Microalloyed Steel,* ISIJ International, 2002, Vol. 42, No. 4, p423-431.

[135] S. F. Medina, *Determination of No-Recrystallisation Temperature in Nb-V-Ti Microalloyed Steel and Discussion of its Definition,* Materials Science and Technology, 1998, No. 14, p217-221.

[136] S. Vervynckt, et al., *Modern HSLA Steels and Role of Non-Recrystallisation Temperature*, International Materials Review, 2012, Vol. 57, No. 4, p187-207.

[137] K. Minami, et al., *Mathematical Modeling of Mean Flow Stress during the Hot Strip Rolling of Nb Steels,* ISIJ International, 1996, Vol. 36, No. 12, p1507-1515.

[138] F. Siciliano, et al., *Mathematical Modelling of the Mean Flow Stress, Fractional Softening and Grain Size during the Hot Strip Rolling of C-Mn Steels,* ISIJ International, 1996, Vol. 36, No. 12, p1500-1506.

[139] S. Solhjoo and R. Ebrahimi, *Prediction of No-Recrystallization Temperature by Simulation of Multi-Pass Flow Stress Curves from Single-Pass Curves,* Journal of Materials Science, 2010, p1-7.

[140] M. G. Akben, I. Weiss and J. J. Jonas, Dynamic Precipitation and Solute Hardening in a V Microalloyed Steel and Two Nb Steels Containing High Levels of Mn, Acta Metallurgica, Vol. 29, p111-121.

[141] H. Andrade, M. Akben, and J. Jonas, *Effect of Molybdenum, Niobium, and Vanadium on Static Recovery and Recrystallization and on Solute Strengthening in Microalloyed Steels,* Metallurgical and Materials Transactions A, 1983, Vol. 14, No. 10, p1967-1977.

[142] S. Yomamto et al., *The Effect of Microalloying Elements on the Recovery and Recrystallization in Deformed Austenite*, from the same reference as [41], 1982, p613-637.

[143] S. Hansen, J. B. Sande, and M. Cohen, *Niobium Carbonitride Precipitation and Austenite Recrystallization in Hot-Rolled Microalloyed Steels,* Metallurgical and Materials Transactions A, 1980, Vol. 11, No. 3, p387-402.

[144] J. Speer and S. Hansen, *Austenite Recrystallization and Carbonitride Precipitation in Niobium Microalloyed Steels,* Metallurgical and Materials Transactions A, 1989, Vol. 20, No. 1, p25-38.

[145] O. Kwon and A.J. DeArdo, *Interactions Between Recrystallization and Precipitation in Hot-Deformed Microalloyed Steels,* Acta Metallurgica et Materialia, 1991, Vol. 39, No. 4, p529-538.

[146] M. Luton, R. Dorvel, and R. Petkovic, *Interaction between Deformation, Recrystallization and Precipitation in Niobium Steels,* Metallurgical and Materials Transactions A, 1980, Vol. 11, No. 3, p411-420.

[147] A. LeBon, J. Rofe-Vernis, and C. Rossard, *Recrystallization and Precipitation during Hot Working of a Nb-Bearing HSLA Steel,* Metal Science, 1975, Vol. 9, p36-40.

[148] H. S. Zurob, et al., *Rationalization of the Softening and Recrystallization Behaviour of Microalloyed Austenite using Mechanism Maps.* Materials Science and Engineering A, 2004, Vol. 382, No. (1-2), p64-81.

[149] X. Liu, et al., *Modelling of Interaction Between Recrystallisation and Precipitation During Multipass Rolling of Niobium Microalloyed Steels,* Materials Science and Technology, 1995, Vol. 11, p469-473

[150] M. Gomez, S.F. Medina, and P. Valles, *Determination of Driving and Pinning Forces for Static Recrystallization during Hot Rolling of a Niobium Microalloyed Steel,* ISIJ International, 2005, Vol. 45, No. 11, p1711-1720.

[151] M. I. Vega, et al., *Recrystallisation Driving Forces Against Pinning Forces in Hot Rolling of Ti-Microalloyed Steels,* Materials Science and Engineering: A, 2006. Vol. 423, No. (1-2), p253-261.

[152] J. J. Jonas and I. Weiss, *Effect of Precipitation on Recrystallization in Microalloyed Steels,* Metal Science, 1979, Vol. 13, p238-245.

[153] I. Weiss and J. Jonas, *Interaction between Recrystallization and Precipitation during the High Temperature Deformation of HSLA Steels,* Metallurgical and Materials Transactions A, 1979, Vol. 10, No. 7, p831-840.

[154] A. Quispe, S. F. Medina, et al., *Influence of Austenite Grain Size on Recrystallisation-Precipitation Interaction in a V-Microalloyed Steel*, Materials Science and Engineering: A 2007, Vol. 447, No. (1-2), p11-18.

[155] W. M. Rainforth, et al., *Precipitation of NbC in a Model Austenitic Steel*, Acta Materialia, 2002, Vol. 50, No. (4), p735-747.

[156] S. F. Medina, and J.E. Mancilla, *Determination of Static Recrystallisation Critical Temperature of Austenite in Microalloyed Steels.* ISIJ International, 1993, Vol. 33, No. 12, p1257-1264.

[157] S. F. Medina, et al., *Model for Static Recrystallisation Critical Temperature in Microalloyed Steels,* Materials Science and Technology, 2001, Vol. 17, p536-544.

[158] S. F. Medina, *The Influence of Niobium on the Static Recrystallization of Hot Deformed Austenite and on Strain Induced Precipitation Kinetics,* Scripta Metallurgica et Materialia, 1995, Vol. 32, No. 1, p43-48.

[159] S. F. Medina and A. Quispe, *Influence of Strain on Induced Precipitation Kinetics in Micro-alloyed Steels,* ISIJ International, 1996, Vol. 36, No. 10, p1295-1300.

[160] B. Dutta and C.M. Sellars, *Effect of Composition and Process Variables on Nb(C, N) Precipitation in Niobium Microalloyed Austenite,* Materials Science and Technology, 1987, Vol. 3, p197-206.

[161] E. Valdes and C.M. Sellars, *Influence of Roughing Rolling Passes on Kinetics of Strain Induced Precipitation of Nb(C, N),* Materials Science and Technology, 1991, Vol. 7, p622-630.

[162] B. Dutta, et al., *Mechanism and Kinetics of Strain Induced Precipitation of Nb(C, N) in Austenite,* Acta Metallurgica et Materialia, 1992, Vol. 40, No. 4, p653-662.

[163] B. Dutta and E. J. Palmiere, *Modelling the Kinetics of Strain Induced Precipitation in Nb Microalloyed Steels*, Acta Materialia, 2001, Vol. 49, No. 5, p785-794.

[164] A. P. Singh, D. Sengupta, et al., *Predicting Microstructural Evolution and Yield Strength of Microalloyed Hot Rolled Steel Plate,* Materials Science and Technology, 2004, Vol. 20, p1317-1325.

[165] R. Colas and C. M. Sellars, *Computed Temperature Profiles of Hot Rolled Plate and Strip during Accelerated Cooling*, Proceeding of International Conference on "*Accelerated Cooling of Rolled Steel"*, edited by G. E. Ruddle and A. F. Crawley, 1987, p121-130.

[166] W. B. Morrison, *Microstructure Control in Practice,* Ironmaking and Steelmaking, 1995, Vol. 22, No. 6, p453-458.

[167] H. Abrams, *Thermal Mechanical Process for Steel Slabs and the Product Thereof*, 1983, U. S. Patent No. 4395296, July 26

[168] J. G. Willams, C. R. Killmore, et. al, *Production of Tough HSLA Heavy Plate Steels with A Moderate Controlled Rolling Processes*, from the same reference as [11], 1985, p567-578.

[169] A. Titlyanov, A. Korovin, and A. Radyuk, *Improving the Temperature Conditions in Controlled Rolling on a TLS 5000 Mill,* Steel in Translation, 2011, Vol. 41, No. 5, p380-382.

[170] A. A. Gorni et al., *Recent Development on Controlled Rolling Technology At Companhia Siderurgica Paulsta – COSIPA*, http://www.gorni.eng.br/e/Gorni_AdvancedSteel_1998.pdf, last time access on 05/12/12.

[171] F. Akio and O. Kazuo, *JFE Steel's Advanced Manufacturing Technologies for High Performance Steel Plates,* JFE Technical Report, 2005, No. 5, p10-15.

[172] J. Wendelstorf, et al., *Spray Water Cooling Heat Transfer at High Temperatures and Liquid Mass Fluxes,* International Journal of Heat and Mass Transfer, 2008, Vol. 51, No. (19-20), p4902-4910.

[173] H. Mabuchi, T. Ishikawa, and Y. Nomiyama, *Further Process in Accelerated Cooling as the New Era of High Tech Steel,* in *Materials Solutions '97 on Accelerated Cooling/Direct Quenching Steels*, 1997, Indianapolis, Indiana, p43-50.

[174] T. Ishikawa, *Ultra-High Crack-Arresting Steel Plate (HIAREST) with Super-Refined Grains in Surface Layers*, 1997, Nippon Steel Technical Report, No. 75, p31-42.

[175] H. Mabuchi, T. Hasegawa, and T. Ishikawa, *Metallurgical Features of Steel Plates with Ultra Fine Grains in Surface Layers and their Formation Mechanism,* ISIJ International, 1999, Vol. 39, No. 5, p477-485.

[176] T. Ishikawa et al., *Steel Plate Excellent in Brittle Crack Propagation Arrest Characteristics and Low Temperature Toughness and Process for Producing Same*, 2000, US Patent 6090226

[177] A. J. DeArdo, *The Influence of Thermomechanical Processing and Accelerated Cooling on Ferrite Grain Refinement in Microalloyed Steels*, Proceeding of International Conference on "*Accelerated Cooling of Steel"*, 1985, Pittsburgh, The Metallurgical Society, p97-115.

[178] W. Schutz, et al., *Extended Property Combinations in Thermomechanically Control Processed Steel Plates by Application of Advanced Rolling and Cooling Technology*. Ironmaking and Steelmaking, 2001, Vol. 28, p180-184.

[179] B. Hutchinson, *Microstructure Development During Cooling of Hot Rolled Steels,* Ironmaking and Steelmaking, 2001, Vol. 28, p145-151.

[180] P. S. Bandyopadhyay, et al., *Evolution of Microstructure and Mechanical Properties of Thermomechanically Processed Ultrahigh-Strength Steel,* Metallurgical and Materials Transactions A, 2011, Vol.42, p2742-2752.

[181] T. Tanaka, *Overview of Accelerated Cooled Steel Plate*, in *Accelerated Cooling of Rolled Steel,* 1987, Winnipeg, Canada: PERGAMON PRESS, p187-208.

[182] L. Myllykoski, et al., *Advanced in the Accelerated Cooling of Plates*, the same reference as [10], 1995, p183-196.

[183] M. Umemoto, Z. Hai Guo, and I. Tamura, *Effect of Cooling Rate on Grain Size of Ferrite in a Carbon Steel,* Materials Science and Technology, 1987, Vol. 3, No. 4, p249-255.

[184] A. A. Gorni, et al., *Accelerated Cooling of Steel Plates: The Time Has Come*, Journal of ASTM International, 2008, Vol. 5, No. 8, p1-7.

[185] C. Ouchi, et.al, *Effects of Interrupted Accelerated Cooling after Controlled Rolling on the Mechanical Properties of Low Alloy Steels,* Transactions ISIJ, 1982, Vol. 22, p608-616.

[186] G. Horn, et al., *Advanced Cooling Technologies for High-Strength Plate Production*, Millennium Steel, 2009, p102-105.

[187] Dilg, C., et al., *Accelerated Cooling during Plate Production,* Steel Research International, 1992, p211-217.

[188] I. Kaszau, *State of the Art in Microalloyed Plate Production*, from the same as the reference [10], 1995, p95-104.

[189] R. K. Gibbs, et al., *The Prediction of Ferrite Grain Size in Niobium Microalloyed Controlled Rolled Steels*, from the same reference as [93], 1993, p173-179

[190] SIROLL MULPIC: *Plate Cooling Technology-AC and DQ Cooling for advanced Material Properties*, from SIEMENS VAI website: http://www.industry.siemens.com/datapool/industry/industrysolutions/metals/siroll/en/SIROLL-Mulpic-en.pdf, last access on 05/12/2012.

[191] M. Brammer, *Plate Mills for Higher-Strength Products*, Ironmaking and Steelmaking, 2006, vol. 33, p353-356.

[192] P. Bhooplapur, M. P. Brammer, and M. J. Steeper, *Upgrading Existing Plate Mills for Higher Strength Product,* Ironmaking and Steelmaking, 2008, Vol. 35, p491-495.

[193] B. Brammer, *Plate Mill Upgrades for High Strength Products*, Millennium Steel, 2008, p161-166.

[194] C. M. Sellars, *Metallurgy Modelling of Thermomechanical Processing*, 50th Hatfield Memorial Lectures Volume 4, edited by Peter Beeley, Maney Publications, London

[195] S. -J. Chen, and A. A. Tseng, *Spray and Jet Cooling in Steel Rolling,* International Journal of Heat and Fluid Flow, 1992, Vol. 13, No. 4, p358-369.

[196] G. Franco, *Master Thesis: Boiling Heat Transfer During Cooling of a Hot Moving Steel Plate by Multiple Top Jets*, 2006, University of British Columbia, Chapter 2.

[197] A. Laasraoui and J. J. Jonas, *Prediction of Temperature Distribution, Flow Stress and Microstructure during the Multipass Hot Rolling of Steel Plate and Strip,* ISIJ International, 1991, Vol. 31, No. 1, p95-105.

[198] W. Chen, et al., *Fundamental Phenomena Governing Heat Transfer During Rolling,* Metallurgical and Materials Transactions A, 1993, Vol. 24, No. 6, p1307-1320.

[199] W. C. Chen, et al., *Mathematical Modelling of Heat Flow and Deformation during Rough Rolling,* Ironmaking and Steelmaking, 1993, Vol. 20, No. 2, p113 -125.

[200] C. Devadas, I. Samarasekera, and E. Hawbolt, *The Thermal and Metallurgical State of Steel Strip during Hot Rolling: Part I. Characterization of Heat Transfer,* Metallurgical and Materials Transactions A, 1991. Vol. 22, No. 2, p307-319.

[201] R. Colas, *Modelling Heat Transfer During Hot Rolling of Steel Strip,* Modelling and Simulation in Materials Science and Engineering, 1995, Vol. 3, No. 4, p437.

[202] S. Serajzadeh, et al., *Prediction of Temperature Distribution in the Hot Rolling of Slabs,* Modelling and Simulation in Materials Science and Engineering, 2002, Vol. 10, p185-203.

[203] S. R. Wang and A. A. Tseng, *Macro- and Micro-Modelling of Hot Rolling of Steel Coupled by a Micro-Constitutive Relationship,* Materials & Design, 1995, Vol. 16, No. 6, p315-336.

[204] A. P. Singh, et al., *Influence of Thermomechanical Processing and Accelerated Cooling on Microstructures and Mechanical Properties of Plain Carbon and Microalloyed Steels,* Materials Science and Technology, 1999, Vol. 15, p121-126.

[205] I. Sankar, I., et.al, *Prediction of Heat Transfer Coefficient of Steel Bars Subjected to Tempcore Process using Nonlinear Modeling,* The International Journal of Advanced Manufacturing Technology, 2010, Vol. 47, No. 9, p1159-1166.

[206] M. Mandal and S. K. Pal, *Pseudo-Bond Graph Modelling of Temperature Distribution in a Through-Process Steel Rolling,* Mathematics and Computers in Simulation, 2008, Vol. 77, No. 1, p81-95.

[207] A. Purcell, *Master Thesis: Mathematical Modelling of Temperature Evolution in the Hot Rolling of Steel*, 2000, McGill University, Montreal, Chapter 2.

[208] S. Serajzadeh, *Prediction of Temperature Variations and Kinetics of Austenite Phase Change on the Run-out Table,* Materials Science and Engineering: A, 2006, Vol. 421, No. (1-2), p260-267.

[209] C. M. Sellars, *Computer Modelling of Hot-Working Processes,* Materials Science and Technology, 1985, Vol. 1, p325-332.

[210] J. D. Fletcher and J. H. Beynon, *Heat Transfer Conditions in Roll Gap in Hot Strip Rolling,* Ironmaking and Steelmaking, 1996, Vol. 23, No. 1, p52-57.

[211] Y. H. Li and C.M. Sellars, *Evaluation of Interfacial Heat Transfer and Its Effects on Hot Forming Processes,* Ironmaking and Steelmaking, 1996, Vol. 23, No. 1, p58-61.

[212] R. Wendelstorf, R., et al., *Effect of Oxide Layers on Spray Water Cooling Heat Transfer at High Surface Temperatures,* International Journal of Heat and Mass Transfer, 2008, Vol. 51, No. (19-20), p4892-4901.

[213] M. Torres and R. Colas, *A Model for Heat Conduction through the Oxide Layer of Steel during Hot Rolling*, Journal of Materials Processing Technology, 2000, Vol. 105, p258-263.

[214] X-T, Li, M-T, Wang and F-S, Du, *A Coupling Thermal Mechanical and Microstructural FE Model for Hot Strip Continuous Rolling Process and Verification,* Materials Science and Engineering: A, 2005, Vol. 408, No. (1-2), p33-41.

[215] J. P. Holman, *Heat Transfer*, edition, London, McGraw-Hill, Chapter 1, p1-19.

[216] S. Serajzadeh, *Thermomechanical Modelling of Hot Slab Rolling,* Materials Science and Technology, 2005, Vol. 21, p93-102.

[217] R. J. Hand, S. R. Foster, and C. M. Sellars, *Temperature Changes During Hot Plane Strain Compression Testing,* Materials Science and Technology, 2000, Vol. 16, p442-450.

[218] C. Devadas and I. V. Samarasekera, *Heat Transfer during Hot Rolling of Steel Strip,* Ironmaking and Steelmaking, 1986, Vol. 13, No. 6, p311-321.

[219] S. Sikdar and A. Mukhopadhyay, *Numerical Determination of Heat Transfer Coefficient for Boiling Phenomenon at Runout Table of Hot Strip Mill,* Ironmaking and Steelmaking, 2004, Vol. 31, No. 6, p495-502.

[220] P. Campbell, et al., *Microstructural Engineering Applied to the Controlled Cooling of Steel Wire Rod: Part III. Mathematical Model-Formulation and Predictions*, Metallurgical and Materials Transactions A, 1991, Vol. 22, No. 11, p2791-2805.

[221] Y. Watanabe, et al., *Integrated Model for Microstructural Evolution and Properties of Steel Plates Manufactured in Production Line,* ISIJ International, 1992, Vol. 32, No.3, p405-413.

[222] X. J. Zhang, P. D. Hodgson, et al., *The Effect of Through-Thickness Strain Distribution on the Static Recrystallization of Hot Rolled Austenitic Stainless Steel Strip*, Journal of Materials Processing Technology, 1996, Vol. 60, No. (1-4), p615-619.

[223] C. -H. Moon and Y. Lee, *An Approximate Model for Local Strain Variation over Material Thickness and Its Applications to Thick Plate Rolling Process*, ISIJ International, 2009, Vol. 49, No. 3, p402-407.

[224] S. X. Zhou, *An Integrated Model for Hot Rolling of Steel Strips,* Journal of Materials Processing Technology, 2003, Vol. 134, No. 3, p338-351.

[225] J. G. Lenard, *Workability and Process Design in Rolling*, from the same reference as the [89], Chapter 18, p263.

[226] X. Duan and T. Sheppard, *Prediction of Temperature Evolution by FEM during Multi-Pass Hot Flat Rolling of Aluminium Alloys*. Modelling and Simulation in Materials Science and Engineering, 2001, Vol. 9, p525-538.

[227] C. M. Sellars, *Computer Modelling of Microstructural Evolution during Hot Working*, from the same the same reference as [15], 1988, p448-457.

[228] M. Pietrzyk, *Finite-Element Simulation of Large Plastic Deformation,* Journal of Materials Processing Technology, 2000, Vol. 106, No. (1-3), p223-229.

[229] M. Pietrzyk and J. G. Lenard, *A Study of Heat Transfer during Flat Rolling,* International Journal for Numerical Methods in Engineering, 1990, Vol. 30, No. 8, p1459-1469.

[230] T. Iguchi and I. Yarita, *3-Dimensional Analysis of Flat Rolling by Rigid-Plastic FEM Considering Sticking and Slipping Frictional Boundary*, ISIJ International, 1991, No 6, p559-565.

[231] M. Pietrzyk, *Through-Process Modelling of Microstructure Evolution in Hot Forming of Steels,* Journal of Materials Processing Technology, 2002, Vol. 125-126, p53-62.

[232] B. Kowalski, *PhD Thesis: Method of Interpretation of Results of Plane Strain Compression Tests for Evaluation of Rheological Parameters of Materials*, 2003, AGH University of Science and Technology, Chapter 2.

[233] C. Boldetti, *PhD Thesis: Multi-scale Measurement and Modelling of Large Deformation of Structural Metals during Thermomechanical Processing*, 2006, University of Sheffield, Chapter 2.

[234] J. H. Beynon and C. M. Sellars, *Strain Distribution Patterns During Plane Strain Compression*, Journal of Testing and Evaluation, 1985, Vol. 13, No. 1, p28-38.

[235] B. Kowalski, C.M. Sellars, and M. Pietrzyk, *Development of a Computer Code for the Interpretation of Results of Hot Plane Strain Compression Tests.* ISIJ International, 2000, Vol. 40, No. 12, p1230-1236.

[236] M. S. Mirza and C.M. Sellars, *Modelling the Hot Plane Strain Compression Test Part 1 - Effect of Specimen Geometry, Strain Rate, and Friction on Deformation,* Materials Science and Technology, 2001, Vol. 17, p1133-1141.

[237] A. Mukhopadhyay, I.C. Howard, and C.M. Sellars, *Development and Validation of a Finite Element Model for Hot Rolling using ABAQUS/STANDARD,* Materials Science and Technology, 2004, Vol. 20, p1123-1133.

[238] O. Pawelski and R. Kaspar, *Physical Simulation of the Thermomechanical Process in Hot Rolling*, from the same reference [15], 1988, p438-447.

[239] M. Pietrzyk, J.G. Lenard, and G.M. Dalton, *A Study of the Plane Strain Compression Test*,* CIRP Annals - Manufacturing Technology, 1993, Vol. 42, No. 1, p331-334.

[240] M. S. Loveday, et al., *Measurement of Flow Stress in Hot Plane Strain Compression Tests,* Materials at High Temperatures, 2006, Vol. 23, p85-118.

[241] A. L. Lacey and M. S. Loveday et al., *Measuring Good Practice Guide No 27: Measuring Flow Stress in Hot Strain Compression Tests,* 2002, National Physical Laboratory (NPL)

[242] S. H. John, *PhD Thesis: Laboratory Simulation of Microstructural Evolution in AISI 430 Ferritic Stainless Steel during the Steckel Mill Process*, 2006, University of Sheffield, Chapters 3 and 5.

[243] S. H. John, *TMC Manual: Testing on the IMMPETUS Thermomechanical Compression (TMC) Test Machine*, University of Sheffield, 2009

[244] A. J. Lacey, *Master Thesis: Interaction of Testing Machine Characteristics and Specimen Geometry in Plane Strain Compression Testing*, 2003, University of Sheffield, Chapter 2.

[245] C. Ouchi, T. Sampei, and I. Kozasu, *The Effect of Hot Rolling Condition and Chemical Composition on the Onset Temperature of γ-α Transformation after Hot Rolling,* Transactions ISIJ, 1982, Vol. 22, p214-222.

[246] ASTM E112-10: *Standard Test Method for Determining Average Grain Size*, 2010, ASTM International, United States.

[247] S. D. Choo and W. Y. Choo, *An Integrated Model for Microstructural Evolution and its Application to the Properties Predictions of Plate Steels*, Proceeding on *42nd Mechanical Working and Steel Processing (MWSP) Conference*, 2000, Toronto, Canada, p407-417.

[248] A. P. Singh, et al., *A Mathematical Model to Predict Microstructural Changes and Final Mechanical Properties of API-Grade Steel Plates Produced by Thermomechanical Control Processing*, Proceeding on 44th Mechanical Working and Steel Processing (MWSP) Conference, 2002, Florida, p1139-1149.

[249] S. J. Lee and Y. K. Lee, *Prediction of Austenite Grain Growth during Austenitisation of Low Alloy Steels,* Materials & Design, 2008, Vol. 29, Vol. No. 9, p1840-1844.

[250] User's Guide Manuel of Abaqus Software, from the website address: http://abaqusdoc.ucalgary.ca/v6.9/, last time accessed on 27th June, 2013

[251] Free Software ImageJ User Guide, from the website address: http://rsbweb.nih.gov/ij/download.html, last time accessed on 13th June, 2013

[252] R. Goodall, *Lecture Notes on Quantification of Microstructure and Texture*, 2009, Materials Science and Engineering Department, University of Sheffield

[253] R. L. Higginson and C. M. Sellars, *Worked Examples in Quantitative Metallography*, 2003, London, Maney, Chapter 2.

[254] G. F. Vander Voort, *Grain Size Measurement*, Practical Applications of Quantitative Metallography, edited by J. L. Mccall and J. H. Steele, 1984, p85-131.

[255] S. Nanba, et al., *Prediction of Microstructure Distribution in the Through Thickness Direction during and after Hot Rolling in Carbon Steels,* ISIJ International, 1992, Vol. 32, No. 3, p377-386.

[256] C. P. Hong and J. J. Park, *Design of Pass Schedule for Austenite Grain Refinement in Plate Rolling of a Plain Carbon Steel,* Journal of Materials Processing Technology, 2003, Vol. 143-144, p758-763.

[257] M. Atkins, *Atlas of Continuous Cooling Transformation Diagram for Engineering Steels*, prepared by staff of British Steel Corporation Swinden House, Sheffield Laboratories, Rotherham, 1980, pp227-229.

[258] A. Kern and U. Schriever, *Exploitation of Computer Modelling For Quality Assurance and Quality Control During the Production of Heavy Plates of Steel*, 2002, Advanced Engineering Materials, No. 4, p215-220.

[259] H.A. Abrams, *Thermal Mechanical Process for Steel Slabs and the Product Thereof*, 1983, Bethlehem Steel Corporation (Bethlehem, PA): United States.

[260] T. Sakai, Y. Saito, et al., *Deformation and Recrystallisation Behaviour of Low Carbon Steel in High Speed Hot Rolling*, Trans ISIJ, 1988, Vol. 28, p1028-1035.

[261] A. A. Gorni, *The Production of Extra-Heavy Plates Using Continuously Cast Slabs,* 2002, http://www.gorni.eng.br/e/heavy_plate.html, last access on 15 July 2013.

[262] J. Majta, et al., *An Integrated Computer Model with Applications for Austenite-to-Ferrite Transformation during Hot Deformation of Nb-Microalloyed Steels,* Metallurgical and Materials Transactions A, 2002, Vol. 33, No. 5, p1509-1520.

[263] B. Mintz, J. R. Banerjee, and K.M. Banks, *Regression Equation for $\overline{Ar_3}$ Temperature for Coarse Grained as Cast Steels,* Ironmaking and Steelmaking, 2011, Vol. 38, No. 3, p197-203.

[264] X. Q. Yuan, Z. Y. Liu, et al., *The Onset Temperatures of γ to α Phase Transformation in Hot Deformed and Non-deformed Nb Micro-alloyed Steels,* ISIJ International, 2006, Vol. 46, No. 4, p579-585.

[265] A. A. dos Santos and R. Barbosa, *Model for Microstructure Prediction in Hot Strip Rolled Steels,* Steel Research International, 2010, Vol. 81, No. 1, p55-63.

[266] Olasolo, M., et al., *Effect of Austenite Microstructure and Cooling Rate on Transformation Characteristics in a Low Carbon Nb-V Microalloyed Steel,* Materials Science and Engineering: A, 2011, Vol. 528, No. 6, p2559-2569.

Appendix A – A Summary Table of Conducted Multipass PSC Tests on TMC Machine

The following summary tables include most of the continuous cooling multipass PSC tests with different test conditions and steel chemical compositions for this PhD research project. Many different multipass PSC tests were carried out, thus for the traceability purposes, every deformed PSC sample was labelled with the alphabet letter indicating the steel grade followed by the individual sample number. For instance, A1 means the first PSC testing of Nb steel A. Therefore, the other letters B, C, D and E are the Nb+Ti steel B, plain carbon steels C and D and dummy steel E (Fe-30wt%Ni-0.05wt%C-0.38wt%Nb) respectively. In terms of PSC testing conditions, the average measured temperatures and input strain of each deformation are shown in the table. Moreover, the default applied strain rates for the 3-pass roughing were 2.082, 2.529 and 2.797 s^{-1} and the gap times during roughing were 5 seconds, while the default input strain rates for the 5-pass finishing were 3.797, 3.911, 3.932, 3.788 and 2.224s^{-1}.

Test conditions + codes		Average Rough Temp. (°C)	Input Roughing strain (and strain rate)	Holding temp	Cooling time (s)	Average Finish Temperature (°C)	Input Finishing strain (and strain rate)	Temp. Drop (°C)	Cooling Time (s) & Media
3R-2CT-ok	**A1**	1019,994,972	0.4+0.4+0.1	972-840	**100**				AIR+WQ
3R+1F-ok	**A2**	1018,993,980	0.4+0.4+0.1	980-830	**100**	**835**	0.14		AIR+WQ
3R+2F ok	**A3**	1021,993,978	0.4+0.4+0.1	978-830	**100**	**835, 866**	0.14+0.13		AIR+WQ
2 passes - ok	**A4**	946, 937	0.4+0.4 (2.5^{-1})						WQ
2 passes - OK	**A5**	859, 863	0.4+0.4 (2.5^{-1})						WQ
2 passes-	**A6**	1160, 1114	0.4+0.4 (2.5^{-1})						WQ

ok									
2 passes ok	**A7**	1190, 1142	0.4+0.4 (2.5^{-1})						WQ
3R+W-BAD	**A8**	1026,1009,992	0.4+0.4+0.1						WQ
8P with IFC – Failed Test	**A9**	1037,1007, 978	0.4+0.4+0.1	990-741 741-790 790-815 815-840 840-864 864-880	58 5 5 10 20 59	870, 873, 867, 838, 859	0.14+0.13+0.12+0.1 +0.14		IFC+WQ
8P- Failed	**A10**	1044, 1017, 991	0.4+0.4+0.1	Same as above cooling profile		871, 862, 857, 837, 841	0.14+0.13+0.12+0.1 +0.14		IFC+WQ
3R-Centre IFC-BAD	**A11**	1234, 1198, 1156	0.2-(1.83)+0.5-(2.17) +0.3-(2.47)	1150-1132 1132-1113 1113-1094 1094-1067 1067-1045	58 20 20 30 29				IFC+WQ
3R-Centre+ air-ok	**A12**	1256, 1203, 1155	0.2-(1.83)+0.5-(2.17) +0.3-(2.47)	1155-1003	348				AIR+WQ
8P less stress	**A13**	1049, 1066, 1025	0.13+0.45+0.45= 1.03	Same as above cooling profile of A9		888,911, 901, 890, 877	0.2+0.17+0.16+0.16 +0.14 = 0.83		WQ

A-3R-Hold ok	**A14**	1044, 1016,987	0.45+0.45+0.15 = 1.03	980-980	348				AIR+WQ
A-3R-Hold Better	**A15**	1054, 1013, 971	0.45+30s+0.45+**3.19s**+0.15 = 1.03	1064-1005 998-968 980-880 880-880	**30** **3.19** 3 120				Mist+WQ
A-8P with IFC in HP Ferrite OK	**A16**	1037, 996, 968	0.45+**5s**+0.45+**5s**+ 0.13	**980-814** **814-741** **741-790** **790-815** **815-840** **840-864** **864-880**	**30** **28** **5** **5** **10** **20** **59**	874, 868, 858, 849, 840	0.2+0.17+0.16+0.16 +0.14 = 0.83	840-400	**44** WQ
A-8P Ferrite ok	**A17**	1042, 997, 961	0.45+**30s**+0.45+**5s** +0.13	Same as above IFC cooling profile of test A16		875, 861, 851, 844, 835	0.2+0.17+0.16+0.16 +0.14 = 0.83	840-400	**20** WQ
A-8P Ferrite ok	**A18**	1036, 1002, 969	0.45+**30s+**0.45+**30 s** +0.13	Same as the IFC cooling profile of test A16		874, 864, 853, 845, 836	0.2+0.17+0.16+0.16 +0.14 = 0.83	840-400	**10** WQ
A-3R-Intense IFC2 GOOD	**A19**	1034, 1005, 977	0.4+**30s**+0.4+**30s**+ 0.1	**970-980** **980-593** **593-721** **721-768** **768-816**	**5** **20** **6** **4.3** **6**				WQ

				816-852 **852-880**	**20** **60**				
A-8P GOOD	**A20**	1032, 1003, 978	0.4+**30s** +0.4+**30s**+0.1	980-880 880-880	261 5	879, 857, 848, 842, 835	0.2+0.17+0.16+0.16 +0.14	820-400	**42** WQ
10mm 3R+W-OK	**A21**	1038, 1000, 970	0.4+**30s**+0.4+**30s**+ 0.1						**WQ**
12mm 8p+Air +84s-Ok	**A22**	1036, 1000, 970	0.4+**30s** +0.4+**30s**+0.1	980-880 880-880	261 5	880, 862, 853, 845, 837	0.2+0.17+0.16+0.16 +0.14	820-400	**84** WQ
12mm 8p+IFC+W -ok	**A23**	1035, 998, 969	0.4+**30s** +0.4+**30s**+0.1	Same as the IFC cooling profile of test A16		868, 855, 847, 843, 836	0.2+0.17+0.16+0.16 +0.14		**WQ**
10mm 8p+air +42s-OK	**A24**	1032, 995, 968	**0.3**+30s+**0.3**+30s+ 0.1	970-880 880-880	261 5	879, 857, 848, 842, 836	**0.14+0.13+0.12+0.1 2+0.12**	820-400	**42** WQ
10mm 8P+IFC+42 s-OK	**A25**	1032, 993, 968	**0.3**+30s+**0.3**+30s+ 0.1	Same as the IFC cooling profile of test A16		866, 854, 845, 838, 832	**0.14+0.13+0.12+0.1 2+0.12**	820-400	**42** WQ
12mm-8p air+42-OK	**A26**	1033, 996, 968	0.4+**30s** +0.4+**30s**+0.1	980-850 850-850	261 5	850, 835, 824, 815, 805	0.2+0.17+0.16+0.16 +0.14	790-400	**42** WQ
12mm 8p air+air-OK	**A27**	1036, 999, 970,	0.4+**30s** +0.4+**30s**+0.1	980-880 880-880	261 5	880, 865, 854, 847, 839	0.2+0.17+0.16+0.16 +0.14	830-760 760-400	**209** **1241** **WQ**
10mm	**A28**	1039, 1003	0.4+**30s**	970-880	261				**WQ**

3p+Air+w-OK		, 971	+0.4+**30s**+0.1	880-880	5				
10mmBar-5p-Less Strain	**A29**					875, 858, 849, 844, 840	**0.14+0.13+0.12+0.12+0.12**	820-400	**126**
10mm Bar 8p less strain	**A30**	980, 940	0.15+0.15 ($3s^{-1}$) gap time 10s			910, 891, 879, 870, 861, 854	0.15+0.15+0.15+0.15+0.15+0.15($3s^{-1}$) gap time 10s	820-400	**126**
10mm-6R+IFC+5F+42-less strain	**A31**	1029,1006, 995,985, 974,965	0.12+0.12+0.12+0.12+0.12+0.12($2.5s^{-1}$) = 0.72, gap time 12s	Same as the IFC cooling profile of test A16		869, 861, 852, 843, 835	**0.14+0.13+0.12+0.12+0.12=0.63**	820-400	**42**
B-3R-2CT-ok	**B1**	1022, 992, 964	0.4+0.4+0.1						WQ
B-Two CT-ok	**B2**	1030,1003,977	0.4+0.4+0.1	977-880 880-870	30 10				WQ
B-Two CT-ok	**B3**	1025, 997, 968	0.4+0.4+0.1	968-900 900-870	30 60				WQ
B-Two CT-ok	**B4**	1033, 986, 956	0.4+0.4+0.1	956-870	300				WQ
B-3R+2F-ok	**B5**	1034, 997, 964	0.4+0.4+0.1	964-880 880-870	30 10	864, 860	0.14+0.13		WQ
B-5F Bad	**B6**			1200-830 830-830	90 10	828,829,834,838, 842	0.14+0.13+0.12+0.1+0.14		WQ

B-1R+1F-2CT-less strain	**B7**	1034	0.4 (5^{-1})	1034-810 810-795	30 4	800	0.4 (5^{-1})		WQ
B-3R Less strain	**B8**	1034, 1020, 1003	0.1+0.4+0.4	1003-870	300				WQ
B centre - 3R-Temp wrong	**B9**	**1200, 1157, 1100**	0.2-(1.83)+0.5-(2.17) +0.3-(2.47)						WQ
B Surface-3R-less strain	**B10**	1078, 1052, 1012	0.35-(3.27)+0.75-(3.34)+0.4-(3.42)						WQ
B-quarter 3R-ok	**B11**	1196, 1149, 1114	0.45+0.45+0.15						WQ
B-surface 3R+IFC ok	**B12**	1087, 1059, 1010	0.35-(3.27)+0.75-(3.34)+0.4-(3.42)	Same as the IFC cooling profile of test A16					IFC +WQ
B-surface 3R+Air OK	**B13**	1087, 1062, 1030	0.35-(3.27)+0.75-(3.34)+0.4-(3.42)	1020-880	348				IFC+WQ
B-Surface 3R+IFC2-ok	**B14**	1087, 1064, 1033	0.35-(3.27)+0.75-(3.34)+0.4-(3.42)	Same as the intense IFC2 cooling profile as the **Test A19**					IFC+WQ
Steel B 6P-low	**B15**	1037, 1016, 993	0.4+0.4+0.1	Same as the IFC cooling profile		871, 887, 887	0.14+0.13+0.12		IFC+WQ

stress								
Steel B 8P-failed	**B16**	1047, 1014, 984	0.4+0.4+0.1	Same as the IFC cooling profile	871, 857, 852, 848, 844	0.14+0.13+0.12+0.1 +0.14		IFC+WQ
Steel B 7 passes failed	**B17**	1046, 1015, 984	0.4+0.4+0.1	980-741	871, 861, 857, 853	0.14+0.13+0.12+0.1		IFC+WQ
Steel B 8 passes failed	**B18**	1038, 1008, 980	0.4+0.4+0.1	Same as the IFC cooling profile of test A16	870, 864, 858, 834, 847	0.14+0.13+0.12+0.1 +0.14		IFC+WQ
Steel B 8p-Less strain	**B19**	1043, 1023, 1004,	0.27+0.27+0.1=0.6 4	Same as the IFC cooling profile of test A16	873, 874, 875, 876, 876	0.14+0.13+0.12+0.1 +0.4		IFC+WQ
Steel B 8p-Less strain	**B20**	1046, 1023, 1006	0.35+0.35+0.15	Same as the IFC cooling profile of test A16	871, 872, 872, 832, 849	0.19+0.18+0.17+0.1 5+0.25		IFC+WQ
B-8p less strain	**B21**	1038, 997, 971	0.18+0.23+0.13	Same as the IFC cooling profile	871,860, 854, 847, 844	0.2+0.17+0.16+0.16 +0.2		IFC+WQ
B-8p Less strain	**B22**	1044, 1009, 981,	0.45+0.45+0.13	983-1063 9 1063-869 340	870,861, 853, 848, 843	0.2+0.17+0.16+0.16 +0.17		Air + WQ
B-8p- Less strain	**B23**	1043, 1006, 977	0.45+0.45+0.13	Same as the IFC cooling profile of test A16	870, 863, 856, 849, 843	0.2+0.17+0.16+0.16 +0.17		IFC+WQ
B-8p-Air – Less strain	**B24**	1042, 1009, 968	0.42+ 0.45+0.13	980-880 157	872, 861, 855, 850, 845	0.2+0.17+0.16+0.16 +0.14	880-760 760-400	209 1241

								WQ	
B-8p-Air – BAD Low stress	**B25**	1054, 1031, 999	0.42+0.45+0.13	980-880	20	875, 885, 882, 877, 870	0.2+0.17+0.16+0.16 +0.14	880-760 760-400 WQ	209 1241
B-3R-Hold ok	**B26**	1050, 1023, 994	0.45+0.45+0.15	980-980	348			WQ	
B-12mm Ferrite ok	**B27**	1035, 1005, 972	0.42+30s+0.45+30 s +0.13	980-880	20	876, 866, 853, 842, 833	0.2+0.17+0.16+0.16 +0.14	880-760 760-400 WQ	**209 1241**
B-12mm Ferrite ok	**B28**	1038, 1009, 973	0.42+30s+0.45+30 s+ 0.13	970-880	266	877, 855, 848, 843, 836	0.2+0.17+0.16+0.16 +0.14	880-760 760-400 WQ	**209 1241**
B-12mm ferrite	**B29**	1039, 1007, 974	0.4+30s+0.4+30s+ 0.1	970-880 880-880	261 5	881, 857, 848, 842, 836	0.2+0.17+0.16+0.16 +0.14	820-400	**22** WQ
B-12mm ferrite	**B30**	1036, 1008, 977	0.4+30s+0.4+30s+ 0.1	970-880 880-880	261 5	883, 861, 853, 845, 838	0.2+0.17+0.16+0.16 +0.14	820-400	**84 WQ**
B-10mm Ferrite	**B31**	1032, 1000, 976	**0.3**+30s+**0.3**+30s+ 0.1	970-880 880-880	261 5	879, 859, 848, 841, 834	**0.14+0.13+0.12+0.1 2+0.12**	820-400	**42 WQ**
B-12mm Ferrite-OK	**B32**	1036, 1005, 977	0.4+30s+0.4+30s+ 0.1	970-880 880-880	261 5	881, 860, 850, 844, 837	0.2+0.17+0.16+0.16 +0.14	820-400	**42 WQ**
10mm B-3R+W-OK	**B33**	1034, 999, 969	0.4+30s+0.4+30s+ 0.1						**WQ**
12mm 8P+266s+	**B34**	1037, 1001, 971	0.4+30s+0.4+30s+ 0.1	970-880 880-880	261 5	881, 866, 857, 850, 842	0.2+0.17+0.16+0.16 +0.14		**WQ**

W-OK									
12mm 8P+IFC+42 -OK	**B35**	1036, 999, 970	0.4+30s+0.4+30s+ 0.1	Same as the IFC cooling profile of test A16		869, 862, 854, 847, 839	0.2+0.17+0.16+0.16 +0.14	820-400	**42 WQ**
10mm 8P+IFC+42 -OK	**B36**	1033, 996, 968	**0.3**+30s+**0.3**+30s+ 0.1	Same as the IFC cooling profile of test A16		867, 855, 845, 841, 835	**0.14+0.13+0.12+0.1 2+0.12**	820-400	**42 WQ**
10mm centre roughing OK	**B37**	1207, 1154, 1123	0.2-(1.83)+0.5-(2.17) +0.3-(2.47) =1						**WQ**
12mm 8p+IFC2+ Air-OK	**B38**	1037, 1003, 971	0.4+30s+0.4+30s+ 0.1	980-593 593-721 721-768 768-816 816-852 852-880	20 6 4.3 6 20 60	870, 857, 852, 846, 839	0.2+0.17+0.16+0.16 +0.14	820-760 760-400	**209** **1241** WQ
12mm 8p+IFC+42 Low T-OK	**B39**	1031, 993, 968,	0.4+30s+0.4+30s+ 0.1	Same as the IFC cooling profile of test A16		825, 809, 799, 793, 786	0.2+0.17+0.16+0.16 +0.14	760-400	**42 WQ**
10mm 10p+42- OK	**B40**	1031, 996, 973, 927,888	**0.15+0.15+0.1+0.1 5+0.15=0.7**	890-870 870-880	20 10	867, 853, 846, 840, 835	**0.14+0.13+0.12+0.1 2+0.12**	820-400	**42 WQ**
10mmBar-	**B41**					878, 865, 853,	0.2+12s+0.17+12s+0	820-760	**209**

5P+Air-Less Strain						843, 831	.16+12s+0.16+13s+0.14 =0.83	760-400	**1241** WQ
10mm 3R+IFC+ W-OK	**B42**	1035, 1004, 974	0.4+30s+0.4+30s+0.1	Same as the IFC cooling profile of test A16					**WQ**
C-3R 2CT Less strain	C1	1023, 984, 952	0.4+0.4+0.1						WQ
C-3R+Hold	C2	1036,1010,979	0.4+0.4+0.1 (5^{-1})	979-810 810-800	20 3				WQ
C-3R+Hold 2CT-ok	C3	1038,1007,974	0.4+0.4+0.1 (10^{-1})	974-810 810-800	30 10				WQ
C 3R+Hold 2CT-OK	C4	1028, 981, 964	0.4+0.4+0.1	964-810 810-800	30 10				WQ
C-2R Less strain	C5	953. 944	0.4+0.4 (2.5 s-1)	1200-950 950-950	82 15				WQ
C-8P Less strain	C6	1037, 1014, 998	0.25+0.25+0.15	Same as the IFC cooling profile		869,874, 874, 831, 856	0.19+0.18+0.17+0.15+0.25		WQ
12mm 8p+Air+wok	C7	1035, 1002, 973	0.4+30s+0.4+30s+0.1	970-880 880-880	261 5	880, 867, 857 847, 837	0.2+0.17+0.16+0.16+0.14		WQ
12mm 8p+Air +42-ok	C8	1037, 1002, 972	0.4+30s+0.4+30s+0.1	970-880 880-880	261 5	880, 866, 857 849, 841	0.2+0.17+0.16+0.16+0.14	820-400	**42 WQ**

12mm 8p+IFC +42 ok	C9	1036, 1002, 972	0.4+30s+0.4+30s+ 0.1	Same as the IFC cooling profile		870, 862, 854 848, 841	0.2+0.17+0.16+0.16 +0.14	820-400	**42 WQ**
10mm 8p+Air +42-ok	C10	1032, 995, 970	**0.3**+30s+**0.3**+30s+ 0.1	970-880 880-880	261 5	879, 869, 855, 845, 836	**0.14+0.13+0.12+0.12+0.12**	820-400	**42 WQ**
10mm 8p+IFC +42-less strain	C11	1031, 996, 970	**0.3**+30s+**0.3**+30s+ 0.1	Same as the IFC cooling profile		867, 858, 848, 841, 835	**0.14+0.13+0.12+0.12+0.12**	820-400	**42 WQ**
10mm 8p+IFC2 +42-ok	C12	1030, 993, 970	**0.3**+30s+**0.3**+30s+ 0.1	Same as the intense IFC2 cooling profile of **Test B38**		867, 860, 849, 840, 833	**0.14+0.13+0.12+0.12+0.12**	820-400	**42 WQ**
10mm 8p+IFC +84-ok	C13	1033, 994, 968	**0.3**+30s+**0.3**+30s+ 0.1	Same as the IFC cooling profile		866, 851, 843, 838, 834	**0.14+0.13+0.12+0.12+0.12**	820-400	**84 WQ**
12mm 8p IFC+42-low Temp-ok	C14	1033, 996, 968	0.4+30s+0.4+30s+ 0.1	Same as the IFC cooling profile		826, 802, 790, 784, 777	0.2+0.17+0.16+0.16 +0.14	820-400	**42 WQ**
10mm-12p -OK	C15	981, 948, 931, 911, 890, 871	0.12+0.12+0.12+0.12+0.12+0.12(2.5s^{-1}) , gap time 12s			830, 811, 796, 785, 777, 771	0.12+0.12+0.12+0.12+0.12+0.12	755-400	**42 WQ**
10mm-13p-OK	C16	972, 953, 932, 912, 892, 872	0.12+0.12+0.12+0.12+0.12+0.12(2.5s^{-}			851, 832, 813, 794, 777, 758,	0.12+0.12+0.12+0.12+0.12+0.12+0.12(2.	755-400	**42 WQ**

			^{1}) = 0.72, gap time 12s			734	$5s^{-1}$) = 0.84, gap time 12s		
Bar 9F+Air-Less strain	C17					967, 939, 934, 951, 962, 963, 959, 950, 956	0.11+0.11+0.11+0.11+0.11+0.11+0.32+0.24+0.17+0.08		
10mm 3R+Air+W-ok	C18	1035, 997, 970	0.4+30s+0.4+30s+0.1	980-880 880-880	261 5				WQ
10mm 3R+IFC+W-2CT-ok	C19	1035, 998, 969	0.4+30s+0.4+30s+0.1	Same as the IFC cooling profile					WQ
D-3R-2CT Less strain	D1	1018, 992, 970	0.4+0.4+0.1	970-840	100				WQ
D-5F Less strain	D2			1200-870 870-870	85 15	865, 864, 859, 856, 853	0.14+0.13+0.12+0.1+0.14		WQ
D-1P-OK	D3	1034	0.4 (2.5 s^{-1})	1040-980 980-980	5 300				WQ Slow rate
D-1P-OK	D4	896	0.4 (2.5 s^{-1})	1200-900 900-900	82 15				WQ
Dummy-8ps-error in Temp. Ferrite	D5	735, 760, 778	0.25+0.28+0.13	778-774	3	774, 792, 796, 800, 802	0.2+0.17+0.16+0.16+0.17	809-981 981-760 760-400	18 191 1241 WQ
D-8Ps	D6	1039, 1007,	0.25+0.28+0.13	973-1067	9	871, 858, 851,	0.2+0.17+0.16+0.16	WQ	

		971		1067-880	339	846, 840	+0.17		
D-8Ps Shear	D7	1040, 1018, 997	0.25+0.28+0.13	997-872	26	875, 877, 874, 870, 865	0.2+0.17+0.16+0.16 +0.14	**840-760 709-400**	**209 1241 WQ**
10mm 8p+IFC +42-2TC-ok	D8	1035, 1000, 972	**0.3**+30s+**0.3**+30s+ 0.1	Same as the IFC cooling profile of the **Test A16**		871, 851, 844, 839, 835	**0.14+0.13+0.12+0.12+0.12**	820-400	**42 WQ**
Steel 68-8p	E1	1027,987,979	0.1+0.1+0.1=0.3	979-940	20	941,919,901,885,873	0.14+0.13+0.12+0.1 +0.14	WQ	WQ
Steel 68-3R-OK	E2	1035, 1007, 983	0.4+0.4+0.1	Same as the IFC cooling profile				WQ	WQ
Steel 68- 8p failed	E3	1035, 1015, 1001,	0.2+0.2+0.15	Same as the IFC cooling profile		869, 877, 879, 879, 881	0.19+0.18+0.17+0.15+0.25	Failed	
Steel 68- 8p	E4	1039, 1015, 1000	0.25+0.25+0.15	Same as the IFC cooling profile		870, 873, 874, 831, 853	0.19+0.18+0.17+0.15+0.25	WQ	WQ

Appendix B – An Example of Constructing and Correcting the Continuous Cooling Multipass Flow Curves from an 8-Pass PSC Test

As clearly shown in Appendix A, many different continuous cooling multipass (mainly the 8-pass) PSC tests were carried out in this research program and some of the corresponding multipass flow curves were presented in the Results chapter. In general, after each multipass PSC test was finished, the data logging that recorded the instantaneous specimen temperature, load, displacement and velocity of the ram at each time step (depending on the frequency setting) was automatically saved in a data file, which then was transferred into the designed Microsoft Excel spreadsheet to construct the corresponding multipass flow curve. For the single pass PSC testing, a good practice guide on the procedures of determination and correction of flow curves was published in 2006 [241], which has been employed and modified in constructing the multipass flow curves with some additional steps. In the following section, an example of determining and correcting the multipass flow curves from an 8-pass PSC test (Test B32) is presented step by step, and in total five major steps are required before the flow curve can be finalised.

B. 1. Obtaining the Relevant Deformation Data

It may useful to notice that the complete data logging included not only the target 8-pass deformation information when the PSC sample was inside the test furnace for the reduction, but also the reheating, holding and cooling temperature profiles when the sample was inside the FTTU. Therefore, the relevant reduction data were obtained by manually removing all the non-deformation data on the spreadsheet, and the resultant curve of applied load and tool-displacement of 8-pass deformation is presented in Figure B1.

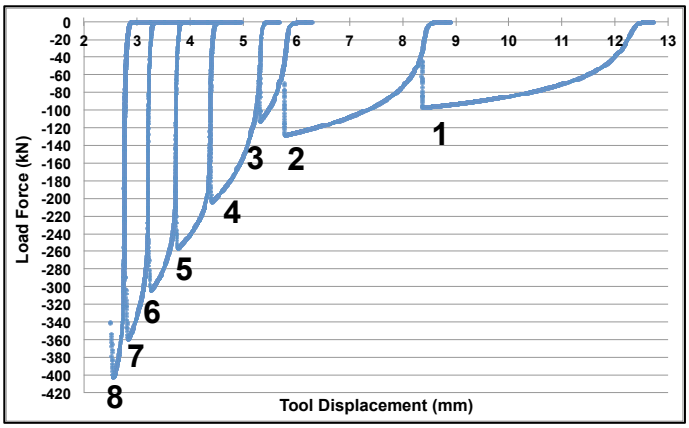

Figure B1: Relationships of tool displacements and applied compressive loads (negative values) of Nb+Ti steel B during 8-pass PSC tests (3R+266s+5F+10ºC/s)

B. 2. Hot Dimensions of PSC Specimen

The next step is to calculate the hot dimensions of PSC specimen during the deformation because at the high testing temperature the steel expands, which in turn depends on its thermal expansion coefficient α (0.000017/^{0}C was used in this project) and initial cold dimensions of the undeformed PSC sample. Therefore, it is important to remember that prior- and post-testing, the thickness and breadth of the PSC specimen at the room temperature are measured in several different places, which were described clearly in the good practice guide [241], and then the average cold measurements were used to determine the hot thickness and breadth of specimen at the high temperatures by using the following equations:

$$h_h = h_o \times \left[1 + \left(T_{Test} - 25\right) \times \alpha\right] \quad \text{(B1)}$$

$$b_h = b_o \times \left[1 + \left(T_{Test} - 25\right) \times \alpha\right] \quad \text{(B2)}$$

$$h_h = h_f \times \left[1 + \left(T_{Test} - 25\right) \times \alpha\right] \quad \text{(B3)}$$

$$b_h = b_f \times \left[1 + \left(T_{Test} - 25\right) \times \alpha\right] \quad \text{(B4)}$$

where h_h and b_h were the initial and final hot thickness and hot width of PSC sample respectively, while h_0 and b_0 were the initial cold and undeformed thickness and width of specimen at room temperature (was set at 25ºC); T_{Test} was the average deformation temperature. For the single pass PSC test, there was only one T_{Test}, but in the continuous cooling 8-pass PSC test, there were 8 different T_{Test}. Therefore, to calculate h_h and b_h, the T_{Test} (1037ºC) of the first deformation was applied in above Equations B1 and B2, which are presented in the following Table B1. The average values of final deformed thickness h_f and width B_f at room temperature were also used to determine the final deformed hot thickness and width at the end of 8-pass reduction, thus the T_{Test} (937ºC) of 8th deformation was applied in Equations B3 and B4, and the calculated results are shown in Table B1 in which w is the width of tool and the instantaneous deformation temperature T_i at each time step was used to determine the hot width of tool.

Table B1: Calculations of hot dimensions (mm) of PSC sample and width of tool at the high deformation temperature according to the cold measurement at room temperature

Average Dimensions			
	Cold (mm)	Hot (mm)	
h_0	11.994	12.200	**1037ºC**
b_0	29.98	30.496	**1037ºC**
h_f	2.804	2.842	**937ºC**
b_f	39.13975	39.680	**937ºC**
w	15	15.226	**T_i**

B. 3. Origin and Machine Compliance Correction

The applied deformation started to take place on the PSC sample when the tool displacement h_{Tool} (presented in Figure B1) was as the same as the calculated hot initial thickness, or when $h_h - h_{Tool} = 0$. However, due to the fine powders of boron nitride lubricant being sprayed on the sample surface before the test, the starting point of the sample deformation is off the origin, which is presented in the initial load-displacement curve (yellow curve) in Figure B2. Therefore, the yellow curve must be corrected for error in setting zero position of tool as well as the machine compliance, and the procedures were described clearly in the good practices guide [241]. In short, a straight line was drawn fitting through the initial part of the load-displacement curve, shown in Figure B2. Then, the entire curve is shifted to the right along the displacement axis (red curve) to make the straight line go through the origin. Finally, the "elastic deformation region" of the red curve was removed or corrected into the actual load-displacement curve, presented in the blue curve in Figure B3.

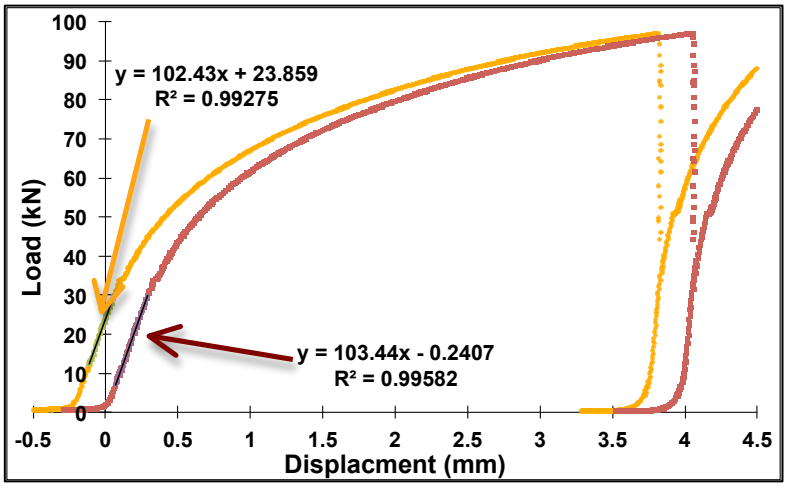

Figure B2: Comparison of the load displacement curves before (yellow curve) and after the origin or zero-offset correction (red curve)

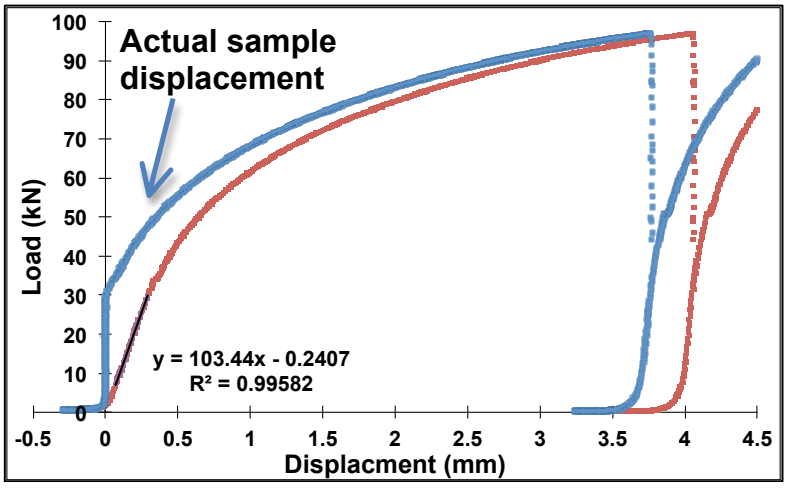

Figure B3: Comparison of the load displacement curves before (blue curve) and after the compliance correction (red curve)

B. 4. Determinations of Equivalent Strain and Equivalent Flow Stress

The rest of the steps, such as calculating the equivalent strain and flow stress, were determined through a series of empirical equations, which were the same as the procedures of constructing the flow curve for the single PSC pass. In brief, based on the actual sample displacement curve in Figure B3, the instantaneous PSC sample thickness h_i at each time step can be determined by subtraction from the initial hot thickness (12.2mm in Table B1), and then through equation $\varepsilon_3 = \ln\left(h_i / h_h\right)$, the instantaneous true strain ε_3 at the thickness direction was calculated. In order to determine the equivalent strain ε_{evm}, presented in Equation 62 in Literature Section 2.6.1, the true strain $\varepsilon_2 = \ln\left(b_i / b_h\right)$ in the breadth direction led to the lateral spread of the specimen also needing to be calculated, which is described clearly in the reference [241]. For determining the equivalent flow stress, the equation $\sigma = 2k / f$ was used, in which $f = \left(-\bar{\varepsilon} / \varepsilon_3\right)$ and the shear stress k depends on the instantaneous pressure $\bar{p} = Load / \left(b_i \times w_h\right)$, and three friction conditions: sliding, partially sticking and sticking. Different friction condition gave dissimilar relationship between the instantaneous pressure and maximum shear stress, which is presented in the good practice guide [241].

B. 5. Correction for the Temperature Rise during Deformation

Finally, to correct the effect of rising temperature during deformation on the flow stress, the following equation (described in reference [241]) was applied, in which the T_{inst} is the instantaneous recorded temperature while the T_{iso} is the desired isothermal or target temperature of each deformation. Therefore, for the continuous cooling 8-pass PSC test, this correction was applied to each pass, with different T_{iso}, and the resultant multipass flow curve (σ_{iso} versus $\bar{\varepsilon}$) is presented in Figure B4.

$$\sigma_{iso} = \sigma + \frac{Q_{def}}{\beta R}\left(\frac{1}{T_{iso}} - \frac{1}{T_{inst}}\right) \tag{B5}$$

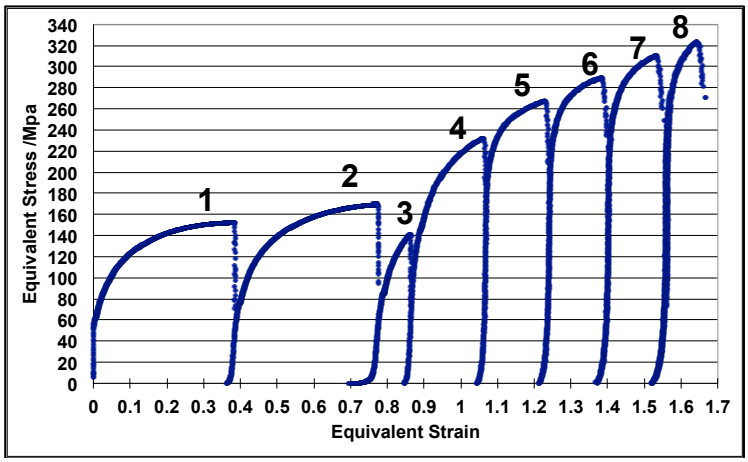

Figure B4: The final multipass flow curve of continuous cooling 8-pass PSC test (B42)